PHOTONS IN ACTION: ASYMMETRIC SYNTHESIS AND POLYMER DEGRADATION

A Dissertation
Submitted to the Graduate Faculty
of the
North Dakota State University
of Agriculture and Applied Science

By

Ramya Raghunathan

In Partial Fulfillment of the Requirements
for the Degree of
DOCTOR OF PHILOSOPHY

Major Department:
Chemistry and Biochemistry

May 2016

Fargo, North Dakota

North Dakota State University
Graduate School

Title

PHOTONS IN ACTION: ASYMMETRIC SYNTHESIS AND POLYMER DEGRADATION

By

Ramya Raghunathan

The Supervisory Committee certifies that this ***disquisition*** complies with North Dakota State University's regulations and meets the accepted standards for the degree of

DOCTOR OF PHILOSOPHY

SUPERVISORY COMMITTEE:

Prof. Jayaraman Sivaguru
Co-Chair

Prof. Mukund P. Sibi
Co-Chair

Prof. Pinjing Zhao

Prof. Kalpana Katti

Approved:

May 13, 2016
Date

Prof. Gregory R. Cook
Department Chair

ABSTRACT

Light is an environmentally benign and renewable source of energy that finds wide application in the field of science. This dissertation explores two areas of chemistry that utilizes light extensively *viz.*, asymmetric phototransformations and photodegradation of polymers. Phototransformation is an elegant method to construct structurally complex and diverse organic scaffolds. However, controlling the excited state in phototransformation to manipulate its stereochemical outcome is a challenge. This dissertation discloses a unique method employing atropisomeric chromophore to tackle asymmetric induction from the excited state. Photodegradation is a safe method to breakdown polymers that pose huge environmental and ecological concerns. Apart from designing polymers with a phototrigger that initiates the breakdown in a programmed fashion, this thesis also demonstrates recovery and reuse of monomers making the strategy sustainable.

Chapter 1 describes the importance of light and basic principles involved in organic phototransformations. In this section, principle differences between asymmetric thermal and photochemical transformations are introduced, methodologies developed in asymmetric phototransformations and the role of light in medicinal/biological system and material science is presented.

Chapter 2 evaluates metal free, thiourea/urea organocatalyst in enantioselective 6π-photocyclization of acrylanilides. Preliminary investigations revealed that the asymmetric induction imparted by thiourea was low. Detailed photophysical analysis provided valuable information on the excited state interaction of the substrate with the catalyst, opening avenues for future development of this strategy.

Chapter 3 demonstrates “axial-point chiral” strategy towards atropselective Paternò-Büchi reactions of oxoamides and chain length dependent [2+2] vs. [5+2]-photocycloaddition of atropisomeric maleimides. Axial chirality dictated high enantioselectivity (>97 %) in the photoproduct, while the solvent and substitution in the reactant controlled the diastereomeric ratio in photoproducts respectively.

Chapters 4-5 report the photodegradation of bio-derived polymers using phototriggers. This method not only enabled us to deconstruct the polymers to its functional monomer(s) but also enabled a pathway to recover and recycle the monomer highlighting the sustainability of the strategy.

In summary this thesis details the role of light in asymmetric phototransformations using organocatalyst and atropisomeric chromophores leading to chiral photoproducts. Further, it describes the photodegradation of biomass-derived polymers and its recoverability and reusability of the monomer as a sustainable approach.

ACKNOWLEDGEMENTS

I would like to take this opportunity to thank all those people who have made my Ph.D. days a memorable and a cherishable one. I would like to extend my sincere and deepest gratitude to my advisors Prof. Jayaraman Sivaguru and Prof. Mukund Sibi for their continuous support, patience and encouragement throughout my Ph.D. study. Over the years, I have learned so much from them, which made me a better scientist and also a better professional. They have always been a great source of inspiration and provided me with knowledge as well as moral support during tough and desperate times.

I would also like to thank my committee members Prof. Pinjing Zhao and Prof. Kalpana Katti for their support and constructive criticism for my research. They have always been very accommodative for my requests in setting up committee meeting and seminars.

I have always felt that our research group/lab is like “home away from home”. In that regards, I would like to sincerely appreciate all the past and the current Sivagroup members - Dr. Barry C Pemberton, Dr. Anoklase Jean-Luc Ayitou, Dr. Elango Kumarasamy, Dr. Nandini Vallavoju, Akila Iyer, Anthony Clay, Sunil Kandappa, Ravichandranath Singathi, Sapna Ahuja, all Sibi group members especially Dr. Selvakumar Sermadurai, Dr. Ramkumar Moorthy, Dr. Gaouyuan Ma, Hariharaputhiran Subramanian, Eric Serum, Krystal Kalliokoski, Joint postdoctorates of the Siva group and the Sibi group - Dr. Saravana Kumar Rajendran and Dr. Retheesh Krishnan. I would also like to thank all Governor school, PICNICs and REU students.

My sincere thanks to all the research groups at NDSU-Zhao group, Cook group, Sun group, Rasmussen Group and Srivatsava Group for their scientific discussions, chemicals and instruments whenever I needed.

I would like to thank the faculty members in the Department of Chemistry and Biochemistry for their support and encouragement during my research. I sincerely thank our staff scientists Dr. Angel Ugrinov, Dr. John Bagu and Daniel Wanner for helping me with X-ray crystallography and NMR studies.

My sincere thanks and appreciation to all the administrative staff -Wendy Leach, Linda Stoetzer, Amy Kain, Dionna Martel, Tina Exner, Jeff Scholl, David Tacke, Cole Larsen and Anthony Quinn- in the department of Chemistry and Biochemistry for their friendly conversation and taking care of all of my administrative responsibilities.

I sincerely thank the NSF (CHE-1213880 and CHE-1465075), NSF-CAREER CHE-0748525 for Prof. Jayaraman Sivaguru and NSF-NDEPSCoR (EPS-IIA-1355466) for the center for sustainable materials, NDSU for the generous support to carry out research.

I sincerely thank the NDSU Graduate School for providing me with a doctoral dissertation fellowship this past year, which helped me concentrate on my research and thesis work. I would also like to thank the Department of Chemistry and Biochemistry for recognizing me with the “Chemistry Graduate Student Scholarship” and “Robert Mary Ann Tucker Research award”.

I would like to thank our research collaborator Prof. Dean Webster and his group members especially Dr. Ivan Hevus and Dr. Songqi Ma for their great collaboration in the polymer project that is detailed in this dissertation and also for teaching me the fundamentals of polymer chemistry.

I would like to thank our research collaborators Prof. Nicholas Turro and Dr. Steffen Jockusch at Columbia University, New York, NY for their collaborative work with respect to photophysical aspects detailed in this dissertation and publications elsewhere.

I want to extend my heartfelt thank you to Dr. Sumathy Sivaguru and Sheryll Clapp FNP-BC for their kindness, sincere caring and concern whenever I was not feeling well that made everything better and are a great encouragement.

My special thanks to my parents (mom, dad, mom-in law, dad-in law) for their unconditional love, trust, blessings and prayers. I would also like to thank all my family members (brothers, sisters-in law, brother-in-law, co-sister-in-law, my two lovely nieces and my two wonderful besties) for their support and encouragement. I strongly believe that, without their wishes this long journey would not have been successful.

Saving the best for the last, a special thanks to my soul mate, my husband and a great friend-Elango Kumarasamy without whom I could not have reached my goals. He has been my pillar of strength and confidence through ups and downs and always made me feel special. Thank you so much for helping me sail through this journey and for being there for me all the times with lots of love, faith, and support. You are the best thing that ever happened to me and you mean world to me!

DEDICATION

To my Mom and Dad

To whom I owe for what I am today and everything I have today

TABLE OF CONTENTS

LIST OF TABLES

LIST OF FIGURES

LIST OF SCHEMES

LIST OF CHARTS

LIST OF EQUATIONS

LIST OF ABBREVIATIONS

Ac.....Acetyl

BINAP.....2,2'-bis(diphenylphosphino)-1,1'-binaphthyl

Ts.....*para*-toluenesulfonyl

MsCl.....Methanesulfonyl chloride

Et_3N.....Triethylamine

Boc.....*tert*-butyloxycarbonyl

dba.....Dibenzylideneacetone

BuLi.....Butyllithium

HAT.....Hydrogen atom transfer

CDI.....1,1'-Carbonyldiimidazole

equiv.....Equivalent(s)

ESI.....Electrospray ionization

PkA.....First eluting enantiomer in the HPLC on a chiral stationary phase

PkB.....Second eluting enantiomer in the HPLC on a chiral stationary phase

d.r......Diastereomeric ratio

ee.....Enantiomeric excess

e.r......Enantiomeric ratio

rac.....Racemic

FTIR.....Fourier transform infrared spectroscopy

FDCA.....Furan dicarboxylic acid

h.....Hours

h.....Planck's constant

HMPA.....Hexamethylphosphoramide

HMF.....Hydroxy methyl furfural

ID .....Inner diameter

IS.....Internal standard

k_B.....Boltzmann's constant

LDA .....Lithium diisopropylamide

LiHMDS.....Lithium bis(trimethylsilyl)amide

NaHMDS.....Sodium bis(trimethylsilyl)amide

M .....Molar

mM .....Millimolar

min .....Minutes

N/A .....Not applicable

NMR.....Nuclear magnetic resonance

Ph.....Phenyl

PMB .....*para*-methoxybenzyl

ppm .....Parts per million

concd .....Concentration

rt.....Room temperature

satd. .....Saturated

Anhyd......Anhydrous

o.....Ortho

m.....Meta

p.....Para

^{t}Bu .....*tert*-butyl

^{i}Pr.....isopropyl

Me .....Methyl

Et.....Ethyl

tol ..... …..Tolyl

Bu..... …..Butyl

Bn..... …..Benzyl

Bz..... …..Benzoyl

TMS ..... …..Trimethylsilyl

TIPS ..... …..Triisopropyl

AcOH ..... …..Acetic acid

Hex..... …..Hexanes

TFA ..... …..Trifluoroacetic acid

TPM ..... …..Triphenyl methane

DCE ..... …..1,2-dichloroethane

DCM..... …..Dichloromethane

$CHCl_3$ ..... …..Chloroform

$CDCl_3$ ..... …..Deuterated chloroform

EtOAc..... …..Ethyl acetate

MCH..... …..Methylcyclohexane

MeCN..... …..Acetonitrile

MeOH..... …..Methanol

EtOH ..... …... Ethanol

IPA ..... …..Isopropyl alcohol (2-propanol)

TFE ..... …..Trifluoroethanol

THF ..... …..Tetrahydrofuran

THF-d_8 ..... …..Deutrated tetrahydrofuran

D_2O ..... …..Deutrated water

DMSO ..... …..Dimethylsulfoxide

DMSO-d_6..... Deuterated dimethylsulfoxide

DMF ..... N,N-dimethylformamide

DI ..... De ionized

Cy..... Cyclohexyl

Cp ..... Cyclopentyl

w/w..... Weight by weight (percentage)

v/v ..... Volume by volume (percentage)

TLC ..... Thin layer chromatography

R*f* ..... Retardation factor

HPLC ..... High Performance Liquid Chromatography

GC..... Gas chromatography

GPC ..... Gel permeation chromatography

TGA..... Thermogravimetric analysis

DSC ..... Differential scanning calorimetry

HRMS ..... High Resolution Mass Spectrometry

ESI ..... Electrospray Ionization

XRD ..... X-ray diffraction

PXRD ..... Powder X-ray diffraction

atm ..... Atmosphere(s)

UV/VIS ..... Ultra-Violet/Visible light

CD..... Circular dichroism

CPL ..... Circularly polarized light

HOMO..... Highest Occupied Molecular Orbital

LUMO..... Lowest Unoccupied Molecular Orbital

NEER ..... Non-Equilibrating Excited Rotamers

ISC ..... ……Intersystem crossing

S_1 or S_n ..... ……First or n^{th} singlet excited state

S_0 ..... ……Ground state (singlet)

T_1 or T_n..... ……First or n^{th} triplet excited state

SET ..... ……Single electron transfer

eT..... …….. Electron transfer

E_T ..... …..Triplet energy of the excited state species

CHAPTER 1. INTRODUCTION TO LIGHT, PRINCIPLES OF PHOTOCHEMISTRY AND ITS APPLICATIONS

1.1. Introduction

Light (photon) plays an important and fascinating role in the evolution and sustenance of the life on our planet. The interaction of human being with light started several thousand years ago when people began using fire, induced by lightening for cooking food, protecting themselves from predators and for warmth.[1] Light is a constant source of energy that cherishes the life on earth and every form of life respond to light in one way or another. Various natural phenomena that occur on earth such as photosynthesis, circadian rhythms and vision cannot function in the absence of light. Even in the modern day medicine, such as treatment of jaundice in infants, light plays an indispensable role.

Ever since we understood the importance of light and it's exhaustive supply of energy, we began to study nature of light and its potential for advancing science and ultimately our way of life. Light is employed in various scientific fields including medicine, life sciences, art and technology to understand, analyze and apply the information. Among different areas of science, chemistry played a critical role in the history of light, leading to the development of devices such as microscope, telescope, optical microscopy etc., and many light induced phenomena/processes.[1] The most important and earliest accounts of light (sunlight) induced processes are burning light of Archimedes, simple oxidation and reduction of metal ions by eminent scientists Archimedes, Joseph Priestley and J. W. Döbereiner respectively.[2] Yet, artificial synthesis of organic molecules using light was only at their imaginary phase or at best in the nascent stage. In 1834, Hermann Trommsdorff reported his observation on the first account of phototransformations on Santonin **1** (Scheme 1.1), a sesquiterpene lactone that turned yellow and burst upon exposure to light.[2-4] Later in 1872 Fausto Sestini and Stanislao Cannizaro jointly pursued detailed study on Santonin and the isolation of photosantonic acid.[3] Other investigations of chemical reaction up on interaction with light includes photodimerization of aromatics with acid derivatives and styrene derivatives by Carl Julius Fritzsche and Carl Theodor Liebermann respectively, geometric isomerization of olefins by W. H. Perkins, photoinduced halogenations by Julian Scharamm, photoreduction of carbonyl compounds by Heinrich Klinger.[2] Though several reports on light induced

reactions emerged on the literature, it was not until 20th century, when Giacomo Ciamician and Paul Silber performed a series of systematic investigations on light based chemical reactions.[3] Since then the role of light in organic chemistry has grown steadily leading to a formation of new branch of chemistry "photochemistry" that dedicatedly explores the interaction of light with organic molecules.

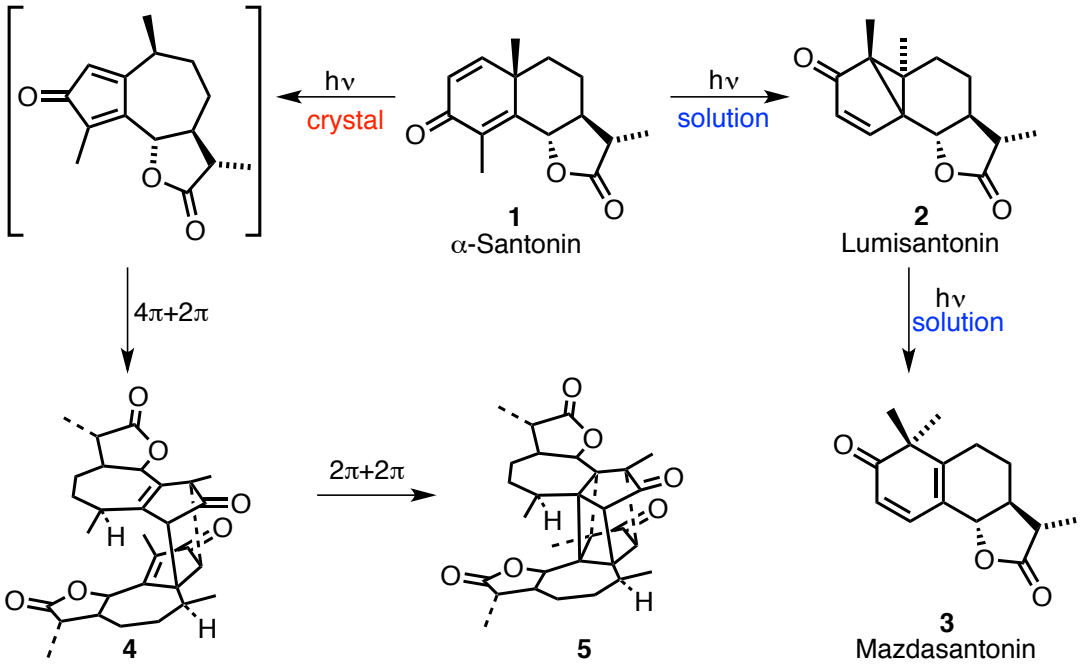

Scheme 1.1: Solid and solution state photoreaction of α-santonin (Reproduced from reference 4 with permission from American Chemical Society, 2007).

1.2. Principles of photochemistry

The study of chemical reactions of molecules upon interaction with light is called photochemistry. An organic molecule in the ground state upon photo excitation is promoted to its higher energy states. Now this molecule in the higher energy undergoes subsequent reaction to result in new molecules. Such a phenomenon often allows one to access structurally complex organic scaffolds in fewer steps that are usually very challenging or inaccessible through conventional thermal chemistry. Not all the organic compounds have the ability to absorb light, it is only the molecules that have chromophores can absorb light. Chromophore is a functionality in a compound that can interact with light and enable the molecule to reach the excited state. In order to understand the course of interaction of light with a chromophore (part of the molecule that absorbs light) it is essential to understand the nature of the light. Light is an

electromagnetic radiation that is a continuous spectrum of waves from low energy - long radio waves (longer wavelength) to high-energy short gamma waves (shorter wavelength) as shown in Figure 1.1. Synthetic organic photochemists are mainly interested in ultraviolet and visible light portion of the electromagnetic spectrum that is capable of inducing an excitation in a given molecule leading to chemical reactivity.

The photochemical transformations can be understood by two fundamental principles of photochemistry. The first law of photochemistry, the Grothuss-Draper law which states that, “a molecule must absorb light to undergo photochemical reaction”. The second law of photochemistry, the Stark-Einstein law that states that “when the photon of energy (resonance) is absorbed by a chromophore in the system, absorbance process takes place where the energy of the photon is transferred to a molecule leading to an electronically excited state”. Such matching energy or resonance energy of photon can cause only one electronic excitation. In other words, an encounter with single photon will only result in the electronic excitation of one molecule.

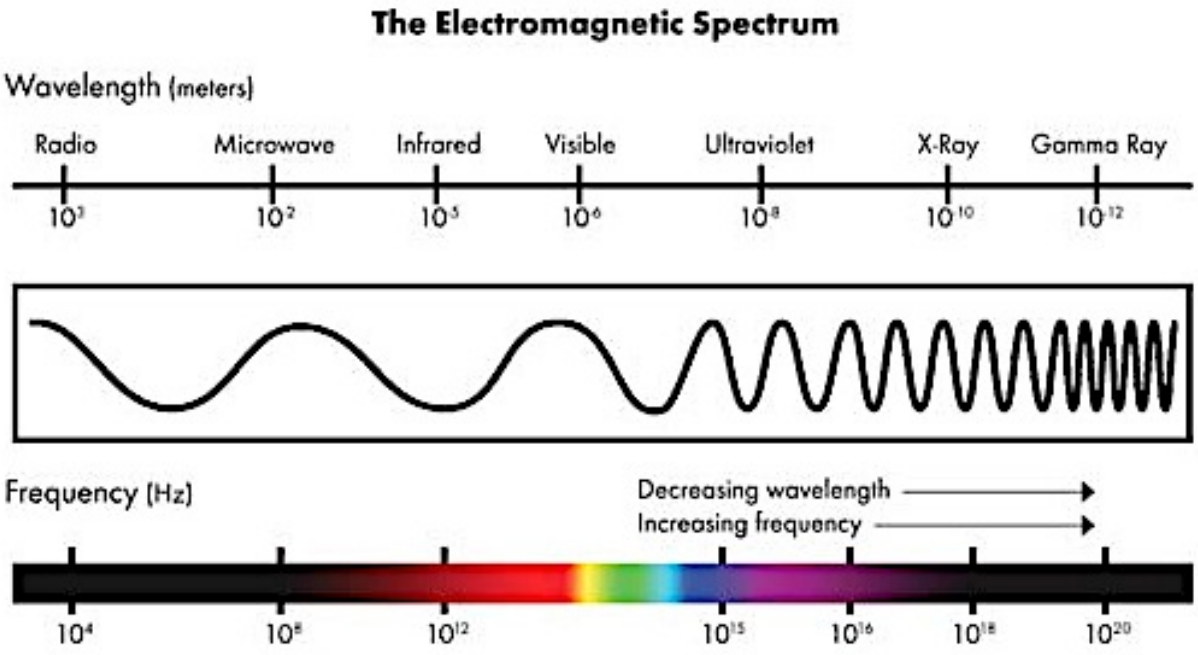

Figure 1.1: Electromagnetic spectrum of light.[5]

The energy absorbed by the chromophore of a molecule depends on the type of atoms and bonds involved in the process of excitation. The energy of the photon required for the excitation is given by Planck-Einstein equation. Once the molecule is excited, it can either be singlet excited state where the

electrons have opposite spin (↑↓- paired) with a net spin of zero (singlet) or triplet where the electron are of same spin (↑↑- unpaired) with a net spin of one (triplet) based upon spin angular momentum as depicted in Figure 1.2.

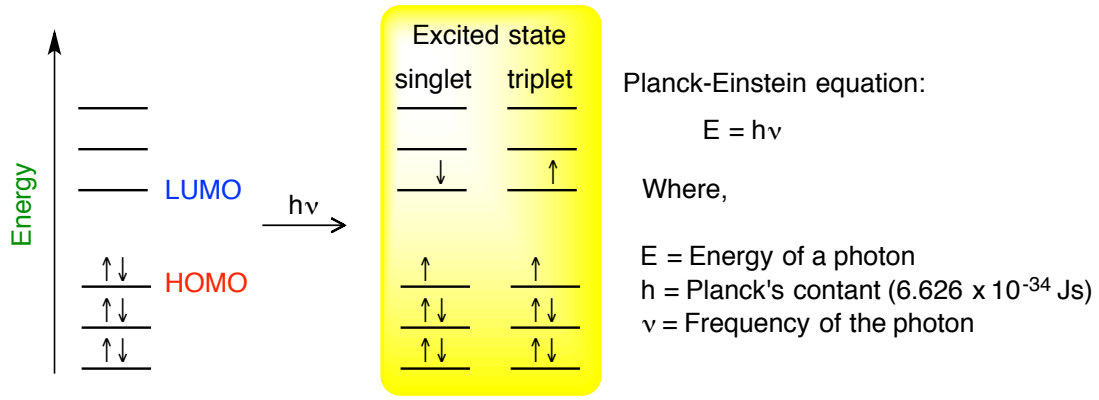

Figure 1.2: Photoexcitation of electron from HOMO to LUMO.

The excited molecules have several pathways to relax to the ground state. These pathways are broadly classified into radiative and non-radiative and are portrayed in the Jablonski diagram (Figure 1.3).

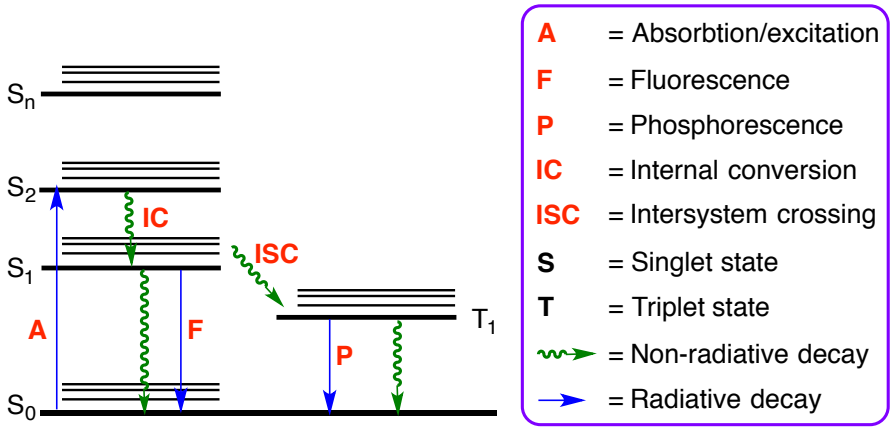

Figure 1.3: Jablonski diagram depicting relaxation processes.

In a non-radiative process, transition from higher to lower electronic state occurs via thermal or vibrational relaxation without the emission of light and this process is known as the internal conversion (IC).

Internal conversion can be further classified into two types depending on whether a change in the spin multiplicity occurs or not. When a relaxation from vibrational level of one electronic state to another vibrational level of its lower electronic state occurs ($S_1 \rightarrow S_0$), spin change is not involved, such a process

is termed as “spin allowed transition”. However if the transition from higher electronic state to lower electronic state occurs with change in spin as in the case of transition from singlet to triplet (S → T), then the process is called as “spin forbidden transition”. This process is also known as intersystem crossing (*ISC*) which occurs typically slower than an IC as it involves change in spin of electrons.

In a radiative relaxation process, the excited species relaxes to the ground state by emitting a photon either by fluorescence or phosphorescence. When an excited singlet state (S_n) returns to ground state (S_0) with the emission of light, the process is termed as fluorescence (F). Whereas if the relaxation to S_0 occurs from triplet excited state (T_n) it is termed as phosphorescence (P). Since this process is “spin forbidden”, phosphorescence is generally slow compared to fluorescence. The approximate time scales for the above-discussed transitions are given in the Table 1.1.

Table 1.1: Timescale for the relaxation pathways from the excited state.[6]

Process	Transition	Timescale (sec)
Light absorption	$S_0 \rightarrow S_n$	*ca*. 10^{-15}
Internal conversion	$S_n \rightarrow S_1$	10^{-14} to 10^{-11}
Vibrational relaxation	$S_n^* \rightarrow S_n$	10^{-12} to 10^{-10}
Intersystem crossing	$S_1 \rightarrow T_1$	10^{-11} to 10^{-6}
Fluorescence	$S_1 \rightarrow S_0$	10^{-9} to 10^{-6}
Phosphorescence	$T_1 \rightarrow S_0$	10^{-3} to 100
Non-radiative decay	$S_1 \rightarrow S_0$ $T_1 \rightarrow S_0$	10^{-7} to 10^{-5} 10^{-3} to 100

Though molecules can be photo-excited upon absorption of photon, not all the excitation leads to desired photoproduct(s). As the excited state is higher in energy, has multiple competing pathways to relax to the ground state and the domination of one path over the other depends on several factors. The efficiency of a photochemical process is given by its quantum yield (Φ) as shown in the equation 1.1. Quantum yield (Φ) is described as the ratio of number of molecules that undergo desired photoreaction to the number of absorbed photon by the molecule undergoing the desired transformation.

$$\text{Quantum Yield } (\Phi) = \frac{\text{Number of molecules undergo desired process}}{\text{Number of photons absorbed}} \qquad \textbf{(Equation 1.1)}$$

1.3. Standards for a photochemical set up

Synthetic photochemistry made significant progress since early 20th century after Ciamician and Silber's systematic investigations of photochemical reactions.[7] The development of ultrafast spectroscopic techniques provided significant understanding of the excited state behavior of the molecule that paved the way for further development in this branch of chemistry. Based on extensive studies and observation by various scientists over time, general standards have been recommended while performing a photochemical reaction. Those guidelines are discussed in detail in the following sections.

1.3.1. Choice of irradiation source

Light is an essential part of a photochemical reaction, therefore choice of light source employed in a given photochemical reaction becomes very important. The chromophore of a molecule is responsible for the light absorption and it can be excited using a resonance wavelength of light. Use of excess energy of light can lead to detrimental effects or unwanted side products leading to poor efficiency in the reaction. The choice of irradiation wavelength should be based on the type of chromophore involved in the photoreaction. Table 1.2 provides some insights on the types of chromophores, their transition and wavelength at which there is maximum absorption.

Table 1.2: Types of chromophore, their transition and maximum absorption wavelength.[8,9]

Chromophore	Transition	λ_{max} (nm)
N=O	$n \rightarrow \pi^*$	~660
C=S	$n \rightarrow \pi^*$	~520
N=N	$n \rightarrow \pi^*$	~350
C=C-C=O	$n \rightarrow \pi^*$	~350
C=O	$n \rightarrow \pi^*$	~280
Benzene	$\pi \rightarrow \pi^*$	~260
C=C-C=O	$\pi \rightarrow \pi^*$	~220
C=C-C=C	$\pi \rightarrow \pi^*$	~220
C=C	$\pi \rightarrow \pi^*$	~180
C-C	$\sigma \rightarrow \sigma^*$	<180
C=H	$\sigma \rightarrow \sigma^*$	<180

The Table 1.2 clearly indicates that most of the chromophores can be excited with wide spectrum of irradiation sources ranging from visible to UV region. The most commonly used broadband irradiation source is a mercury lamp. The lamp is usually placed in an immersion well enclosed by quartz glass jacket with continuous flow of water that acts as a heat sink and prevents over heating of the lamp. Mercury lamps can be divided into 3 types: low, medium and high pressure based on their spectral output and intensity. Among them, medium pressure mercury lamp is the widely used light source for organic phototransformations. However, broadband light is not suitable in a situation where selective excitation of a chromophore is needed in a molecule that has other excitable chromophores. In situations like these a narrow bandwidth of light sources are employed which often prove to be very selective and useful in preventing undesired products or decomposition.[10] There are several photochemical set ups available in the market that can be fitted with narrow bandwidth light bulbs such as Rayonet® reactors that can be fitted with variety of light sources including ~250 nm, ~300 nm, ~350 nm, ~420 nm, LEDs which comes in multiple wavelengths (violet LED, blue LED, green LED , red LED etc.,), common fluorescence lamp (CFL) that emits light in the visible region or monochromatic laser irradiation.

1.3.2. Choice of photochemical apparatus

Apart from narrow bandwidth light source, the choice of glasswares for a photochemical reaction can also allow us to bring about selective excitation of a desired chromophore. The specific make up of a glassware can act like a filter thereby allowing only certain wavelength of light to penetrate through the reaction vessel. Various types of glasswares are available in the market and these include Uranium (>350 nm cut off) Pyrex (< 290 nm cut off), Corex (<260 nm cut off), Vycor (<220 nm cut off) and Quartz (<190 nm cut off). Apart from the listed glassware/filters, there are specially designed glass filters and filter solutions are also available that are used to cut off undesired wavelength of light.[11]

1.3.3. Choice of solvents

The choice of solvent can play a crucial role in the outcome of a photochemical reaction. Often times, the poor choice of solvent lead to undesired side products and decomposition of the reactants or

products. As the solvent molecules can be excited using an appropriate light source, it becomes imperative to choose a solvent that does not absorb light in a given reaction. Further, solvent can also be taken to our advantage to accelerate a reaction (as a sensitizer), provide useful insights about the reaction mechanisms, control by-product formation and also influence the ratios of the photoproducts (in the case of formation of more than one photo product). Below are few parameters that are to be followed when choosing a solvent

1. Solvent should be free of impurities as presence of impurities can affect the reactions.
2. The solvent must completely dissolve the reactant(s) to give a homogenous solution to avoid scattering and reflection of the light.
3. The solvent must be optically transparent at the wavelength of excitation where the reactant(s) only absorb.
4. The solvent should not adversely affect the excited state of a molecule and enable its decay.
5. The concentration of the reaction mixture has to be optimized such that the reactants in the solvent itself should not act as a filter leading to internal filter effect.

Table 1.3 lists some of the common organic solvents and their approximate cut off wavelength:[12-14]

Table 1.3: Common organic solvents used in the photoreactions and their UV-cut off.

Entry	Solvent	Dielectric constant	UV Cut-off (nm)
1	*n*-hexanes	1.9	195
2	Cyclohexane	2.0	215
3	Carbon tetrachloride	2.2	265
4	Benzene	2.3	280
5	Toluene	2.4	285
6	1,4-Dioxane	2.2	230
7	Chloroform	4.8	245
8	Diethyl ether	4.3	215
9	Methylene chloride	9.1	230
10	Tetrahydrofuran	7.5	245
11	Ethyl acetate	6.0	255
12	Acetone	21.0	330
13	Acetonitrile	36.6	190
14	Dimethylsulfoxide	47.0	277
15	Ethanol	24.6	204
16	Methanol	32.6	205
17	Acetic acid	6.2	250
18	Water	78.5	185

1.3.4. The choice of sensitizers

Sensitizers are photochemical catalysts that act as a light antenna and transfer its excited state energy to the reactant there by bringing about a photochemical reaction. Sensitizers are used when the desired reactants are poor light absorbers or their excited state is short lived. In such cases the sensitizer absorbs light and transfers its energy (or electron) to reactant to initiate the photochemical reaction. In order to perform this task, the sensitizer should absorb light efficiently and should have long life time to transfer its energy or electron to the reactants. Importantly, the sensitizer should be photostable to perform the energy transfer multiple times. The Table 1.4 is the lists some of the most commonly used sensitizers [15]

Table 1.4: List of triplet sensitizers and their triplet energies.

Entry	Sensitizers	E_T (kcal·mol $^{-1}$)
1	6,9-Dicyanoanthracne	~42
2	Anthracene	~43
3	Benzil	~53
4	Biacetyl	~56
5	2-acetyl-napthalene	~59
6	Naphthalene	~61
7	Thioxanthone	~63
8	Biphenyl	~66
9	Fluorenone	~66
10	Benzophenone	~69
11	Acetophenone	~74
12	Xanthone	~74
13	Acetone	~78
14	Pyridine	~85

1.4. Role of light in asymmetric organic synthesis

The importance of accessing optically pure (chiral) molecule, especially in the pharmaceutical industry and drug discovery is increasing exponentially. Such significance was given to chiral molecules after the tragedy involved in the use of undesired isomer of thalidomide drug in the year 1957 that led to child birth with abnormalities.[16] Since then, the field of asymmetric synthesis has evolved into a powerful method in organic synthesis that focused to obtain optically pure molecules. While the demand for new drugs are increasing, there is also a growing concern for developing methods to access those drugs with greener protocol. In this regard, phototransformations holds promise as it provides access to structurally complex organic scaffolds with multiple stereogenic centers in fewer steps.[17-19] In addition, photochemical transformations employs environmentally benign reagent – “light” giving a sense of greener perspective in achieving structural complexity in the molecule. While accessing complexity in an organic molecule seemed to be easy with the use of light, obtaining them with desired chiral purity proved to be a challenging task. The difficulty in achieving high stereocontrol is due to the short-lived excited state of the molecule, which makes it challenging to control and tune the excited state for a favorable stereochemical

outcome. The other issue involved in the stereocontrol is that the excited state is much higher in energy and subsequent processes are barrier less that presents challenges in tuning the energetics of a reaction. An important criterion to achieve high stereoselectivity in a photoreaction is the preorganization of the reactants. Preorganization sets the reactants in an appropriate conformation such that the excited state can be channeled to a desired reaction pathway. In this vein, many research groups have looked at various strategies to obtain stereoselective phototransformations by employing methods that were successful in thermal transformations. Unfortunately, the successful methods in thermal reactions such as chiral perturbers, chiral auxiliaries etc., only resulted in moderate success. The fundamental challenge involved in obtaining high enantioselectivity in the photoreaction is poor interaction of the chiral perturbers to bring about desired chiral induction during short-lived excited state of the chromophore undergoing the chemical transformations.

In a conventional thermal reaction, the chiral inductors interact with prochiral reactants resulting in diastereomeric transition states (Figure 1.4A). The extent of interaction with the reactant will dictate the selectivity in the product. For example, a differential activation energy of ~3 kcal·mol^{-1} at room temperature (298 K) is sufficient to result in >99% enantioselectivity. But this situation cannot be extended to photochemical transformations. In a photochemical reaction, upon shining light, the reactants are promoted to higher excited states that are short-lived and highly energetic. The high-energy excited species is unable to distinguish the small diastereomeric energy difference imparted by the chiral perturbers thus leading to poor selectivity (Figure 1.4B) in the resulting product. To address this bottleneck, photochemists have attempted various strategies with limited success.[20] The following subsection provides a brief overview of those endeavors.

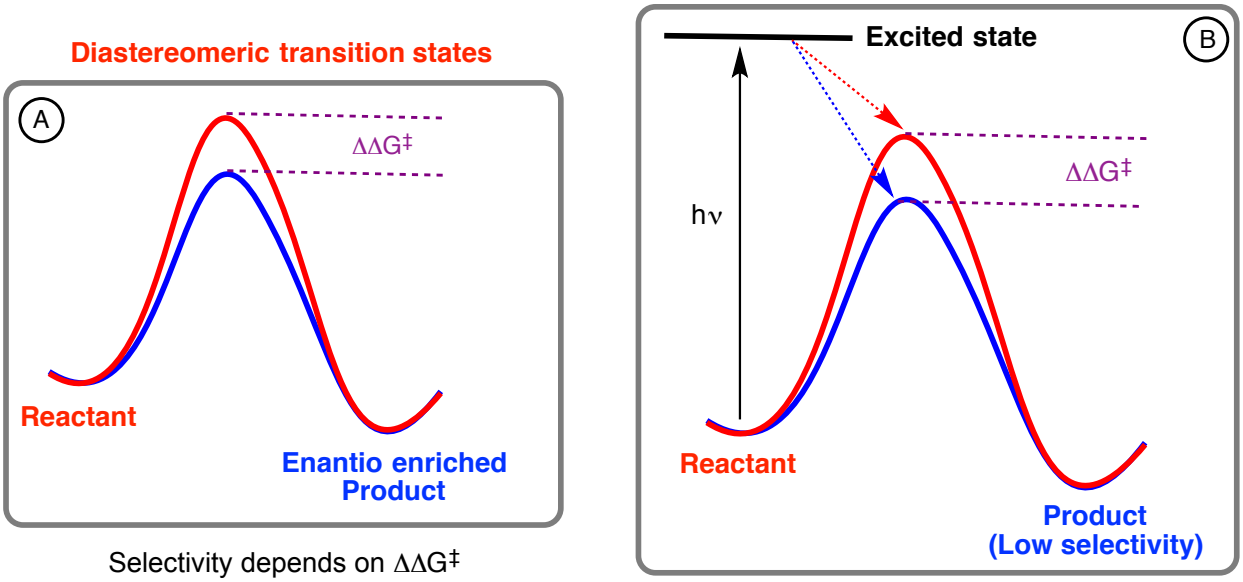

Figure 1.4: Representation of diastereomeric transition state in A) thermal and B) photoreaction.

1.4.1. Asymmetric phototransformations using chiral light source

Circularly polarized light (CPL) is a chiral electromagnetic radiation and in principle up on interaction with the racemic reactant(s) it should yield enantioenriched product. Indeed, photoreaction-using CPL was the earliest performed asymmetric phototransformations. The potential of using CPL was first suggested by Le Bel and Van't Hoff in the 19th century.[21,22] A prochiral molecule up on interacting with CPL gets promoted to the excited state with a preference of one enantiomer over the other leading to enantioenriched product. In principle asymmetric phototransformations influenced by CPL can be classified into three categories as depicted in Figure 1.5.[23] They are a) photo resolution where the inter convertible enantiomers are deracemized (Figure 1.5A) b) asymmetric synthesis where the optically active compound is synthesized from prochiral substrate (Figure 1.5 B) and c) photo destruction where one of the enantiomer in the racemate is preferentially destroyed leading to enantioenrichment (Figure 1.5C).

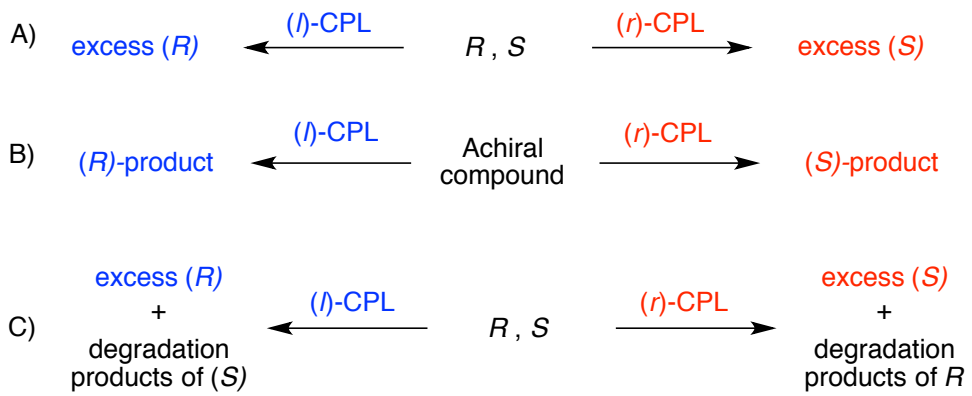

Figure 1.5: Classification of CPL induced symmetric transformation A) photo resolution, B) asymmetric synthesis, C) photo destruction. (Reproduced from reference 20 with permission from Wiley-VCH, 1999).

Though Le bel and Van't Hoff considered CPL for obtaining optically active molecule, it was not until 1929, when Kuhn and coworkers first experimentally reported the photo resolution of racemic ethyl 2-bromopropanoate **6** and 2-azido-*N*,*N*-dimethylpropanamide **7** (Scheme 1.2).[8,24,25] They proposed that the photo resolution took place via homolytic cleavage of α-C-Br or α-C-N_3 followed by recombination in a stereocontrolled fashion. The anisotropy factor (g) (measure of excitation of one enantiomer over the other towards CPL) played a crucial role in dictating the chirality in the product.

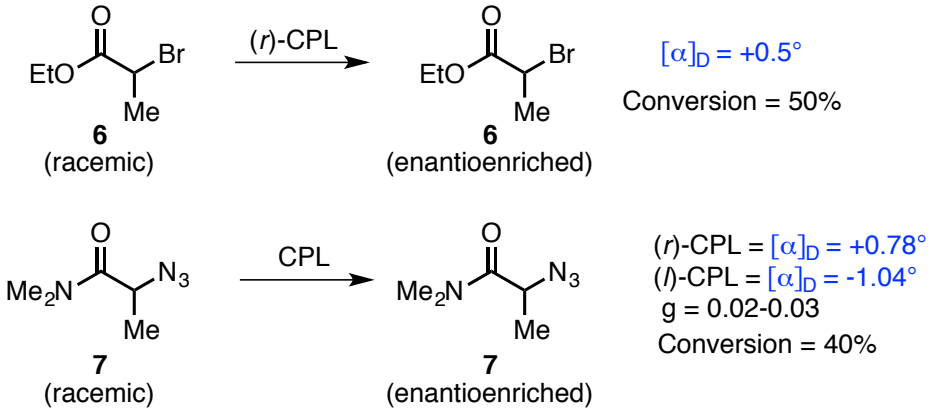

Scheme 1.2: Photo resolution of ethyl 2-bromopropanoate **6** (top) and 2-azido-*N*,*N*-dimethylpropanamide **7** (bottom) using CPL.

In 1971, Kagan and coworkers reported asymmetric synthesis of hexahelicenes **12** using CPL.[26] They were successful in achieving optically active hexahelicenes by oxidative 6π-photocyclization of 1,2-diarylethanes **8** and **9** in the presence of iodine (Scheme 1.3).

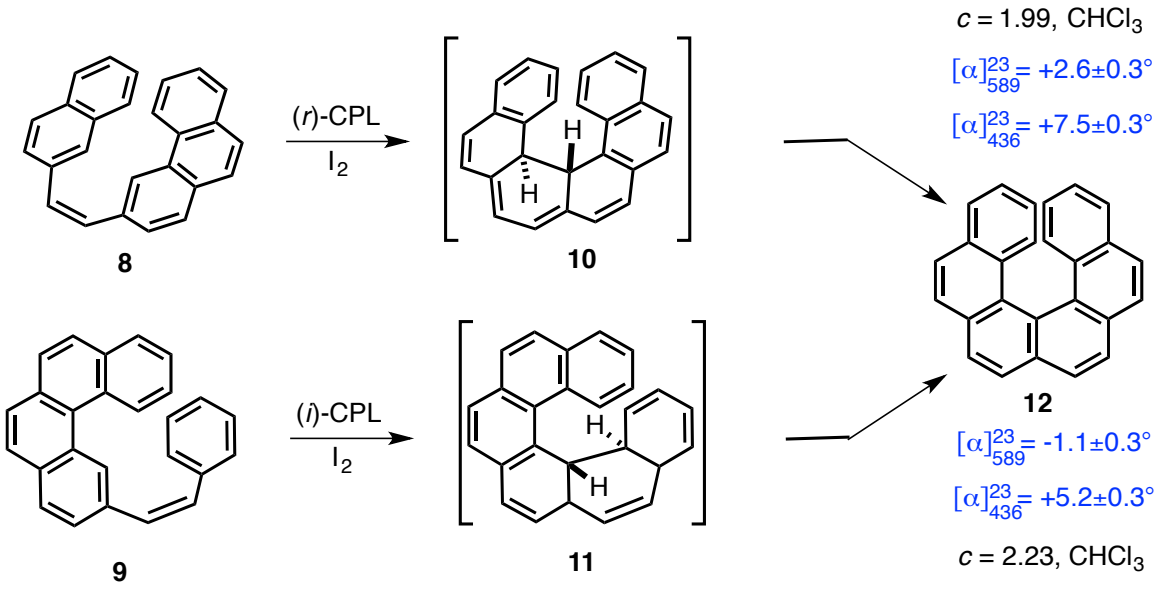

Scheme 1.3: Oxidative 6π-photocyclization of 1,2-diarylethanes **8**-**9** induced by CPL.

Bonner and coworkers demonstrated the first asymmetric photolysis of prebiotically important amino acid (*rac*)-Leucine **13** using CPL generated by Nd/YAG laser (Scheme 1.4). [27] They obtained 1.98 % *ee*, 2.50 % *ee* with (*r*)-CPl and (*l*)-CPL respectively as shown in Scheme 1.4.

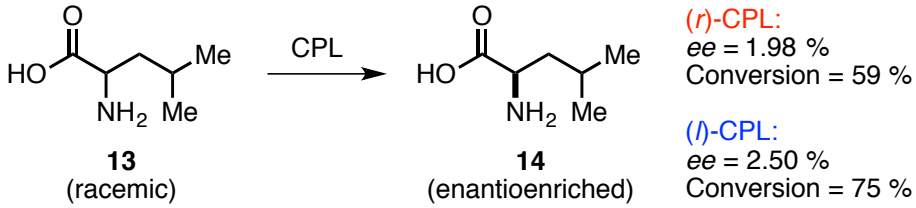

Scheme 1.4: Asymmetric photolysis of amino acid **13** by laser induced CPL.

While many groups were working towards enantioenriched prebiotically important molecules, Soai and coworkers in 2005 developed a method that will be of synthetic use in large-scale preparation (Scheme 1.5). They demonstrated the process by employing CPL on racemic pyrimidyl alcohol **15**.[28,29] The photodecomposition of alcohol **15** resulted in enantioenriched alkanol, which acted as cryptochiral (special case of chirality raised due to electronic properties of the molecule) source auto catalyzing the reaction between 2-alkynylpyrimidine carbaldehyde **16** and diisopropylzinc **17** leading to enantioenriched pyrimidyl alkanol **15**.

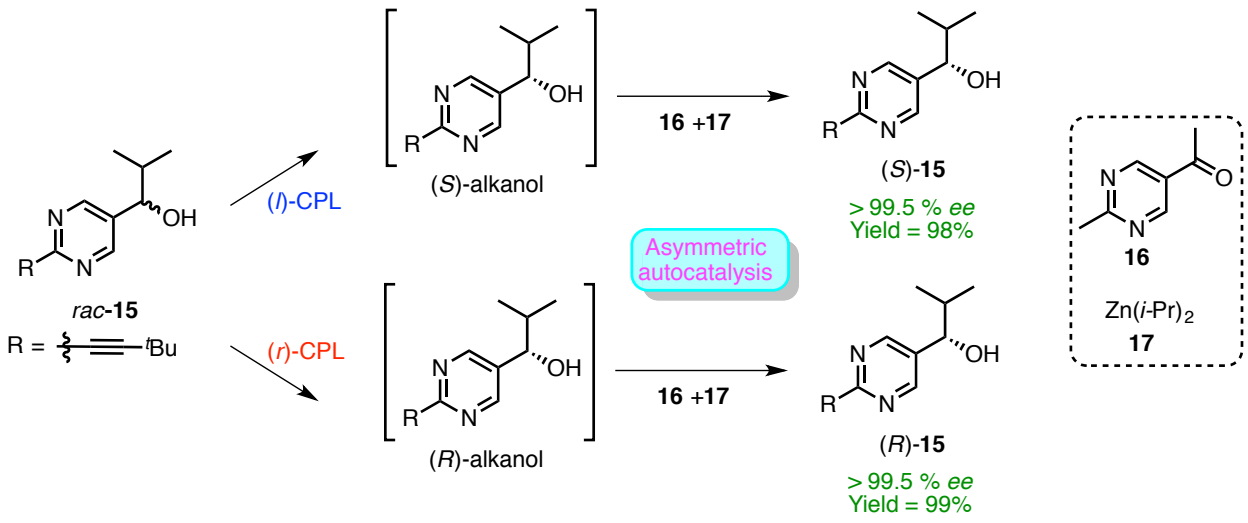

Scheme 1.5: Asymmetric autocatalysis of pyrimdyl alcohol **15** using CPL.

Employing asymmetric photodestruction method, Rau and coworkers reported resolution of tetramethyl-tetraaza-spirononadiene **18** by using circularly polarized light. Based on their experimental studies they believed that the (*S*)-isomer underwent photolysis to a greater extent compared to (*R*)-isomer that led to enantioenrichment in the product (Scheme 1.6).[30]

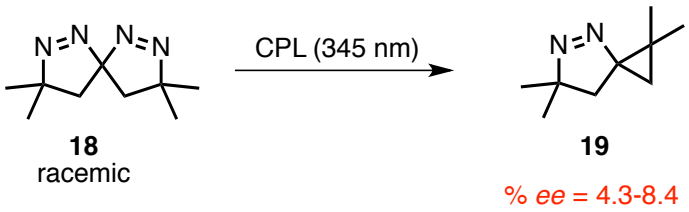

Scheme 1.6: Asymmetric photo destruction of **18** using CPL.

1.4.2. Solid state asymmetric phototransformations

Solid-state (crystalline state) photoreaction is one of the earliest methods for asymmetric phototransformations that dates back to early 20th century.[31-33] The success of solid-state photoreactions relies on the crystalline lattice of the system and they are termed as “topochemically controlled reactions”. This approach (solid state) holds a unique place as they can give rise to optically active photoproduct starting from achiral reactant without any external influence. Such studies are called as “absolute asymmetric synthesis”.[34] Two fundamental aspects are involved in asymmetric solid-state photoreactions. They are a) inducing chiral crystals and b) performing topochemically-controlled reactions. In order to

carry out successful solid-state asymmetric phototransformations, crystals should be generated in one of the 65 chiral space groups out of 230 unique space groups available.[35] In addition to this, the relative distance between the reacting partners should be approximately < 4.2 Å (Schmidt distance).[36]

Schmidt and coworkers elegantly demonstrated the solid-state [2+2]-photodimerization of cinnamic acid derivative **20** that yielded cyclobutane photoproducts (Scheme1.7).[37-39] On the contrary, in solution, *cis-trans* isomerization of the double bond was the dominant pathway. The formation of the photoproducts in solid-state irradiation was determined by the polymorph of the crystals of the cinnamic acid derivative. While the α-polymorph and the β-polymorph resulted in photoproducts **22** and **23** respectively, γ-form did not yield the desired photoproduct. They attributed the failure of photoreaction to the distance of the reacting double bonds i.e. 4.7-5.1 Å, which does not comply with the optimal distance (<4.2 Å) criteria proposed by Schmidt. Based on the insights gained from their investigation, they further extended their methodology for bimolecular photocycloaddition of the butadiene derivatives.[40]

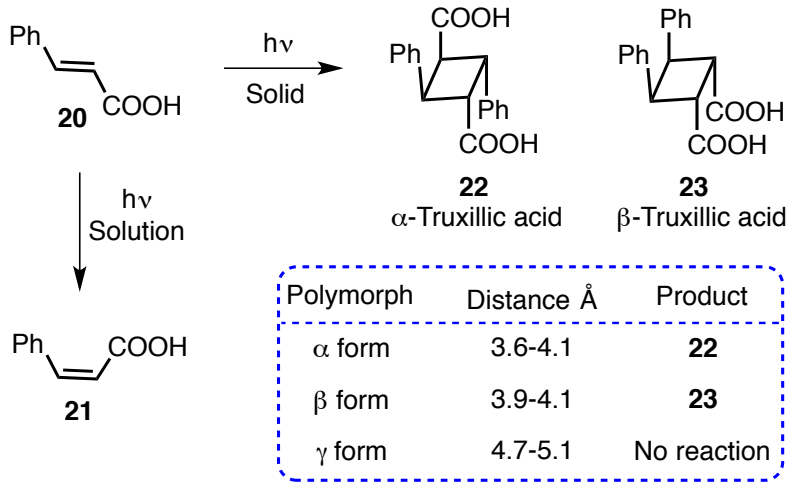

Scheme 1.7: Solid-state [2+2]-photodimerization of cinnamic acid derivatives **20**. (Reproduced from reference 38 with permission from American Chemical Society,1987).

Employing the same strategy, Scheffer and coworkers reported first absolute asymmetric di-π methane rearrangement and Norrish-Yang cyclization.[41] Irradiation of achiral dibenzobarralene diester derivative **24** crystallized from cyclohexane (crystallized in a $P2_12_12_1$) resulted in semibulvalene product **25** with >95 % *ee* (Scheme 1.8). The *ee* obtained was the highest reported for an absolute asymmetric synthesis at that time.

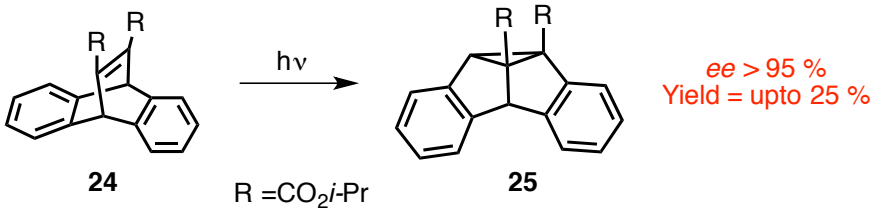

24 **25**

Scheme 1.8: Asymmetric di-π methane rearrangement of dibenzobarralene diester derivative **24**.

The same group had demonstrated the Norrish-Yang reaction in adamantyl-*p*-chloroacetophenone derivative **26** (Scheme 1.9). The reaction proceeded via hydrogen abstraction by excited state ketone through a six membered transition state leading to the formation of cyclobutanol derivative **27**.

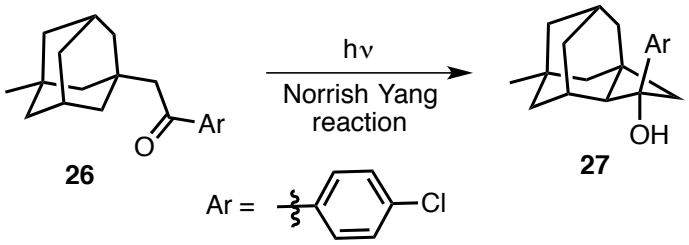

26 **27**

Scheme 1.9: Norrish Yang reaction of adamantyl derivative **26**.

Although, the topochemically controlled reactions opened avenues to access enantioenriched photoproduct, it was not a universal method to obtain stereoselectivity as this technique solely dependent on the criteria that the "achiral substrate should crystallize in a chiral space group". With crystallographic technique at the developing stage it was hard to predict if the molecule had crystallized in a chiral space group. In order to ensure the molecule crystallizes in a chiral space group a different strategy was envisioned. In this technique, a chiral auxiliary was attached to achiral reactant either covalently or ionically that influenced the molecule to crystallize in a chiral space group.[42] In covalent type, the chiral auxiliary is tethered to achiral substrate via covalent bond (Figure 1.6 A) whereas in ionic model, the tethering is via a salt bridge such as ammonium ion or carboxylate anion (Figure 1.6 B).

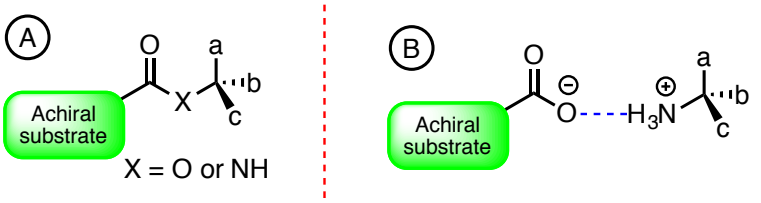

Figure 1.6: Different ways to tether chiral auxiliary on carboxylic acid derivatives A) Covalent, B) Ionic.

The ionic chiral auxiliary approach was advantageous compared to covalent because ionic type showed high melting points. This effect proved to be advantageous in resisting melting when the crystals were irradiated for longer period of time for higher conversion. Further, ionic chiral auxiliary are easy to detach after the photoreaction revealing enantioenriched building blocks. Scheffer and coworkers documented the first report on ionic auxiliary tethered asymmetric photoreaction by investigating di-π methane rearrangement of dibenzobarralene derivative **28** as shown in Scheme 1.10.[43]

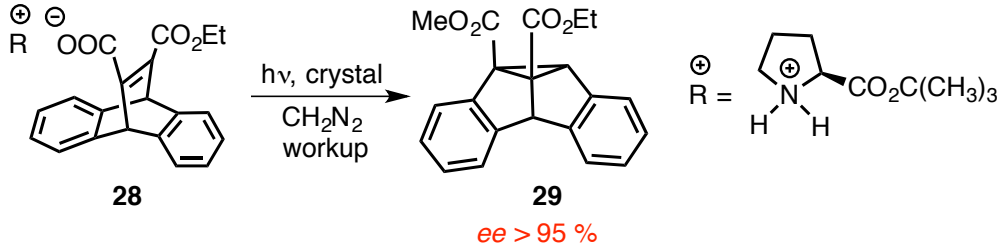

Scheme 1.10: Asymmetric di-π methane rearrangement of dibenzobarralene derivative **28** using ionic chiral auxiliary.

They employed a variety of optically active amines as chiral auxiliaries, which were tethered to the ester by simply mixing with the amine in methanol or ether resulting in chiral salts that were filtered and irradiated. After the irradiation, the solution was worked up with diazomethane to obtain semibulvalene product **29** with very high enantiomeric excess (>95 % ee when proline *tert* –butyl ester was employed). X-ray analysis showed that the enantioselectivity of the reaction is conformationally controlled similar to dibenzobarralene diester derivative **24** that underwent stereoselective di-π methane rearrangement. Following their successful demonstration of chiral auxiliary based di-π methane rearrangement, the same group elaborated their research to Norrish-Yang reaction using chiral auxiliary attached amino ketone derivative **30**. Irradiation of **30** afforded *cis* and *trans* cyclobutanol product **31** with 91 % *ee* and **32** (>12:1 ratio) via hydrogen abstraction respectively along with cleavage product **33** (Scheme 1.11).[44] High *ee* was attributed to the geometric orientation and the molecular motion of the

substrate in the crystalline state. The predominant formation of **33** was due to competitive hydrogen abstraction and cleavage of 1,4 biradical.

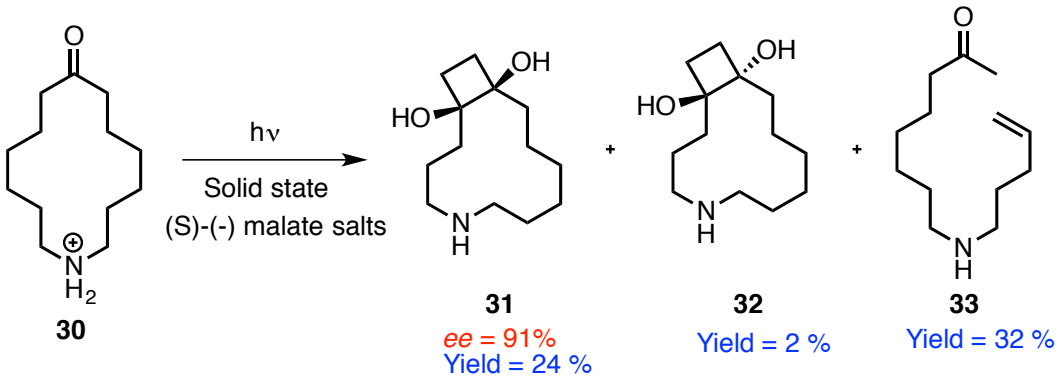

Scheme 1.11: Norrish Yang reaction of salts of amino ketone **30**.

1.4.3. Asymmetric phototransformations by supramolecular approach

Inspired by the biological processes that utilize molecular confinement to perform desired task, photochemists employed supramolecular hosts to organize and direct the short-lived excited state species to perform the desired phototransformation. The supramolecular host with the ability to accommodate guest molecules acts as a container to hold molecule through non-covalent interactions in a reaction-ready state. This conformationally locked reactant, upon photo excitation undergoes specific transformation. The energies of non-covalent interactions in the supramolecular complexes can vary from <1.2 to 84 kcal·mol $^{-1}$.[45] The presence of supramolecular host has the potential to alter the kinetics and the selectivity of a given reaction. Such host-guest approach is widely used in catalysis, drug delivery system, molecular machines etc., Few of the well-defined and successful supramolecular hosts that are employed for asymmetric phototransformations include cyclodextrins, zeolites, cucurbiturils, micelles etc.,[46,47] Ramamurthy and coworkers had employed chirally modified zeolites for stereoselective 4π-photocyclization of tropolone derivatives **34** (Scheme 1.12).[48-50] In their work, they used photochemically inert and optically pure ephedrine as a chiral inductor, which was adsorbed on to the NaY zeolite prior to loading of the reaction mixture containing tropolone ether. The irradiation was performed as a powder or slurry in hexane to yield bicyclic photoproduct **35** with 78 % *ee*. The selectivity was attributed to the interaction between tropolone ether and ephedrine within the zeolite cavity ordered by cation-π .cation-

carbonyl interaction. In addition to this three point interaction, the cation present in the zeolite also played a crucial role in determining the selectivity.

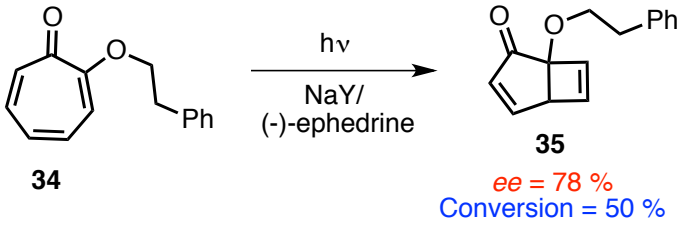

34 **35**

ee = 78 %
Conversion = 50 %

Scheme 1.12: 4π-Photocyclization of tropolone derivatives **34** in zeolite.

Inoue and coworkers[51] utilized γ-cyclodextrins as supramolecular host and illustrated photodimerization of anthracene carboxylate **36** as shown in Scheme 1.13. The anthracene derivative **36** and the cyclodextrin formed a 2:1 guest-host complex in the ground state, which up on irradiation resulted in photoproducts **37**, **38**, **39** and **40**. The *syn*-HT photoproduct had an *ee* of 41 % and *anti*-HH resulted in < 5 % *ee* at 0 °C.

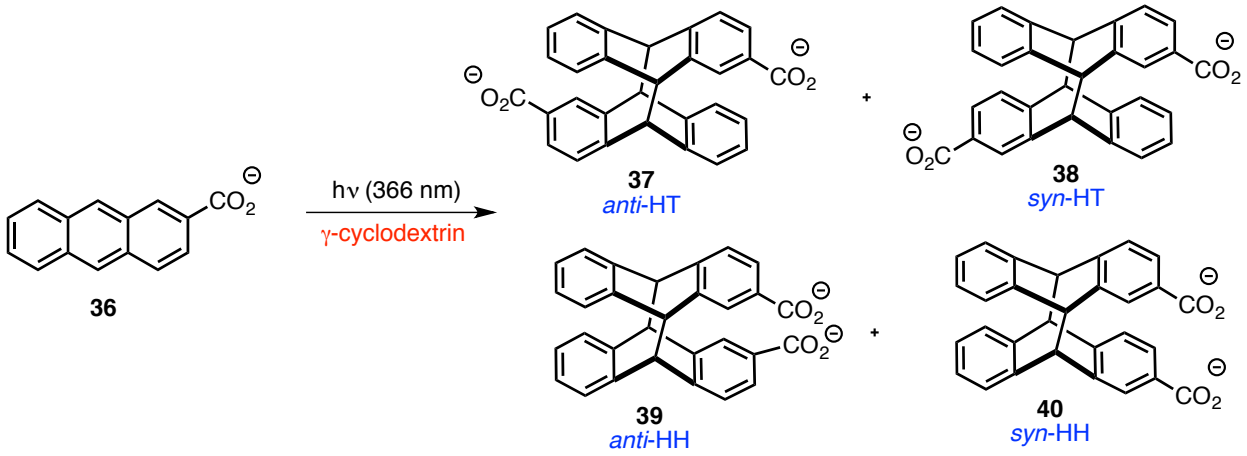

36

37 *anti*-HT

38 *syn*-HT

39 *anti*-HH

40 *syn*-HH

Scheme 1.13: Photodimerization of anthracene carboxylate **36** in supramolecular host-cyclodextrin.

Sivaguru and coworkers demonstrated photodimerization of 6-methyl coumarin **41** in the presence of catalytic amount of cucurbit[8]uril (CB[8]) in water (Scheme 1.14).[52,53] The photodimerization was effective in the presence of 10 mol% of CB[8] resulting in *syn*-dimer as major product with the ratio of *syn* HT:HH = 70:30 whereas in absence of CB[8] photodimerization resulted in 10% conversion with mixture of products. Based on their detailed kinetic and photophysical analysis, they proposed a catalytic cycle for the photodimerization. The first step of the catalytic cycle involved the formation of 1:1 host:guest complex followed by 1:2 host:guest complex with the former as the rate determining step.

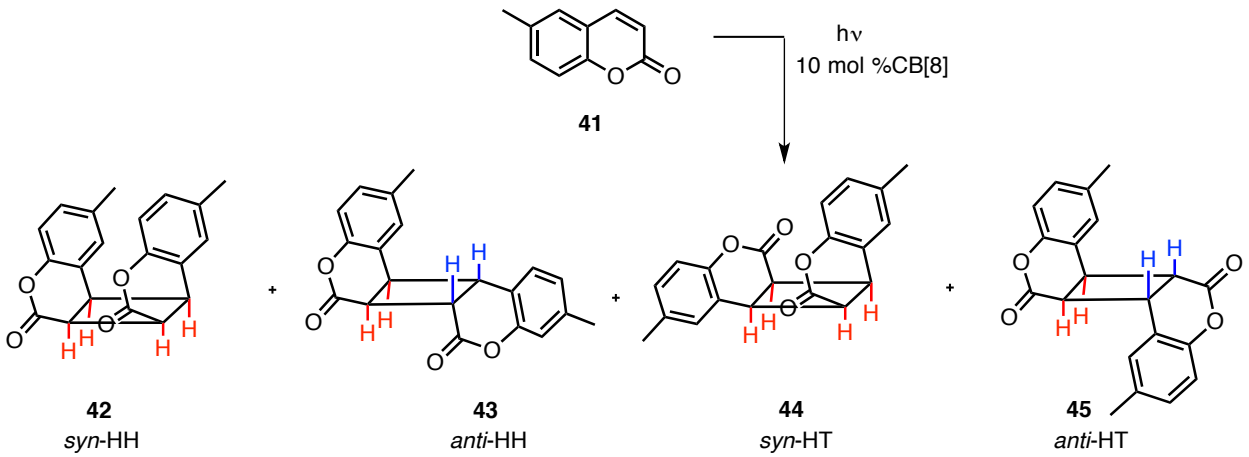

Scheme 1.14: CB[8] mediated photodimerization of 6-methyl coumarin **41**

Ramamurthy and coworkers reported the dimerization of acenaphthylene **46** using octa-acid as the host (Scheme 1.15).[54] They had performed both direct irradiation and triplet-sensitized irradiation with Eosin. Direct irradiation resulted in *syn* dimer **47** and the triplet-sensitized irradiation yielded both *syn* **47** and *anti* dimer **48** in a ratio 60:40. High selectivity was credited to the restricted mobility of the reactants in direct irradiation.

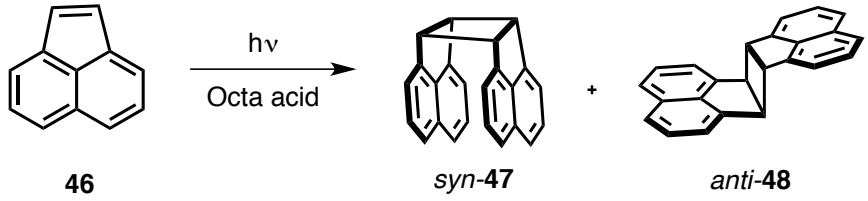

Scheme 1.15: Octa-acid mediated photodimerization of acenaphthylene **46**.

1.4.4. Asymmetric phototransformations by H-bonding template

The previous section described the success of employing supramolecular host as a reaction vessel to obtain stereoselectivity in the desired photochemical transformation. However, the selectivity in the photoproduct(s) depends on the effective binding of host with guest and also the orientation of the guest inside the cavity. In contrast to this approach, chemists explored the use of chiral templates that interact with the reactant through H-bonding and provide necessary stereodifferentiation for higher selectivity. One of the earliest examples of stereoselective photocycloaddition by H-bonding template was elegantly demonstrated by Nakamura and coworkers in 1996 (Scheme 1.16).[55] They used stoichiometric

Kemp triacid as a host that was appended to coumarin derivative **49**. The photoreaction between Kemp triacid tethered coumarin **49** and butyl thymine **50** in benzene afforded *cis-syn*/*cis-anti* cross adduct **51** in a ratio of 96:4. However in this approach, the H-bonding Kemp triacid derivative that provided stereoselectivity was still covalently bound to the photoproduct. In order for a strategy that employs sub stoichiometric amount of host paving way for true catalysis required further development.

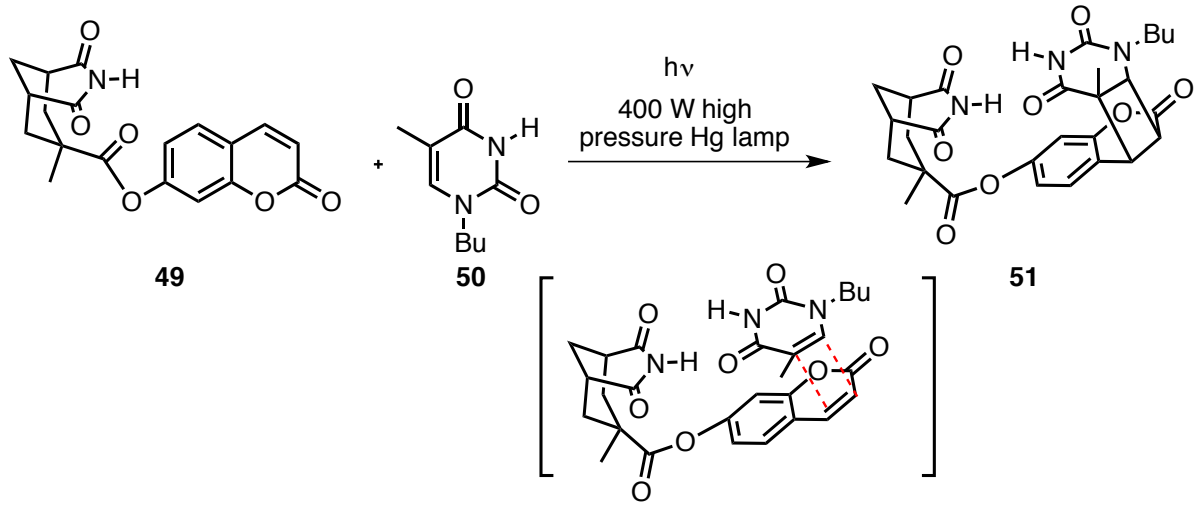

Scheme 1.16: Kemp triacid-based photocycloaddition of coumarin **49** and butyl thymine **50**.

Based on Nakamura's work, Bach and coworkers developed H-bonding catalysis using Kemp triacid derivative and demonstrated its efficacy towards enantioselective [2+2]-photocycloaddition of quinolone (Scheme 1.17).[56] They subjected 2-quinolone derivative **52** to intramolecular [2+2]-photocycloaddition in the presence of H-bonding catalyst **53** in toluene as a solvent that yielded cyclobutane derivatives **54** and **55** with up to 88 % *ee*. The substrate bound to the chiral template through H-bonding and the tetrahydronaphthalene group on the template shielded one of the enantiotopic faces of the substrate leading to enantio enrichment in the resulting photoproducts.

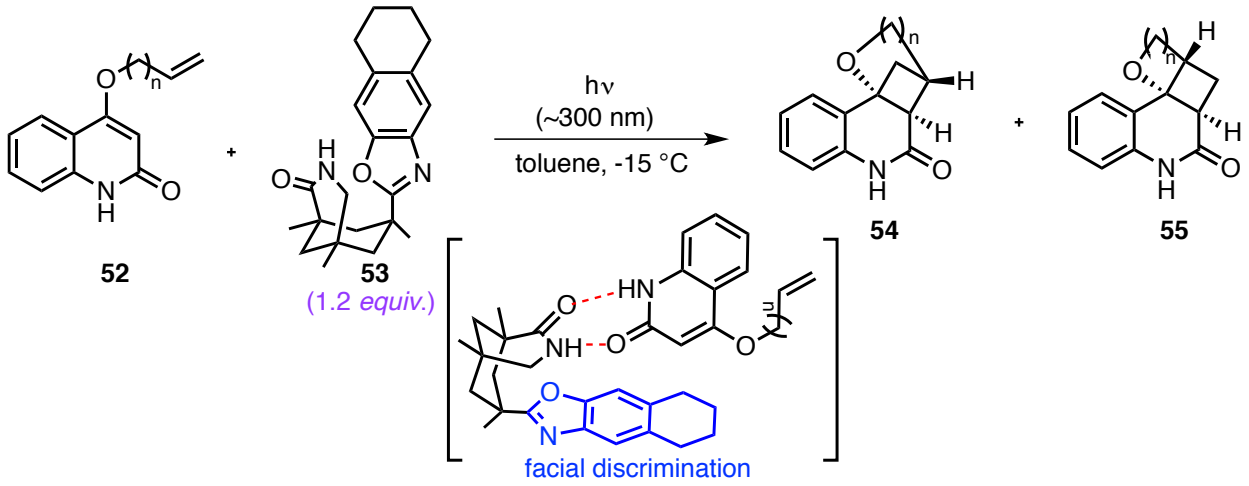

Scheme 1.17: Photocycloaddition of quinolone **50** using chiral template.

The same group developed a strategy in which a sensitizer was appended to the Kemp triacid template to perform triplet-sensitized photoreactions (Scheme 1.18).[57] Using their sensitizer template **57**, they demonstrated enantioselective visible light photocatalysis of quinolone derivative **56**. In the presence of chiral thioxanthone template **57,** the intramolecular [2+2]-photocycloaddition of quinolone **56** proceeded efficiently leading to product **58** with high enantioselectivity (92 %) and conversion (90 %). The reaction proceeded via energy transfer from the excited thioxanthone to the substrate and since the reactant was bound to the chiral template the stereo induction was efficient leading to enantioenriched photoproducts.

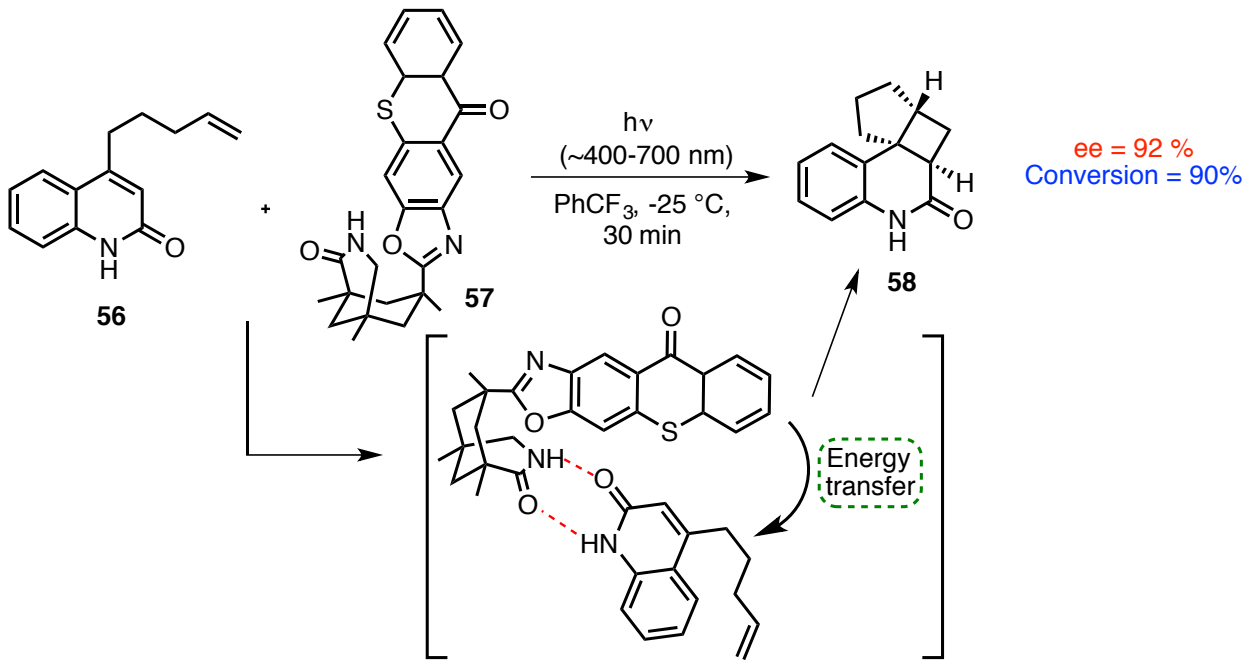

Scheme 1.18: Photocycloaddition of quinolone **56** using thioxanthone based chiral template **57**.

Recently Sivaguru, Sibi and coworkers demonstrated the use of novel atropisomeric binaphthyl thiourea organocatalyst **60** for intramolecular [2+2]-photocycloaddition of coumarin derivative **59** as shown in Scheme 1.20.[58] The use of organocatalyst for photocatalysis has its advantages including easy handling of the reagents, non-metal based reaction conditions and most importantly the ease of synthesis and modification of the catalysts. The enantioselective reaction of coumarin **59** yielded tricyclic photoproduct **60** with 69-96% *ee* at low catalyst loading of 1-30 mol%. Detailed photophysical analysis revealed that the reaction proceeded via static and dynamic complexes allowing an energy transfer from the exciplex (static and dynamic excited state complex). They also proposed dual catalytic cycle depending up on the catalyst loading.

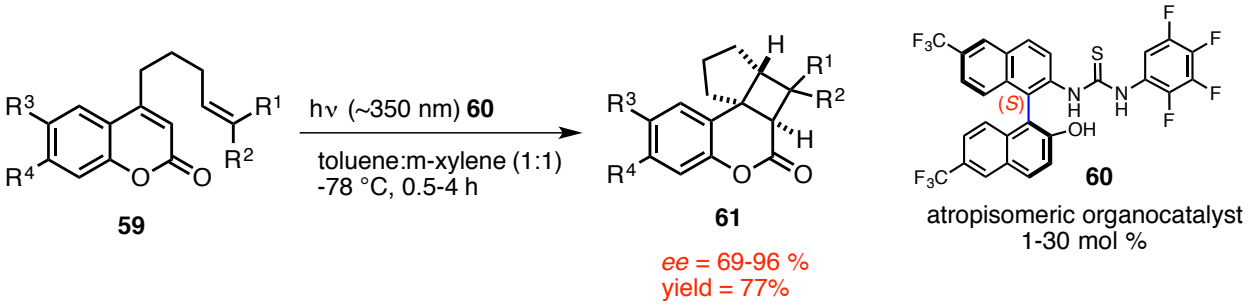

Scheme 1.19: Photocycloaddition of coumarin **59** using atropisomeric thiourea catalyst **60**.

The same group also demonstrated intermolecular [2+2]-photocycloaddition of coumarin **62** with alkene **63** catalyzed by achiral thiourea catalyst **64**. Irradiation of coumarin **62** and alkene **63** in presence of catalyst **64** afforded cyclobutane photoproduct **65** (Scheme 1.20).[59] Detailed photophysical investigations on the substrate and the catalyst revealed that the reaction occurred via a combination of minimized aggregation of the coumarin **62**, altered excited lifetime and enhanced intersystem crossing influenced by the catalyst.

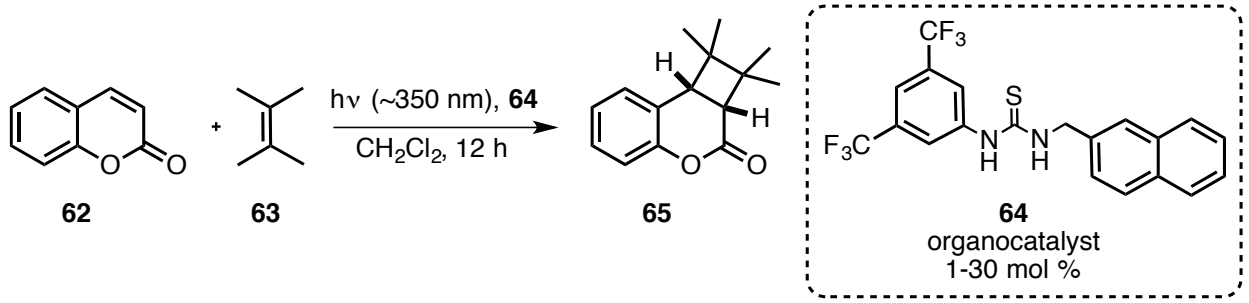

Scheme 1.20: Intermolecular photocycloaddition of coumarin **62** using thiourea catalyst **64**.

1.4.5. Asymmetric phototransformations influenced by axial chirality

Axial chirality can be defined, as a stereoisomerism arising from non-planar arrangement of four groups about a chiral axis. In other words axially chiral compounds lack a stereogenic center but exist as a pair of enantiomers. Atropisomers are class of axially chiral compounds where the chirality originates from the restricted rotation around a single bond that in turn rely on the sterics around the axis. Such axially chiral compounds was first identified in 1922 by Christie and Kenner in 6,6'-dinitrobiphenyl-2,2'-dicarboxylic acid **66**,[60] but the term "atropisomer" was coined by Richard Kuhn in 1933.[61] Early investigations on these molecules were mainly focused on physical characteristics such as racemization

barrier, conformational analysis etc. But later taking advantage of its unique chirality, several reports emerged that demonstrated an efficient way to transfer axial chirality from the substrate to the point chirality in the product.

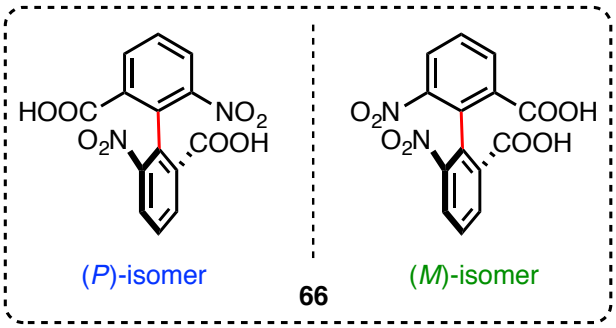

Figure 1.7: First reported axially chiral compound 6,6'-dinitrobiphenyl-2,2'- dicarboxylic acid **66**.

Curran and Clayden were the first to demonstrate the application of atropisomeric compounds for asymmetric thermal transformations[62] and Curran named such reactions as "atropselective reactions".[63] In 1994, Curran and coworkers were the first to report atropselective reactions of axially chiral maleimides and anilides derivatives. They demonstrated the cycloaddition of benzonitrile oxide to racemic acrylanilide **67** that gave isoxazoline derivative **68** and **69** as shown in Scheme 1.21 with high diastereoselectivity (*dr* >97:3).[64]

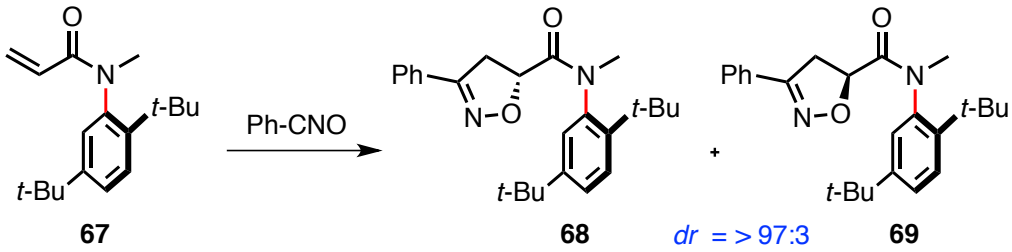

Scheme 1.21: Cycloaddition of benzonitrile oxide to acrylanilides **67**.

The same group illustrated the transfer of axial chirality in the reactant to point chirality in the product with high enantioselectivity by radical cyclization of axially chiral acrylanilides **70** as shown in Scheme 1.22.[65] In this reaction, the racemization barrier of the reactant was high enough (ΔG = 30.8 kcal·mol $^{-1}$) to perform reaction at ambient temperature without eroding the optical purity of axial chirality, whereas the racemization barrier for the radical intermediate was lower than the reactant due to loss of Iodo group that acted as one of the steric. In spite of the loss of iodo group, the transfer of chirality was

efficient since the radical cyclization occurred at much faster time scale than the competing racemization. This reaction resulted in oxindole derivative **71** with moderate yield and high enantioselectivity.

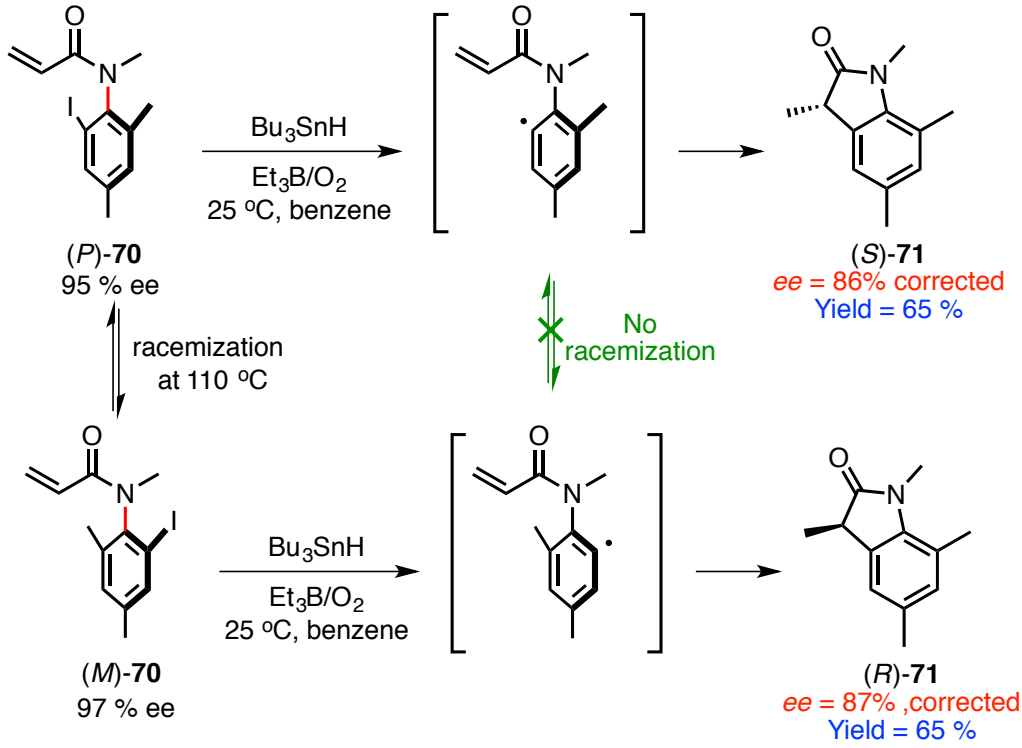

Scheme 1.22: Radical cyclization of atropisomeric acrylanilides **70**. (Reproduced from reference 64 with permission from American Chemical Society, 1999).

In 1996, Clayden and coworkers reported stereoselective reduction of ketone on axially chiral naphthamide derivative **72** that resulted in high diastereoselectivity in the corresponding alcohol **73** with *anti*:*syn* ratio up to 99:1 (Scheme 1.23).[66] High selectivity was observed when bulky nucleophile such as $LiBHEt_3$ was employed. In addition to using bulky nucleophile, the selectivity in the product also depended on the ability of atropisomeric compound to direct the nucleophile.

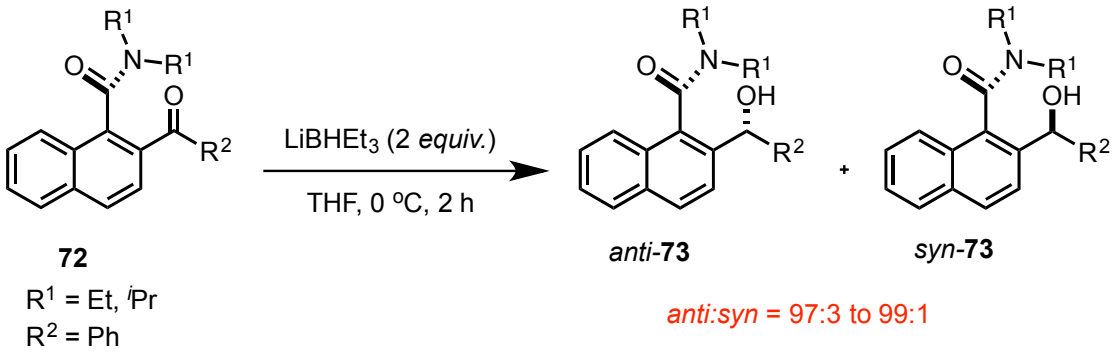

Scheme 1.23: Diastereoselective reduction of atropisomeric amide derivative **72**.

After eminent works by Curran and Clayden, there was an immense growth in the research of atropisomeric compound in thermal chemistry. But atropisomers in photochemical reaction was not explored to the extent it was in thermal chemistry. Bach and coworkers investigated stereoselective Paternò-Büchi reaction with atropisomeric enamides **74** and benzaldehyde **75** which resulted in moderate diastereoselectivity in the resulting oxetane (Scheme 1.24).[67] However, in this example, the atropisomeric enamide was only in the ground state that reacted with excited benzaldehyde and the excited state photochemistry of atropisomeric system was not investigated.

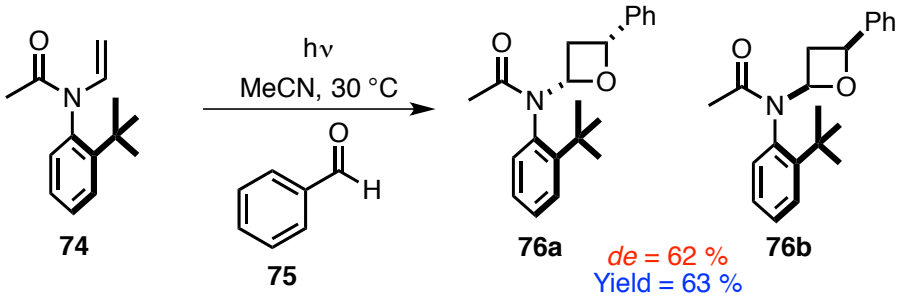

Scheme 1.24: Paternò-Büchi reaction of atropisomeric enamide **74** with benzaldehyde.

During this time, Sakamoto and coworkers introduced a new concept called “frozen chirality” where chiral crystals were obtained from achiral substrates.[35] In this strategy, the chirally enriched reactant could be irradiated at low temperature in a suitable solvent so that the absolute chirality remains intact during the phototransformations. They demonstrated this elegant concept by performing photocycloaddition of chiral naphthamide **77** generated from achiral naphthamide with 9-cyanoanthracene **78** in THF or THF/MeOH at -20 °C resulting in 95 % *ee* in the photoproduct **79** (Scheme 1.25).[68]

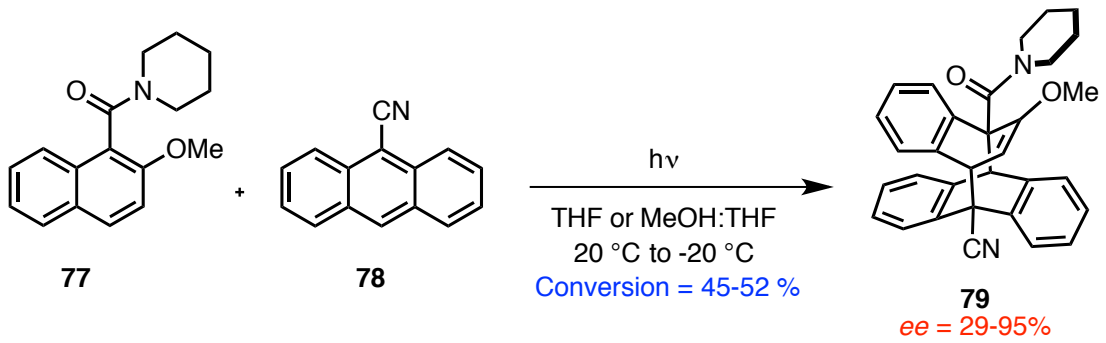

Scheme 1.25: Photocycloaddition of anthracene derivative with napthamides obtained through frozen chirality concept.

They have also reported benzophenone sensitized [2+2]-photocycloaddition of coumarin carboxamide **80** with various alkenes **82** (Scheme 1.26).[69] Upon irradiation, the reaction yielded products **83** and **84** with *ee* up to 99% and *endo*:*exo* ratio up to 1:0.

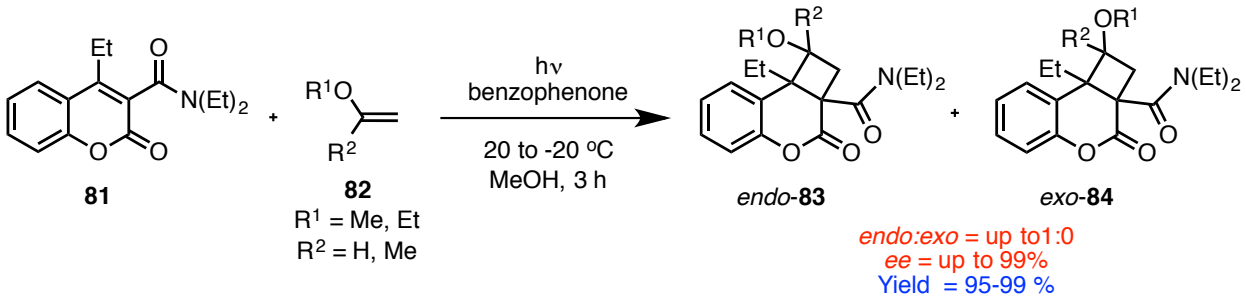

Scheme 1.26: Photocycloaddition of coumarin derivative **81** with alkenes **82**.

Though achieving enantioselectivity via frozen chirality is a promising avenue, once again this strategy had challenges in crystallizing achiral molecules in a chiral space group as discussed earlier. More over, the chiral crystal in solution has to resist racemization during irradiation, which was a major hurdle in this technique. As discussed in the previous section, controlling the short lived excited state especially in solution was much more challenging. In order to find a solution to this bottleneck, Sivaguru and coworkers carried out detailed investigation on photochemistry of atropisomeric chromophores as an avenue to perform atropselective photochemical reaction in solution. Their concept of "Axial to Point Chiral Transfer" was inspired by success of atropisomers in thermal chemistry discussed in previous section and Havinga's Non-Equilibration of Excited Rotamers (NEER) principle in photochemical transformations. The NEER principle, put forth by Havinga which states that "species formed upon π-π* excitation of the various *transoid* and *cisoid* ground-state rotamers of a conjugated alkene will not

equilibrate during the short excited-state lifetime due to the increased bond order of the ground state C-C single bonds".[70] One of the interesting examples where NEER principle operates is in the photoreactivity of previtamin D.[71,72] The study reveals that the rotamers do not interconvert in the excited state even though the products formed from the excited state is unstable due to steric interaction. Initially this principle was put forward for singlet reaction and later it was proven for triplet-sensitized reactions as well. Below schematic (Figure 1.8) represents the hybrid of NEER principle and atropisomers that enabled Sivaguru and co-workers to perform atropselective phototransformations in leading to chirally enriched building blocks. The optically pure rotamers/atropisomers A and B that interconvert in the ground state (with a given rate constant determined by energy barrier) when photo-excited is promoted to the excited state with same rotamer ratio as in the ground state. This short-excited state species do not interconvert due to NEER principle and thus lead to specific photoproducts that is dictated by their ratio in ground state. If one could design atropisomers such that we have precise control over the ratio of rotamers in the ground state, then we could extend that control to the photoproducts leading to complete "axial to point chiral transfer".

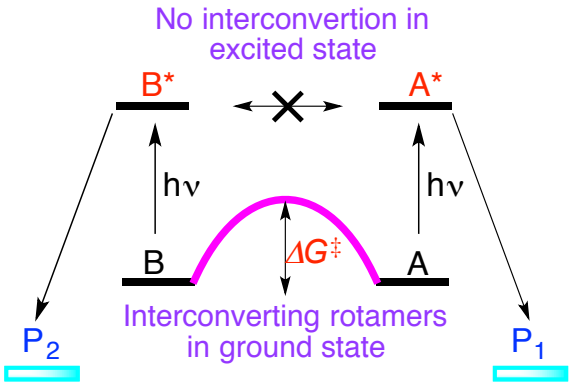

Figure 1.8: Schematic representation of NEER principle.

In an effort to validate this principle, Sivaguru and coworkers reported highly enantiospecific photoreactions with various atropisomeric chromophores. For example they reported *conrotatory* 6π-photocyclization of acrylanildes derivatives **85** resulting in *cis* and *trans* photoproducts **86** and **87** (Scheme 1.27).[73,74]

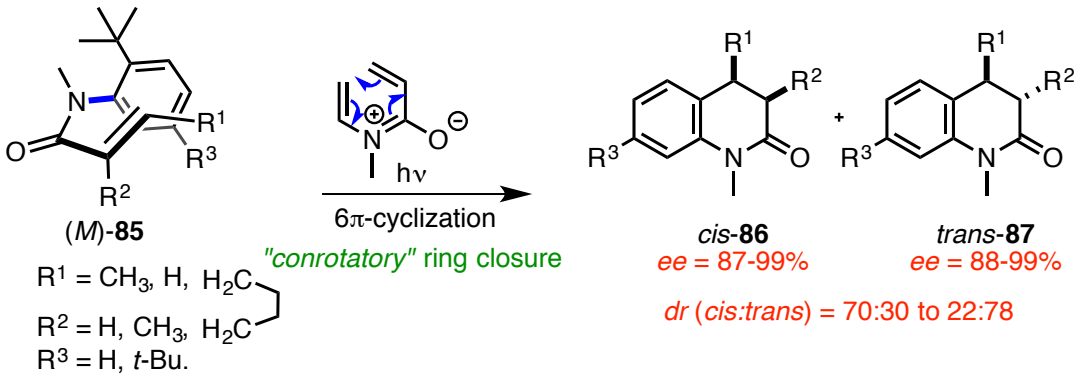

Scheme 1.27: Atropselective 6π-photocyclization of acrylanildes **85**.

The photoreaction occurred via cyclization at the *ortho* carbon holding the *t*-Bu group followed by loss of isobutene relieving the steric strain in the product. The diastereoselectivity and the enantioselectivity were influenced by the substitutions on the alkene and the type of mechanism involved in the photoreaction (singlet or triplet). In the singlet pathway, the zwitterionic intermediate underwent stereospecific *conrotatory* ring closure to form enolate intermediate. This process is followed by non-stereospecific hydrogen migration to afford both *cis* and *trans* photoproducts **86** and **87**. Whereas the triplet-sensitized reaction proceeded through radical pathway via a cyclization followed by stereospecific H-abstraction leading to photoproduct with high enantioselectivity.[75] They also demonstrated atropselective photoreaction in solid state[76] and in the presence of alkali metal ions[77] to achieve high selectivity in acrylanilide derivatives. To further explore this strategy, they reported stereospecific Norrish-Yang cyclization of atropisomeric α-oxoamides **88** yielding β-lactam as a major photoproduct **89** with high enantioselectivity (Scheme 1.28).[78,79]

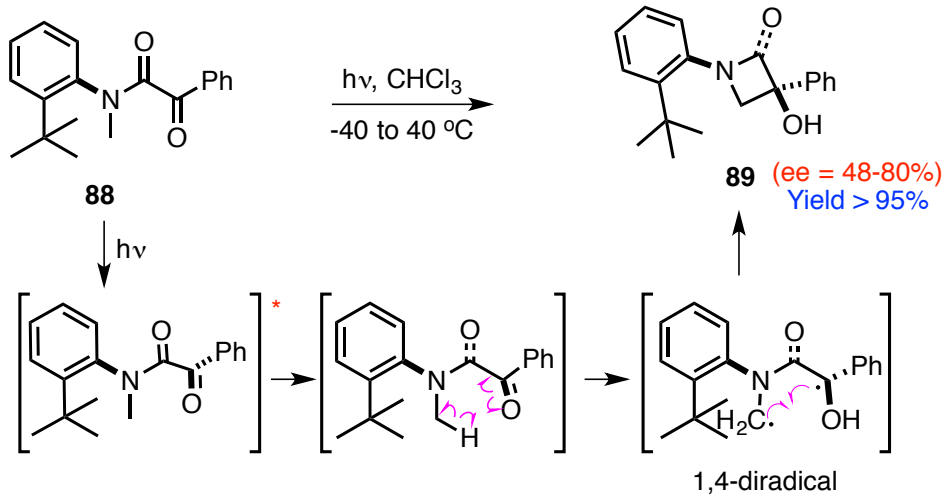

Scheme 1.28: Atropselective Norrish-Yang cyclization of α-oxoamides **88**.

In 2011, Sivaguru and coworkers, demonstrated atropselective 4π-ring closure of 2-pyridones **90** leading to enantioenriched β-lactam **91** as photoproduct via "*dis"* outward ring closure (Scheme 1.29).[80] Based on their extensive physical characterization studies, the enantioselectivity of the photoproduct was highly dependent on solvent, reaction temperature and the type of face shielding i.e the formation of inter and intra molecular hydrogen bond of the substrate with the solvent and the steric features of the compound.

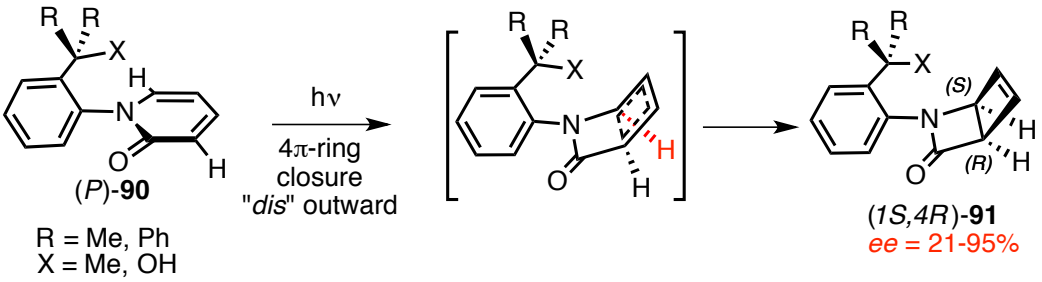

Scheme 1.29: Atropselective 4π-ring closure of 2-pyridones **90**.

The same group had also demonstrated the [2+2]-photocycloaddition of atropisomeric acrylimides **92** resulting in exclusive cross [2+2] photoadduct **93** with excellent *ee* and *de* (Scheme 1.30).[81] On the contrary, the non-atropisomeric acrylimide (without *t*-Bu group at the *ortho* position) resulted in a mixture of straight and cross addition product **93** and **94**. This is one of the interesting examples as it clearly showed the effect of axial chirality in influencing the selectivity of the reaction.

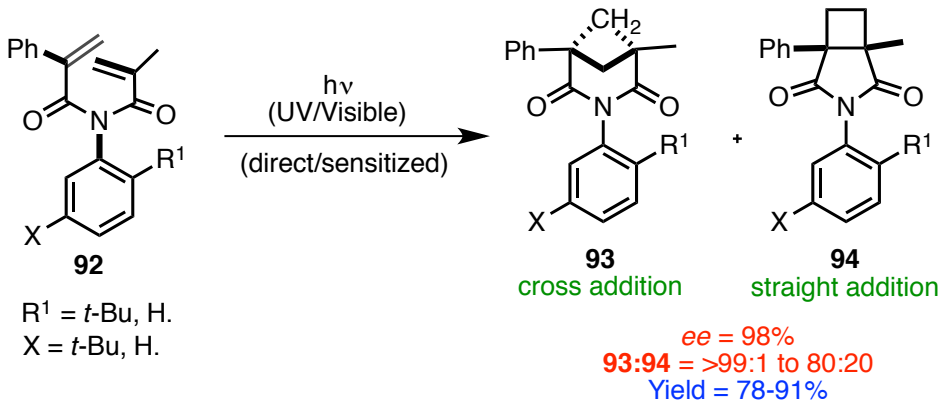

Scheme 1.30: Atropselective [2+2]-photocycloaddition of acrylimides **92**.

1.5. Role of light in biological systems and medicine

Light, as discussed plays a vital role in various fields of science. One of the important fields where the use of light was significantly explored and appreciated is in the biological systems and therapies. The following subsection provides a glimpse of those endeavors.

1.5.1. Role of light in biological system

Light has a very important role in biological processes. All these processes are initiated by absorption of light by the chromophore, which undergoes photochemical transformations and the biological systems respond to these changes in initiating a change/response. One such transformation is *cis-trans* isomerization of a C=C bond upon interaction with light. One of the fascinating examples where such a process plays a critical role in biological system is the vision process in living organisms (Scheme 1.31). This process is initiated on the surface of the retina where photoreceptor cells - rods and cones are activated upon interaction with light. During this interaction, the 11-*cis*-retinal **95**, which is bound to the protein opsin (the bound complex is called Rhodopsin) isomerizes to all *trans*-retinal **96** (all trans-retinal bound complex is called Bathorhodopsin) in 200 femtoseconds.[82-84] This fast photochemical process causes change in the structure of the protein (Bathorhodopsin → Lumirhodopsin→ Metarhodopsin I → Metarhodopsin II) generating a nerve impulse to the brain, which then interprets those signals and

constructs an image. During this process the all 11-*trans* retinal is expelled, which upon further enzymatic reaction is converted to 11-*cis* retinal for the cycle to continue (Scheme1.31).[85,86]

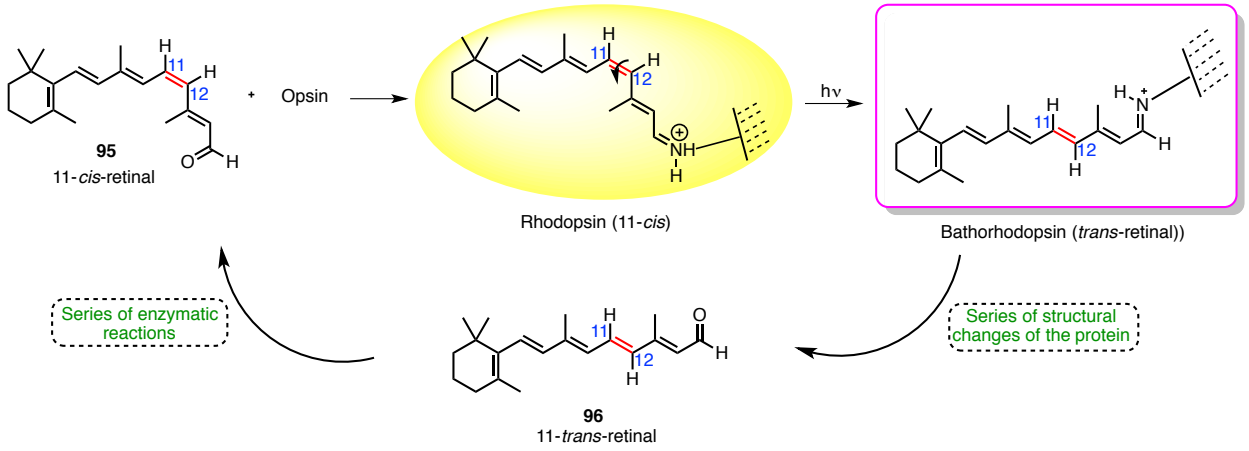

Scheme 1.31: Schematic representation of vision process.

Such *cis-trans* isomerization initiated by light is also responsible for the growth in plants. Plants use light for photosynthesis. They posses a light sensitive pigment bound to the protein called phytochrome, which acts as a biological clock regulating the growth and development of plants. Phytochrome can exist in two forms namely Pr **97** (*cis* form-inactive) and Pfr **98** (*trans* form-active). Upon interaction with light, phytochrome undergo *cis-trans* isomerization (Scheme 1.32)[87,88] around C_{15} –C_{16} bond resulting in altering the gene expression thus dictating the growth of the plants. Such also occur in bacteria and other microorganism, which acts as circadian rhythm for their movements.

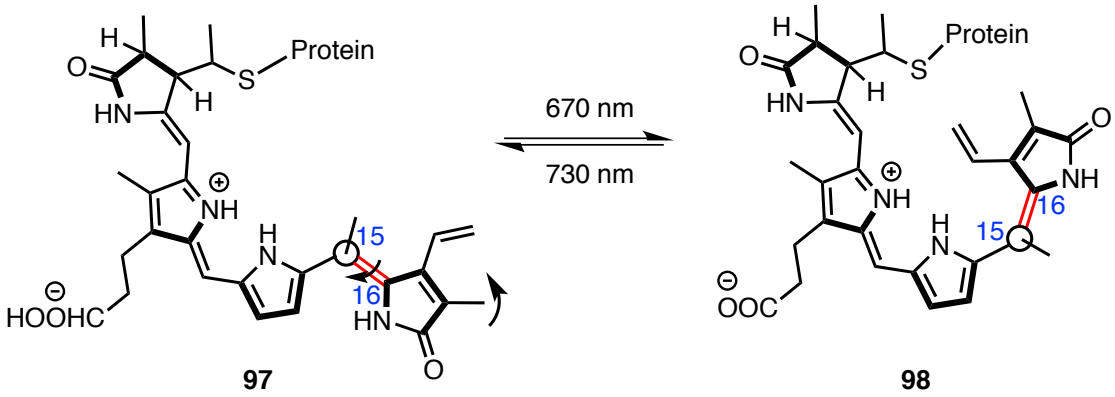

Scheme 1.32: Schematic representation of growth of plants by phytochrome receptor.

1.5.2. Role of light in medicinal therapies

Light has been used for the treatment of several diseases over 3000 years. Ancient Egyptian, Indian and Chinese civilizations employed light for the treatment of psoriasis, rickets, vitiligo etc.,[89] Even though the therapeutic properties of light were known for several years it was only after Niels Finsen's extensive work using light to treat small-pox, discharge of smallpox pustules and cutaneous tuberculosis in the late 19th century led to the modern day light therapies.[90]

One of the important treatments, which doctors stumbled upon, is the use of light in the treatment of jaundice in babies known as neonatal jaundice.[91] This disease occurs as a result of accumulation of bilirubin, which is a breakdown product of heme catabolism. Bilirubin is insoluble in water due to the presence of intramolecular hydrogen bonding thus making it hydrophobic in nature. This hydrophobicity, prevents their excretion from humans and gets deposited on the skin and other internal organs leading to jaundice. When babies suffering from jaundice are exposed to light, *cis-trans* photoisomerization of the double bond in bilirubin at C_4, C_{15} carbons occurs leading to the loss of intramolecular hydrogen bonding making it hydrophilic and water-soluble. Due to its change in solubility profile upon *cis-trans* isomerization, hydrophilic bilirubin can be excreted out of the body. This is one of the less expensive, non-invasive and painless treatments for babies ailing from jaundice and is still the only treatment for newborns in neonatal care that is practiced in many countries. The process of converting hydrophobic bilirubin to hydrophilic bilirubin is depicted in the Scheme 1.33.[91]

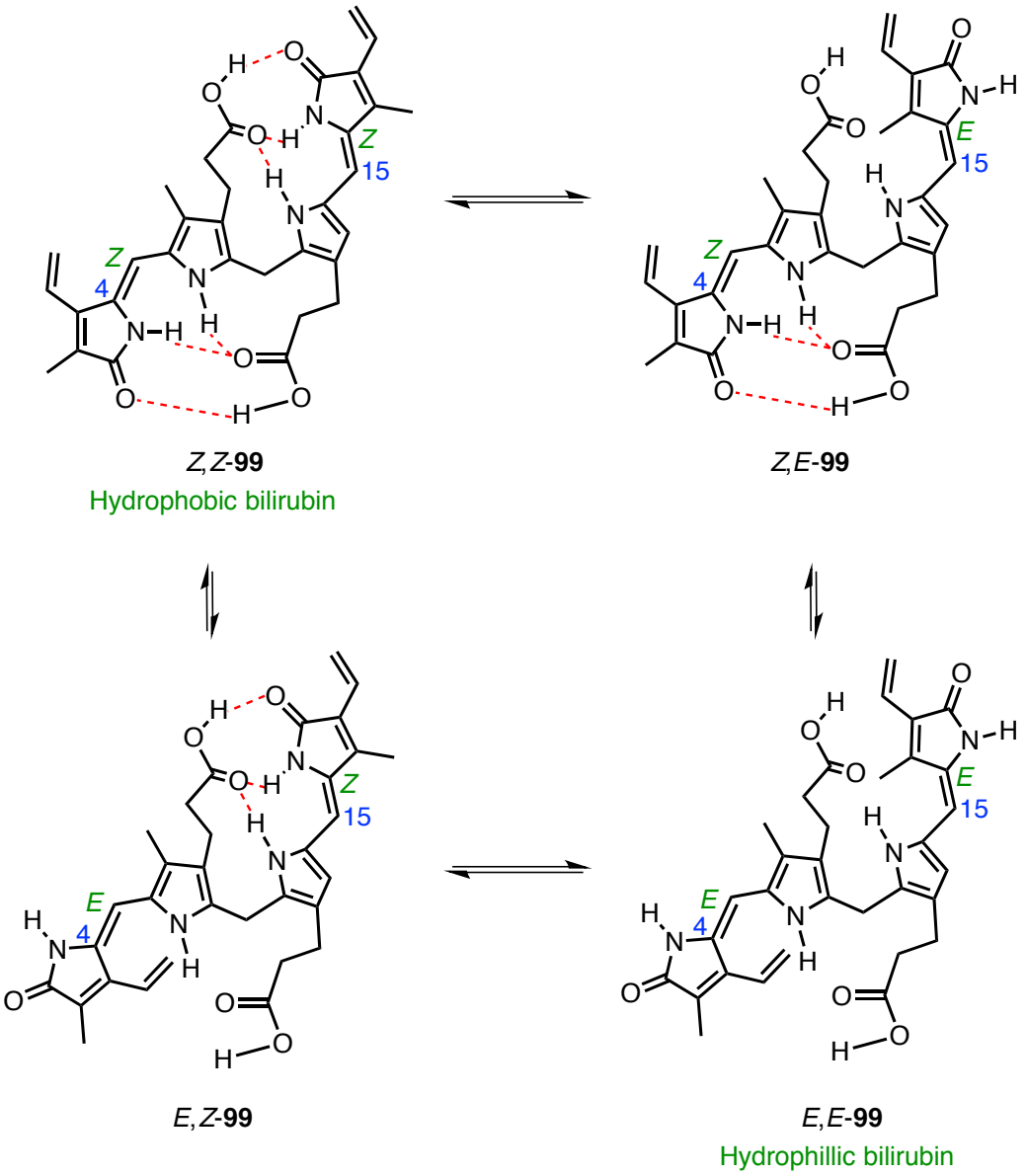

Scheme 1.33: Schematic representation of *cis-trans* isomerization in bilirubin **99**.

Another break through treatment in the field of medicine where light plays a crucial role is photodynamic therapy (PDT). In 1903, Herman Von Tappeiner and A. Jesionek, based on two independent reports made by German medical student[92] and a neurologist from France[93] respectively, treated skin tumors with eosin and white light.[94] They called this phenomenon as “photodynamic action”.[95] Following their preliminarily experiments, various trials involving different reagents and light led to modern photodynamic therapy. PDT is a treatment that destroys target cells employing three components *viz.*, a photosensitizer, tissue oxygen and light. The first step in this process involves intake of the

photosensitizer intravenously, which is taken up by inflammatory cells in vessel wall or can be applied topically. The second step is activating the sensitizer by suitable wavelength of light, which then kills the damaged cells. The activation of sensitizer and the destroying of the target cell involve two mechanisms (type I and type II vide infra). In both the mechanisms, the photosensitizer interacts with light and gets promoted to singlet excited state which then intersystem crosses to triplet state. In type I, the triplet state sensitizer directly react with the target cell by transferring an electron to the cell membrane giving rise to radicals which then reacts with oxygen to form the reactive oxygen species leading to cell death (via radical chemistry). In type II, the triplet-excited sensitizer interacts with the tissue oxygen leading to singlet oxygen, which destroys the damaged cell. Type II is the most prevalent mechanism (Figure 1.9).[96,97] The elegance of this therapy is, they are target specific as the photosensitizer is activated only in precise area (spatial control) of the tissue so that cells in the proximal area are not affected. In other words since the half life of singlet oxygen in biological system is <0.04 μs, the area of action will be <0.02 μm.[98] The main advantage of this method is quick curing process, minimal side effect and target specificity.

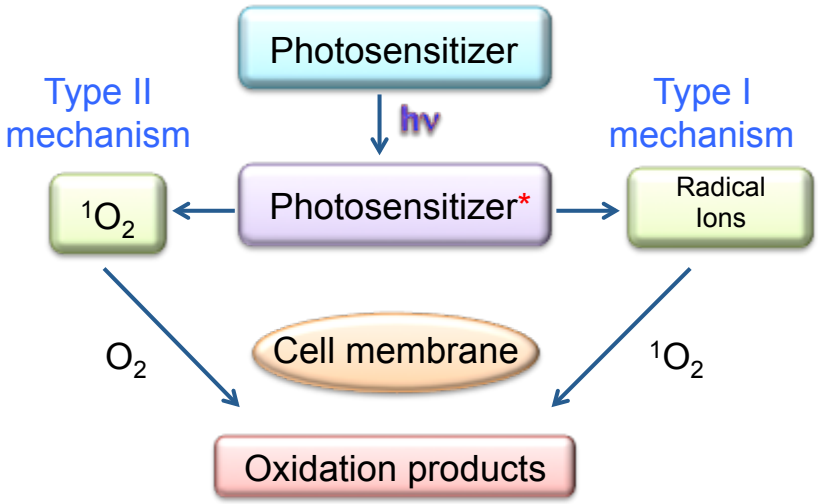

Figure 1.9: Mechanism of action in PDT.

Porphyrin is one of the extensively used photosensitizer in PDT. Porphyrin has four pyrrole rings connected via methane units. Initial studies with porphyrin sensitizer was performed by W. Hausmann in *Paramecium* - a genus of unicellular protozoan and reported that it killed the cells.[99] Even though many scientists explored the study of PDT with modified porphyrin such as haematoporphyrin derivate (HPD)

for various diseases, it was not until 1972 when Diamond and coworkers demonstrated that porphyrin derivatives could be employed as a photosensitizer to kill cancer cells.[100] *In vivo* studies in 1972 by Diamond and coworkers revealed that it suppressed the gliomas (type of tumor in brain) growth in mice. But complete cure of the tumor was not reported. Later in 1975, Dougherty and coworkers reported that HPD (haematoporphyrin derivate) completely destroyed the mammary tumor and bladder carcinoma in mice.[101] These studies led to the first human trials with HPD in 1976 by Kelly and coworkers, where he successfully treated 5 patients with recurrent bladder carcinoma which failed to respond to the conventional radio- and chemotherapy. [102]

Later Dougherty and coworkers performed detailed investigations on 7 patients with malignant melanomas, 3 patients with colon carcinomas, 5 patients with breast carcinomas on chest wall, 2 patients with recurring basal cell carcinomas using HPD sensitizer. 2.5 mg/kg-5.0 mg/kg doses were injected intravenously. After 3 days of injection of sensitizer, the patients were exposed to red light (100 milliwatts/sq cm) for 20 mins ranging from one to several days depending up on the stage and the reoccurrence of tumor. Tumor response and the normal tissue were monitored for 7 days and followed up at least once in 4 weeks to ensure the absence of recurrence. Complete disappearance or complete tumor response was noticed with 2.5 mg/kg of HPD dose with slight to no erythyma on the skin.[103]

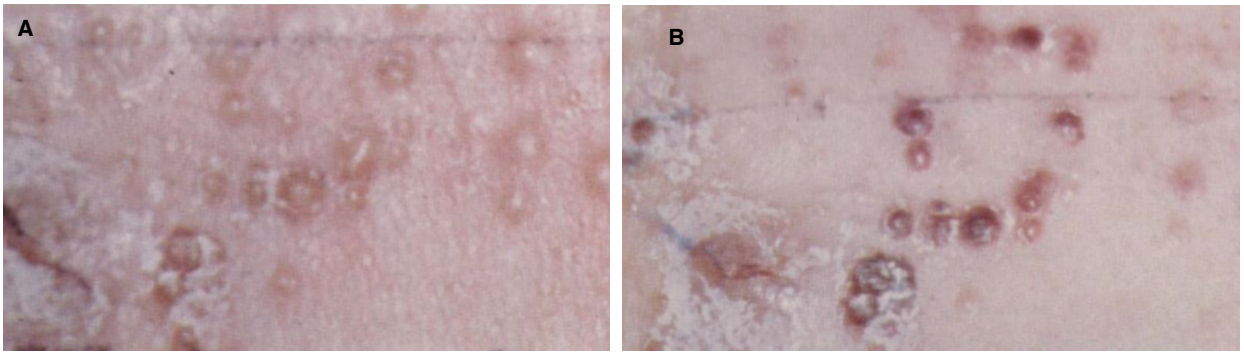

Figure 1.10: Breast carcinoma A) Before treatment B) after 1 day of irradiation showing erythema. Complete response obtained after 120 h (Reproduced from reference 102 with permission from American Association for Cancer Research, 1998).

Continuous efforts by scientists – Dougherty, McCaughen and many more led PDT for brain, breast, head and neck pancreatic treatment (both precancerous or cancerous conditions) etc.,[96] The clinical application was approved using HPD with trade name Photofrin[104] in 1993 in Canada and later to

various parts of the world. Below are few clinically approved sensitizer used for various types of cancer (Table 1.5).

Table 1.5: Few clinically approved sensitizers for PDT.[96]

Sensitizer	Trade name	Type of cancer	Wavelength (nm)
HPD	Photofrin	Cervical, oesophagel, brain tumors, bladder, breast cancer	630
Boronated protophyrin	BOPP	Brain tumor	630
Lutetium texaphyrin	Lutex	Cervical, prostrate and brain tumor	732
Pthalocyanine-4	Pc4	Cutaneous/subcutaneous lesion form diverse solid tumor origins	670
Taporfin Sodium	Talaporfin	Solid tumor from diverse origins	664

1.5.3. Role of light in drug delivery

Drug delivery system can be defined as a system that has the ability to release an active molecule upon stimuli. The most important criteria to be met in qualifying as a good drug delivering system are i) the delivery of the drug has to be at the appropriate site and ii) controlled rate of drug release at the target site. With this goal, any system, which responds to an external stimuli such as heat, light, change in pH etc., can be successfully employed for drug delivery.[105] Among these different types, the one based on light responsive system have received great attention since they are greener, they can be target specific and most importantly light can be used in biological systems. Most of the light based drug delivery system uses a photosensitive unit, which is commonly called as phototriggers. Phototrigger acts as a protecting group, which provides spatial and temporal release of various chemicals, upon shining light. Based upon their action they are often called as photoreleasable -, photoremovable-, photosensitive- and photoactivatable group. Compounds protected by photo protecting group are also called as caged compounds. The compounds in the caged form will be in their inactive form, but upon irradiation, turns to active form and releases the chemicals.[106,107] J. A Barltrop and Schofield reported the first observation on photosensitive group in 1962 on the release of amino acid **104** from carbamate **100** upon shining light as shown in scheme 1.34.[108]

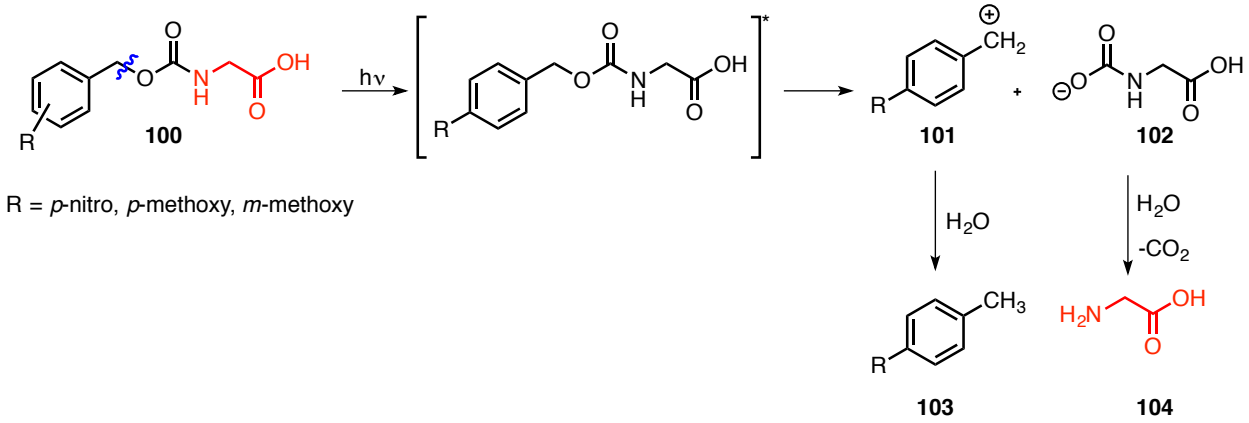

Scheme 1.34: First observation on photosensitive group on release of amino acid **104**.

Followed by this observation there were several reports made by Barton, Woodward and co-workers.[109,110] But it was popularized by Engels and coworkers[111] and Hoffman and coworkers[112] as they extended this strategy to biological systems wherein they achieved photorelease of cyclic adenosine monophosphate and ATP respectively in late 1970s. From that point forward there have been numerous reports on photoremovable group in different fields including drug release, material science and organic synthesis. The phototrigger should possess certain properties in order to be used in the drug delivery system. Several researchers have listed those properties and the compiled list was given by Lester and Sheehan,[113-115] that includes:

1. The caged substrate, substrate, and photoproduct should have good solubility in water for biological studies; for synthetic purpose this property can be relaxed.
2. Quantum yield for the release of active component should be efficient (ϕ_{rel} >0.10).
3. The release of active substrate should be a primary photochemical process.
4. Excitation wavelength should be preferably >300 nm especially for biological systems.
5. Photochemical by-products should not interfere with the system investigated.

Photoremovable protecting group, which lacks one or two of the desirable properties, can be still useful but absence of more properties will not be ideal for the intended investigation.

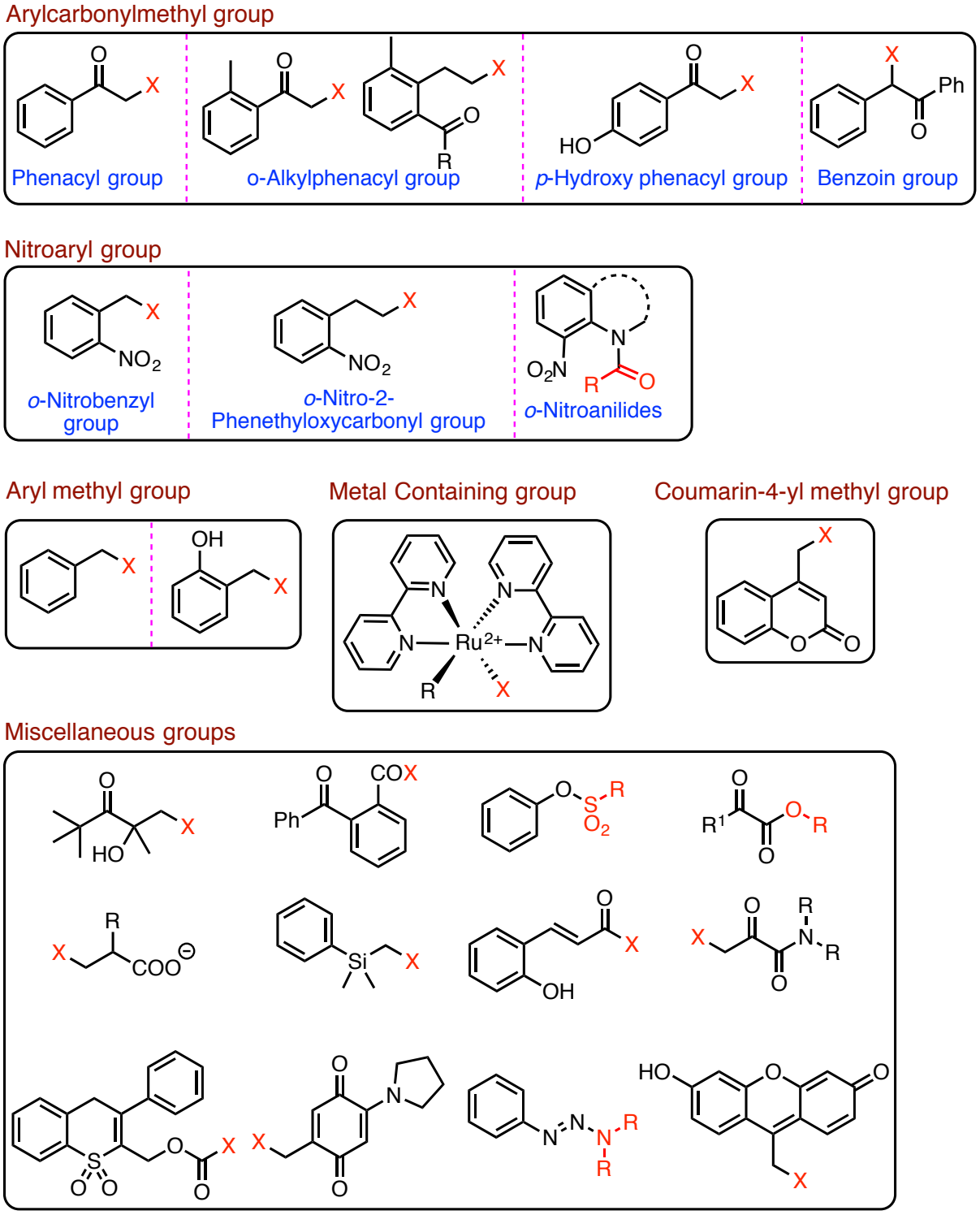

Figure 1.11: Selected examples of phototriggers.[106]

These phototriggers undergo a photolytic cleavage by absorbing a photon thereby triggering the release of the active component. There are several pathways[116] that the phototrigger could take to perform the release and some of them are listed below

Norrish type II reaction:

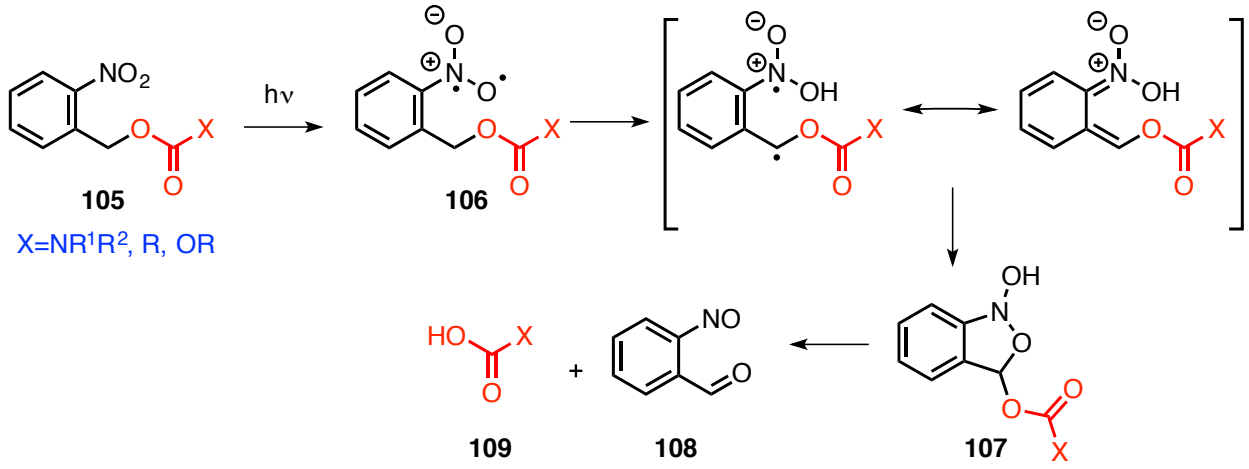

Scheme 1.35: Photocleavage of nitroaryl derivative **105** by Norrish type-II reaction.

Nitroaryl group **105** undergoes Norrish type-II reaction via intramolecular abstraction of γ-hydrogen by excited carbonyl (n,π*) resulting in the formation of 1,4 diradical followed by cyclization resulting in photorelease of acid derivative **109** (Scheme1.35). Alternate mechanism which involves β-cleavage also possible that is dictated by the spin states involved in the reaction.[110]

Norrish type I reaction:

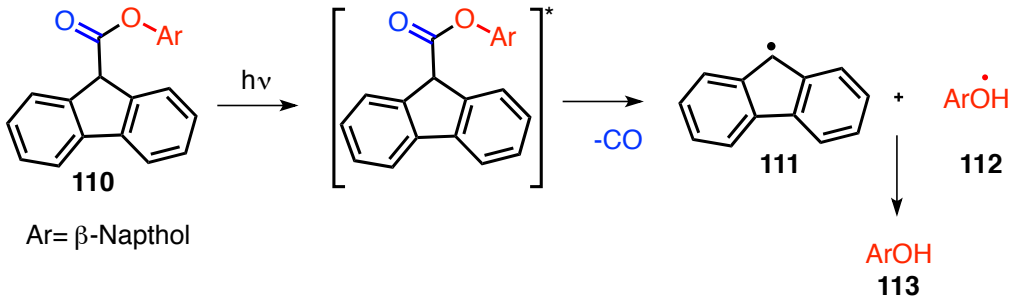

Scheme 1.36: Photocleavage of fluorene derivative **110** by Norrish type-I reaction.

Fluorene carboxylate derivative **110** undergoes Norrish type-I cleavage via homolytic cleavage of excited carbonyl group leading to fluorene radical **111** and aryloxy radical **112** along with the release of

carbon monoxide (Scheme 1.36). The aryloxy radical **112** can abstract a hydrogen leading to the formation of the desired product **113**.[117]

Photoisomerization:

Cinnamyl ester, upon absorption of photon undergoes *cis-trans* isomerization that places the functional group in the suitable orientation for the release of the enzyme (Scheme 1.37).[118,119]

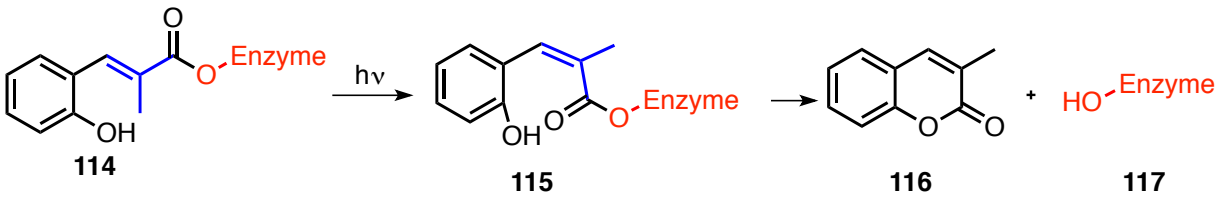

114 **115** **116** **117**

Scheme 1.37: Photo release of enzyme 117 by isomerization reaction.

Based on their properties, the utility of phototriggers has been extended to wide range of disciplines including, multistep synthesis, drug delivery, polymers, and modern agriculture. Taking advantage of the properties of phototriggers, several drug delivery systems were developed that were used for treating various diseases. For example, Pradeep Singh and coworkers demonstrated the use of perylene-3-yl methanol nanoparticles as a phototrigger, and nanocarrier for the release of anticancer drug chlorambucil (Scheme 1.38). The perylene-chlorambucil photocaged compound **118** (Pb-Cbl) was synthesized according to the reported literature.[120] Reprecipitation technique was adopted to use this photocaged compound for drug delivery. The shape and size of the nanocarrier was found to be globular and 30 nm respectively. Irradiation of photocaged Pb-Cbl under visible light (>410 nm) in 125W medium pressure Hg lamp with filter (1 M $NaNO_2$) resulted in the release of the drug chlorambucil **120** and the nanocarrier **119**.[121] The progress of release of the drug was monitored by reverse phase HPLC, which showed an efficient release within 20 min of irradiation. They also illustrated the temporal control of their strategy by light ON-OFF where only drug release occurred up on irradiation. This strategy was extended to *in vitro* studies in HeLa cells and validated their method in the biosystem.

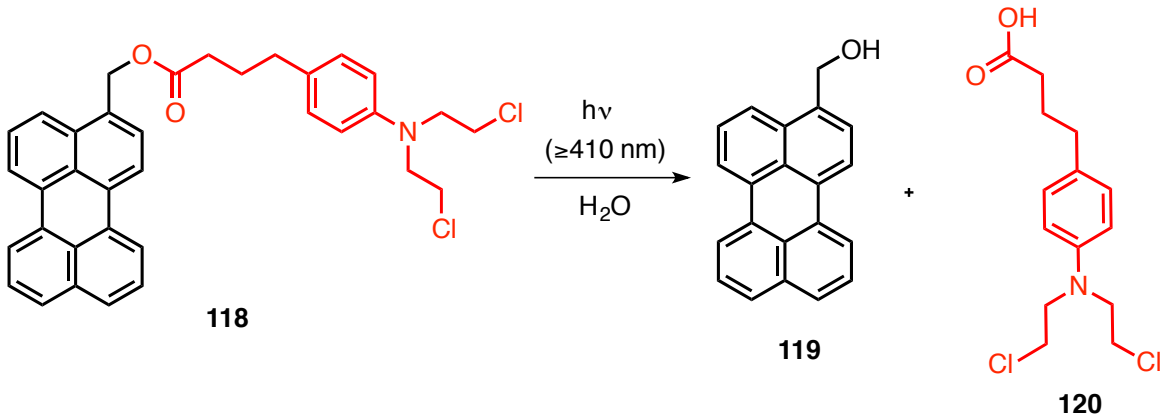

Scheme 1.38: Photorelease of chlorambucil **120** under visible light in HeLa cells.

In another example, Friedman and coworkers established the release of insulin,[122] which was covalently linked to the (poly ethylene glycol) resin (Scheme 1.39). Insulin is an important drug for the treatment of type I diabetes. This drug is usually injected in the patient multiple times in a day. Though other approaches such as transdermally delivering insulin using cannula are available it is not patient friendly. Therefore, in order to address this Friedman and coworkers designed a method to release the drug using a photocleavable linker attached to the drug insulin that is covalently linked to resin. In an attempt to prove their concept, they used (polyethylene glycol) resin to which nitro phenyl derivative linked with insulin was attached via click reaction.

Irradiation of the polymer linked insulin **121** was performed using two different lamps i) 30W black-ray fluorescent lamp and ii) 365 nm LED. Based on the detailed kinetic studies, 365 nm LED released the drug 32 times faster than the fluorescent UV lamp. They followed the release of the drug **122** using HPLC with authentic insulin as a reference. They also showed ON-OFF studies to prove that light is necessary for the release of the drug demonstrating the control over the process of release multiple times. In their long-term goal they were interested in using biodegradable resin so that after the release of the drug, the insoluble resin could be biodegraded and excreted from the body.

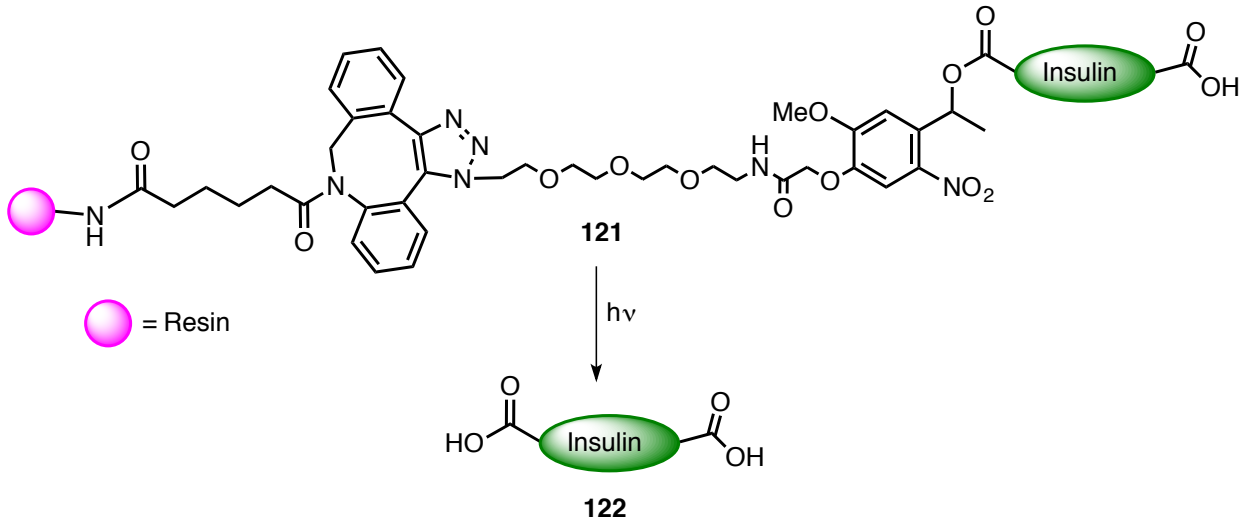

Scheme 1.39: Photo release of insulin **122** using 365 nm LED.

1.6. Role of light in polymers/materials

As the need for customizable, new and specialty polymeric materials in various fields are increasing day by day, scientists have looked at employing light for developing such polymeric materials. Light is used for initiating many physiochemical changes in polymers such as structure and size modifications, stimuli responsive polymers with spatio-temporal control etc., It has also been used to study the relationship between the structure and the property of a polymer, to synthesize as well as degrade polymers and functionalize the polymer. Such polymers have found wide applications from photolithographic applications to *invivo* biomedical applications. The following section will highlight those efforts taken in the field of materials.

1.6.1. Role of light lithography

In modern times, most of the electronic devices such as laptops, cell phones etc., rely on microchips developed from various semiconductor devices. Though the function of microchip can be explained by physics or engineering techniques, the fabrication of those electronic devices can be explained by technique called photolithography.[123] This process was first developed in the year 1959.[124,125] The word lithography literally means “writing on stones”. In semiconductor lithography, a specific geometric shape is inscribed on a silicon wafer that acts a stone using light and photomask. The

main process in photolithography involves a) preparation of silicon layers with SiO_2 surface. b) spin coating the photoresist (polymer) to approximately 1μm thickness. c) placing a photomask of desired geometric shape on the photoresist and d) irradiating photoresist and the photomask with UV light. Up on irradiation, the unmasked area undergoes polymerization or degradation of polymers making it insoluble/soluble respectively leaving a pattern. After the formation of patterned polymer on the SiO_2 substrate, the unwanted SiO_2 substrate is etched away leaving behind the pattern. The photoresist can be of two types *viz*., positive resist and negative resist. In the case of negative resist, the photoresist contain pre-polymer mixture with photoinitiator such as 2,2-dimethoxy-2-phenyl acetophenone (DMPA) therefore upon exposure to light DMPA breaks down into reactive radical species thus initiating the polymerization resulting in insoluble polymer leaving a pattern as shown in Figure 1.12 B. On the other hand, the photoresist containing a photocleavable group attached to a polymer resulting in degradation of polymer (making it soluble) after irradiation as depicted in the Figure 1.12. [126] In order to have a precise control over the shape of the pattern it is important for photoresist polymer to undergo polymerization /degradation efficiently. As polymerization-using photoinitiator was a very fast process, more emphasis was given in developing degradable polymers. Turro and coworkers demonstrated one such effort using nitrobenzyl phototrigger for linear and star polymer using click reactions.[127]

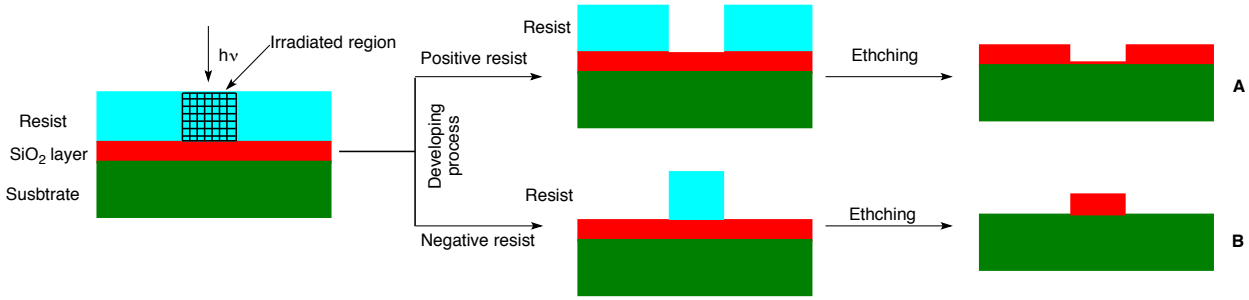

Figure 1.12: Pictorial representation different type of resist. (Reproduced from reference 125 with permission from American Chemical Society).

In 2004, Doh and coworkers demonstrated the use of photolithography technique in patterning bio macromolecules (Scheme 1.40).[128] The conventional photoresists are developed with organic solvents, which is too harsh for biomolecules such as proteins. So, they developed a photoresist (positive type) using *o*-nitrobenzyl cleavable linker with methyl methacrylate and poly(ethylene glycol) methacrylate that could be developed using pH buffer so that the process is compatible with biomolecules. Upon

exposure of polymer **123** to light, the nitro benzyl group cleaved that resulted in pattern and also leaving behind a carboxylic acid anion **124** that could be further developed using buffer. They also extended this work to different proteins as well as immune cells.

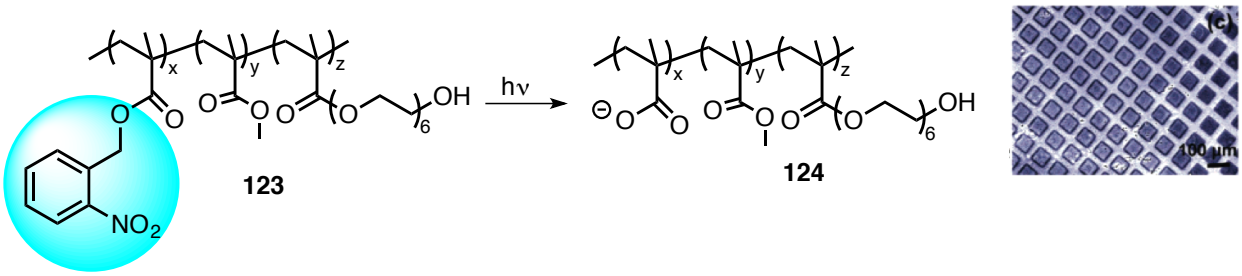

Scheme 1.40: Protein patterning using **123**. (Right) UV exposed and methylene blue stained photoresist. (Reproduced from reference 127 with permission from American Chemical Society, 2004).

In 2011, Carlborg and coworkers demonstrated thio-ene based patterning for microfluidic devices. They illustrated this method by applying polyethylene glycol based thiol with ene in the presence of Isopropyl thioxanthone as a photoinitiator. Upon irradiation, the thiol-ene undergo stepwise polymerization with quantitative yield followed by development of the resist that led to pattern on the device.[129]

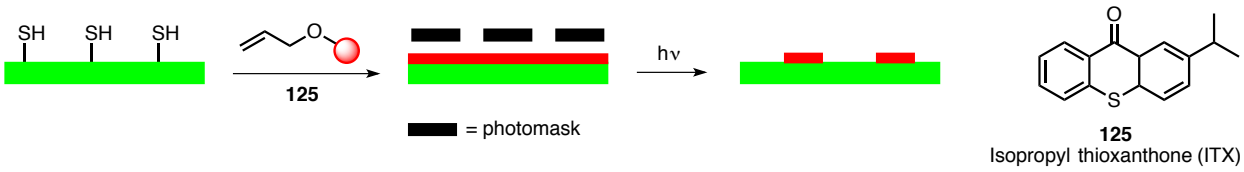

Figure 1.13: Pictorial representation of thiol-ene reaction for pattern microfluidic device.

1.6.2. Role of light in smart materials

Smart materials are materials that will change few of its properties up on external stimuli such as pH, stress, temperature, electric or magnetic field, light etc., Two characteristic examples of this are self-healing polymers (SHP) and shape memory polymers (SMP). SHPs can repair any damage (breaking of chemical bond or polymer chains) inside the polymeric material, or on its surface while the SMPs can transition from temporary shape to permanent shape.[130] One of the stimuli that is widely used for self-healing polymers and shape memory polymers is light. The advantages of using light is a) they can be delivered to specific site (spatial control) and b) the process can be stopped and activated whenever required (temporal control).

Self-healing process in polymers can be performed by three different approaches i) photo-crosslinking reaction ii) photo triggered metathesis and iii) photo thermal effect. In 2004, Chung and coworkers reported first photo crosslinking healing of polymer employing [2+2]-photocycloaddition of cinnamoyl derivative (Scheme 1.41). They first made a thin, hard, transparent polymer with cinnamate monomer -1,1,1-tris(cinnamoylmethyl)ethane (TCE) using light >280 nm. The formation of cycloaddition product **126** was followed by disappearance of C=C double bond in the cinnamoyl derivative by FTIR. The resultant cyclobutane derivative was subjected to mechanical stress (grinding) to break the cyclobutane ring to form **127** that was again irradiated with light for 120 s to form **126**.[131] By comparing the flexural strength of the originally synthesized film, cracked and self-healed polymer, they reported the efficiency to be 14 %. The efficiency was increased to 26 % by performing the healing process at 100 °C.

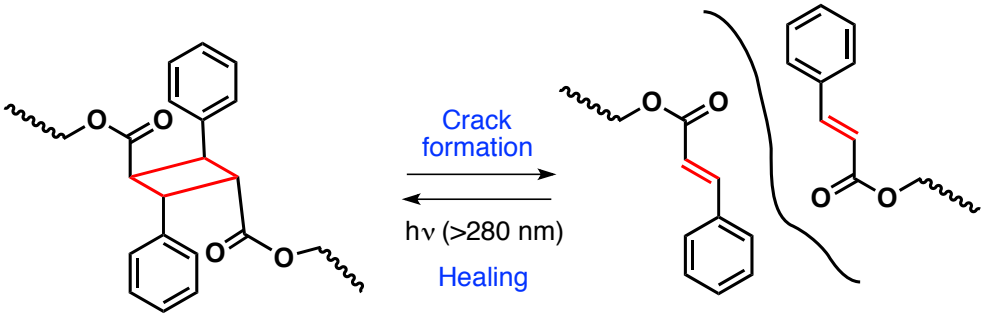

Scheme 1.41: Crack formation and healing process of cinnamoyl derivative.

The idea of using light for self-healing process by photoinduced reactive radical on a cracked surface was demonstrated by Ghosh and Urban in 2009.[132] Following upon their strategy, there had been considerable development in the photoinduced metathesis reaction on covalent bonds such as disulfides, trithiocarbonates and allyl sulfide. Matyjaszewski demonstrated one such study by synthesizing cross-linked polymer by RAFT polymerization of *n*-butyl acrylate **128** and trithiocarbonates (TTC) **129** cross linker (Scheme1.42).[133] Upon UV irradiation **130**, the TTC unit breaks leading to reactive radicals, which react among themselves thereby healing the crack by re-crosslinking the material. They also demonstrated that self-healing can be performed multiple times by cutting the polymer into 3 pieces and fusing them by irradiating in MeCN solution. They showed that the healing is not just a physical entanglement rather chemically fused by swelling the reformed polymer in anisole for 6 h, which did not show any polymer dissociation.

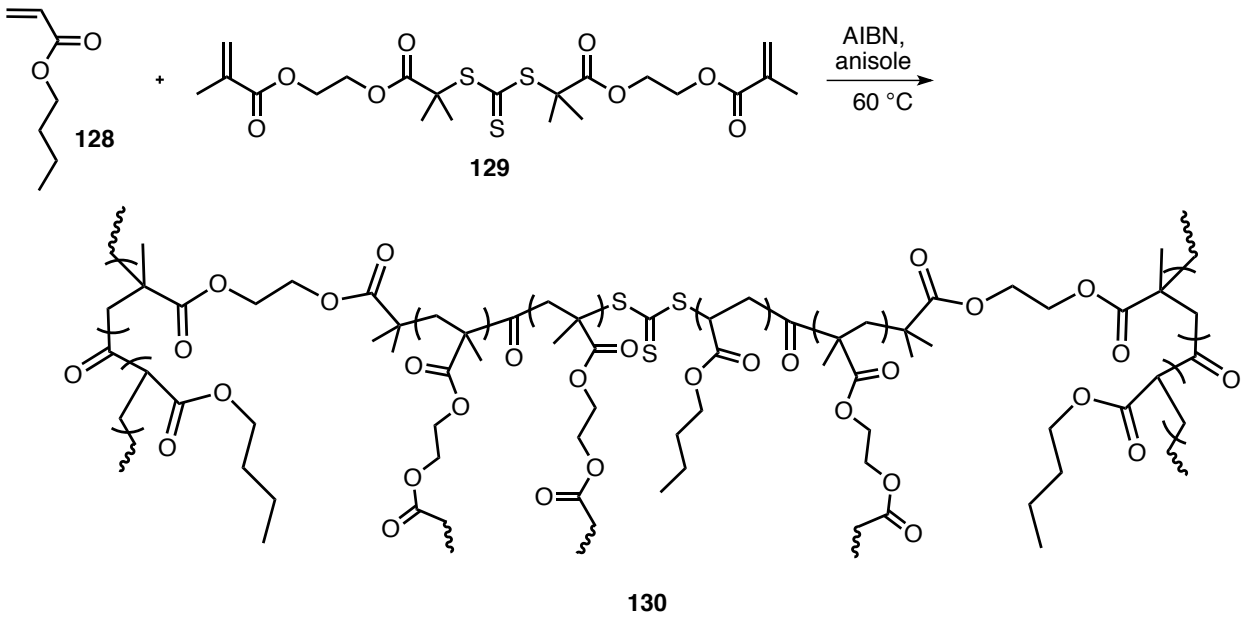

128 129 130

Scheme 1.42: Synthesis of a cross-linked polymer **130**.

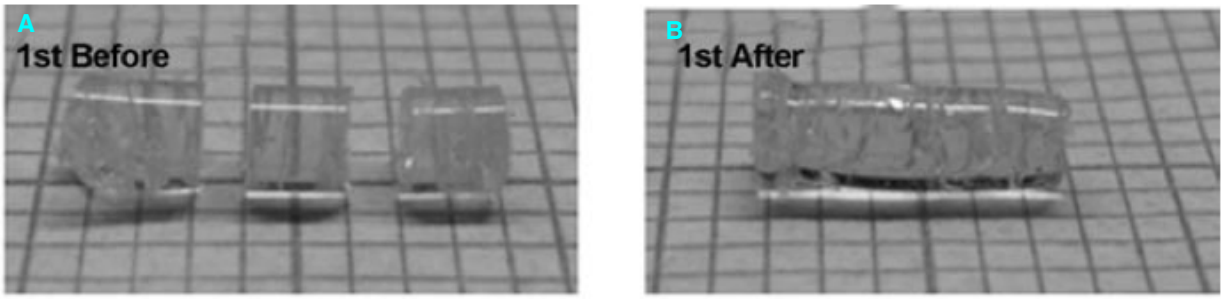

Figure 1.14: Self healing of polymer 130 A) cut into 3 pieces B) healing upon UV irradiation. (Reproduced from reference 132 with permission from Wiley-VCH, 2011).

Another approach to self heal the polymers is by photo thermal method. Weder and coworkers[134] illustrated this approach using metallo supramolecular polymer synthesized from poly(ethyle-co-butylene),the ligand 2,6-bis(1'-methyl-benzimidazoyl)pyridine and metal ion either Zn^{2+} or La^{3+} (Scheme 1.43). Up on irradiation of mechanically cracked polymer, the ligand absorbs light generating heat above 175 °C, at that temperature the ligand–metal binding is dissociated resulting depolymerization on the cracked surface. The low viscous polymer obtained due to depolymerization diffuses in the crack and mend the defects. Once the light is turned off, heating is stopped which resulted in the formation of metal-ligand coordination. The healing of the polymer was confirmed by atomic force microscope images (AFM).

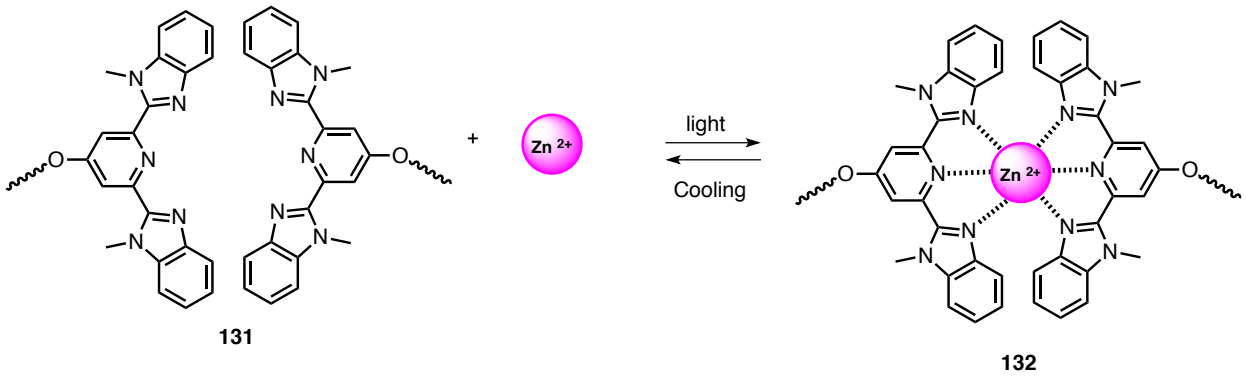

131 132

Scheme 1.43: Self-healing of polymer **132** by photo thermal process.

Similar to self-healing smart materials, shape memory smart materials are fast developing class of polymers that can remember two or more of its temporary shapes apart from their permanent shape. The temporary shapes were obtained by deformation at a temperature greater than its transition temperature (glass transition temperature or melting point of the polymer) and the permanent shape of the polymer was regained by cooling below its transition temperature. Light induced shape memory polymers can be obtained by two main methods. The most widely used method is photo thermal method as discussed in the self-healing polymers. The other method employed is the reversible photochemical reaction. In photo thermal method, the shape memory polymer should contain an additive or filler, which can absorb the light and generate heat. Most commonly used additives are carbon nanotube, gold nanoparticle, gold nanorods, organic dyes etc.,[130]

In 2012, Chen and coworkers[135] used single walled carbon nanotube (SWNT) as an additive in Nafion polymer (sulfonated tetrafluoroethylene based fluoropolymer) that had the ability to remember three or more temporary shapes. They employed near infrared (NIR) laser for this process. Absorption of 808 nm NIR (6 mW mm^{-2}) by SWNT generates heat (T = 70-75 °C) followed by cooling resulted in the formation of first temporary shape-coiled form (Figure 1.15 b). Second temporary shape was obtained by using localized 808 nm NIR (25 mW mm^{-2}) which rises the temperature between 140-150 °C resulting in coiled form with a bend (Figure 1.15 c). Uncoiling of the material took place in the oven at 75 °C resulting in the bend structure (Figure 1.15 d). Unbending of the material was performed by irradiation using 808 nm NIR (T = 140-150 °C).

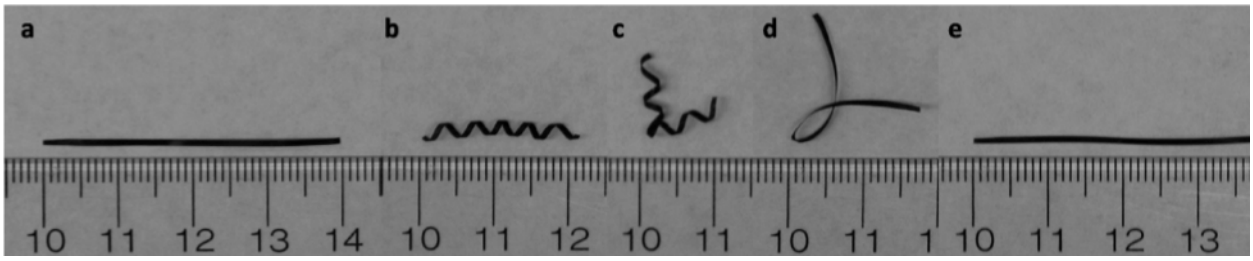

Figure 1.15: Shape memory Nafion polymer with SWNT. a) permanent shape b) first temporary shape 808 nm NIR (6 mW mm^{-2}, T = 70-75 °C) c) first temporary shape localized 808 nm NIR (25 mW mm^{-2}, T = 140-150 °C) d) uncoiling in over at 75 °C d) unbending to permanent shape using 808 nm NIR light (T = 140-150 °C). (Reproduced from reference 134 with permission from American Chemical Society, 2012).

While the photo thermal process is the most widely used method, Lindlein and coworkers[136] reported first example of the shape memory polymer using reversible photo crosslinking reaction using cinnamic acid and cinnamylidene acetic acid as photo switching groups. Following this precedence many groups reported the use of various photochemical reaction in memorizing the shape of the polymer. One of the interesting developments reported in shape memory polymers that employed light was the use of azo-liquid crystal polymer (LCN) reported by White and coworkers (Figure 1.16).[137] They synthesized the polymer starting from acrylate monomer RM 257 **133** and 4,4'-bis[6-(acryloxy)-hexyloxy] azobenzene **134**. The polymer was made into film and subjected to irradiation by 442 nm circularly polarized light to undergo *trans-cis* and *cis-trans* isomerization at room temperature (below the 40 °C) resulting in a bend structure. The bent form was stable in the absence of light and regained its permanent shape by irradiating with light.

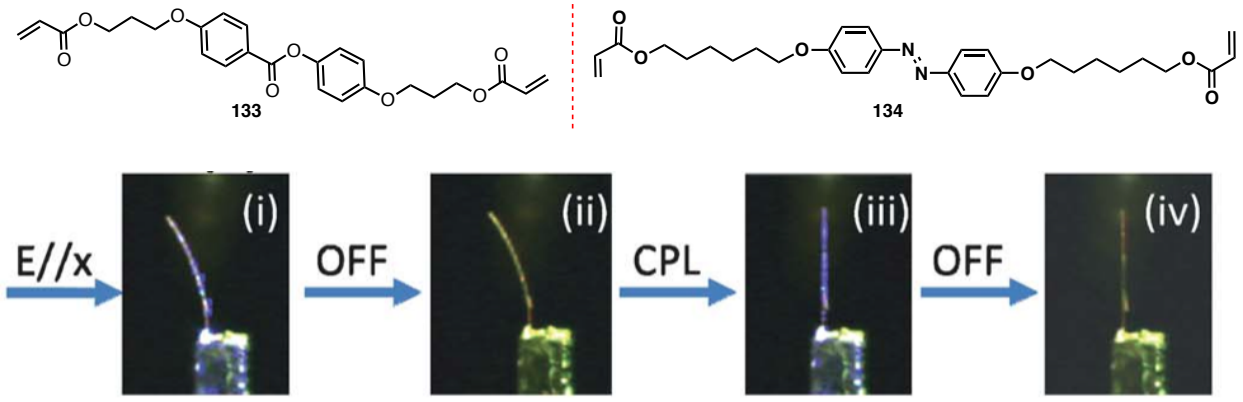

Figure 1.16: (Top) Shape memory polymers synthesized using **133** and **134**. (Bottom) i) Bending of the thin film upon excitation of circularly polarized 442 nm visible light ii) stable bent form of the film upon turning off of light iii) regaining permanent shape after irradiation of light iv) stable permanent form after turning off light. (Reproduced from reference 136 with permission from The Royal Society of Chemistry, 2011).

The applications of such shape memory polymers are largely used in many industrial applications such as robotics, engines etc., they also find vast applications in medicinal field such as orthopedic and various ophthalmic devices. These smart materials could also be potentially used as orthodontics wires. With such demand in developing new devices and strategies, light plays a significant role in realizing those goals with greener perspective.

1.7. Summary and outlook

The use of light in our day to day activities as well as for its role in different fields such as organic synthesis, medicine and materials has seen tremendous growth in recent years. In this regard various successful strategies and techniques employing light were reported in the literature especially in obtaining stereoselectivity in the field of organic synthesis, in drug delivery and in materials that includes lithography, degradable polymer and smart materials. Chapter one provides a glimpse of critical role played by light in various fields of science. With an aim to further explore new prospects in chemistry that utilizes light, the second and third chapters in this thesis describe strategies to obtain stereoselectivity in photochemical transformations using organocatalyst and atropisomeric chromophores respectively. The fourth and fifth chapters details elaborately about the use of phototrigger in the degradation of polymer and the reusability of the polymers.

1.8. References

(1) Forbes, M. D. E. What We Talk About When We Talk About Light. *ACS Cent. Sci* **2015**, *1*, 354-363.

(2) Roth, H. D. The Beginnings of Organic Photochemistry. *Angew. Chem. Int. Ed.* **1989**, *28*, 1193-1207.

(3) Roth, H. D. A Tribute to Stanislao Cannizzaro, Chemical Informationist and Photochemist. *Photochem. Photobiol. Sci.* **2011**, *10*, 1849-1853.

(4) Natarajan, A.; Tsai, C. K.; Khan, S. I.; McCarren, P.; Houk, K. N.; Garcia-Garibay, M. A. The Photoarrangement of α-Santonin is a Single-Crystal-to-Single-Crystal Reaction: A Long Kept Secret in Solid-State Organic Chemistry Revealed. *J. Am. Chem. Soc.* **2007**, *129*, 9846-9847.

(5) Introduction to Electromagnetic Spectrum. http://westernreservepublicmedia.org/ubiscience/electromagnetic.htm. (accessed February 2, 2016).

(6) Turro, N. J. R., V.; Scaiano, J. C. : *Modern Molecular Photochemistry of Organic Molecules*; University Science Books: Sausalito, CA, 2010.

(7) Ciamician, G. The Photochemistry of the Future. *Science* **1912**, *36*, 385-394.

(8) Ayitou, A. J.-L. Stereospecific Photochemical Transformations Involving Axially Chiral Acrylanilides and α-Oxoamides. North Dakota State University, ND, March 2013.

(9) Kumarasamy, E. Stereospecific Phototransformations of Atropisomeric Chromophores. North Dakota State University, ND, October 2014.

(10) Turro, N. J.; Ramamurthy, V.; Cherry, W.; Farneth, W. The Effect of Wavelength on Organic Photoreactions in solution. Reactions from Upper Excited States. *Chem. Rev.* **1978**, *78*, 125-145.

(11) Stegemeyer, H. Photoluminescence of Solutions. Von C. A. Parker. Elsevier Publishing Co., Amsterdam-London-New York 1968. 1. Aufl., XVI, 544 S., 188 Abb., 53 Tab., geb. Dfl. 85,–. *Angew. Chem.* **1969**, *81*, 1007-1008.

(12) Reichardt, C.; Welton, T.: Solvent Effects on the Absorption Spectra of Organic Compounds. In *Solvents and Solvent Effects in Organic Chemistry*; Wiley-VCH Verlag GmbH & Co. KGaA, 2010; pp 359-424.

(13) *Handbook of Photochemistry, Third Edition*; Taylor & Francis Group, LLC, 2006. pp. 583-600.

(14) Common Organic Solvents: Table of Properties. https://www.organicdivision.org/orig/organic_solvents.html. (accessed February 12, 2016).

(15) Monati, M.; Credi, A.; Prodi, L.; Gandolfi, M. T.: *Hand book of photochemistry*; 3 ed.; CRC press, 2006.

(16) Kim, J. H.; Scialli, A. R. Thalidomide: The Tragedy of Birth Defects and the Effective Treatment of Disease. *Toxicol. Sci.* **2011**, *122*, 1-6.

(17) Penkett, C. S.; Woolford, J. A.; Day, I. J.; Coles, M. P. The Double [3 + 2] Photocycloaddition Reaction. *J. Am. Chem. Soc.* **2009**, *132*, 4-5.

(18) Cornelisse, J. The Meta Photocycloaddition of Arenes to Alkenes. *Chem. Rev.* **1993**, *93*, 615-669.

(19) Bach, T.; Hehn, J. P. Photochemical Reactions as Key Steps in Natural Product Synthesis. *Angew. Chem. Int. Ed.* **2011**, *50*, 1000-1045.

(20) In *Chiral Photochemistry*; Inoue, Y., Ramamurthy, V., Eds.; Marcel Dekker: New York, 2004; Vol. 11.

(21) Le Bel, J. A. Sur les Relations qui Existent Entre les Formulas Atomiques de corps Organiques et le Pouvior Rotatiore de leurs Dissolutions. *Bull. Soc. Chim. Fr.* **1874**, *22*, 337-347.

(22) Van't Hoff, J. H.: *Die Lagerung der Atom and Raume*; 2 ed., 1894. pp. 30.

(23) Feringa, B. L.; van Delden, R. A. Absolute Asymmetric Synthesis: The Origin, Control, and Amplification of Chirality. *Angew. Chem. Int. Ed.* **1999**, *38*, 3418-3438.

(24) Kuhn, W.; Braun, E. Photochemische Erzeugung optisch aktiver Stoffe. *Die Naturwissenschaften* **1929**, *17*, 227-228.

(25) Kuhn, W.; Knopf, E. Photochemische Erzeugung optisch aktiver Stoffe. *Naturwissenschaften* **1930**, *18*, 183.

(26) Kagan, H.; Moradpour, A.; Nicoud, J. F.; Balavoine, G.; Tsoucaris, G. Photochemistry with Circularly Polarized Light. Synthesis of Optically Active Hexahelicene. *J. Am. Chem. Soc.* **1971**, *93*, 2353-2354.

(27) Flores, J. J.; Bonner, W. A.; Massey, G. A. Asymmetric Photolysis of (RS)-Leucine with Circularly Polarized Ultraviolet Light. *J. Am. Chem. Soc.* **1977**, *99*, 3622-3625.

(28) Kawasaki, T.; Sato, M.; Ishiguro, S.; Saito, T.; Morishita, Y.; Sato, I.; Nishino, H.; Inoue, Y.; Soai, K. Enantioselective Synthesis of Near Enantiopure Compound by Asymmetric Autocatalysis Triggered by Asymmetric Photolysis with Circularly Polarized Light. *J. Am. Chem. Soc.* **2005**, *127*, 3274-3275.

(29) Sato, I.; Sugie, R.; Matsueda, Y.; Furumura, Y.; Soai, K. Asymmetric Synthesis Utilizing Circularly Polarized Light Mediated by the Photoequilibrium of Chiral Olefins in Conjunction with Asymmetric Autocatalysis. *Angew. Chem. Int. Ed.* **2004**, *43*, 4490-4492.

(30) Blume, R.; Rau, H.; Schuster, O. Molar Ellipticity of the Pure Enantiomer by Partial Photoresolution. Photoreaction of 4,4,4',4'-Tetramethyl-2,2,3',3'-tetraazaspiro[4.4]nona-2,2'-diene. *J. Am. Chem. Soc.* **1976**, *98*, 6583-6586.

(31) Ciamician, G.; Silber, P. Chemische Lichtwirkungen. *Berichte der deutschen chemischen Gesellschaft* **1902**, *35*, 4128-4131.

(32) Ostromisslensky, I. Untersuchungen im Gebiete der Spiegelbildisomerie. *Berichte der deutschen chemischen Gesellschaft* **1908**, *41*, 3035-3046.

(33) Stobbe, H. S., F. K. Lichtreaktionen der *trans*-und *cis*-Zimtsäuren. *Chem. Ber* **1922**, *55*, 2225-2245.

(34) Green, B. S.; Lahav, M.; Rabinovich, D. Asymmetric Synthesis via Reactions in Chiral Crystals. *Acc. Chem. Res.* **1979**, *12*, 191-197.

(35) Sakamoto, M. Absolute Asymmetric Synthesis from Achiral Molecules in the Chiral Crystalline Environment. *Chem. Eur. J.* **1997**, *3*, 684-689.

(36) Schmidt, G. M. J. Photodimerization in the Solid State. *Pure Appl. Chem.* **1971**, *27*, 647-678.

(37) Cohen, M. D.; Schmidt, G. M. J. 383. Topochemistry. Part I. A survey. *J. Chem. Soc.* **1964**, 1996-2000.

(38) Schmidt, G. M. J. 385. Topochemistry. Part III. The crystal chemistry of some trans-cinnamic acids. *J. Chem. Soc.* **1964**, 2014-2021.

(39) Ramamurthy, V.; Venkatesan, K. Photochemical Reactions of Organic Crystals. *Chem. Rev.* **1987**, *87*, 433-481.

(40) Elgavi, A.; Green, B. S.; Schmidt, G. M. J. Reactions in Chiral Crystals. Optically Active Heterophotodimer Formation from Chiral Single Crystals. *J. Am. Chem. Soc.* **1973**, *95*, 2058-2059.

(41) Evans, S. V.; Garcia-Garibay, M.; Omkaram, N.; Scheffer, J. R.; Trotter, J.; Wireko, F. Use of Chiral Single Crystals to Convert Achiral Reactants to Chiral Products in High Optical yield: Application to the Di-π-methane and Norrish type II Photorearrangements. *J. Am. Chem. Soc.* **1986**, *108*, 5648-5650.

(42) Scheffer, J. R.; Xia, W.: Asymmetric Induction in Organic Photochemistry via the Solid-State Ionic Chiral Auxiliary Approach. In *Organic Solid State Reactions* Toda, F., Ed.; Springer Berlin Heidelberg: Berlin, Heidelberg, 2005; pp 233-262.

(43) Gudmundsdottir, A. D.; Scheffer, J. R. Asymmetric Induction in the Solid State Photochemistry of Salts of Carboxylic Acids with Optically Active Amines. *Tetrahedron Lett.* **1990**, *31*, 6807-6810.

(44) Cheung, E.; Netherton, M. R.; Scheffer, J. R.; Trotter, J. In the Footsteps of Pasteur:Asymmetric Induction in the Solid-State Photochemistry of Ammonium Carboxylate Salts. *J. Am. Chem. Soc.* **1999**, *121*, 2919-2920.

(45) Anslyn, E. V. D., D. A.: *Modern Physical Organic chemistry*; University Sciene Books, Sausalito, CA, 2006.

(46) Pemberton, B. C.; Raghunathan, R.; Volla, S.; Sivaguru, J. From Containers to Catalysts: Supramolecular Catalysis within Cucurbiturils. *Chem. Eur. J.* **2012**, *18*, 12178-12190.

(47) Vallavoju, N.; Sivaguru, J. Supramolecular Photocatalysis: Combining Confinement and Non-Covalent Interactions to Control Light Initiated Reactions. *Chem. Soc. Rev.* **2014**, *43*, 4084-4101.

(48) Sivasubramanian, K.; Kaanumalle, L. S.; Uppili, S.; Ramamurthy, V. Value of Zeolites in Asymmetric Induction During Photocyclization of Pyridones, Cyclohexadienones and Naphthalenones. *Org. Biomol. Chem.* **2007**, *5*, 1569-1576.

(49) Joy, A.; Scheffer, J. R.; Ramamurthy, V. Chirally Modified Zeolites as Reaction Media:Photochemistry of an Achiral Tropolone Ether. *Org. Lett.* **1999**, *2*, 119-121.

(50) Joy, A.; Ramamurthy, V. Chiral Photochemistry within Zeolites. *Chem. Eur. J.* **2000**, *6*, 1287-1293.

(51) Nakamura, A.; Inoue, Y. Supramolecular Catalysis of the Enantiodifferentiating [4 + 4] Photocyclodimerization of 2-Anthracenecarboxylate by γ-Cyclodextrin. *J. Am. Chem. Soc.* **2002**, *125*, 966-972.

(52) Pemberton, B. C.; Kumarasamy, E.; Jockusch, S.; Srivastava, D. K.; Sivaguru, J. Photophysical Aspects of 6-Methylcoumarin–Cucurbit[8]uril Host–Guest Complexes. *Can. J. Chem.* **2011**, *89*, 310-316.

(53) Pemberton, B. C.; Barooah, N.; Srivatsava, D. K.; Sivaguru, J. Supramolecular Photocatalysis by Confinement-Photodimerization of Coumarins Within Cucurbit[8]urils. *Chem. Commun.* **2010**, *46*, 225-227.

(54) Kaanumalle, L. S.; Ramamurthy, V. Photodimerization of Acenaphthylene Within a Nanocapsule: Excited State Lifetime Dependent Dimer Selectivity. *Chem. Commun.* **2007**, 1062-1064.

(55) Mori, K.; Murai, O.; Hashimoto, S.; Nakamura, Y. Highly Regio- and Stereoselective Photocycloaddition Between Coumarin and Thymine by Molecular Recognition. *Tetrahedron Lett.* **1996**, *37*, 8523-8526.

(56) Bach, T.; Bergmann, H.; Harms, K. Enantioselective Intramolecular [2+2]-Photocycloaddition Reactions in Solution. *Angew. Chem. Int. Ed.* **2000**, *39*, 2302-2304.

(57) Alonso, R.; Bach, T. A Chiral Thioxanthone as an Organocatalyst for Enantioselective [2+2] Photocycloaddition Reactions Induced by Visible Light. *Angew. Chem. Int. Ed.* **2014**, *53*, 4368-4371.

(58) Vallavoju, N.; Selvakumar, S.; Jockusch, S.; Sibi, M. P.; Sivaguru, J. Enantioselective Organo-Photocatalysis Mediated by Atropisomeric Thiourea Derivatives. *Angew. Chem. Int. Ed.* **2014**, *53*, 5604-5608.

(59) Vallavoju, N.; Selvakumar, S.; Pemberton, B. C.; Jockusch, S.; Sibi, M. P.; Sivaguru, J. Insights into the Mechanistic Aspects of Organo-photocatalysis Mediated by Thioureas. *Angew. Chem. Int. Ed* **2016**, *55*, 5446-5451.

(60) Christie, G. H.; Kenner, J. The Molecular Configurations of Polynuclear Aromatic Compounds. *J. Chem. Soc., Trans.* **1922**, *121*, 614-620.

(61) Kuhn, R. *Molekulare Asymmetrie in Stereochemie,* **1933**, 803.

(62) Mikami, K.; Aikawa, K.; Yusa, Y.; Jodry, J. J.; Yamanaka, M. Tropos or Atropos? That is the Question! *Synlett* **2002**, 1561-1578.

(63) *Prof. Dennis Curran coined the term "atropselective reaction" that involve axially chiral molecules*

(64) Curran, D. P.; Qi, H.; Geib, S. J.; DeMello, N. C. Atroposelective Thermal Reactions of Axially Twisted Amides and Imides. *J. Am. Chem. Soc.* **1994**, *116*, 3131-3132.

(65) Curran, D. P.; Liu, W.; Chen, C. H.-T. Transfer of Chirality in Radical Cyclizations. Cyclization of *o*-Haloacrylanilides to Oxindoles with Transfer of Axial Chirality to a Newly Formed Stereocenter. *J. Am. Chem. Soc.* **1999**, *121*, 11012-11013.

(66) Clayden, J.; Westlund, N.; Wilson, F. X. Asymmetric Induction Using Atropisomers: Diastereoselective Additions to 2-Acyl-1-naphthamides. *Tetrahedron Lett.* **1996**, *37*, 5577-5580.

(67) Bach, T.; Schröder, J.; Harms, K. Diastereoselective Photocycloaddition of an Axial Chiral Enamide. *Tetrahedron Lett.* **1999**, *40*, 9003-9004.

(68) Sakamoto, M.; Unosawa, A.; Kobaru, S.; Saito, A.; Mino, T.; Fujita, T. Asymmetric Photocycloaddition in Solution of a Chiral Crystallized Naphthamide. *Angew. Chem. Int. Ed.* **2005**, *44*, 5523-5526.

(69) Sakamoto, M.; Kato, M.; Aida, Y.; Fujita, K.; Mino, T.; Fujita, T. Photosensitized 2 + 2 Cycloaddition Reaction Using Homochirality Generated by Spontaneous Crystallization. *J. Am. Chem. Soc.* **2008**, *130*, 1132-1133.

(70) Havinga, E.; Schlatmann, J. L. M. A. Remarks on the Specificities of the Photochemical and Thermal Transformations in the Vitamin D Field. *Tetrahedron* **1961**, *16*, 146-152.

(71) Maessen, P. A.; Jacobs, H. J. C.; Cornelisse, J.; Havinga, E. Photochemistry of Previtamin D3 at 92 K; Formation of an Unstable Tachysterol$_3$ Rotamer. *Angew. Chem. Int. Ed.* **1983**, *22*, 718-719.

(72) Jacobs, H. J. C. Photochemistry of Conjugated Trienes: Vitamin D Revisited. *Pure Appl. Chem.* **1995**, *67*, 63-70.

(73) Ayitou, A. J.-L.; Sivaguru, J. Light-Induced Transfer of Molecular Chirality in Solution: Enantiospecific Photocyclization of Molecularly Chiral Acrylanilides. *J. Am. Chem. Soc.* **2009**, *131*, 5036-5037.

(74) Ayitou, A.; Pemberton, B. C.; Kumarasamy, E.; Vallavoju, N.; Sivaguru, J. Fun with Photons: Selective Light Induced Reactions in Solution and in Water Soluble Nano-containers. *Chimia* **2011**, *65*, 202-209.

(75) Ayitou, A. J.-L.; Sivaguru, J. Reactive Spin State Dependent Enantiospecific Photocyclization of Axially Chiral α-Substituted Acrylanilides. *Chem. Commun.* **2011**, *47*, 2568-2570.

(76) Ayitou, A. J.-L.; Vallavoju, N.; Ugrinov, A.; Sivaguru, J. Enantiospecific 6π-Photocyclization of Atropisomeric α-Substituted Acrylanilides in the Solid-State: Role of Crystalline Confinement on Enantiospecificity. *Photochem. Photobiol. Sci.* **2011**, *10*, 1380-1383.

(77) Ayitou, A. J.-L.; Clay, A.; Kumarasamy, E.; Jockusch, S.; Sivaguru, J. Enantiospecific Photochemical 6π-Ring Closure of α-Substituted Atropisomeric Acrylanilides - Role of Alkali Metal Ions. *Photochem. Photobiol. Sci.* **2014**, *13*, 141-144.

(78) Ayitou, A. J.-L.; Jesuraj, J. L.; Barooah, N.; Ugrinov, A.; Sivaguru, J. Enantiospecific Photochemical Norrish/Yang Type II Reaction of Nonbiaryl Atropchiral α-Oxoamides in Solution: Axial to Point Chirality Transfer. *J. Am. Chem. Soc.* **2009**, *131*, 11314-11315.

(79) Jesuraj, J. L.; Sivaguru, J. Photochemical Type II Reaction of Atropchiral Benzoylformamides to Point Chiral Oxazolidin-4-ones. Axial Chiral Memory Leading to Enantiomeric Resolution of Photoproducts. *Chem. Commun.* **2010**, *46*, 4791-4793.

(80) Kumarasamy, E.; Jesuraj, J. L.; Omlid, J. N.; Ugrinov, A.; Sivaguru, J. Light-Induced Enantiospecific 4π Ring Closure of Axially Chiral 2-Pyridones: Enthalpic and Entropic Effects Promoted by H-Bonding. *J. Am. Chem. Soc.* **2011**, *133*, 17106-17109.

(81) Iyer, A.; Jockusch, S.; Sivaguru, J. Dictating Photoreactivity through Restricted Bond Rotations: Cross-Photoaddition of Atropisomeric Acrylimide Derivatives under UV/Visible-Light Irradiation. *J. Phys. Chem. A* **2014**, *118*, 10596-10602.

(82) Peteanu, L. A.; Schoenlein, R. W.; Wang, Q.; Mathies, R. A.; Shank, C. V. The First Step in Vision Occurs in Femtoseconds: Complete Blue and Red Spectral Studies. *Proc. Natl. Acad. Sci.* **1993**, *90*, 11762-11766.

(83) Wang, Q.; Schoenlein, R. W.; Peteanu, L. A.; Mathies, R. A.; Shank, C. V. Vibrationally Coherent Photochemistry in the Femtosecond Primary Event of Vision. *Science* **1994**, *266*, 422-424.

(84) Mathies, R. A.: The Femtosecond cis-trans Isomerization in Vision: a Classic Barrierless Photochemical Reaction. In *Ultrafrast Processes in Chemistry and Photobiology*; Blackwell Science, Cambridge, 1995.

(85) Liu, R. S. H. S., Y.; Ramamurthy, V.: *Photochemistry in Organized and Constrained Media*; VCH, Newyork, 1991. pp. 817.

(86) " I have seen the light?" Vision and Light Induced Molecular changes. http://www.chemistry.wustl.edu/~edudev/LabTutorials/Vision/Vision.html (accessed December 24, 2015).

(87) Weiler, E. W. Sensory Principles of Higher Plants. *Angew. Chem. Int. Ed.* **2003**, *42*, 392-411.

(88) Rüdiger, W.; Thümmler, F. Phytochrome, the Visual Pigment of Plants. *Angew. Chem. Int. Ed.* **1991**, *30*, 1216-1228.

(89) Spikes, J. D.: *Primary Photoprocesses in Biology and Medicine*; Plenum Press, New York, 1985. pp. 209-227.

(90) Finsel, N. R.: *Phototherapy*; Edward Arnold, London, 1901.

(91) Lightner, D. A.; McDonagh, A. F. Molecular Mechanisms of Phototherapy for Neonatal Jaundice. *Acc. Chem. Res.* **1984**, *17*, 417-424.

(92) Raab, O. Uber die Wirkung Fluoreszierender Stoffe auf Infusorien. *Zeitung Biol.* **1900**, *39*, 524-526.

(93) Prime, J.: *Les accidents toxiques par l'eosinate de sodium*; Jouve and Boyer, Paris, 1900.

(94) von Tappeiner, H. J., A. Therapeutische versuche mit fluoreszierenden stoffen. *Muench Med. Wochenschr.* **1903**, *47*, 2042-2044.

(95) von Tappeiner, H. J., A.: *Die sensiblilisierende Wirkung fluoreszierender Substanzer Gesammte Untersuchungen uber die photodynamische Erscheinerung*; Voger, F. C., Leipzig, 1907.

(96) Dolmans, D. E. J. G. J.; Fukumura, D.; Jain, R. K. Photodynamic Therapy for Cancer. *Nat Rev Cancer* **2003**, *3*, 380-387.

(97) Lovell, J. F.; Liu, T. W. B.; Chen, J.; Zheng, G. Activatable Photosensitizers for Imaging and Therapy. *Chem. Rev.* **2010**, *110*, 2839-2857.

(98) Moan, J.; Berg, K. The Photodegradation of Porphyrins in Cells can be used to Estimate the Lifetime of Singlet Oxygen. *Photochem. Photobiol.* **1991**, *53*, 549-553.

(99) Hausmann, W. Die sensiblisierende Wirkung des Hematoporphyrins. *Biochem. Zeitung* **1911**, *30*, 276-316.

(100) Diamond. I.; Granelli, S. G. M., A. F.; Nielsen, S.; Wilson, C. B.; Jaenicke, R. Photodynamic Therapy of Malignant Tumours. *Lancet.* **1972**, *2*, 1175-1177.

(101) Dougherty, T. J., Grindey, G. B.; Fiel, R.; Weishaupt, K. R.; Boyle, D. G. Photoradiation Therapy. II. Cure of Animal Tumors with Hematoporphyrin and Light. *J. Natl Cancer Inst.* **1975**, *55*, 115-121.

(102) Kelly, J. F. S., M. E. Hematoporphyrin Derivative: A Possible Aid in the Diagnosis and Therapy of Carcinoma of the Bladder. *J. Urol.* **1976**, *115*, 150-151.

(103) Dougherty, T. J. K., J. E.; Goldfarb, A.; Weishaupt, K. R.; Boyle, D.; Mittleman, A. Photoradiation Therapy for the Treatment of Malignant Tumors. *Cancer Res.* **1978**, *38*, 2628-2635.

(104) Dougherty, T. J. Hematoporphyrin as a Photosensitizer of Tumors. *Photochem. Photobiol.* **1983**, *38*, 377-379.

(105) Alvarez-Lorenzo, C.; Bromberg, L.; Concheiro, A. Light-sensitive Intelligent Drug Delivery Systems. *Photochem. Photobiol.* **2009**, *85*, 848-860.

(106) Klán, P.; Šolomek, T.; Bochet, C. G.; Blanc, A.; Givens, R.; Rubina, M.; Popik, V.; Kostikov, A.; Wirz, J. Photoremovable Protecting Groups in Chemistry and Biology:Reaction Mechanisms and Efficacy. *Chem. Rev.* **2013**, *113*, 119-191.

(107) Herrmann, A. Controlled Release of Volatiles under Mild Reaction Conditions: From Nature to Everyday Products. *Angew. Chem. Int. Ed.* **2007**, *46*, 5836-5863.

(108) Barltrop, J. A.; Schofield, P. Photosensitive Protecting Groups. *Tetrahedron Lett.* **1962**, *3*, 697-699.

(109) Barton, D. H. R.; Chow, Y. L.; Cox, A.; Kirby, G. W. Photosensitive Protection of Functional Groups. *Tetrahedron Lett.* **1962**, *3*, 1055-1057.

(110) Patchornik, A.; Amit, B.; Woodward, R. B. Photosensitive Protecting Groups. *J. Am. Chem. Soc.* **1970**, *92*, 6333-6335.

(111) Engels, J.; Schlaeger, E. J. Synthesis, Structure, and Reactivity of Adenosine Cyclic 3',5'-phosphate-benzyltriesters. *J. Med. Chem.* **1977**, *20*, 907-911.

(112) Kaplan, J. H.; Forbush, B.; Hoffman, J. F. Rapid Photolytic Release of Adenosine 5'-triphosphate from a Protected analog: Utilization by the Sodium:Potassium pump of Human Red Blood Cell Ghosts. *Biochemistry* **1978**, *17*, 1929-1935.

(113) Sheehan, J. C.; Umezawa, K. Phenacyl Photosensitive Blocking Groups. *J. Org. Chem.* **1973**, *38*, 3771-3774.

(114) Lester, H. A. N., J. M. Physiological and Pharmacological Manipulations with Light Flashes. *Ann, Rev. Biophys. Bioeng.* **1982**, *11*, 151-175.

(115) Givens, R. S. C., P. G. I.; Yousef, A. L.; Lee, J,-I.: Photoremovable Protecting groups. In *CRC Handbook of Organic Photochemistry and Photobiology*; 2nd ed.; CRC press: Boca Raton, FL, 2004.

(116) Bochet, C. G. Photolabile protecting groups and linkers. *J. Chem. Soc., Perkin Trans. 1* **2002**, 125-142.

(117) Banerjee, A.; Falvey, D. E. Protecting Groups That Can Be Removed through Photochemical Electron Transfer:Mechanistic and Product Studies on Photosensitized Release of Carboxylates from Phenacyl Esters. *J. Org. Chem.* **1997**, *62*, 6245-6251.

(118) Turner, A. D.; Pizzo, S. V.; Rozakis, G. W.; Porter, N. A. Photochemical Activation of Acylated α-Thrombin. *J. Am. Chem. Soc.* **1987**, *109*, 1274-1275.

(119) Turner, A. D.; Pizzo, S. V.; Rozakis, G.; Porter, N. A. Photoreactivation of Irreversibly Inhibited Serine Proteinases. *J. Am. Chem. Soc.* **1988**, *110*, 244-250.

(120) Jana, A.; Ikbal, M.; Singh, N. D. P. Perylen-3-ylmethyl: Fluorescent Photoremovable Protecting Group (FPRPG) for Carboxylic Acids and Alcohols. *Tetrahedron* **2012**, *68*, 1128-1136.

(121) Jana, A.; Devi, K. S. P.; Maiti, T. K.; Singh, N. D. P. Perylene-3-ylmethanol: Fluorescent Organic Nanoparticles as a Single-Component Photoresponsive Nanocarrier with Real-Time Monitoring of Anticancer Drug Release. *J. Am. Chem. Soc.* **2012**, *134*, 7656-7659.

(122) Jain, P. K.; Karunakaran, D.; Friedman, S. H. Construction of a Photoactivated Insulin Depot. *Angew. Chem. Int. Ed.* **2013**, *52*, 1404-1409.

(123) Chen, Y.; Pépin, A. Nanofabrication: Conventional and Nonconventional Methods. *Electrophoresis* **2001**, *22*, 187-207.

(124) Noyce, R. N. Semiconductor Device-And-Lead Structure. U.S Patent 2,981,877.

(125) Kilby, J. Miniturized Electronic Circuits. U.S Patent 3,138,743.

(126) Reichmanis, E.; Thompson, L. F. Polymer Materials for Microlithography. *Chem. Rev.* **1989**, *89*, 1273-1289.

(127) Johnson, J. A.; Finn, M. G.; Koberstein, J. T.; Turro, N. J. Synthesis of Photocleavable Linear Macromonomers by ATRP and Star Macromonomers by a Tandem ATRP−Click Reaction:Precursors to Photodegradable Model Networks. *Macromolecules* **2007**, *40*, 3589-3598.

(128) Doh, J.; Irvine, D. J. Photogenerated Polyelectrolyte Bilayers from an Aqueous-Processible Photoresist for Multicomponent Protein Patterning. *J. Am. Chem. Soc.* **2004**, *126*, 9170-9171.

(129) Carlborg, C. F.; Haraldsson, T.; Oberg, K.; Malkoch, M.; van der Wijngaart, W. Beyond PDMS: Off-Stoichiometry Thiol-ene (OSTE) Based Soft Lithography for Rapid Prototyping of Microfluidic Devices. *Lab on a Chip* **2011**, *11*, 3136-3147.

(130) Habault, D.; Zhang, H.; Zhao, Y. Light-triggered Self-healing and Shape-memory Polymers. *Chem. Soc. Rev.* **2013**, *42*, 7244-7256.

(131) Chung, C.-M.; Roh, Y.-S.; Cho, S.-Y.; Kim, J.-G. Crack Healing in Polymeric Materials via Photochemical [2+2] Cycloaddition. *Chem. Mater.* **2004**, *16*, 3982-3984.

(132) Ghosh, B.; Urban, M. W. Self-Repairing Oxetane-Substituted Chitosan Polyurethane Networks. *Science* **2009**, *323*, 1458-1460.

(133) Amamoto, Y.; Kamada, J.; Otsuka, H.; Takahara, A.; Matyjaszewski, K. Repeatable Photoinduced Self-Healing of Covalently Cross-Linked Polymers through Reshuffling of Trithiocarbonate Units. *Angew. Chem. Int. Ed.* **2011**, *50*, 1660-1663.

(134) Burnworth, M.; Tang, L.; Kumpfer, J. R.; Duncan, A. J.; Beyer, F. L.; Fiore, G. L.; Rowan, S. J.; Weder, C. Optically Healable Supramolecular Polymers. *Nature* **2011**, *472*, 334-337.

(135) Kohlmeyer, R. R.; Lor, M.; Chen, J. Remote, Local, and Chemical Programming of Healable Multishape Memory Polymer Nanocomposites. *Nano Lett.* **2012**, *12*, 2757-2762.

(136) Lendlein, A.; Jiang, H.; Junger, O.; Langer, R. Light-induced Shape-memory Polymers. *Nature* **2005**, *434*, 879-882.

(137) Lee, K. M.; Koerner, H.; Vaia, R. A.; Bunning, T. J.; White, T. J. Light-activated Shape Memory of Glassy, Azobenzene Liquid Crystalline Polymer Networks. *Soft Matter* **2011**, *7*, 4318-4324.

CHAPTER 2. ASSESSING THIOUREA/UREA CATALYSTS FOR ENANTIOSELECTIVE 6π-PHOTOCYCLIZATION OF ACRYLANILIDES

2.1. Introduction

Photocyclization reactions can be defined as intramolecular processes leading to the formation of ring system (carbo-or heterocyclic) by formation of new σ-bond.[1] This process can either take place via concerted mechanism e.g. electrocyclic reactions or by multi step processes e.g. Norrish-Yang cyclization. Electrocyclic ring closing reactions are unimolecular pericyclic reactions where a new σ-bond is formed between terminal conjugated π-system. This type of reaction is widely used in the synthesis of natural products.[2,3] This concerted reaction can take place either by photochemical or by thermal methods. Depending on the total number of π electrons involved in the reaction and the type of reaction e.g. photochemical or thermal, the cyclization can occur by *conrotatory* or *disrotatory* pathways. In *conrotation*, the atomic orbitals at the terminal position turn in the same direction or in other words the atomic orbital rotate either in clockwise or counter clockwise direction. In *disrotation*, the terminal atomic orbitals rotate in opposite direction with respect to each other (one atomic orbital turns clockwise and the other turns counter clockwise) as depicted in the Figure 2.1.[4,5]

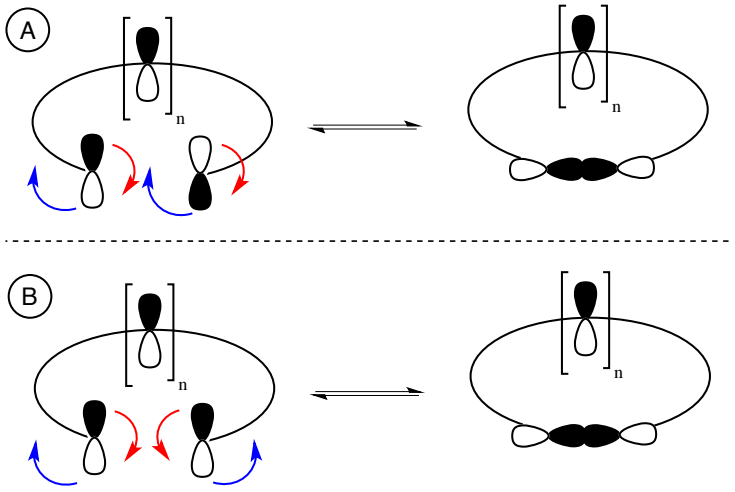

Figure 2.1: Pictorial representation of A. *con*-rotation, B. *dis*-rotation.

Woodward-Hoffmann rules[6] and Fukai Frontier model theory (FMO)[7] put forward certain guidelines to predict if a given cyclization is allowed or forbidden under given reaction conditions

(photochemical or thermal) (Table 2.1). Based on these rules, the type of rotation determines the stereospecificity of the resulting products. For example, cyclization of 2,4,6-octatriene **135** (4n+2 electron system) takes place only via *disrotation* in thermal reaction where the ground state (HOMO configuration) is involved in the bond forming process leading to *cis* product **136**-*cis*. However, in the photochemical set up, upon excitation, one electron is promoted to form HOMO* to LUMO*. This change in the electronic configuration requires *conrotation* for bond formation resulting in the t*rans* photoproduct **136**-*trans* (*disrotation* is not favored photochemically) (Figure 2.2). Thus these guidelines are indispensible for understanding and explaining the stereospecificity of the resulting product.[8-10]

Table 2.1: Woodward-Hoffman rules for electro cyclization.

No. of electrons	Thermal	Photochemical
4n (n=integer)	*Conrotatory*	*Disrotatory*
4n+2	*Disrotatory*	*Conrotatory*

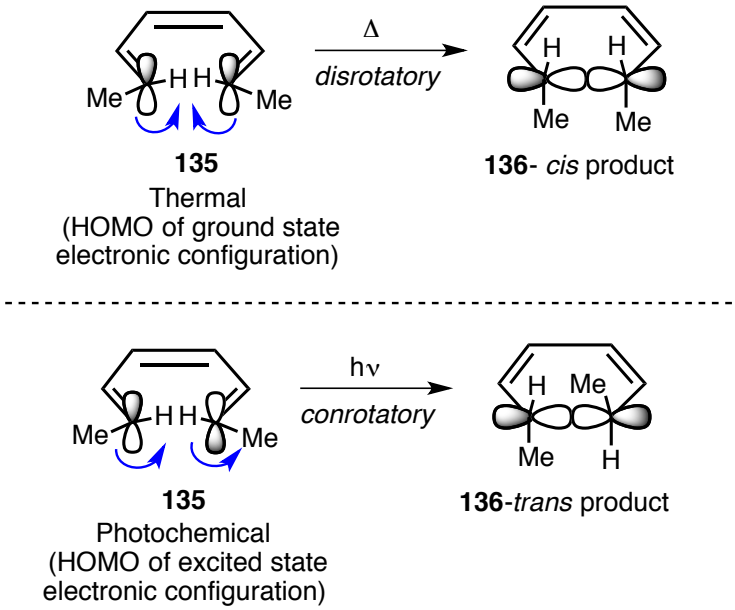

Figure 2.2: FMO analysis cyclization of 2,4,6-octatriene top: ground state reaction (Thermal) bottom: excited state reaction (photochemical).

2.2. 6π-Photocyclization of acrylanilides

6π-Photocyclization of acrylanilides resulting in 3,4-dihydroquinolin-2(H)-one was first reported by Chapman and coworkers.[11-13] During their study on the photochemistry of unsaturated acids and their

derivatives, they observed non-oxidative cyclization of alkyl-substituted acrylanilides to diastereomeric photoproducts *cis* and *trans* alkyl substituted 3,4-dihydroquinoline derivatives **138** (Scheme 2.1).

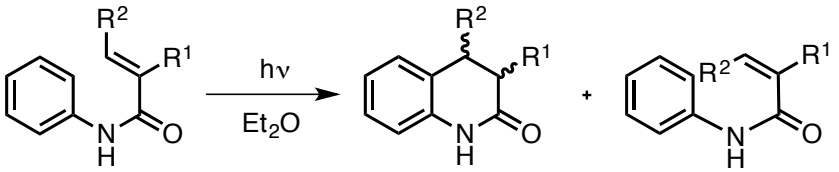

137 **138** **139**

a) $R^1 = R^2 = Me$; b) $R^1 = H$, $R^2 = Me$; c) $R^1 = Me$, $R^2 = H$

Scheme 2.1: First report on photocyclization of acrylanilides.

Based on their observations, Ninomiya and coworkers had performed detailed study on 6π-photocyclization of acrylanilides including the influence of the substituents and the role of solvents such as diethyl ether, benzene and methanol in determining the ratio of the resulting *cis*/*trans* products (Scheme 2.2). Their study revealed that in an aprotic solvent, *trans* product **141**-*trans* was obtained due to the tautomerization via thermal suprafacial 1,5 hydrogen shift whereas in protic solvent or in presence of Brønsted acid, *cis* photoproduct **141**-*cis* was obtained.[14,15]

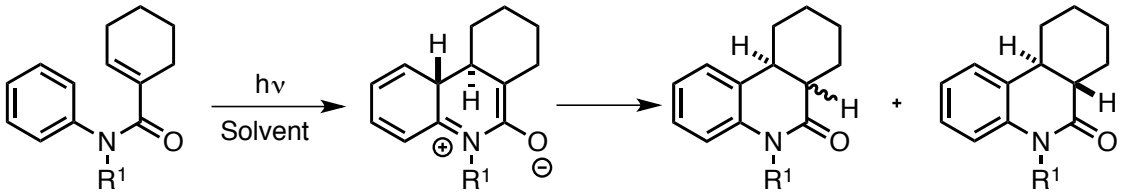

140 **141**-*cis* **141**-*trans*

Scheme 2.2: Photocyclization of anilides: role of solvent effects.

Most of the research efforts to control the excited state of the substrate to obtain high enantioselectivity in the photoproduct(s) employed supramolecular assemblies; solid-state irradiation etc., In that regard, Toda and coworkers reported an enantioselective solid-state 6π-photocyclization of acrylanilides using inclusion crystal (recrystallization of host and guest in stoichiometric ratio from a solvent) of acrylanilides with tartaric acid-derived 1,4-dioxaspiro-[4.4]-nonanes and -[4.5]-decanes. The reaction predominantly yielded *trans* photoproduct with 41-70 % yield and up to 98 % enantioselectivity due to its chiral conformation in the crystalline environment provided by the chiral host.[16,17] The first enantioselective 6π-photocyclization of acrylanilides **142** in solution was reported by Ninomiya and

coworkers. The zwitterionic intermediate formed during the 6π-photocyclization was enantioselectively protonated using an external chiral proton source (+)-di(*p*-toluyl)tartaric acid (DTTA) that resulted in enantiomerically enriched 3,4-dihydroquinolin-2(H)-one products **143** (Scheme 2.3).[18]

Building upon their work, Bach and coworkers[19] have studied the effect of chiral Kemp host in enantioselective 6π-photocyclization of acrylanilides **142**. They employed chiral Kemp triacid host, which binds to the guest using its two-point hydrogen-bonding site. Such orientation provides a chiral environment for the substrate and facilitates enantioselective 6π-photocyclization to yield enantioenriched products. They were able to achieve up to 57 % *ee* for the *trans* photoproduct at -55 °C and 45% *ee* for *cis* photoproduct at -15 °C in toluene.

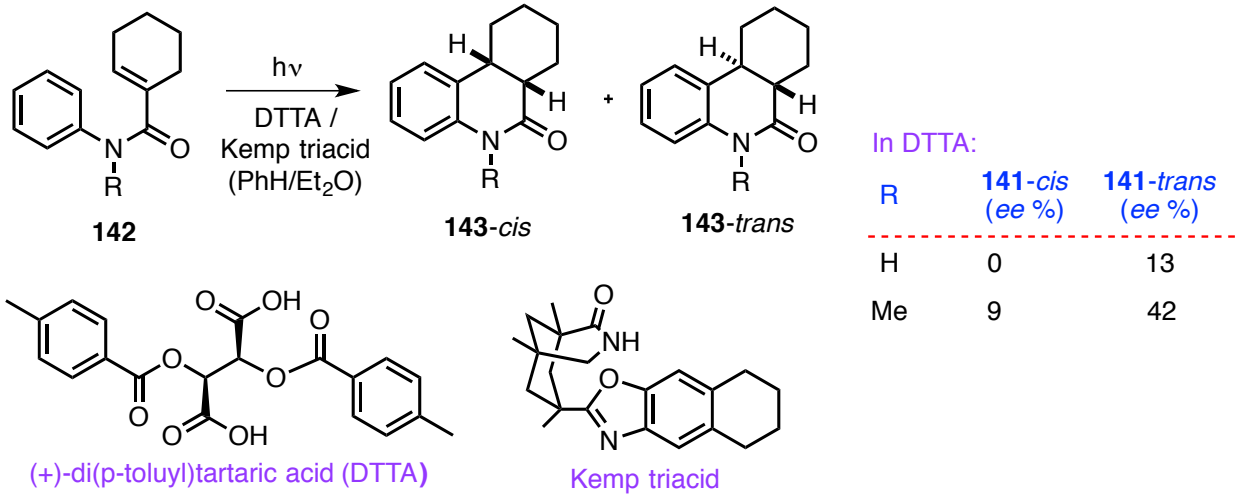

Scheme 2.3: Enantioselective 6π-photocyclization of acrylanilides **142** in solution.

One of the successful reports on enantioselective 6π-photocyclization in solution was documented by Sivaguru and coworkers.[20-24] They employed atropisomeric acrylanilides derivative **144** to achieve conformational orientation and steric predisposition for the enantioselective cyclization to occur. In this substrate-controlled reaction, they were able to achieve enantioselectivity up to 99% in the photoproducts **145** (Scheme 2.4). They were able to fine-tune the selectivity with spin (direct/sensitized) as well as by using solid-state reactivity and also using alkali metal ions. In recent years, many researchers have been working towards developing photocatalytic system for stereoselective synthesis.

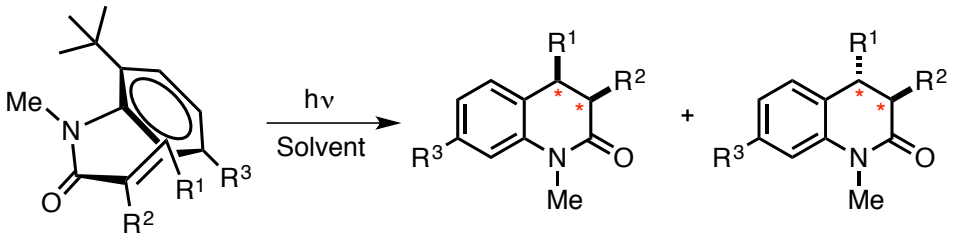

144 **145**-*cis* **145**-*trans*

Scheme 2.4: Atropselective 6π-photocyclization of atropisomeric acrylanilides in solution.

One of the emerging strategies that is gaining rapid interest in the synthetic community is photoredox catalysis.[25-30] In this strategy, the substrate undergoes a one electron oxidation or reduction initiated by a transition metal catalyst leading to a ground state radical anion or a radical cation. This process leads to an increase in reactivity of the substrate from the ground state. During the reaction cycle the substrate is not in the excited state. So, this strategy may not be suitable to induce selectivity in reactions that originates from the excited state. This opens up avenues to explore different approaches to control or manipulate the substrate in the excited state to achieve chiral induction. One such approach is to use of an organocatalyst that activates the substrates through hydrogen bonding (H-bonding). H-bond can be defined as an "X-H---A" interaction, where XH acts as proton donor to A.[31] They can be classified as 3 types as in Table 2.2.

Table 2.2: Classification and properties of hydrogen bonding.[32]

	Strong	**Moderate**	**Weak**
X-H----A interaction (type of bonding)	Mostly covalent	Mostly electrostatic	Electrostatic
Bond angle X-H----A (°)	175-180	130-180	90-150
Length of H-bond H-----A (Å)	1.2-1.5	1.5-2.2	2.2-3.2
Bond energy (kcal·mol^{-1})	14-40	4-15	<4

Thiourea/urea catalyst coordinates with the substrate through its double H-bond interaction leading to the activation and acceleration of a given reaction. If a chiral (thio) urea catalyst is employed, then in principal the interaction can lead to chiral induction in the given transformation. The advantages of using (thio)urea-based organocatalysts are[33]

- Metal free catalysis
- Relative ease of synthesis from inexpensive reagents
- Robustness and exceptional stability
- Inertness towards moisture and less demanding conditions (inert atmosphere, inert towards moisture, low temperature)

Sivaguru, Sibi and coworkers successfully demonstrated the use of atropisomeric thiourea catalyst for enantioselective intramolecular [2+2]-photocycloaddition of 4-alkenyl substituted coumarins **59** (Scheme 2.5).The enantioselective photoreactions took place via hydrogen bonding interaction via energy sharing mechanism leading to 69-96% *ee* in the photoproduct **61** at low catalyst loading of 1-30 mol%.[34,35]

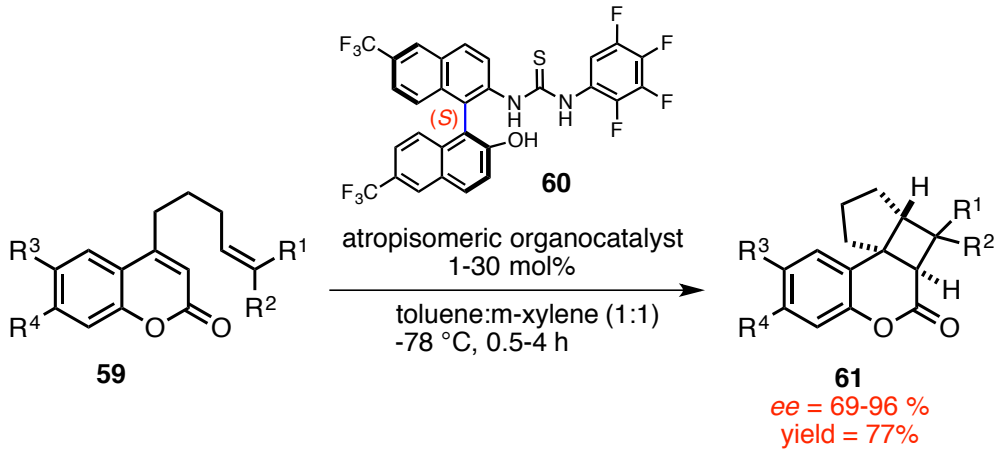

Scheme 2.5: Enantioselective [2+2]-photocycloaddition of 4-alkenyl coumarins **59** using atropisomeric thiourea catalysts.

As a continuing effort along these lines, we have investigated organocatalyst-based enantioselective 6π-photocyclization of acrylanilides in solution. The thiourea/urea catalysts employed this investigation are listed in Scheme 2.6 and were synthesized according to the procedures reported in the literature. To develop a catalytic method for 6π-photocyclization of acrylanilides, we evaluated six thiourea/urea catalysts with different backbones. They are phenylethyl thiourea derivative **147a**, binaphthyl based bis-aryl thiourea **147b**, C_2-symmetrical bis-thioureas **147c** and **147d**, mono functional chiral thiourea **147e** and mono-functional chiral urea catalyst **147f**.

2.3. Catalyst screening for 6π-photocyclization of acrylanilides

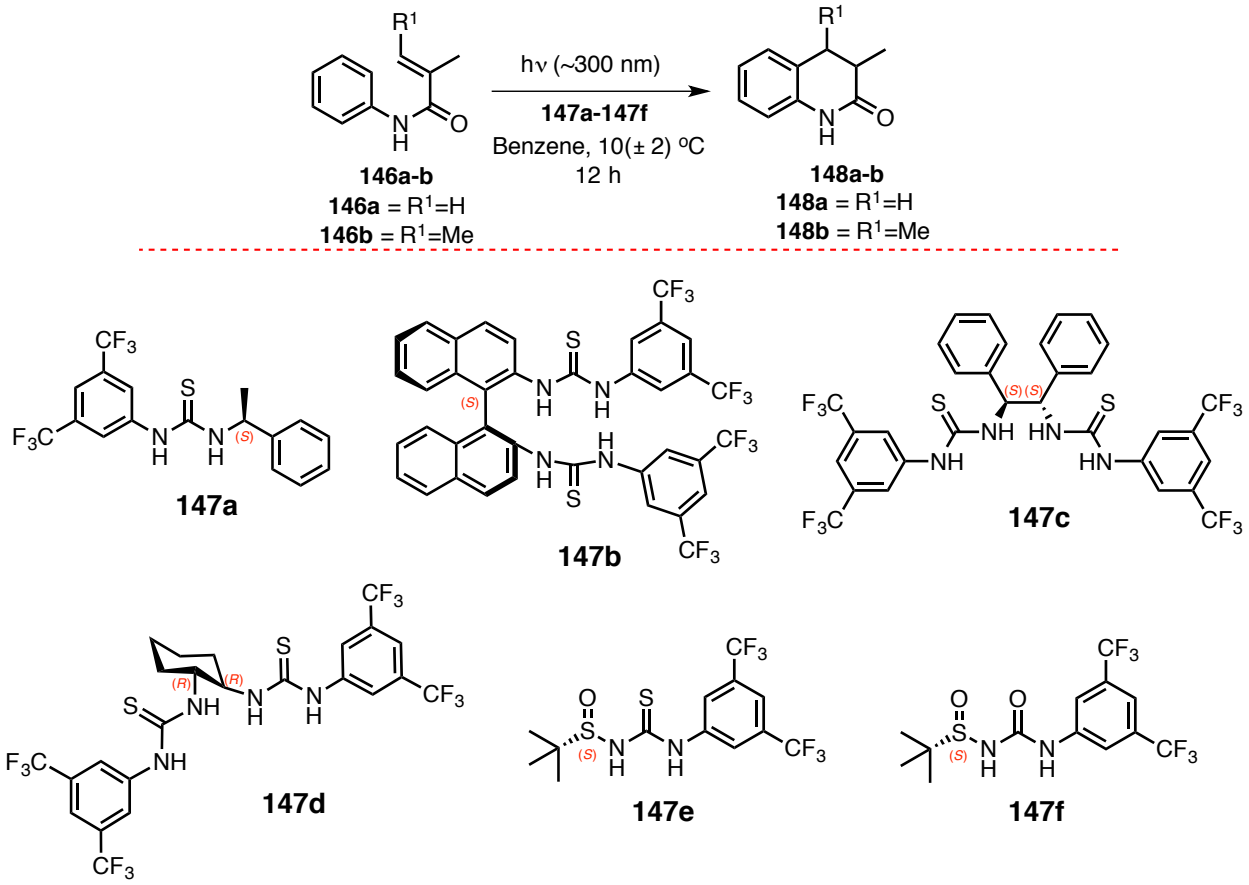

Scheme 2.6: Irradiation of **146a** with 100 mol% of catalyst **147a**-**147f**.

The photoreaction of the N-phenyl methacrylamide **146a-b** was carried out with 100 mol% of the catalyst **147a**-**147f** at 10 °C in benzene. The reaction mixture was degassed by nitrogen bubbling for 5–10 min. The irradiation was performed using a Rayonet reactor equipped with ~ 300 nm light bulbs (14 Watts x 16 bulbs) for 12 h. After the photoreaction, to monitor the reaction progress, an aliquot (~0.5 mL) of the reaction mixture was taken in a GC vial and was diluted by adding methanol (1 mL). The samples were then analyzed by gas chromatography on a chiral stationary phase to ascertain the enantiomeric excess in the photoproduct. For conversion yield and mass balance studies, after irradiation, an appropriate amount of internal standard (triphenylmethane) was added to the reaction mixture. The solvent was evaporated under reduced pressure and was dried under high vacuum. The crude reaction mixture was analyzed by ^{1}H-NMR spectroscopy ($CDCl_3$ as solvent). From the integral value of respective peaks, NMR yield was calculated.

Analysis of Table 2.3 revealed that the background reaction i.e., in the absence of catalyst, proceeded to completion to yield racemic photoproduct. However, in the presence of thiourea catalyst, the conversion was low compared to background reaction, but noticeable amount of enantiomeric excess (*ee*) was observed. The phenylethyl thiourea catalyst **147a** gave a moderate conversion with 13 % *ee*. Upon changing the catalyst to binaphthyl based bis-aryl derivative **147b**, the *ee* was lowered to 7 %. The C_2 - symmetrical bis –thiourea catalyst **147c** and **147d** only resulted in racemic mixture, whereas the monofunctionalized thiourea catalyst gave low enantioselectivity. Interestingly, the urea catalyst **147f** gave highest conversion for the catalyzed reaction but only resulted in 9 % *ee*.

Table 2.3: Enantioselective 6π-photocyclization of **1** with thioureas / urea **147a**-**147f** [a].

Entry	Substrate	Catalyst	NMR yield (%)[b]	% *ee*[c]
1	**146a**	None	100	Racemic
2	**146a**	**147a**	53	13
3	**146a**	**147b**	28	7
4	**146a**	**147c**	35	Racemic
5	**146a**	**147d**	31	Racemic
6	**146a**	**147e**	-	7
7	**146a**	**147f**	89	9
8	**146b**	None	-	Racemic
9	**146b**	**147a**	-	Racemic

[a] Reactions were carried out in benzene at 10±2 °C for 12 h with 1 equivalent of catalyst. All the samples were degassed with N_2 bubbling for 5-10 min prior to irradiation. Values are an average of two trials. [b] NMR yield was determined by ^{1}H-NMR spectroscopy using triphenylmethane as an internal standard. [c] From GC analysis using chiral stationary phase (error: ±3%).

2.4. Catalyst loading studies for 6π-photocyclization of acrylanilides

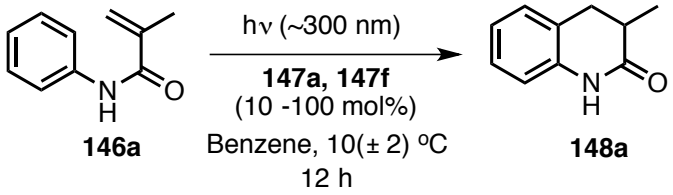

146a **148a**

Scheme 2.7: Irradiation of **146a** with 10 - 100 mol% of catalyst **147a** and **147f**.

The photoreaction of the N-phenyl methacrylamide with varying catalyst loading (10 – 100 mol%) of **147a** and **147f** were irradiated at 10 °C in benzene using a Rayonet reactor equipped with ~ 300 nm light bulbs (14 Watts x 16 bulbs) for 12 h. The reaction mixture was degassed by nitrogen bubbling for 5–

10 min. Then the resultant solution was irradiated in Rayonet reactor at 10 °C (± 2 °C) for 12 h. After the photoreaction, to monitor the reaction, an aliquot (~0.5 mL) of the reaction mixture was taken in a GC vial and was diluted by adding 1 mL of methanol. The samples were then analyzed by gas chromatography on a chiral stationary phase to ascertain the enantiomeric excess in the photoproduct.

Inspection of Table 2.4 shows that catalyst loading of 50 mol% was efficient in obtaining a higher ee in the photoproduct. For example, 50 mol% of **147a** catalyst resulted in 13 % *ee* and further increase in catalyst loading did not result in an increase of enantioselectivity in the photoproduct. Similar results were observed when **147f** was employed. Interestingly, the higher loading of **147f** catalyst resulted in higher conversions. This is on contrary to **147a** catalyst where the conversion started to depreciate.

Table 2.4: Enantioselective 6π-photocyclization of **146a** with varying catalyst **147a**-**147**f loading[a]

Entry	Catalyst (mol%)	NMR yield (%)[b]	% *ee*[c]
1	**147a** (10)	54	9
	147a (50)	49	13
	147a (100)	53	13
2	**147f** (10)	56	7
	147f (50)	59	9
	147f (100)	89	9

[a] Reactions were carried out in benzene at 10±2 °C for 12 h. All the samples were degassed with N_2 bubbling for 5-10 min prior to irradiation. Values are an average of two trials. [b] NMR yield was determined by ^{1}H-NMR spectroscopy using triphenylmethane as internal standard. [c] From GC analysis using chiral stationary phase (error: ±3%).

2.5. 6π-photocyclization of acrylanilides under sensitized conditions

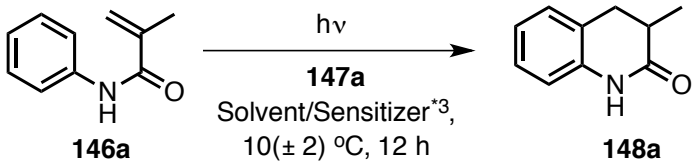

146a **148a**

Scheme 2.8: Irradiation of N-phenylacrylanilide **146a** with triplet sensitizer.

N-Phenylmethacrylamide **146a** (1mM), thiourea **147a** and an appropriate sensitizer (acetone (E_T = 78 kcal·mol $^{-1}$) or xanthone (E_T = 74 kcal·mol $^{-1}$)) were dissolved in respective solvent in a Pyrex test tube and were degassed by bubbling nitrogen for 5–10 min. The resultant solution was irradiated in Rayonet reactor equipped with ~ 300 nm light bulbs / 350 nm light bulbs at 10±2 °C for 12 h. After the

photoreaction, to monitor the reaction, an aliquot (~0.5 mL) of the reaction mixture was taken in a GC vial and was diluted by adding 1 mL of methanol. The samples were then analyzed by chiral gas chromatography to ascertain the enantiomeric excess in the photoproduct. For conversion yield and mass balance studies, after irradiation, an appropriate amount of internal standard (triphenylmethane) was added to the reaction mixture. The solvent was evaporated under reduced pressure and was dried under high vacuum. The crude reaction mixture was analyzed by ^{1}H-NMR spectroscopy ($CDCl_3$ as solvent). From the integral value of respective peaks, NMR yield was calculated.

The results of the sensitized irradiations with acetone (both as solvent and sensitizer) or xanthone in benzene are shown in Table 2.5. The studies revealed that in the presence of a sensitizer the conversion of the reaction was low compared to non-sensitized reaction. Similarly, the enantioselectivity of the reaction was also affected where the sensitized reaction only yielded racemic mixture for all the substrates under our condition in our study.

Table 2.5: 6π-photocyclization of **146a** under sensitized conditions[a].

Entry	Catalyst	Solvent/Sensitizer[*3]	Irradiation source	NMR yield (%)[c]	% *ee*[d]
1	None	Acetone[b]/-	300 nm	24	Racemic
2	**147a**	Acetone[b]/-	300 nm	10	Racemic
3	None	Benzene/Xanthone	350 nm	22	Racemic
4	**147a**	Benzene/Xanthone	350 nm	7	Racemic
5	None	Benzene/Xanthone	300 nm	15	Racemic
6	**147a**	Benzene/Xanthone	300 nm	17	Racemic

[a] All the samples were degassed with N_2 bubbling for 5-10 min prior to irradiation. Values are an average of two trials. [b] Acetone as solvent and sensitizer. [c] NMR yield was determined by ^{1}H-NMR spectroscopy using triphenylmethane as internal standard. [d] From GC analysis using chiral stationary phase (error : ±3 %).

2.6. Temperature dependent studies for 6π-photocyclization of acrylanilides

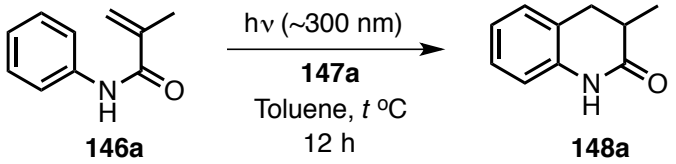

146a **148a**

Scheme 2.9: Irradiation of **146a** at different temperature.

N-Phenylmethacrylamide **146a** (1mM) and thiourea **147a** were dissolved in toluene in a Pyrex

test tube. The reaction mixture was degassed by nitrogen bubbling for 5–10 min. The resultant solution was irradiated in Rayonet reactor equipped with ~ 300 nm light bulbs for 12 h at a given temperature as shown in Table 2.6. After the photoreaction, to monitor the reactions, an aliquot (~0.5 mL) was taken in a GC vial and was diluted by adding 1 mL of methanol. Then the samples were analyzed by chiral gas chromatography to ascertain the enantiomeric excess in the photoproduct. For conversion yield and mass balance studies, after irradiation, an appropriate amount of internal standard (triphenylmethane) was added to the reaction mixture. The solvent was evaporated under reduced pressure and was dried under high vacuum. The crude reaction mixture was analyzed by ^{1}H-NMR spectroscopy ($CDCl_3$ as solvent). From the integral value of respective peaks, NMR yield was calculated.

Inspection of the Table 2.6 clearly showed that the temperature of the reaction did not have any noticeable influence in the product *ee* values while it affected the conversion. For example, in the presence of catalyst **147a**, conversion was 21 % with 10 % *ee* at -60 ^{o}C and at 25 ^{o}C, the conversion was 93 % with 9 % *ee*.

Table 2.6: Temperature dependent studies 6π-photocyclization of **146a**.[a]

Entry	Catalyst	Temp °C	NMR yield (%)[b]	% *ee*[c]
1	None	-60	54	Racemic
		-30	78	Racemic
		0	80	Racemic
		25	97	Racemic
2	**147a**	-60	21	10
		-30	43	9
		0	51	9
		25	93	9

a] All the samples were degassed with N_2 bubbling for 5-10 min prior to irradiation. Values are an average of two trials. [b] NMR yield was determined by ^{1}H-NMR spectroscopy using triphenylmethane as internal standard. [c] From GC analysis using chiral stationary phase (error: ±3 %).

2.7. Photophysical studies of 6π- photocyclization of acrylanilides

Detailed photophysical studies were performed to understand the interaction between the substrate and the catalyst. UV-Vis absorption spectra of **146a**, catalyst **147a** and the 1:1 mixture of **146a** and **147a** were recorded in toluene and ethanol (Figure 2.3A and Figure 2.3B). No emission was observed at room temperature therefore, in order to understand the interaction, steady state luminescence were recorded at 77 K. Based on the spectra (Figure 2.3C) it was evident that there was

luminescence from the catalyst **147a** and no luminescence from the substrate. Also, it was interesting to note that the luminescence of the catalyst was quenched by the substrate indicating the interaction of the excited-state catalyst and the substrate. To corroborate this interaction, we performed luminescence studies in a polar protic solvent such as ethanol (Figure 2.3D). We envisioned that the hydrogen bonding ability of the catalyst with the substrate would be disrupted by the protic solvent that also can act as a H-bonding agent. As expected, in ethanol glass at 77 K, the luminescence of **147a** was not quenched by substrate. This was further substantiated by photoreaction wherein we obtained a racemic photoproduct in ethanol solvent compared to 13 % *ee* in benzene. These studies clearly showed that interaction mediated by hydrogen bonding between the substrate and the catalyst was critical for the observed enantioselectivity in the reaction that was manifested as the quenching of the luminescence of the catalyst in presence of substrate.

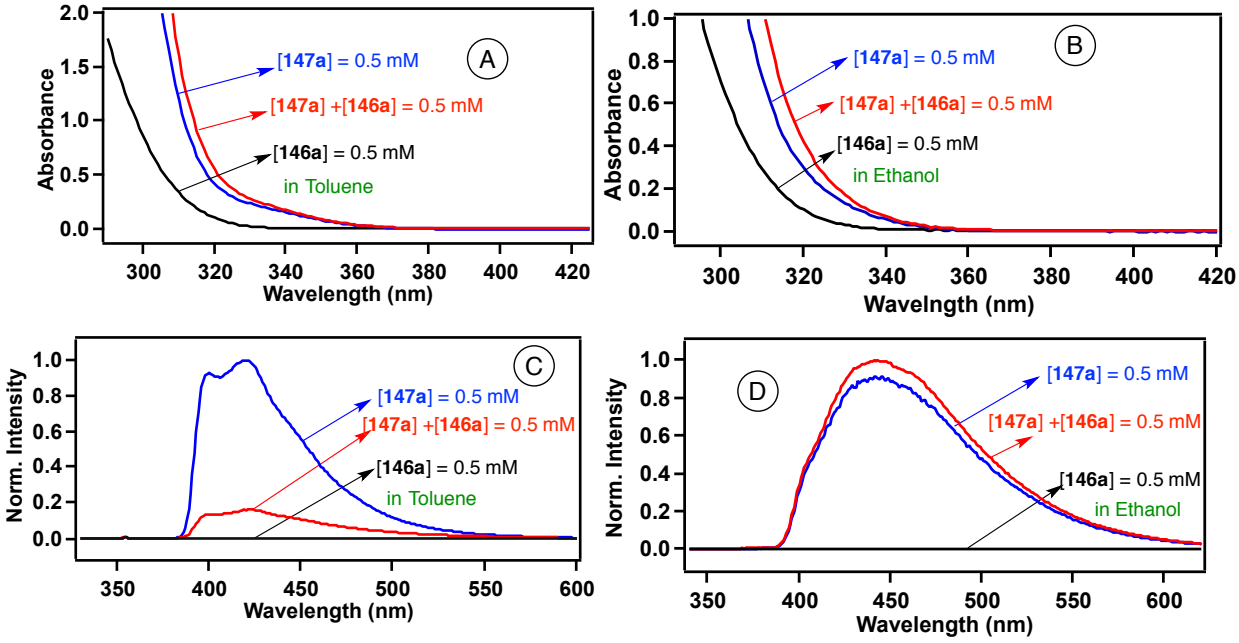

Figure 2.3: (A) UV-Vis spectra of **146a** (black), **147a** (blue) and **147a**+**146a** (red) (1:1 mixture) in toluene. (B) UV-Vis spectra of **146a** (black), **147a** (blue) and **147a**+**146a** (red) (1:1 mixture) in ethanol.(C) Luminescence spectra of **146a** (black), **147a** (blue) and **147a**+**146a** (red) (1:1 mixture) at 77 K in toluene. (D) Luminescence spectra of **146a** (black), **147a** (blue) and **147a**+**146a** (red) (1:1 mixture) at 77 K in ethanol at 320 nm excitation.

2.8. Mechanistic rationale for 6π-photocyclization of acrylanilides

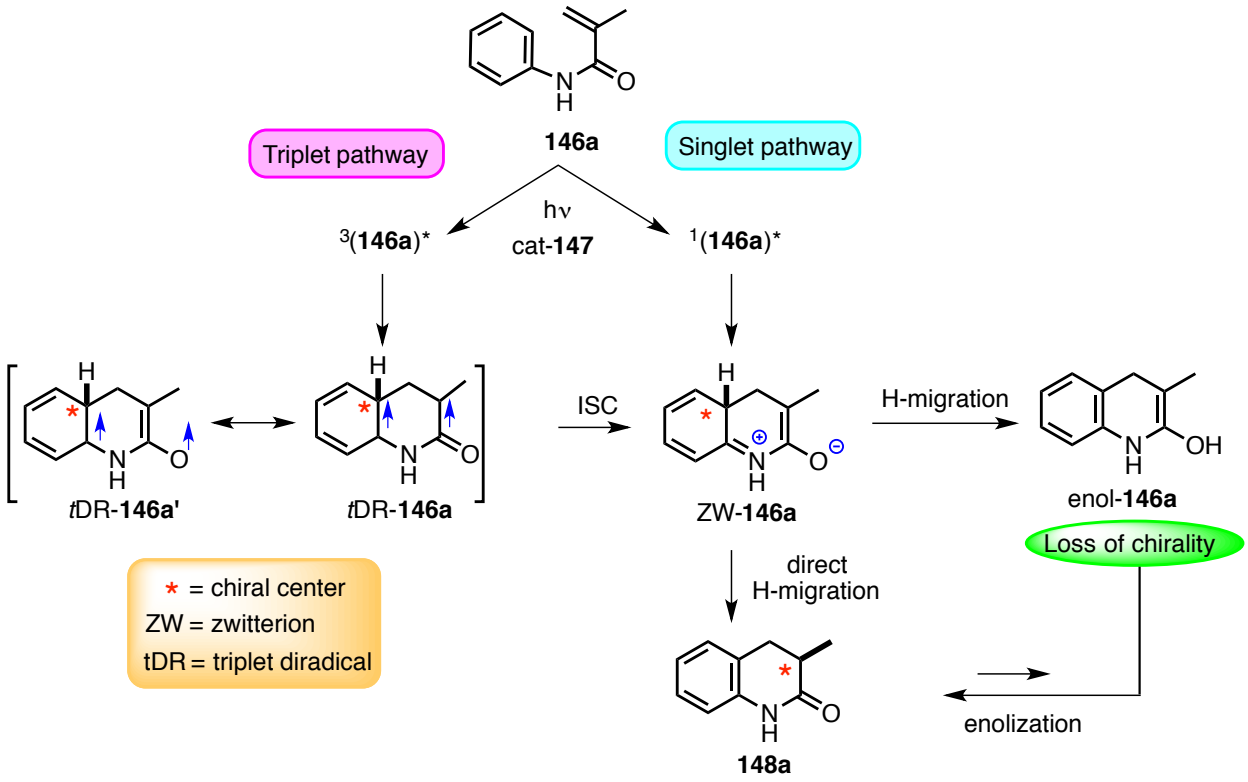

Scheme 2.10: Mechanistic rationale for 6π-photocyclization of **146a**.

Based on the literature precedence, 6π-photocyclization of **146a** can occur either via a singlet-excited state or via a triplet excited state. Based on the photochemical reactivity paradigm and the ππ* excited state in acrylanilides, it is highly plausible that the reaciton can proceed either via a zwitterionic intermediate from a singlet excited state and a diradicaloid intermediate from the triplet excited state. Depending upon our experimental conditions, in the presence of catalyst **147**, both a zwitterionic intermediate ZW-**146a** and a triplet diradical intermediate *t*DR-**146a** are possible. If reactions takes place via triplet pathway, it forms *t*DR-**146a** (and *t*DR-**146a'**) and has to intersystem cross to singlet to form the product. The ZW-**146a** thus formed via a direct or sensitized irradiation will lead to photoproduct **148** via direct hydrogen migration or via an enol intermediate (Scheme 2.10). We believe that the partition of the reactive pathways either via ZW-**146a** intermediate (where a chiral form is preserved) and/or via the enol intermediate (where the chirality is destroyed) determines the enantiomeric excess in the photoproduct. From our photophysical studies, it is evident that the catalyst and substrate interact in the excited state

and this interaction is facilitated by hydrogen bonding. In spite of the observable interaction, the low enantioselectivity is likely a reflection of a combination of factors *viz.,* a) with respect to the mode of cyclization; b) formation of an enol intermediate that destroys the chirality; c) relative reactivity of the zwitterion intermediate leading to enol formation that competes with direct hydrogen migration. The blend of these aspects are likely reflected in the observed low enantioselectivity in the product irrespective of the catalyst-substate interaction(s) in the excited state.

2.9. Summary and outlook

We have developed a catalytic process for the 6π-photocyclization of acrylanildes derivative employing thiourea/urea catalyst leading to 3,4 dihydroquinolin-2-one. Photophysical studies clearly showed the interaction between the catalyst and the substrate where the luminescence of the catalyst was efficiently quenched by the substrate. In spite of the interaction of the catalyst and the substrate, we observed low enantioselectivity due to combination of several factors like mode of cyclization of the substrate while bound to the catalyst, formation of enol intermediate that destroys the chirality and the relative reactivity of the zwitterion intermediate that competes with enol formation and direct hydrogen migration. However our preliminary studies showed the interaction of the catalyst and the susbtrate which opens up avenues for exploring the system further to get better selectivity in the photocyclization of acrylanilide systems.

2.10. Experimental section

2.10.1. General methods

All commercially obtained reagents/solvents were used as received; chemicals were purchased from TCI®, Alfa Aesar®, Sigma-Aldrich®, and Acros® and were used as received without further purification. Dry Benzene solvent was purchased from Merck® Chemicals. Unless stated otherwise, reactions were conducted in oven-dried glassware. ^{1}H-NMR and ^{13}C-NMR spectra were recorded on Bruker and Varian 400 MHz (100 MHz for ^{13}C) and on 500 MHz (125 MHz for ^{13}C) spectrometers. Data for ^{1}*H*-NMR are reported as chemical shift (δ ppm) with the corresponding integration values. Coupling constants (*J*) are

reported in hertz (Hz). Standard abbreviations indicating multiplicity were used as follows: s (singlet), b (broad), d (doublet), t (triplet), q (quartet), m (multiplet) and ABq (AB quartet). Data for ^{13}C-NMR spectra are reported in terms of chemical shift (δ ppm). Analytical gas chromatography analyses were performed on Varian 3900® equipped with auto-injector CP-8410 for automated sample injection, a chiral stationary phase: Supelco betadex-225 30 x 0.25 mm and a flame ionization detector. Instrumental settings as indicated below were used.

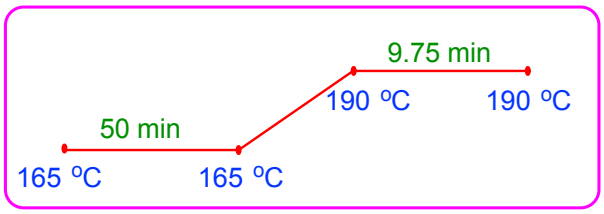

Figure 2.4: Pictorial representation of GC oven program.

GC Oven program: Injector temperature: 250 °C, Injection volume: 5 µL ,Split ratio: 20:1, Detector temperature: 280 °C, Gas flow: He (29 mL/min), H_2 (30 mL/min), air (300 mL/min). Total run time: 61 min

When necessary, the compounds were purified by combiflash chromatography equipped with dual wavelength UV-Vis absorbance detector (Teledyne ISCO®) using ethyl acetate-hexanes as the mobile phase and Redisep cartridge filled with silica (Teledyne ISCO®) as stationary phase. In some cases, compounds were purified by column chromatography on silica gel (Sorbent Technologies®, silica gel standard grade: Porosity 60 Å, Particle size: 230 x 400 mesh, Surface area: 500 – 600 m^2/g, Bulk density: 0.4 g/mL, pH range: 6.5 – 7.5). The Retention Factor (R*f*) values were recorded using a 5-50 % ethyl acetate-hexanes as mobile phase and on Sorbent Technologies® Silica Gel TLC plates (200 mm thickness w/UV254).

2.10.2. General methods employed for photochemical reactions

An RPR-200 photochemical reactor (Southern New England Ultraviolet Company®) equipped with 16 (~300 nm) 14 watts lamps was used for photochemical reactions. To monitor the progress of the reaction, an aliquot (~0.5 mL) of the reaction mixture was taken in a GC vial and was diluted by adding 1 mL of methanol. The samples were analyzed by gas chromatography on a chiral stationary phase to ascertain the enantiomeric excess in the photoproduct. For conversion yield and mass balance studies,

after irradiation for specific time intervals, an appropriate amount of internal standard (triphenylmethane) was added to the reaction mixture. The solvent was evaporated under reduced pressure and was dried under high vacuum. The crude reaction mixture was analyzed by ^{1}H-NMR spectroscopy ($CDCl_3$ as solvent). From the integral value of respective peaks, % conversion and mass balance was calculated using the formula

$$mol_a = mol_i \; X \left(\frac{\text{Integral of analyte}}{\text{Integral of Int. Std}} \right) X \frac{N_a}{N_i} \qquad \textbf{(Equation 2.1)}$$

Where, N_a and N_i are the number of nuclei giving rise to the relevant analyte and internal standard signals respectively. Similarly mol_a and mol_i are the molarity of analyte and the internal standard in deuterated chloroform, respectively. All photoreactions were performed in duplicates.

2.10.3. General methods employed for photophysical studies

Spectrophotometric solvents (Sigma-Aldrich®) were used wherever necessary unless or otherwise mentioned. UV quality fluorimeter cells with range until 190 nm were purchased from Luzchem®. Low temperature luminescence measurements were performed using a quartz tube (3 mm inner diameter) that fit in a liquid N_2 filled quartz Dewar jacket with an optical window. Absorbance measurements were performed on an Agilent Cary 300 UV-Vis spectrometer®. Emission spectra were recorded on a Horiba Scientific Fluorolog 3 spectrometer® (FL3-22) equipped with double-grating monochromators, dual lamp housing containing a 450-watt CW xenon lamp and a UV xenon flash lamp (FL-1040), Fluorohub/MCA/MCS electronics® and R928 PMT detector. Emission and excitation spectra were corrected in all the cases for source intensity (lamp and grating) and emission spectral response (detector and grating) by standard instrument corrections provided in the instrument software.

2.11. General procedure for the synthesis of organocatalyst 147a-147f

2.11.1. Synthetic protocol for catalysts 147a, 147c and 147d

147a,[36] **147c**[37] and **147d**[38] was synthesized according to a procedure reported in the literature. To a solution of the corresponding amine (1.5 mmol) in dry THF (3-5 mL), 3,5-bis(trifluoromethyl)phenyl

isothiocyanate (1.5 mmol) was added at room temperature. The reaction mixture was stirred at 50 °C for 6-48 h. The reaction progress was monitored by TLC. After completion of the reaction, the reaction mixture was concentrated under reduced pressure and the residue was purified by flash chromatography on silica gel to afford the pure product (84 - 97% yield).

2.11.2. Synthetic protocol for catalyst 147b

The compound **147b** was synthesized according to a procedure reported in the literature.[39] To a solution of (*S*)-1,1′′-binaphthyl-2,2′′-diamine (0.72 mmol) in dry dichloromethane (1.5 mL), 3,5-bis(trifluoromethyl)phenyl isothiocyanate (1.5 mmol) was added at room temperature. The reaction mixture was stirred at room temperature for 12 h. After completion of the reaction (monitored by TLC), the resultant mixture was concentrated under reduced pressure and the residue was purified by flash chromatography on silica gel to afford the pure product (82% yield).

2.11.3. Synthetic protocol for catalyst 147e

The compound **147e** was synthesized according to a procedure reported in the literature.[40] To a stirred solution of (*S*)-*tert*-butanesulfinamide (1.0 mmol) in dry THF (10 mL) at -78 °C, butyllithium in hexanes (1.1 mmol) was added slowly to the reaction mixture. The resultant solution was stirred for 15 min. Then 3,5-bis(trifluoromethyl)phenyl isothiocyanate was added and stirred at room temperature for 5 h. The reaction mixture was quenched by addition of water and extracted with CH_2Cl_2. The combined organic layer was dried over *anhyd.* Na_2SO_4, filtered and the solvent was removed under reduced pressure to get the crude product. The crude residue was purified by flash chromatography on silica gel to afford the pure product (67% yield).

2.11.4. Synthetic protocol for catalyst 147f

The compound **147f** was synthesized according to a procedure reported in the literature.[40] To a stirred solution of (*S*)-*tert*-butanesulfinamide (1.0 mmol) in dry THF (10 mL) at -78 °C, butyllithium in hexanes (1.1 mmol) was added slowly to the reaction mixture. The resultant solution was stirred for 15

min. Then 3,5-bis(trifluoromethyl)phenyl isocyanate was added and stirred at room temperature for 5 h. The reaction mixture was quenched by addition of water and extracted with CH_2Cl_2. The combined organic layer was dried over *anhyd.* Na_2SO_4, filtered and the solvent was removed under reduced pressure to get the crude product. The crude residue was purified by flash chromatography on silica gel to afford the pure product (90% yield).

2.12. General irradiation procedure for enantioselective phototransformations and characterization of the photoproducts

2.12.1. Catalyst screening studies

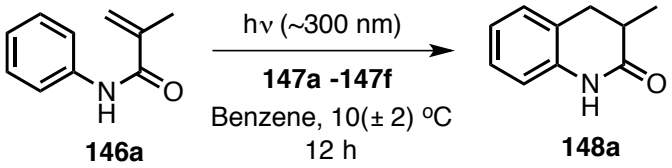

146a **148a**

Scheme 2.11: Irradiation of **146a** with 100 mol% of catalyst **147a**-**147f**.

N-Phenylmethacrylamide **146a** (1mM) and thiourea **147a**–**147f** were dissolved in Benzene in a Pyrex test tube. The reaction mixture was degassed by nitrogen bubbling for 5–10 min. Then the resultant solution was irradiated in Rayonet reactor equipped with ~ 300 nm light bulbs at 10±2 °C for 12 h. The samples were analyzed by gas chromatography on a chiral stationary phase to ascertain the enantiomeric excess in the photoproduct. For conversion yield and mass balance studies, after irradiation, an appropriate amount of internal standard (triphenylmethane) was added to the reaction mixture. The solvent was evaporated under reduced pressure and was dried under high vacuum. The crude reaction mixture was analyzed by ^{1}H-NMR spectroscopy ($CDCl_3$ as solvent). From the integral value of respective peaks, NMR yield was calculated.

2.12.2. Catalyst loading studies

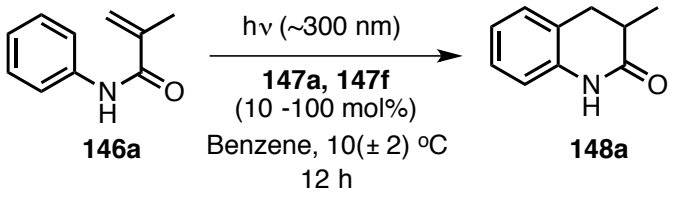

Scheme 2.12: Irradiation of **146a** with 10 - 100 mol% of catalyst **147a**, **147f**.

N-Phenylmethacrylamide **146a** (1mM) and 10-100 mol% of the catalyst **147a** and **147f** were dissolved in benzene in a Pyrex test tube. The reaction mixture was degassed by nitrogen bubbling for 5–10 min. Then the resultant solution was irradiated in Rayonet reactor at 10 °C (± 2 °C) for 12 h. The progress of the reaction was monitored by GC to ascertain the enantiomeric excess in the photoproduct.

2.12.3. Solvent studies

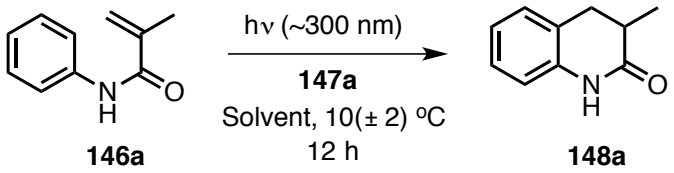

Scheme 2.13: Irradiation of **146a** with 100 mol% of catalyst **147a** in different solvent.

N-Phenylmethacrylamide **146a** (1mM) and 100 mol% of the catalyst **147a** was dissolved in respective solvent in a Pyrex test tube. The reaction mixture was degassed by nitrogen bubbling for 5–10 min. Then the resultant solution was irradiated in Rayonet reactor at 10 °C (± 2 °C) for 12 h. The progress of the reaction was monitored by GC to ascertain the enantiomeric excess in the photoproduct.

Table 2.7: Solvent dependent studies 6π-photocyclization of **146a**.[a]

Solvent	**% Enantioselectivity**[b]	
	Without catalyst **147a**	With catalyst **147a**
Benzene	Racemic	13
Ethanol	Racemic	Racemic
Methyl tetrahydrofuran	Racemic	Racemic

[a] Reactions were carried out at 10±2 °C for 12 h. Values are an average of two trials. [b] From GC analysis using chiral stationary phase (error : ±3 %).

^{1}H-NMR (400 MHz, $CDCl_3$, δ ppm): 1.27-1.28 (d, 3H, J= 2 Hz), 2.62-2.75 (m, 2H), 2.95-3.00 (m, 1H), 6.79-6.81 (m, 1H), 6.94-6.98 (m, 1H), 7.12-1.17 (m, 2H), 8.73 (b, 1H).

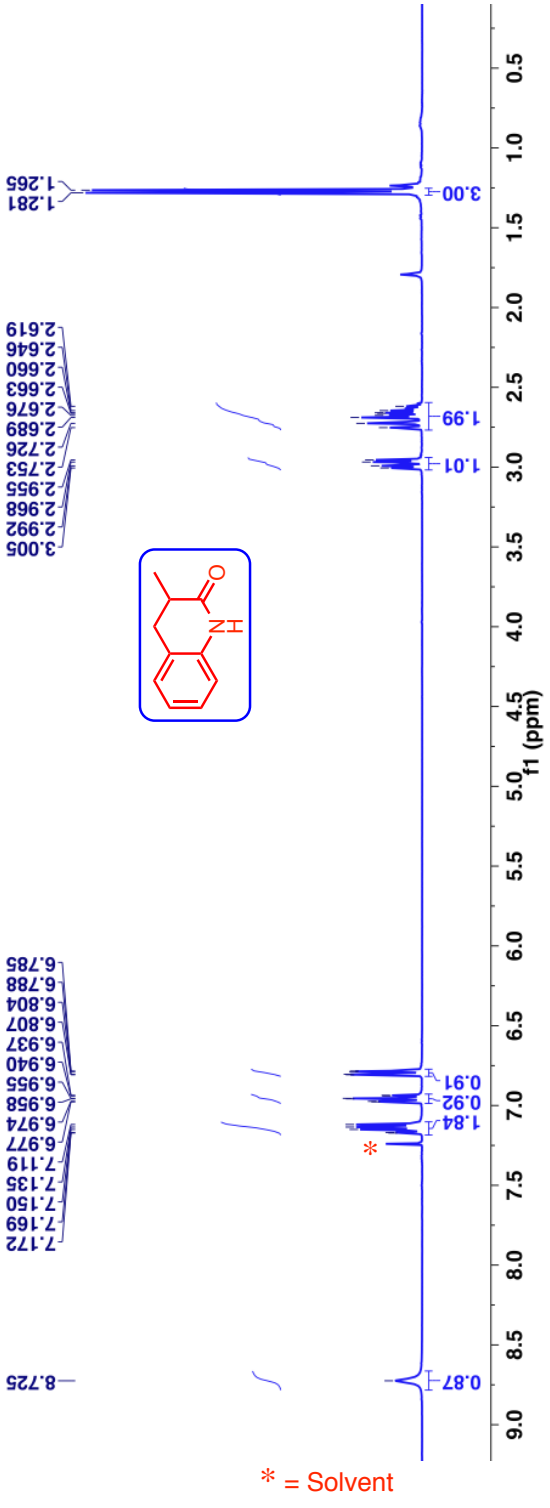

Figure 2.5: ^{1}H-NMR (400 MHz, $CDCl_3$, δ ppm of acrylanilide photoproduct **148a**.

^{13}C-NMR (100 MHz, $CDCl_3$, δ ppm): 15.6, 33.6, 35.2, 115.4, 123.1, 123.7, 127.7, 128.3, 137.4, 174.9.

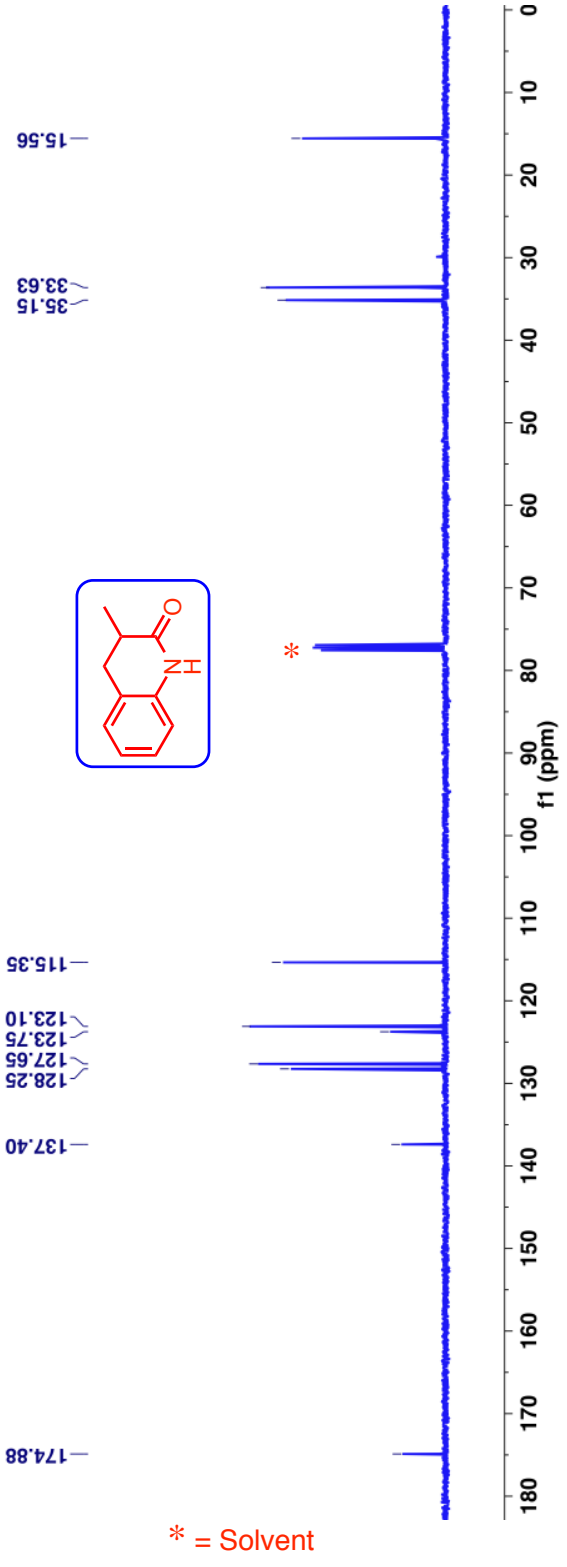

Figure 2.6: ^{13}C-NMR (100 MHz, $CDCl_3$, δ ppm of acrylanilide photoproduct **148a**.

2.13. References

(1) Braslavsky, S. E.: Glossary of Terms Used in Photochemistry, 3rd edition (IUPAC Recommendations 2006). In *Pure Appl. Chem.*, 2007; Vol. 79; pp 293.

(2) Hoffmann, N. Photochemical Reactions as Key Steps in Organic Synthesis. *Chem. Rev.* **2008**, *108*, 1052-1103.

(3) Bach, T.; Hehn, J. P. Photochemical Reactions as Key Steps in Natural Product Synthesis. *Angew. Chem. Int. Ed.* **2011**, *50*, 1000-1045.

(4) Carey, F. A. S., R. J.: *Advanced Organic Chemistry Part A Structure and Mechanisms*; 2nd ed.; Plenum Press, New York N.Y., 1984.

(5) March, J.: *Advanced Organic Chemistry Reactions, Mechanisms and Structure*; 3rd ed.; John Wiley & Sons, New York, 1985.

(6) Hoffmann, R.; Woodward, R. B. Conservation of Orbital Symmetry. *Acc. Chem. Res.* **1968**, *1*, 17-22.

(7) Fukui, K.; Yonezawa, T.; Shingu, H. A Molecular Orbital Theory of Reactivity in Aromatic Hydrocarbons. *J. Chem. Phys.* **1952**, *20*, 722-725.

(8) Woodward, R. B.; Hoffmann, R. Stereochemistry of Electrocyclic Reactions. *J. Am. Chem. Soc.* **1965**, *87*, 395-397.

(9) Woodward, R. B.; Hoffmann, R. The Conservation of Orbital Symmetry. *Angew. Chem. Int. Ed.* **1969**, *8*, 781-853.

(10) Longuet-Higgins, H. C.; Abrahamson, E. W. The Electronic Mechanism of Electrocyclic Reactions. *J. Am. Chem. Soc.* **1965**, *87*, 2045-2046.

(11) Cleveland, P. G. C. O. L. Non-oxidative Photocyclization of Alkyl-substituted Acrylic Acid Anilides to Dihydrocarbostyrils. *Chem. Commun.(Lond.)* **1967**, 1064-1067.

(12) Chapman, O. L.; Adams, W. R. Photochemical Isomerization of α, β-Unsaturated Acids to β-Lactones and α, β-Unsaturated Amides to β-Lactams. *J. Am. Chem. Soc.* **1967**, *89*, 4243-4244.

(13) Chapman, O. L.; Adams, W. R. Photochemical Transformations. XXII. Photoisomerization of Substituted Acrylic Acids and Acrylamides to β-Lactones and β-Lactams. *J. Am. Chem. Soc.* **1968**, *90*, 2333-2342.

(14) Ninomiya, I.; Yamauchi, S.; Kiguchi, T.; Shinohara, A.; Naito, T. Photocyclisation of Enamides. Part V. Photocyclisation of α,β-Unsaturated Anilides. *J. Chem. Soc., Perkin Trans. 1* **1974**, 1747-1751.

(15) Ninomiya, I.; Kiguchi, T.; Yamauchi, S.; Naito, T. Photocyclisation of Enamides. Part IX. Syntheses of Benzonaphthyridines by Photocyclisation of N-Pyridylcyclohex-1-enecarboxamides and Pyridine-(N-cyclohex-1-enyl)carboxamides. *J. Chem. Soc., Perkin Trans. 1* **1976**, 1861-1865.

(16) Tanaka, K.; Toda, F. Solvent-Free Organic Synthesis. *Chem. Rev.* **2000**, *100*, 1025-1074.

(17) Tanaka, K.; Kakinoki, O.; Toda, F. Control of the Stereochemistry in the Photocyclisation of Acrylanilides to 3,4-Dihydroquinolin-2(1H)-ones. Delicate Dependence on the Host Compound. *J. Chem. Soc., Chem. Commun.* **1992**, 1053-1054.

(18) Naito, T. T., Y.; Ninomiya, I. Asymmetric Photocyclization of N-α,β-Unsaturated Acylanilides. *Heterocycles* **1984**, *22*, 237-240.

(19) Bach, T.; Grosch, B.; Strassner, T.; Herdtweck, E. Enantioselective [6π]-Photocyclization Reaction of an Acrylanilide Mediated by a Chiral Host. Interplay between Enantioselective Ring Closure and Enantioselective Protonation. *J. Org. Chem.* **2003**, *68*, 1107-1116.

(20) Ayitou, A. J.-L.; Sivaguru, J. Light-Induced Transfer of Molecular Chirality in Solution: Enantiospecific Photocyclization of Molecularly Chiral Acrylanilides. *J. Am. Chem. Soc.* **2009**, *131*, 5036-5037.

(21) Clay, A.; Kumarasamy, E.; Ayitou, A. J.-L.; Sivaguru, J. Photochemistry of Atropisomers: Non-biaryl Atropisomers for Stereospecific Phototransformations. *Chem. Lett.* **2014**, *43*, 1816-1825.

(22) Ayitou, A. J.-L.; Ugrinov, A.; Sivaguru, J. 6π-Photocyclization of *O*-tert-butylacrylanilides. N-Substitution Dictates the Regiochemistry of Cyclization. *Photochem. Photobiol. Sci.* **2009**, *8*, 751-754.

(23) Ayitou, A. J.-L.; Clay, A.; Kumarasamy, E.; Jockusch, S.; Sivaguru, J. Enantiospecific Photochemical 6π-Ring Closure of α-Substituted Atropisomeric Acrylanilides - Role of Alkali Metal Ions. *Photochem. Photobiol. Sci.* **2014**, *13*, 141-144.

(24) Ayitou, A. J.-L.; Vallavoju, N.; Ugrinov, A.; Sivaguru, J. Enantiospecific 6π-Photocyclization of Atropisomeric α-Substituted Acrylanilides in the Solid-State: Role of Crystalline Confinement on Enantiospecificity. *Photochem. Photobiol. Sci.* **2011**, *10*, 1380-1383.

(25) Whitten, D. G. Photoinduced Electron Transfer Reactions of Metal Complexes in Solution. *Acc. Chem. Res.* **1980**, *13*, 83-90.

(26) Nicewicz, D. A.; MacMillan, D. W. C. Merging Photoredox Catalysis with Organocatalysis: The Direct Asymmetric Alkylation of Aldehydes. *Science* **2008**, *322*, 77-80.

(27) Condie, A. G.; González-Gómez, J. C.; Stephenson, C. R. J. Visible-Light Photoredox Catalysis: Aza-Henry Reactions via C−H Functionalization. *J. Am. Chem. Soc.* **2010**, *132*, 1464-1465.

(28) Hurtley, A. E.; Lu, Z.; Yoon, T. P. [2+2] Cycloaddition of 1,3-Dienes by Visible Light Photocatalysis. *Angew. Chem. Int. Ed.* **2014**, *53*, 8991-8994.

(29) Arceo. E., B. G., Bergonzini. G., Melchiorre. P. Enantioselective Direct α-Alkylation of Cyclic Ketones by Means of Photo-organocatalysis. *Chem. Sci.* **2014**, *5*, 2438-2442.

(30) Hari, D. P.; Schroll, P.; König, B. Metal-Free, Visible-Light-Mediated Direct C–H Arylation of Heteroarenes with Aryl Diazonium Salts. *J. Am. Chem. Soc.* **2012**, *134*, 2958-2961.

(31) Steiner, T. The Hydrogen Bond in the Solid State. *Angew. Chem. Int. Ed.* **2002**, *41*, 48-76.

(32) Jeffrey, G. A.: *An Introduction to Hydrogen Bonding*; Oxford University Press, Oxford, 1997.

(33) Organocatalysis. http://www.organic-chemistry.org/topics/organocatalysis.shtm. (accessed December 16, 2015).

(34) Vallavoju, N.; Selvakumar, S.; Jockusch, S.; Sibi, M. P.; Sivaguru, J. Enantioselective Organo-Photocatalysis Mediated by Atropisomeric Thiourea Derivatives. *Angew. Chem. Int. Ed.* **2014**, *53*, 5604-5608.

(35) Vallavoju, N.; Selvakumar, S.; Jockusch, S.; Prabhakaran, M. T.; Sibi, M. P.; Sivaguru, J. Evaluating Thiourea Architecture for Intramolecular [2+2]□Photocycloaddition of 4-Alkenylcoumarins. *Adv. Synth. Catal.* **2014**, *356*, 2763-2768.

(36) Mori, K. Y., T.; Maddaluno, J.; Nakano,K.; Ichikawa, Y.; Kotsuki, H. Organocatalytic Asymmetric Hetero-Diels-Alder Reaction of Oxindoles under High Pressure. *Synlett* **2011**, *14*, 2080-2084.

(37) Bian, G.; Fan, H.; Yang, S.; Yue, H.; Huang, H.; Zong, H.; Song, L. A Chiral Bisthiourea as a Chiral Solvating Agent for Carboxylic Acids in the Presence of DMAP. *J. Org. Chem.* **2013**, *78*, 9137-9142.

(38) Sohtome, Y.; Tanatani, A.; Hashimoto, Y.; Nagasawa, K. Development of Bis-thiourea-Type Organocatalyst for Asymmetric Baylis–Hillman Reaction. *Tetrahedron Lett.* **2004**, *45*, 5589-5592.

(39) Fleming, E. M.; McCabe, T.; Connon, S. J. Novel axially chiral bis-arylthiourea-based organocatalysts for asymmetric Friedel–Crafts type reactions. *Tetrahedron Lett.* **2006**, *47*, 7037-7042.

(40) Robak, M. T.; Trincado, M.; Ellman, J. A. Enantioselective Aza-Henry Reaction with an N-Sulfinyl Urea Organocatalyst. *J. Am. Chem. Soc.* **2007**, *129*, 15110-15111.

CHAPTER 3. ATROPSELECTIVE PHOTOCYCLOADDITION OF AXIALLY CHIRAL CHROMOPHORES*

3.1. Introduction

Light induced transformations holds a unique place in the field of asymmetric organic synthesis and are often employed to access structurally complex and chirally enriched molecule in fewer steps.[1-3] Thus, photochemical reactions often serve as a complementary strategy to thermal reactions in obtaining structurally complex building blocks. Though phototransformations are elegant, they are inherently fast processes, which poses a challenge to control the excited state reactivity often resulting in poor selectivity. As a solution to this challenge, many research groups have performed reactions in confined media, employed supramolecular templates, carried out reactions in the solid-state, which has led to an improvement in controlling selectivity in the photoproduct(s).[4-8] In spite of this improvement, achieving stereoselectivity in photoreactions in solution remains a longstanding challenge. As a possible solution to this bottleneck, Sivaguru and coworkers introduced a concept of "axial to point chiral transfer" that employed atropisomeric chromophores to perform various asymmetric photoreactions with good control over stereochemistry. In this vein, we have successfully demonstrated 6π-photocyclization,[9-11] 4π-photocyclization,[12,13] [2+2]-photocycloaddition[14] and Norrish-Yang reactions.[15,16]

---

*The material in Sections 3.2-3.6 of this chapter was co-authored by Ramya Raghunathan (RR), Elango Kumarasamy (EK), Akila Iyer (AI), Dr. Angel Ugrinov (AU) and Dr. J. Sivaguru (JS). RR, EK, AI in consultation with JS synthesized all the compounds and carried out all the experiments. AU recorded XRD data and solved the structures reported in this chapter. SJ performed photophysical studies detailed in this chapter. EK, RR, AI and JS came up with the mechanistic rationale and the conclusion described in this chapter.

The material in Sections 3.7-3.14 of this chapter was co-authored by Ramya Raghunathan (RR), Elango Kumarasamy (EK), Dr. Steffen Jockusch (SJ), Dr. Angel Ugrinov (AU) and Dr. J. Sivaguru (JS). RR and EK in consultation with JS synthesized all the compounds and carried out all the experiments. A part of the results based on the atropisomeric maleimide system that is not reported in this thesis is a part of EK's thesis. AU recorded XRD data and solved the structures reported in this chapter. SJ performed photophysical studies detailed in this chapter. RR, EK, SJ and JS came up with the mechanistic rationale and the conclusion described in this chapter.

The material in Sections 3.15-3.22 of this chapter was co-authored by Ramya Raghunathan (RR), Elango Kumarasamy (EK), Dr. Angel Ugrinov (AU), Dr. Steffen Jockusch and Dr. J. Sivaguru (JS). RR and EK in consultation with JS synthesized all the compounds and carried out all the experiments. AU recorded XRD data and solved the structures reported in this chapter. RR, EK, SJ and JS came up with the mechanistic rationale and the conclusion described in this chapter.

To further broaden the scope of this methodology we have carried out investigations on Paternò-Büchi reactions of atropisomeric oxoamides, and photocycloaddition ([2+2]-[5+2]) of maleimides.

3.2. Paternò-Büchi reaction of atropisomeric oxoamides

The [2+2] photocycloaddition reaction between excited state of a carbonyl group and an alkene generating an oxetane ring is called as Paternò-Büchi reaction. Oxetanes are constituents of many biologically active natural products like taxol, merrilactone A, oxetin etc.,[17] Emajuele Paternò was the first to observe this reaction in 1909 while performing a photochemical reaction between benzophenone **149** and amylene **150**, which resulted in [2+2] photoadduct **151** (Scheme 3.1).[18] It was not until 1954, when George Hermann Büchi reported the exact identification of the photoproduct as an oxetane. Since then, there are many reports in the field of synthetic chemistry that utilizes Paternò-Büchi reaction.[19]

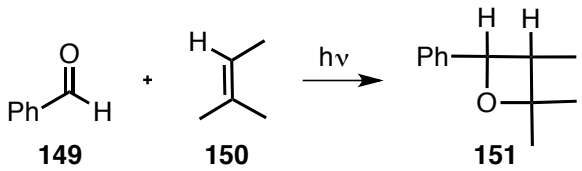

Scheme 3.1: An example of a Paternò-Büchi reaction.

The mechanism of these cycloaddition reactions depends on the interactions of the orbitals (n or π^*) of the two components that initiate the process and also the electronics and the sterics of alkene (electron rich or electron poor). However the most simplified mechanism describes that the carbonyl group serves as a light absorbing chromophore resulting in an excited state carbonyl **152** that can be singlet or a triplet. The excited carbonyl then reacts with the alkene **153** counterpart to form the oxetane photoproduct **154** via a 1,4 biradical formation (singlet or triplet; Scheme 3.2). The 1,4 biradical intermediate formed during the reaction has been characterized spectroscopically. The diradical intermediate has been trapped by biradical quenchers. Though in few instances, it has been shown that the exciplex formation precede the formation of biradical intermediates, and their role in the regio-stereoselectivity is not well understood or explored.[20,21] Also, for the reaction between electron rich alkenes and electron-poor carbonyl compounds, electron transfer mechanism is a potential alternative

pathway. The regio- and stereo-chemistry of the addition is dictated by the stereoelectronic of the excited state and the reactivity of carbonyl compound.

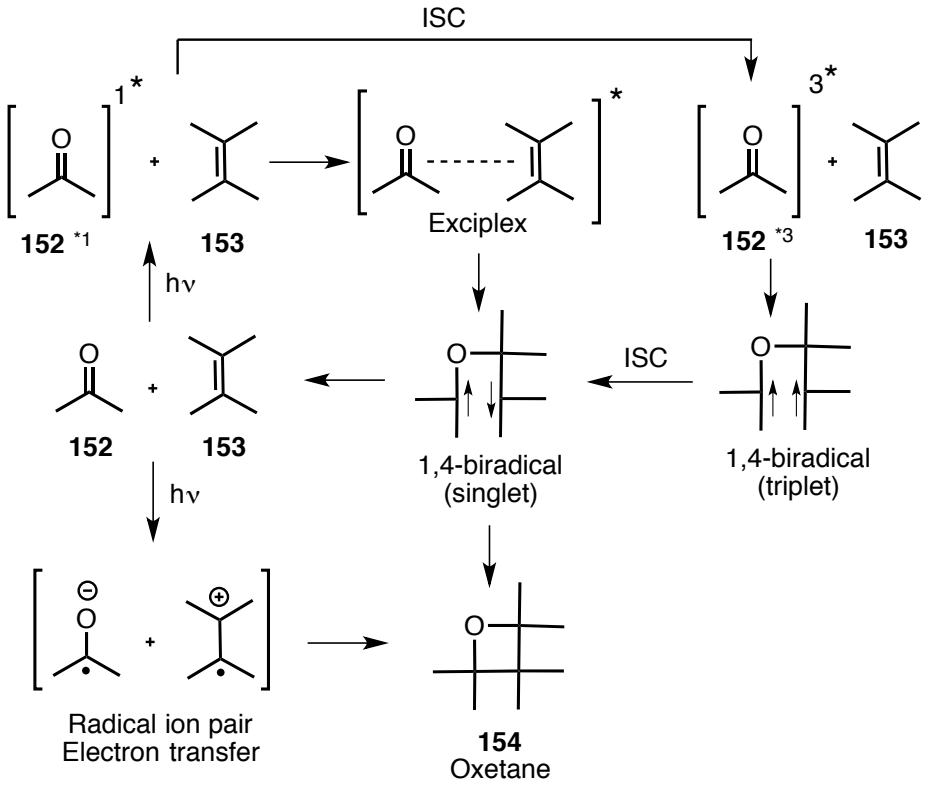

Scheme 3.2: General mechanism of Paternò-Büchi reactions.

The Paternò-Büchi reactions can be widely performed with different type of alkenes and carbonyl derivatives. However, its application in synthesis is limited because of its regioselectivity. Many research groups have probed control of the regioselectivity in these reactions. From these investigations, it can be concluded that the regioselectivity can be controlled by the substituents on the alkene and the type of the carbonyl that participates in the reaction. The photocycloaddition of benzophenone **155** and isobutene **156** gave two regioisomers **157** and **158** in 90:10 ratio (Scheme 3.3).[22,23] Similarly the cycloaddition of β-unsubstituted enol ether to benzophenone gave the cycloadducts in a 3:1 ratio.[24]

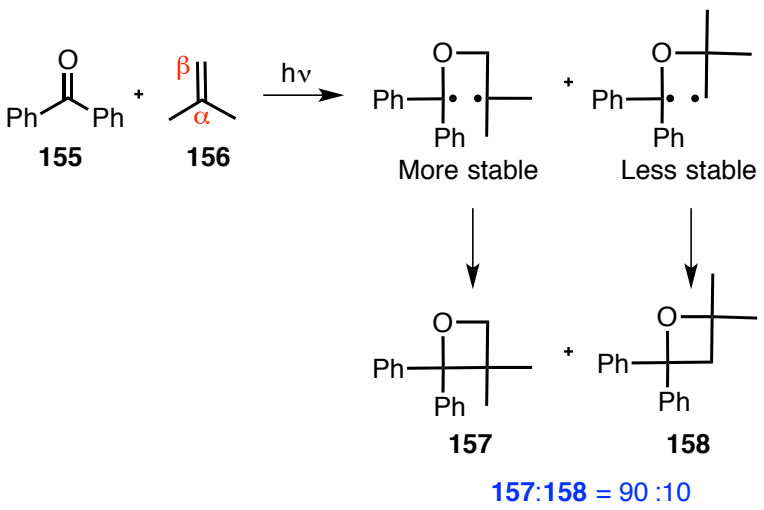

Scheme 3.3: Regioselectivity in Paternò-Büchi reactions.

Diastereoselectivity in Paternò-Büchi reactions can be either a simple/non-induced diastereoselectivity where the stereogenic center will be generated in the photoproduct without any stereogenic element existing in the starting materials or induced diastereoselectivity, where a stereogenic center will be generated from substrates that already have at least one stereogenic center. Griesbeck and coworkers have extensively studied on the non-induced diastereoselectivity employing dihydrofuran and furan with prochiral carbonyl derivatives.[25] They examined [2+2]-photocycloaddition of 2,3 dihyrdofuran **160** with different aliphatic and aromatic aldehydes **159** which resulted in high diastereoselectivity up to 91:9 for pivaldehyde (aliphatic aldehyde) and 98:2 for mesitaldehyde, 2,4-di-*tert*-butyl-6-methylbenzaldehyde (aromatic aldehyde) (Scheme 3.4). The formation of *endo* product is attributed to the spin-orbit coupling geometries of triplet 1,4 biradical. This model[26] was also able to explain the Paternò-Büchi reactions of enamine photocycloaddition described by Bach and coworkers.[27,28]

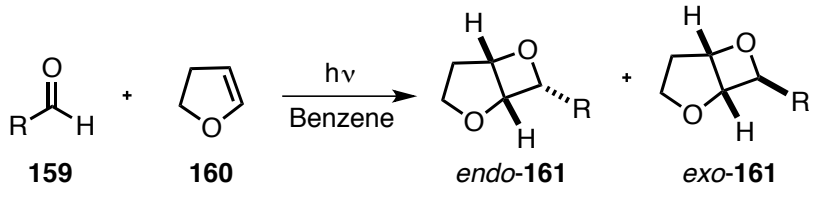

Aliphatic aldehyde		Aromatic aldehyde	
R =	*dr* = *endo*:*exo*	R =	*dr* = *endo*:*exo*
Me	45:55	Ph	88:12
Et	58:42	*o*-Tol	92:8
i-Bu	67:33	Mes.	>98:2
t-Bu	91:9	2,4-di-*t*-Bu-6-Me-Ph	>98:2

Scheme 3.4: Non-induced diastereoselectivity in Paternò-Büchi reactions.

The first example of induced diastereoselectivity in Paternò-Büchi reaction was reported by Gotthardt and Lenz in 1979 by using a chiral carbonyl compound.[29] They used enantiomerically pure (-)-menthyl ester of phenylglyoxalic acid **162** with tetramethylethylene **153**, which resulted in oxetane photoproducts **163** and **164** with a diastereomeric excess of 32% (Scheme 3.5).

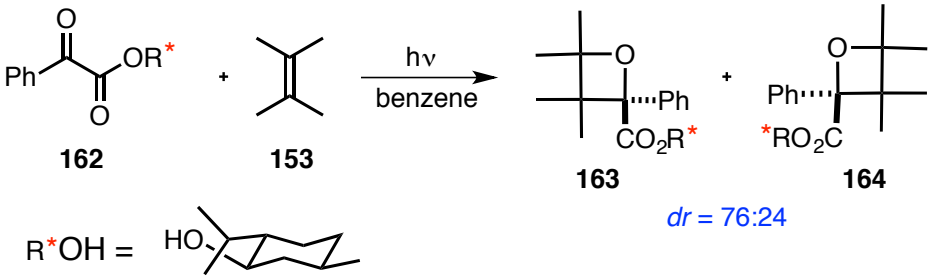

Scheme 3.5: Photocycloaddition of chiral phenylglyoxylates **162** with tetramethylethylene **153**.

In 1991 Scharf and coworkers reported a highly diastereoselective Paternò-Büchi reaction involving chiral phenyl glyoxylates.[30,31] Although the sterogenic center in the phenyl glyoxylates are localized in the alcohol part of the α-keto ester, which is distant from the reactive triplet excited carbonyl group, they were able to achieve exceedingly high diastereoselectivity. For example, the photocycloaddition of 1,3-dioxole **165** and with phenyl glyoxalic acid ester **162** gave the cycloadducts with high diastereoselectivity (Scheme 3.5).

While research on induced diastereoselectivity from chiral carbonyl unit was studied by different groups, Bach and coworkers investigated an alternative strategy that involved the use of chiral alkene

units to obtain selectivity in the Paternò-Büchi reactions (Scheme 3.6).[32-34] They investigated the photocycloaddition of chiral silylenolethers **167** with benzaldehyde **149**. The substituent R at the γ-position of silylenolethers was varied to understand and evaluate the influence of steric and the electronic effects on the selectivity.

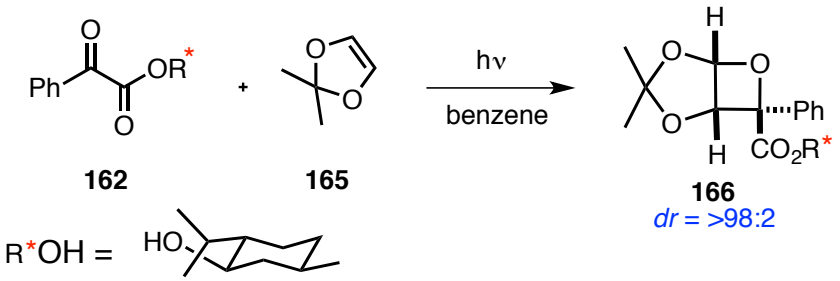

162 **165** **166**

dr = >98:2

Scheme 3.6: Photocycloaddition of chiral phenylglyoxylates **162** with 1,3 dioxole **165**.

Diastereoselectivity in the oxetane was increased as the bulkiness of the R substituent increased. For. e.g. when R was ethyl, the *dr* was 61:39; however when R was *t*-Bu the *dr* increased to 95:5 (Scheme 3.7). This facial diastereoselectivity was explained based on the 1,3 allylic strain model.[35]

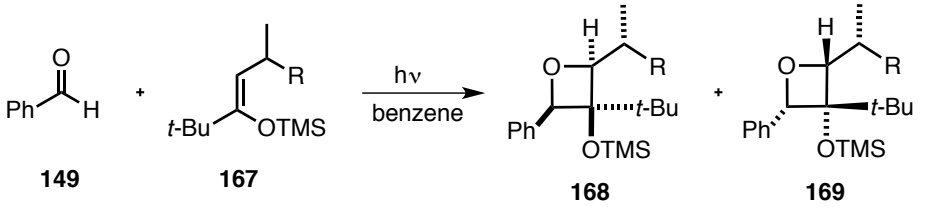

149 **167** **168** **169**

R =	*dr* (**168**:**169**)
Et	61 : 39
i-Pr	70 : 30
Ph	71 : 29
t-Bu	95 : 5

Scheme 3.7: Photocycloaddition of benzaldehyde **149** with silylenol ether **167**.

Sakamoto and coworkers have extensively worked on stereoselective and enantioselective intramolecular Paternò-Büchi reactions involving N-(α,β-unsaturated carbonyl)benzoylformamides **170** both in solid-state and in solution.[36,37] They carried out detailed experimental investigations on various structural parameters and described the importance of structural features that is necessary to access chirally enriched oxetane product. Irradiation of N-(α,β-unsaturated carbonyl)benzoylformamides **170** resulted in cross [2+2] intramolecular cycloaddition between the carbonyl and the alkenyl double bonds. Systematic studies on the efficiency of the reactions were performed by varying the substituents on **170** One key factor that determined the reactivity of **170** towards Paternò-Büchi reactions is the conformational distribution of imides. The imides can exist in 4 different conformers namely *E*,*E* or s-*trans*, s-*trans*, E,Z or s-*trans*, s-*cis*, *Z*,*E* or s-*cis*, s-*trans* and *Z*,*Z* or s-*cis*, s-*cis* as shown in the Figure 3.1.

Cyclic imides that are in *E*,*E* or s-*trans*, s-*trans* conformations have the reacting species (carbonyl and alkene group) (Scheme 3.8) are in close proximity that results in the oxetane product. However for **170** in other conformations, the reacting species are not suitably oriented to undergo Paternò-Büchi reaction to yield oxetane photoproduct.

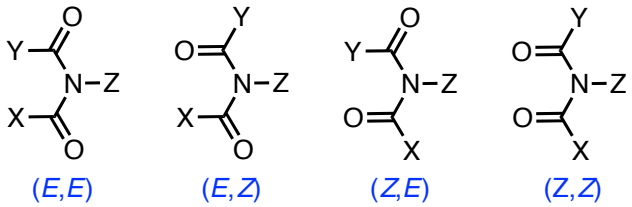

Figure 3.1: Conformers of N-(α,β-unsaturated carbonyl)benzoylformamides.

When the reactions was performed in solution, the interconversion of conformers to *E*,*E* or s-*trans*, s-*trans* takes place rapidly resulting in facile formation of oxetane photoproduct. Whereas in solid-state such conformational interconversion not feasible as it will involve series of changes in the molecular orientation. Also, apart from interconversion, two other parameters that determine the photocycloaddition in the solid-state are the distance and the dihedral angle between the carbonyl and the alkenyl groups. Based on their experiments, the *E*,*E* or s-*trans*, s-*trans* gave good yield and up to 99% ee. Though few substrates crystallized in *E*,*Z* or s-*trans*, s-*cis* conformer which only resulted in 50 % yield with *ee* value of 88% (resulted attributed to the distance and dihedral angle).

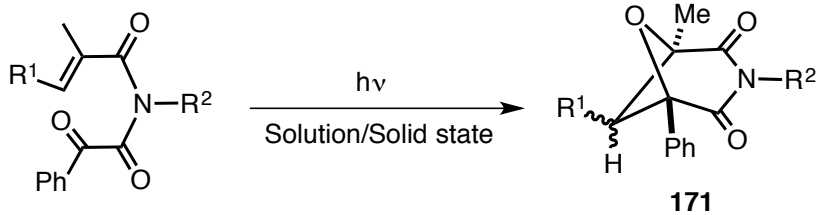

170 **171**
syn and *anti*-2

Scheme 3.8: Phototransformations of N-(α,β-unsaturated carbonyl)benzoylformamides **170**.

Based on the literature precedence and the importance of oxetane moiety in the many biologically active natural products, atropisomeric oxoamides were designed to evaluate intramolecular atropselective Paternò-Büchi phototransformations in solution and in the solid state. The newly synthesized atropisomeric oxoamides and their intermediates listed in the following Chart 3.1

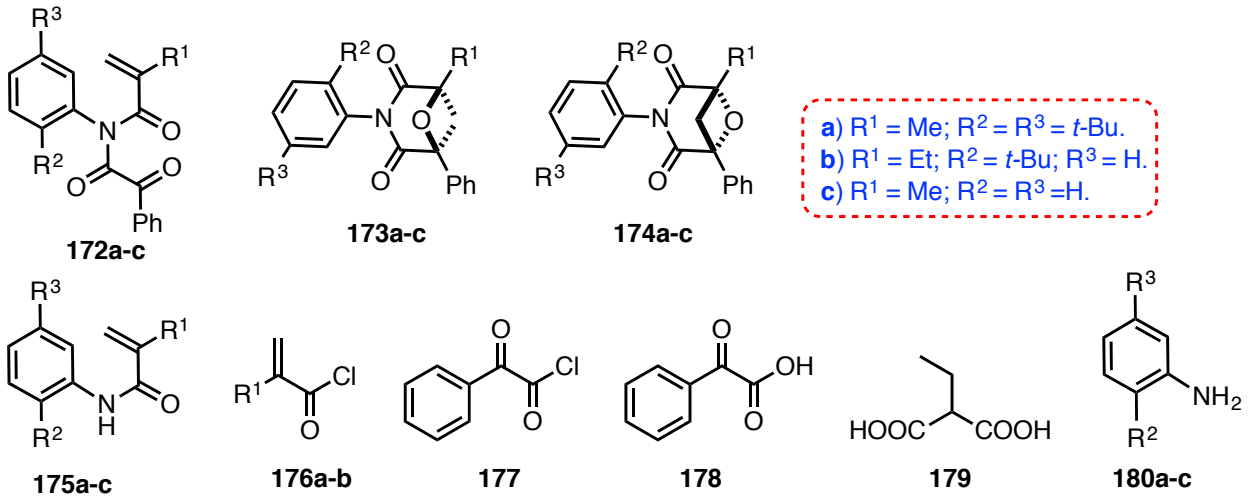

Chart 3.1: Structures of atropisomeric oxoamides, their photoproducts and the precursors for the synthesis.

The newly synthesized atropisomeric oxoamides **172** were characterized by NMR spectroscopy, mass spectrometry and single crystal XRD analysis. HPLC analysis showed *P* and *M* isomers were originated due to the restricted bond rotation around N-C(aryl) axis. *P* and *M* isomers were separated using HPLC on a chiral stationary phase. The optical purity of the isomers was confirmed by optical rotation and by analysis on a chiral stationary phase.

3.3. Racemization barrier in atropisomeric oxoamides

One of the important features of an atropisomeric compound is its ability to racemize at higher temperatures. Such racemization will erode the absolute configuration of the isomer leading to poor selectivity in the atropselective transformations. Therefore it becomes important to ascertain the barrier for N-C(aryl) rotation. Due to slow racemization of these compounds at room temperature, we carried out racemization kinetics on optically pure atropisomeric oxoamides **172a** and **172b** at 50 °C in polar acetonitrile (MeCN) and non-polar benzene solvents.

The decrease in the enantiomeric excess (*ee*) over time was monitored using HPLC on a chiral stationary phase. The first order kinetic plot of ln (% *ee*) vs. time gave the rate constant of racemization (k_{rac}). The activation energy barrier, half-life and rate of racemization were calculated from the following equation.[38]

$$k_{rac} = k\left(\frac{k_B T}{h}\right) e^{-\Delta G^{\ddagger}_{rac}/RT} \qquad \textbf{(Equation 3.1)}$$

$$\Delta G^{\ddagger}_{rac} = -RT \ln\left(\frac{h k_{rac}}{k T k_B}\right) \qquad \textbf{(Equation 3.2)}$$

The half-life of racemization ($\tau_{1/2rac}$), was calculated using the rate constant of racemization k_{rac} (assuming $1\text{-}P_0 = 0$ at $t = 0$)

$$\ln\left(\frac{\chi_{eq}}{\chi_{eq} - \chi}\right) = \ln\left(\frac{R_0}{2R - R_0}\right) = \ln\left(\frac{R + S}{R - S}\right) = 2k_{enant}\, t \qquad \textbf{(Equation 3.3)}$$

$$\ln\left(\frac{R_0}{R_0 - \chi}\right) = k_{rac}\, t \qquad \textbf{(Equation 3.4)}$$

Where,

$k_{rac} = 2k_{enant}$; R_0 is the initial concentration of the (*R*)-enantiomer;

$\chi = R_0 - R$, S (concentration of the racemate at time *t)*; and

k_{rac} is the rate constant for racemization

Note: $R_0 = R + S$

At 50% *ee,* the equation becomes:

$$\tau_{1/2rac} = \frac{\ln 2}{2k_{enant}} \quad or \quad \frac{\ln 2}{k_{rac}} \qquad \textbf{(Equation 3.5)}$$

The course of racemization (% *ee*) was monitored by HPLC analysis on a chiral stationary phase at various time intervals. The activation energy barrier is provided in Table 3.1.

Analysis of the kinetic parameters of atropisomeric oxoamides **172** provided insights into the energy barrier to rotation around the N-C(aryl) chiral axis (Table 3.1). For example, in the case of **172a** in MeCN at 50 °C, the half-life for racemization ($\tau_{1/2}$) was 6.4 days, corresponding to a racemization rate constant (k_{rac}) of 1.26×10^{-6} s^{-1} and an activation energy barrier ($\Delta G^{\ddagger}_{rac}$) of 27.7 kcal·mol^{-1}. Upon changing to a non-polar benzene solvent, the half-life for racemization ($\tau_{1/2}$) was reduced to 3.8 days at 50 °C,

corresponding to a racemization rate constant (k_{rac}) of 2.11 × 10^{-6} s^{-1} and an activation energy barrier ($\Delta G^{\ddagger}_{rac}$) of 27.4 kcal·$mol^{-1}$. The racemization kinetic studies shows that non-bonding interactions and the solvent polarity played a critical role in the rates and the half-life of racemization. These studies also suggested that the newly synthesized atropisomeric oxoamides can resist racemization at ambient temperature (due to high-energy barrier for racemization at 50 °C) and can be employed for atropselective photoreactions without any racemization.

Table 3.1: Rate constant, half-life and energy barrier for racemization on atropisomeric oxoamides **172a-b**.

Entry	Compound	Solvent	Parameters		
			$\tau_{1/2}$ (days)	k_{rac} (s^{-1})	$\Delta G^{\ddagger}_{rac}$ (kcal·mol^{-1})
1	**172a**	MeCN	6.4	1.26 × 10^{-6}	27.7
2	**172a**	Benzene	3.8	2.11 × 10^{-6}	27.4
3	**172b**	MeCN	3.5	2.27 × 10^{-6}	27.3
4	**172b**	Benzene	2.1	3.81 × 10^{-6}	27.0

The racemization kinetics was followed by HPLC analysis on a chiral stationary phase. Values carry an error of ±5%.

3.4. Intramolecular Paternò-Büchi reaction of atropisomeric α-oxoamides 172

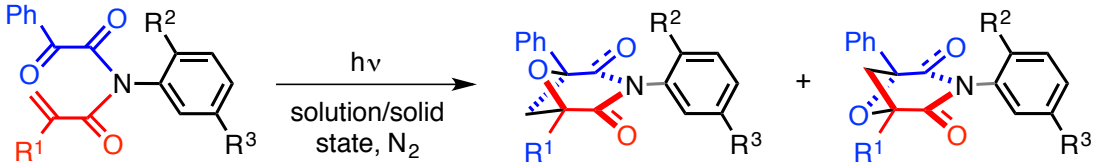

172 **173** **174**

a) R^1=Me; R^2=R^3=*t*-Bu; **b**) R^1=Et; R^2=*t*-Bu; R^3=H
c) R^1=Me; R^2=R^3=H

Scheme 3.9: Intramolecular Paternò-Büchi reaction of atropisomeric α-oxoamides **172**.

The newly synthesized, optically pure atropisomeric oxoamides were irradiated at room temperature in benzene and acetonitrile solvent using either 450 W medium pressure Hg lamp placed inside a water-cooled jacket with a Pyrex cut off filter or a Rayonet reactor equipped with ~ 350 nm bulbs (14 Watts x 16 bulbs) under constant flow of nitrogen. After the photoreaction, the solvent was evaporated and the crude photoproduct(s) were purified by either preparative TLC or column chromatography. Solid-state photoreactions were carried out on chiral crystals obtained from preparative

HPLC separations of atropisomeric oxoamides followed by crystallization. The crystals were sandwiched between a glass substrate that was irradiated for a given time interval. After the reaction, the resulting product was analyzed by several analytical tools to estimate the stereoselectivity.

Analysis using NMR spectroscopy, HPLC and X-ray diffraction revealed that the presence of two diastereomeric photoproducts *viz*., photoproduct **173** where the relative orientation of the oxygen atom in the oxetane ring was *syn* to the N-aryl *ortho-tert*-butyl substituent while in photoproduct **174**, the relative orientation was *anti*. The NMR spectroscopic and the HPLC analysis of the crude reaction mixture revealed the *dr* values and the enantiomeric excess in the resulting photoproducts respectively.

Analysis of Table 3.2 reveals that the Paternò-Büchi reaction of atropisomeric α-oxoamides proceeded smoothly to furnish oxetane photoproducts **173** and **174** in excellent yields (78-91%) and mass balance (>90%). The enantiomeric excess of the photoproduct of all the oxoamides were analyzed and found to be >97 %. This was a clear indication of the influence of stable chiral axis that facilitated efficient “Axial to Point Chiral Transfer” during Paternò-Büchi reaction resulting in enantioenriched photoproducts. Apart from providing sufficient sterics that resulted in higher energy barrier, the presence of bulky *ortho-tert*-butyl substituent on the N-phenyl ring influences the formation of *s-trans*, *s-trans* conformer in the solution leading to enhanced reactivity. As a control study, **172c** was synthesized that lacked the bulky *ortho-tert*-butyl and it showed diminished reactivity (30% yield). The slow reactivity reflected conformational distribution where the *s-trans*, *s-trans* was not present as a major conformer in the solution.

Table 3.2: Intramolecular Paternò-Büchi of atropisomeric α-oxoamides **172a-c**[a]

Entry	Compound[b]	Solvent	*dr* (**173:174**)[c]	*% ee*[d,e]	Yield[f]
1	(-)-**172a**	MeCN	71:29	98 (*R,R,M*)-**173a**	78
2	(+)-**172a**	MeCN		98 (*S,S,P*)-**173a**	
3	(-)-**172a**	Benzene	55:45	97 (*R,R,M*)-**173a**	90
4	(+)-**172a**	Benzene		97 (*S,S,P*)-**173a**	
5	(*M*)-**172b**	MeCN	82:18	99 (*R,R,M*)-**173b**	81
6	(*P*)-**172b**	MeCN		98 (*S,S,P*)-**173b**	
7	(*M*)-**172b**	Benzene	78:22	99 (*R,R,M*)-**173b**	78
8	(*P*)-**172b**	Benzene		98 (*S,S,P*)-**173b**	
9	(*M*)-**172b**	Crystal	15:85	98 (A)-**174b**	-
10	(*P*)-**172b**	Crystal		98 (B)-**174b**	-
11	**172c**	MeCN	-	-	30

[a]Reported values are an average of 3 runs with ±3% error. 2.5 h irradiation for **172a–c**, 12 h irradiation for **172c**. [b](+) and (-) represent the sign of optical rotation, refer to experimental section. [c]The diastereomeric ratio (dr) was determined using ^{1}H-NMR spectroscopy. [d]From HPLC analysis. A and B refer to the elution order for a given pair of enantiomers. Absolute configuration from single crystal XRD using Flack parameter. [e]Identical ee values for both **172** and **173**. [f]Isolated yield.

The diastereomeric ratio (*dr*) in the photoproducts was influenced by polarity of the solvent. For example, *dr* value **173:174** from the reaction of **172a** in polar MeCN was 71:29 and in non-polar benzene, the *dr* value was 55:45. The dr values for substrate **172b** showed a modest increase in both MeCN and benzene. To enhance the diastereoselectivity in the photoproducts, we carried out photoreaction in the solid state, as we were successful in crystallizing the optically pure isomer of **172b**. Irradiation of optically pure crystal of **172b** gave dr values of 15:85. Though the dr values in solution as well as in the solid state were comparable, we observed reversal of diastereomers i.e., in solid-state reaction photoproduct **174b** was formed as the major product. A closer look at the crystal structure of **172b** showed that the distance between the keto carbonyl functionality and the alkene double bond is at an optimal distance viz., OC····CH_2=C is ~3.083 Å and CO····C=CH_2 is 2.986 Å (Figure 3.2) for undergoing photochemical transformation resulting in photoproduct **174b** as the major product.

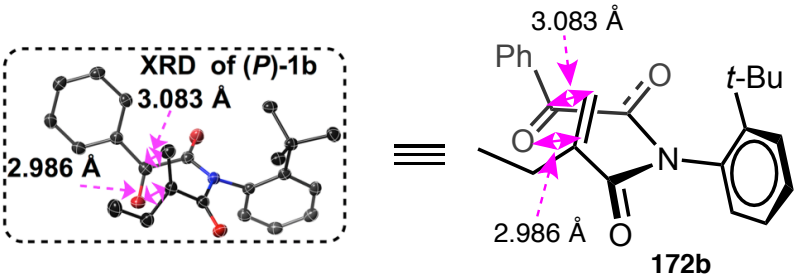

Figure 3.2: Crystal structure of optically pure oxoamide **172b**.

3.5. Mechanistic rationale for Paternò-Büchi reaction of atropisomeric α-oxoamides

On the basis of photochemical investigations, it is evident that apart from the structural features of the oxoamides, other characteristics such as conformers arising from atropisomerism, excited state reactivity of ketones with electron deficient alkenes plays a vital role in the observed reactivity and selectivity in Paternò-Büchi reaction of atropisomeric α-oxoamides. We believe that the half-filled π* orbital of the carbonyl group initiated the photoreaction by charge transfer to the LUMO of π* orbital of the electron deficient alkene resulting in the formation of oxetane photoproducts.

Based on the stereochemistry of the photoproducts, in addition to the *s-trans*,*s-trans* geometry at CO-N bond, the conformation of CO-CC bond plays a vital role. Four conformers viz., *conf*-**A**, *conf*-**B**, *conf*-**C**, *conf*-**D** arising from *s-trans*,*s-trans* geometry of **172** dictates the product ratio and the selectivity. As observed in the case of oxetane **173** and **174**, it is likely that *conf*-**D** and *conf*-**A** gives rise to the oxetane photoproducts. Photo excitation of *conf*-**D** and *conf*-**A** leads to a 1,4 diradical. Based on the overlap of $\pi^*_{C=O}$ and $\pi^*_{C=C}$, it is likely that diradical DR1 (DR1-(D) and DR1-(A)) is formed that cyclize to form products **173** and **174** respectively. The other diradicals (DR2, DR3, DR4) are also feasible depending upon the orbital coefficient, steric, electronic feature present in the system as well as the substitution on the alkene bond. In solution state, since **173** was formed as the major isomer, it is believed that *conf*-**D** is preferred compared to *conf*-**A**. In solid state, it is ascertained from the crystal structure that *conf*-**A** was predominant resulting in oxetane **174** as the major product (Scheme 3.10).

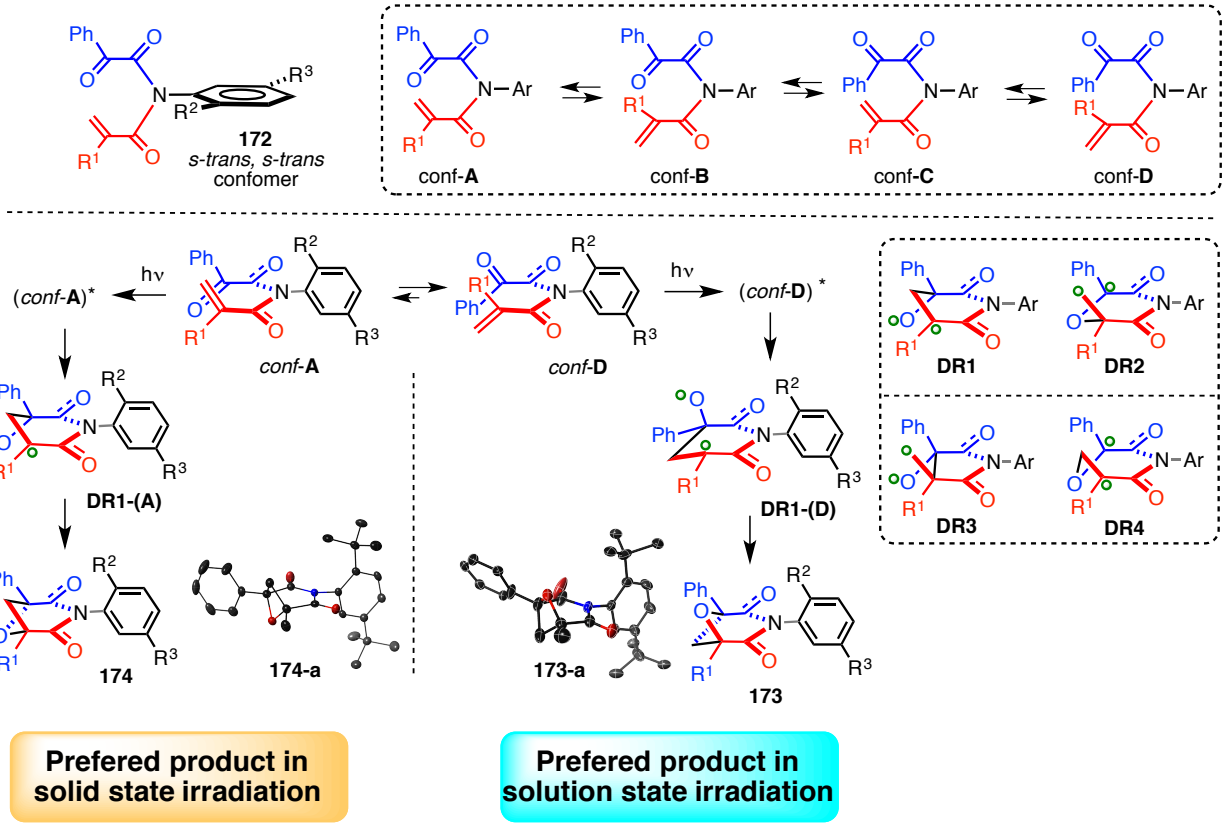

Scheme 3.10: Mechanistic rationale for Intramolecular Paternò-Büchi reaction of atropisomeric α-oxoamides **172**.

3.6. X-Ray crystal structure data for atropisomeric α-oxoamides and its photoproducts

Structure determination: Single crystal X-ray diffraction data of the compounds **172, 173 and 174** were collected on a Bruker Apex Duo diffractometer with a Apex 2 CCD area detector at T = 100K. Cu radiation was used. All structures were process with Apex 2 v2010.9-1 software package (SAINT v. 7.68A, XSHELL v. 6.3.1). Direct method was used to solve the structures after multi-scan absorption corrections.

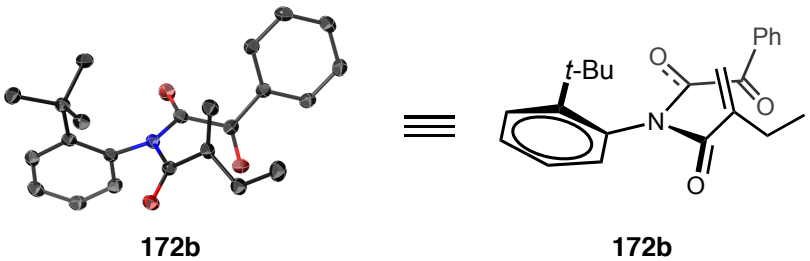

Figure 3.3: Crystal structure of (-)-(*M*)-**172b** (Crystallized from: hexanes/2-propanol).

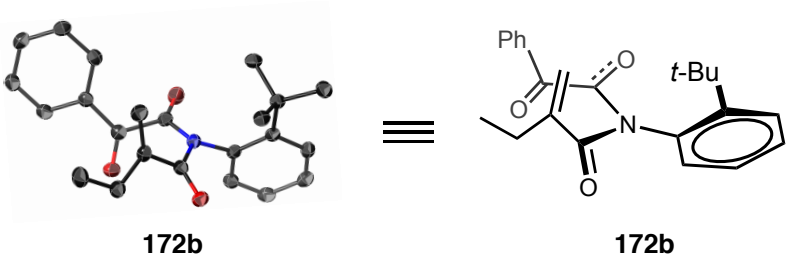

172b **172b**

Figure 3.4: Crystal structure of (-)-(*P*)-**172b** (Crystallized from: hexanes/2-propanol).

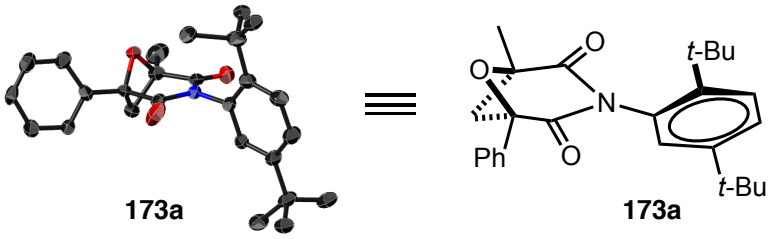

173a **173a**

Figure 3.5: Crystal structure of (-)-(*R,R,M*)-**173a** (crystallized from: hexanes/chloroform).

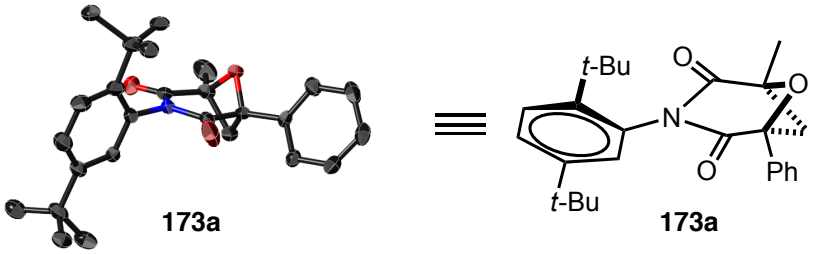

173a **173a**

Figure 3.6: Crystal structure of (+)-(*S,S,P*)-**173a** (crystallized from: hexanes/2-propanol).

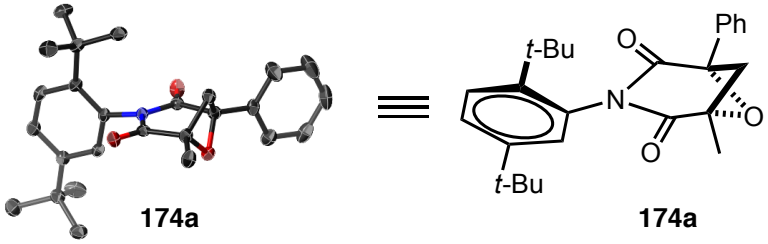

174a **174a**

Figure 3.7: Crystal structure of **174a** (crystallized from: hexanes/chloroform).

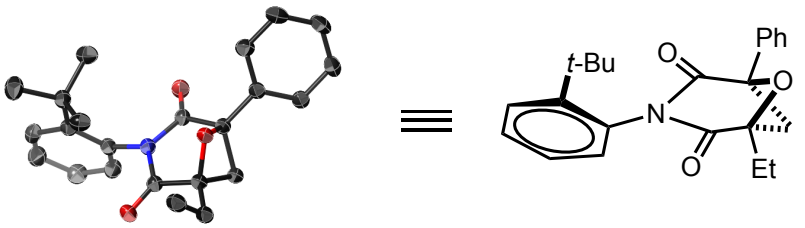

173b **173b**

Figure 3.8: Crystal structure of (+)-(*R,R,M*)-**173b** (crystallized from: hexanes/chloroform).

3.7. [2+2]-Photocycloaddition of maleimides - Introduction

Maleimides are one of the interesting and resourceful substrates that have numerous applications not only in the ground state (thermal transformations) but also in the excited state (photochemical transformations). This chromophore is highly reactive and functionalizable due to the presence of electron deficient double bond and imide carbonyl groups. Photochemical transformations especially photocycloaddition involving maleimides are well explored in the literature. Few examples of photocycloaddition undergone by maleimides includes [2+2],[39] [4+2][40] and [5+2][41,42] and are represented in the Scheme 3.11. Many prominent research groups have explored phototransformations employing maleimides and thiomaleimides extensively resulting in cyclobutane photoproducts.[39,43-45]

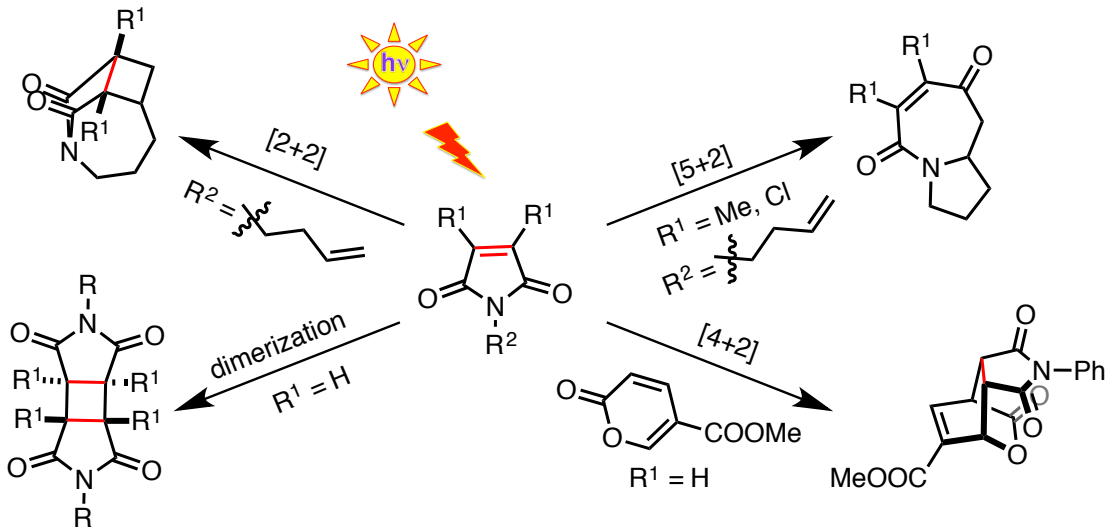

Scheme 3.11: Diverse photochemical transformations of maleimides.

One of the interesting results reported by Milburn and co-workers in the photoreactivity of the maleimides is to access chemoselective photoproducts depending on the type of irradiation conditions.[45]

Upon direct irradiation of N-alkyl maleimides in acetonitrile solvent resulted in the [5+2] photocycloaddition through N-CO bond cleavage leading to azepinone derivative **182**, whereas up on sensitized irradiation in acetonitrile, N-alkyl maleimides **181** underwent [2+2] photocycloaddition that led to cyclobutane photoproducts **183** (Scheme 3.12). These products are very useful in the synthesis of complex polycyclic molecules.

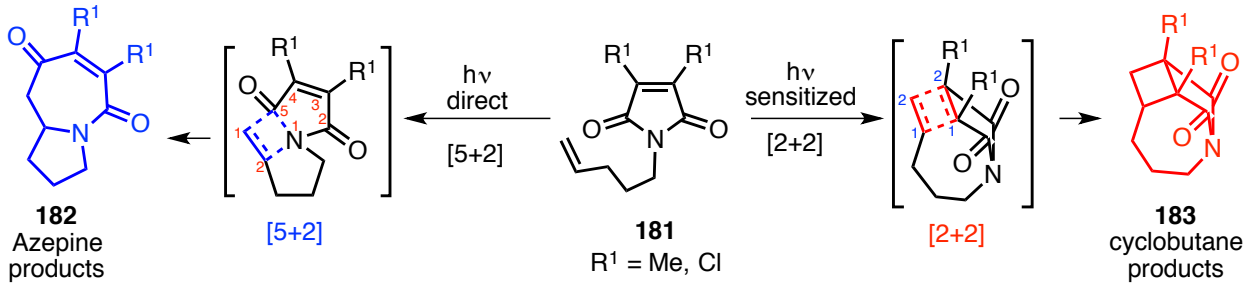

Scheme 3.12: [2+2] and [5+2]-photochemical transformations of maleimides.

In another investigation, Baker and coworkers reported efficient formation of cyclobutane photoproducts (Scheme 3.13) through intra and intermolecular [2+2] photocycloaddition of various thiomaleimides **184**, **186**, **188**,**189** (Figure 3.9).[39]

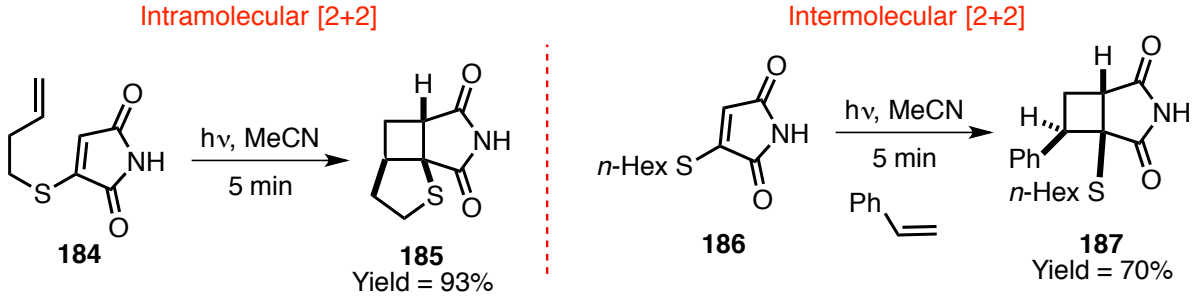

Scheme 3.13: Intra- and intermolecular [2+2]-photocycloaddition of thiomaleimides.

Comparison of UV-Vis spectrum of unsubstituted maleimides (λ_{max} of 273 nm), mono thiomaleimides (λ_{max} of 339 nm) and dithiomaleimide (λ_{max} of 393 nm) explained that these sulfur substituted maleimides shows bathochromic shift along with increase in the extinction coefficient allowing for increase in the efficiency of photocycloaddition.

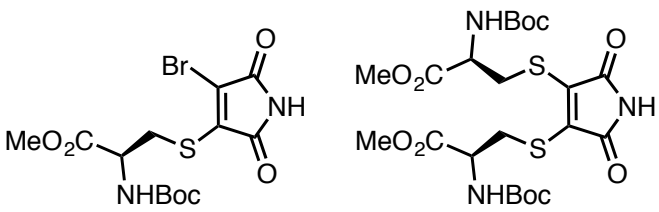

Figure 3.9: [2+2]-photocycloaddition of thiomaleimides.

Though these compounds undergo variety of photocycloaddition reactions yielding synthetically useful moieties, stereoselective phototransformations of maleimides remained unexplored. Milburn and coworkers[43] were one of the first to report a diastereoselective intramolecular [2+2]-photocycloaddition of tetrahydrophthalimides **190**. In these substrates the reacting alkene unit was tethered to chiral valinol and phenylgylcinol units that provides necessary diastereoselectivity in the photocycloaddition (Scheme 3.14). However, the diastereoselectivity between the *endo* and the *exo* photoproducts was only moderate at best.

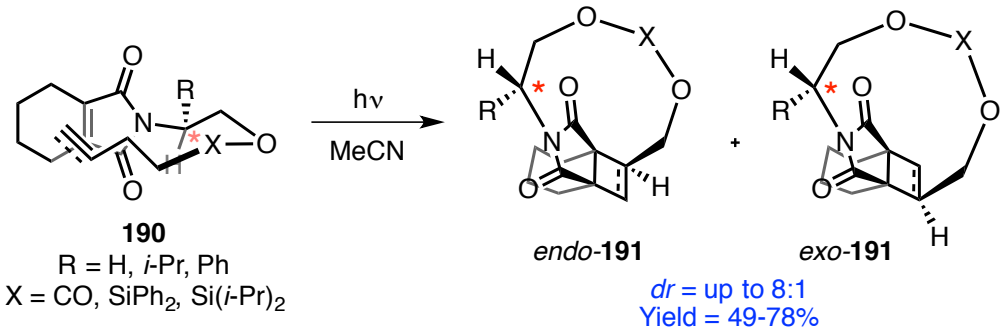

190
R = H, *i*-Pr, Ph
X = CO, $SiPh_2$, $Si(i\text{-}Pr)_2$

Scheme 3.14: [2+2]-Photocycloaddition of tetrahydrophthalimides.

Based on this literature precedence and utility of these building blocks in the organic synthesis, we designed atropisomeric maleimides (Chart 3.2) to investigate them in stereospecific phototransformations. The synthesized atropisomeric maleimides and their precursors listed in the Chart 3.2

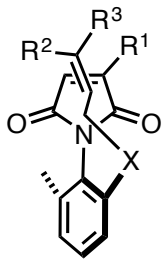

192a-b
192d-f

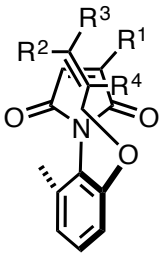

192c

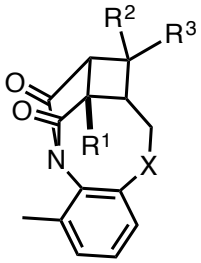

193a-b,
193d-f

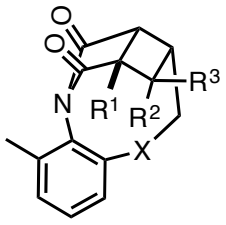

194a-b,
194d-f

a) R^1 = Me; R^2-R^3 = Me; X = O;
b) R^1,R^2 = Me; R^3 = H; X = O
d) R^1 = Br; R^2-R^3 = H; X = O;
e) R^1 = Ph; R^2-R^3 = H; X = CH_2
f) R^1 = imidazole; R^2-R^3 = H; X = O.

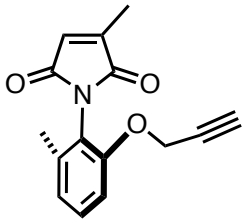

192g

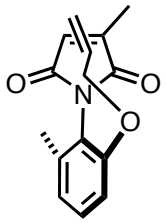

192h

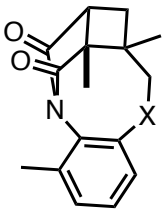

193c

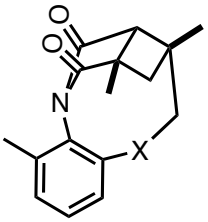

194c

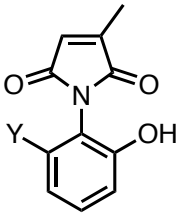

195

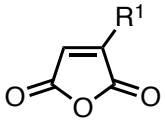

196
a) R^1 = Me;
b)R^1 = Ph;
c)R = Br

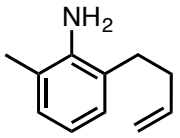

197

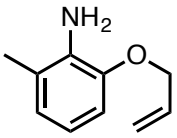

198

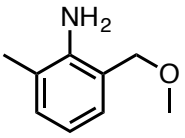

199

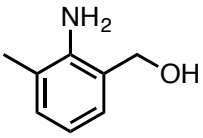

200

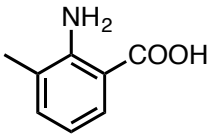

201

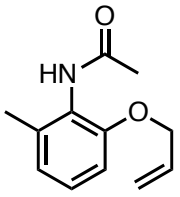

202
Y = Me; X=O

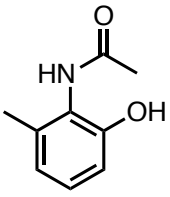

203

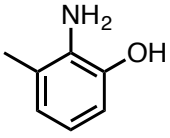

204

Chart 3.2: Structures of atropisomeric maleimides, their photoproducts and the precursors for the synthesis.

3.8. Photoreactivity of N-aryl atropisomeric maleimides towards cycloaddition reaction

Based on the pioneering work by Milburn and co workers, it is known that N-alkenyl maleimide derivatives undergo both [2+2]- and [5+2]-photocycloaddition depending on the irradiation conditions.[45] We were interested in investigating atropisomeric maleimides towards photocycloaddition. One of the interesting observations made during this course of [2+2]-photocycloaddition was the chain length dependent control over the chemoselectivity. For example, when maleimides with a butenyl chain **192** was irradiated only [2+2]-photocycloaddition products **193** and **194** was observed under both direct and sensitized. However, when the atropisomeric maleimides with an allyl chain group **205a** was exposed to direct irradiation conditions only [5+2] product **206a** and **207a** were obtained. Sensitized irradiation of allyl chain substituted maleimides resulted only in the isomerization of the double bond resulting in styrene type products (Scheme 3.15).

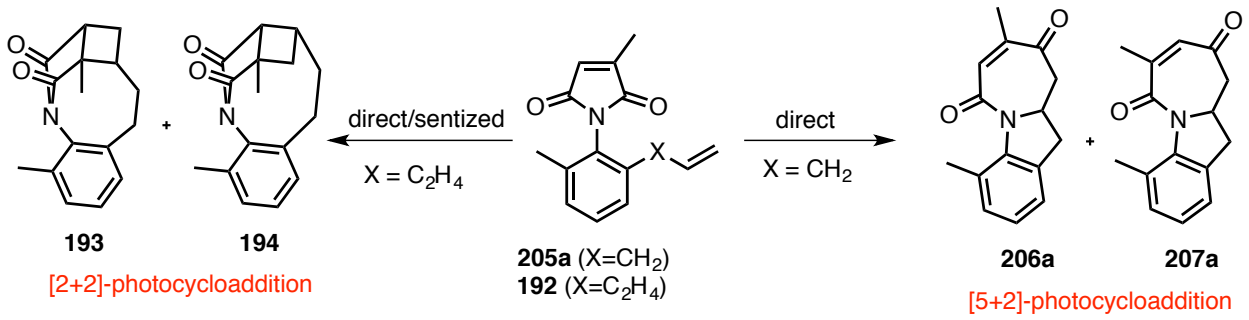

Scheme 3.15: Photoreactivity of N-aryl maleimides with varying chain length.

We believe that the formation of [5+2] adduct is the consequence of molecular constraint on the maleimides and the kinetics of the reactions ([2+2] vs [5+2]). In [5+2] photocycloaddition, the length of the allyl chain was short preventing it form reaching the maleimide double bond to undergo [2+2] photocycloaddition. Therefore upon irradiation, the N-CO bonds cleave, resulting in the insertion of allyl double bond. On the other hand, the butenyl-substituted maleimides is long enough to reach the maleimide double bond to undergo [2+2] photocycloaddition (Sections 3.6-3.13), [5+2]-photocycloaddition of allyl maleimide derivative is discussed in detail in sections 3.14-3.21.

3.9. Racemization barrier in atropisomeric maleimide

N-Aryl maleimides prefers to be twisted at N-C_{aryl} axis due to steric hindrance between the imide carbonyl and *ortho* hydrogens. However simple hydrogen will not provide enough sterics to be atropisomeric. In this aspect, the newly synthesized atropisomeric maleimides with methyl group at the 6-position of the phenyl ring played a crucial role in providing stable atropisomers by increasing the energy barrier for N-C_{aryl} bond rotation. Racemization of optically pure atropisomeric maleimides **192a** was carried out in toluene at 100 °C. The progress of the racemization (% *ee*) was monitored by HPLC analysis on a chiral stationary phase at different time intervals.

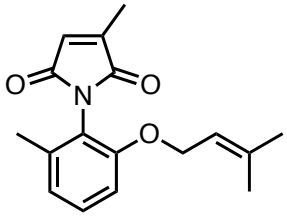

192a

192a, Toluene, 100 °C	
k_{rac} (s^{-1})	= 2.22 x 10^{-6}
$\tau_{1/2}$ (days)	= 3.6
$\Delta G^{\ddagger}_{rac}$ (kcal/mol)	= 31.7

Figure 3.10: Racemization kinetics of **192a.**

Inspection of the kinetic parameters on atropisomeric maleimides **192a** gave insights on the energy barrier to rotation around N-C_{aryl} axis (Figure 3.10). The half-life for racemization ($\tau_{1/2}$) was 3.6 days at 100 °C, corresponding to a racemization rate constant (k_{rac}) of 2.22 × 10^{-6} s^{-1} and an activation energy barrier ($\Delta G^{\ddagger}_{rac}$) of 31.7 kcal·$mol^{-1}$. Such a high racemization barrier allowed us to carry out atropselective photoreaction without the loss of optical purity.

3.10. Intramolecular [2+2]-photocycloaddition of atropisomeric maleimides

The photoreactions of newly synthesized atropisomeric maleimides **192** were subjected to different irradiation conditions and solvent that resulted in [2+2] photoadducts with complete chemoselectivity over competing [5+2] photocycloaddition. Three different sets of irradiation conditions were examined (a) direct irradiation; (b) sensitized irradiation under UV light (e.g., using xanthone as a sensitizer in a Rayonet reactor at ~350 nm); and (c) metal-free sensitized irradiation under visible-light (e.g., using thioxanthone as a sensitizer in a Rayonet reactor at ~420 nm). After the photoreaction, the

solvent was evaporated under reduced pressure and the photoproduct(s) were purified by column chromatography.

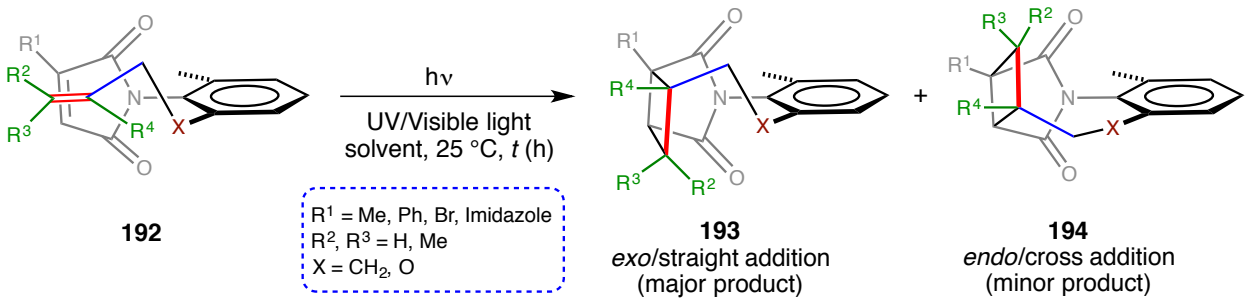

Scheme 3.16: [2+2] photocycloaddition of atropisomeric maleimides **192.**

Crude ^{1}H-NMR spectroscopic analysis revealed the presence of diastereomeric photoproducts *viz*., *exo*-photoproduct **193** and *endo*-photoadduct **194**. In the major *exo*-photoproduct, the carbon bearing the terminal alkene tether is away from the carbon bearing the R^1 substituent. On the other hand, in the minor *endo*-photoproduct, the carbon of the terminal alkene is towards the carbon bearing the R^1 substituent. Several control studies were performed to optimize conditions to provide insights about the solvent choice, sensitizer and type of irradiation.

3.11. Control experiments for atropselective [2+2]-photocycloaddition of maleimides

The optimized conditions for the photoreactions were obtained after series of screening reactions carried out on atropisomeric maleimides. These experiments played a vital role in optimizing the solvent, choice of irradiation, sensitizer temperature and time. The following table summarizes the results of those experiments (Table 3.3)

Table 3.3: Control experiments for atropselective [2+2]-photocycloaddition of maleimides **192**.

Entry	Compd	Solvent	Conditions	*dr* (**193:194**)	Convn (%)	MB (%)
1	**192a**	Acetone	bb, rt, 75 min	79:21	53[a]	-
2	**192a**	MeCN	Xanthone, 350 nm, rt, 1 h	79:21	60[a]	-
3	**192e**	MeCN	Xanthone, 350 nm, rt, 8 h	>99:1	> 99	93
4	**192e**	MeCN	Thioxanthone, 420 nm, rt, 1 h	>99:1	82 [a]	-
5	**192f**	Acetone	bb, rt, 30 min	Decomposed		
6	**192f**	MeCN	Thioxanthone, 420 nm, rt, 1 h	>99:1	74 [a]	-
7	**192g**	Acetone	bb, rt, 60 min	Decomposed		

Note: MeCN- acetonitrile; bb- broad band (450W mercury lamp); rt- room temperature; The reactions were run with ~3.9 mM concentration either under constant bubbling of N_2 or N_2 degassed solution. Convn- conversion, MB- mass balance. ~300, ~350 and ~420 nm irradiations were carried out in a Rayonet reactor. [a] Isolated yield.

Investigation of Table 3.3 shows that the photocycloaddition reaction progressed more efficiently under sensitization. For example, triplet sensitized reactions i.e. in the presence xanthone and thioxanthone; reaction was complete within 1 h (entry 2, 4 and 6) without any decomposition. The alkyne-substituted maleimide **192g** did not result in the desired [2+2] photoadduct even under sensitized irradiation (acetone, xanthone and thioxanthone) rather led to dimerization and decomposition. Various other control studies were performed that includes (a) solvent screening (b) thioxanthone sensitizer loading and (c) analysis of dr in photoproducts in different solvents. These experiments were performed with **192h** as a model compound.[46,47] The conversion was moderate to high in several solvents (MeOH, MeCN, ethyl acetate, chloroform, CH_2Cl_2 etc.,).[46] The photoproduct was not stable in THF and the conversion was low in benzene and methyl cyclohexane. The efficiency of employing thioxanthone sensitizer in promoting the visible light mediated [2+2]-photocycloaddition was evident from the Table 3.3 (entries 4 and 6). Therefore sensitizer-loading studies were performed with **192h**. A 60% conversion was achieved using 5 mol% of thioxanthone, but in order to ensure that the catalyst always absorbs the light thereby preventing the decomposition of the starting materials (optical shield), 30 mol% loading was used. The dr ratio in the photoproducts was not affected significantly by changing the solvent from polar

MeOH to non-polar toluene or MCH. Based on these control experiments, the stereospecific photoreactions were carried out under optimized conditions i.e., with 30 mol % of xanthone (Rayonet reactor at ~350 nm) or thioxanthone (Rayonet reactor at ~420 nm) as sensitizers in MeCN as solvent.[46,47]

3.12. Atropselective [2+2]-photocycloaddition of maleimides 192

The photoreaction was performed in optimized reaction conditions i.e., MeCN as solvent and sensitizer-xanthone or thioxanthone to access the enantio- and diastereoenriched photoproducts. The photoreaction was monitored by TLC. After complete consumption of the starting material, the solvent was evaporated under reduced pressure and the photoproducts were isolated by column chromatography. The diastereomeric ratio of the photoproducts was analyzed by crude NMR spectroscopy and the HPLC analysis revealed the enantiomeric excess in the photoproduct(s) (Scheme 3.17).

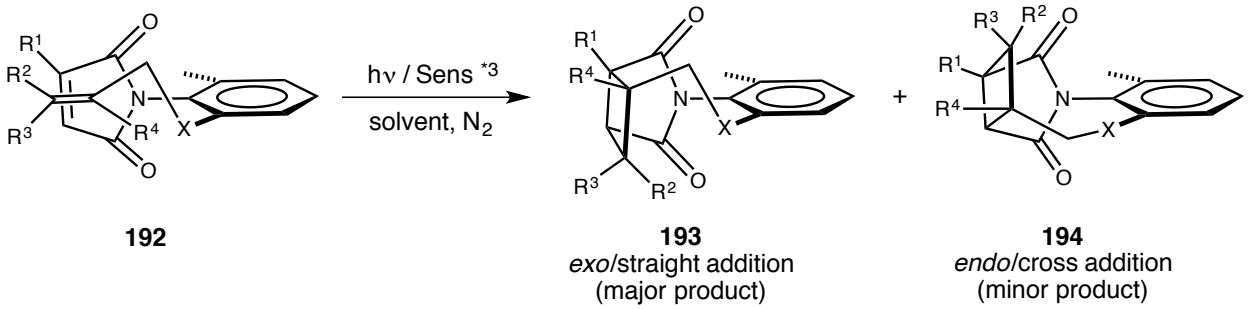

192

193
exo/straight addition
(major product)

194
endo/cross addition
(minor product)

Scheme 3.17: Atropselective [2+2] photocycloaddition of atropisomeric maleimides **192**.

Investigation of Table 3.4 clearly revealed, the enantioselectivity of photoproducts in all the atropisomeric maleimides investigated were >98%. This is a reflection of higher energy barrier for the newly synthesized atropisomeric maleimides. The diastereomeric ratio (*exo*:*endo*) in the photoproducts was dictated by the substituents at the alkenyl tether (R^2-R^4) and the maleimide double bond (R^1). So in order to evaluate the influence of the substituents on the alkenyl and the maleimide ring, we systematically varied the substituents. When R^1 was Me as in the case of **192a**, the *dr* value was 79:21, however when R^1 was changed to Br as in **192d**, the *dr* decreased to 69:31. Complete control over the *dr* was obtained when R^1 was substituents with bulky phenyl and imidazole **192e** and **192f**.

Table 3.4: Intramolecular [2+2]-photocycloaddition of atropisomeric maleimides **192**[a,b]

Entry	Substrate	Major photoproduct	Isolated Yield [%], *dr* (**193:194**),[c] % *ee*
1	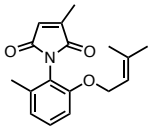	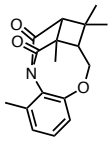	60 (79:21)[f]
	(+)-**192a**	(-)-**193a**	> 98% *ee*
	(-)-**192a**	(+)-**193a**	> 98% *ee*
2	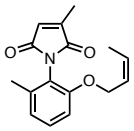	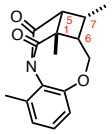	90[d] (84:16)
	(+)-**192b**	(A)-(1*R*,5*S*,6*R*,7*S*)-**193b** [d]	> 98% *ee*
	(-)-**192b**	(B)-(1*S*,5*R*,6*S*,7*R*)-**193b** [d]	> 98% *ee*
3	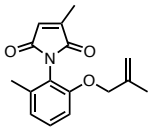	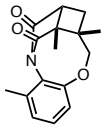	77 (62:38)
	192c	**193c**	
4	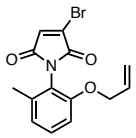	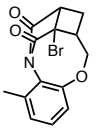	82 (69:31)
	192d	**193d**	
5	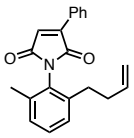	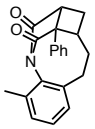	82 (> 99:1)
	192e	**193e**	
6	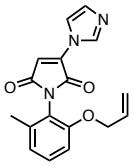	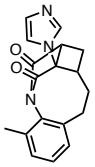	74 (>99:1)
	192f	**193f**	
7	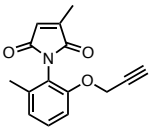	Dimers / Decomposition	
	192g		

[a]Irradiation of **192a** was performed with 30 mol % xanthone as the triplet sensitizer in acetonitrile solvent at room temperature using a Rayonet reactor equipped with 300 nm lamps. Irradiations of **192e**, and **192f** were performed with 30 mol% thioxanthone as the triplet sensitizer in acetonitrile solvent at room temperature using a Rayonet reactor equipped with 420 nm lamps. For all other substrates, the photoreactions were performed in acetone at room temperature using a 450 W medium-pressure Hg lamp with a Pyrex cutoff filter. [b]The ee values were obtained from HPLC analysis on a chiral stationary phase, and the results are averages of three runs with an error of ±3%. The absolute configuration was determined by XRD with Flack parameters. [c]The ratios were determined by ^{1}H NMR spectroscopy of the crude samples. [d]Yield based on ^{1}H NMR spectroscopy using triphenylmethane as an internal standard.

To understand the effect of R^1 substitution, we continued the investigation by changing the substitution on the alkene tether. The gem dimethyl substitution at the alkene tether as in the case of **192a** did not alter the *dr* values compared to **192 h** (79:21).[46] On the other hand, monomethyl substitution as in the case of **192b** resulted in a *dr* 84:16. Internal substitution on the alkene carbon **192c** lowered the *dr* values. We changed the alkene reacting partner to alkyne **192g** envisaging cyclobutene photoproduct, but the reaction did not give the desired photoproduct rather it formed dimeric products with significant decomposition. The presence of oxygen on the alkenyl tether in the photoproduct **193a** provided avenues

to cleave the tether after the photoreaction. The ether cleavage of the photoproducts proceeded smoothly and furnished N-aryl phenols **230** and **231**. However, the imide cleavage did not yield the desired product.

These results showed that maleimides undergo [2+2]-photocycloaddition with degree of stereocontrol. The *dr* ratio is influenced by R^1 substituent on maleimide double bond and R^2-R^4 substituent in the alkene tether.

3.13. Mechanistic rationale for stereospecific [2+2]-photocycloaddition

Detailed photophysical investigation revealed some of the salient features of the results (a) the maleimides as such, had very poor intersystem crossing quantum yield and very low triplet population upon direct irradiation and (b) the triplet excited state of thioxanthone (sensitizer) is quenched by maleimides to generate triplet maleimides suggesting that excited state thioxanthone acted as a donor while the maleimide functioned as an acceptor. Based on the photophysical and photochemical experiment we believe that the intramolecular [2+2]-photocycloaddition of maleimides proceeded via triplet pathway (Scheme 3.18). We believe the electron rich alkene likely interacted with the half filled π orbital of the $\pi\pi^*$ excited state of the maleimide.

Since this [2+2]-photocycloaddition required a triplet sensitizer, the product formation takes place in two steps. The first step is the formation of 1,4 diradical (DR1-DR4) and the second step is the cyclization step, in which triplet 1,4 diradical intersystem crosses to form singlet 1,4 diradical and combines to form photoproducts **193** and **194**. The formation of *exo* and *endo* product can be explained based on their conformational equilibrium and the type of radical formed. On the basis of conformational equilibrium, the *exo* product was likely formed from *conf*-A in which the CH_2 group of the alkenyl tether is pointed away from the R^1 substituent of the maleimide double bond. In the initial step it could likely lead to the formation of DR1 or DR2. Similarly the *endo* photoproduct was likely formed from conformer *conf*-B in which the CH_2 group of the alkenyl tether is pointed towards the R^1 substitution of the maleimide double bond. In this case diradical DR3 or DR4 will likely formed. These 1,4 diradicals intersystem crosses to form singlet 1,4 diradical and cyclize to the photoadducts.

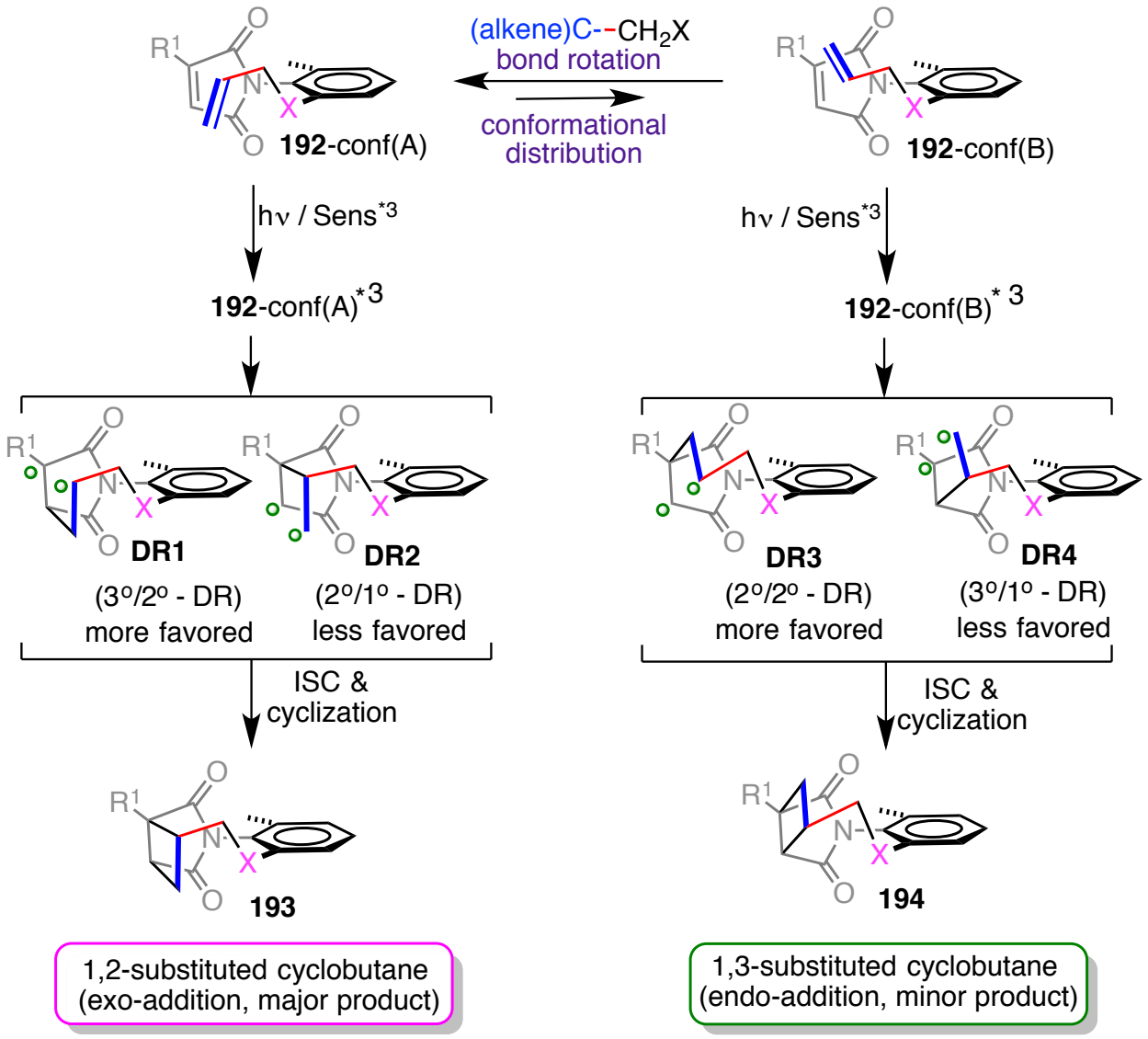

Scheme 3.18: Mechanistic rationale of atropisomeric maleimides **192**.

To obtain deeper knowledge on the type of radical formed; scrambling studies of **192b** were performed with the maleimides that has a methyl substituent at the terminal carbon at the alkenyl tether (*cis* alkene) (Scheme 3.19). The analysis of the photoproducts of maleimides **193b** showed only *endo* and *exo* photoproduct and trace of scrambled photoproducts.

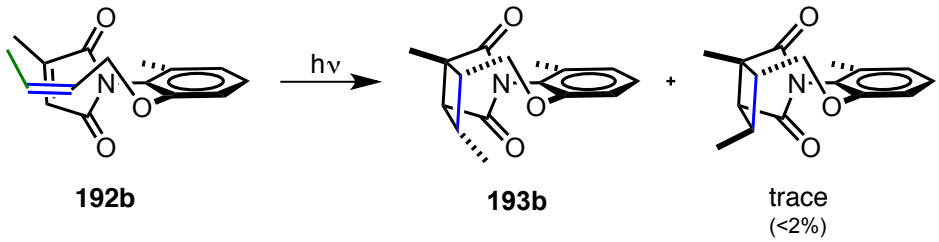

Scheme 3.19: Scrambling studies of maleimides **192b**.

The absence of scrambled photoproducts with respect to the alkene substituent (Scheme 3.19) reflected two scenarios. In the first scenario, the 1,4 diradical DR1 was likely more favored over DR2 leading to major *exo* product. Similarly, 1,4 diradical DR3 was likely more favored over DR4 for the minor *endo* product. In the second case, the 1,4 diradical DR2 formed in the initial step, cyclizes at much faster rate compared to bond rotation to retain the stereospecificity of the *exo* photoproduct. However, the second scenario is unlikely because the photoreaction takes place via a triplet pathway. So, the 1,4 diradical formed has to intersystem cross to singlet state, which provides sufficient time for scrambling to occur. Hence the lack-scrambling product likely indicates the first scenario as plausible mechanism.

3.14. X-Ray crystal structure data for atropisomeric maleimides and its photoproducts

Structure determination: Single crystal X-ray diffraction data of the compound **193b** was collected on a Bruker Apex Duo diffractometer with a Apex 2 CCD area detector at T = 100K. Cu radiation was used. All structures were processed with Apex 2 v2010.9-1 software package (SAINT v. 7.68A, XSHELL v. 6.3.1). Direct method was used to solve the structures after multi-scan absorption corrections. Details of data collection and refinement are given in the table below.

Table 3.5 Crystal structure data for cyclobutane photoproduct **193b**.

	(*1R,5S,6R,7S*)-**193b**	(*1S,5R,6S,7R*)-**193b**
Formula	$C_{16}H_{17}NO_3$	$C_{16}H_{17}NO_3$
FW	271.30	271.30
cryst. size_max [mm]	0.25	0.19
cryst. size_mid [mm]	0.22	0.15
cryst. size_min [mm]	0.14	0.07
cryst. system	Orthorhombic	Orthorhombic
Space Group, Z	$P2_12_12_1$, 4	$P2_12_12_1$, 4
a [Å]	10.4155(4)	10.4007(7)
b [Å]	10.8207(4)	10.8621(7)
c [Å]	11.9003(4)	11.9388(8)
α [Å]	90	90
ß [Å]	90	90
γ [Å]	90	90
V [Å^3]	1341.20(8)	1348.77(15)
ρ_{calc} [g/cm^3]	1.344	1.336
μ [mm^{-1}]	0.756	0.752
Radiation Type	Cu	Cu
F(000)	576	576
no of measured refl.	6957	6310
no of indep. refl.	2368	2369
no of refl. (I ≥ 2σ)	2309	2204
Resolution [Å]	0.84	0.84
R1/wR2 (I ≥ 2σ)[a] [%]	4.86/13.23	6.80/19.80
R1/wR2 (all data) [%]	4.96/13.31	7.16/20.27

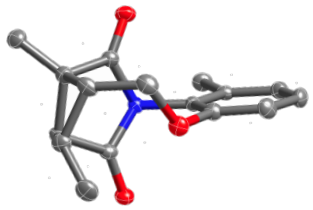

193b

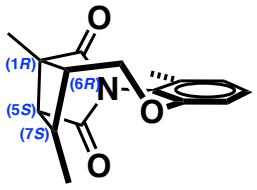

193b

(A is the first isomer that elutes from chiral stationary phase in HPLC analysis)

Figure 3.11: Photoproduct (A)-(*1R,5S,6R,7S)*- **193b** (crystallized from: hexanes:$CHCl_3$)

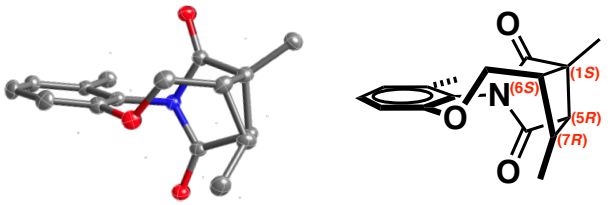

193b **193b**

(B is the Second isomer that elutes from chiral stationary phase in HPLC analysis)

Figure 3.12: Photoproduct (B)-(*1S,5R,6S,7R)*-**193b** (crystallized from: hexanes:$CHCl_3$)

3.15. [5+2]-Photocycloaddition of maleimides-introduction

In the previous section on [2+2]-photocycloaddition of atropisomeric of maleimides, we have reported that the maleimide chromophore underwent facile photocycloaddition with very high enantioselectivity, diastereoselectivity and good isolated yield. As a further extension in the study of maleimide chromophore, we looked at the [5+2]-photocycloaddition of maleimide. One of the interesting observations made during the [2+2]-photocycloaddition study is the chemoselectivity of the photocycloaddition i.e. [2+2] vs. [5+2], which was determined by the chain length of the alkenyl tether (Scheme 3.20). When the maleimide has a 4-carbon alkene (butenyl) tether it underwent [2+2]-photocycloaddition exclusively whereas reaction with a 3-carbon alkene (allyl) tether, it exclusively led to [5+2]-photoproduct(s) (photocycloaddition through N-CO bond cleavage leading to azepinone derivative).

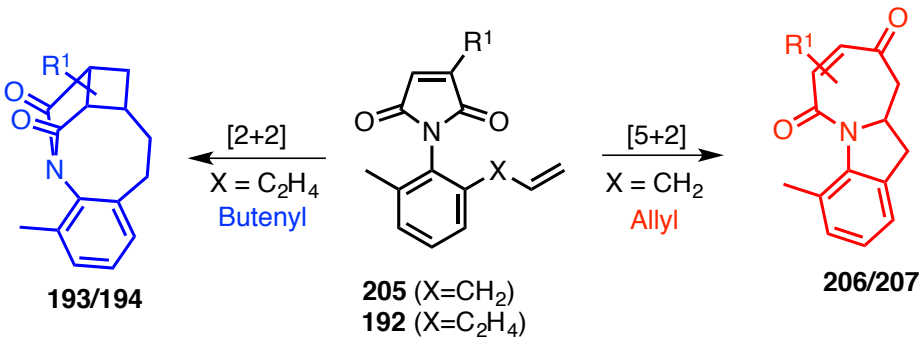

193/194 **205** (X=CH_2) **192** (X=C_2H_4) **206/207**

Scheme 3.20: [2+2] and [5+2]-Photochemical transformations of maleimides.

In 1977, Mazzocchi and coworkers[48] reported [5+2] photoproducts **210** when they were exploring the photocycloaddition of dienes towards N-alkylphthalimides **208** (Scheme 3.21). Though they did not name it as [5+2] photoproduct, they deciphered the structure to be *anti* and *syn* azepinone derivatives.

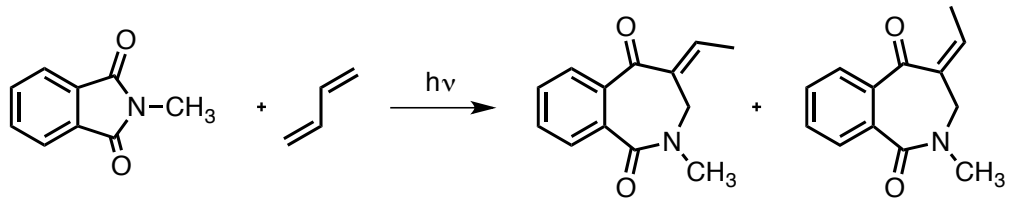

208 **209** *anti*-**210** *syn*-**210**

Scheme 3.21: Photocycloaddition of dienes to N-alkylphthalimides.

Following this observation, Mazzocchi et al., reported series of papers on the mechanism of the formation of azepinone photoproducts.[49-51] Similar observation, were made by Milburn and workers in 1998[52] when they were investigating the photocycloaddition of pentenyl substituted imide derivatives **212** (Scheme 3.22). The photoreaction resulted in a tricyclic azepinone product **213** rather than the anticipated cyclobutane photoproduct **212**. They have elaborated their observation from simple alkene to complex alkene tether leading to [5+2] photoproduct in quantitative yield as a single diastereoisomer (Scheme 3.23).

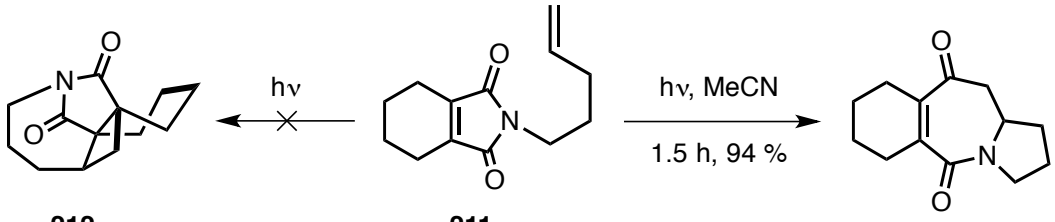

212 **211** **213**

Scheme 3.22: [5+2]-Photocycloaddition of maleimides with simple alkene tethers.

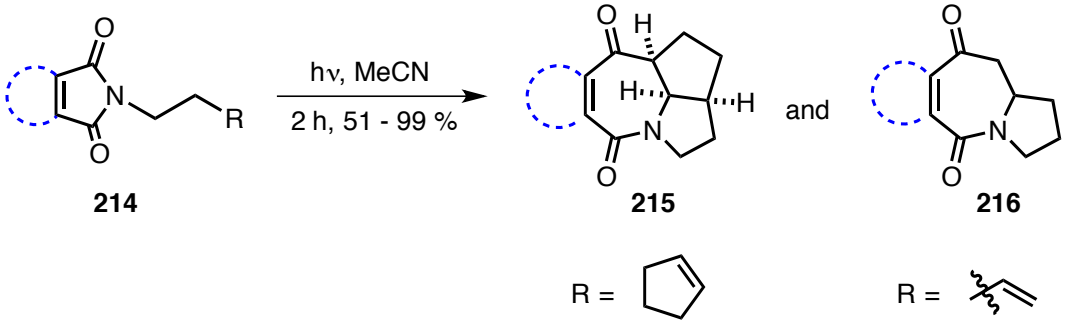

214 **215** **216**

Scheme 3.23: [5+2]-Photocycloaddition of maleimides with complex alkene tethers.

With the intention of increasing the scope of these reactions to access novel organic building blocks, Milburn and co-workers have incorporated diverse functionality into the alkenyl tether. Maleimides with chiral substitution on the alkenyl tether **217** resulted in inseparable *cis*/*trans* isomers **218**.[42] The ratio of the *cis*/*trans* isomers was affected by the position of this substitution as shown in Scheme 3.24. Increase in the formation of *cis* isomer was observed on substituting methyl group at position 3 whereas substitution at position 4 or 5 resulted in a single isomer (Scheme 3.24).

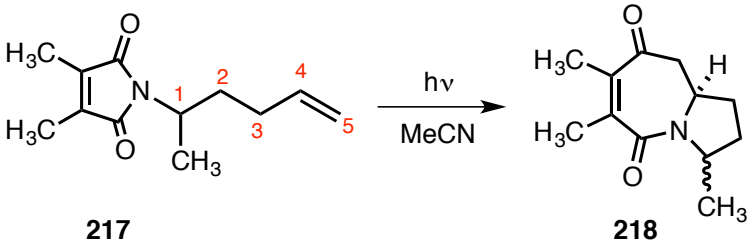

217 **218**

CH_3 Position	*cis*/*trans* ratio
1	1.27 : 1
2	1:1
3	3:1

Scheme 3.24: Photocycloaddition of maleimide derivative **217**.

Milburn and co workers have also explored other possible mechanism for observed [5+2]-photocycloaddition of maleimides apart from the pathways proposed by Mazzocchi, Fischer and De Schreyver et al. Based on their detailed photophysical and theoretical studies, they proposed that the [5+2] products can be formed via stepwise processes where singlet excited state is formed by n-π^* excitation followed by α-cleavage of N-CO bond.[53]

Due to the advantage of [5+2]-photocycloaddition in accessing structurally complex building blocks in a single step, the same group has demonstrated that this powerful strategy could be used for accessing several natural products. For example, they have demonstrated the synthesis of (-)-Cephalotaxine, one of the alkaloids isolated from plum yews that are potential drugs for the treatment of leukemia (Scheme 3.25).[54]

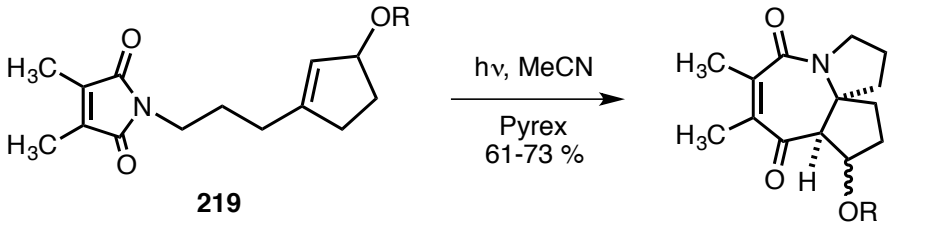

219

220
(-) - Cephalotaxine

Scheme 3.25: Photocycloaddition of maleimide derivative **219** towards natural product **220**.

Based on literature precedence, it is clear that the azepinone derivatives are biologically useful scaffolds and has its importance in natural product synthesis. Unfortunately, there are no reports on an asymmetric approach for the [5+2]-photocycloaddition reaction that would yield enantioenriched azepinone products. Therefore, we were interested in utilizing our strategy of “axial to point chiral transfer” to access enantioenriched azepinone derivatives. We designed atropisomeric maleimides with 3-carbon alkenyl chain (allyl) to undergo intramolecular stereospecific [5+2]-photocycloaddition. The atropisomeric maleimides and their intermediates listed in the following Chart 3.3 were synthesized according to procedures reported in literature.

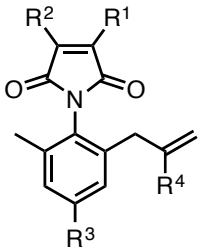

205(a-i)

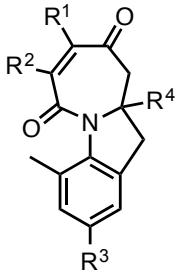

206(a-h)

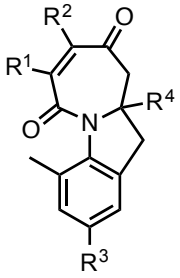

207(a-e), 207(g-h)

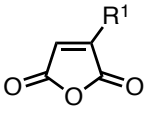

221a-e
a) R^1 = H; b) R^1 = Me;
c) R^1 = Br
d) R^1 = Ph; e) R^1 = CF_3

a) R^1-R^4 = H
b) R^1 = Me; R^2-R^4 = H
c) R^1 = Br; R^2-R^4 = H
d) R^1 = Ph; R^2-R^4 = H
e) R^1 = Ph; R^2 = H; R^3-R^4 = Me
f) R^1 = OMe; R^2-R^4 = H
g) R^1 = CF_3; R^2-R^4 = H
h) R^1 = Me; R^2 = Br; R^3-R^4 = H
i) R^1 = $(Me)_2$; R^2-R^4 = H

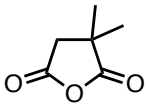

221f

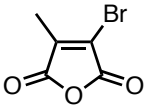

221h

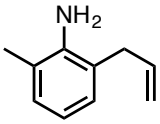

222

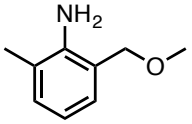

199

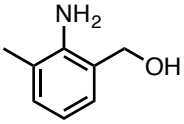

200

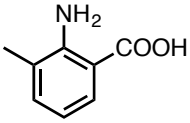

201

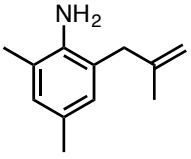

223

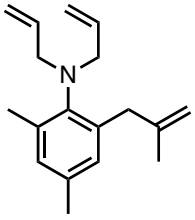

224

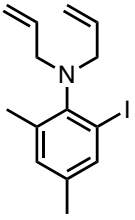

225

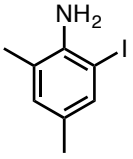

226

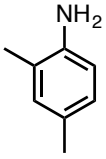

227

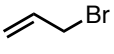

228

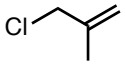

229

Chart 3.3: Structures of atropisomeric ally maleimides, their photoproducts and the precursors for the synthesis.

3.16. Racemization barrier in atropisomeric allyl maleimides

As discussed in section 3.8, atropisomeric compounds are bound to racemize at elevated temperature, which will lead low selectivity during the phototransformations. Though the atropisomeric maleimides with a butenyl chain gave insights on the energy barrier, it is important to evaluate the rotation barrier for the newly synthesized maleimides derivatives with an allyl substituent.

Inspection of the Table 3.6 indicates that the atropisomeric maleimides with a 3-carbon (allyl) chain are stable at the elevated temperature (100 °C). For instance, **205c** displayed a half life of racemization of 23 days, with racemization constant of ~3.5 × 10^{-7} s^{-1} and activation energy barrier of 33.0 kcal·mol^{-1}. No significant change in the racemization barrier was observed on varying the substituent on the maleimides ring. These studies suggested that these atropisomeric maleimides could be subjected to phototransformations without racemization.

Table 3.6: Racemization kinetics of atropisomeric maleimides **205**.

Entry	Compound	Parameters		
		$\tau_{1/2}$ (days)	k_{rac} (s^{-1})	$\Delta G^{\ddagger}_{rac}$ (kcal·mol^{-1})
1	**205c**	23	3.5 × 10^{-7}	33.0
2	**205d**	32	2.5 × 10^{-7}	33.3
3	**205e**	26	3.1 × 10^{-7}	33.1
4	**205f**	17	4.6 × 10^{-7}	32.8

3.17. Intramolecular [5+2]-photocycloaddition of atropisomeric maleimides

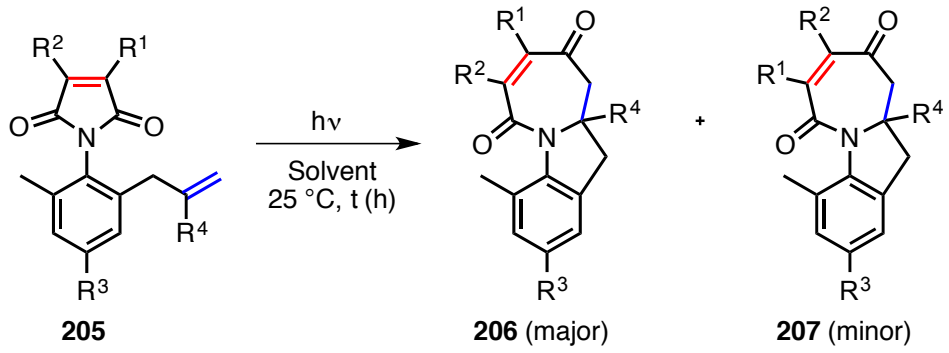

205 **206** (major) **207** (minor)

Scheme 3.26: Photocycloaddition or atropisomeric maleimides **205**.

The photoreactions of newly synthesized atropisomeric maleimides **205** in the optimized solvent were irradiated in a Rayonet reactor equipped with ~300 nm lamp (16 lamp × 14 watt). After the

photoreaction, the solvent was evaporated under reduced pressure and the photoproduct(s) were purified by either preparative TLC or column chromatography. Crude ^{1}H-NMR spectroscopic analysis revealed the presence of two diastereomeric photoproducts major **206** and minor **207** due to the regiochemistry of addition across the N-CO bond. ^{1}H-NMR analysis of the crude product revealed the *dr* values and the HPLC analysis disclosed the enantiomeric excess in the photoproducts respectively.

3.18. Solvent screening for [5+2]-photocycloaddition of atropisomeric maleimides

Solvent plays a key role in the outcome of the photoreactions. Therefore, various solvents were screened for the photoreaction of atropisomeric maleimide **205a**. For the experiment, maleimide **205a** in a given solvent (~3.9 mM concentration) was degassed with N_2 for 15 min and then sealed for photoreaction. This solution was irradiated in a Rayonet reactor (~300 nm) for 3 h. After 3 h, internal standard (triphenylmethane) was added and this solution was concentrated under reduced pressure to obtain the crude reaction mixture. ^{1}H-NMR spectroscopy was recorded on the crude reaction mixture and from the integral values the conversion and mass balance were calculated based on the equation 2.1.

Analysis of the Table 3.7 shows that the conversion and mass balance of the photoreaction is similar in all the solvents except ethyl acetate and chloroform where decomposition was observed. Based on these results we chose acetonitrile as solvent for further photoreactions.

Table 3.7: Optimization of solvent with maleimide **205a**.

Entry	Solvent	NMR Yield (%) (% mass balance)
1	Acetonitrile	26 (60)
2	Ethyl acetate	Decomposed
3	Dichloromethane	20 (59)
4	Chloroform	Decomposed
5	Benzene	33 (50)
6	MCH	35 (59)

Note: The reported value carry an error of ±5%.

3.19. Photoreaction of atropisomeric allyl maleimide in various atmospheric conditions

In a typical experiment, maleimide **205a** in MeCN (~3.9 mM concentration) was bubbled with Nitrogen or Oxygen for 8-10 min. For irradiation under air, the reaction mixture was irradiated without bubbling. The resultant solution was irradiated in a Rayonet reactor (~300 nm or ~350 nm) for 3 h. After the reaction, a stock solution of internal standard (triphenylmethane) was added and this solution was concentrated under reduced pressure to obtain the crude reaction mixture. ^{1}H-NMR spectrum was recorded on the crude reaction mixture and from the integral values the conversion and mass balance were calculated using equation 2.1 (Table 3.8)

Table 3.8: Photoreaction of **205a** at various atmospheric conditions.

Entry	Condition	NMR Yield (%)
1	Nitrogen	23
2	Oxygen	22
3	Air	26

Note: The reported value carry an error of ±5%.
Values are average of two trials.

3.20. Atropselective [5+2]-photocycloaddition of atropisomeric maleimides 205

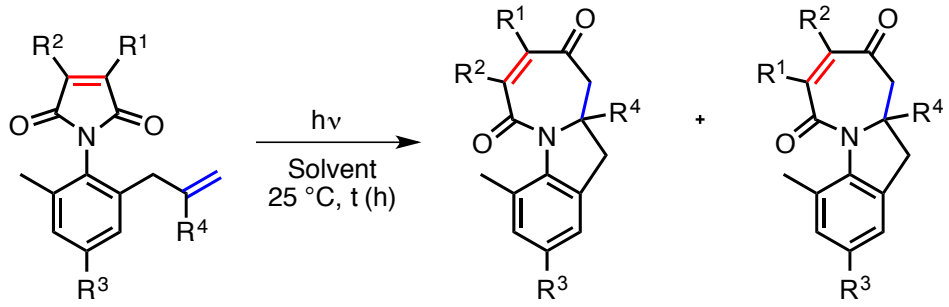

205 **206** (major) **207** (minor)

Scheme 3.27: [5+2]-Photocycloaddition of atropisomeric maleimides **205**.

The photoreaction was carried out with optically pure atropisomeric maleimides in optimized solvent –MeCN with the irradiation conditions mentioned in section 3.19. After irradiation, the solvent was evaporated under reduced pressure and the photoproducts were isolated by preparative thin layer

chromatography and characterized by NMR spectroscopy, mass spectrometry, single crystal XRD, $[\alpha]_D$ and by HPLC. HPLC analysis of the photoproducts on a chiral stationary phase gave the optical purity of the photoproducts.

The results of [5+2]-photoreaction of the atropisomeric maleimides showed few noteworthy features. a) The presence of the maleimide double bond is necessary for the [5+2]-photocycloaddition to take place, as the succinimide derivative **205i** did not undergo photocycloaddition under the irradiation conditions (Table 3.9 entry 9). b) Direct irradiation resulted in the desired photoproducts, rather than the sensitized irradiation, which led to isomerization of the alkene tether giving rise to styrene type derivative and c) the conversion of products was very low ~14 - 26 % except for **205d**. This is due to high extinction coefficient of the photoproducts **206** and **207** compared to the reactant **205**. Hence the photoproduct acts as an internal filter thereby preventing complete conversion. Reviewing Table 3.9 discloses that the maleimides which were subjected to enantiospecific reaction resulted in > 98 % ee. This indicated that the chirality in the starting material was efficiently transferred to photoproducts due to the high N-C_{aryl} rotational barrier. However, *dr* values of the photoproducts are influenced by the substituent on the maleimides. Therefore, substitution on the maleimides ring was systematically varied to understand its effect on the dr between **206** and **207**. When R^1 is a methyl as in **205b** the *dr* value was 60:40. Slight increase in the dr values was observe when R^1 was replaced with Br as in **205c** (*dr* = 65:35) and when R^1 = Ph as **205d**, the dr was 70:30. Substitution on the alkene tether as in **205e** did not affect the dr (74:26) but it showed significant influence on reactivity. Compound **205e** displayed slow reactivity compared to **205d** (without the internal substitution), which is evident from the conversion (**205e** = 14% and **205d** = 50%) due to the steric in the reacting alkene during transition state. Disubstitution on the maleimides also did not affect the dr as in the case of **205h**, dr = 69:31. On understanding that the substitution so far showed only weak electronic perturbation on the reactivity, we went on to investigate on strong electron donating and withdrawing substitution. When R^1 = OMe, we observed complete control over dr 99:1 in addition to the >98 % enantioselectivity. Minor methoxy was synthesized separately to confirm the absence of minor photoproduct by comparing it with the crude reaction mixture. While the strong activating group on the maleimide ring resulted in complete control over the dr and ee, the deactivating

group CF_3 as in **205g** resulted in the slight reversal of the *dr* (favoring the minor photoproduct) with >98 % ee.

Table 3.9: Intramolecular [5+2]-photocycloaddition of atropisomeric maleimides.[a]

Entry	Substrate	Major photoproduct	Yield [%],[b] *dr* (**206:207**),[c] % *ee*[d]
1	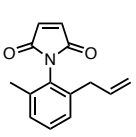	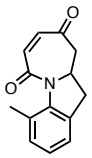	26
	205a	**206a**	
2	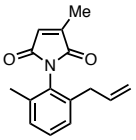	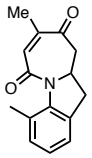	15 (60:40)
	205b	**206b**	
3	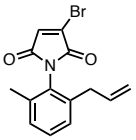	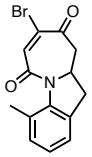	16 (65:35)
	(+)-**205c**	(B)-**206c**	> 98% *ee*
	(-)-**205c**	(A)-**206c**	> 98% *ee*
4	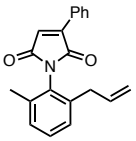	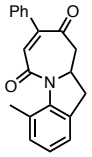	50 (70:30)
	(+)-**205d**	(B)-**206d**	> 98% *ee*
	(-)-**205d**	(A)-**206d**	> 98% *ee*
5	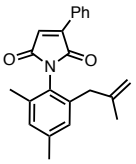	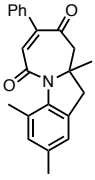	14 (74:26)
	(+)-**205e**	(A)-**206e**	> 98% *ee*
	(-)-**205e**	(B)-**206e**	> 98% *ee*
6	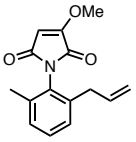	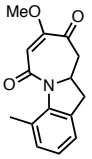	18 (99:1)
	(-)-**205f**	(A)-**206f**	> 98% *ee*
	(+)-**205f**	(B)-**206f**	> 98% *ee*
7	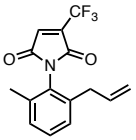	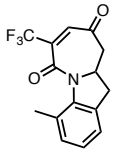	26 (45:55)
	(+)-**206g**	(A)-**207g**	> 98% *ee*
	(-)-**206g**	(B)-**207g**	> 98% *ee*
8	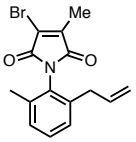	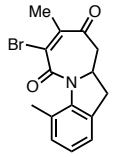	18 (69:31)
	205h	**206h**	
9	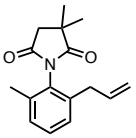	No reaction	-
	205i		

a) Irradiation of substrates in MeCN was performed using Rayonet reactor equipped with ~300 nm bulbs except for **205d** and **205e** for which ~350 nm bulbs was employed. For all the substrates photoreactions were performed in MeCN as solvent. b) Yield based on ^{1}H-NMR spectroscopy using triphenylmethane as an internal standard. c) The dr ratio were determined by ^{1}H-NMR spectroscopy of crude reaction mixture. d) The ee values were obtained form HPLC analysis on a chiral stationary phase, and the results are average of three runs with an error of ±3. (+) and (−) represent the sign of optical rotation (MeOH at 25 °C). A and B refer to the order of HPLC elution for a given pair of enantiomers.

3.21. Mechanistic rationale of [5+2]-photocycloaddition of atropisomeric maleimides 205

Based on the UV-Vis experiments (Section 3.32) it is evident that the lowest excited state of atropisomeric maleimides **205** is $n\pi^*$ configuration with slight mixing of $\pi\pi^*$ in the case of **205d** and **205e**. The mixing of $\pi\pi^*$ was substantiated by higher extinction coefficient (at ε_{340} **205d** = 2044 $M^{-1}\cdot cm^{-1}$ and **205e** = 2644 $M^{-1}\cdot cm^{-1}$) and slight bathochromic shift upon changing the solvent from methylcyclohexane (non-polar) to methanol (polar). Furthermore these types of maleimide derivatives have low intersystem crossing and very low triplet quantum yield.[47] Based on our experiments and literature precedence,[44,55] we believe that the [5+2]-photocycloaddition occurs from $n\pi^*$ excited state and the involves singlet-excited species. This was corroborated by the outcome of the a) photoreaction under triplet sensitized irradiation (acetone as solvent and sensitizer) which resulted in isomerization and not the desired [5+2]-photoproduct b) the product yield remained unaffected under nitrogen or oxygen or aerated conditions. [5+2]-photocycloaddition of alkenyl substituted maleimides and N-alkenyl phthalimides were studied in literature and different mechanism has been put forth. For example, Mazzocchi and coworkers[49-51] based on their extensive studies on N-alkenyl phthalimides proposed that the photocycloaddition of alkene to zwitterionic resonance form of maleimide, which then undergoes fragmentation of N-C(CO) bond to form [5+2] product. Alternatively Milburn and coworkers[53] suggested α-cleavage of N-C(CO) bond originating from $n\pi^*$ of the excited N-alkenyl maleimides. Gaining insights from literature and based on our experimental observations, we propose that atropisomeric maleimides likely undergoes reaction from $n\pi^*$ excited state of **205**. (Scheme 3.28)

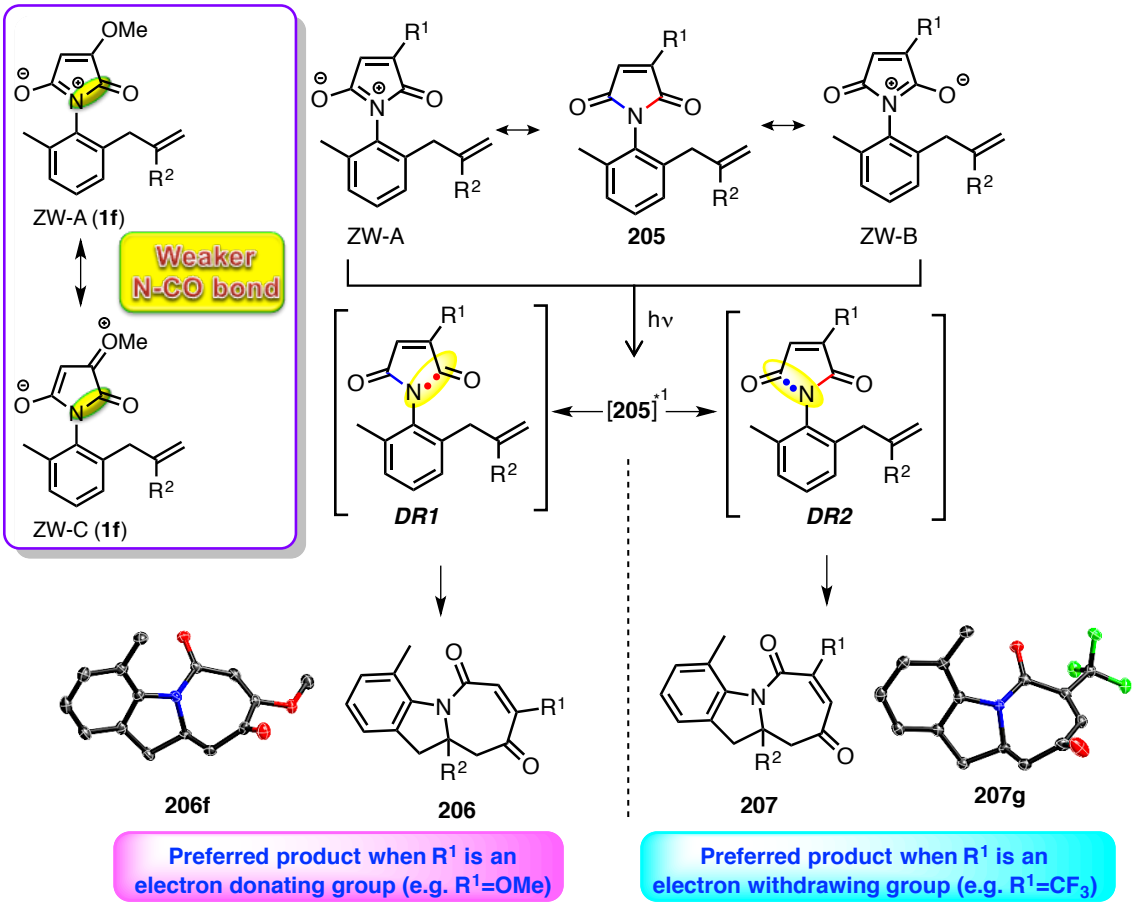

Scheme 3.28: Mechanistic rationale of [5+2] maleimides **205**.

Based on the photochemical paradigm, the nπ* singlet excited state leads to cleavage of N-C(CO) bond resulting in a diradical (DR) which combines to form the [5+2]-photoproducts. Since the maleimides **205** is unsymmetrically substituted, the cleavage of N-C(CO) can take place on either side (shown in red and blue) resulting in regioisomeric photoproducts **206** and **207**. It is evident from the results that the *dr* between **206** and **207** is influenced by the R^1 substituent on the maleimide ring. If the R is electron donating group as in the case of **205f** (R^1=OMe), N-C(CO) which is nearest to the R^1 substituent will be weaker due to mesomeric effect leading to diradical DR1 over DR2 which adds to the alkene to form **206** as the major photoproduct. If R^1 is electron withdrawing group such as CF_3, the cleavage of the N-C(CO) which is farthest from the R^1 substituent (blue bond) is preferred resulting in DR2 compared to DR1 resulting in the formation of **207** as a major photoproduct.

3.22. X-Ray crystal structure data for atropisomeric maleimides and its photoproducts

Structure determination: Single crystal X-ray diffraction data of the compounds **206** and **207** were collected on a Bruker Apex Duo diffractometer with a Apex 2 CCD area detector at T = 100K. Cu radiation was used. All structures were processed with Apex 2 v2010.9-1 software package (SAINT v. 7.68A, XSHELL v. 6.3.1). Direct method was used to solve the structures after multi-scan absorption corrections. Details of data collection and refinement are given in the table below

Table 3.10: Crystal structure data for atropisomeric maleimides **205** and its photoproducts **206** and **207**.

	(*10R*)-**206b** (PkA)	(*10S*)-**206b** (PkB)	**206c**	**207**	**206f**	**206g**	**207g**
Formula	$C_{15}H_{15}NO_2$	$C_{15}H_{15}NO_2$	$C_{14}H_{12}BrNO_2$	$C_{14}H_{12}BrNO_2$	$C_{15}H_{15}NO_3$	$C_{15}H_{12}F_3NO_2$	$C_{15}H_{12}F_3NO_2$
FW	241.29	241.29	306.16	306.16	257.29	295.26	295.26
cryst. size_max	0.24	0.22	0.24	0.301	0.227	0.16	0.2
cryst. size_mid	0.17	0.20	0.166	0.23	0.221	0.11	0.182
cryst. size_min	0.14	0.12	0.06	0.21	0.045	0.05	0.075
cryst. system	Orthorhombic	Orthorhombic	Monoclinic	Orthorhombic	Monoclinic	Monoclinic	Triclinic
Space Group, Z	'$P2_12_12_1$', 4	'$P2_12_12_1$', 4	'$P12_{1/n}1$', 4	'$P2_12_12_1$', 4	'$P12_{1/n}1$', 8	'$P\ 1\ 2_{1/c}\ 1$', 4	'$P12_11$', 2
a [Å]	7.9647(2)	7.9650(2)	18.1984(5)	8.5431(8)	16.9222(7)	9.6309(3)	8.7121(3)
b [Å]	9.5076(3)	9.5073(4)	7.3629(2)	9.8089(8)	7.6509(3)	7.8723(2)	11.7093 (3)
c [Å]	16.0492(5)	16.0506(4)	19.2858(5)	14.6636(12)	20.5384(8)	17.2740(3)	14.2353(4)
α [Å]	90	90	90	90	90	90	76.9998(11)
ß [Å]	90	90	108.4870(10)	90	109.285(2)	96.9200(12)	72.3793(11)
γ [Å]	90	90	90	90	90	90	69.8941(6)
V [$Å^3$]	1215.33(6)	1215.44(5)	2450.81(11)	1228.79(18)	2509.90(18)	1300.13(6)	1287.79(7)
ρ_{calc} [g/mm^3]	1.319	1.319	1.665	1.665	1.362	1.508	1.523
μ [mm^{-1}]	0.704	0.704	4.534	3.338	0.779	1.117	1.128
Radiation Type	Cu	Cu	Cu	Cu	Cu	Cu	Cu
F(000)	512	512	1236	616	1088	608	608
no of measured refl.	7249	9006	34112	9446	15458	15086	16410
no of indep. refl.	2119	2206	4323	2719	4309	2304	4407
no of refl. (I ≥ 2σ)	2077	2165	3735	2542	3820	2001	4025
Resolution [Å]	0.84	0.84	0.84	0.84	0.84	0.84	0.84
R1/wR2 (I ≥ 2σ)[a] [%]	2.77/6.79	2.66/6.56	3.21/7.78	0.00/4.25	0.000/28.73	4.50/11.28	3.51/8.72
R1/wR2 (all data)[%]	2.83/6.84	2.72/6.61	3.84/8.22	0.001/4.36	0.000/29.02	5.08/11.69	3.83/8.93

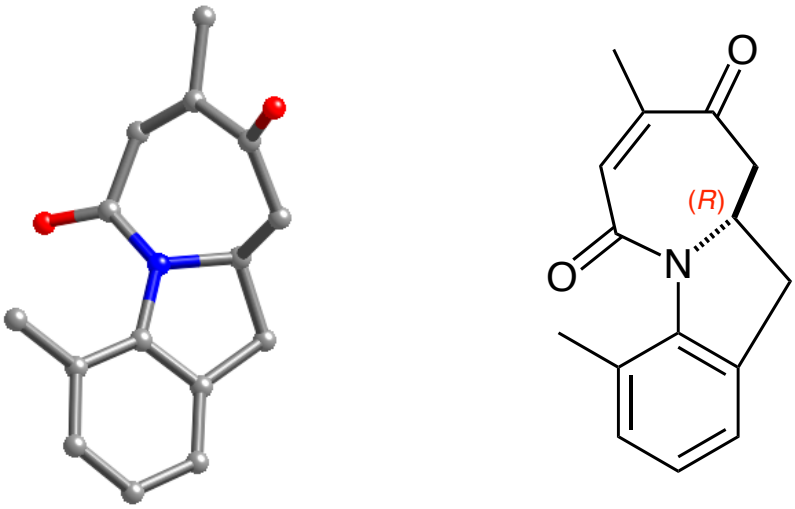

Figure 3.13: Photoproduct (*10R*)-**206b** (crystallized from hexanes:$CHCl_3$).

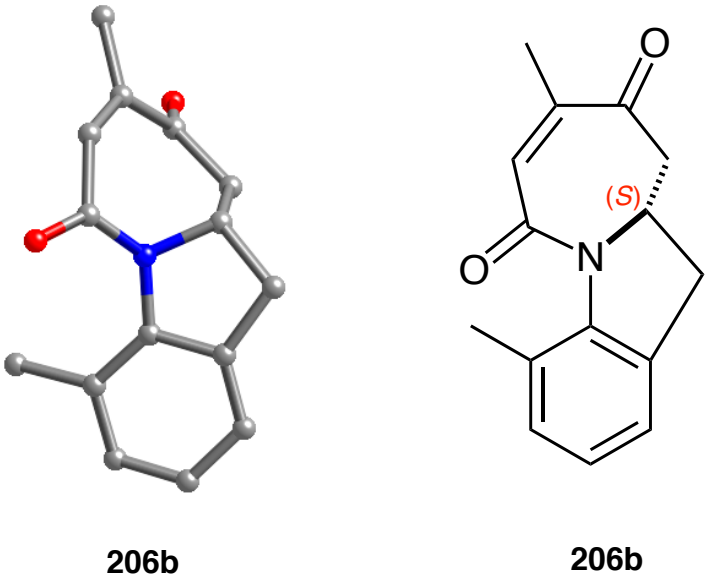

Figure 3.14: Photoproduct (*10S*)-**206b** (crystallized from hexanes:$CHCl_3$).

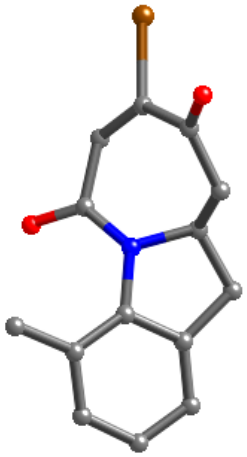

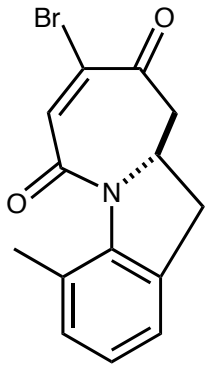

206c **206c**

Figure 3.15: Photoproduct **206c** (crystallized from hexanes:$CHCl_3$).

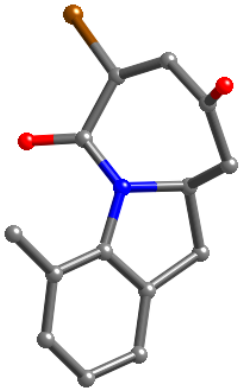

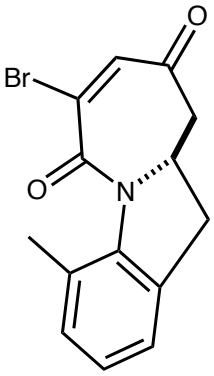

207c **207c**

Figure 3.16: Photoproduct **207c** (crystallized rom hexanes:$CHCl_3$).

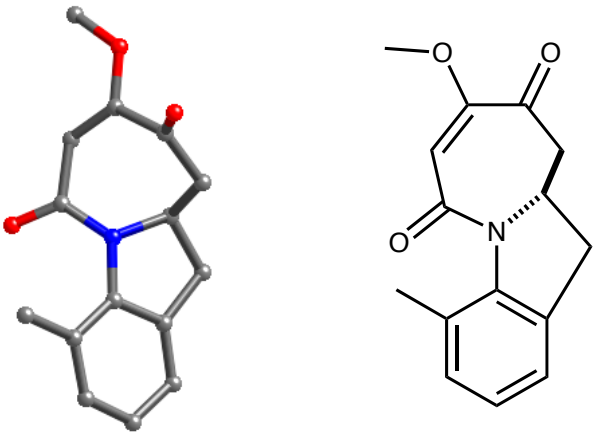

206f **206f**

Figure 3.17: Photoproduct **206f** (crystallized from hexanes:$CHCl_3$).

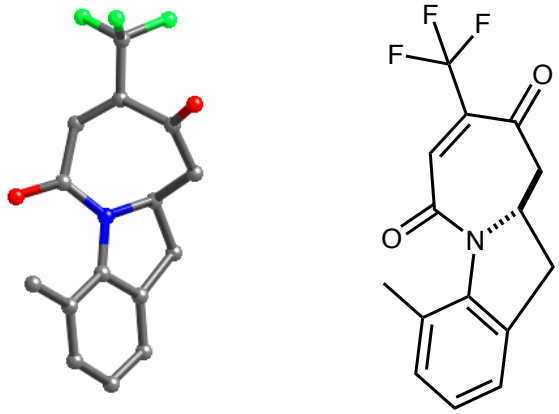

206g **206g**

Figure 3.18: Photoproduct **206g** (crystallized from hexanes:$CHCl_3$).

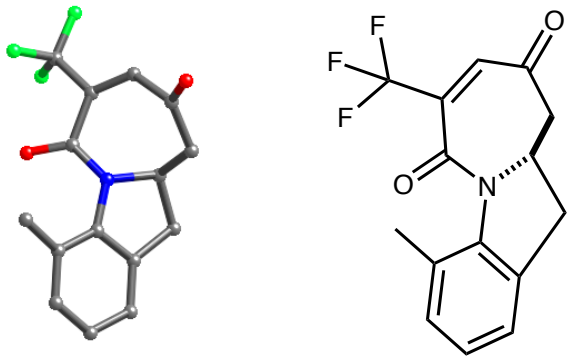

207g **207g**

Figure 3.19: Photoproduct **207g** (crystallized from hexanes:$CHCl_3$).

3.23. Summary and Outlook

The atropisomeric chromophores designed for Paternò-Büchi reaction proceeded smoothly to yield diastereomeric photoproducts. The reactivity and the selectivity was dependent on the degree of overlap of orbital between excited ketone and the electron deficient alkene and the solvent employed for the photoreaction. The conformational aspect of the atropisomeric oxoamides dictates the stereoselectivity. Further, the diastereoselectivity was easily reversed by simply switching the reaction medium from solution to solid-state conditions.

The [2+2]-photocycloaddition of maleimides resulted in several interesting features. The control over the chemoselectivity of atropisomeric maleimides ([2+2] vs. [5+2]) was dictated by the chain length of the alkene tether and not on the irradiation conditions as in the case of N-alkenyl maleimides. The substituent on the maleimide and the alkene tether played a crucial role in the regioselectivity of the photoproducts. The photocycloaddition proceeds smoothly under UV/Visible light/ household lamp resulting in diastereomeric products (*exo* and *endo*). The irradiation conditions provided an opportunity to merge the visible light with flow set up, which showed promise in the scalability of the photoreactions. Detailed photophysical experiments gave insights on the excited states, which helped in deciphering the mechanism.

We have also successfully demonstrated the atropisomeric maleimides can be employed for atropselective [5+2] photocycloaddition leading to azepinone type products with high enantioselectivity.

We have also discussed the role of electrons imparted by the substituent R^1 on the maleimide ring in determining the dr values in the photoproducts. Substitution of electron donating group on the maleimide ring lead to complete stereocontrol in the photoproduct. This method opens up avenues for synthesizing enantioenriched azepinone type products.

3.24. Experimental section for atropselective photoreactions

3.24.1. General methods

All commercially obtained reagents/solvents were used as received; chemicals were purchased from Alfa Aesar®, Sigma-Aldrich®, Acros organics®, TCI America®, Mallinckrodt®, and Oakwood® Products, and were used as received without further purification. Unless otherwise stated, reactions were conducted in oven-dried glassware under nitrogen atmosphere. Unless otherwise state demineralized water (DI water) was used for work up procedures. ^{1}H-NMR and ^{13}C-NMR spectra were recorded on Varian 400 MHz (100 MHz for ^{13}C) and on 500 MHz (125 MHz for ^{13}C) spectrometers. Data from the ^{1}H-NMR spectroscopy are reported as chemical shift (δ ppm) with the corresponding integration values. Coupling constants (*J*) are reported in hertz (Hz). Standard abbreviations indicating multiplicity are used as follows: s (singlet), b (broad), d (doublet), t (triplet), q (quartet), m (multiplet) and virt (virtual). Data for ^{13}C NMR spectra are reported in terms of chemical shift (δ ppm). High-resolution mass spectrum data in Electrospray Ionization mode were recorded on a Bruker – Daltronics® BioTof mass spectrometer in positive (ESI+) ion mode. HPLC analyses were performed on Waters® HPLC equipped with 2525 pump or on Dionex® Ultimate 3000 HPLC. Waters® 2767 sample manager was used for automated sample injection on Waters® HPLC or Ultimate 3000 sample injector was used for injection on Dionex® HPLC. All HPLC injections on Waters® HPLC were monitored using a Waters® 2487 dual wavelength absorbance detector at 254 and 270 nm or on Dionex®. HPLC were monitored using a diode array detector (DAD3000125). Analytical and semi-preparative injections were performed on chiral stationary phase using various columns as indicated below.

i) Regis® PIRKLE COVALENT (*R*,*R*) WHELK–01

a) 25 cm x 4.6 mm column for analytical injections.

b) 25 cm x 10 mm column for semi-preparative injections.

ii) CHIRACEL® OD-H

a) 0.46 cm x 25 cm column for analytical injections.

b) 10 mm x 25 cm column for semi-preparative injections.

iii) CHIRALPAK® IC

a) 0.46 cm x 25 cm column for analytical injections.

b) 10 mm x 25 cm column for semi-preparative injections

iv) CHIRALPAK® AD-H

a) 0.46 cm x 15 cm column for analytical injections.

b) 10 mm x 25 cm column for semi-preparative injections.

v) CHIRALCEL – OD-3

a) 0.46 cm x 15 cm column for analytical injections.

vi) CHIRAPAK – AD-3

a) 0.46 cm x 15 cm column for analytical injections.

Masslynx software version 4.1 was used to monitor/analyze the HPLC injections on Waters® and to process HPLC traces. Chromeleon 7 software was used to monitor and process HPLC injections on Dionex® HPLC. Igor Pro® Software version 6.0 was used to process the HPLC graphics. Optical activity values were recorded on JASCO® DIP – 370 digital polarimeter. When necessary, the compounds were purified by combiflash equipped with dual wavelength UV-Vis absorbance detector (Teledyne ISCO) using hexanes:ethyl acetate as the mobile phase and Redisep® cartridge filled with silica (Teledyne ISCO) as stationary phase. In some cases, compounds were purified by column chromatography on silica gel (Sorbent Technologies®, silica gel standard grade: porosity 60 Å, particle size: 230 x 400 mesh, surface area: 500 – 600 m^2/g, bulk density: 0.4 g/mL, pH range: 6.5 – 7.5). Unless indicated, the Retardation Factor (R*f*) values were recorded using a 5-50% hexanes:ethyl acetate as mobile phase and on Sorbent Technologies®, silica Gel TLC plates (200 mm thickness w/UV_{254}).

3.25. General procedure for synthesis of α-oxoamide derivative 172 and their precursors

3.25.1. Synthesis of 2-methylenebutanoyl chloride 176b

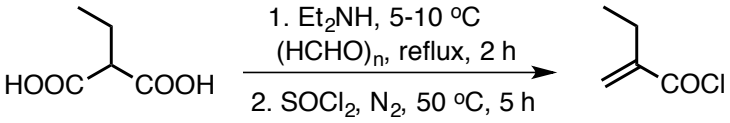

179 **176b**

Scheme 3.29: Synthesis of 2-methylenebutanoyl chloride **176b**.

2-Methylenebutanoyl chloride was synthesized according to the literature reported procedure.[56] To a solution of ethyl malonic acid (**179**)(1.85 g, 1.0 equiv.) in dry ethyl acetate (40 mL) at 0 ^{o}C under N_2 atmosphere diethylamine (2.17 mL, 1.5 equiv.) was added. The mixture was stirred for 5 min followed by the addition of paraformaldehyde (0.67 g, 1.5 equiv) in 2 portions. The resulting mixture was stirred for 5 mins and then moved to oil bath where it was refluxed for 2 h. The mixture was cooled to room temperature and quenched with water. The pH of the solution was adjusted to 1 by carefully adding c*onc.* HCl and extracted with ethyl acetate (3 X 15 mL). The combined organic layer was dried over *anhy.* Na_2SO_4, filtered and the solvent was removed under reduced pressure to yield crude product as pale yellow oil. The crude product was directly taken to next stage without further purification.

To the crude product under N_2 atmosphere added thionyl chloride (1.54 mL, 1.0 equiv.). The mixture was heated to 50 °C and maintained for 3 h. After 3 h, the excess thionyl chloride was removed under reduced pressure while the temperature was maintained at 25 °C. The vacuum was released under N_2 and the residue was taken up in DCM and directly taken to next step without further analysis or purification.

3.25.2. Synthesis of phenylglyoxalyl chloride 177

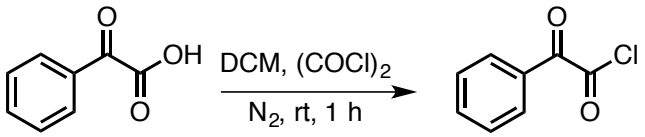

178 **177**

Scheme 3.30: Synthesis of phenylglyoxalyl chloride **177**.

To a solution of phenylglyoxylic acid (**178**) (1.1 g, 7.33 mmol, 1.0 equiv.) in DCM (10 mL) at room temperature added a two drops of DMF (catalytic). To this solution oxalyl chloride (2.5 equiv) was slowly added during which white effervescence was observed. The mixture was further stirred for 1 h and the solvent and excess oxalyl chloride was removed under reduced pressure while the temperature was maintained at 25 °C. The vacuum was released under N_2 and the residue was taken up in DCM and directly taken to next step without further analysis or purification.

3.25.3. Synthesis of substituted amide derivatives 175a-c

180a-c **176a-b** **175a-c**

Scheme 3.31: Synthesis of substituted amide derivatives **175a-c**.

To a solution of aniline (1.0 g, 1.0 equiv), triethylamine (2.0 equiv) in dry DCM (15 mL) at 0 °C under N_2 atmosphere corresponding acyl chloride (1.1 equiv) was added. The resulting solution was slowly allowed to warm to room temperature over 6 h. After the reaction, water was added, stirred and the layers were separated. The organic layer was washed with DM water (2 X 15 mL), dried over *anhy.* Na_2SO_4, filtered and the solvent was removed under reduced pressure to yield crude product. The crude product was purified by combiflash using hexanes:ethyl acetate mixture.

TLC condition - R_f = 0.32 (80% hexanes:20% ethyl acetate) for **175a** (Yield = 85 %)

TLC condition - R_f = 0.28 (50% hexanes:50% ethyl acetate) for **175b** (Yield = 76 %)

TLC condition - R_f = 0.52 (50% hexanes:50% ethyl acetate) for **175c** (Yield = 93 %)

^{1}H-NMR (400 MHz, $CDCl_3$, δ ppm): 7.76 (s, 1H), 7.57 (bs, 1H), 7.31-7.29 (m, 1H), 7.17-7.13 (m, 1H), 5.83 (s, 1H), 5.46 (s, 1H), 2.08 (s, 3H), 1.39 (s, 9H) and 1.297 (s, 9H).

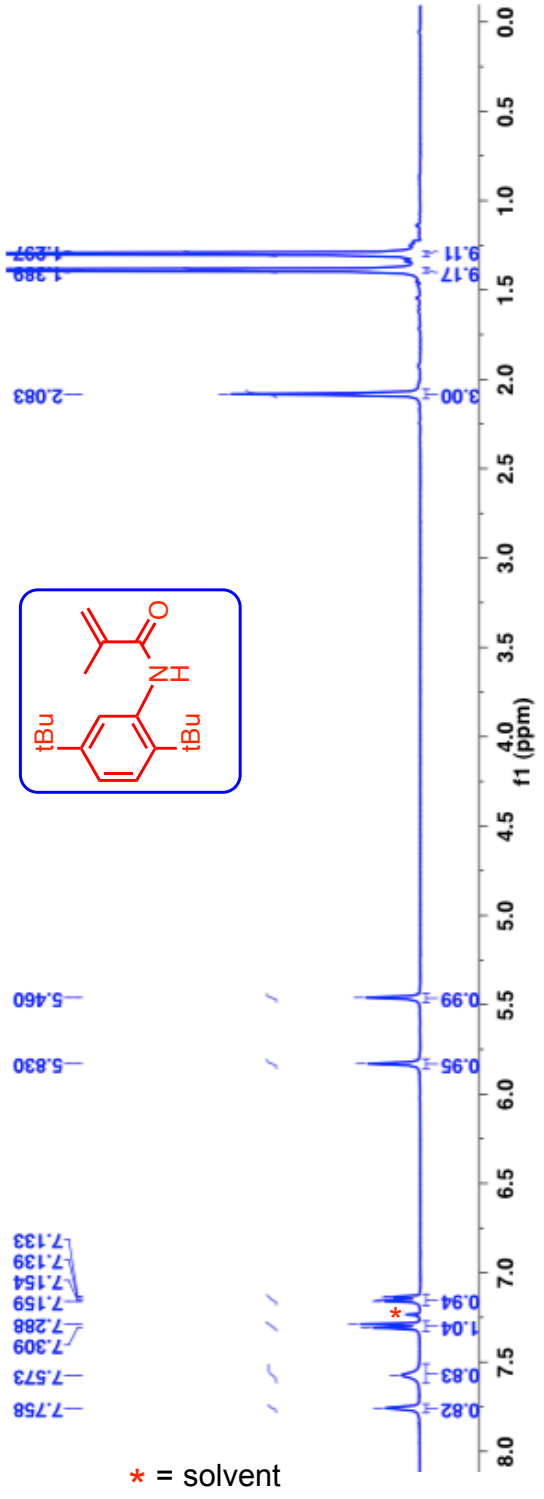

Figure 3.20: ^{1}H-NMR (400 MHz, $CDCl_3$, δ ppm) spectrum 2,5 di-*tert*-butylphenyl methacrylamide **175a**.

^{13}C-NMR (100 MHz, $CDCl_3$, δ ppm): 166.5, 149.9, 141.3, 138.9, 135.0, 126.3, 124.4, 122.9, 119.9, 34.5, 34.3, 31.4, 30.9 and 19.2.

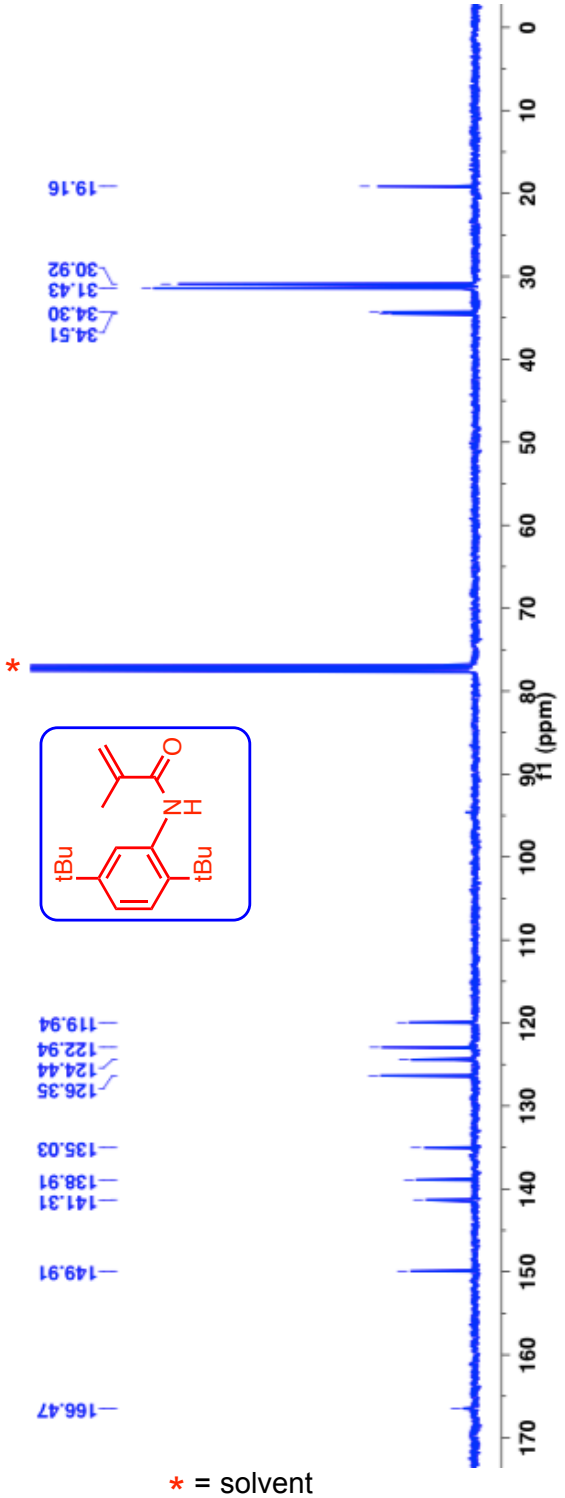

Figure 3.21: ^{13}C-NMR (100 MHz, $CDCl_3$, δ ppm) spectrum 2,5 di-*tert*-butylphenyl methacrylamide **175a**.

^{1}H-NMR (400 MHz, $CDCl_3$, δ ppm): 7.65-7.63 (m, 1H), 7.57 (bs, 1H), 7.38-7.36 (m, 1H), 7.23-7.11 (m, 2H), 5.72 (s, 1H), 5.39 (s, 1H), 2.43 (q, *J*=7.2 Hz, 2H) 1.39 (s, 9H) and 1.13 (t, *J*=7.2 Hz, 3H).

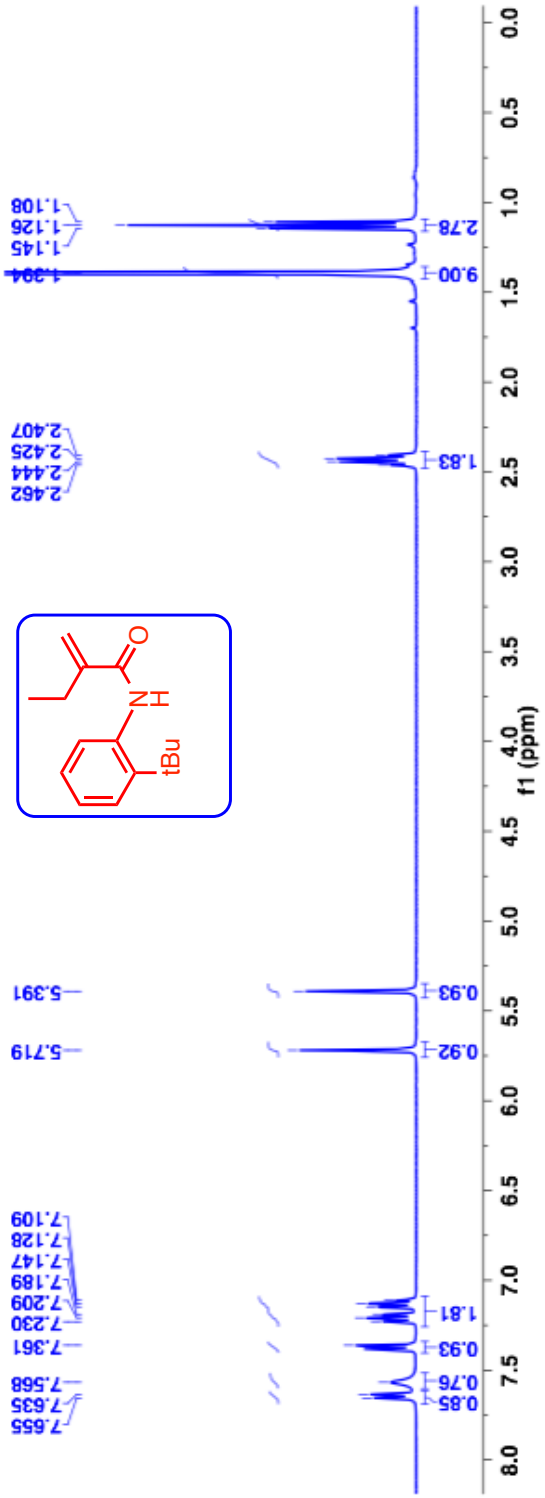

Figure 3.22: ^{1}H-NMR (400 MHz, $CDCl_3$, δ ppm) spectrum 2-*tert*-butylphenyl ethacrylamide **175b**.

^{13}C-NMR (100 MHz, $CDCl_3$, δ ppm): 167.2, 148.3, 142.4, 135.4, 127.7, 127.0, 126.7, 126.2, 116.7, 34.7, 30.8, 25.7 and 12.7.

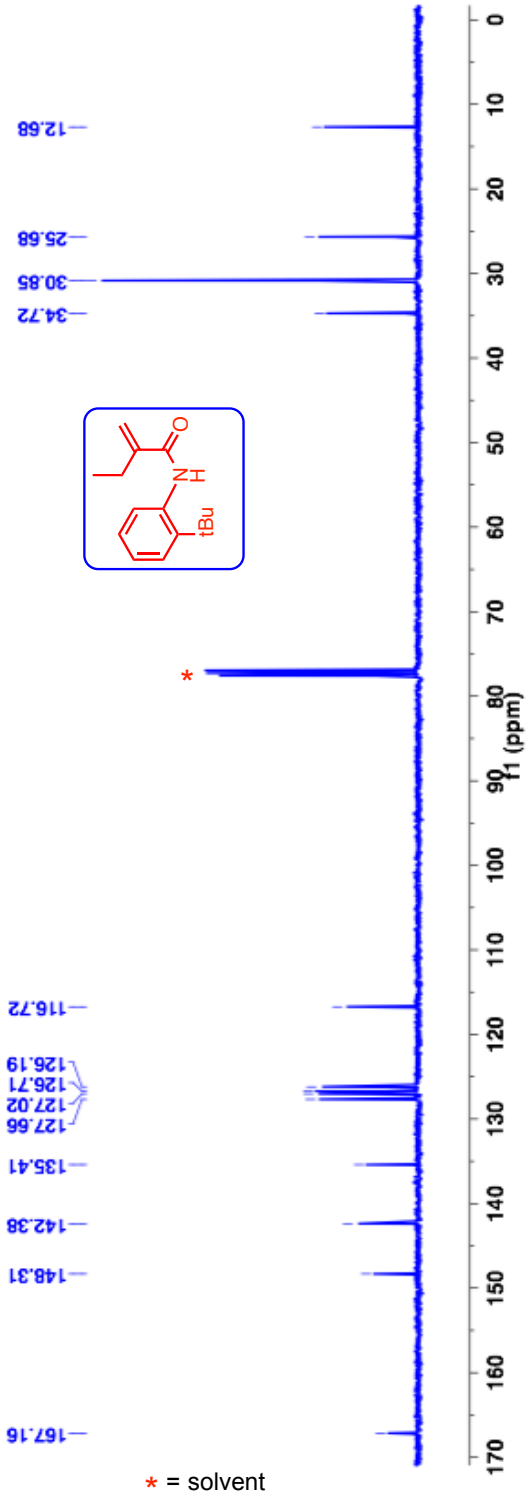

Figure 3.23: ^{13}C-NMR (100 MHz, $CDCl_3$, δ ppm) spectrum 2-*tert*-butylphenyl ethacrylamide **175b**.

HRMS-ESI (m/z) ([M + Na]$^+$):

Calculated : 254.1515

Observed : 254.1513

|Δm| : 0.8 ppm

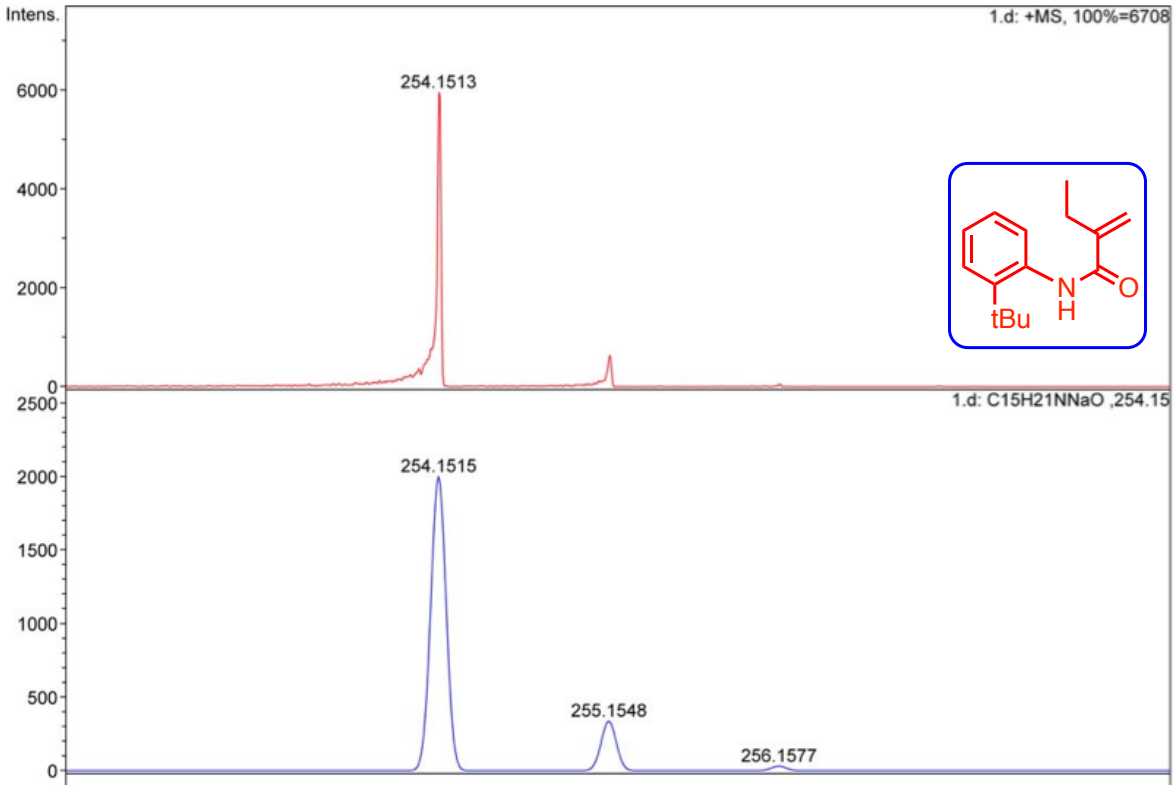

Figure 3.24: HRMS of 2-*tert*-butylphenyl ethacrylamide **175b**.

^{1}H-NMR (400 MHz, $CDCl_3$, δ ppm): 7.69 (bs, 1H), 7.55-7.53 (m, 2H), 7.30-7.26 (m, 2H), 7.098-7.06 (m, 1H), 5.75 (s, 1H), 5.40 (s, 1H) and 2.01 (s, 3H).

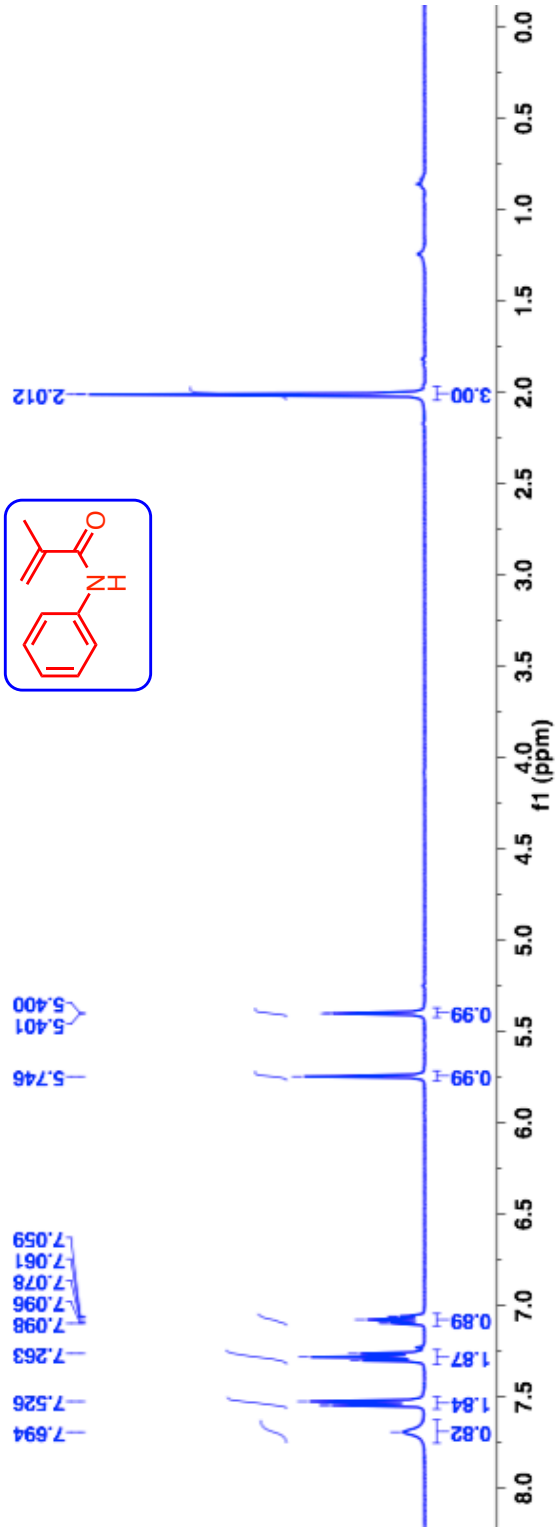

Figure 3.25: ^{1}H-NMR (400 MHz, $CDCl_3$, δ ppm) spectrum Phenyl methacrylamide **175c**.

^{13}C-NMR (100 MHz, $CDCl_3$, δ ppm): 166.96, 141.1, 138.0, 129.1, 124.6, 120.3, 120.0 and 18.96.

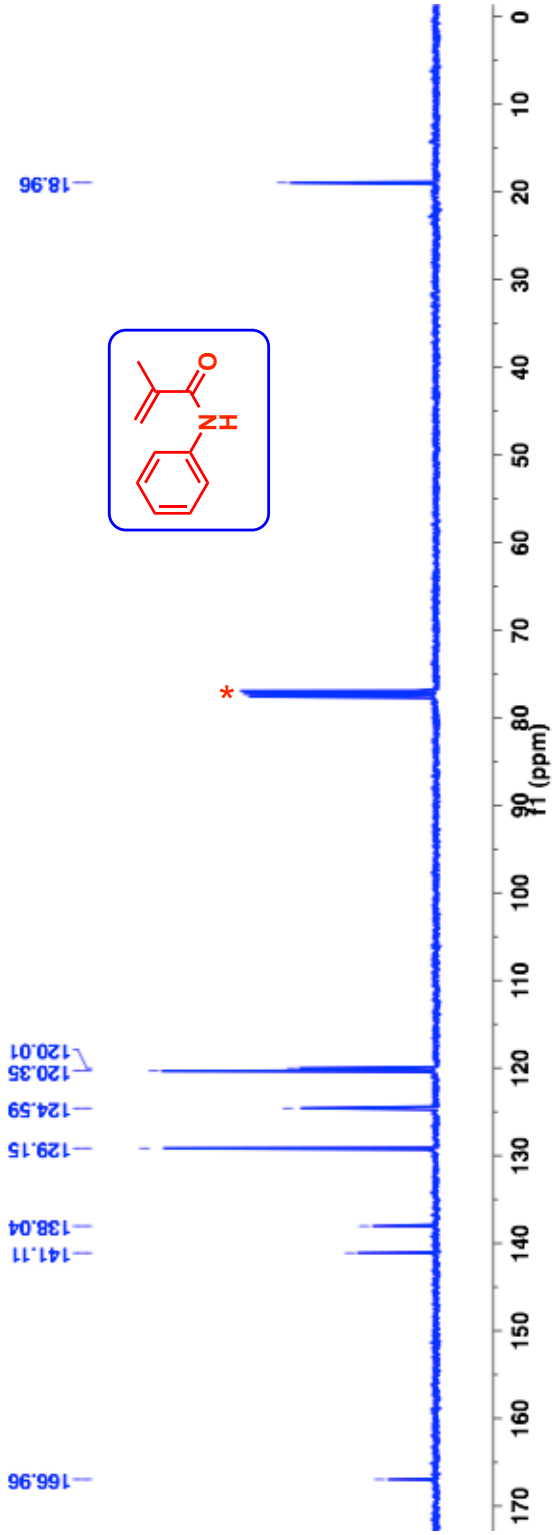

* = solvent

Figure 3.26: ^{13}C-NMR (100 MHz, $CDCl_3$, δ ppm) spectrum Phenyl methacrylamide **175c**.

3.25.4. Synthesis of α-oxoamides derivatives 172a-c

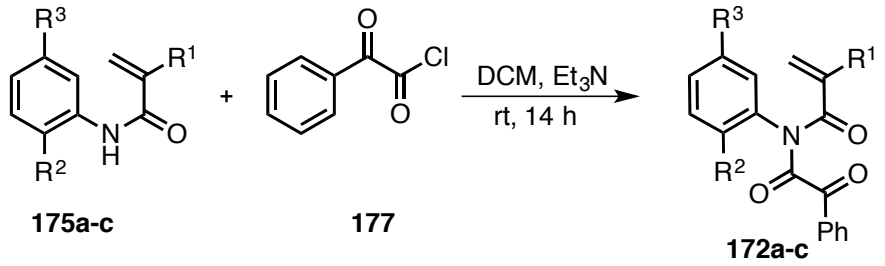

Scheme 3.32: Synthesis of substituted amide derivatives **172a-c**.

To a solution of corresponding amide (**175 a-c**) (1.0 g, 1.0 equiv.) in dry DCM (15 mL) at 0 °C under N_2 atmosphere triethylamine (2.3 equiv.) was added followed by the addition of corresponding acid chloride (**177**) (2.0 equiv.). The resulting solution was slowly allowed to warm to room temperature over 14 h. After the reaction, water was added, stirred and the layers were separated. The organic layer was washed with DM water (2 X 15 mL), dried over *anhy.* Na_2SO_4, filtered and the solvent was removed under reduced pressure to yield crude product. The crude product was purified by combiflash using hexanes:ethyl acetate mixture.

TLC condition - R_f = 0.43 (80% hexanes:20% ethyl acetate) for **172a** (Yield = 84 %)

TLC condition - R_f = 0.33 (50% hexanes:50% ethyl acetate) for **172b** (Yield = 64 %)

TLC condition - R_f = 0.32 (50% hexanes:50% ethyl acetate) for **172c** (Yield = 70 %)

^{1}H-NMR (400 MHz, $CDCl_3$, δ ppm): 8.01-7.98 (m, 2H), 7.62-7.59 (m, 1H), 7.52-7.48 (m, 3H), 7.41-7.38 (m, 1H), 5.42 (s, 1H), 5.28- 5.28 (m, 1H), 1.80-1.799 (m, 3H), 1.399 (s, 9H) and 1.29 (s, 9H).

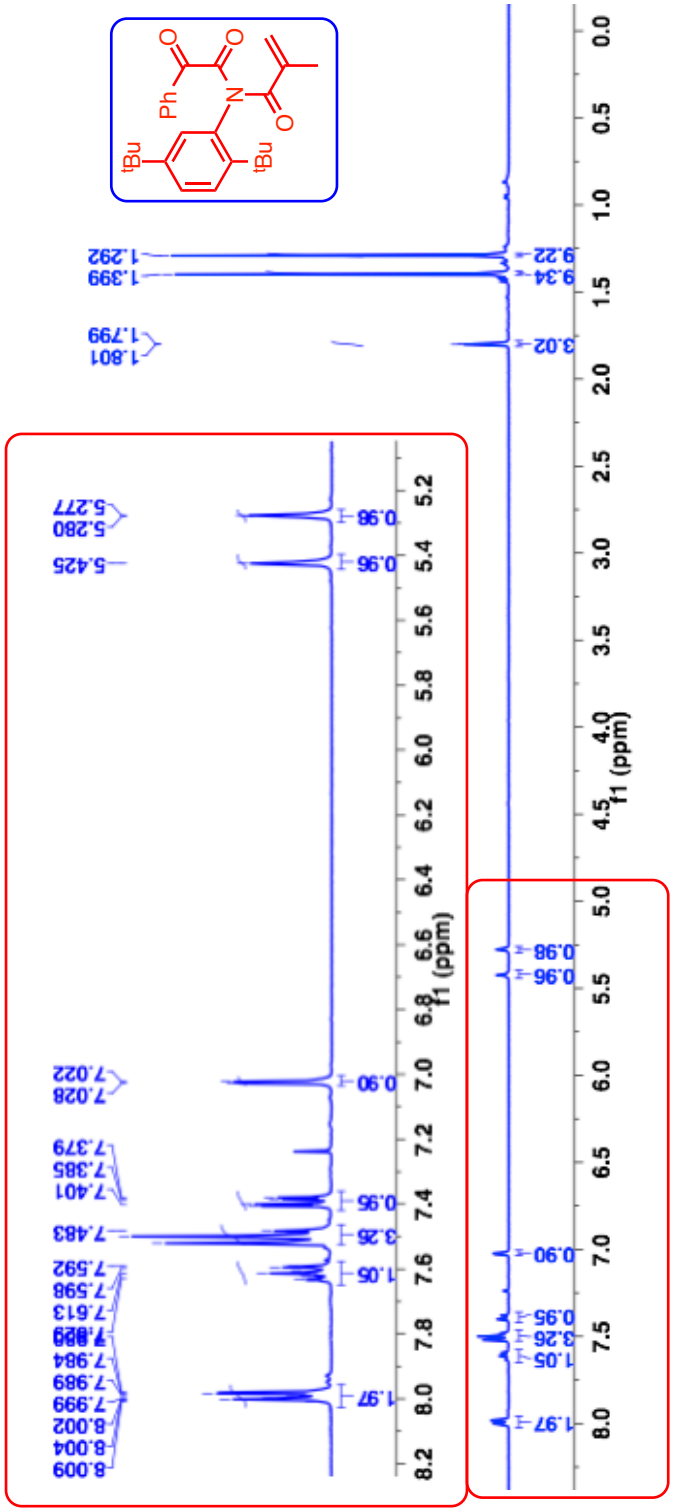

Figure 3.27: ^{1}H-NMR (400 MHz, $CDCl_3$, δ ppm) spectrum of oxoamide derivative **172a**.

^{13}C-NMR (100 MHz, $CDCl_3$, δ ppm): 186.7, 172.6, 170.96, 150.5, 144.8, 141.0, 135.9, 134.4, 133.3, 129.9, 129.4, 129.0, 128.7, 126.8, 125.7, 125.6, 125.2, 35.8, 34.4, 32.0, 31.3 and 19.9.

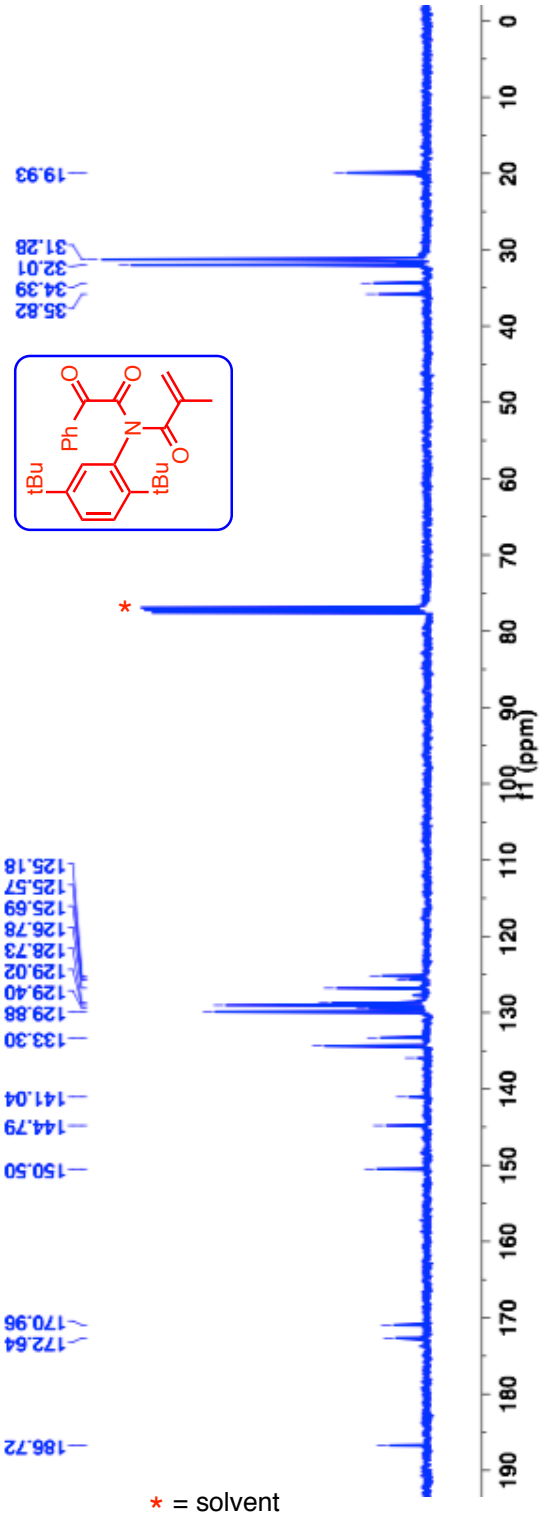

Figure 3.28: ^{13}C-NMR (100 MHz, $CDCl_3$, δ ppm) spectrum of oxoamide derivative **172a**.

HRMS-ESI (m/z) ([M + Na]$^+$):

Calculated : 428.2196

Observed : 428.2201

|Δm| : 1.2 ppm

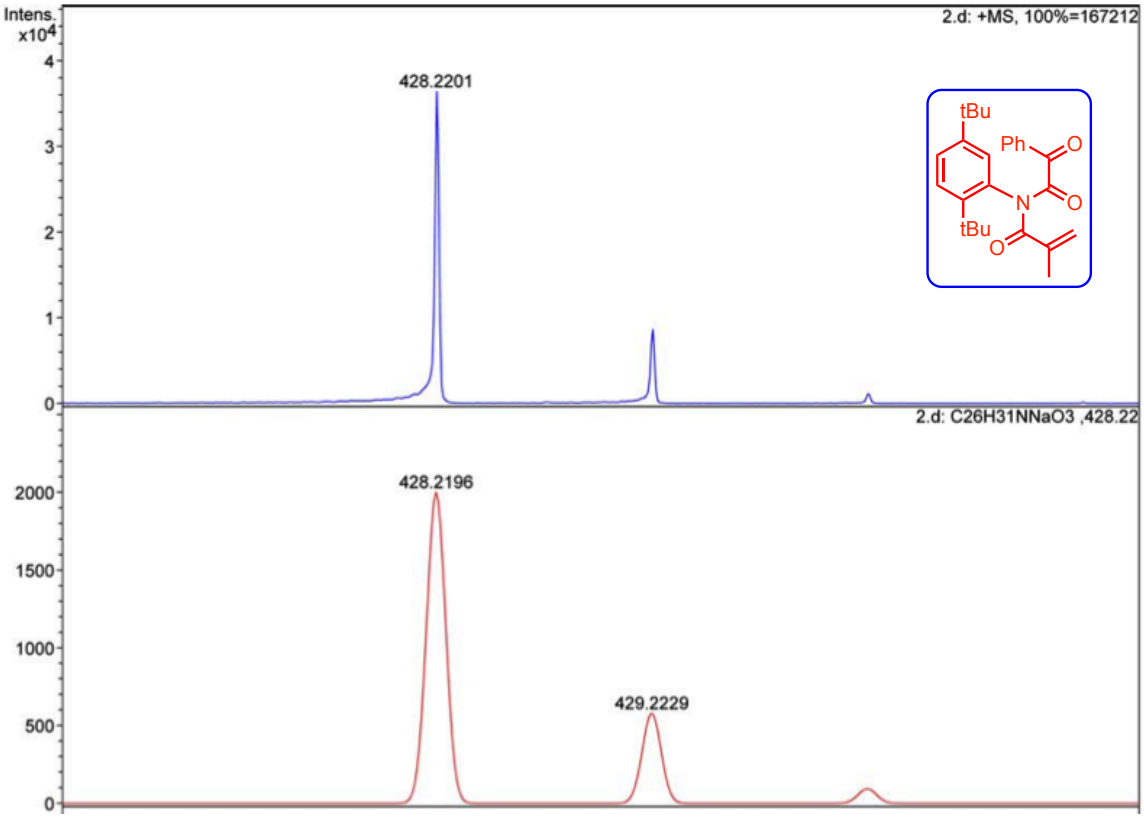

Figure 3.29: HRMS of oxoamide derivative **172a**.

HPLC analysis conditions:

For analytical conditions,

I). Column : (*R*,*R*) WHELK–01

Abs. detector wavelength : 254 nm and 270 nm

Mobile phase : Hexanes:2-propanol = 95:5

Flow rate : 1.0 mL/min

Retention times (min) : ~ (-)-9.44 and ~ (+)-11.98

For preparative conditions,

I). Column : (*R*,*R*) WHELK–01

Abs. detector wavelength : 254 nm and 270 nm

Mobile phase : Hexanes:2-propanol = 95:5

Flow rate : 3.0 mL/min

Retention times (min) : ~ (-)-14.0 and ~ (+)-17.37

Optical rotation $[\alpha]_D^{22}$:

HPLC retention time (*R*,*R*) WHELK–01 at ~ 9.44 min, (*c* ≈ 0.772 %, MeOH) = -22.05 deg.

HPLC retention time (*R*,*R*) WHELK–01 at ~ 11.98 min, (*c* ≈ 0.772 %, MeOH) = +22.91 deg.

^{1}H-NMR (400 MHz, $CDCl_3$, δ ppm): 8.01-7.99 (m, 2H), 7.61-7.59 (m, 2H), 7.51-7.47(m, 2H), 7.41-7.36 (m, 1H), 7.29-7.287 (m, 1H), 7.10-7.08 (m, 1H), 5.49 (s, 1H), 5.23 (t, *J*=1.6 Hz, 1H) 2.35-2.12 (m, 2H), 1.43 (s, 9H) and 0.92 (t, *J*= 7.4 Hz, 3H).

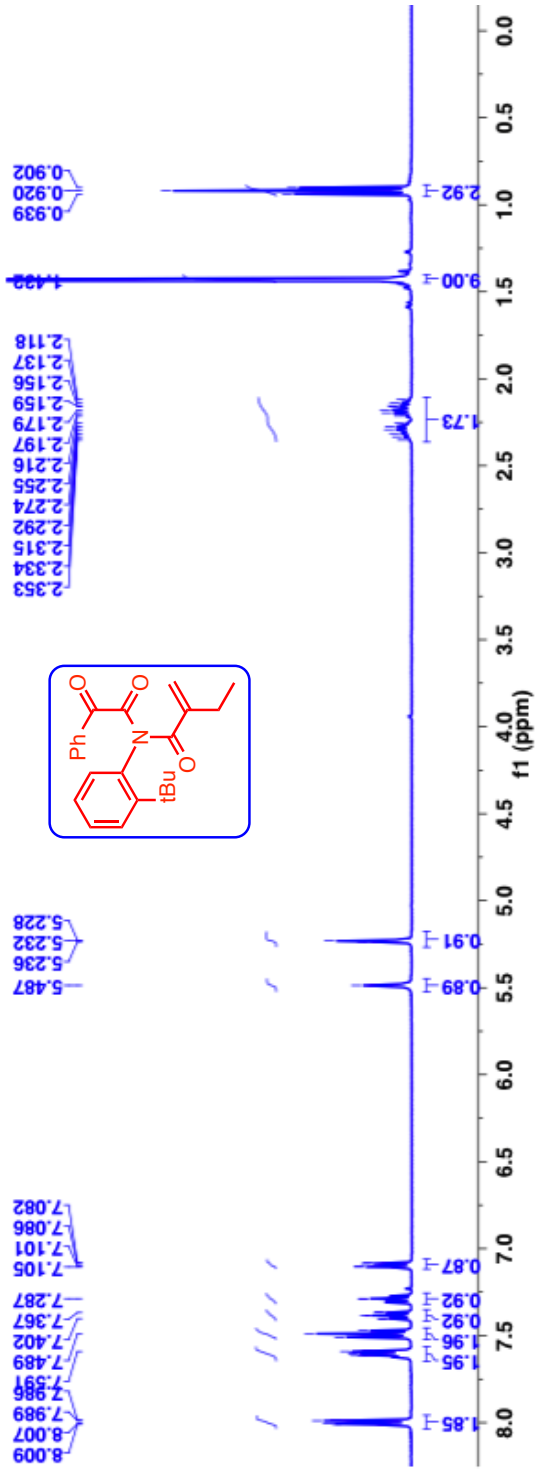

Figure 3.30: ^{1}H-NMR (400 MHz, $CDCl_3$, δ ppm) spectrum of oxoamide derivative **172b**.

^{13}C-NMR (100 MHz, $CDCl_3$, δ ppm): 186.6, 172.8, 170.7, 148.0, 147.0, 146.9, 135.1, 134.5, 133.3, 131.7, 129.9, 129.7, 129.1, 127.6, 122.7, 36.2, 31.98, 25.7 and 11.5.

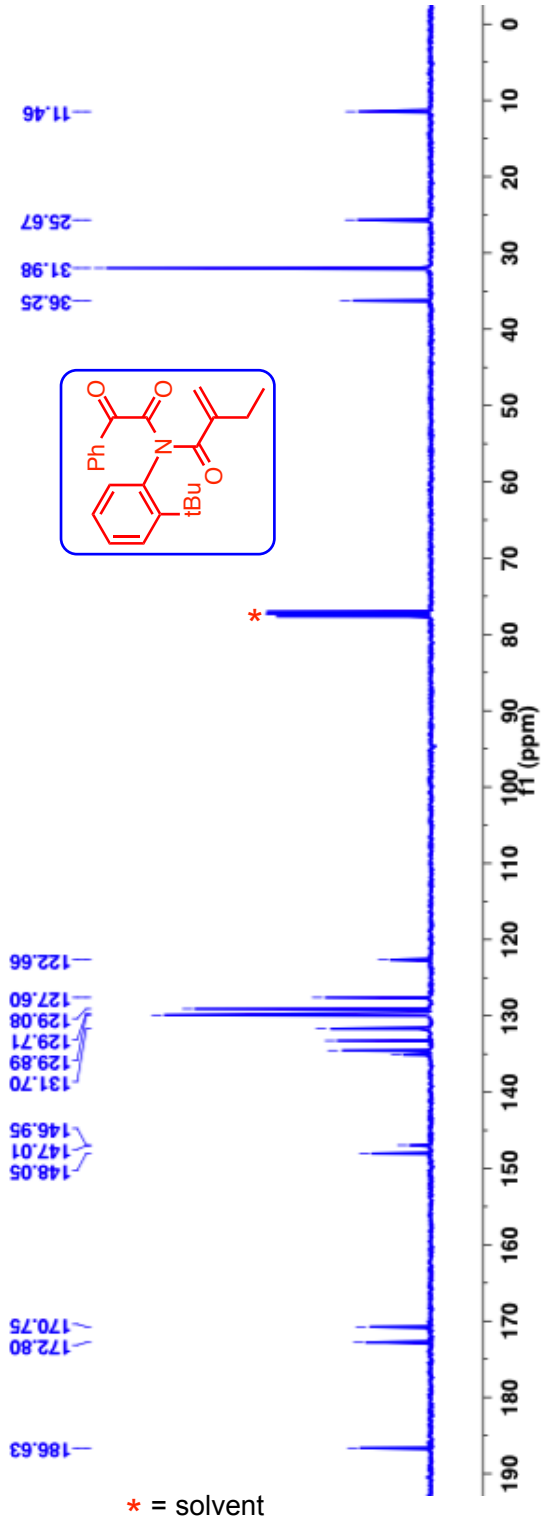

Figure 3.31: ^{13}C-NMR (100 MHz, $CDCl_3$, δ ppm) spectrum of oxoamide derivative **172b**.

HRMS-ESI (m/z) ([M + Na]$^+$):

Calculated : 386.1727

Observed : 386.1730

|Δm| : 0.8 ppm

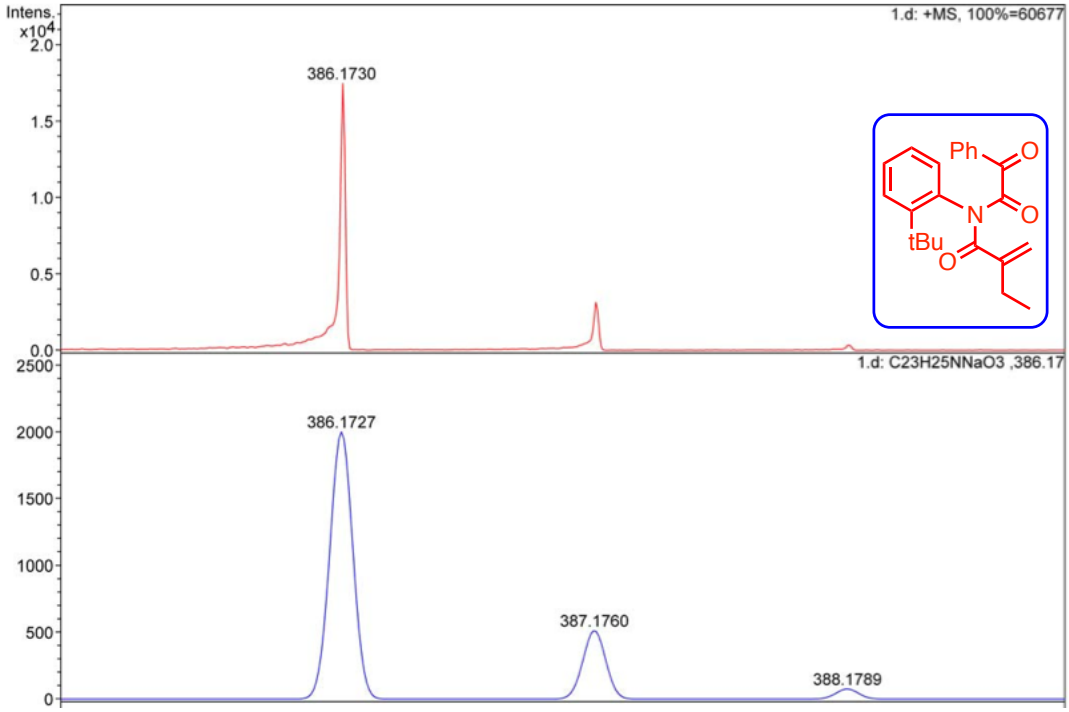

Figure 3.32: HRMS of oxoamide derivative **172b**.

HPLC analysis conditions:

For analytical conditions,

I). Column : CHIRALPAK-AD-H

Abs. detector wavelength : 254 nm and 270 nm

Mobile phase : Hexanes:2-propanol = 90:10

Flow rate : 1.0 mL/min

Retention times (min) : ~ 5.66 [*M*-(-)-**172b**] and 13.58 [*P*-(+)-**172b**]

For preparative conditions,

I). Column : CHIRALPAK-AD-H

Abs. detector wavelength : 254 nm and 270 nm

Mobile phase : Hexanes:2-propanol = 95:5

Flow rate : 3.0 mL/min

Retention times (min) : ~ 10.80 [*M*-(-)-**172b**] and ~ 29.77 [*P*-(+)-**172b**]

(The absolute crystal structure was obtained by single crystal XRD using Flack parameters)

Optical rotation $[\alpha]_D^{22}$:

HPLC retention time CHIRALPAK-AD-H at ~ 5.66 min, (*c* ≈ 2.00 %, MeOH) = -65.06 deg.

HPLC retention time CHIRALPAK-AD-H at ~ 13.58 min, (*c* ≈ 2.00 %, MeOH) = +64.08 deg.

^{1}H-NMR (400 MHz, $CDCl_3$, δ ppm): 7.99-7.97 (m, 2H), 7.598-7.58 (m, 1H), 7.50-7.38 (m, 5H), 7.23-7.21 (m, 2H), 5.55 (s, 1H), 5.38 (s, 1H) and 1.74 (m, 3H).

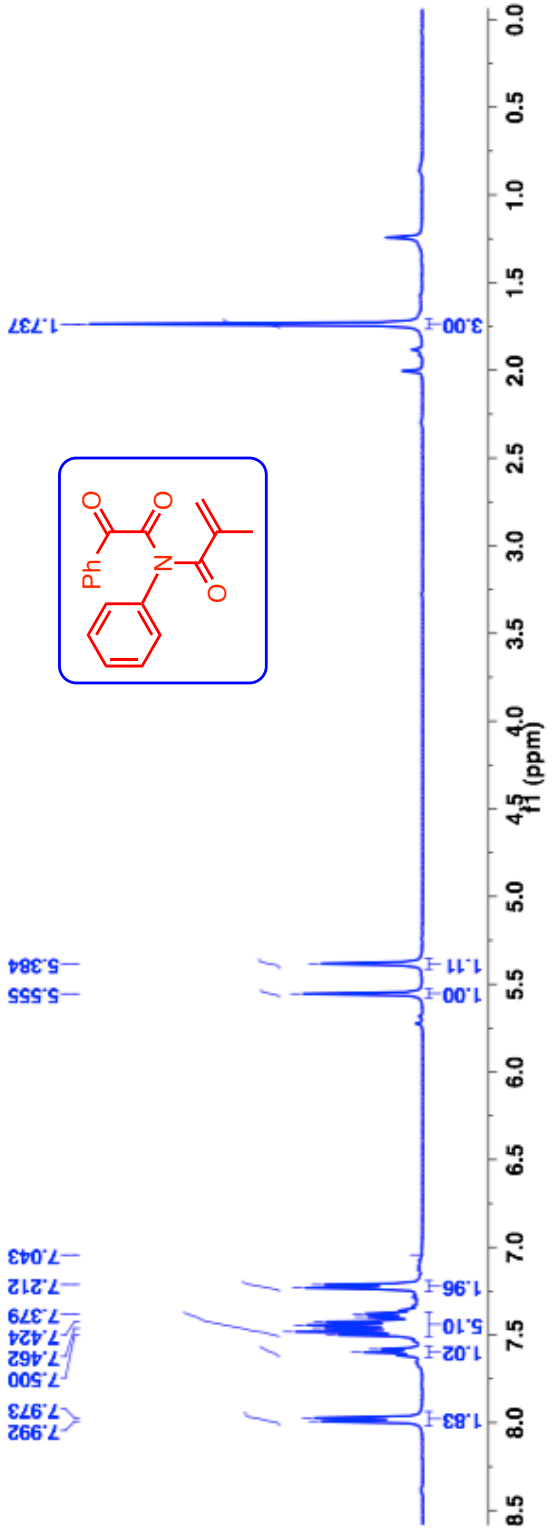

Figure 3.33: ^{1}H-NMR (400 MHz, $CDCl_3$, δ ppm) spectrum of oxoamide derivative **172c**.

^{13}C-NMR (100 MHz, $CDCl_3$, δ ppm): 187.4, 173.2, 169.99, 139.3, 136.8, 134.5, 132.97, 130.0, 129.8, 129.0, 128.99, 127.9, 126.6 and 18.96.

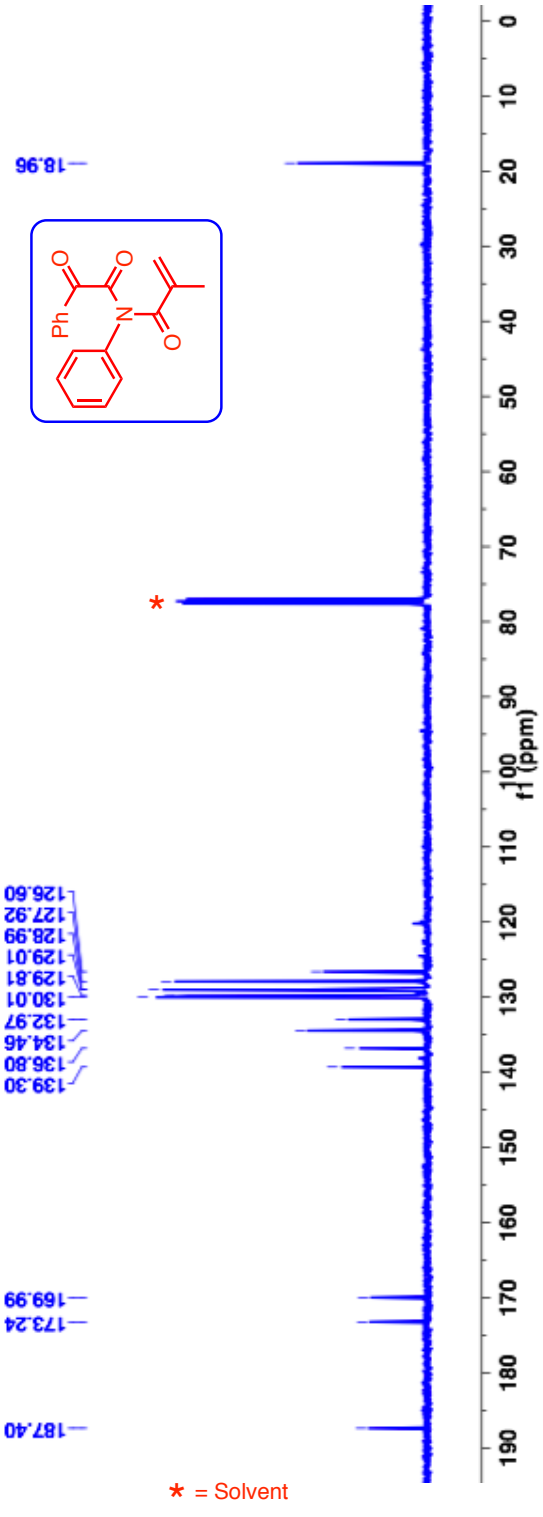

Figure 3.34: ^{13}C-NMR (100 MHz, $CDCl_3$, δ ppm) spectrum of oxoamide derivative **172c**.

3.26. General irradiation procedure Paternò-Büchi reaction of atropisomeric α-oxoamides and characterization of photoproducts

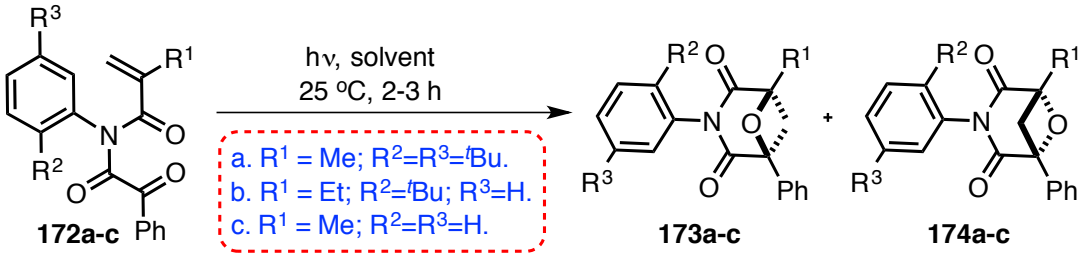

Scheme 3.33: Photoreaction of oxoamide derivatives **172a-c**.

A solution (~ 3 mM concentration/1mg in 1mL) of optically pure axially chiral α-oxoamides **172a-b** and achiral **172c** in benzene or acetonitrile were irradiated at 25 °C for a given time interval in Pyrex tube with a 450 W medium pressure mercury lamp placed inside a water cooled quartz well under a constant flow of nitrogen or in a rayonet reactor equipped with 16 (12 Watt) ~350 nm bulbs under constant flow of nitrogen. After irradiation, the solvent was evaporated under reduced pressure and the photoproducts were isolated by preparative thin layer chromatography. For large scale reactions, the photosylate was purified by combiflash using hexanes:ethyl acetate mixtures. The photoproducts were then characterized by NMR spectroscopy, mass spectrometry, single crystal XRD, $[\alpha]^{T}_{D}$ and HPLC analysis of the photosylate on a chiral stationary phase gave the optical purity of the photoproducts.

Note: For compound **172a** the reaction was monitored by ^{1}H-NMR spectroscopy, as TLC monitoring was difficult due to the overlap of R_f for starting material and the product.

TLC condition - R*f* = 0.56 for **173a** and 0.73 for **174a** respectively (80% hexanes:20% ethyl acetate)

TLC condition - R*f* = 0.46 for **173b** and 0.59 for **174b** respectively (80% hexanes:20% ethyl acetate)

TLC condition - R*f* = 0.24 for **173c** (50% hexanes:50% ethyl acetate)

^{1}H-NMR (400 MHz, $CDCl_3$, δ ppm): 7.55-7.53 (m, 1H), 7.46-7.38 (m, 6H), 6.90 (d, *J*=2 Hz, 1H), 3.50-3.30 (ABq, 2H), 1.74 (s, 3H), 1.36 (s, 9H) and 1.34 (s, 9H).

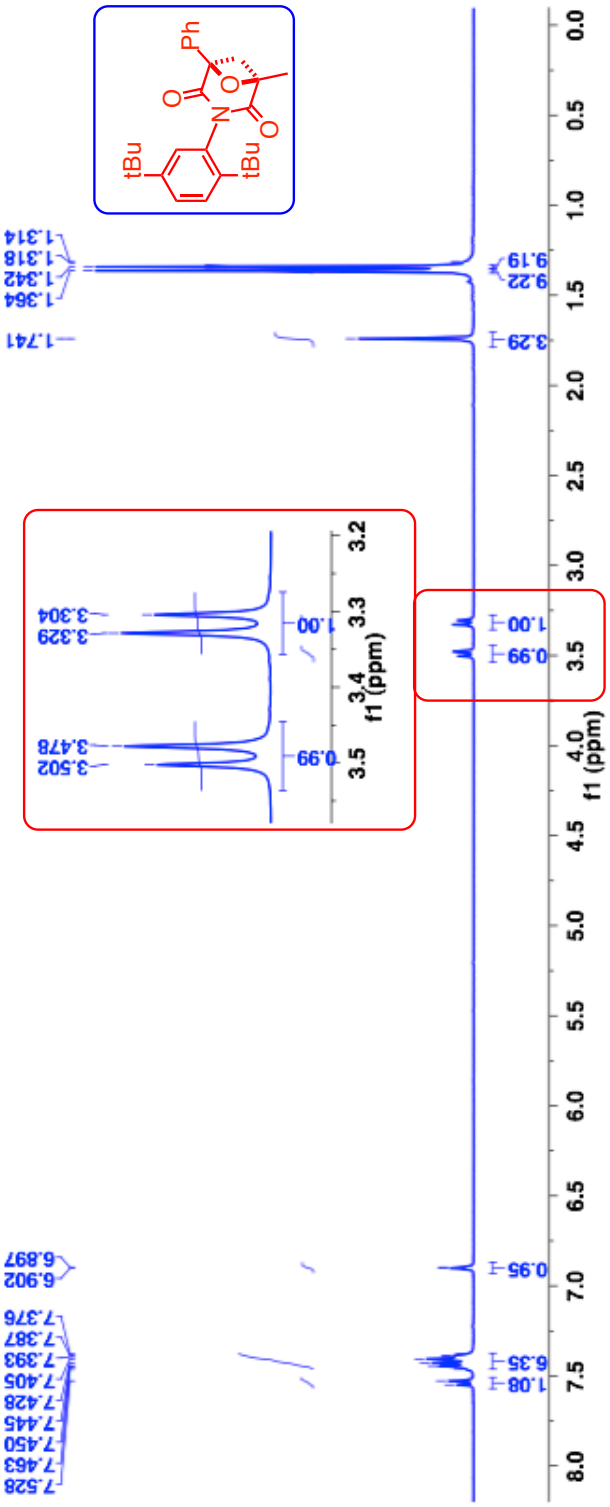

Figure 3.35: ^{1}H-NMR (400 MHz, $CDCl_3$, δ ppm) spectrum of oxetane photoproduct **173a**.

^{13}C-NMR (100 MHz, $CDCl_3$, δ ppm): 173.7, 172.8, 150.4, 145.2, 136.0, 131.1, 129.1, 128.6, 128.5, 127.8, 126.9, 125.7, 84.8, 82.9, 48.3, 35.4, 34.4, 31.7, 31.5 and 20.3.

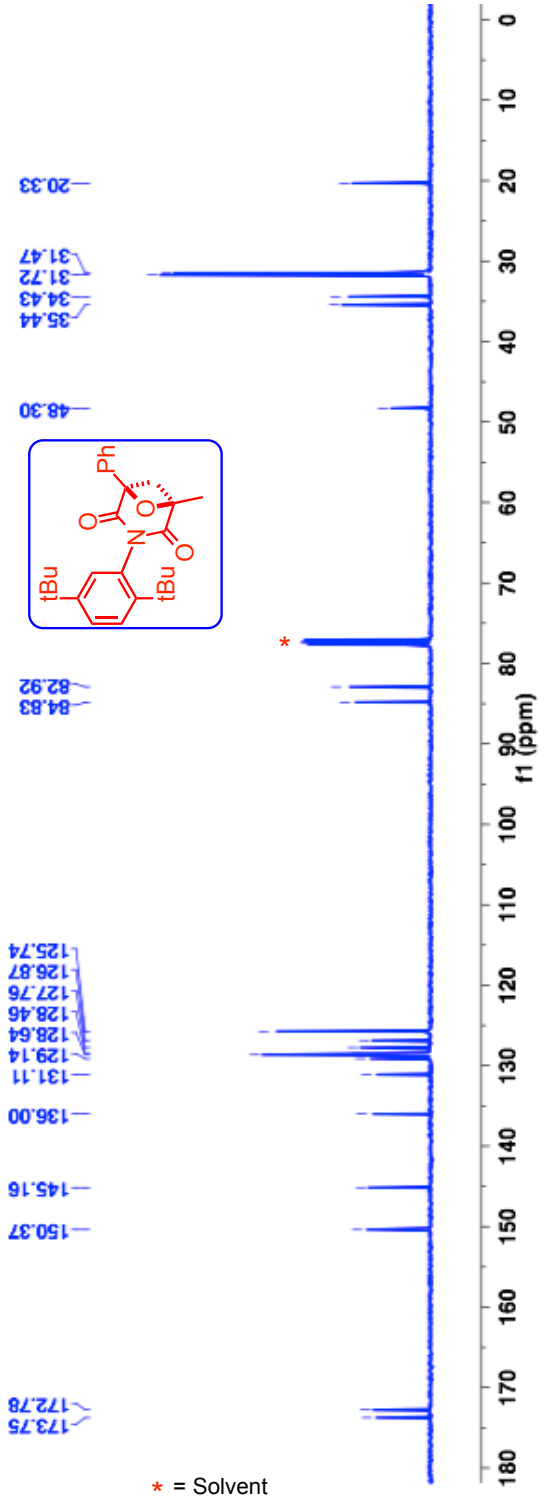

Figure 3.36: ^{13}C-NMR (100 MHz, $CDCl_3$, δ ppm) spectrum of oxetane photoproduct **173a**.

HRMS-ESI (m/z) ([M + Na]$^+$):

Calculated : 428.2196

Observed : 428.2184

|Δm| : 2.8 ppm

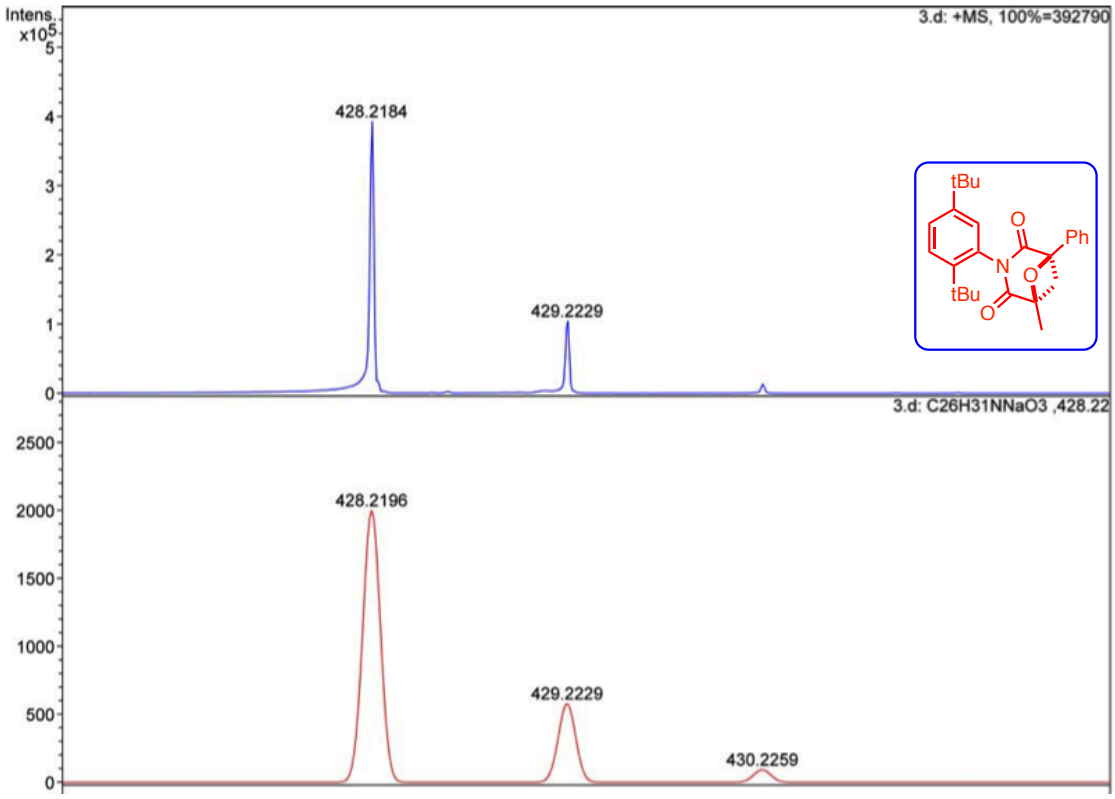

Figure 3.37: HRMS of oxetane photoproduct **173a**.

HPLC analysis conditions:

For analytical conditions,

I). Column : CHIRALPAK-AD-H

Abs. detector wavelength : 254 nm and 270 nm

Mobile phase : Hexanes:2-propanol = 98:2

Flow rate : 1.0 mL/min

Retention times (min) : ~ (+)-4.64 and (-)-7.95

For preparative conditions,

I). Column : CHIRALPAK-AD-H

Abs. detector wavelength : 254 nm and 270 nm

Mobile phase : Hexanes:2-propanol = 99:1

Flow rate : 3.0 mL/min

Retention times (min) : ~ (+)-7.53 and (-)-15.10

Optical rotation $[\alpha]_D^{22}$:

HPLC retention time CHIRALPAK-AD-H at ~ 4.64 min, (*c* ≈ 1.10 %, MeOH) = +22.27 deg.

HPLC retention time CHIRALPAK-AD-H at ~ 7.95 min, (*c* ≈ 1.10 %, MeOH) = -23.41 deg.

^{1}H-NMR (400 MHz, $CDCl_3$, δ ppm): 7.53-7.50 (m, 1H), 7.46-7.38 (m, 6H), 6.92 (d, *J*=2 Hz, 1H), 3.40-3.339 (ABq, 2H), 1.74 (s, 3H), 1.35 (s, 9H) and 1.298 (s, 9H).

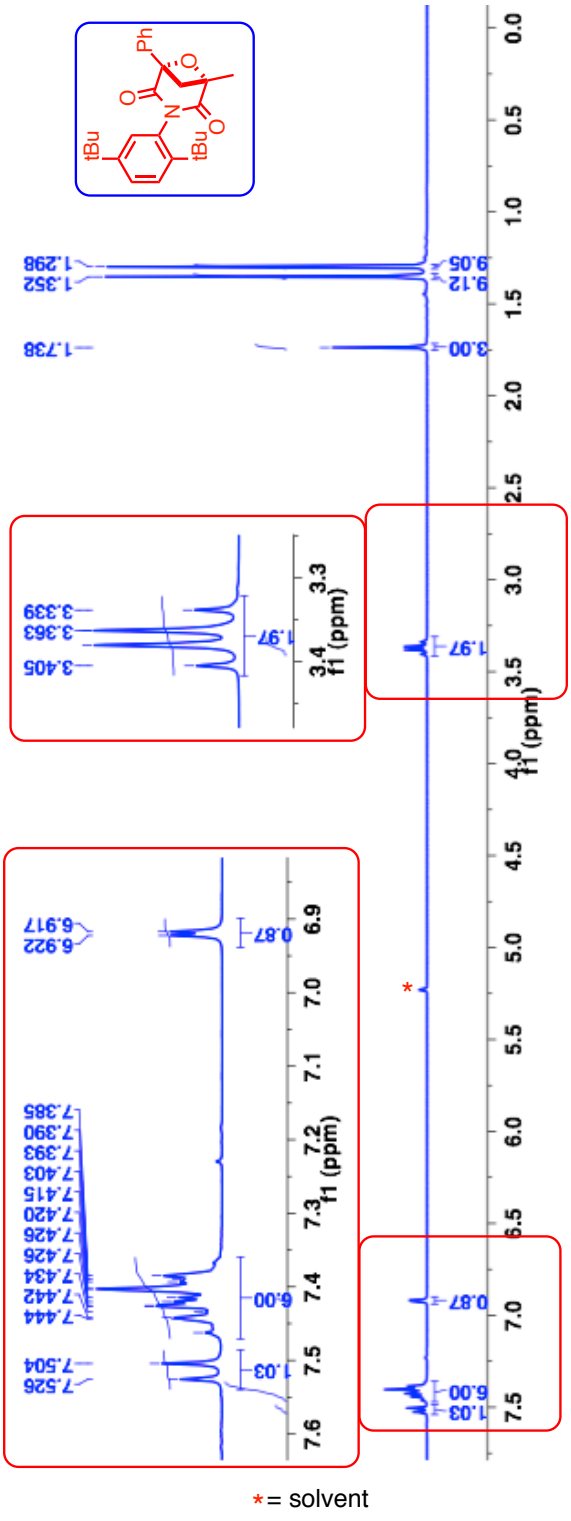

*= solvent

Figure 3.38: ^{1}H-NMR (400 MHz, $CDCl_3$, δ ppm) spectrum of oxetane photoproduct **174a**.

^{13}C-NMR (100 MHz, $CDCl_3$, δ ppm): 173.4, 172.4, 150.6, 144.9, 135.98, 131.1, 129.1, 128.7, 128.6, 127.8, 126.8, 125.6, 84.6, 82.7, 46.2, 35.6, 34.4, 31.96, 31.4 and 20.4.

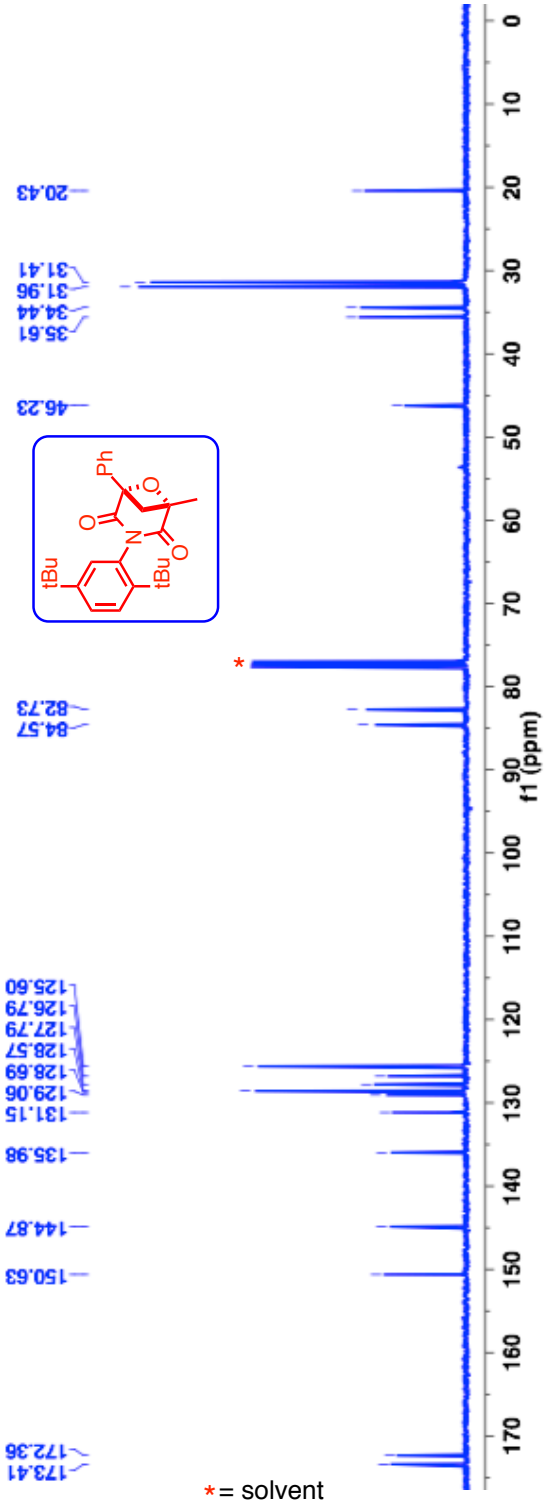

Figure 3.39: ^{13}C-NMR (100 MHz, $CDCl_3$, δ ppm) spectrum of oxetane photoproduct **174a**.

HRMS-ESI (m/z) ([M + Na]$^+$):

Calculated : 428.2196

Observed : 428.2197

|Δm| : 0.2 ppm

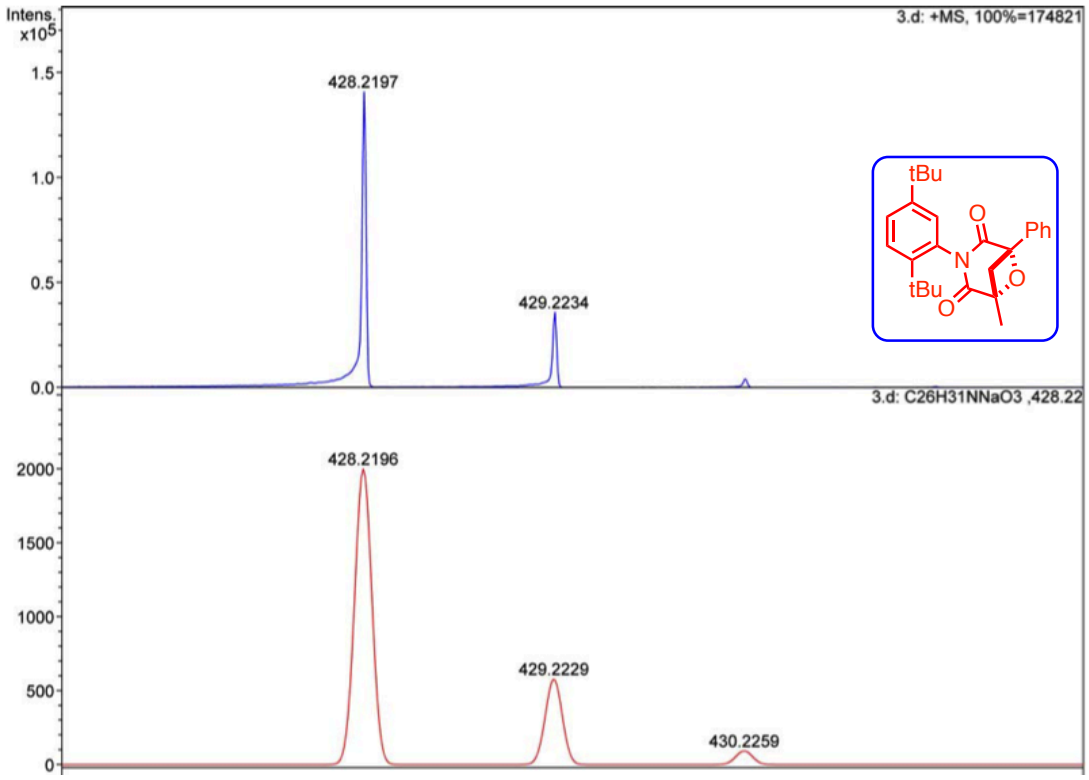

Figure 3.40: HRMS of oxetane photoproduct **174a**.

HPLC analysis conditions:

For analytical conditions,

I). Column : (*R*,*R*) WHELK–01

Abs. detector wavelength : 254 nm and 270 nm

Mobile phase : Hexanes:2-propanol = 98:2

Flow rate : 1.0 mL/min

Retention times (min) : ~ 10.25 [**PkA**] and ~ 20.52 [**PkB**]

(**PkA** and **PkB** refers to the order of elution of the isomers in the HPLC on the chiral stationary phase)

^{1}H-NMR (400 MHz, $CDCl_3$, δ ppm): 7.61-7.59 (m, 1H), 7.46-7.38 (m, 6H), 7.32-7.30 (m, 1H), 6.98-6.96 (m, 1H), 3.47-3.14 (ABq, 2H), 2.16-2.03 (m, 2H), 1.36 (s, 9H) and 1.11 (t, *J*=7.46 Hz, 3H)

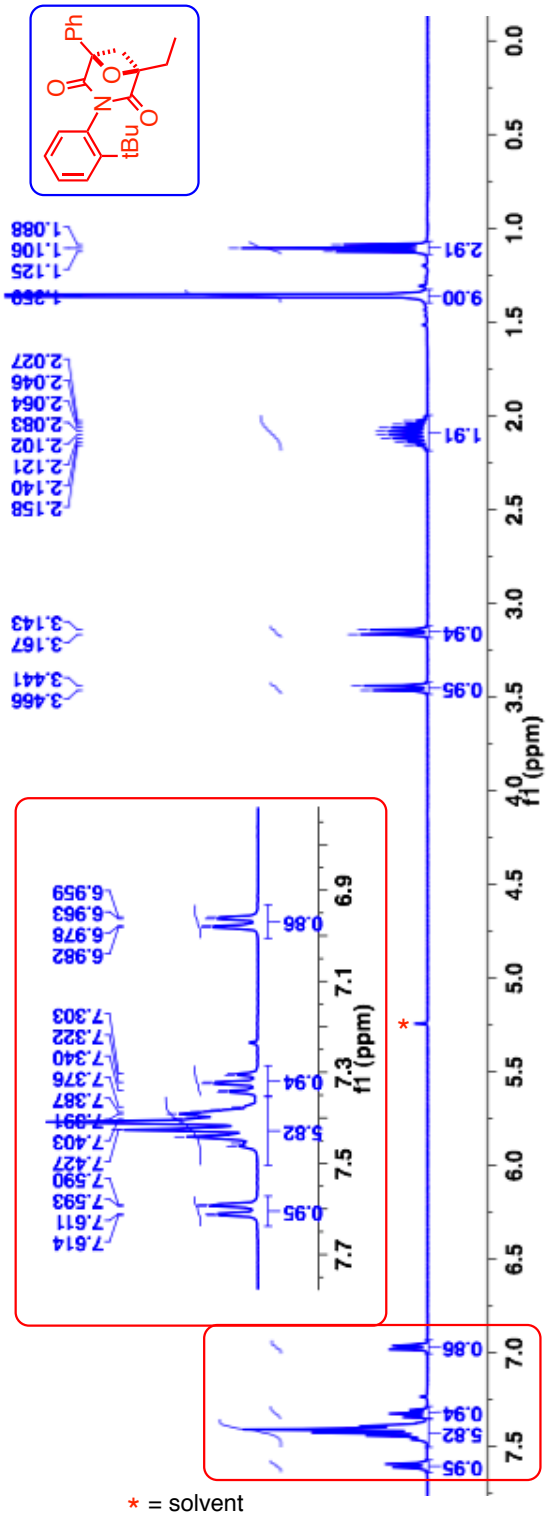

Figure 3.41: ^{1}H-NMR (400 MHz, $CDCl_3$, δ ppm) spectrum of oxetane photoproduct **173b**.

^{13}C-NMR (100 MHz, $CDCl_3$, δ ppm): 173.5, 172.7, 148.5, 136.0, 131.7, 131.1, 129.7, 129.1, 128.8, 128.6, 127.5, 125.6, 85.4, 84.5, 46.2, 35.8, 31.6, 26.2 and 6.9.

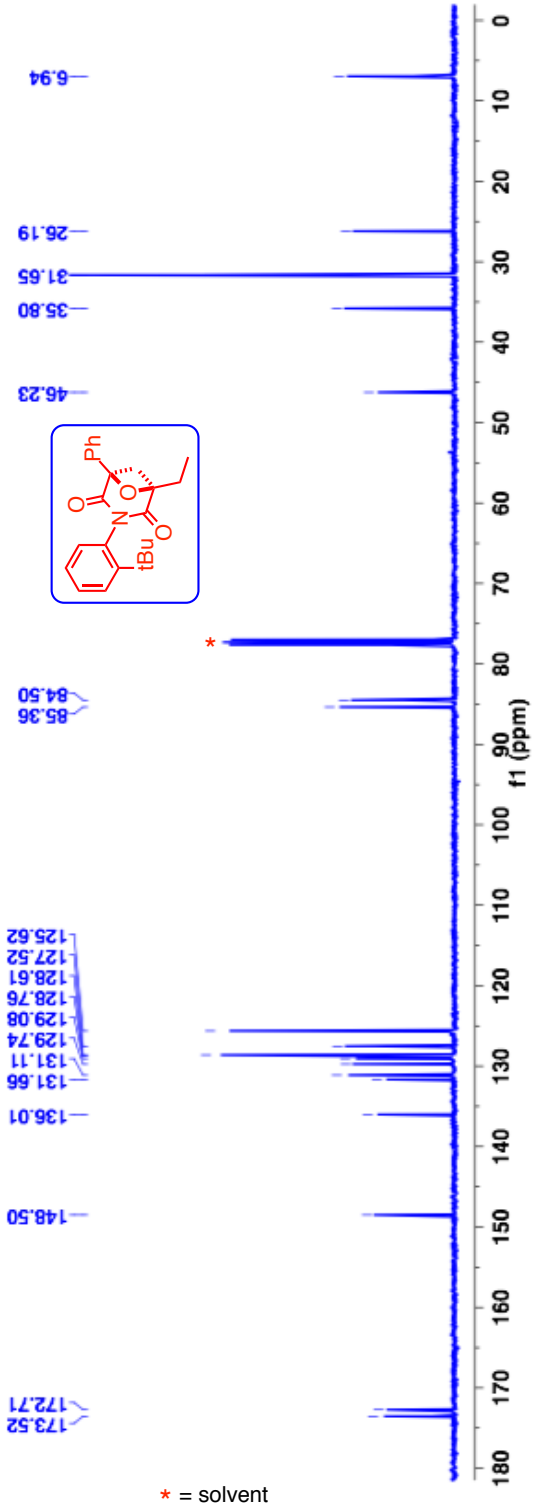

Figure 3.42: ^{13}C-NMR (100 MHz, $CDCl_3$, δ ppm) spectrum of oxetane photoproduct **173b**.

HRMS-ESI (m/z) ([M + Na]$^+$):

Calculated : 386.1727

Observed : 386.1728

|Δm| : 0.3 ppm

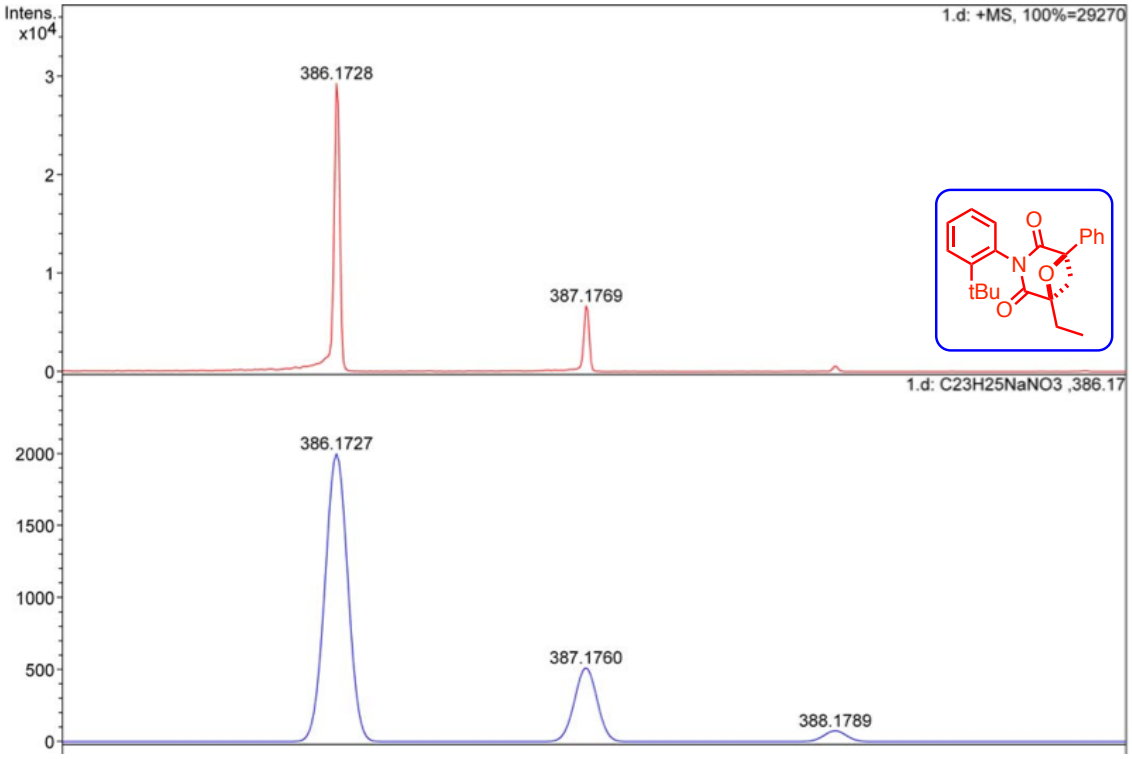

Figure 3.43: HRMS of oxetane photoproduct **173b**.

HPLC analysis conditions:

For analytical conditions,

I). Column : CHIRALPAK-AD-H

Abs. detector wavelength : 254 nm and 270 nm

Mobile phase : Hexanes:2-propanol = 90:10

Flow rate : 1.0 mL/min

Retention times (min) : ~ (-)-6.34 and (+)-10.92

For preparative conditions,

I). Column : (*R*,*R*) WHELK–01

Abs. detector wavelength : 254 nm and 270 nm

Mobile phase : Hexanes:2-propanol = 98:2

Flow rate : 3.0 mL/min

Retention times (min) : ~ (+)-21.00 and (-)-28.14

Optical rotation $[\alpha]_D^{24}$:

HPLC retention time CHIRALPAK-AD-H at ~ 6.34 min, (*c* ≈ 1.83 %, $CHCl_3$) =-11.91 deg.

HPLC retention time CHIRALPAK-AD-H at ~ 10.92 min, (*c* ≈ 1.83 %, $CHCl_3$) = +11.92 deg.

^{1}H-NMR (400 MHz, $CDCl_3$, δ ppm): 7.59 (m, 1H), 7.43-7.35 (m, 6H), 7.27-7.23 (m, 1H), 6.999-6.98 (m, 1H), 3.39-3.24 (ABq, 2H), 2.09-2.03 (m, 2H), 1.35 (s, 9H) and 1.08 (t, *J*= 7.6 Hz, 3H).

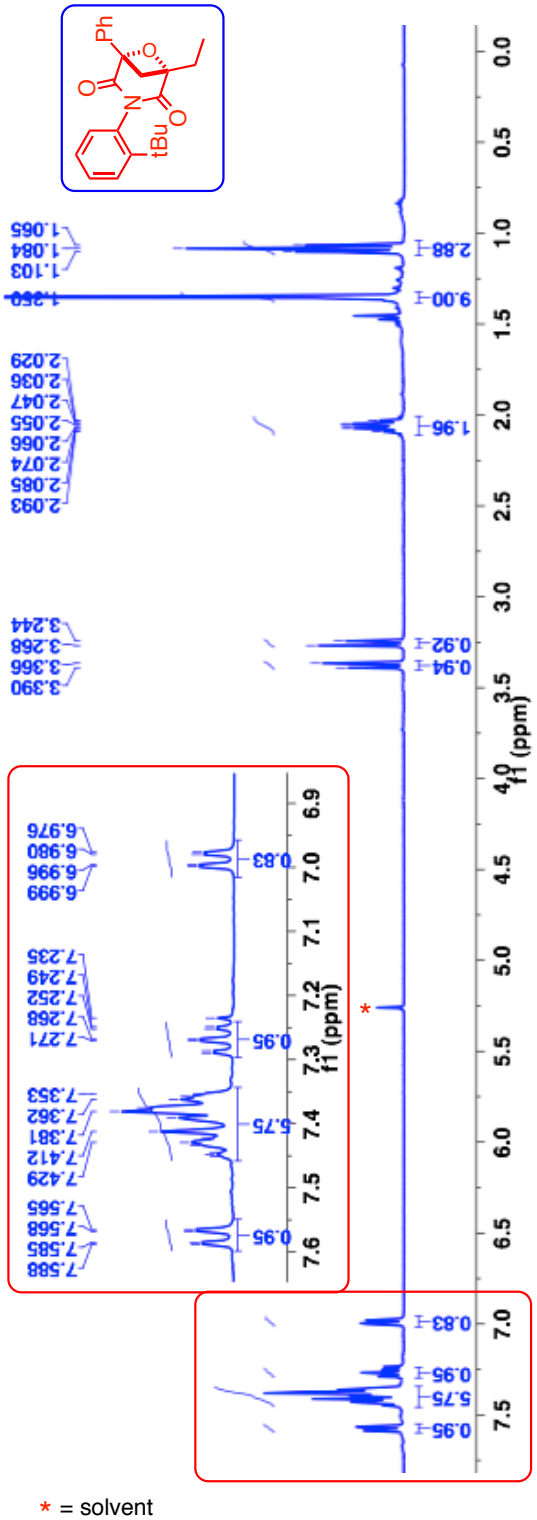

Figure 3.44: ^{1}H-NMR (400 MHz, $CDCl_3$, δ ppm) spectrum of oxetane photoproduct **174b**.

^{13}C-NMR (100 MHz, $CDCl_3$, δ ppm): 173.2, 172.4, 148.2, 135.9, 131.7, 131.1, 129.6, 129.0, 129.0, 128.5, 127.7, 125.6, 85.0, 84.4, 43.1, 36.0, 31.9, 25.9 and 6.94.

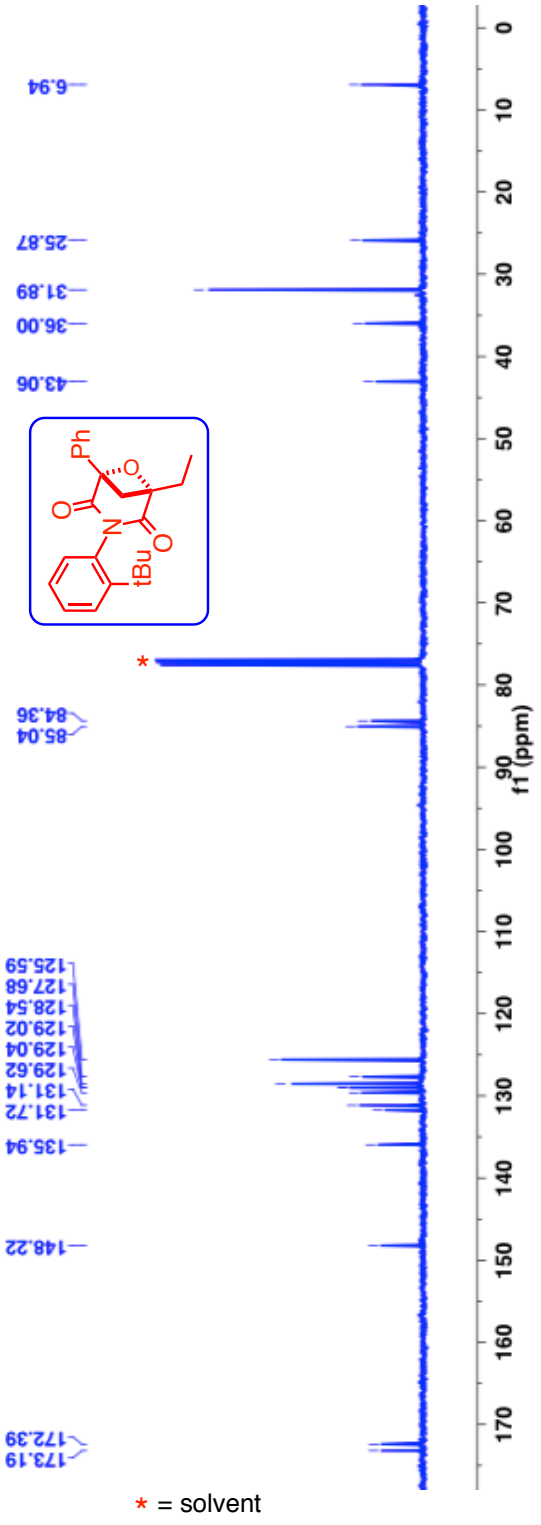

Figure 3.45: ^{13}C-NMR (100 MHz, $CDCl_3$, δ ppm) spectrum of oxetane photoproduct **174b**.

HRMS-ESI (m/z) ([M + Na]$^+$):

Calculated : 386.1727

Observed : 386.1731

|Δm| : 1.0 ppm

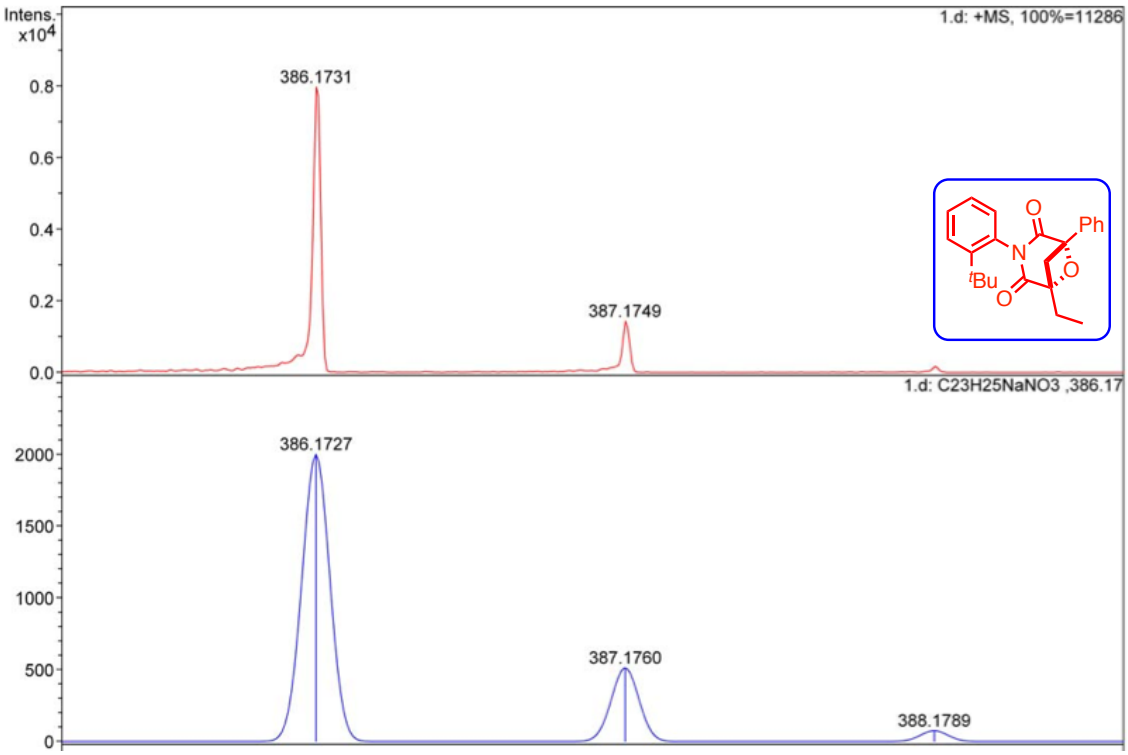

Figure 3.46: HRMS of oxetane photoproduct **174b**.

HPLC analysis conditions:

For analytical conditions,

I). Column : (*R*,*R*) WHELK–01

Abs. detector wavelength : 254 nm and 270 nm

Mobile phase : Hexanes:2-propanol = 90:10

Flow rate : 1.0 mL/min

Retention times (min) : ~ 9.15 (**PkA**) and 11.72 (**PkB**)

(**PkA** and **PkB** refers to the order of elution of the isomers in the HPLC on the chiral stationary phase)

^{1}H-NMR (400 MHz, $CDCl_3$, δ ppm): 7.49-7.34 (m, 8H), 7.27-7.25 (m, 2H), 3.42-3.31 (ABq, 2H) and 1.72 (s, 3H).

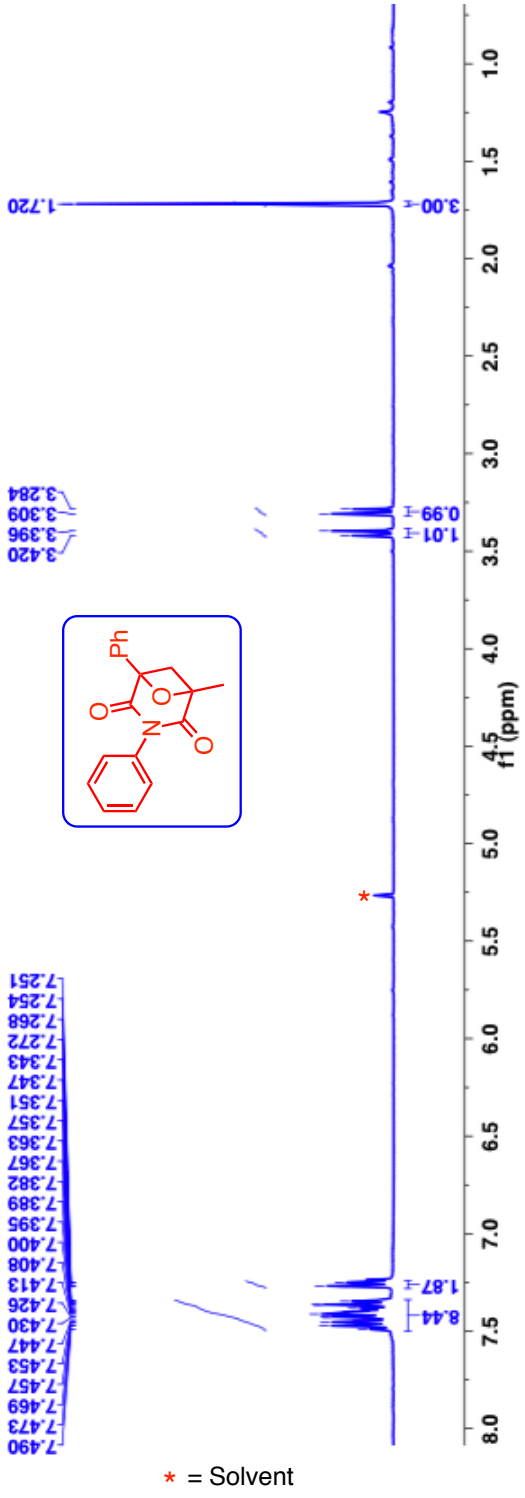

Figure 3.47: ^{1}H-NMR (400 MHz, $CDCl_3$, δ ppm) spectrum of oxetane photoproduct **173c**.

^{13}C-NMR (100 MHz, $CDCl_3$, δ ppm): 172.9, 171.98, 135.8, 132.8, 129.4, 129.1, 129.09, 128.6, 128.4, 125.5, 84.7, 82.9, 48.2 and 20.3.

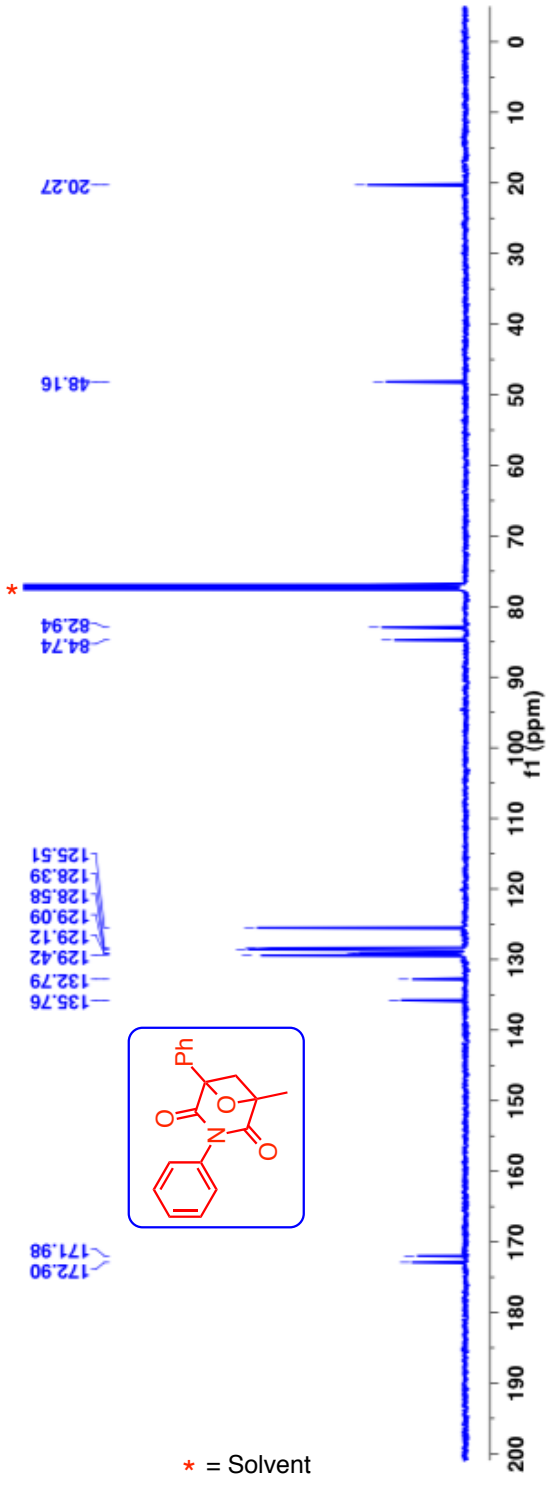

Figure 3.48: ^{13}C-NMR (100 MHz, $CDCl_3$, δ ppm) spectrum of oxetane photoproduct **173c**.

3.27. UV-Vis spectrum of α-oxoamides and its photoproducts

The UV-Vis spectra of oxoamides **172a-c** and its photoproducts **173** and **174** were measured in acetonitrile.

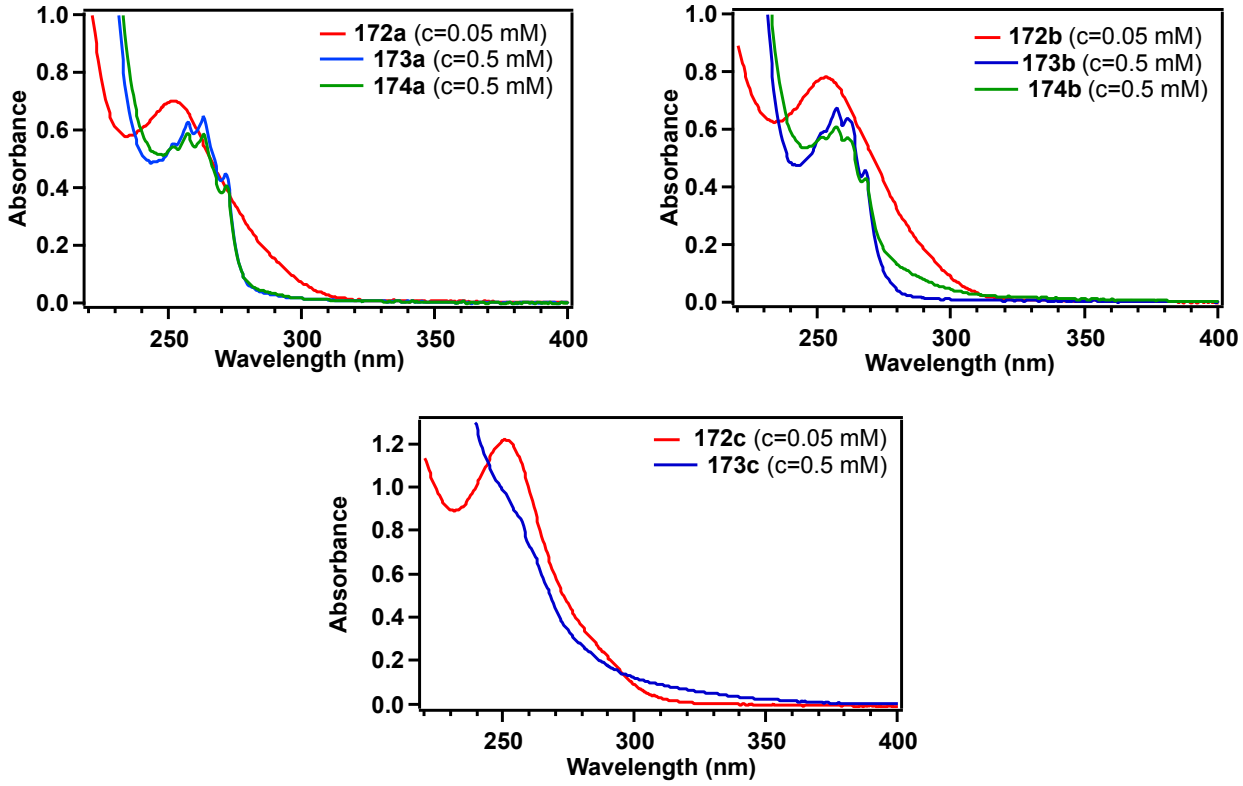

Figure 3.49: UV-Vis spectra of oxoamides **172a-c** and its photoproducts **173** and **174**.

3.28. General procedure for synthesis of maleimide derivatives for [2+2] photocycloaddition and their precursors

3.28.1. Synthesis of acetamide derivative 203

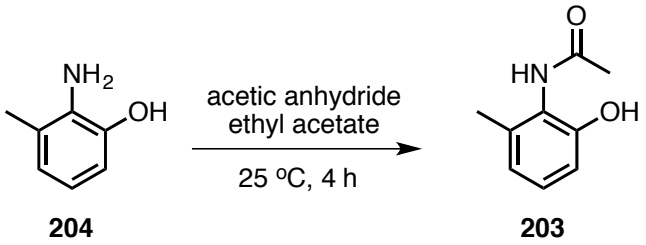

204 **203**

Scheme 3.34: Synthesis of acetamide derivative **203**.

The acetamide derivative was synthesized according to a procedure reported in the literature.[57] To a solution of corresponding aniline **204** (3.0 g, 1.0 *equiv.*) in ethyl acetate (30 mL) at 0 °C, acetic anhydride (2.3 *equiv.*) was added slowly over 15 min. The mixture was allowed to warm to room temperature over 4 h during which a solid started to precipitate out of the solution. The mixture was concentrated under reduced pressure to leave ~10% of the initial ethyl acetate. To this slurry hexanes (50 mL) was added, stirred for 10 min and filtered. The solid residue was washed with hexanes (15 mL), dried and directly taken for the next step without further purification.

R*f* = 0.20 (50% hexanes:50% ethyl acetate), Yield for **203** = 94%

^{1}H-NMR (400 MHz, CD_3OD, δ ppm): 7.00-6.96 (m, 1H), 6.699-6.68 (m, 2H), 2.16 (s, 3H) and 2.14 (s, 3H).

^{13}C-NMR (100 MHz, CD_3OD, δ ppm): 175.7, 156.7, 140.3, 131.5, 127.1, 125.0, 117.6, 25.3 and 20.9.

3.28.2. Synthesis of *o*-allylated acetamide derivative 202

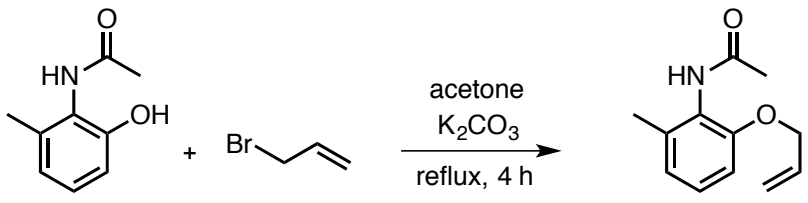

203 **202**

Scheme 3.35: Synthesis of *o*-allylated acetamide derivative **202**.

To a solution of acetamide derivative **203** (3.5 g, 1 *equiv.*) in dry acetone (35 mL) *anhyd.* potassium carbonate (3.0 *equiv.*) and allyl bromide (2.5 *equiv.*) were added at 25 °C. The resulting mixture was refluxed for 4 h. After the completion of the reaction, the mixture was cooled to 25 °C, filtered through celite and the solid was washed with acetone (15 mL). The combined organic layer was concentrated and the residue was taken up in DCM (50 mL) and washed with DI water (2 × 15 mL) and brine solution (1 × 15 mL). The organic layer was dried over *anhyd.* Na_2SO_4, filtered and the solvent was removed under reduced pressure to get the crude product. The crude product was directly taken to next step without further purification.

R*f* = 0.75 (95% DCM:5% methanol), Yield for **202** = 88%

^{1}H-NMR (400 MHz, CD_3OD, δ ppm): 7.12-7.06 (m, 1H), 6.82-6.797 (m, 2H), 6.07-5.97 (m, 1H), 5.41-5.35 (m, 1H), 5.22-5.19 (m, 1H), 4.52-4.499 (m, 2H), 2.17 (m, 3H) and 2.12 (m, 3H).

^{13}C-NMR (100 MHz, CD_3OD, δ ppm): 175.2, 158.2, 141.1, 137.6, 131.5, 128.6, 126.2, 119.8, 114.2, 72.9, 25.3 and 20.9.

3.28.3. Synthesis of *o*-allylated aniline derivative 198

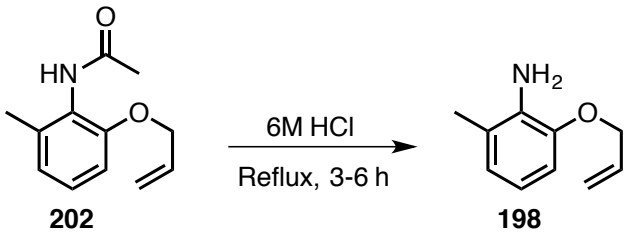

202 **198**

Scheme 3.36: Synthesis of *o*-allylated acetamide derivative **198**.

To *o*-allylated acetamide derivative **202** (2.9 g), 6M HCl (7 mL) was added at 25 °C. The resulting mixture was refluxed for 3-6 h. After the completion of the reaction, the mixture was cooled to 0 °C. The pH of the reaction mixture was adjusted to 14 by slowly adding 4M NaOH solution without allowing the internal temperature to rise above 10 °C. The aqueous layer was extracted with ethyl acetate. The combined organic layer was dried over *anhyd.* Na_2SO_4, filtered and the solvent was removed under reduced pressure to get the crude product. The crude product was purified by combiflash using hexanes: ethyl acetate mixture (80:20).

R*f* = 0.80 (80% hexanes: 20% ethyl acetate), Yield for **198** = 78%

^{1}H-NMR (400 MHz, $CDCl_3$, δ ppm): 6.74-6.43 (m, 3H), 6.15-6.04 (m, 1H), 5.44-5.39 (m, 1H), 5.30-5.27(m, 1H), 4.57-4.55 (m, 2H), 3.79 (bs, 2H) and 2.19 (s, 3H).

^{13}C-NMR (100 MHz, $CDCl_3$, δ ppm): 146.1, 134.8, 133.9, 123.1, 123.0, 117.7, 117.5, 109.9, 69.6 and 17.4.

3.28.4. Synthesis of 2-amino benzyl alcohol derivative 200

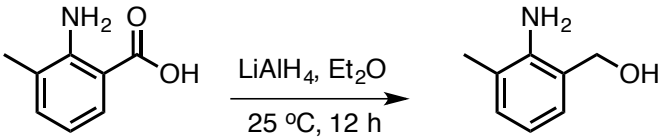

201 **200**

Scheme 3.37: Synthesis of 2-amino benzyl alcohol derivative **200**.

The benzyl alcohol derivative was synthesized according to a procedure reported in the literature.[58]To a slurry of lithium aluminum hydride (2.5 *equiv.*) in dry THF (50 mL) under N_2 atmosphere at 0 °C, a solution anthranillic acid derivative **201** (4.0 g, 1.0 *equiv.*) in dry THF (50 mL) was added over a period of 15 min without allowing the internal temperature to rise above 5 °C. The resulting mixture was allowed to warm to room temperature over 12 h. After the reaction, the mixture was cooled to 0 °C and quenched with saturated Na_2SO_4 solution over 15 min. To the resulting solid mixture DCM (CH_2Cl_2, 75 mL) was added, stirred for 15 min, filtered and the filtered solid residue was washed with DCM (50 mL). The combined organic layer was dried over *anhyd.* Na_2SO_4, filtered and the solvent was removed under reduced pressure to get the crude product. The crude product was directly taken to next step without further purification.

R*f* = 0.45 (50% hexanes: 50% ethyl acetate), Yield for **200** = 90%

^{1}H-NMR (400 MHz, $CDCl_3$, δ ppm): 7.03-7.01 (m, 1H), 6.92-6.90 (m, 1H), 6.65-6.61 (m, 1H), 4.61 (s, 2H), 3.40 (bs, 3H) and 2.15 (m, 3H).

^{13}C-NMR (100 MHz, $CDCl_3$, δ ppm): 144.3, 130.7, 127.3, 124.4, 122.9, 117.9, 64.7 and 17.5.

3.28.5. Synthesis of 2-methoxymethylaniline derivative 199

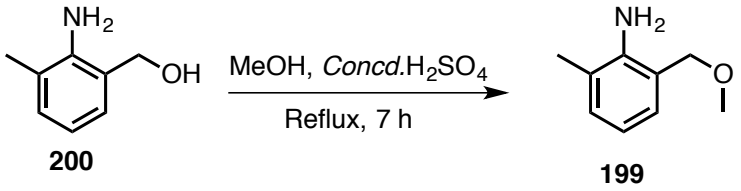

200 **199**

Scheme 3.38: Synthesis of 2-methoxymethylaniline derivative **199**.

To a solution of aminobenzyl alcohol derivative **200** (5.0 g, 1.0 *equiv.*) in methanol (40 mL) at 0 °C, *concd*. H_2SO_4 (1.1 *equiv.*) was added over 5 min. The resulting mixture was heated to 50 °C for 7 h. After the reaction, the mixture was cooled to 10 °C and neutralized with saturated Na_2CO_3 solution carefully, during which a brisk effervescence was observed. The aqueous layer was extracted with DCM (3 × 40 mL). The combined organic layer was dried over *anhyd.* Na_2SO_4, filtered and the solvent was removed under reduced pressure to get the crude product. The crude product was purified by combiflash using a hexanes: ethyl acetate mixture.

R*f* = 0.80 (50% hexanes: 50% ethyl acetate), Yield for **199** = 77%

^{1}H-NMR (400 MHz, $CDCl_3$, δ ppm): 7.05-7.03 (m, 1H), 6.96-6.94 (m, 1H), 6.6-6.62 (m, 1H), 4.49 (s, 2H), 4.12 (bs, 2H), 3.33 (s, 3H) and 2.17 (s, 3H).

^{13}C-NMR (100 MHz, $CDCl_3$, δ ppm): 144.6, 130.7, 128.3, 122.5, 121.5, 117.5, 74.1, 57.6,and 17.5.

3.28.6. Synthesis of 2-(butenyl)aniline 197

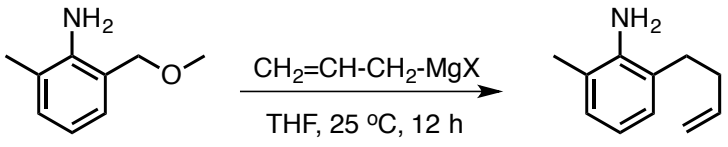

199 **197**

Scheme 3.39: Synthesis of 2-(butenyl)aniline derivative **197**.

To a solution aniline derivative **199** (5.3 g, 1.0 *equiv.*) in dry THF (40 mL) at 0 °C, allyl magnesium halide (2.0 M in THF, 2.2 *equiv.*) was added slowly over 15 min. The resulting mixture was allowed to warm to room temperature over 12 h. After the reaction, the mixture was cooled to 0 °C and quenched with *dil.* HCl. The aqueous layer was extracted with DCM (3 × 50 mL). The combined organic

layer was dried over *anhyd*. Na_2SO_4, filtered and the solvent was removed under reduced pressure to get the crude product. The crude product was purified by combiflash using a hexanes: ethyl acetate mixture. R*f* = 0.60 (90% hexanes: 10% ethyl acetate), Yield for **197** = 75%

^{1}H-NMR (400 MHz, $CDCl_3$, δ ppm): 6.95-6.93 (m, 2H), 6.68-6.64 (m, 1H), 5.9-5.83 (m, 1H), 5.15-4.97 (m, 2H), 3.77 (bs, 2H), 2.61-2.57 (m, 2H), 2.40-2.35 (m, 2H) and 2.18 (s, 3H).

^{13}C-NMR (100 MHz, $CDCl_3$, δ ppm): 142.4, 138.4, 128.6, 127.4, 125.6, 122.4, 118.3, 115.2, 33.1, 31.2 and 17.98.

3.28.7. Synthesis of citraconicimide derivative 195

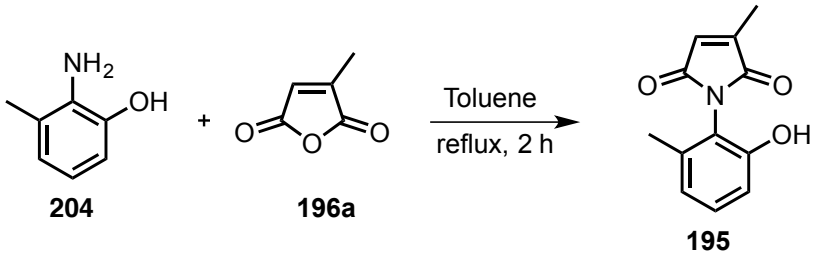

204 **196a** **195**

Scheme 3.40: Synthesis of citraconicimide derivative **195**.

To a solution of aniline **204** (5.0 g, 40.6 mmol) in toluene (25 mL) at 25 °C, citraconic anhydride **196a** (5.46 g, 48.7 mmol) was added with stirring in a round bottom flask. The resulting mixture was refluxed for 2 h after which it was cooled to room temperature and the mixture was diluted with hexanes (50 mL). The precipitated solid was filtered and washed with hexanes (20 mL) and dried under vacuum. The crude product was directly taken to next step without further purification.

R*f* = 0.40 (50% hexanes: 50% ethyl acetate), Yield for **195** = 94%.

^{1}H-NMR (400 MHz, CD_3OD, δ ppm): 7.14-7.098 (m, 1H), 6.74-6.72 (m, 2H), 6.58 (s, 1H), 2.11 (s, 3H) and 2.04 (s, 3H).

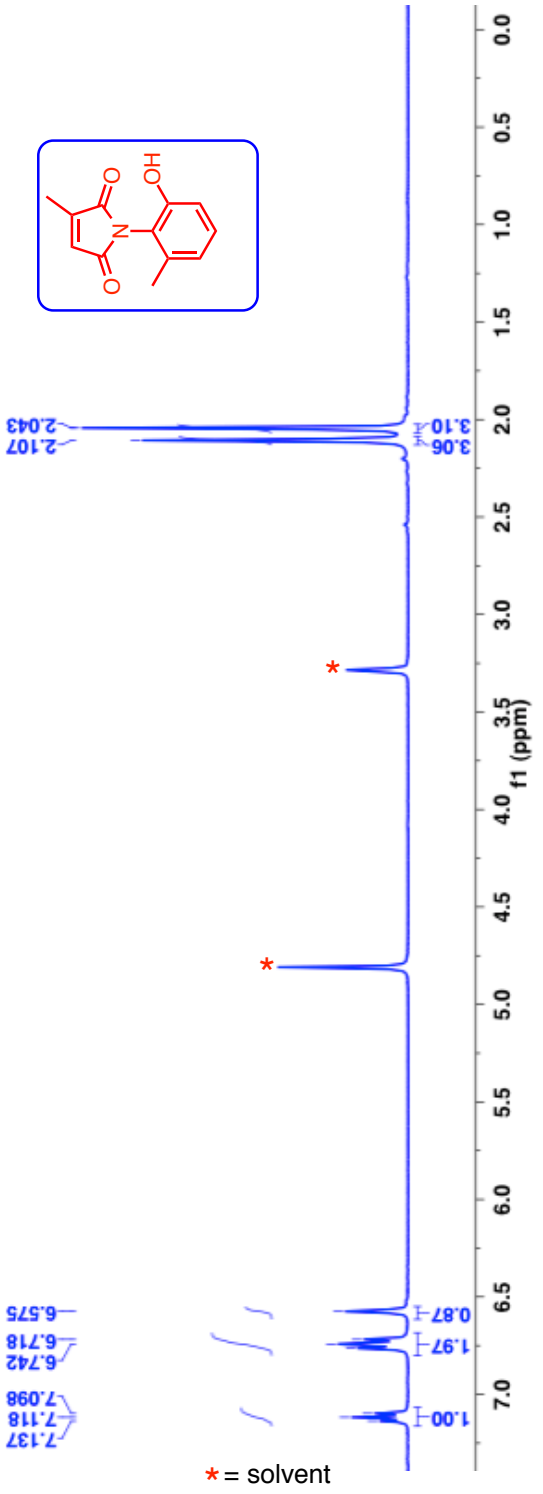

Figure 3.50: ^{1}H-NMR (400 MHz, $CDCl_3$, δ ppm) spectrum of hydroxy maleimide derivative **195**.

^{13}C-NMR (100 MHz, CD_3OD, δ ppm): 175.4, 174.5, 158.3, 150.5, 142.7, 133.7, 131.7, 124.8, 122.3, 117.3, 20.5 and 13.7.

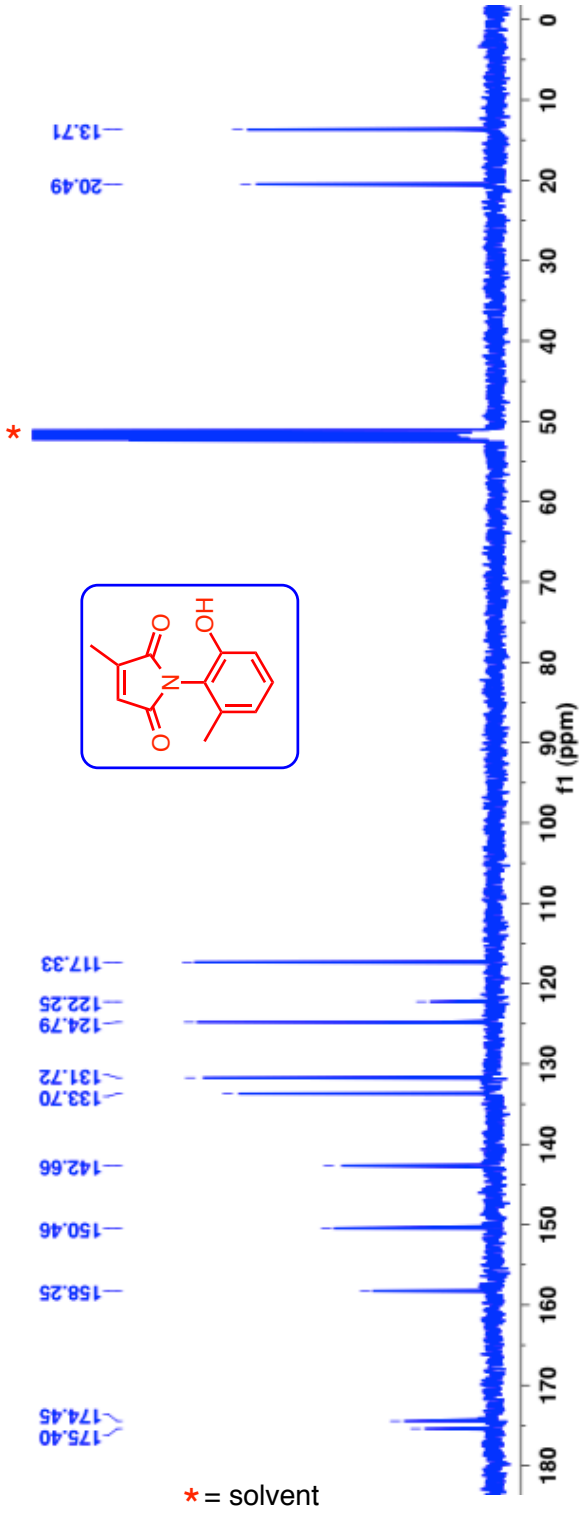

Figure 3.51: ^{13}C-NMR (100 MHz, $CDCl_3$, δ ppm) spectrum of hydroxy maleimide derivative **195**.

HRMS-ESI (m/z) ([M + Na]$^+$):

Calculated : 240.0631

Observed : 240.0639

|Δm| : 3.3 ppm

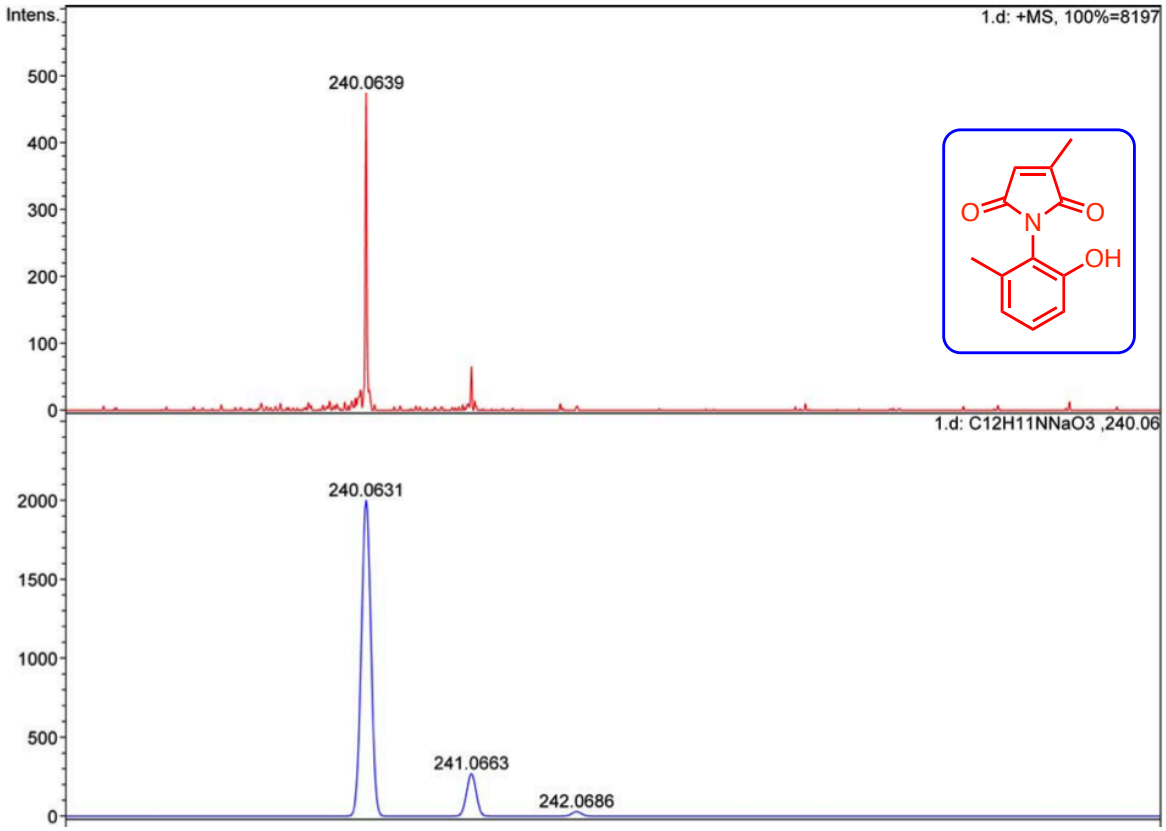

Figure 3.52: HRMS of hydroxy maleimide derivative **195.**

3.28.8. Synthesis of atropisomeric maleimide derivatives 192a-c

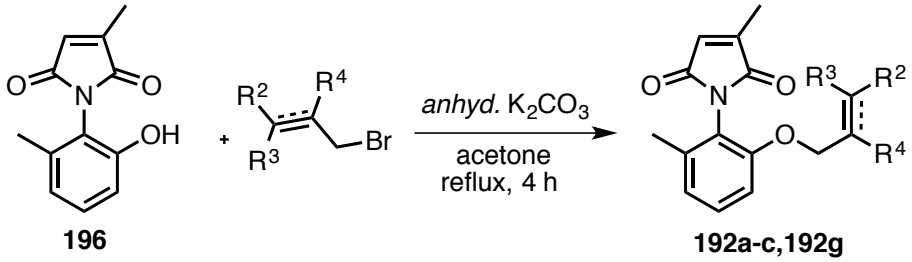

Scheme 3.41: Synthesis of atropisomeric maleimide derivative **192a-c**.

To a mixture of citraconicimide derivative **196** (1.0 g, 1.0 *equiv.*) and *anhyd.* potassium carbonate (3.0 *equiv.*) in dry acetone (10 mL), corresponding allyl bromide (2.5 *equiv.*) was added in a round bottom flask. The resulting mixture was refluxed for 4 h or until the complete consumption of citraconicimide. The reaction mixture was cooled to room temperature and filtered through celite bed. The solid was washed with acetone and the combined organic layer was concentrated to get the crude product. The crude product was purified by combiflash using a hexanes:ethyl acetate mixture.

TLC condition - R_f = 0.80 (50% hexanes:50% ethyl acetate) for **192a**, (Yield = 66%).

TLC condition - R*f* = 0.45 (80% hexanes:20% ethyl acetate) for **192b**, (Yield = -).

TLC condition - R*f* = 0.85 (50% hexanes:50% ethyl acetate) for **192c**, (Yield = 43%).

TLC condition - R*f* = 0.6 (50% hexanes:50% ethyl acetate) for **192g**, (Yield = 74 %)

^{1}H-NMR (400 MHz, $CDCl_3$, δ ppm): 7.22-7.18 (m, 1H), 6.84-6.82 (m, 1H), 6.78-6.76 (m, 1H), 6.42-6.41 (q, *J* = 1.6 Hz, 1H), 5.29-5.25 (m, 1H), 4.45-4.43 (m, 2H), 2.11 (s, 3H), 2.09-2.08 (d, *J* = 2 Hz, 3H), 1.68 (s, 3H) and 1.62 (s, 3H).

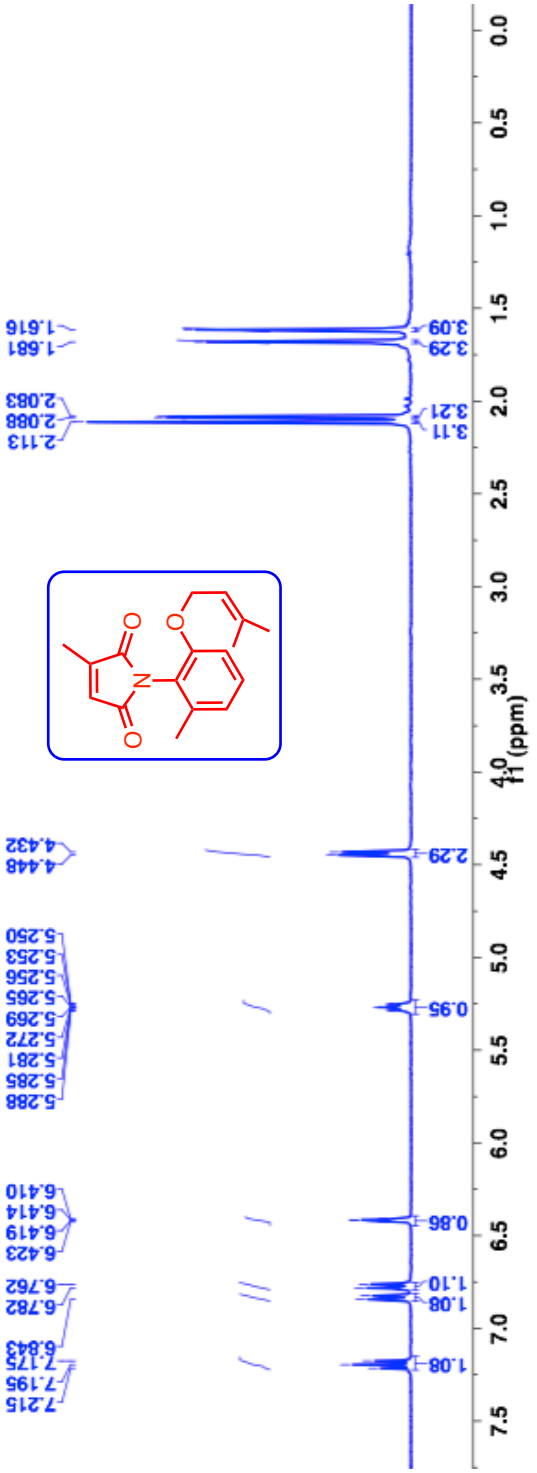

Figure 3.53: ^{1}H-NMR (400 MHz, $CDCl_3$, δ ppm) spectrum of maleimide derivative **192a**.

^{13}C-NMR (100 MHz, $CDCl_3$, δ ppm): 171.1, 170.0, 155.3, 146.1, 138.97, 137.5, 130.1, 128.0, 122.6, 120.1, 119.95, 110.9, 65.8, 25.9, 18.4, 17.95 and 11.3.

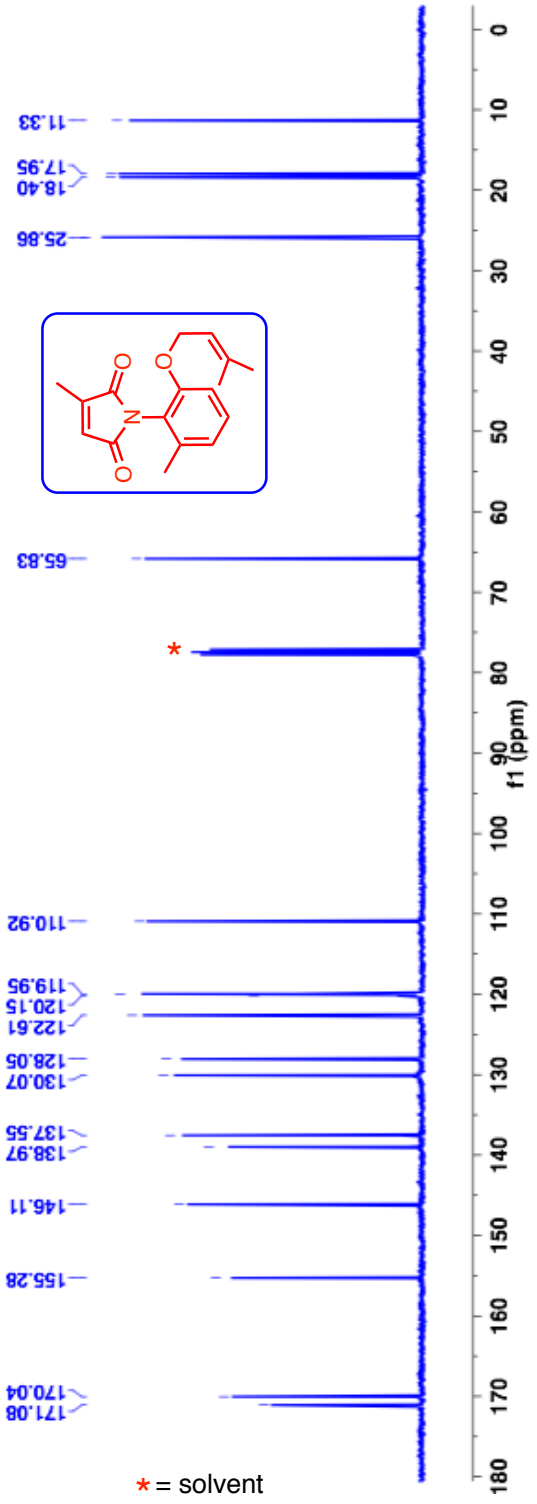

Figure 3.54: ^{13}C-NMR (100 MHz, $CDCl_3$, δ ppm) spectrum of maleimide derivative **192a**.

HRMS-ESI (m/z) ([M + Na]$^+$):

Calculated : 308.1257

Observed : 308.1253

|Δm| : 1.3 ppm

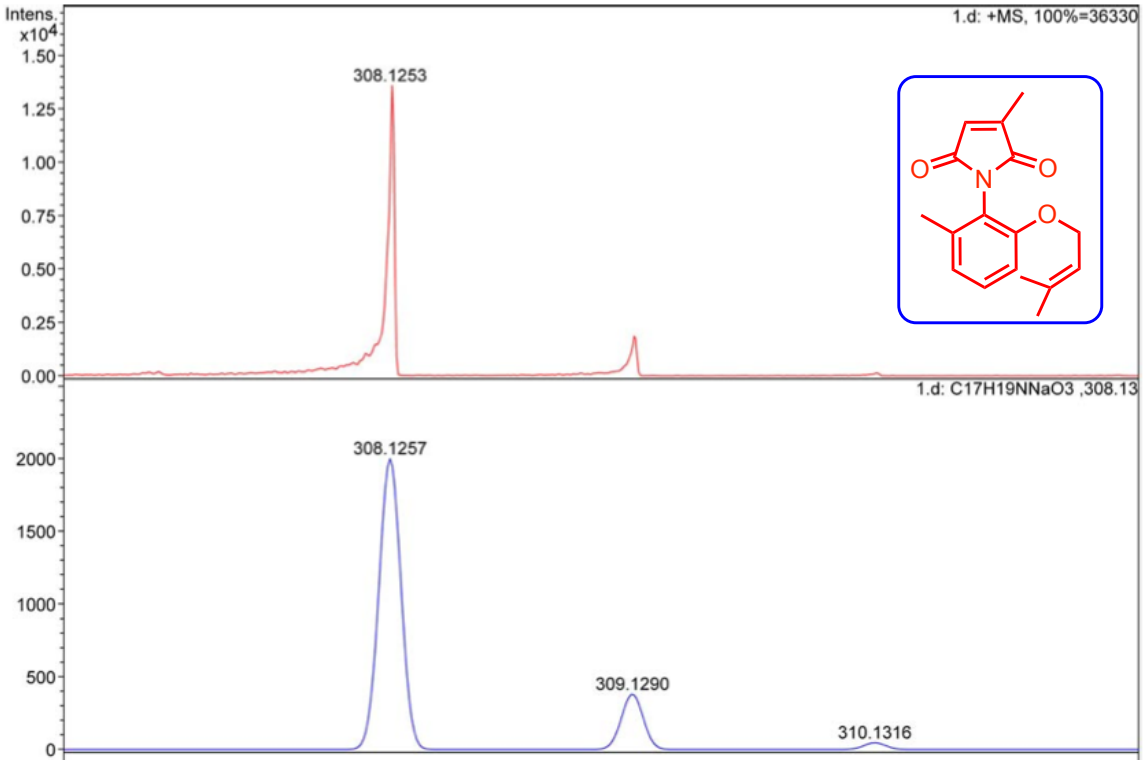

Figure 3.55: HRMS of maleimide derivative **192a**.

HPLC analysis conditions:

For analytical conditions,

I). Column : CHIRALPAK-ADH

Abs. detector wavelength : 254 nm and 270 nm

Mobile phase : Hexanes:2-propanol = 95:5

Flow rate : 1.0 mL/min

Retention times (min) : ~ 9.03 [(+)-**192a**] and ~ 10.47 [(-)-**192a**]

For preparative conditions,

I). Column : CHIRALPAK-ADH

Abs. detector wavelength : 254 nm and 270 nm

Mobile phase : Hexanes:2-propanol = 99:1

Flow rate : 3.0 mL/min

Retention times (min) : ~ 31.89 [(+)-**192a** and ~ 40.74 [(-)-**192a**]

Optical rotation $[\alpha]_D^{24}$:

HPLC retention time (CHIRALPAK-ADH) at ~ 9.03 min, (*c* ≈ 1.29 %, MeOH) = +23.73 deg

HPLC retention time (CHIRALPAK-ADH) at ~ 10.47 min, (*c* ≈ 1.29 %, MeOH) = -22.35 deg.

^{1}H-NMR (400 MHz, $CDCl_3$, δ ppm): 7.24-7.20 (m, 1H), 6.87-6.85 (m, 1H), 6.79-6.77 (m, 1H), 6.45 (q, *J* = 1.6 Hz, 1H), 5.67-5.58 (m, 1H), 5.53-5.46 (m, 1H), 4.53 (d, *J* = 6.4 Hz, 2H), 2.14 (d, *J* = 1.6 Hz, 3H), 2.13 (s, 3H) and 1.64 (d, *J* = 6.4 Hz, 3H).

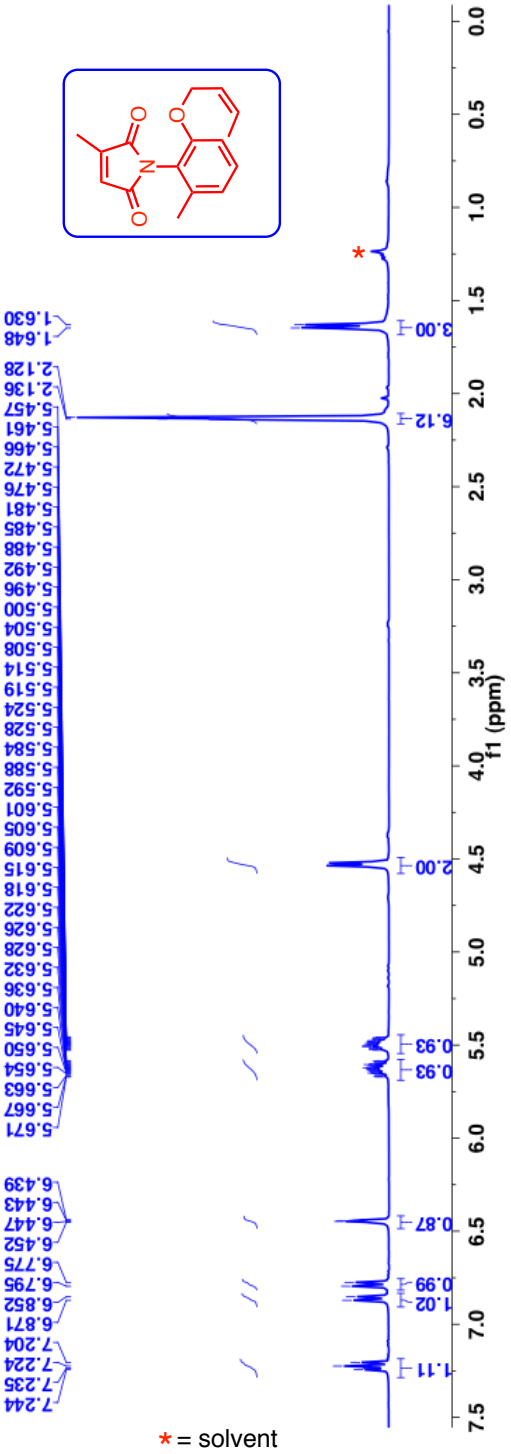

Figure 3.56: ^{1}H-NMR (400 MHz, $CDCl_3$, δ ppm) spectrum of maleimide derivative **192b**.

^{13}C-NMR (100 MHz, $CDCl_3$, δ ppm): 171.1, 170.1, 155.1, 146.2, 139.1, 130.1, 128.5, 128.0, 125.7, 122.8, 120.1, 110.7, 64.7, 17.97, 13.6 and 11.4.

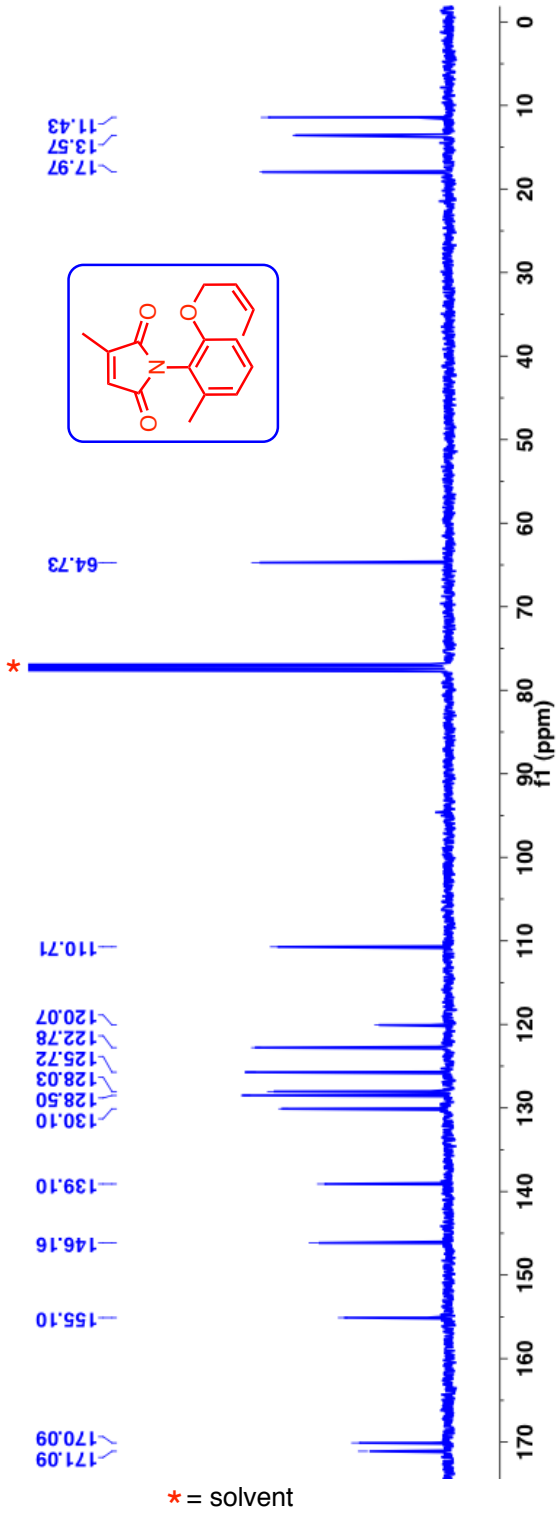

Figure 3.57: ^{13}C-NMR (100 MHz, $CDCl_3$, δ ppm) spectrum of maleimide derivative **192b**.

HRMS-ESI (m/z) ([M + Na]$^+$):

Calculated : 294.1101

Observed : 294.1102

|Δm| : 0.3 ppm

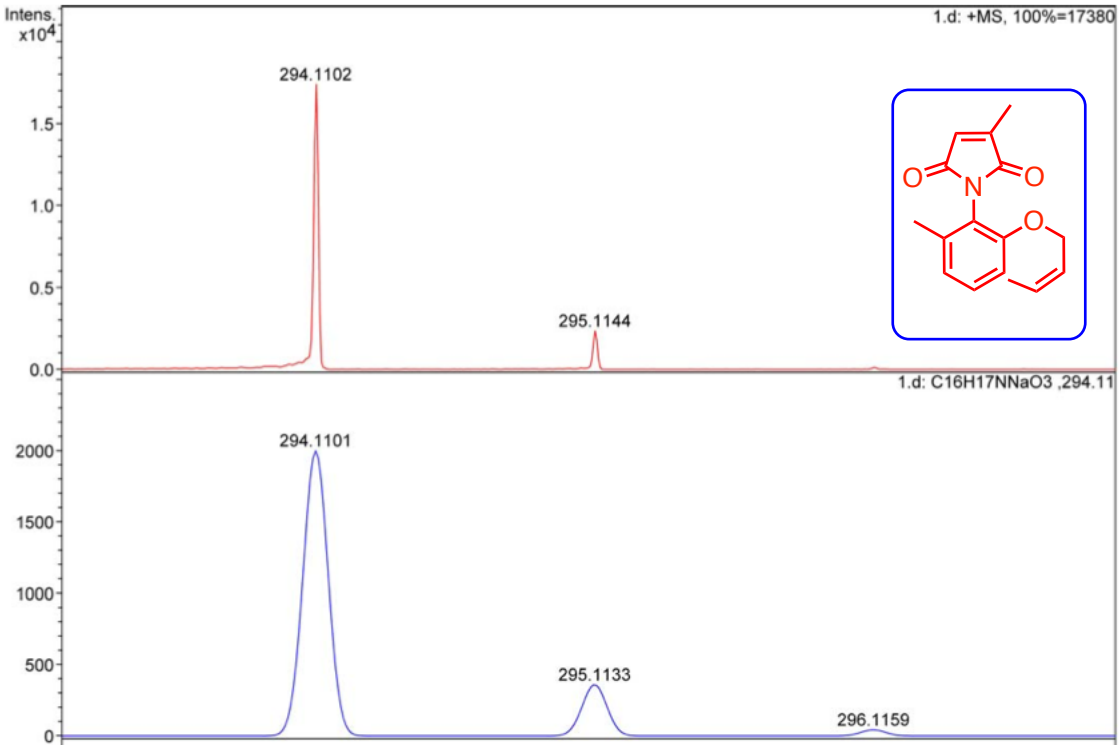

Figure 3.58: HRMS of maleimide derivative **192b**.

HPLC analysis conditions:

For analytical conditions,

I). Column : CHIRALPAK-ADH

Abs. detector wavelength : 254 nm and 270 nm

Mobile phase : Hexanes:2-propanol = 95:5

Flow rate : 1.0 mL/min

Retention times (min) : ~ 8.55 [(+)-**192b**] and ~ 9.69 [(-)-**192b**]

For preparative conditions,

I). Column : CHIRALPAK-ADH

Abs. detector wavelength : 254 nm and 270 nm

Mobile phase : Hexanes:2-propanol = 99:1

Flow rate : 3.0 mL/min

Retention times (min) : ~ 31.58 [(+)-**192b**] and ~ 38.47 [(-)-**192b**]

Optical rotation $[\alpha]_D^{23}$:

HPLC retention time (CHIRALPAK-ADH) at ~ 8.55 min, (*c* ≈ 1.0 %, MeOH) = +30.04 deg

HPLC retention time (CHIRALPAK-ADH) at ~ 9.65 min, (*c* ≈ 1.0 %, MeOH) = -30.14 deg.

^{1}H-NMR (400 MHz, $CDCl_3$, δ ppm): 7.23-7.19 (m, 1H), 6.87-6.85 (m, 1H), 6.77-6.75 (m, 1H), 6.45 (q, *J* = 1.74 Hz, 1H), 4.92 (s, 1H), 4.87 (m, 1H), 4.35 (s, 2H), 2.14 (s, 3H), 2.13-2.12 (m, 3H) and 1.67 (s, 3H).

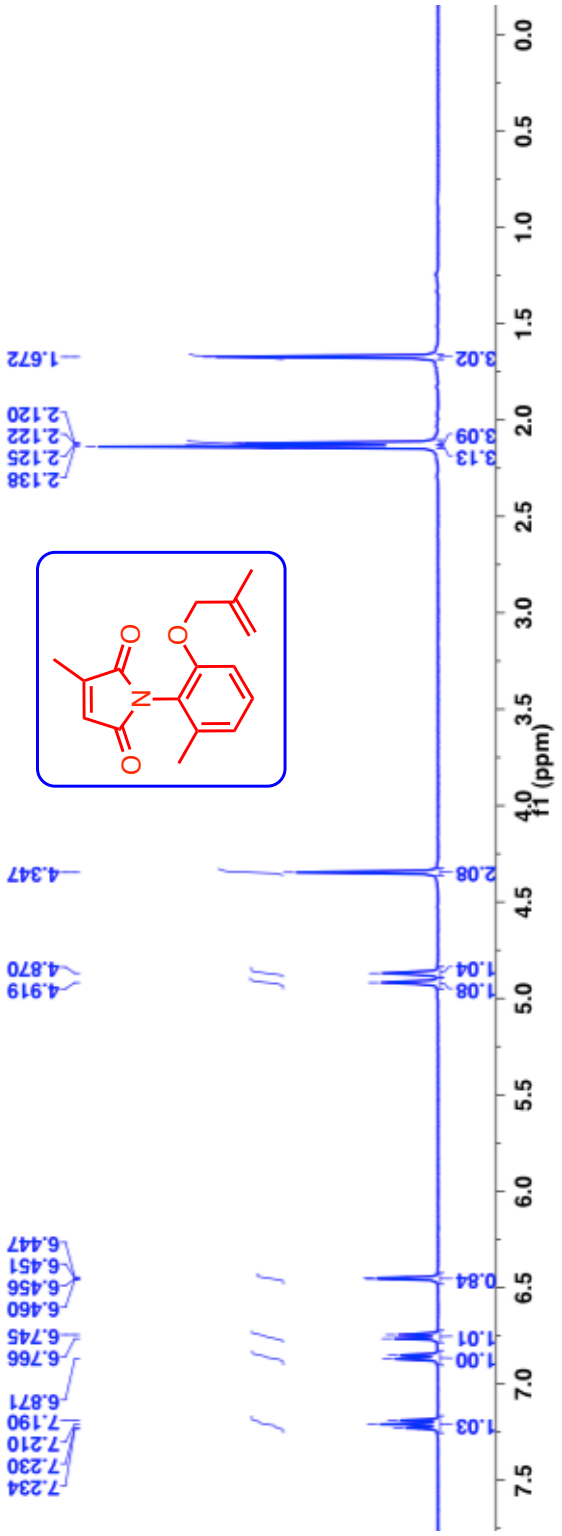

Figure 3.59: ^{1}H-NMR (400 MHz, $CDCl_3$, δ ppm) spectrum of maleimide derivative **192c**.

^{13}C-NMR (100 MHz, $CDCl_3$, δ ppm): 171.1, 170.1, 154.9, 146.3, 140.4, 139.1, 130.1, 128.0, 122.8, 119.8, 112.5, 110.5, 71.97, 19.4, 17.93 and 11.4.

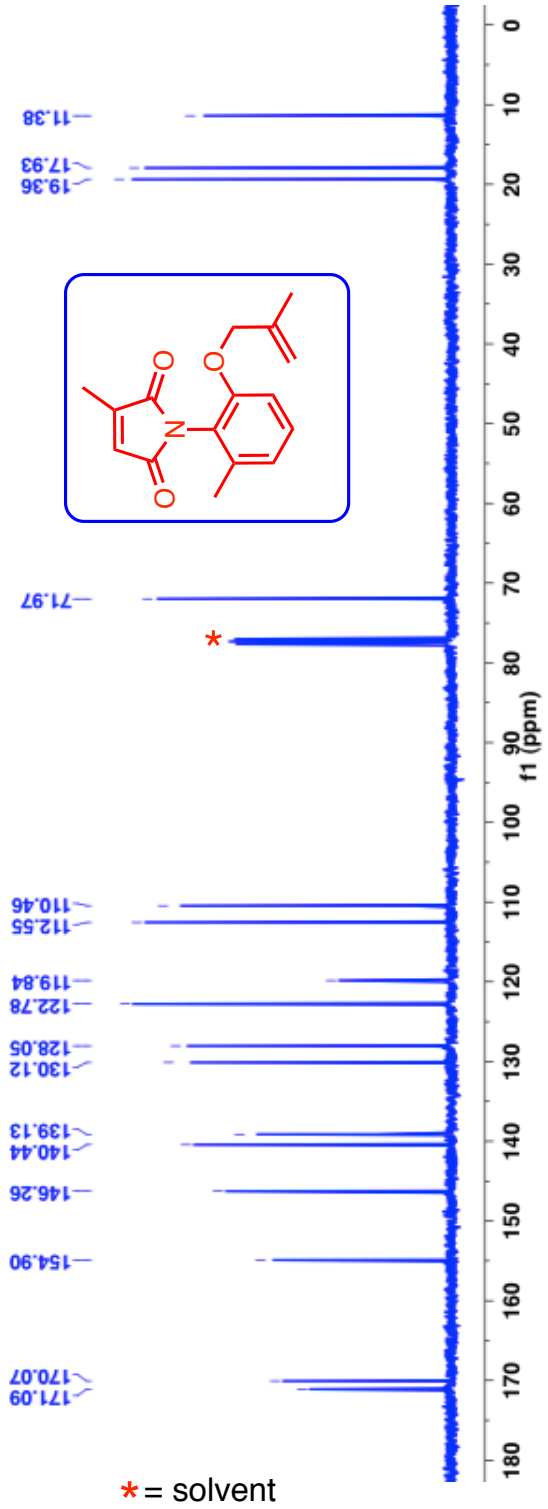

Figure 3.60: ^{13}C-NMR (400 MHz, $CDCl_3$, δ ppm) spectrum of maleimide derivative **192c**.

HRMS-ESI (m/z) ([M + Na]$^+$):

Calculated : 294.1101

Observed : 294.1098

|Δm| : 1.0 ppm

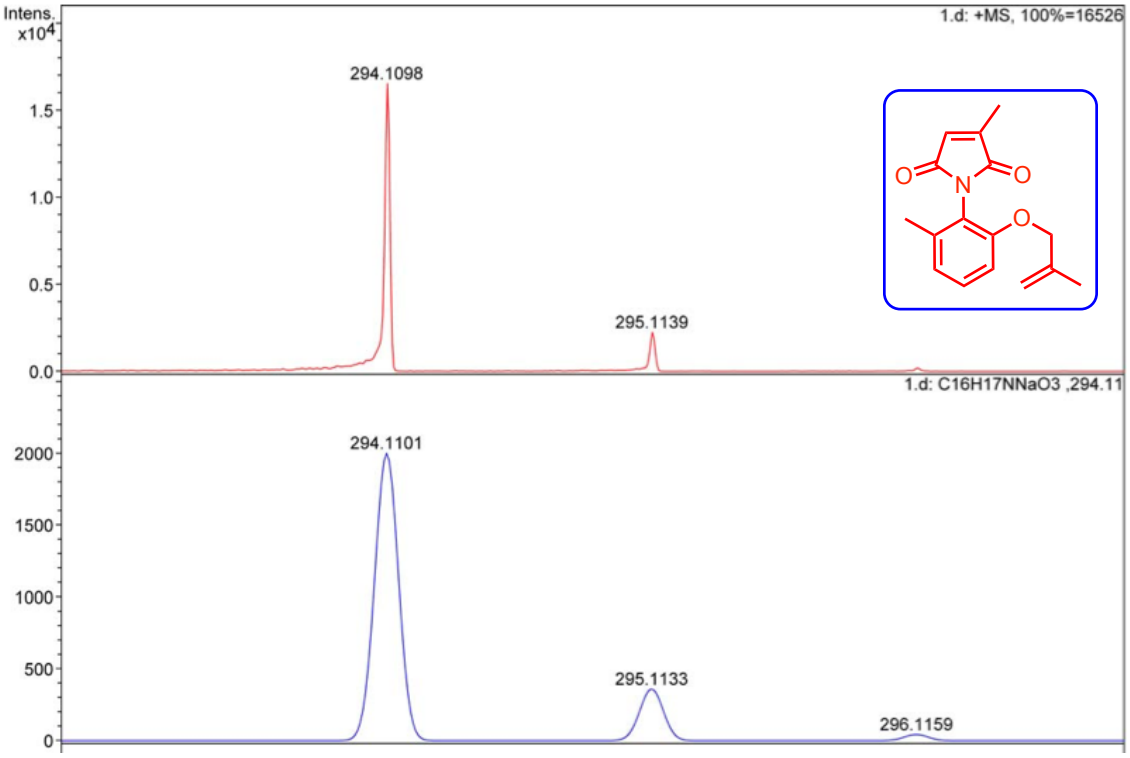

Figure 3.61: HRMS of maleimide derivative **192c**.

^{1}H-NMR (400 MHz, $CDCl_3$, δ ppm): 7.28-7.24 (m, 1H), 6.95-6.91 (m, 2H), 6.46 (q, *J* = 1.8 Hz, 1H), 4.61 (d, *J* = 2.4 Hz, 2H), 2.45 (t, *J* = 2.4 Hz, 1H), 2.15 (d, *J* = 1.8 Hz, 3H) and 2.13 (s, 3H).

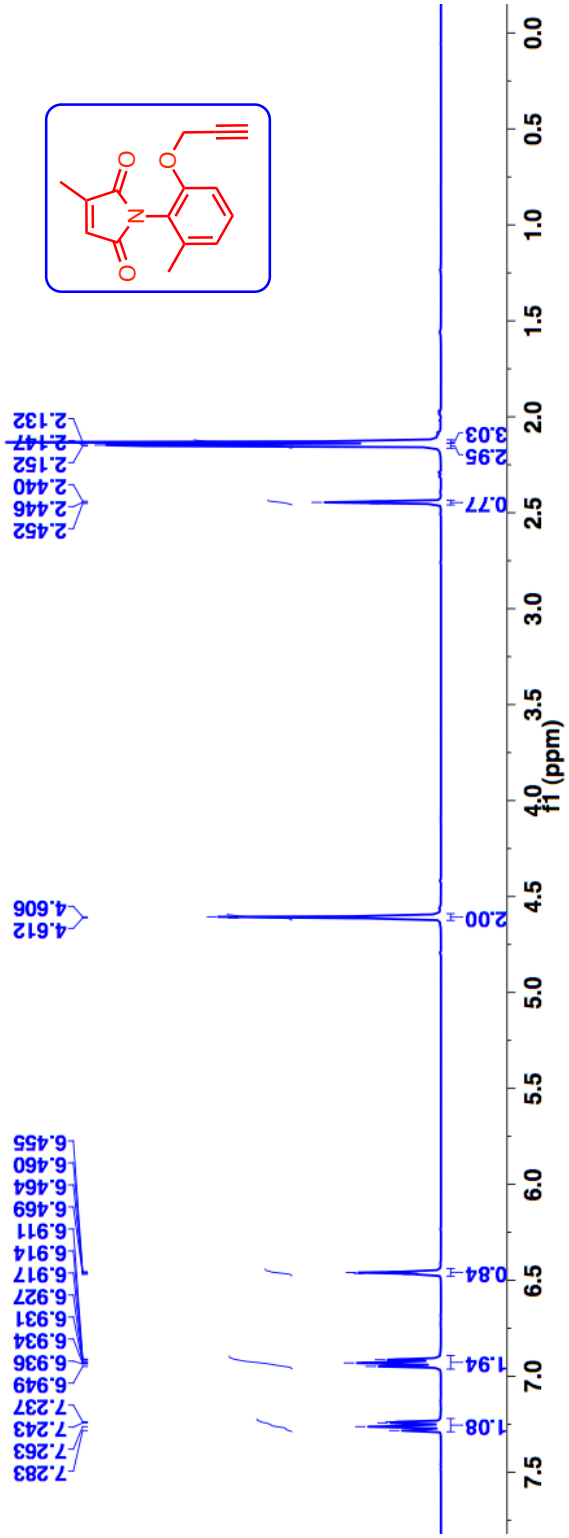

Figure 3.62: ^{1}H-NMR (400 MHz, $CDCl_3$, δ ppm) spectrum of maleimide derivative **192g**.

^{13}C-NMR (100 MHz, $CDCl_3$, δ ppm): 170.9, 169.8, 154.1, 146.2, 139.3, 130.1, 128.1, 123.8, 120.2, 111.1, 78.3, 76.0, 56.8, 17.99 and 11.5.

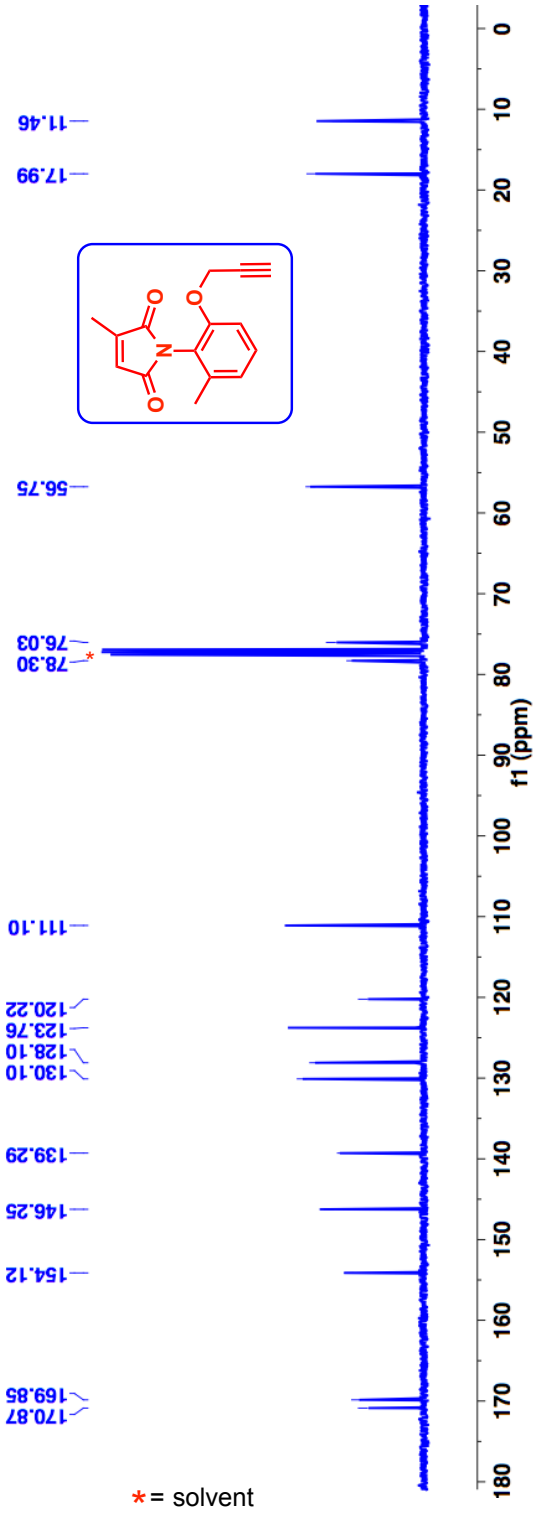

Figure 3.63: ^{13}C-NMR (100 MHz, $CDCl_3$, δ ppm) spectrum of maleimide derivative **192g**.

HRMS-ESI (m/z) ([M + Na]$^+$):

Calculated : 278.0788

Observed : 278.0777

|Δm| : 3.9 ppm

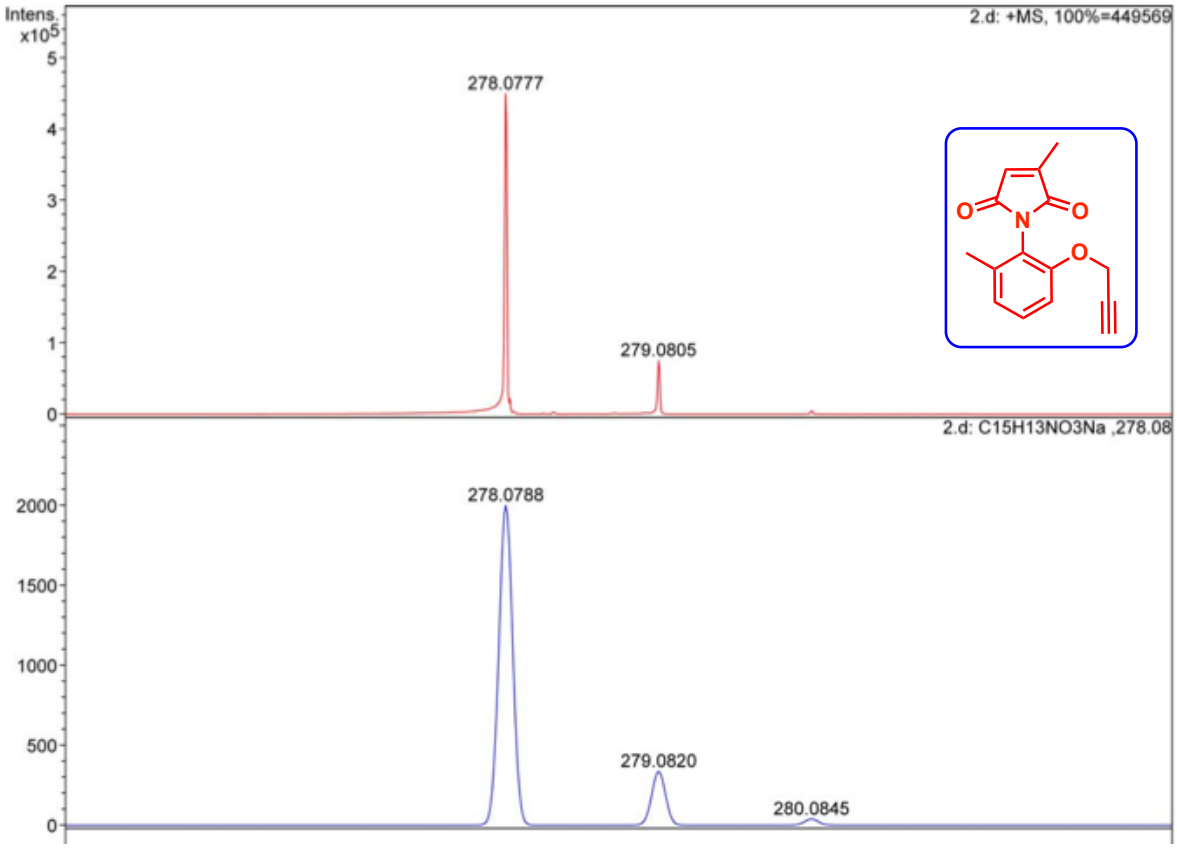

Figure 3.64: HRMS of maleimide derivative **192g**.

3.28.9. Synthesis of atropisomeric maleimide derivative 192d

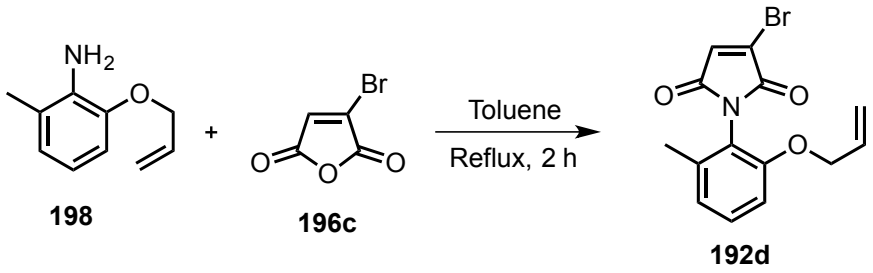

Scheme 3.42: Synthesis of atropisomeric maleimide derivative **192d**.

The bromocitraconic anhydride **196c** was synthesized according a procedure reported in the literature.[59] A mixture of aniline **198** (1.0 g, 1.0 *equiv.*) and anhydride **196c** (1.1 *equiv.*) in toluene (5 mL) was refluxed for 2 h. The reaction mixture was cooled to room temperature and the solvent was evaporated to get the crude product. The crude product was purified by combiflash using a hexanes:ethyl acetate mixture.

TLC condition - R_f = 0.43 (80% hexanes:20% ethyl acetate) for **192d** (Yield = 84 %)

^{1}H-NMR (400 MHz, $CDCl_3$, δ ppm): 7.27-7.23 (m, 1H), 7.01-7.00 (m, 1H), 6.89-6.87 (m, 1H), 6.79-6.77 (m, 1H), 5.92-5.82 (m, 1H), 5.27-5.17 (m, 2H), 4.49-4.48 (m, 2H) and 2.15 (m, 3H).

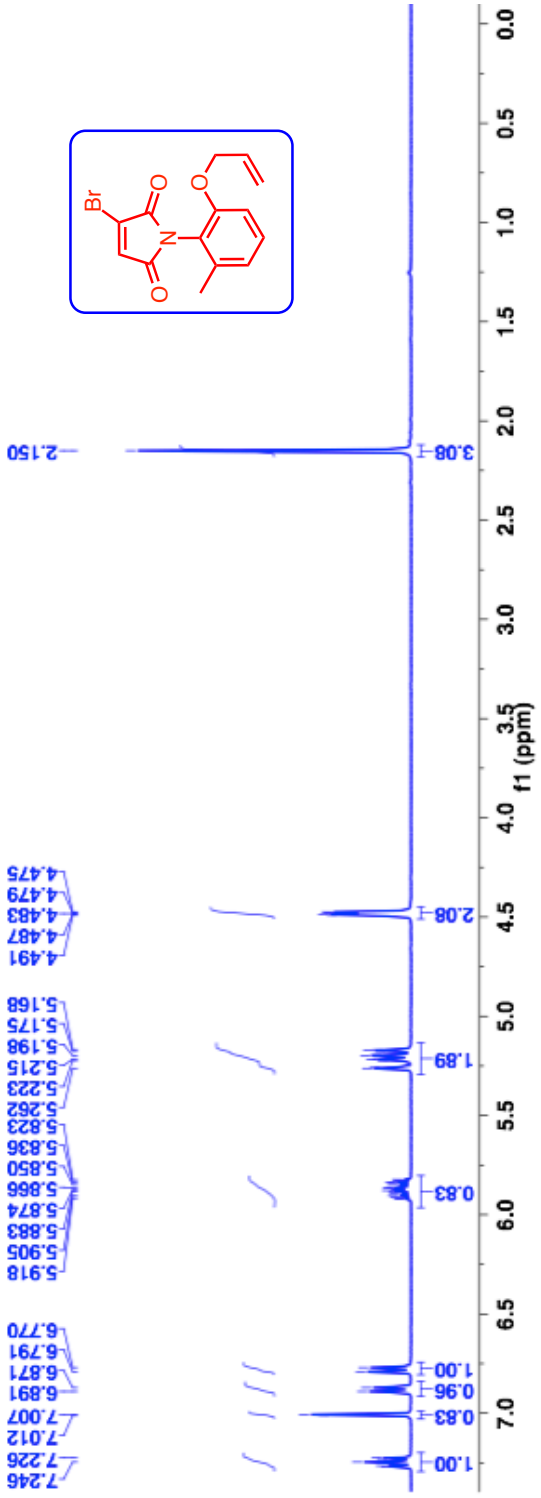

Figure 3.65: ^{1}H-NMR (400 MHz, $CDCl_3$, δ ppm) spectrum of maleimide derivative **192d**.

^{13}C-NMR (100 MHz, $CDCl_3$, δ ppm): 167.7, 164.5, 154.7, 139.1, 132.8, 132.7, 131.9, 130.6, 122.97, 119.3, 117.5, 110.8, 69.2 and 17.9.

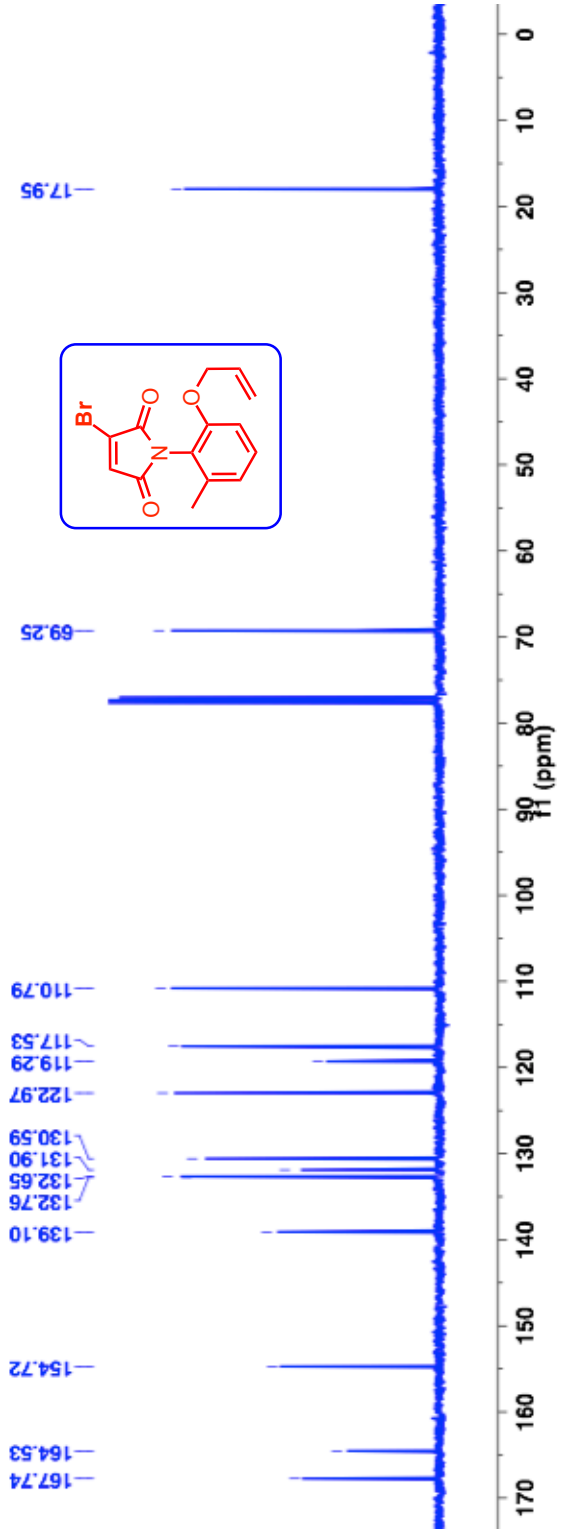

Figure 3.66: ^{13}C-NMR (400 MHz, $CDCl_3$, δ ppm) spectrum of maleimide derivative **192d**.

HRMS-ESI (m/z) ([M + Na]$^+$):

Calculated : 345.9874

Observed : 345.9875

|Δm| : 0.3 ppm

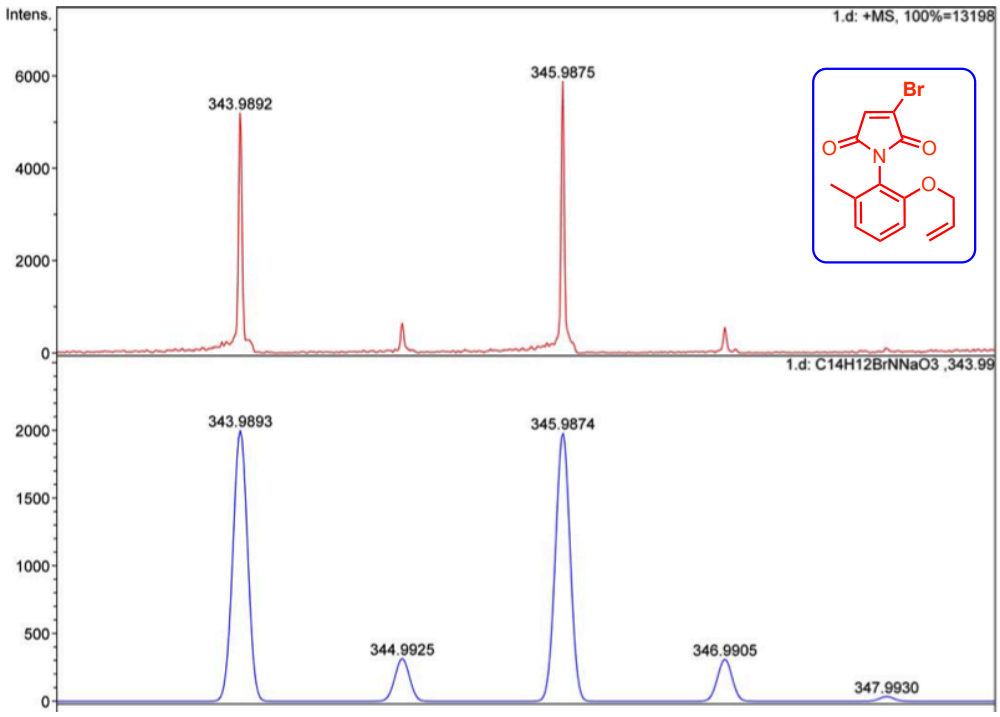

Figure 3.67: HRMS of maleimide derivative **192d**.

HPLC analysis conditions:

For analytical conditions,

I). Column : CHIRALPAK-ADH

Abs. detector wavelength : 254 nm and 270 nm

Mobile phase : Hexanes:2-propanol = 98:2

Flow rate : 1.0 mL/min

Retention times (min) : ~ 12.42 [**PkA**] and ~ 13.44 [**PkB**]

(**PkA** and **PkB** refers to the order of elution of the isomers in HPLC on a chiral stationary phase)

3.28.10. Synthesis of maleimide derivatives 192e and 192f

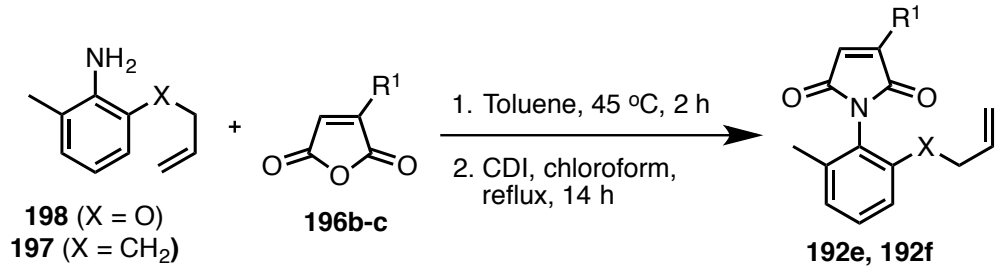

198 (X = O)
197 (X = CH_2)

196b-c

192e, 192f

Scheme 3.43: Synthesis of atropisomeric maleimide derivative **192e-f**.

The maleimide derivatives **192e and 192f** were synthesized according to the literature reported procedure.[12] To a solution of corresponding aniline derivative **197** or **198** (10 mmol) in toluene (20 mL) at 25 °C, substituted maleic anhydride **196b-c** (10.1 mmol) was added. The resulting mixture was heated to 45 °C and maintained for 2 h. After the reaction, the mixture was cooled to room temperature and the residue was diluted with hexanes (50 mL). The precipitated solid was filtered, washed with hexanes (20 mL) and dried under vacuum. The crude product was directly taken to next step without further purification.

To the crude product from above reaction dissolved in chloroform under N_2 atmosphere 1,1'-carbonyldiimidazole (12 mmol) was added. The resulting solution was refluxed for 14 h. After the reaction, the solution was cooled to room temperature and DI water was added. The mixture was stirred and the layers were separated. The organic layer was washed with DI Water (2 × 100 mL), cold aqueous 2N HCl (2 × 75 mL or until the imidazole byproduct was removed) and brine solution (1 × 100 mL). The organic layer was dried over *anhyd.* Na_2SO_4, filtered and the solvent was evaporated under reduced pressure to get the crude product. The crude product was purified by combiflash using a hexanes:ethyl acetate mixture (90:10).

Note: During the addition of 1,1'-carbonyldiimidazole evolution of CO_2 gas was observed.

TLC condition - R*f* = 0.55 (80% hexanes:20% ethyl acetate) for **192e**, (Yield = 70%).

TLC condition - R*f* = 0.50 (90% DCM: 10% MeOH) for **192f**, (Yield = 68%).

^{1}H-NMR (400 MHz, $CDCl_3$, δ ppm): 8.04-8.01 (m, 2H), 7.50-7.48 (m, 3H), 7.33-7.29 (m, 1H), 7.21-7.18 (m, 2H), 6.92 (s, 1H), 5.85-5.75 (m, 1H), 5.02-4.93 (m, 2H), 2.58-2.54 (m, 2H), 2.33-2.28 (m, 2H) and 2.17 (s, 3H).

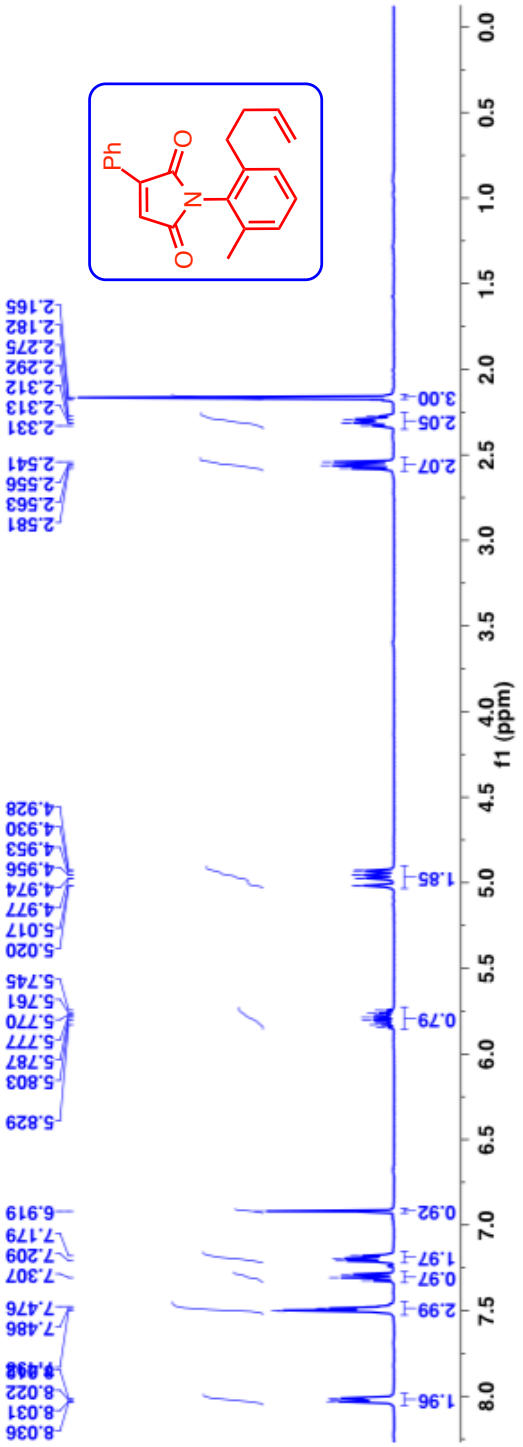

Figure 3.68: ^{1}H-NMR (400 MHz, $CDCl_3$, δ ppm) spectrum of maleimide derivative **192e**.

^{13}C-NMR (100 MHz, $CDCl_3$, δ ppm): 170.0, 169.7, 143.99, 141.1, 137.9, 137.4, 131.6, 129.7, 129.4, 129.3, 129.0, 128.95, 128.9, 127.7, 124.2, 115.4, 34.5, 31.5 and 18.3.

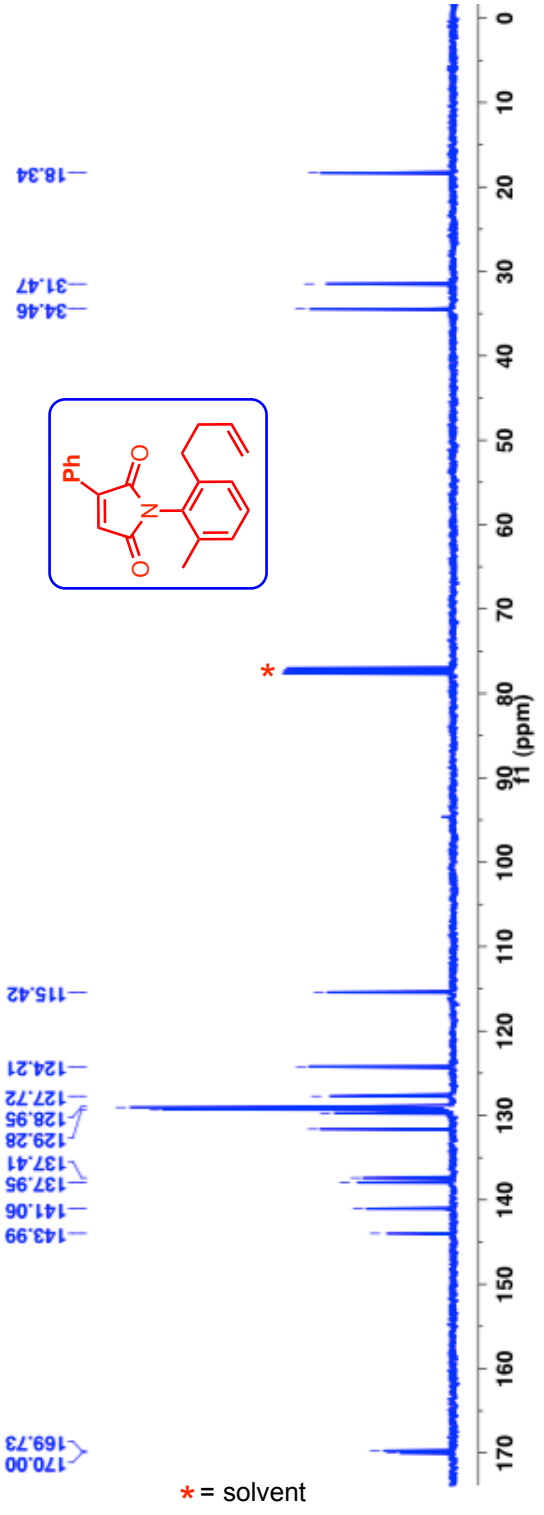

Figure 3.69: ^{1}H-NMR (400 MHz, $CDCl_3$, δ ppm) spectrum of maleimide derivative **192e**.

HRMS-ESI (m/z) ([M + Na]$^+$):

Calculated : 340.1308

Observed : 340.1299

|Δm| : 2.6 ppm

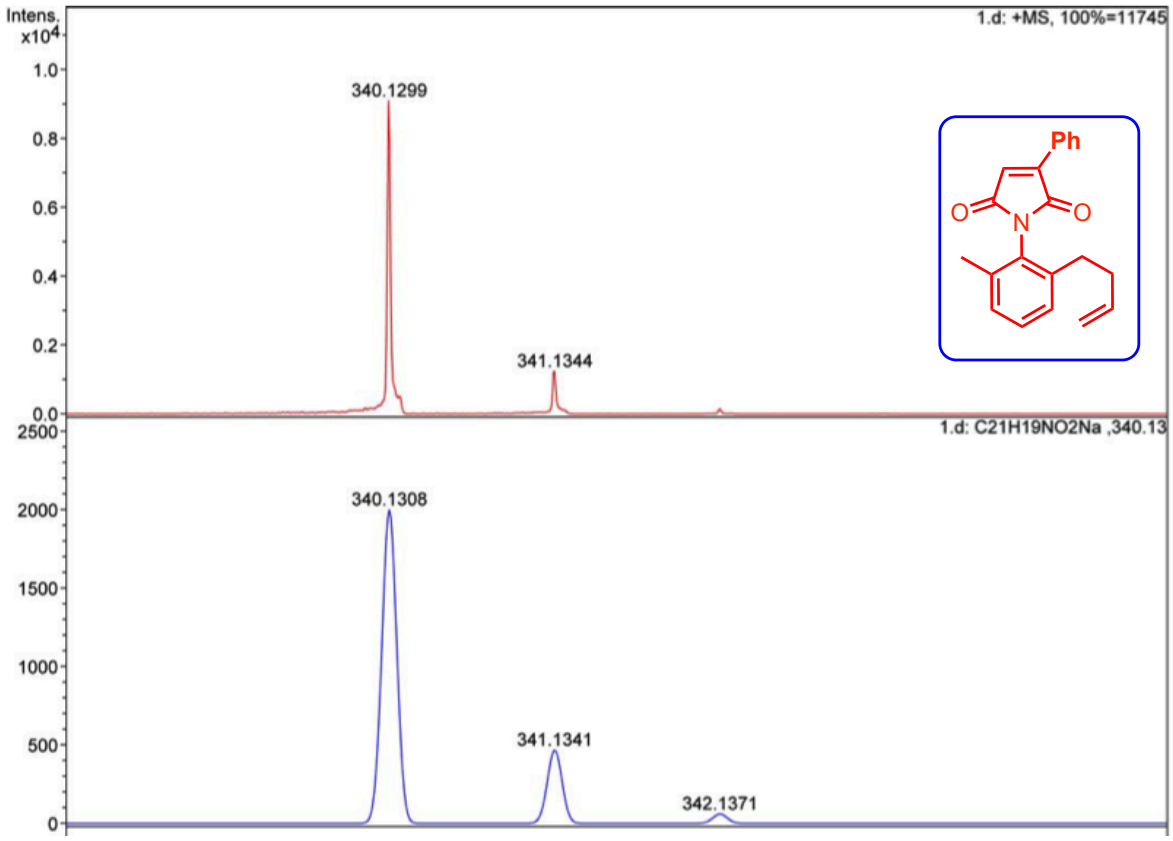

Figure 3.70: HRMS of maleimide derivative **192e**.

^{1}H-NMR (400 MHz, $CDCl_3$, δ ppm): 8.52 (s, 1H), 7.52 (s, 1H), 7.28-7.23 (m, 2H), 6.90-6.88 (m, 1H), 6.80-6.78 (m, 1), 6.398 (s, 1H), 5.91-5.82 (m, 1H), 5.26-5.15 (m, 2H), 4.50-4.49 (m, 2H) and 2.18 (s, 3H).

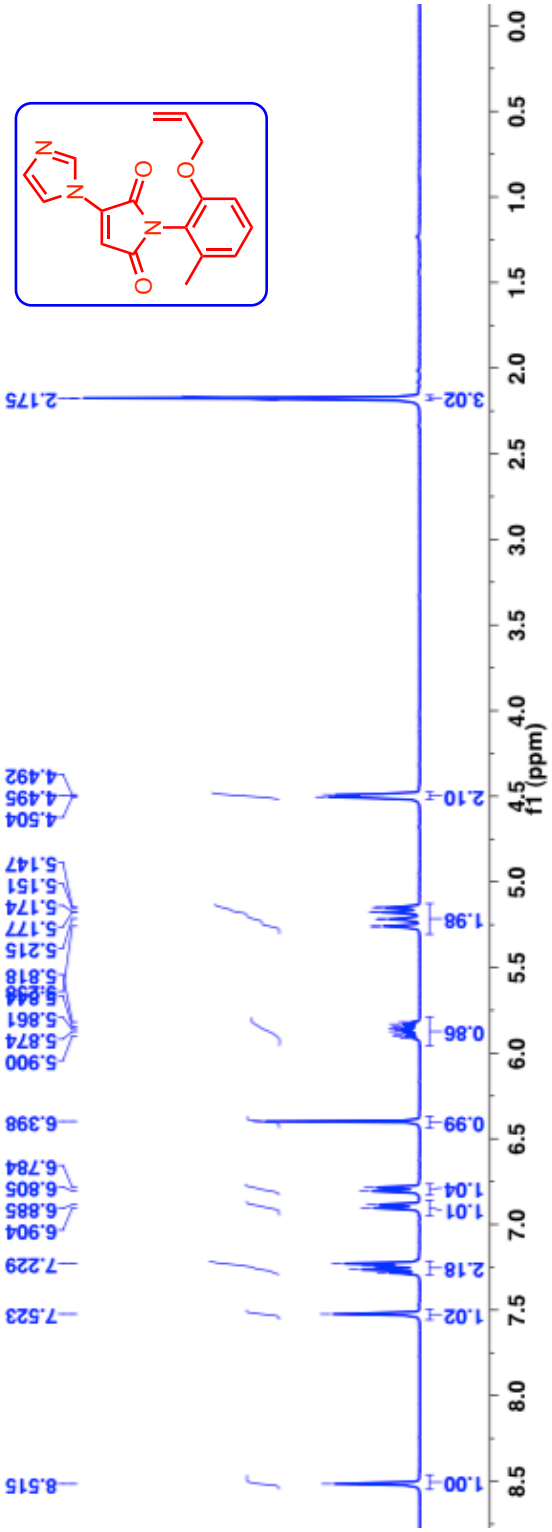

Figure 3.71: ^{1}H-NMR (400 MHz, $CDCl_3$, δ ppm) spectrum of maleimide derivative **192f**.

^{13}C-NMR (100 MHz, $CDCl_3$, δ ppm): 167.9, 164.98, 154.8, 139.2, 138.7, 137.2, 132.7, 132.1, 130.7, 123.0, 118.8, 117.7, 117.6, 110.8, 109.4, 69.3 and 17.99.

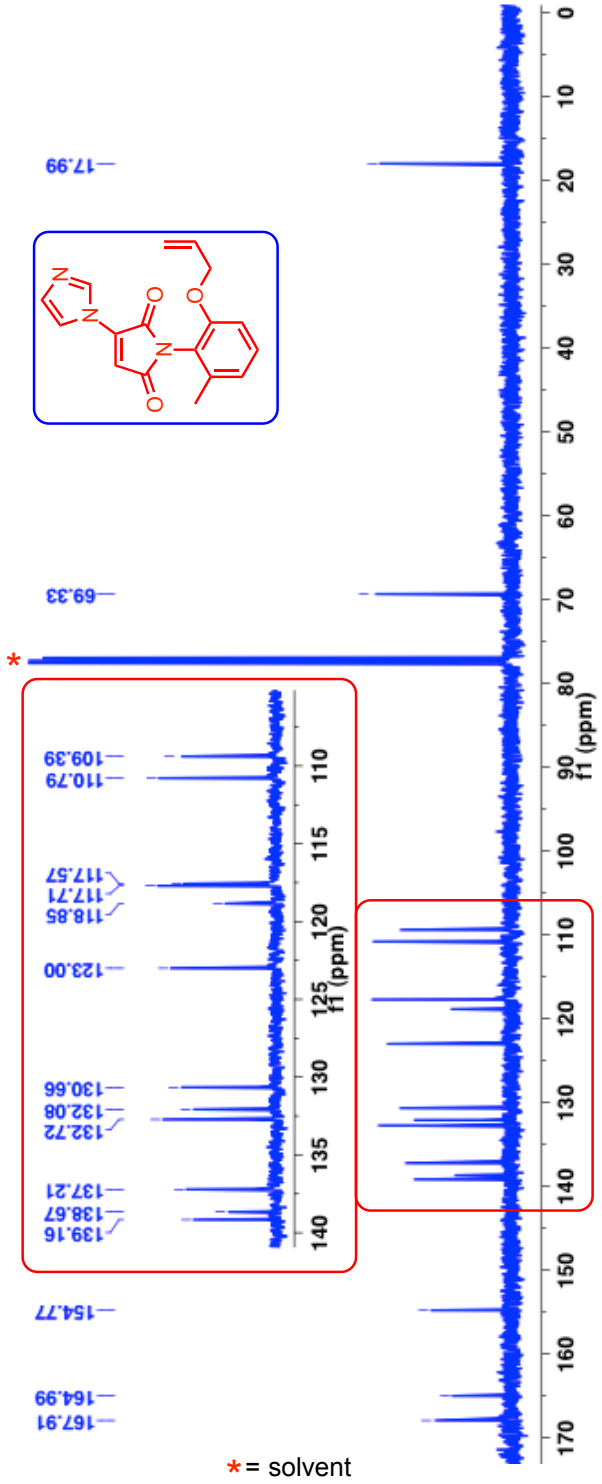

Figure 3.72: ^{13}C-NMR (100 MHz, $CDCl_3$, δ ppm) spectrum of maleimide derivative **192f**.

HRMS-ESI (m/z) ([M + Na]$^+$):

Calculated : 332.1006

Observed : 332.1001

|Δm| : 1.5 ppm

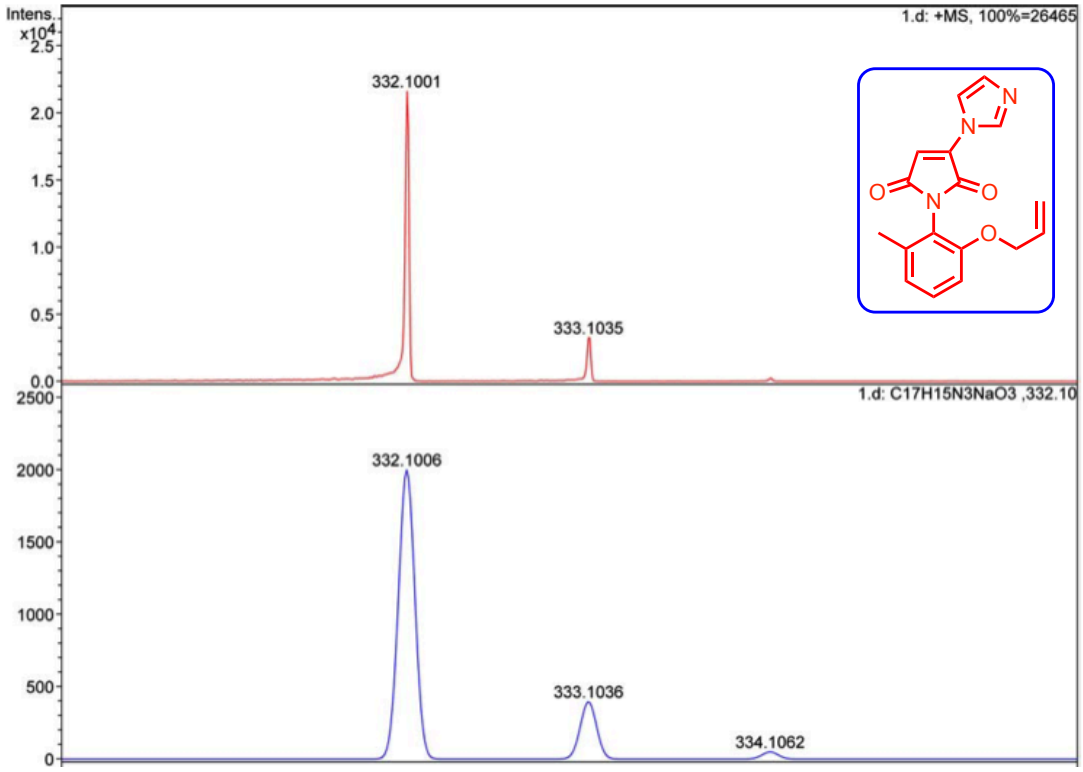

Figure 3.73: HRMS of maleimide derivative **192f**.

3.29. UV-Vis spectrum of atropisomeric maleimides and its photoproducts

The UV-Vis spectra of atropisomeric maleimides and its photoproducts were measured in acetonitrile.

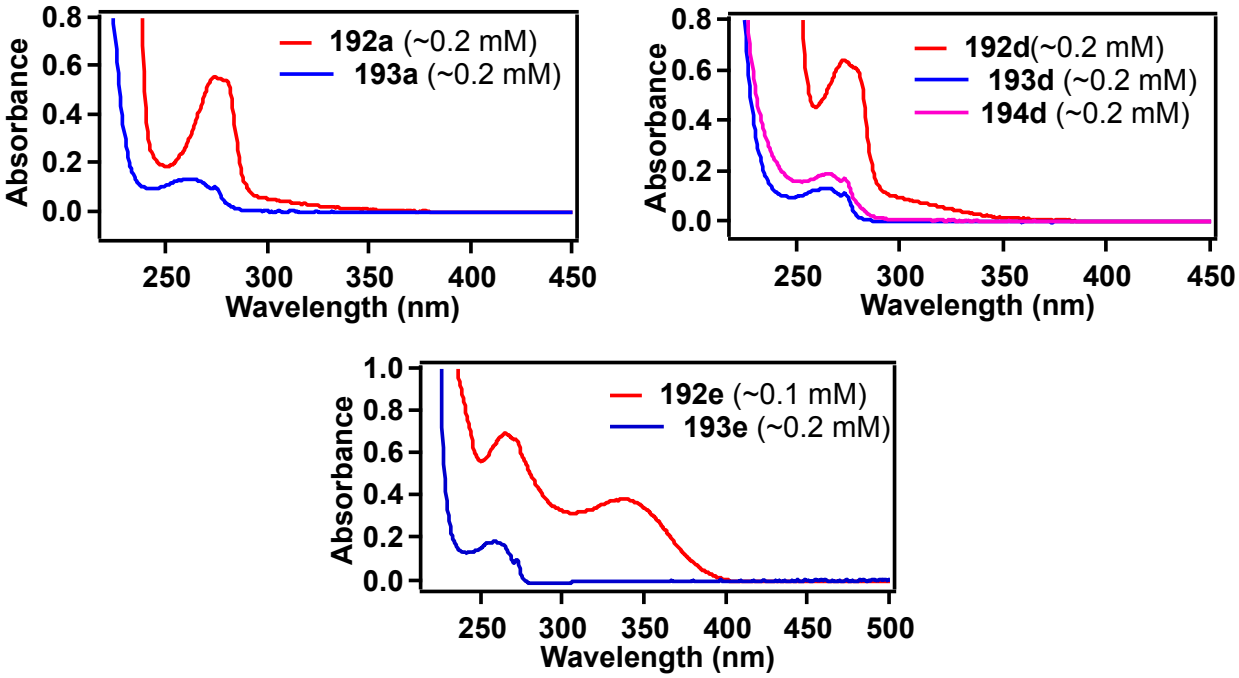

Figure 3.74: UV-Vis spectra of maleimides **192** and its photoproducts **193** and **194** in acetonitrile.

3.30. General irradiation procedures and characterization of photoproducts

3.30.1. Process for photoreaction of atropisomeric maleimides 192

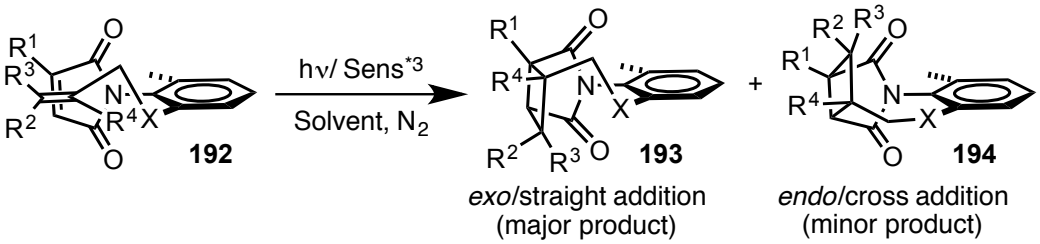

Scheme 3.44: General irradiation procedure for maleimides **192**.

Enantiospecific reactions: A solution of optically pure atropisomeric maleimides obtained from HPLC preparative separation on a chiral stationary phase (2.5-4.0 mM or 1 mg/1 mL) in appropriate solvent (acetone or MeCN) or with the combination of MeCN/30 mol% sensitizer (xanthone or thioxanthone) was irradiated in either one of the following procedures. a) The solution in a Pyrex tube was irradiated with a 450W medium-pressure mercury lamp under constant flow of nitrogen for a given time interval. b) Irradiated in a Rayonet reactor fitted with bulb of desired wavelength. After the irradiation, the solvent was evaporated under reduced pressure and the photoproducts were isolated by preparative thin layer chromatography and characterized by NMR spectroscopy, mass spectrometry, single crystal XRD, CD, $[\alpha]_D$ and by HPLC. HPLC analysis of the photolysate on a chiral stationary phase gave the optical purity of the photoproducts.

Large-scale reactions: Large-scale reactions were carried out on racemic maleimides as batches (4 × 20 mL test tubes per batch). After the irradiation the solutions were combined and the solvent was evaporated under reduced pressure. The residue was purified by combiflash using a hexanes:ethyl acetate mixture as mobile phase.

In some cases (**192e** and **192f**) N_2 degassed solutions of maleimides placed in a merry-go-round (8 x 10 mL test tubes) were irradiated in a Rayonet reactor for given time period. After the irradiation, the solutions were combined and the solvent was evaporated under reduced pressure. The residue was purified by combiflash using a hexanes:ethyl acetate mixture as mobile phase.

Conversion and mass balance were obtained from NMR integration of the crude photosylate against triphenylmethane as an internal standard using the equation 2.1 (Chapter 2)

The *dr* of the photoproducts **193** and **194** were calculated from the crude reaction mixture after the photoreaction.

TLC condition - R*f* = 0.30 (80% hexanes:20% ethyl acetate) for **193a**

TLC condition - R*f* = 0.25 (50% hexanes:50% ethyl acetate for **193b**

TLC condition - R*f* = 0.18 (80% hexanes:20% ethyl acetate) for **193c**

TLC condition - R*f* = 0.20 (80% hexanes:20% ethyl acetate)for **194c**

TLC condition - R*f* = 0.35 (80% petroleum ether:20% ethyl acetate) for **193d**

TLC condition - R*f* = R*f* = 0.25 (80% petroleum ether:20% ethyl acetate for **194d**

TLC condition - R*f* = 0.35 (50% hexanes:50% ethyl acetate) for **193e**

TLC condition - R*f* = 0.40 (90% DCM:10% MeOH) for **193f**

^{1}H-NMR (400 MHz, $CDCl_3$, δ ppm): 7.20-7.16 (m, 1H), 7.06-7.04 (m, 1H), 6.92-6.90 (m, 1H), 4.57 (dd, *J* = 14.4, 4.8 Hz, 1H), 3.87 (d, *J* = 14.4Hz, 1H), 2.92-2.91(m, 1H), 2.35 (s, 3H), 2.18-2.16 (m, 1H), 1.68 (s, 3H), 1.61 (s, 3H) and 1.37 (s, 3H).

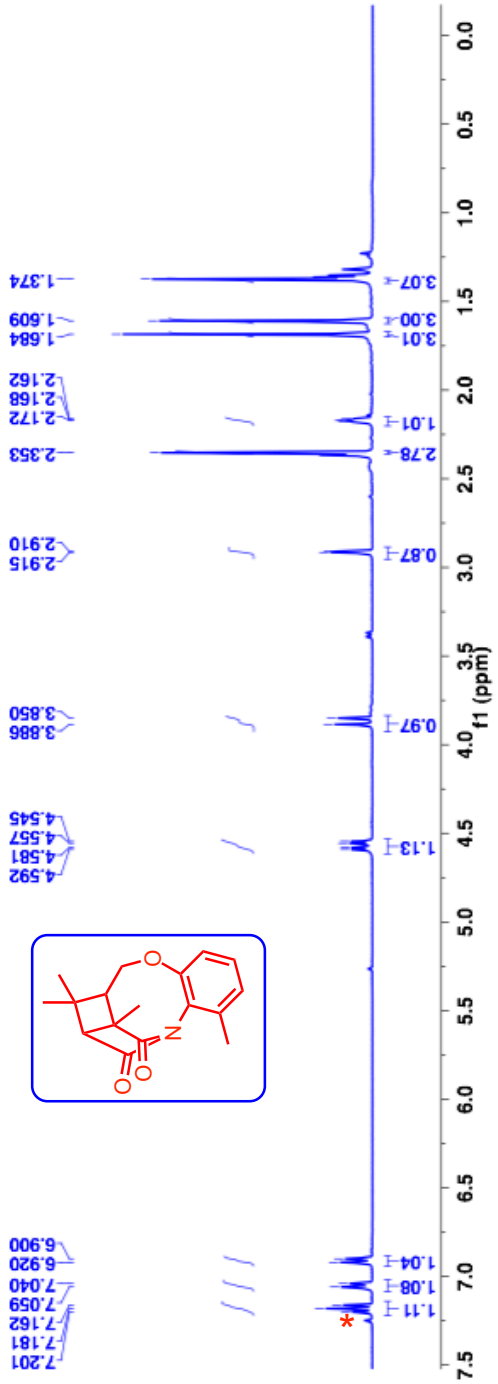

Figure 3.75: ^{1}H-NMR (400 MHz, $CDCl_3$, δ ppm) spectrum of maleimide photoproduct **193a**.

^{13}C-NMR (100 MHz, $CDCl_3$, δ ppm): 183.2, 179.3, 155.9, 139.2, 132.17, 129.9, 126.5, 120.4, 74.1, 58.6, 54.5, 48.9, 41.2, 32.6, 22.5, 17.9 and 17.6.

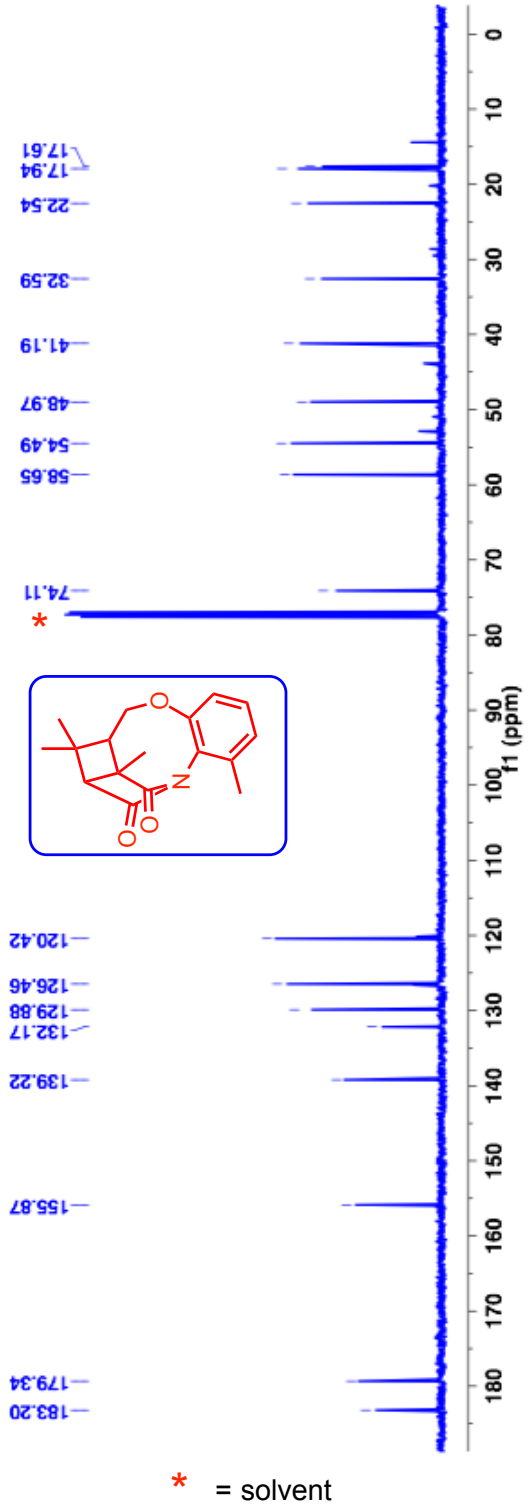

Figure 3.76: ^{13}C-NMR (100 MHz, $CDCl_3$, δ ppm) spectrum of maleimide photoproduct **193a**.

HRMS-ESI (m/z) ([M + Na]$^+$):

Calculated : 308.1257

Observed : 308.1249

|Δm| : 2.6 ppm

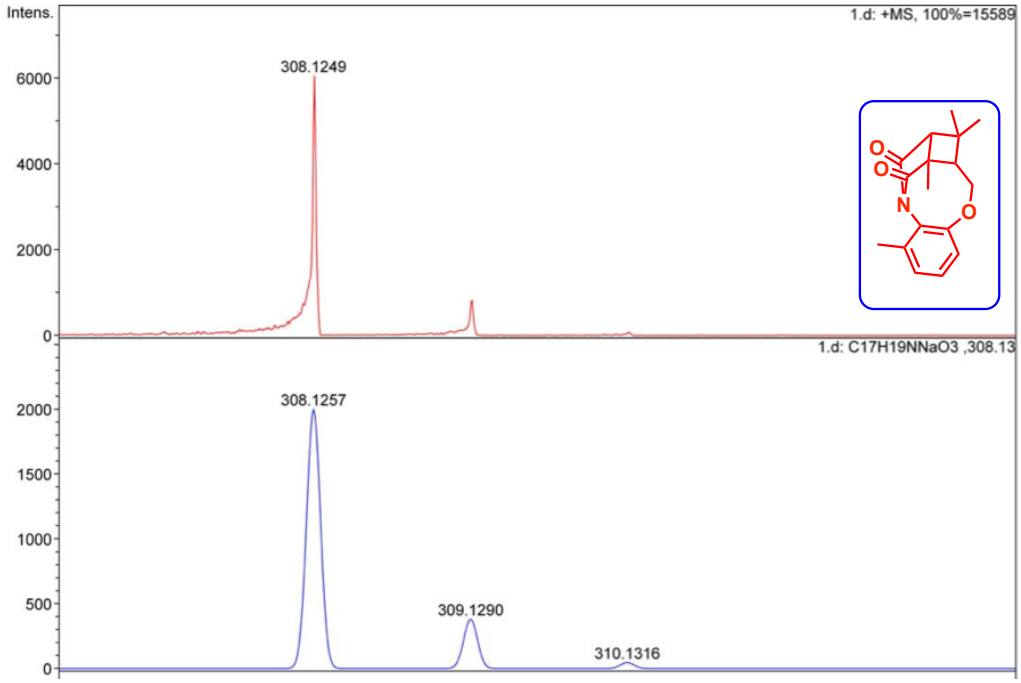

Figure 3.77: HRMS of maleimide photoproduct **193a**.

HPLC analysis conditions:

For analytical conditions,

I). Column : CHIRALPAK-OD-H

Abs. detector wavelength : 254 nm and 270 nm

Mobile phase : Hexanes:2-propanol = 90:10

Flow rate : 1.0 mL/min

Retention times (min) : ~ 15.87 [PkA-**193a**] and ~ 20.57 [PkB-**193a**]

For preparative conditions,

I). Column : CHIRALPAK-OD-H

Abs. detector wavelength : 254 nm and 270 nm

Mobile phase : Hexanes:2-propanol = 95:5

Flow rate : 3.0 mL/min

Retention times (min) : ~ 35.30 [PkA-**193a**] and ~ 45.40 [PkB-**193a**]

^{1}H-NMR (400 MHz, $CDCl_3$, δ ppm): 7.19-7.15 (m, 1H), 7.06-7.04 (m, 1H), 6.93-6.91 (m, 1H), 4.61-4.54 (m, 1H), 3.88-3.80 (m, 1H), 3.61-3.51 (m, 1H), 3.10 (dd, *J* = 9.2, 2.4 Hz, 1H), 2.45 – 2.41 (m, 1H), 2.36 (s, 3H), 1.54 (s, 3H) and 1.34 (d, *J* = 7.2 Hz, 3H).

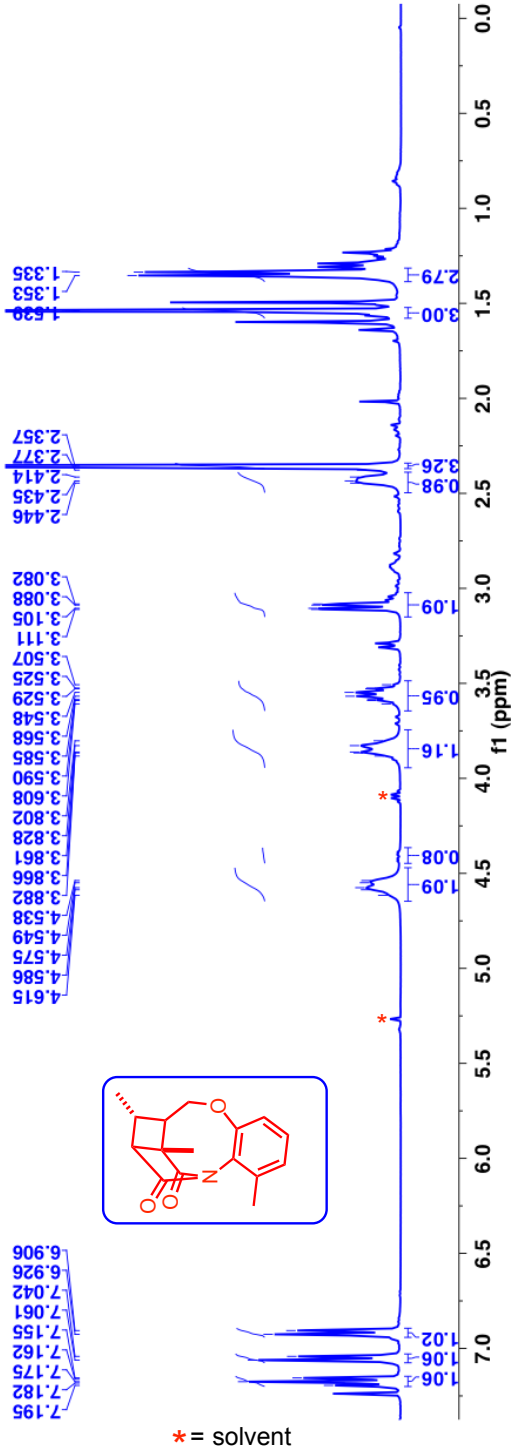

Figure 3.78: ^{1}H-NMR (400 MHz, $CDCl_3$, δ ppm) spectrum of maleimide photoproduct **193b**.

^{13}C-NMR (100 MHz, $CDCl_3$, δ ppm): 182.3, 179.3, 156.0, 139.2, 132.4, 129.7, 126.6, 120.1, 74.9, 53.1, 50.7, 48.6, 33.6, 19.5, 17.6 and 15.3.

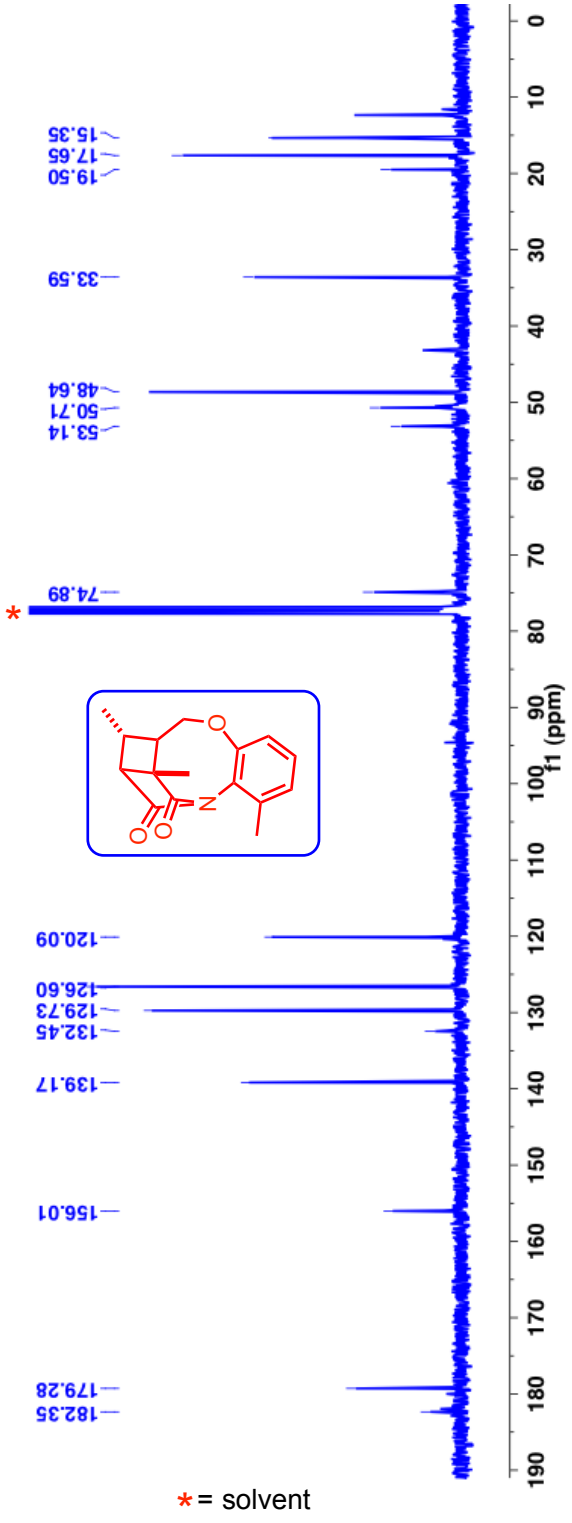

Figure 3.79: ^{13}C-NMR (100 MHz, $CDCl_3$, δ ppm) spectrum of maleimide photoproduct **193b**.

HRMS-ESI (m/z) ([M + Na]$^+$):

Calculated : 294.1101

Observed : 294.1094

|Δm| : 2.4 ppm

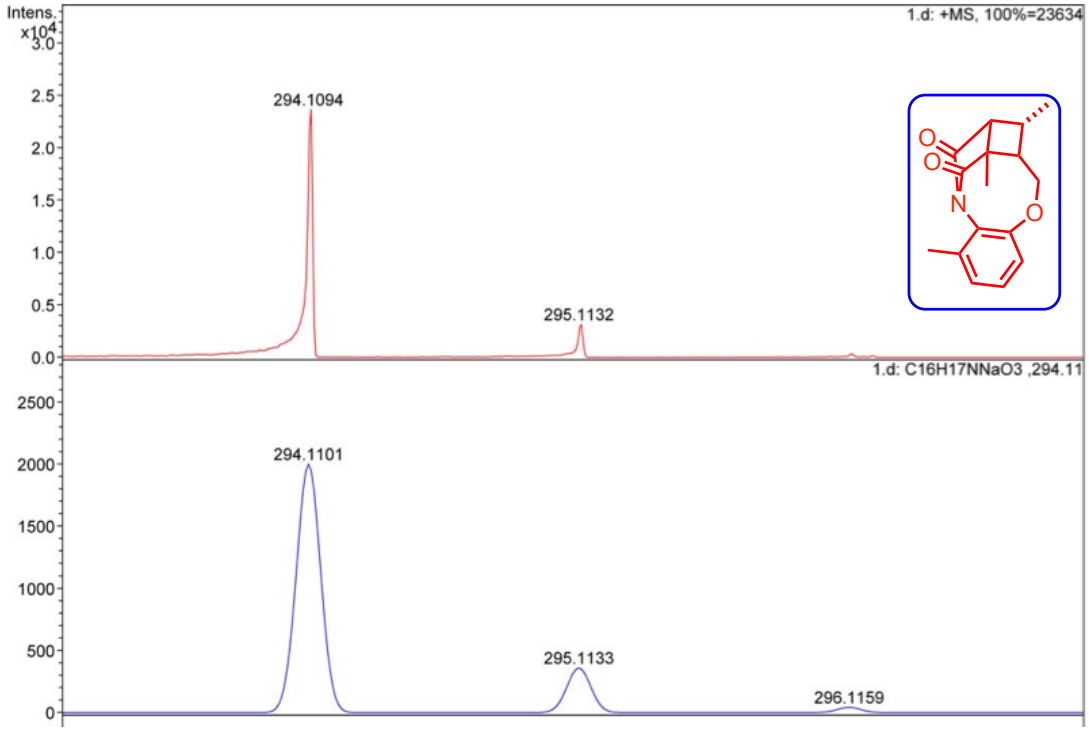

Figure 3.80: HRMS of maleimide photoproduct **193b**.

HPLC analysis conditions:

For analytical conditions,

I). Column : CHIRALPAK-AD-H

Abs. detector wavelength : 254 nm and 270 nm

Mobile phase : Hexanes:2-propanol = 95:5

Flow rate : 1.0 mL/min

Ret. tim. (min): ~9.84 [(PkA)-(*1R,5S,6R,7S*)-**193b**] and ~11.53 [(PkB)-(*1S,5R,6S,7R*)-**193b**]

(**PkA** and **PkB** refers to the order of elution of the isomers on the chiral stationary phase)

^{1}H-NMR (400 MHz, $CDCl_3$, δ ppm): 7.20-7.16 (m, 1H), 7.07-7.05 (m, 1H), 6.95-6.93 (m, 1H), 4.02 (d, *J* = 13.5 Hz, 1H), 3.56 (d, *J* = 13.2 Hz, 1H), 2.98 (dd, *J* = 10, 1.6 Hz, 1H), 2.77 (dd, *J* = 12.4, 1.6 Hz, 1H), 2.55 (dd, *J* = 12.0, 10.0 Hz, 1H), 2.36 (s, 3H), 1.45 (s, 3H) and 1.02 (s, 3H).

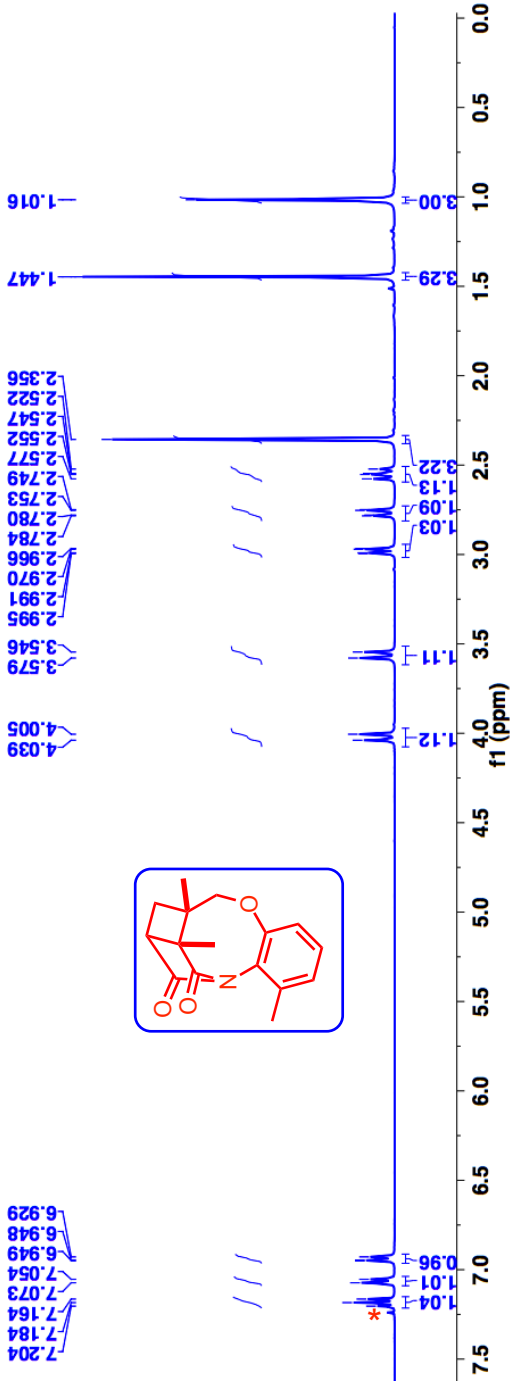

* = solvent

Figure 3.81: ^{1}H-NMR (400 MHz, $CDCl_3$, δ ppm) spectrum of maleimide photoproduct **193c**.

^{13}C-NMR (100 MHz, $CDCl_3$, δ ppm): 182.8, 182.7, 155.8, 139.2, 132.6, 129.7, 126.7, 120.1, 80.7, 54.1, 48.8, 41.99, 32.5, 20.9, 17.6, and 12.96.

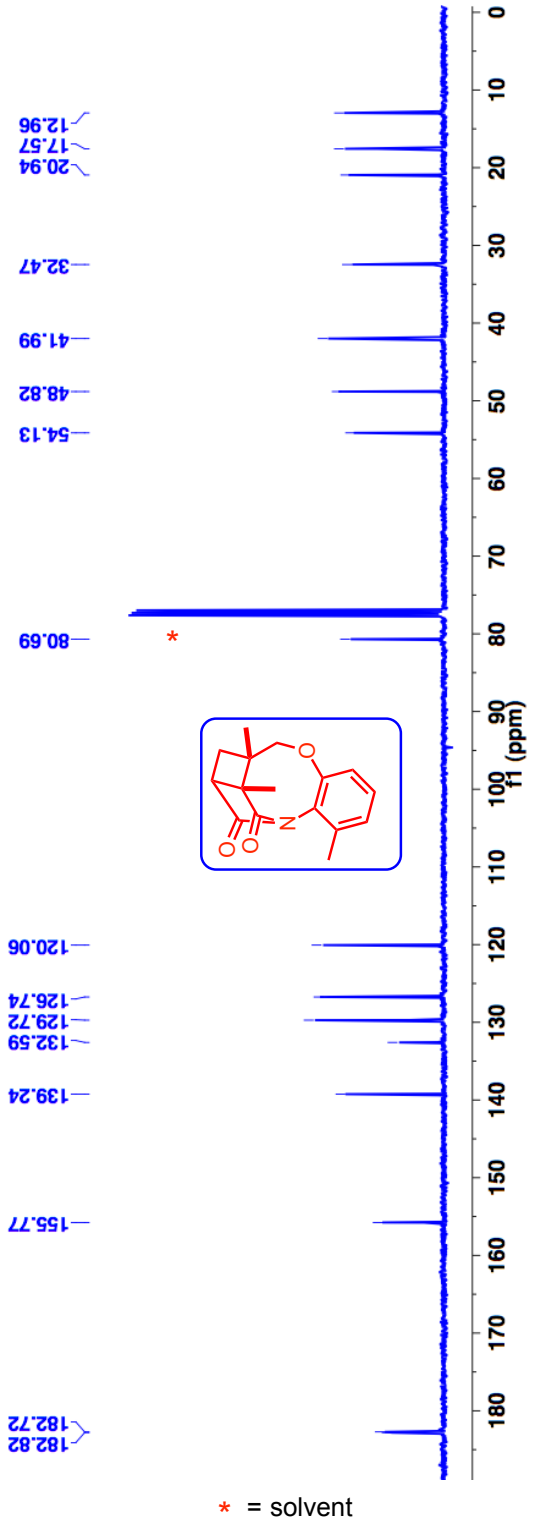

Figure 3.82: ^{13}C-NMR (100 MHz, $CDCl_3$, δ ppm) spectrum of maleimide photoproduct **193c**.

HRMS-ESI (m/z) ([M + Na]$^+$):

Calculated : 294.1101

Observed : 294.1088

|Δm| : 4.4 ppm

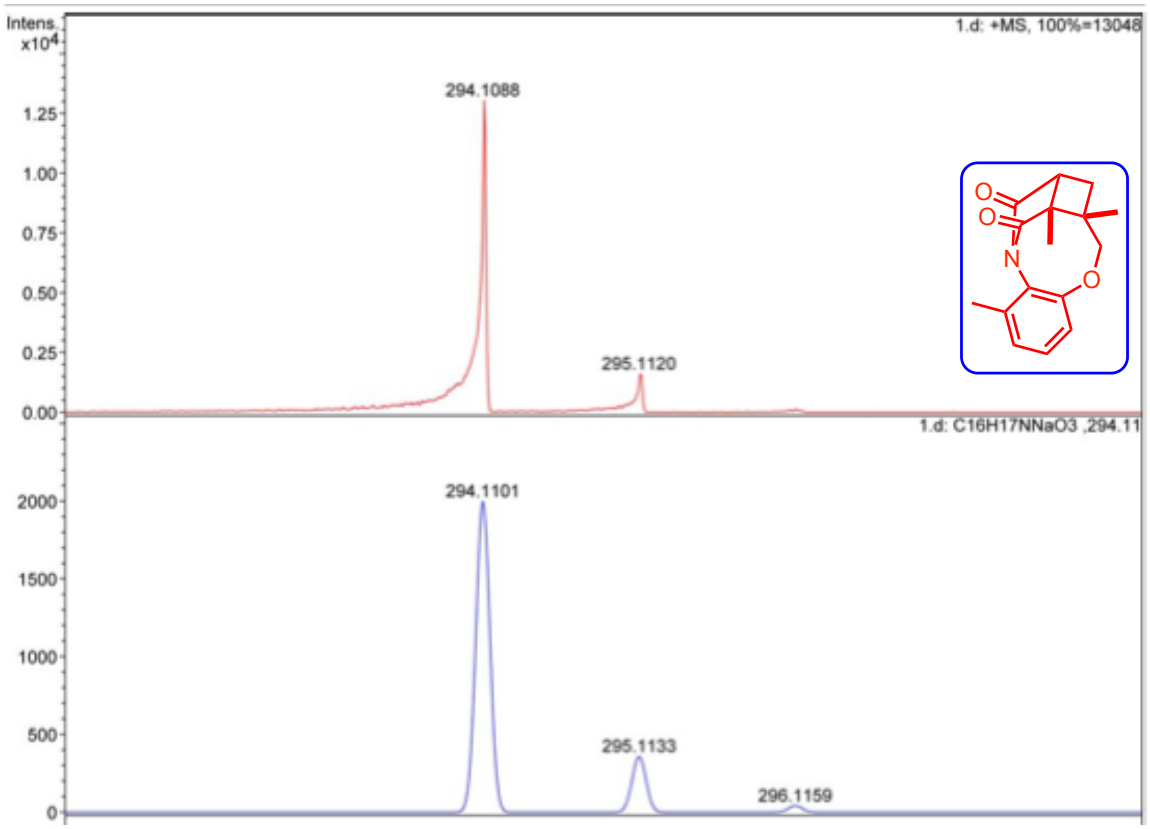

Figure 3.83: HRMS of maleimide photoproduct **193c**.

^{1}H-NMR (400 MHz, $CDCl_3$, δ ppm): 7.20-7.16 (m, 1H), 7.07-7.05 (m, 1H), 6.94-6.92 (m, 1H), 3.97 (d, *J* = 13.6 Hz, 1H), 3.59 (d, *J* = 13.2 Hz, 1H), 3.09 (s, 1H), 2.98 (d, *J* = 12.4 Hz, 1H), 2.36 (s, 3H), 2.21 (d, *J* = 12.4 Hz, 1H), 1.52 (s, 3H) and 1.20 (s, 3H).

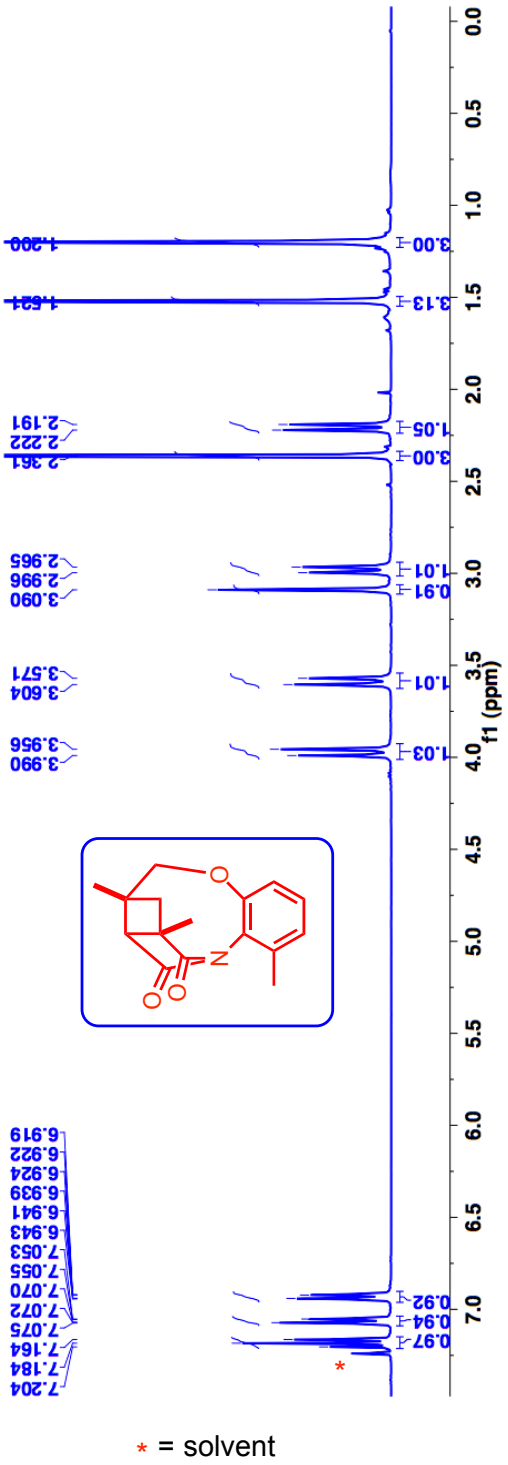

Figure 3.84: ^{1}H-NMR (400 MHz, $CDCl_3$, δ ppm) spectrum of maleimide photoproduct **194c**.

^{13}C-NMR (100 MHz, $CDCl_3$, δ ppm): 185.6, 179.6, 155.96, 139.3, 132.4, 129.7, 126.8, 120.2, 79.7, 58.2, 44.0, 41.6, 41.1, 26.5, 20.2 and 17.6.

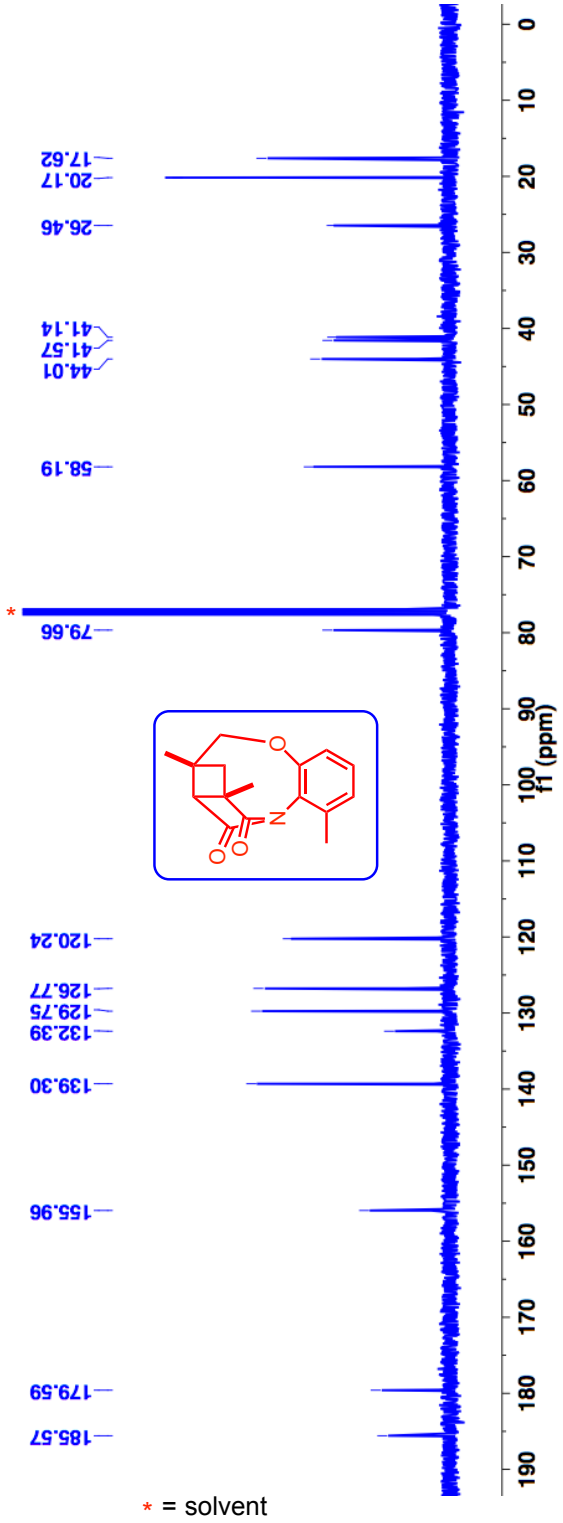

Figure 3.85: ^{13}C-NMR (100 MHz, $CDCl_3$, δ ppm) spectrum of maleimide photoproduct **194c**.

HRMS-ESI (m/z) ([M + Na]$^+$):

Calculated : 294.1101

Observed : 294.1098

|Δm| : 1.0 ppm

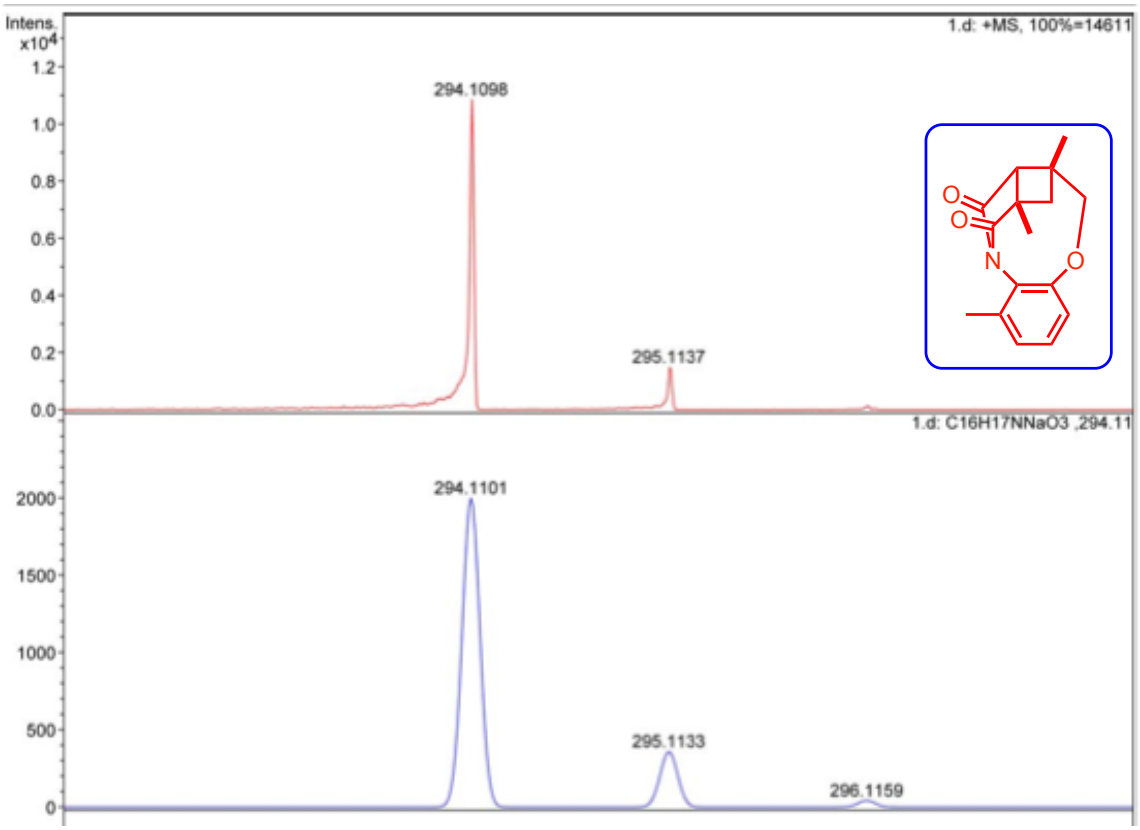

Figure 3.86: HRMS of maleimide photoproduct **194c**.

^{1}H-NMR (400 MHz, $CDCl_3$, δ ppm): 7.24-7.199 (m, 1H), 7.10-7.08 (m, 1H), 6.98-6.96 (m, 1H), 4.37 (dd, *J* =14.0, 4.8 Hz, 1H), 3.79 (d, *J* =14 Hz, 1H), 3.50-3.48 (m, 1H), 3.396-3.32 (m, 1H), 3.15-3.12 (m, 1H), 2.66 (d, *J* =12 Hz, 1H) and 2.37 (s, 3H).

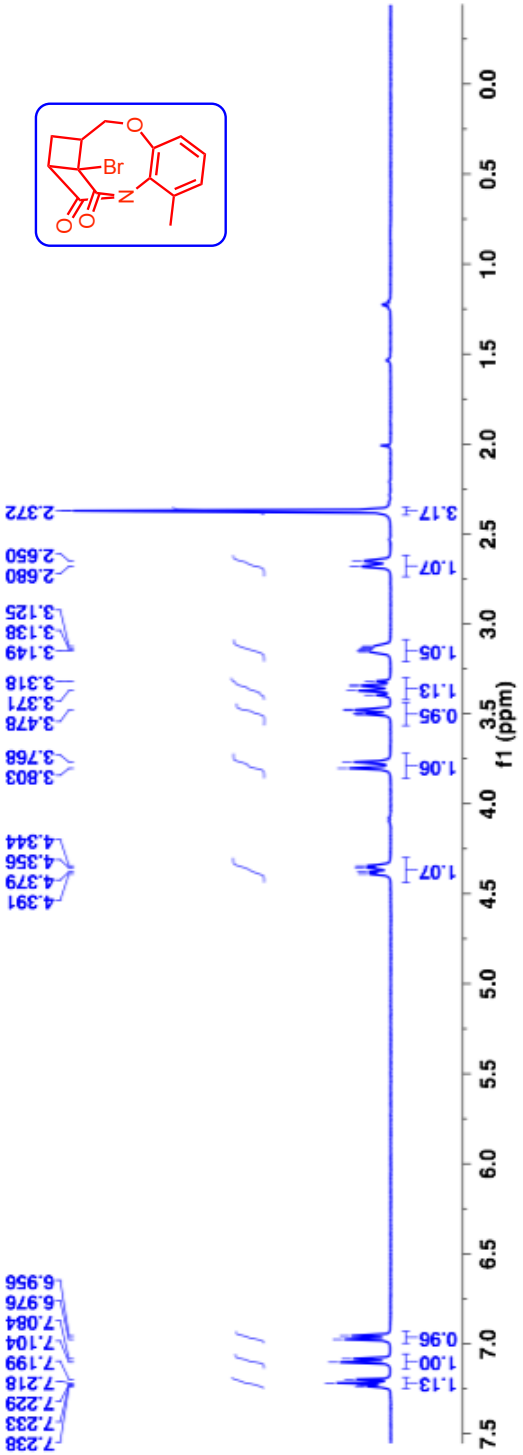

Figure 3.87: ^{1}H-NMR (400 MHz, $CDCl_3$, δ ppm) spectrum of maleimide photoproduct **193d**.

^{13}C-NMR (100 MHz, $CDCl_3$, δ ppm): 178.9, 175.1, 156.0, 139.6, 131.9, 130.3, 127.1, 120.5, 73.7, 55.2, 53.4, 47.5, 24.4 and 17.6.

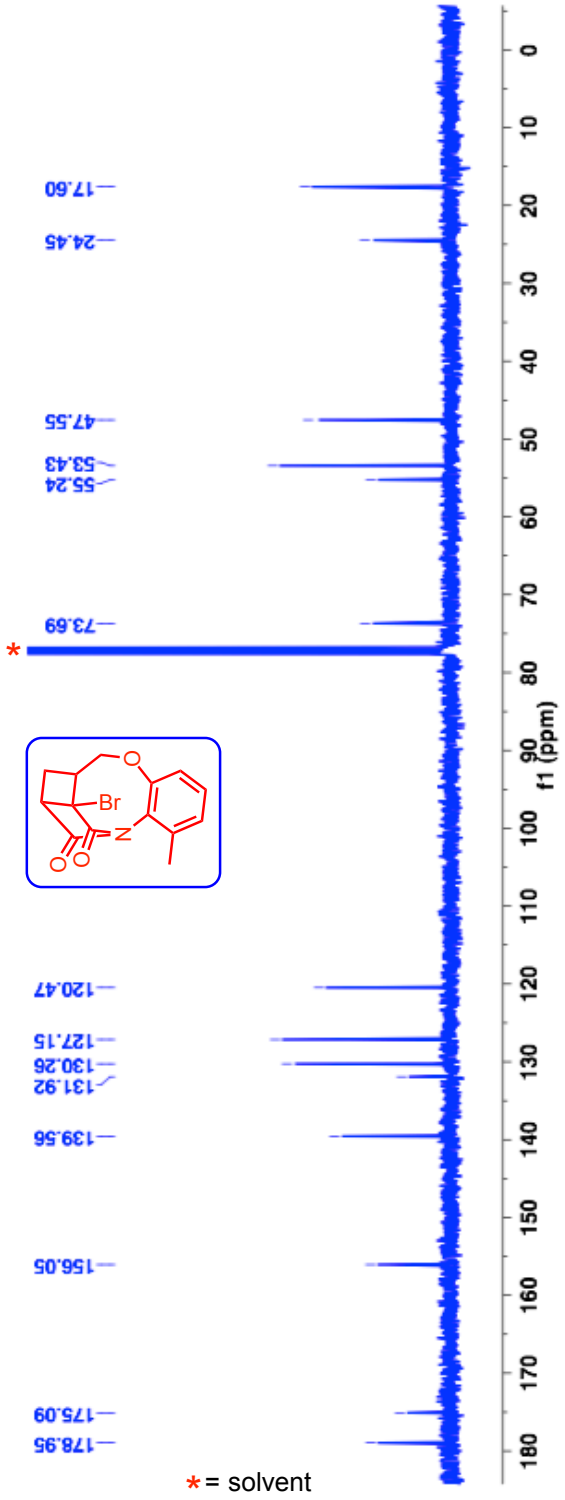

Figure 3.88: ^{13}C-NMR (400 MHz, $CDCl_3$, δ ppm) spectrum of maleimide photoproduct **193d**.

HRMS-ESI (m/z) ([M + Na]$^+$):

Calculated : 343.9893

Observed : 343.9896

|Δm| : 0.9 ppm

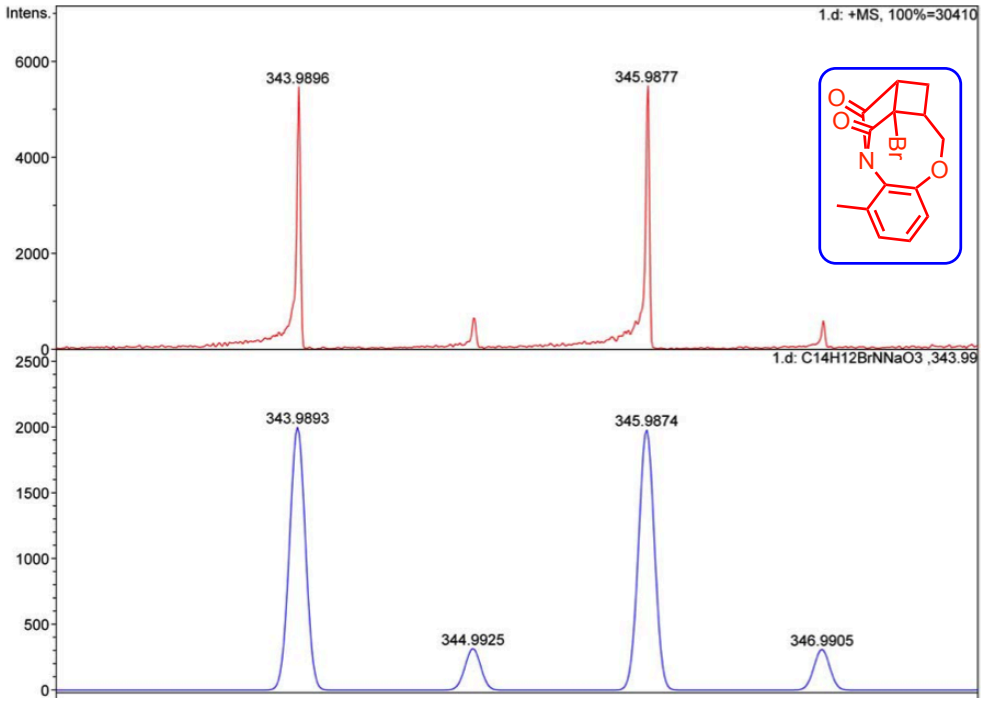

Figure 3.89: HRMS of maleimide photoproduct **193d**.

^{1}H-NMR (400 MHz, $CDCl_3$, δ ppm): 7.25-7.21 (m, 1H), 7.11-7.09 (m, 1H), 6.98-6.96 (m, 1H), 4.43-4.39 (m, 1H), 3.99-3.95 (m, 1H), 3.63 (d, *J* =13.6 Hz, 1H), 3.22-3.199 (m, 3H) and 2.39 (s, 3H).

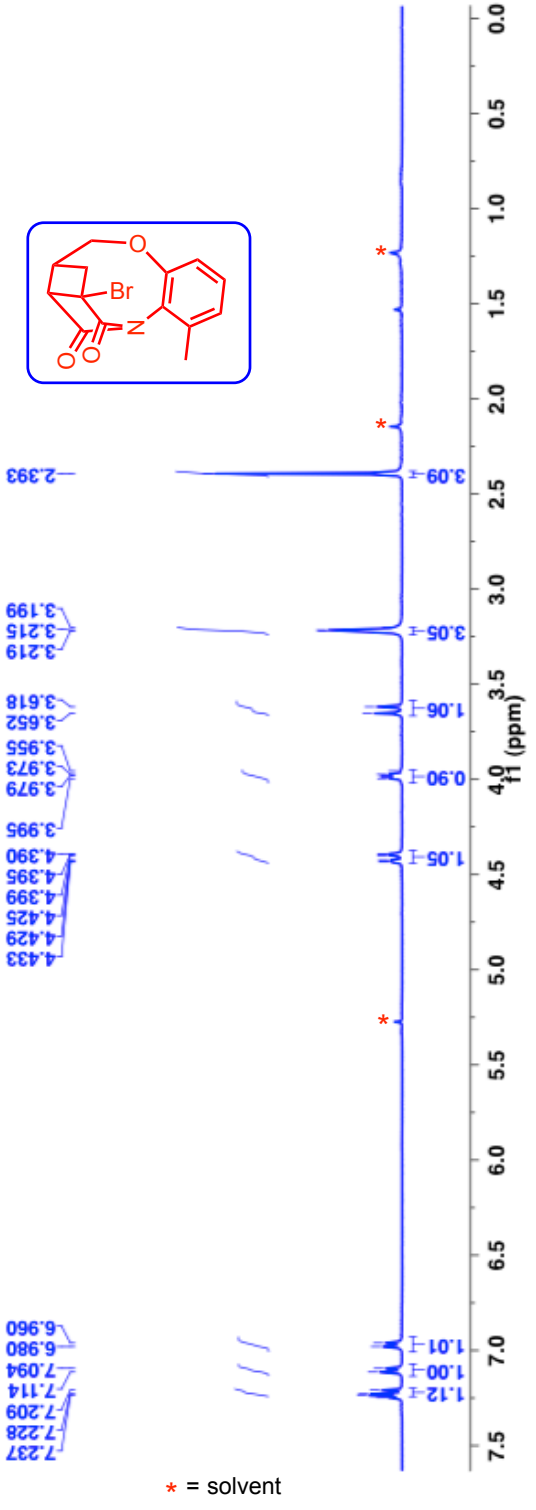

Figure 3.90: ^{1}H-NMR (400 MHz, $CDCl_3$, δ ppm) spectrum of maleimide photoproduct **194d**.

^{13}C-NMR (100 MHz, $CDCl_3$, δ ppm): 178.3, 176.8, 155.97, 139.4, 132.1, 130.2, 127.2, 120.4, 73.4, 55.9, 45.6, 39.2, 37.2 and 17.7.

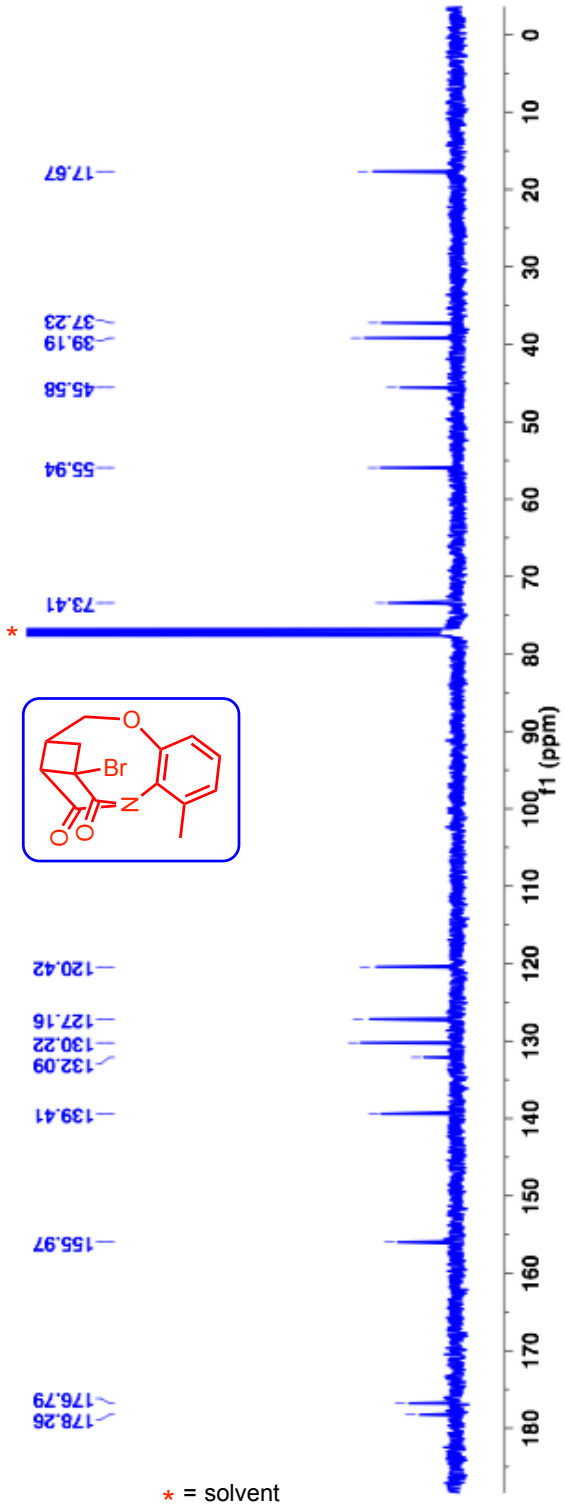

Figure 3.91: ^{13}C-NMR (100 MHz, $CDCl_3$, δ ppm) spectrum of maleimide photoproduct **194d**.

HRMS-ESI (m/z) ([M + Na]$^+$):

Calculated : 343.9893

Observed : 343.9899

|Δm| : 1.7 ppm

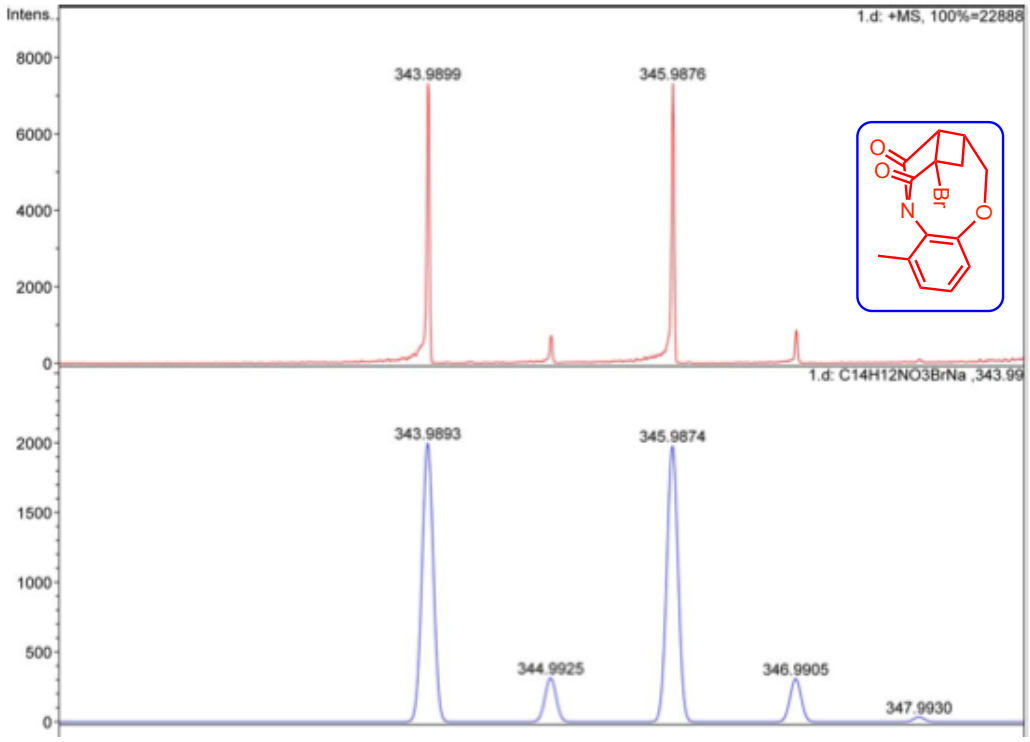

Figure 3.92: HRMS of maleimide photoproduct **194d**.

^{1}H-NMR (400 MHz, CD_2Cl_2, δ ppm): 7.54-7.51 (m, 2H), 7.48-7.44 (m, 2H), 7.39-7.35 (m, 1H), 7.297-7.24 (m, 2H), 7.17-7.13 (m, 1H), 3.75-3.72 (m, 1H), 3.29-3.24 (m, 1H), 3.13-3.05 (m, 1H), 2.96-2.89 (m, 1H), 2.77-2.70 (m, 1H), 2.37-2.34 (m, 1H), 2.29 (s, 3H), 2.26-2.22 (m, 1H) and 2.01-1.95 (m, 1H).

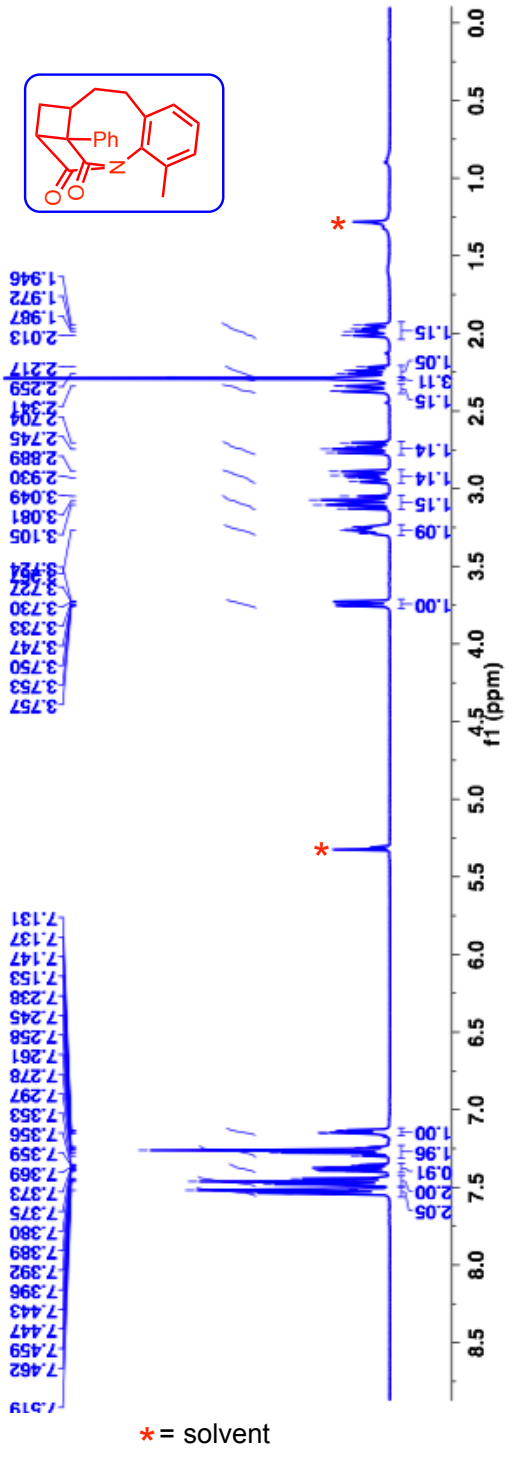

Figure 3.93: ^{1}H-NMR (400 MHz, $CDCl_3$, δ ppm) spectrum of maleimide photoproduct **193e**.

^{13}C-NMR (100 MHz, CD_2Cl_2, δ ppm): 181.5, 180.0, 143.6, 139.9, 137.9, 136.8, 131.3, 131.1, 131.09, 130.7, 129.8, 128.97, 60.0, 51.2, 44.5, 30.4, 29.97, 26.6 and 19.2.

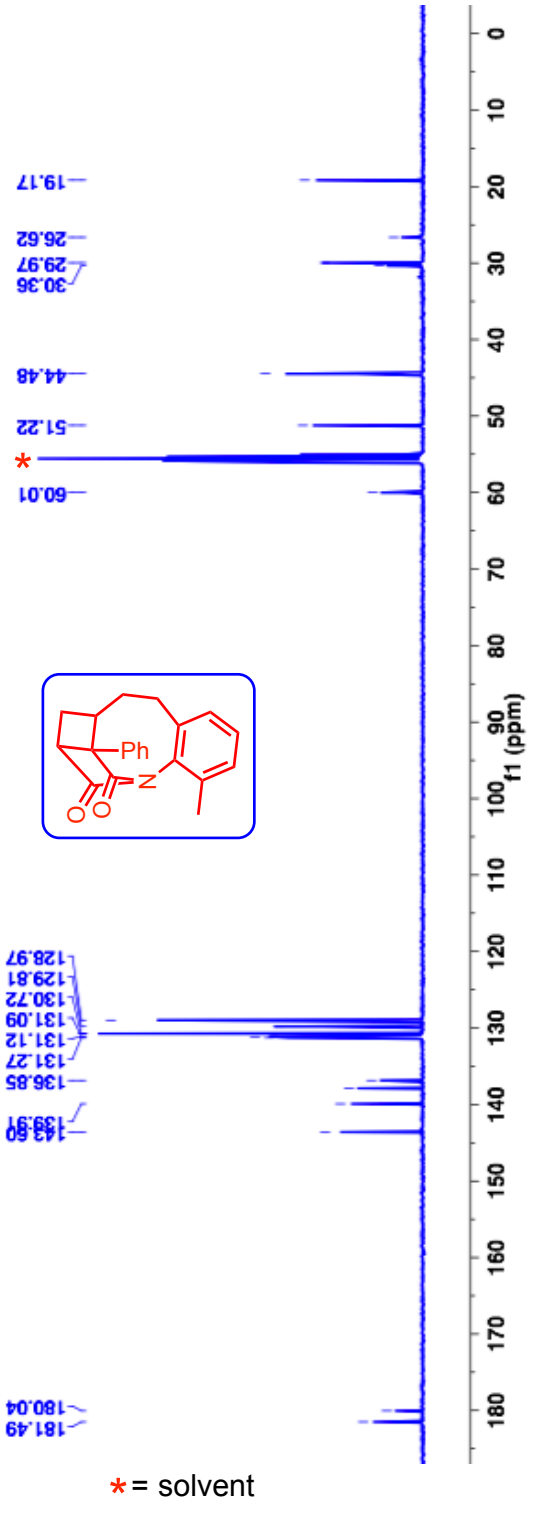

Figure 3.94: ^{13}C-NMR (100 MHz, $CDCl_3$, δ ppm) spectrum of maleimide photoproduct **193e**.

HRMS-ESI (m/z) ([M + Na]$^+$):

Calculated : 340.1308

Observed : 340.1293

|Δm| : 4.4 ppm

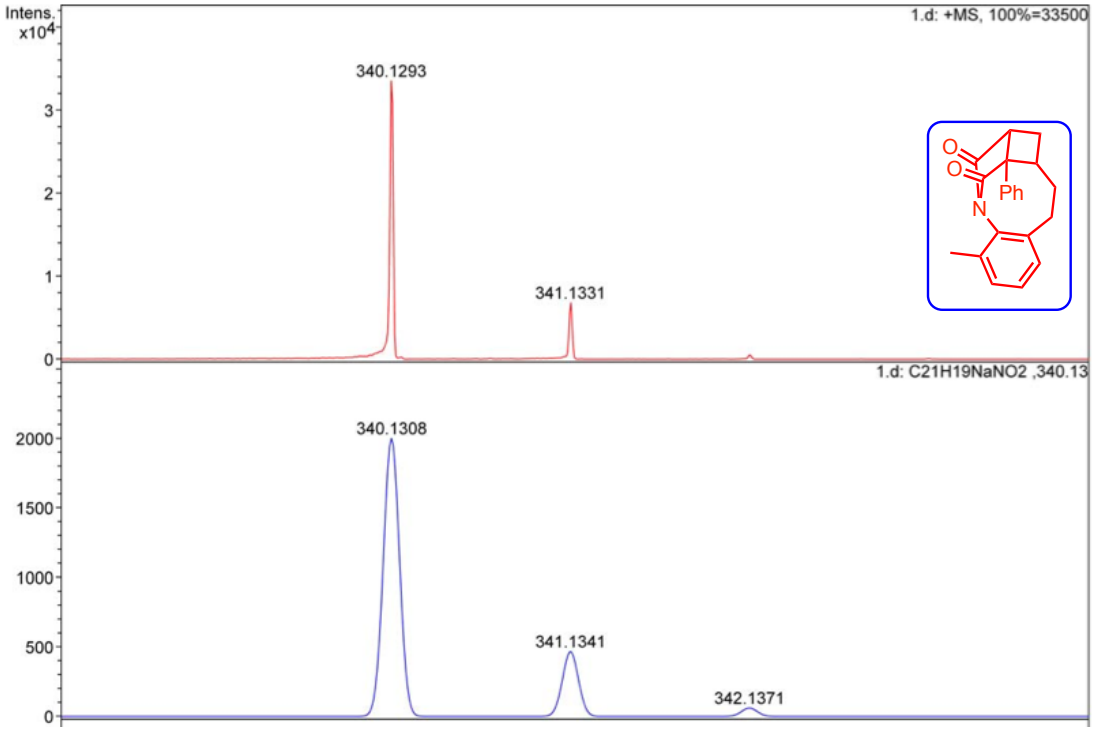

Figure 3.95: HRMS of maleimide photoproduct **193e**.

^{1}H-NMR (400 MHz, DMSO-d6, δ ppm): 8.04 (s, 1H), 7.50 (s, 1H), 7.30-7.26 (m, 1H), 7.15-7.13 (m, 1H), 7.05-7.01 (m, 2H), 4.49-4.44 (m, 1H), 4.02-3.99 (m, 1H), 3.78-3.74 (m, 1H), 3.32-3.29 (m, 1H), 3.20-3.12 (m, 1H) 2.38-2.35 (d, *J* = 11.2 Hz, 1H) and 2.27 (s, 3H).

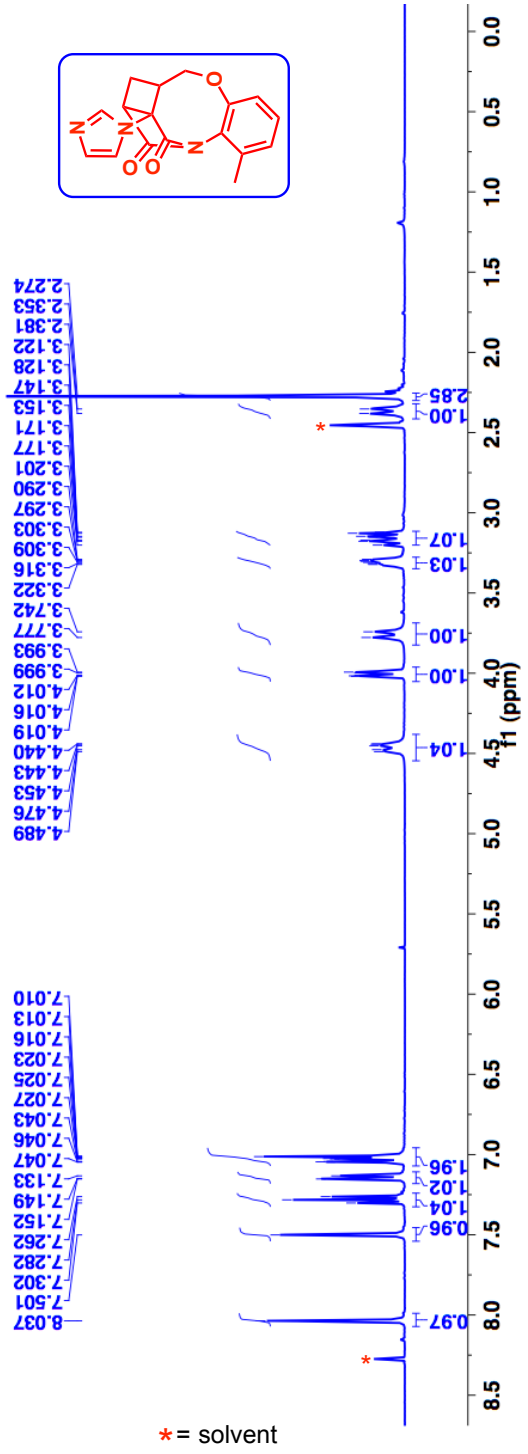

Figure 3.96: ^{1}H-NMR (400 MHz, $CDCl_3$, δ ppm) spectrum of maleimide photoproduct **193f**.

^{13}C-NMR (100 MHz, DMSO-d6, δ ppm): 184.1, 180.97, 161.8, 144.3, 142.2, 136.6, 135.3, 133.8, 131.6, 125.6, 124.3, 79.3, 73.0, 53.7, 48.1, 29.0 and 22.3.

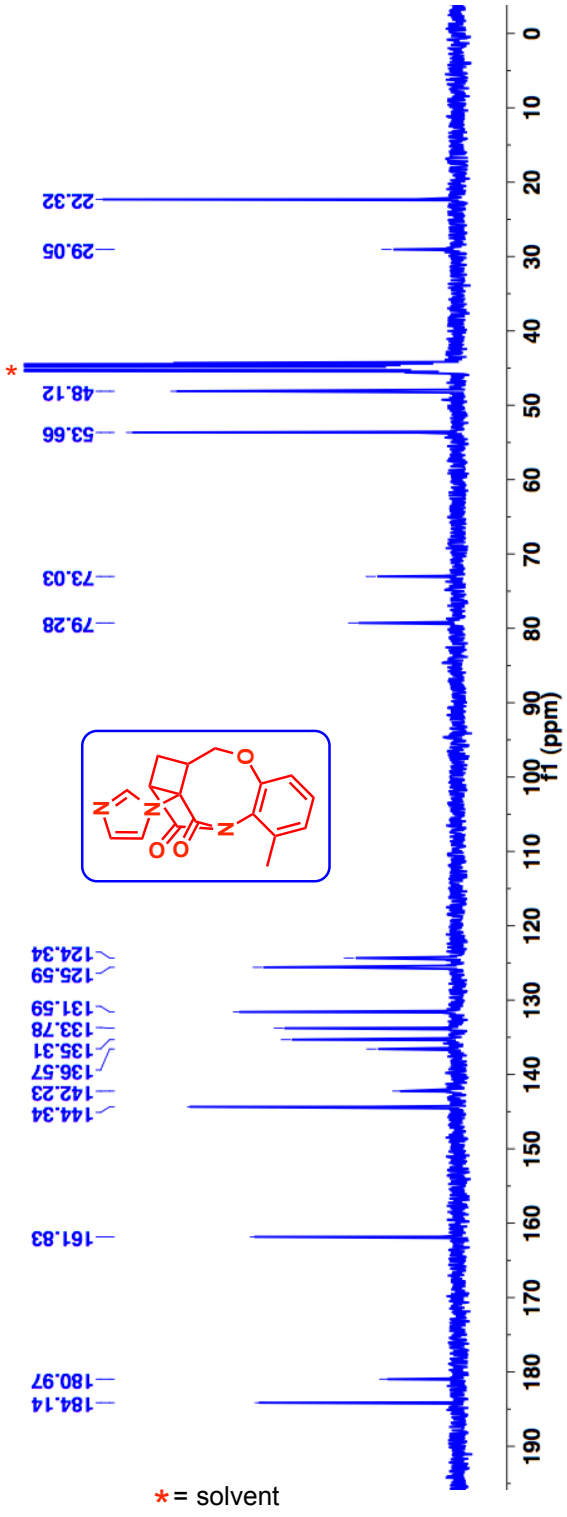

Figure 3.97: ^{13}C-NMR (100 MHz, $CDCl_3$, δ ppm) spectrum of maleimide photoproduct **193f**.

HRMS-ESI (m/z) ([M + H]$^+$):

Calculated : 310.1186

Observed : 310.1179

|Δm| : 2.3 ppm

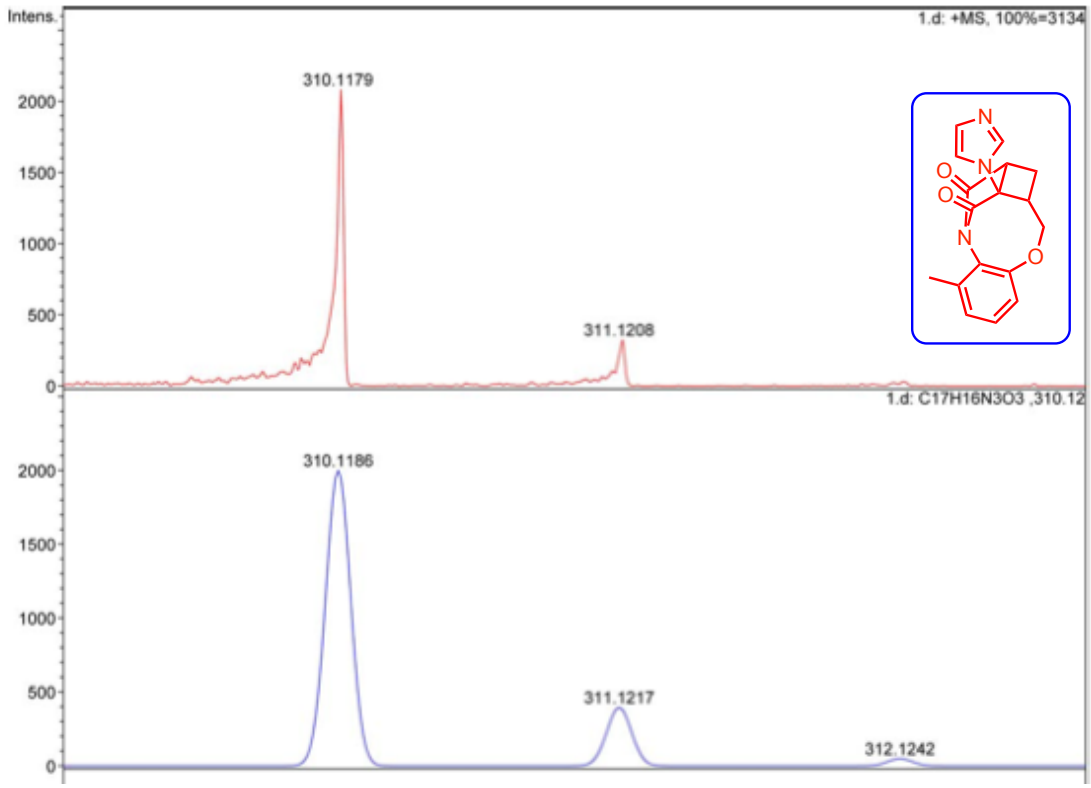

Figure 3.98: HRMS of maleimide photoproduct **193f**.

3.31. Cleavage of maleimide photoproduct 193a

3.31.1. Cleavage of maleimide photoproduct 193a using *Concd.*HCl:TFA

193a **230**

Scheme 3.45: Ether cleavage of photoproduct **193a** using *Concd*.HCl-TFA mixture.

Imide **193a** was taken in a sealed flask/vial to which a 1:1 mixture of *concd*. HCl and trifluoroacetic acid (2 mL) was added at 0 °C and stirred for 5 min. The vial was sealed and transferred to an oil bath and heated to 110 °C for 24 h. After the reaction, the mixture was cooled to 0 °C, diluted with DI water (15 mL) and washed with saturated $NaHCO_3$ solution (10 mL). The organic layer was dried over *anhyd.* Na_2SO_4, filtered and the solvent was removed under reduced pressure to get the crude product. The crude product was purified by combiflash using a hexanes:ethyl acetate mixture.

TLC condition - R*f* = 0.35 (50% hexanes:50% ethyl acetate), Yield = 62%

^{1}H-NMR (400 MHz, CD_3OD, δ ppm): 7.16-7.12 (m, 1H), 6.77-6.74 (m, 3H), 3.78-3.74 (m, 2H), 2.82 (s, 1H), 2.49 (dd, *J* = 10.0, 6.4 Hz, 1H), 1.996 (s, 3H), 1.53 (s, 3H), 1.43 (s, 3H) and 1.27 (s, 3H).

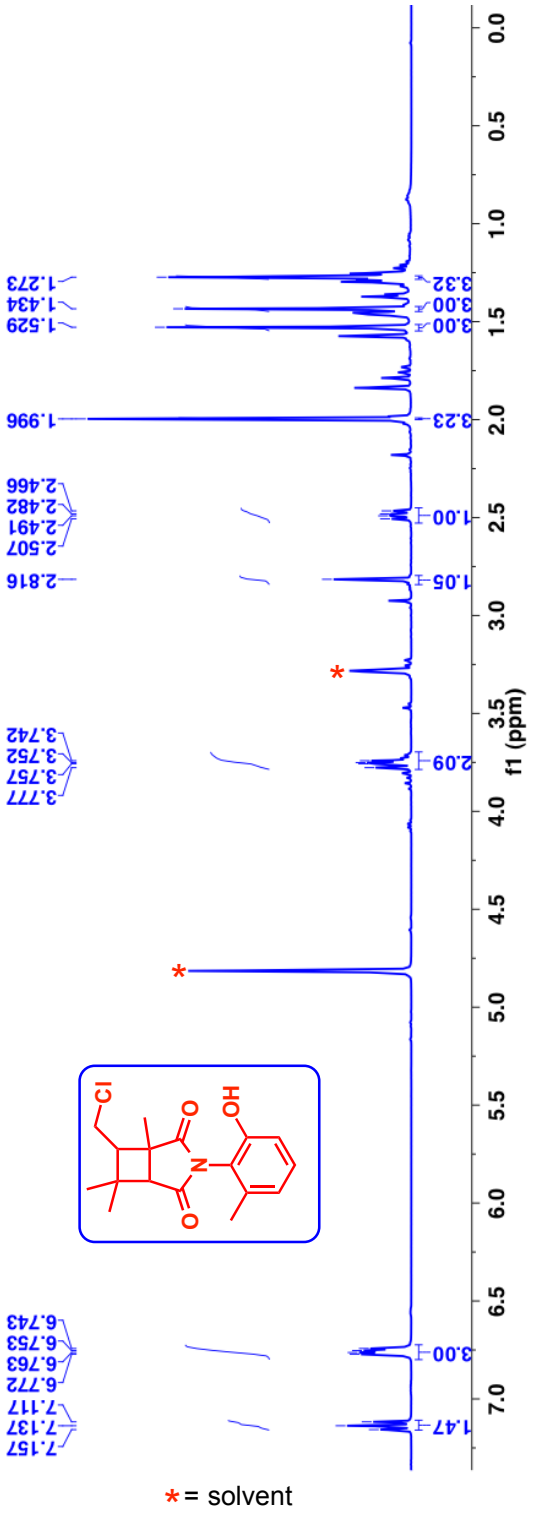

Figure 3.99: ^{1}H-NMR (400 MHz, $CDCl_3$, δ ppm) spectrum of ether cleaved photoproduct **230**.

^{13}C-NMR (100 MHz, CD_3OD, δ ppm): 183.7, 180.9, 157.2, 141.5, 133.96, 124.9, 122.7, 117.3, 57.7, 57.2, 47.9, 45.2, 40.4, 36.4, 24.98, 21.4 and 20.2.

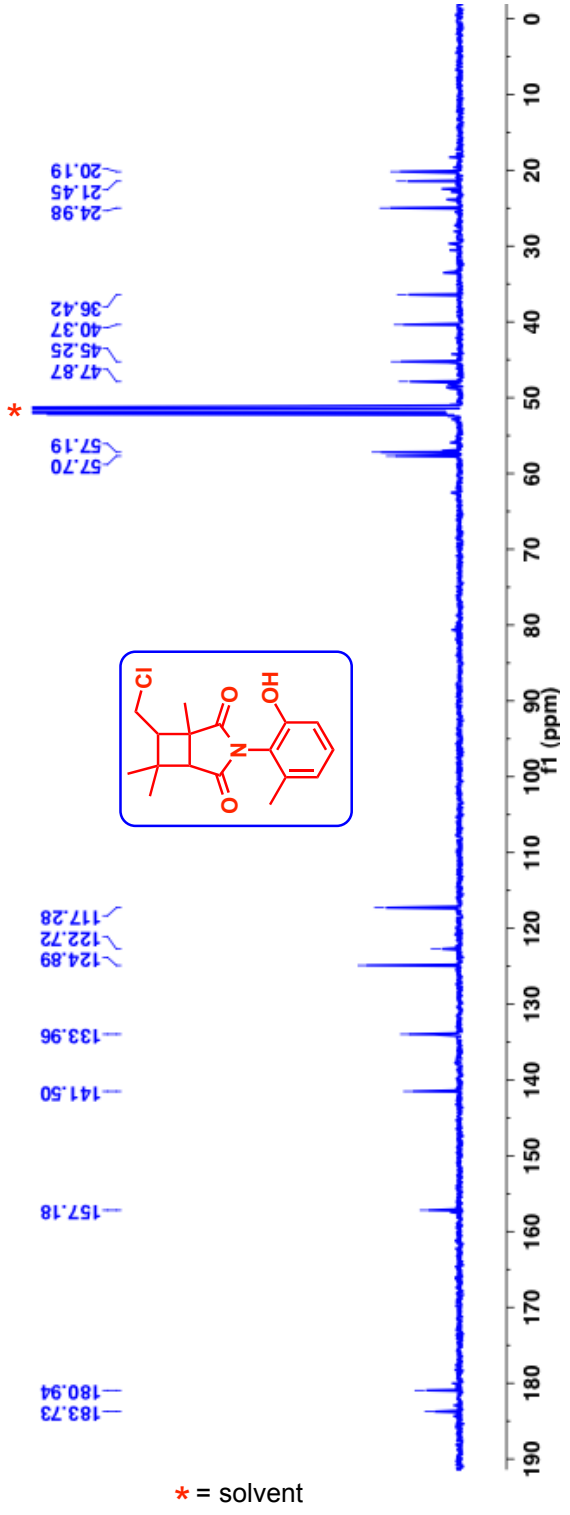

Figure 3.100: ^{13}C-NMR (400 MHz, $CDCl_3$, δ ppm) spectrum of ether cleaved photoproduct **230**.

HRMS-ESI (m/z) ([M + Na]$^+$)

Calculated : 344.1024

Observed : 344.1024

|Δm| : 0.0 ppm

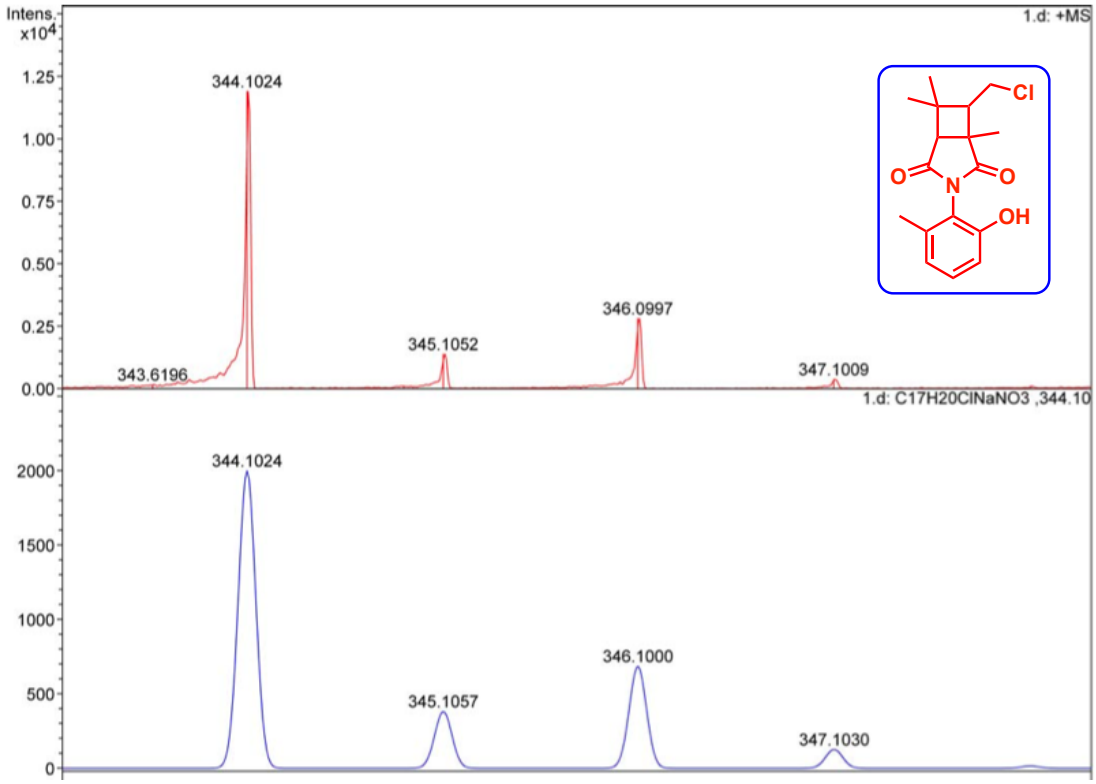

Figure 3.101: HRMS of ether cleaved photoproduct **230**.

3.31.2. Cleavage of maleimide photoproduct 193a using BBr_3

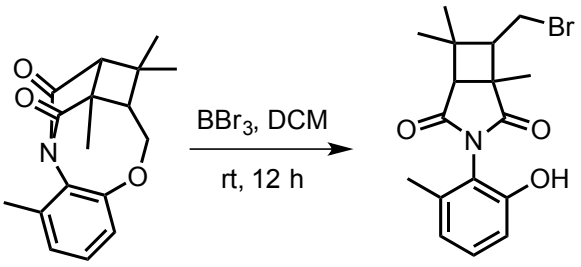

193a **231**

Scheme 3.46: Cleavage of photoproduct **193a** using BBr_3

To a solution of imide**193a** (50 mg, 0.17 mmol) in dry DCM (5 mL) at -78 °C under N_2 atmosphere BBr_3 (1M solution in DCM, 1.75 mL, 10.0 *equiv.*) was added. The resulting mixture was allowed to warm to room temperature over 12 h. After the reaction, the solution was cooled to 0 °C and quenched with saturated $NaHCO_3$ solution. The aqueous layer was extracted with DCM (2 × 10mL). The combined organic layer was dried over *anhyd.* Na_2SO_4, filtered and the solvent was removed under reduced pressure to get the crude product. The product was purified by combiflash using a hexanes:ethyl acetate mixture.

Note: **193a** had small amount of inseparable regioisomers **194a**, so the resulting product contained cleavage product from **194a**.

TLC condition - R*f* = 0.30 (80% hexanes:20% ethyl acetate), Yield = 70%

^{1}H-NMR (400 MHz, $CDCl_3$, δ ppm): 6.93-6.89 (m, 1H), 6.75-6.73 (m, 1H), 6.51 (s, 1H, O**H**), 6.41-6.39 (m, 1H), 3.59 (dd, *J* = 10.8, 5.6 Hz, 1H), 3.51-3.46 (m, 1H), 2.75 (s, 1H), 2.59 (dd, *J* = 10.8, 5.6 Hz, 1H), 2.02 (s, 3H), 1.56 (s, 3H), 1.45 (s, 3H) and 1.28 (s, 3H).

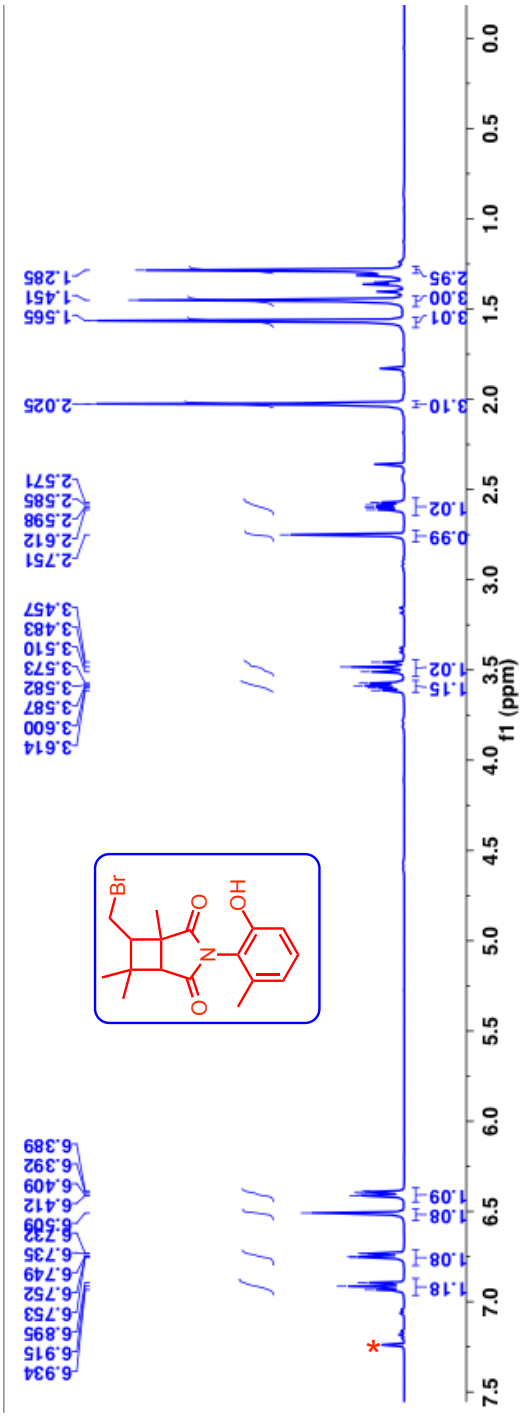

Figure 3.102: ^{1}H-NMR (400 MHz, $CDCl_3$, δ ppm) spectrum of cleavage photoproduct **231**.

^{13}C-NMR (100 MHz, $CDCl_3$, δ ppm): 179.6, 176.8, 151.99, 137.2, 130.5, 122.3, 118.3, 114.4, 54.0, 53.8, 45.4, 37.6, 33.4, 29.3, 22.6, 18.1 and 17.6.

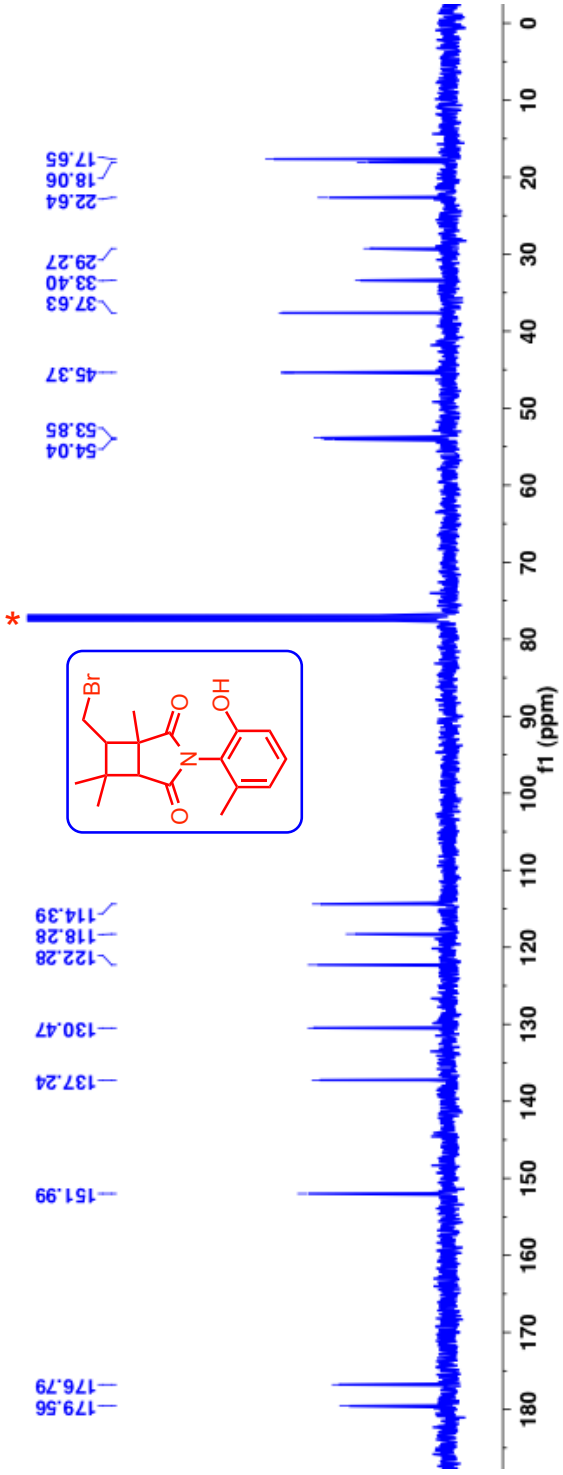

Figure 3.103: ^{13}C-NMR (100 MHz, $CDCl_3$, δ ppm) spectrum of cleavage photoproduct **231**.

HRMS-ESI (m/z) ([M + Na]$^+$):

Calculated : 388.0519

Observed : 388.0529

|Δm| : 2.6 ppm

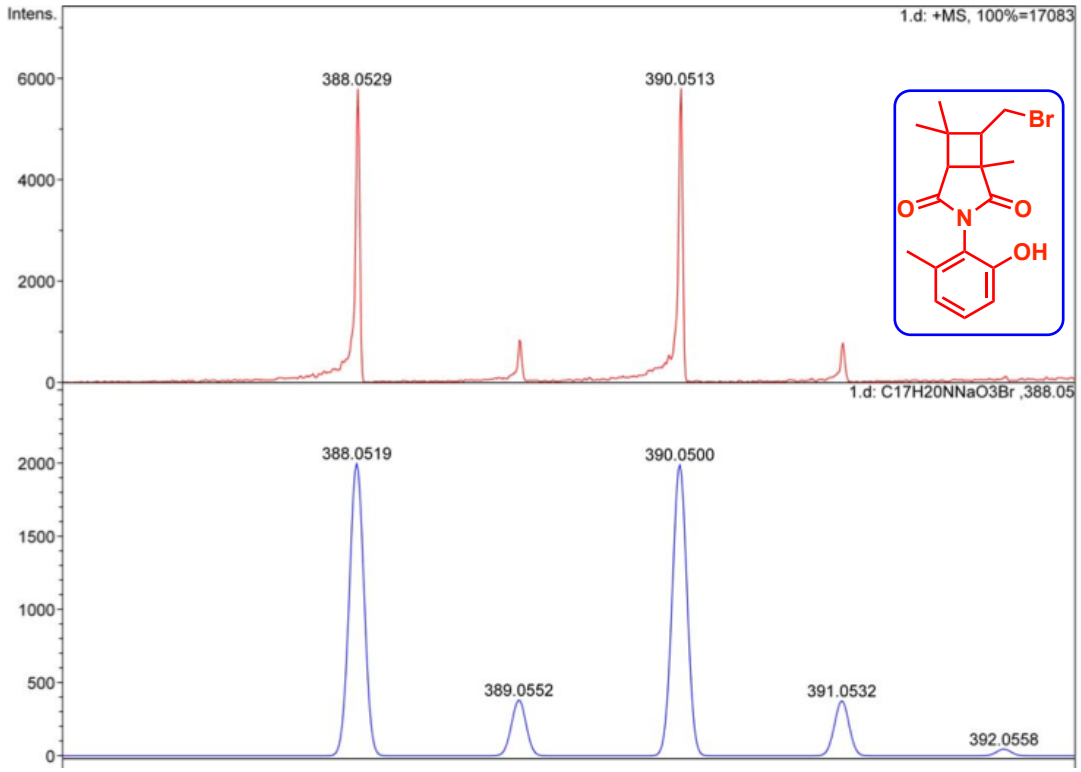

Figure 3.104: HRMS of cleavage photoproduct **231**.

3.31.3. Reduction of maleimide photoproduct 193a using $LiAlH_4$

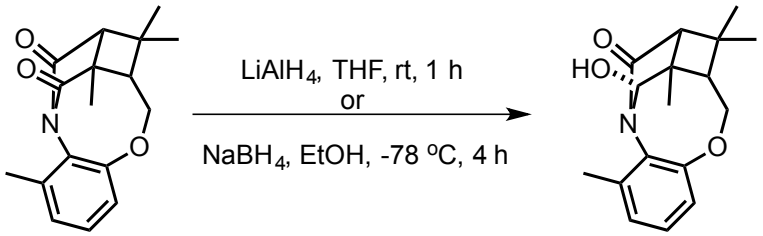

193a **232**

Scheme 3.47: $LiAlH_4$ reduction of photoproduct **193a**.

To a solution of imide **193a** (50 mg) in dry THF (5 mL) at 0 °C under N_2 atmosphere $LiAlH_4$ (5.0 *equiv.*) was added. The resulting mixture was allowed to warm to room temperature and stirred for 1 h. After the reaction, the mixture was cooled to 0 °C and quenched with saturated NH_4Cl solution. The aqueous layer was extracted with ethyl acetate (2 × 10 mL). The combined organic layer was dried over *anhyd.* Na_2SO_4, filtered and the solvent was removed under reduced pressure to get the crude product. The product was purified by combiflash using a hexanes:ethyl acetate mixture.

TLC condition - R*f* = 0.30 (50% hexanes:50% ethyl acetate)

^{1}H-NMR (400 MHz, CD_3OD, δ ppm): 7.10-7.06 (m, 1H), 6.90-6.86 (m, 2H), 5.01-5.00 (m, 1H), 4.63 (d, *J* = 13.6 Hz, 1H), 4.34 (dd, *J* = 13.2, 4.4 Hz, 1H), 3.89–3.79 (m, 1H, exchangeable), 2.30 (dd, *J* = 6.0, 3.2 Hz, 1H), 2.19 (s, 3H), 1.85 (t, *J* = 4.0 Hz, 1H), 1.50 (s, 3H), 1.44 (s, 3H) and 1.29 (s, 3H).

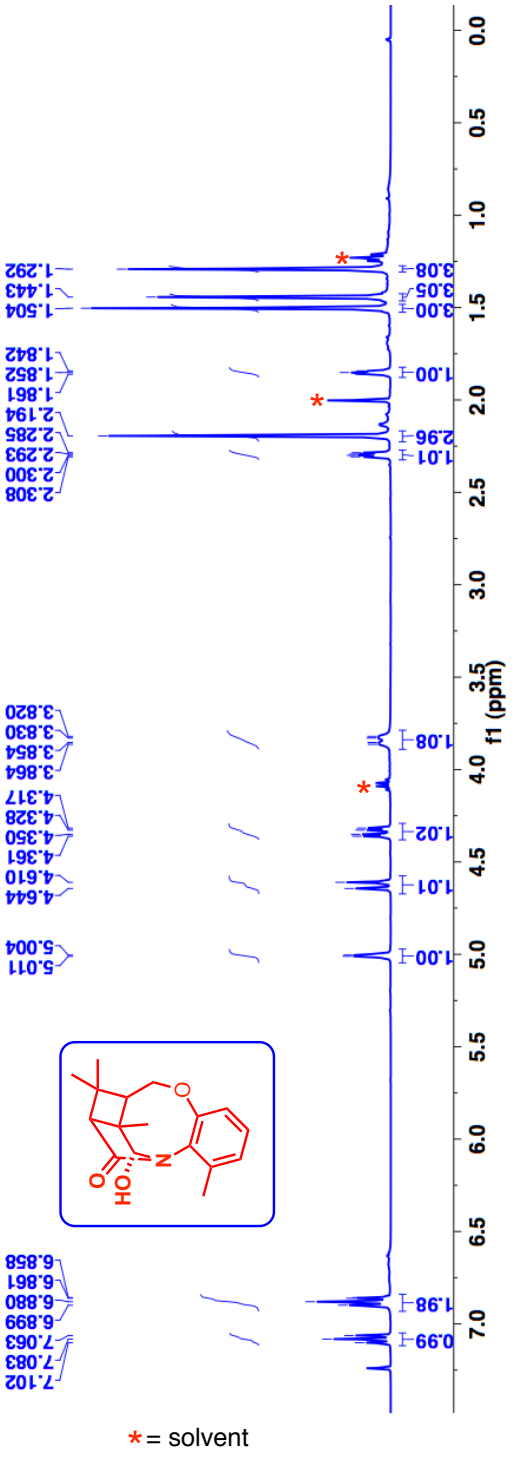

Figure 3.105: ^{1}H-NMR (400 MHz, $CDCl_3$, δ ppm) spectrum of reduction of photoproduct **232**.

^{13}C-NMR (100 MHz, CD_3OD, δ ppm): 178.9, 158.2, 138.6, 131.96, 128.7, 125.4, 119.8, 89.3, 73.5, 56.0, 55.5, 46.3, 40.4, 32.2, 22.95, 22.7 and 17.98.

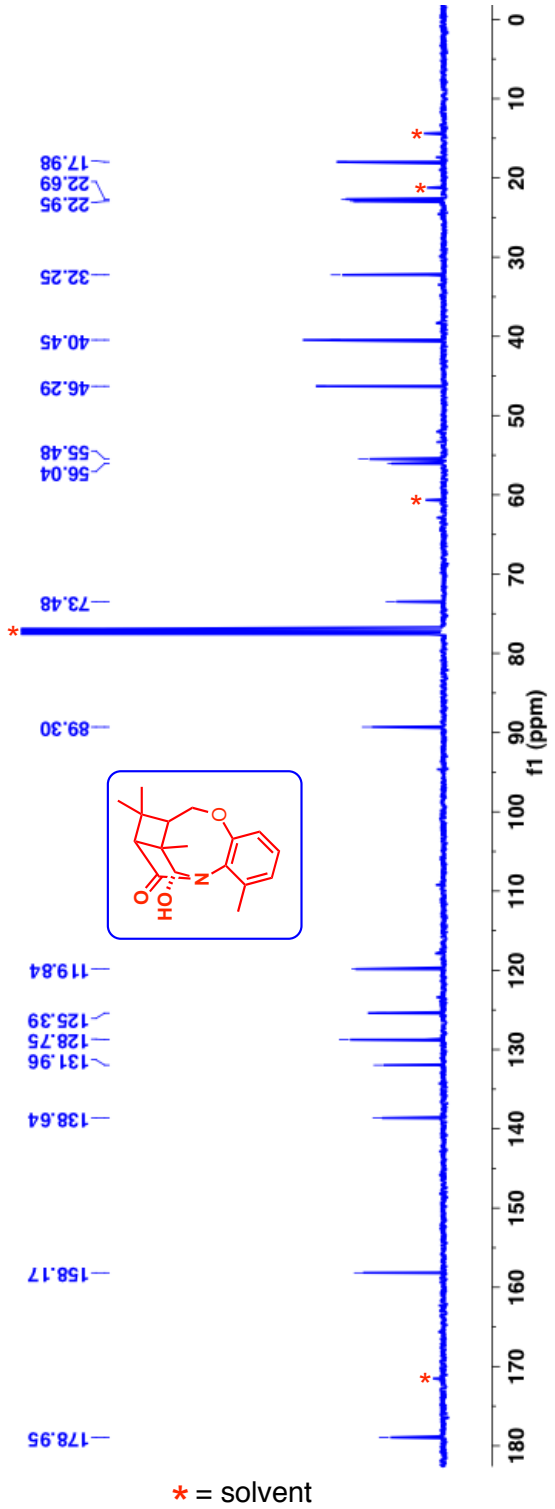

Figure 3.106: ^{13}C-NMR (400 MHz, $CDCl_3$, δ ppm) spectrum of reduction of photoproduct **232.**

HRMS-ESI (m/z) ([M + Na]$^+$):

Calculated : 310.1414

Observed : 310.1419

|Δm| : 1.6 ppm

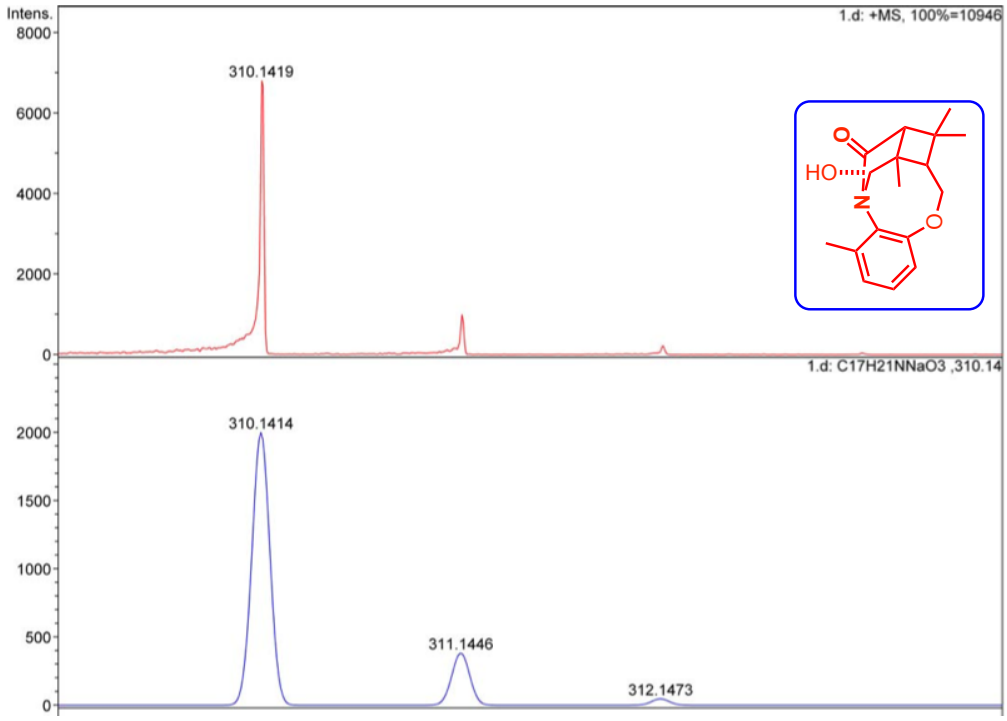

Figure 3.107: HRMS of reduction of photoproduct **232.**

3.32. General procedure for synthesis of maleimide derivatives for [5+2] photocycloaddition and their precursors

3.32.1. Synthesis of 2-(allyl)aniline 222

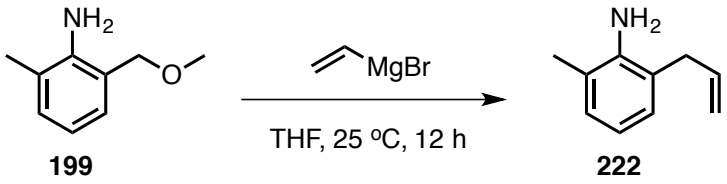

199 **222**

Scheme 3.48: Synthesis of 2-(allyl)aniline derivative **222**.

To a solution aniline derivative **199** (5.3 g, 1.0 *equiv.*) in dry THF (40 mL) at 0 °C, allyl magnesium halide (2.0 M in THF, 2.2 *equiv.*) was added slowly over 15 min. The resulting mixture was allowed to warm to room temperature over 12 h. After the reaction, the mixture was cooled to 0 °C and quenched with *dil.* HCl. The aqueous layer was extracted with DCM (3 × 50 mL). The combined organic layer was dried over *anhyd.* Na_2SO_4, filtered and the solvent was removed under reduced pressure to get the crude product. The crude product was purified by combiflash using a hexanes: ethyl acetate mixture. R*f* = 0.40 (80% hexanes: 20% ethyl acetate), Yield for **222** = 55%

^{1}H-NMR (400 MHz, $CDCl_3$, δ ppm): 7.03-6.95 (m, 2H), 6.69-6.66 (m, 1H), 6.12-5.94 (m, 1H), 5.20-5.12 (m, 2H), 3.68 (bs, 2H), 3.38-3.34(m, 2H) and 2.22 (s, 3H).

^{13}C-NMR (100 MHz, $CDCl_3$, δ ppm): 143.0,136.1,128.8,128.0,123.3,122.3118.1,116.1,36.8 and 17.6.

3.32.2. Synthesis of 2-iodo-4,6-dimethyl aniline 226

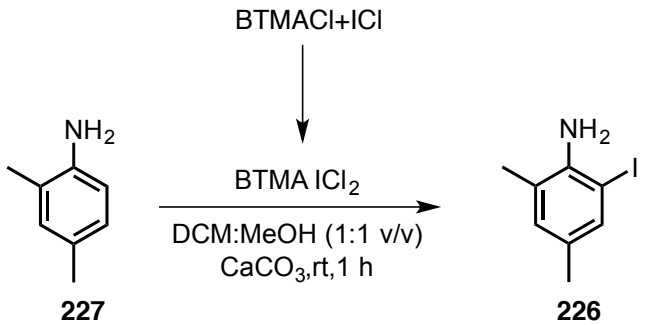

227 **226**

Scheme 3.49: Synthesis of 2-iodo-4,6-dimethylaniline **226**.

Synthesis of iodinating agent benzyltrimethylammonium dichloroiodate (BTMA ICl_2): The compound was synthesized using previously reported procedure.[60] To a solution of iodinemonochloride (3.0 g, 18.6 mmol) in DCM (37 mL) at room temperature added a solution of benzyltrimethylammonium chloride (3.5 g, 18.6 mmol) in DI water (22 mL) slowly over 10 mins. The resulting mixture was stirred at room temperature for 30 mins. The layers were separated and the organic layer was washed with DI water (10 mL), dried over *anhyd.* Na_2SO_4, filtered and the solvent was removed under reduced pressure to get the crude product as a brownish yellow solid. The crude product was directly used for iodination reaction without further purification (isolated crude product yield: 98%).

Note: The iodine monochloride was purchased as 1M solution in DCM, which was again diluted using required amount of DCM. The crude BTMA ICl_2 can also be recrystallized in DCM: Ether mixture.

To a mixture of aniline (1.0 g, 8.2 mmol) and calcium carbonate (1.4 g) in DCM:methanol (50:50 mixture, 50 mL) at room temperature added a solution of benzyltrimethylammonium dichloroiodate (2.9 g, 8.2 mmol) in DCM (30 mL) slowly over 30 mins. The resulting mixture was stirred at room temperature for 1 h. After the reaction, the mixture was filtered through celite bed under vacuum and the bed was washed with DCM (50 mL). The combined filtrate was concentrated under reduced pressure. The residue was taken up in 5% $NaHSO_3$ aqueous solution (40 mL) and the aqueous layer was extracted with diethyl ether (3 x 30 mL). The combined organic layer was dried over *anhyd.* Na_2SO_4, filtered and the solvent was removed under reduced pressure to get the crude product. The crude product was purified by combiflash using hexanes:ethyl acetate mixture (95:5) to get the title compound as a brownish solid (isolated yield = 67%).

TLC condition - R*f* = 0.35 (95% hexanes:5% ethyl acetate)

^{1}H-NMR (400 MHz, $CDCl_3$, δ ppm): 7.34 (s, 1H) and 6.82 (s, 1H),3.90 (bs, 2H), 2.18 (s, 3H), 2.16 (s, 3H).

^{13}C-NMR (100 MHz, $CDCl_3$, δ ppm): 142.5, 137.0, 131.6, 129.5, 122.7, 85.0, 20.0 and 19.1.

3.32.3. Synthesis of N-diallyl-2-iodo-4,6-dimethylaniline 225

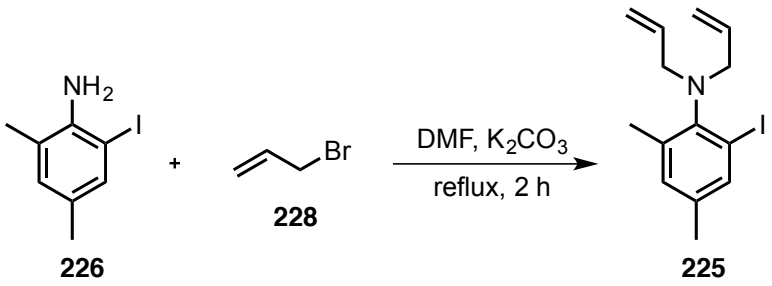

226 **228** **225**

Scheme 3.50: Synthesis of N-diallyl-2-iodo-4,6-dimethylaniline **225**.

The compound was synthesized according to a literature reported procedure.[61] Mixture of aniline (5 g, 20.2 mmol), allyl bromide (4.4 mL, 50.9 mmol) and sodium carbonate (6.4 g, 60.6 mmol) in DMF (150 mL) was heated to 150 °C in a sealed tube and maintained for 2 h. After the reaction, the mixture was cooled to room temperature and poured into cold DI water (200 mL). The aqueous layer was extracted with diethyl ether (3 x 50 mL). The combined organic layer was washed with DI water (2 x 50 mL) to remove traces of DMF, dried over *anhy.* Na_2SO_4, filtered and the solvent was removed under reduced pressure to get the crude product. The crude product was purified by combiflash using hexanes:ethyl acetate mixture (98:2) to get the title compound as a pale yellow oil (isolated yield = 90%).

TLC condition - R*f* = 0.90 (90% hexanes:10% ethyl acetate)

^{1}H-NMR (400 MHz, $CDCl_3$, δ ppm): 7.52 (s, 1H), 6.90 (s, 1H), 5.97 - 5.87 (m, 2H), 5.14 - 5.09 (m, 2H), 5.02 - 4.99 (m, 2H), 3.74 - 3.60 (m, 4H), 2.27 (s, 3H) and 2.20 (s, 3H).

^{13}C-NMR (100 MHz, $CDCl_3$, δ ppm): 147.7, 139.0, 138.1, 137.0, 136.9, 132.4, 116.6, 104.6, 56.2, 20.3 and 20.0.

3.32.4. Synthesis of N-diallyl-2,4-dimethyl-6-allyl-aniline derivative 224

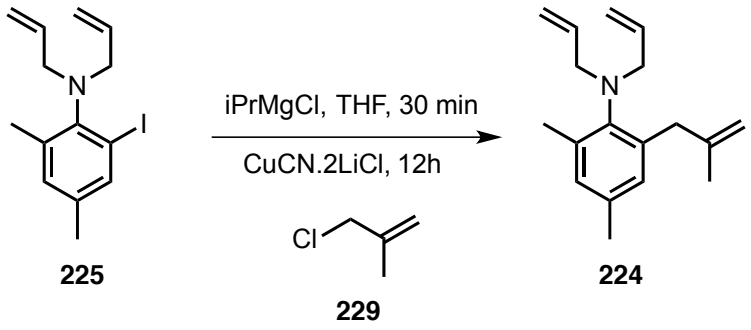

225 **229** **224**

Scheme 3.51: Synthesis of N-diallyl-2,4-dimethyl-6-allyl-aniline derivative **224**.

The compound was synthesized according to the literature reported procedure.[62] To a solution of N-diallyl-2-iodo aniline derivative **225** (5.9 g, 18.0 mmol) in dry THF (120 mL) at -15 °C under N_2 atmosphere added iPrMgCl.LiCl (1.3M in THF, 15.2 mL, 19.8 mmol) slowly over 10 mins. The mixture was maintained at -15 °C for 45 mins after which 3-chloro-2-methylpropene (2.13 mL, 21.6 mmol) and CuCN.2LiCl (0.16 mL, 0.9 mmol) was added. The reaction mixture was slowly allowed to warm to room temperature over 12 h. The reaction mixture was quenched with *Satd.* NH_4Cl solution (50 mL), stirred and the layers were separated. The aqueous layer was extracted with diethyl ether (2 X 75 mL). The combined organic layer was dried over *anhyd.* Na_2SO_4, filtered and the solvent was removed under reduced pressure to get the crude product. The crude product was purified by combiflash using hexanes:ethyl acetate mixture (95:5) to get the title compound as a pale yellow oil (isolated yield = 92%).

TLC condition - R*f* = 0.75 (100% hexanes)

^{1}H-NMR (400 MHz, $CDCl_3$, δ ppm): 6.79 (s, 2H), 5.86-5.76 (m, 2H), 5.09- 5.08 (m, 1H), 5.05- 5.03 (m, 1H), 4.99-4.96 (m, 2H), 4.82-4.81 (m, 1H), 4.58- 4.578 (m, 1H), 3.64-3.51 (m, 4H), 3.37 (s, 2H), 2.25 (s, 3H), 2.22 (s, 3H) and 1.697 (s, 3H).

^{13}C-NMR (100 MHz, $CDCl_3$, δ ppm): 145.9, 138.96, 137.5, 137.3, 134.7, 130.1, 129.6, 128.6, 116.1, 112.1, 56.8, 40.2, 23.0, 21.0 and 19.9.

3.32.5. Synthesis of 2,4-dimethyl-6-allyl-aniline derivative 223

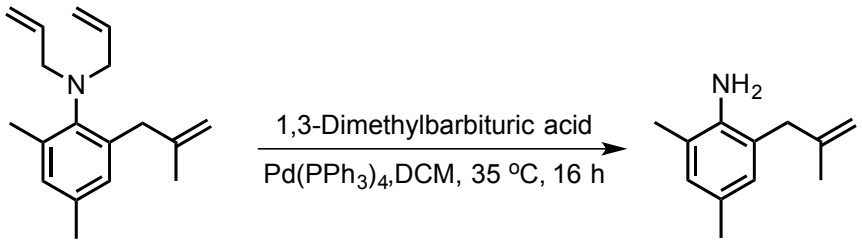

224 **223**

Scheme 3.52: Synthesis of 2,4-dimethyl-6-allyl-aniline derivative **223**.

The compound was synthesized according to the literature reported procedure.[14] In a flame dried flask charged $Pd(PPh_3)_4$ (183 mg, 0.16 mmol) and 1,3-dimethylbarbituric acid (12.8 g, 82 mmol). To this mixture added a solution of N-diallyl-6-(2-methylallyl)-aniline derivative **224** (4.2 g, 16.4 mmol) in dry DCM (100 mL) via cannula. The resulting solution was heated to 35 ^oC and maintained for 16 h. After the reaction the mixture was cooled to room temperature and the solvent was removed under reduced pressure. The residue was taken in a *Satd*. Na_2CO_3 solution (250 mL) and the aqueous layer was extracted with diethyl ether (3 X 75 mL). The combined organic layer was washed with *Satd*. Na_2CO_3 solution (2 X 50 mL), dried over *anhyd.* Na_2SO_4, filtered and the solvent was removed under reduced pressure to get the crude product. The crude product was purified by combiflash using hexanes:ethyl acetate mixture (95:5) to get the title compound as a pale yellow oil (isolated yield = 92%).

Note: The product accompanied by inseparable Di-allylated 1,3- dimethylbarbituric acid byproduct. So the mixture was taken to next step where it gets removed by filtration after the reaction. The relative percentage of the product was determined by ^{1}H-NMR spectroscopy.

TLC condition - R*f* = 0.35 (100% hexanes)

^{1}H-NMR (400 MHz, $CDCl_3$, δ ppm): 6.78 (s, 1H), 6.72 (s, 1H), 4.85 – 4.84 (m, 1H), 4.73 – 4.728 (m, 1H), 3.54 (bs, 2H), 3.24 (s, 2H), 2.20 (s, 3H), 2.13 (s, 3H) and 1.71 (s, 3H).

^{13}C-NMR (100 MHz, $CDCl_3$, δ ppm): 144.0, 141.0, 129.61, 129.56, 127.2, 123.5, 122.6, 111.7, 41.6, 22.5, 20.6 and 17.7.

3.32.6. Synthesis of atropisomeric maleimide derivatives 205a-d, 205g, 205i

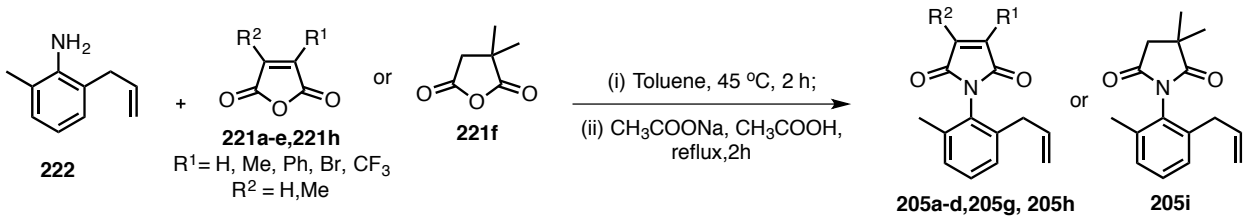

Scheme 3.53: Synthesis of atropisomeric maleimide derivatives **205a-d**, **205g** and **205i**.

To a solution of aniline derivative **222** (500 mg, 1.1 *equiv.*) in toluene (5 mL) corresponding anhydride **221a-e, 221f, 221h** and (1.0 *equiv.*) was added and the resulting mixture was heated to 50 °C for 2 h. After the reaction, the solvent was concentrated and the residue was directly taken to next step. To the residue from the above reaction in glacial acetic acid (5 mL), *anhyd.* sodium acetate (236 mg, 2.88 mmol) was added. The resulting mixture was refluxed for 2 h. After the reaction, the mixture was cooled to room temperature and diluted with ethyl acetate (20 mL). The organic layer was washed with DI water (2 x 15 mL), saturated $NaHCO_3$ solution (2 × 15 mL), dried over *anhyd.* Na_2SO_4, filtered and concentrated under reduced pressure to yield crude product. The crude product was purified by combiflash using a hexanes:ethyl acetate mixture.

R*f* = 0.80 (80% hexanes:20% ethyl acetate) for **205i** (Yield = 80 %)

^{1}H-NMR (400 MHz, $CDCl_3$, δ ppm): 7.27-7.23 (m, 1H), 7.16-7.12 (m, 2H), 5.84-5.74 (m, 1H), 5.03-4.97 (m, 2H), 3.18 (d, *J*=6.8 Hz, 2H), 2.71 (s, 2H), 2.08 (s, 3H), 1.421 (s, 3H) and 1.42 (s, 3H).

^{13}C-NMR (100 MHz, $CDCl_3$, δ ppm): 182.2, 175.03, 137.97, 136.2, 136.1, 130.3, 129.8, 129.4, 128.3, 116.6, 44.2, 40.8, 36.5, 26.4, 25.6, and 17.9.

HRMS-ESI (m/z) ($[M + Na]^+$): Calculated: 280.1308; Observed: 280.1310; |Δm|: 0.8 ppm.

TLC condition - R*f* = 0.45 (80% hexanes:20% ethyl acetate) for **205a** (Yield = 54 %)

TLC condition - R*f* = 0.65 (80% hexanes:20% ethyl acetate) for **205b** (Yield = 60 %)

TLC condition - R*f* = 0.50 (80% hexanes:20% ethyl acetate) for **205c** (Yield = 67 %)

TLC condition - R*f* = 0.50 (80% hexanes:20% ethyl acetate) for **205d** (Yield = 78 %)

TLC condition - R*f* = 0.60 (80% hexanes:20% ethyl acetate) for **205g** (Yield = 40 %)

3.32.7. Synthesis of atropisomeric maleimide derivative 205e

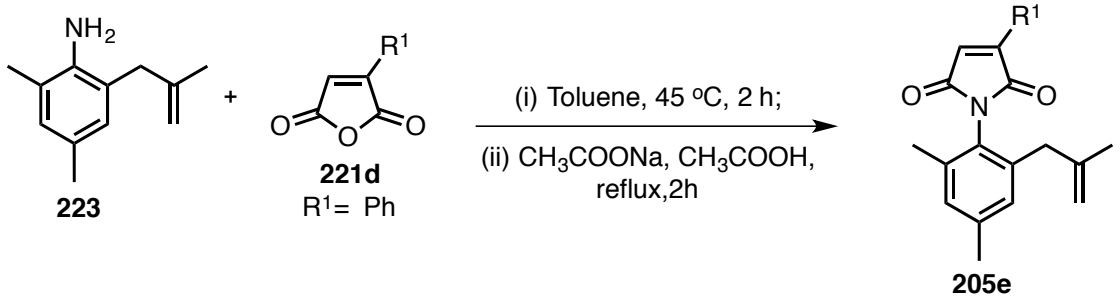

Scheme 3.54: Synthesis of atropisomeric maleimide derivatives **205e**.

To a solution of aniline derivative **223** (500 mg, 1.1 *equiv.*) in toluene (5 mL) corresponding anhydride **221d** (1.0 *equiv.*) was added and the resulting mixture was heated to 50 °C for 2 h. After the reaction, the solvent was concentrated and the residue was directly taken to next step. To the residue from the above reaction in glacial acetic acid (5 mL), *anhyd.* Sodium acetate (236 mg, 2.88 mmol) was added. The resulting mixture was refluxed for 2 h. After the reaction, the mixture was cooled to room temperature and diluted with ethyl acetate (20 mL). The organic layer was washed with DI water (2 x 15 mL), saturated $NaHCO_3$ solution (2 × 15 mL), dried over *anhyd.* Na_2SO_4, filtered and concentrated under reduced pressure to yield crude product. The crude product was purified by combiflash using a hexanes:ethyl acetate mixture.

TLC condition - R*f* = 0.2 (95% hexanes:5% ethyl acetate) for **205e** (Yield = 68 %)

3.32.8. Synthesis of atropisomeric maleimide derivative 205f

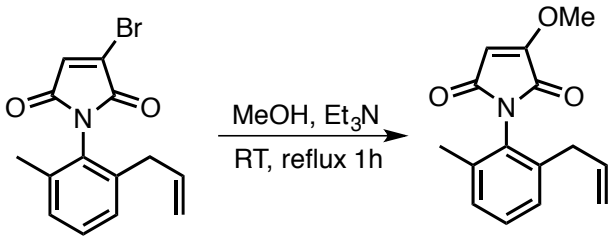

205c **205f**

Scheme 3.55: Synthesis of atropisomeric maleimide derivatives **205f**.

To a solution of bromo maleimide derivative **205c** (500 mg, 1.0 *equiv.*) in MeOH (5 mL) triethylamine in MeOH (1.1 *equiv.*) was added and the resulting mixture refluxed for 1 h. After the reaction, the solvent was concentrated and the reaction mixture was quenched with DI water. The aqueous layer is extracted with DCM (20 mL). The combined organic layer was dried over *anhyd.* Na_2SO_4, filtered and concentrated under reduced pressure to yield crude product. The crude product was purified by combiflash using a hexanes:ethyl acetate mixture.

TLC condition - R*f* = 0.40 (50% hexanes:50% ethyl acetate) ,Yield = 63 %

^{1}H-NMR (400 MHz, $CDCl_3$, δ ppm): 7.27-7.23 (m, 1H), 7.16-7.12 (m, 2H), 5.81-5.71 (m, 1H), 4.98-4.93 (m, 2H), 3.19-3.17 (d, J = 6.4 Hz, 2H) and 2.07 (s, 3H).

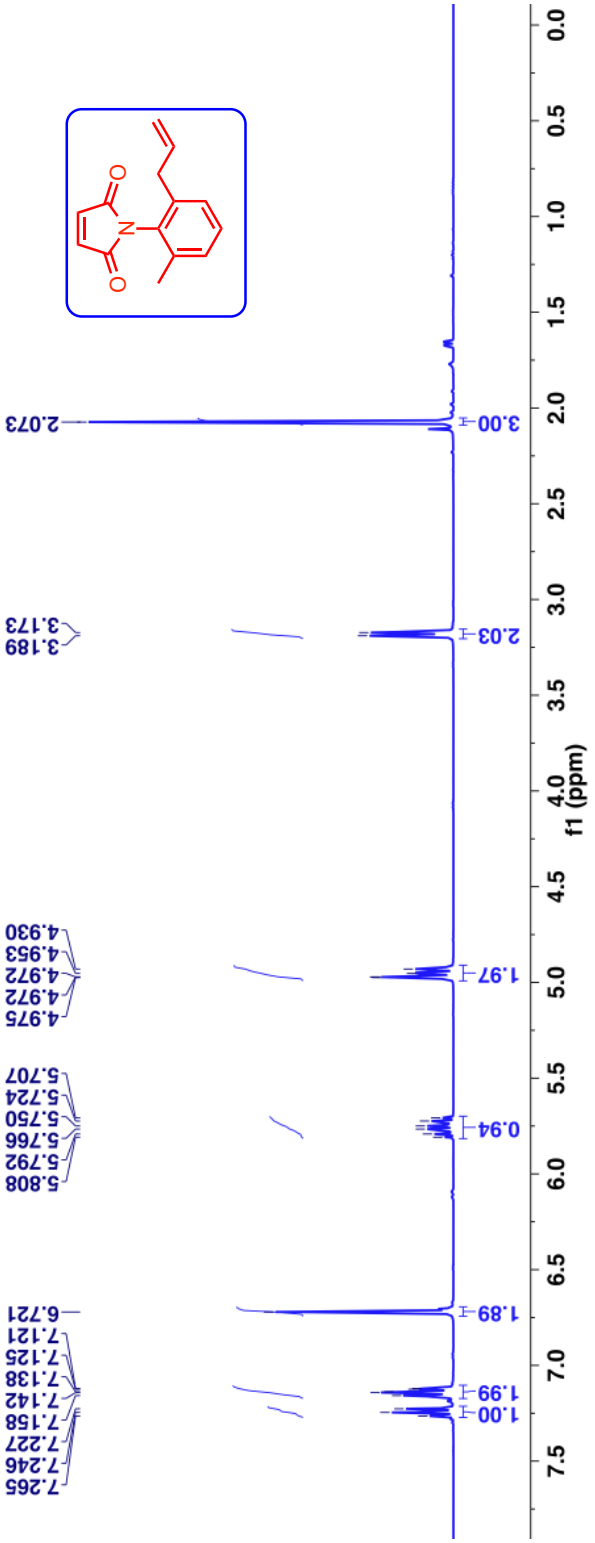

Figure 3.108: ^{1}H-NMR (400 MHz, $CDCl_3$, δ ppm) spectrum of allyl maleimide **205a**.

^{13}C-NMR (100 MHz, $CDCl_3$, δ ppm): 169.9, 130.3, 137.6, 136.1, 134.5, 129.9, 129.4, 129.3, 128.3, 116.6, 36.9 and 18.1.

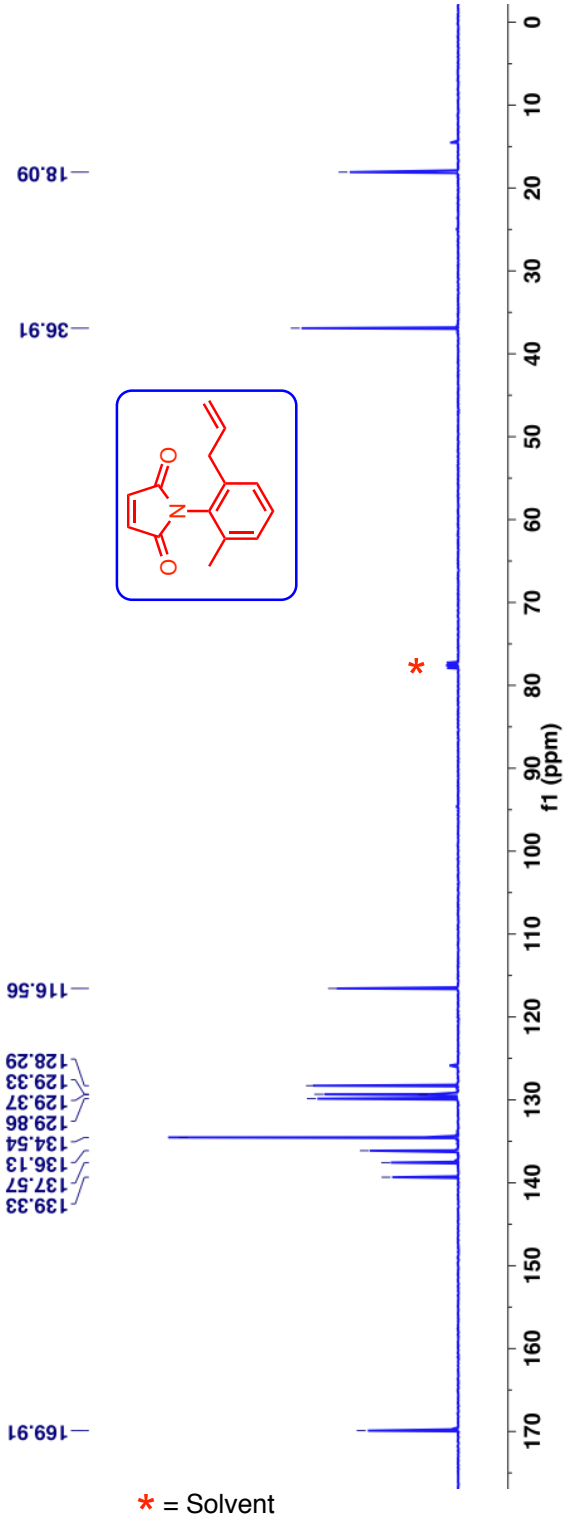

Figure 3.109: ^{13}C-NMR (100 MHz, $CDCl_3$, δ ppm) spectrum of allyl maleimide **205a**.

^{1}H-NMR (400 MHz, $CDCl_3$, δ ppm): 7.28-7.24 (m, 1H), 7.17-7.12 (m, 2H), 6.46-6.45 (q, J = 5.2 Hz 1H), 5.82-5.72 (m, 1H), 4.98-4.93 (m, 2H), 3.19-3.17 (d, J = 6.8 Hz, 2H), 2.14-2.14 (d, J = 2 Hz, 2H) and 2.09 (s, 3H).

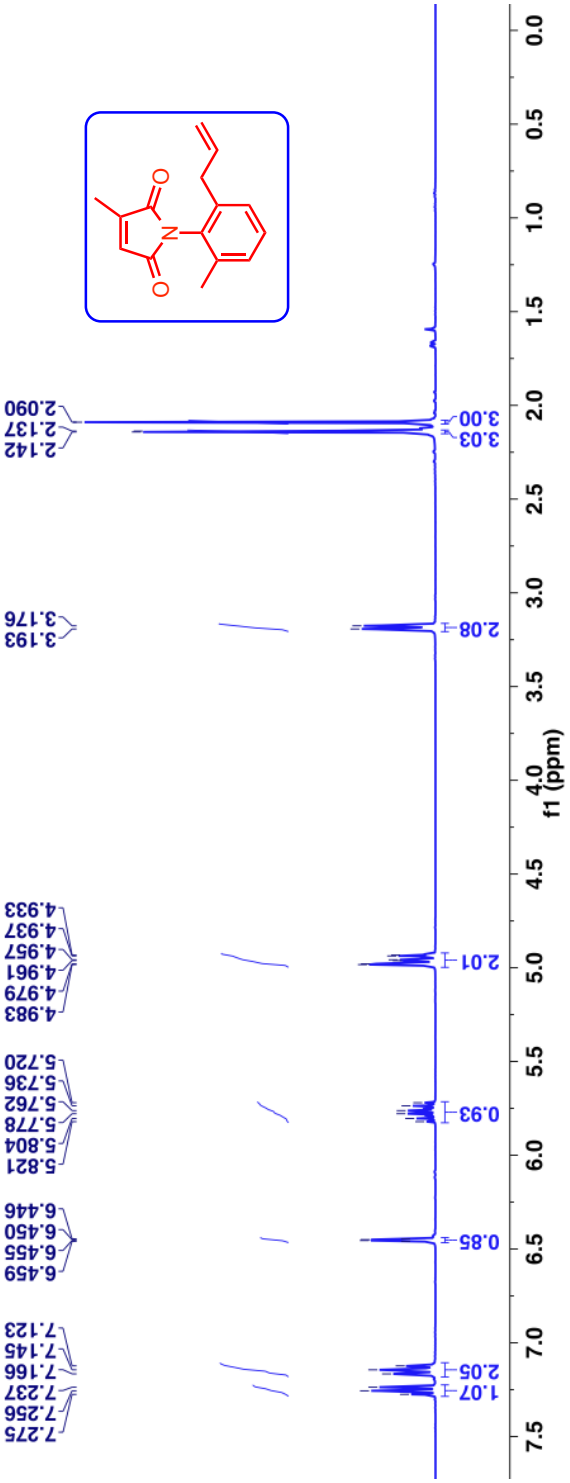

Figure 3.110: ^{1}H-NMR (400 MHz, $CDCl_3$, δ ppm) spectrum of allyl maleimide **205b**.

^{13}C-NMR (100 MHz, $CDCl_3$, δ ppm): 170.9, 169.9, 146.1, 139.3, 137.5, 136.2, 129.7, 129.6, 129.3, 128.2, 127.8, 116.4, 36.9, 18.2 and 11.4.

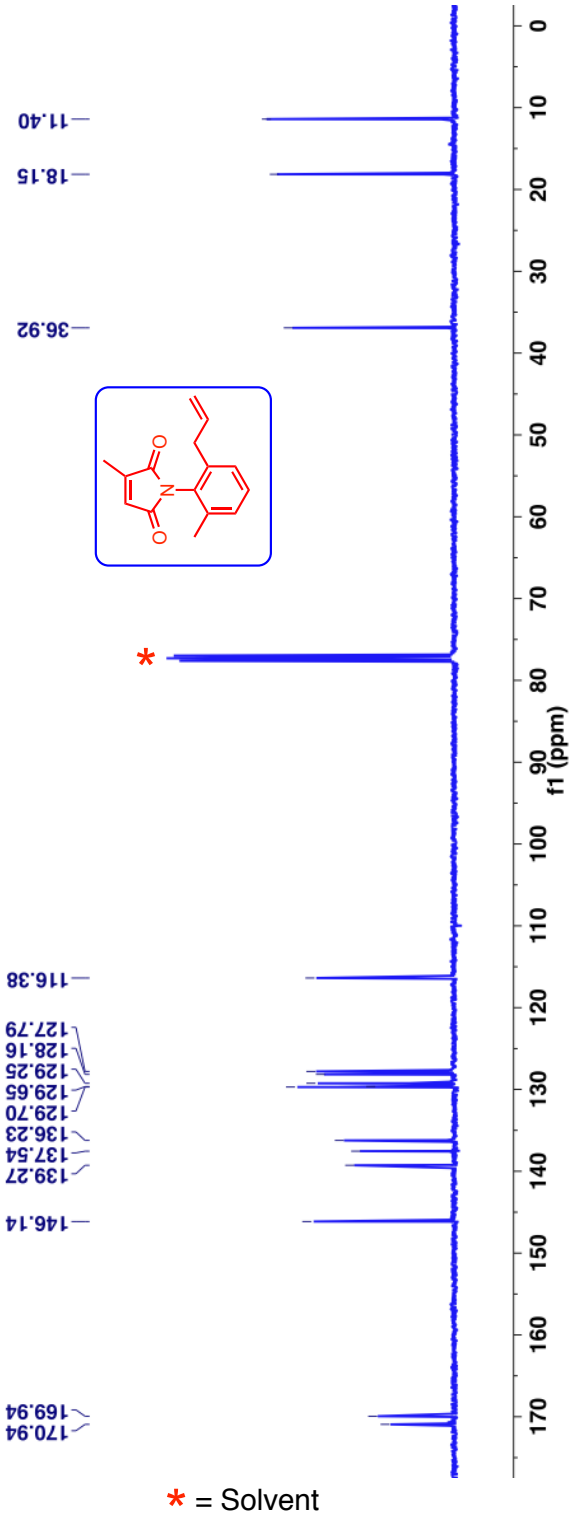

Figure 3.111: ^{13}C-NMR (100 MHz, $CDCl_3$, δ ppm) spectrum of allyl maleimide **205b**.

^{1}H-NMR (400 MHz, $CDCl_3$, δ ppm): 7.30-7.26 (m, 1H), 7.18-7.14 (m, 2H), 6.99 (s,1H), 5.81-5.71 (m, 1H), 5.00-4.94 (m, 2H), 3.20-3.19 (d, J = 6.8 Hz, 2H) and 2.10 (s, 3H).

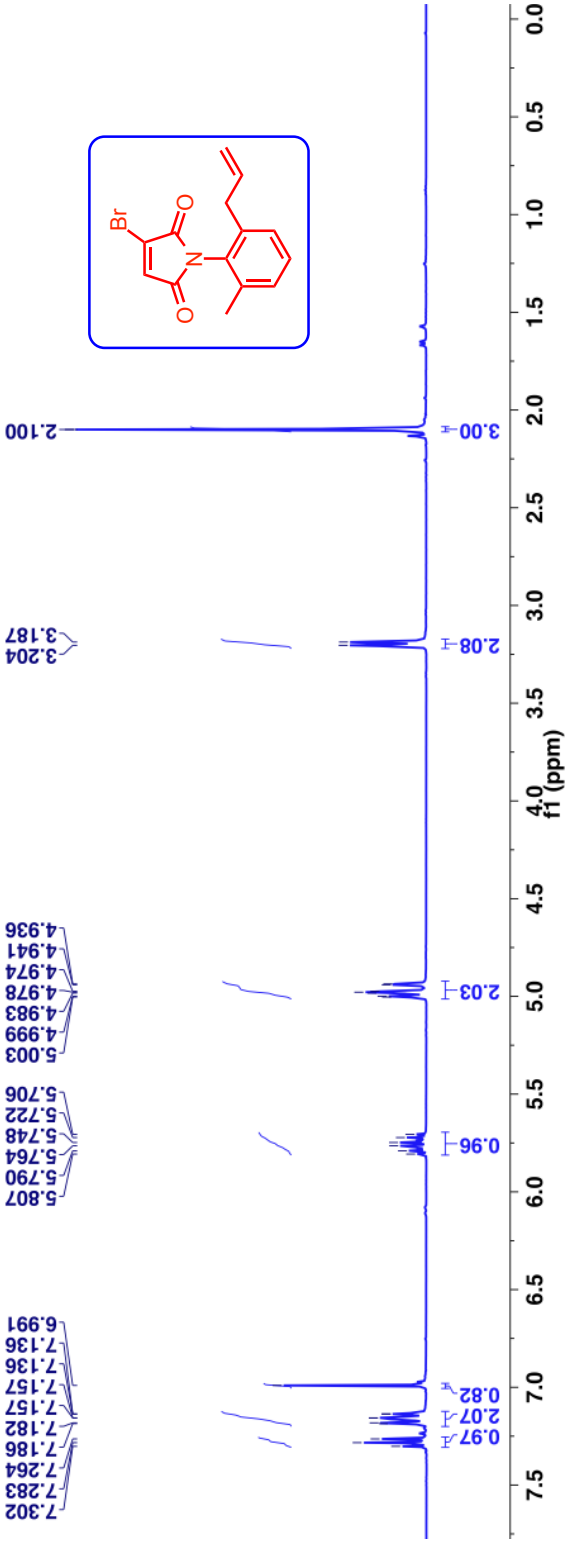

Figure 3.112: ^{1}H-NMR (400 MHz, $CDCl_3$, δ ppm) spectrum of allyl maleimide **205c**.

^{13}C-NMR (100 MHz, $CDCl_3$, δ ppm): 167.7, 164.4, 139.2, 137.5, 136.0, 132.3, 131.9, 130.2, 129.5, 129.1, 128.4, 116.7, 37.1 and 18.1.

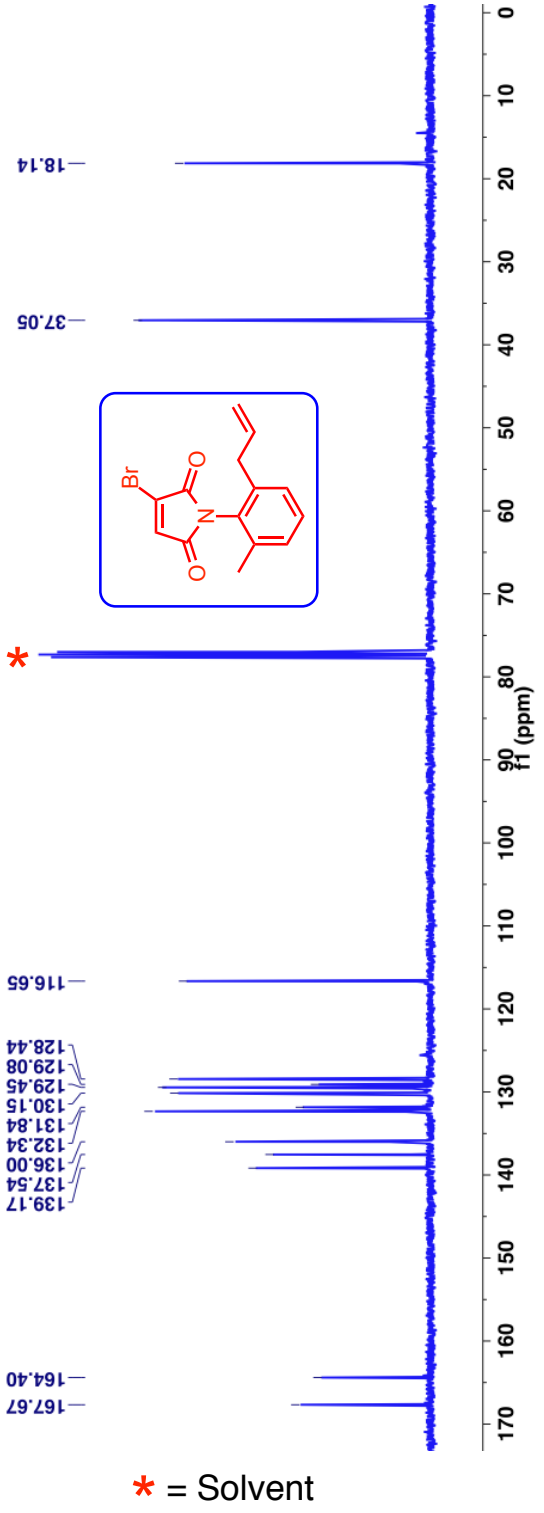

Figure 3.113: ^{13}C-NMR (100 MHz, $CDCl_3$, δ ppm) spectrum of allyl maleimide **205c**.

HPLC analysis conditions:

For analytical conditions,

I). Column : CHIRALPAK-IC

Abs. detector wavelength : 254 nm and 270 nm

Mobile phase : Hexanes:2-propanol = 98:2

Flow rate : 1.0 mL/min

Retention times (min) : ~ 6.72 [(+)-**205c**] and ~ 7.40 [(-)-**205c**]

For preparative conditions,

I). Column : CHIRALPAK-IC

Abs. detector wavelength : 254 nm and 270 nm

Mobile phase : Hexanes:2-propanol = 99:1

Flow rate : 3.0 mL/min

Retention times (min) : ~ 13.05 [(+)-**205c** and ~ 15.30 [(-)-**205c**]

Optical rotation $[\alpha]_D^{22}$:

HPLC retention time (CHIRALPAK-IC) at ~ 6.72 min, (*c* ≈ 0.383 %, $CHCl_3$) = +8.33 deg

HPLC retention time (CHIRALPAK-IC) at ~ 7.40 min, (*c* ≈ 0.383 %, $CHCl_3$) = -8.85 deg.

^{1}H-NMR (400 MHz, $CDCl_3$, δ ppm): 8.03-8.00 (m, 2H), 7.49-7.48 (m, 3H), 7.32-7.29 (m, 1H), 7.23-7.21 (m, 2H), 6.90 (s, 1H),5.91-5.80 (m, 1H), 5.04-5.00 (m, 2H), 3.31-3.29 (d, J = 6.4 Hz, 2H) and 2.1 (s, 3H).

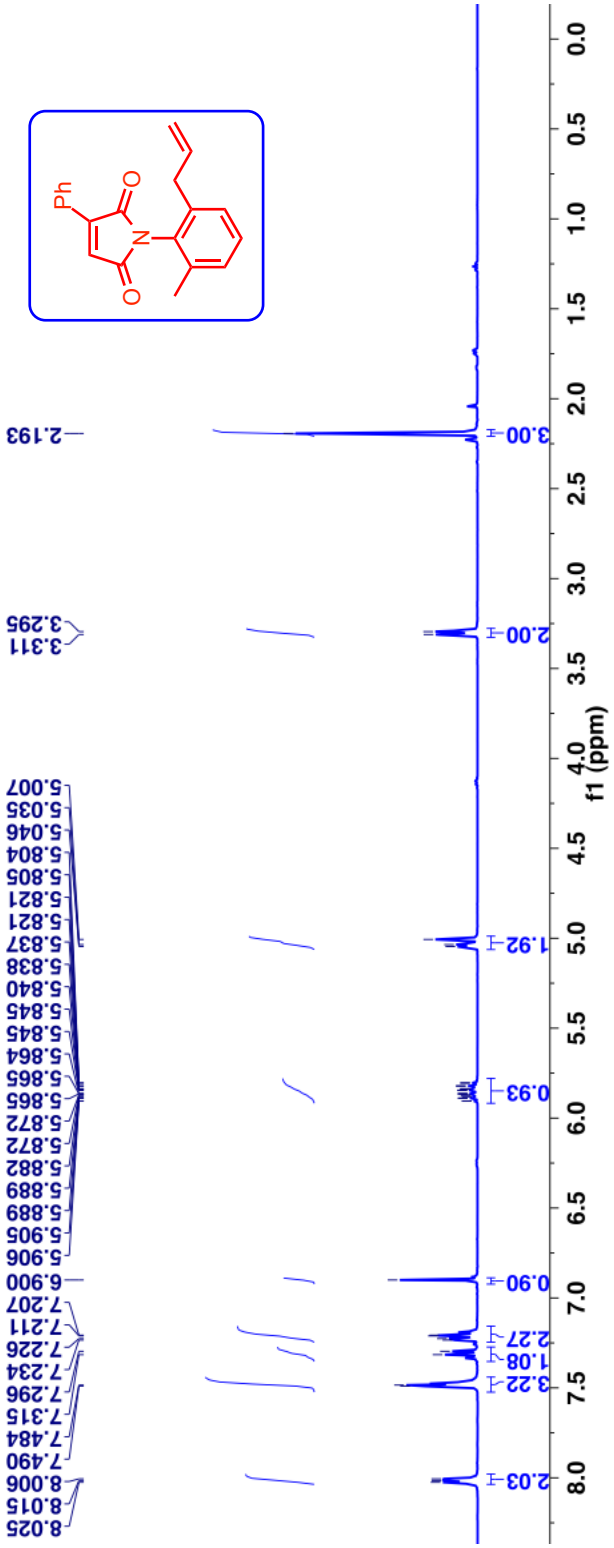

Figure 3.114: ^{1}H-NMR (400 MHz, $CDCl_3$, δ ppm) spectrum of allyl maleimide **205d**.

^{13}C-NMR (100 MHz, $CDCl_3$, δ ppm): 169.9, 169.5, 144.1, 139.4, 137.7, 136.3, 131.6, 129.8, 129.8, 129.4, 129.3, 129.1, 128.9, 128.3, 124.3, 116.6, 37.1 and 18.3.

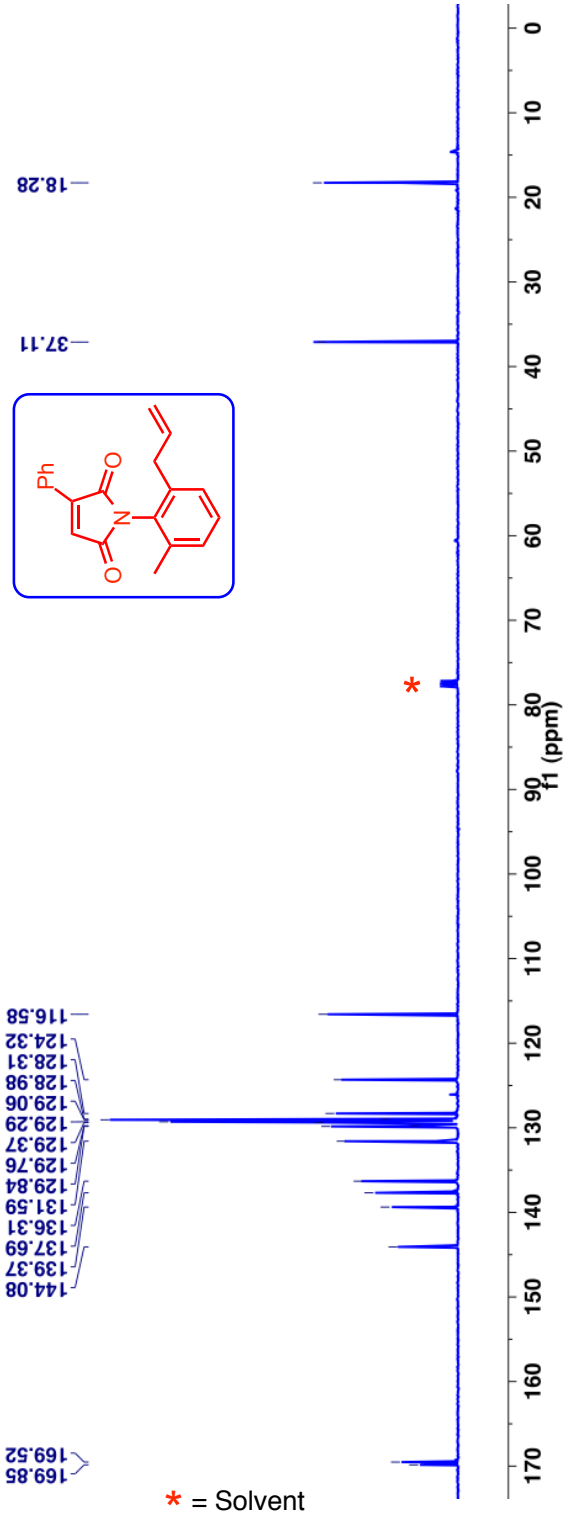

Figure 3.115: ^{13}C-NMR (100 MHz, $CDCl_3$, δ ppm) spectrum of allyl maleimide **205d**.

HPLC analysis conditions:

For analytical conditions,

I). Column : CHIRALPAK-ADH

Abs. detector wavelength : 254 nm and 270 nm

Mobile phase : Hexanes:2-propanol = 95:5

Flow rate : 1.0 mL/min

Retention times (min) : ~ 7.17 [(+)-**205d**] and ~ 7.72 [(-)-**205d**]

For preparative conditions,

I). Column : CHIRALPAK-ADH

Abs. detector wavelength : 254 nm and 270 nm

Mobile phase : Hexanes:2-propanol = 99:1

Flow rate : 3.0 mL/min

Retention times (min) : ~ 31.95 [(+)-**205d** and ~ 36.02 [(-)-**205d**]

Optical rotation $[\alpha]_D^{22}$:

HPLC retention time (CHIRALPAK-ADH) at ~ 7.17 min, (*c* ≈ 0.231 %, $CHCl_3$) = +7.10 deg

HPLC retention time (CHIRALPAK-ADH) at ~ 7.72 min, (*c* ≈ 0.231 %, $CHCl_3$) = -7.45 deg.

^{1}H-NMR (400 MHz, $CDCl_3$, δ ppm): 7.98-7.96 (m, 2H), 7.48-7.46 (m, 3H), 7.02-6.98 (d, J = 16.4, 2H), 6.85 (s, 1H), 4.72 (s, 1H), 4.62 (s, 1H), 3.19 (s, 2H), 2.34 (s, 3H), 2.12 (s, 3H), and 1.59 (s, 3H).

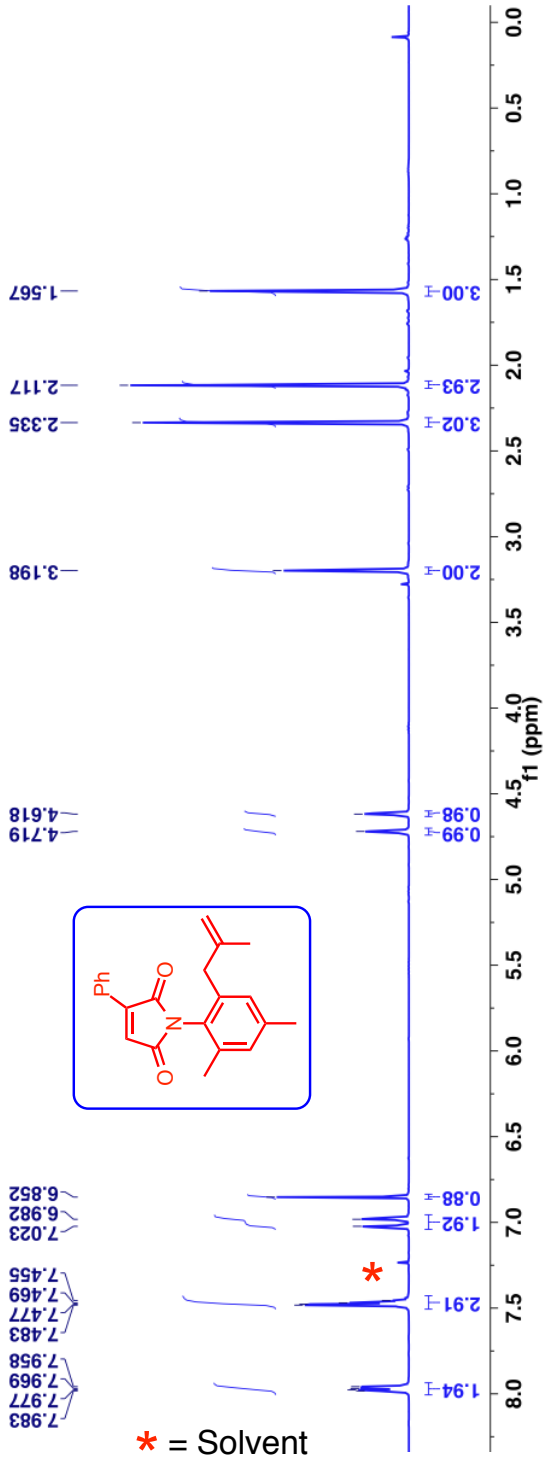

Figure 3.116: ^{1}H-NMR (400 MHz, $CDCl_3$, δ ppm) spectrum of allyl maleimide **205e**.

^{13}C-NMR (100 MHz, $CDCl_3$, δ ppm): 169.7, 169.6, 144.0, 139.5, 138.5, 137.3, 131.5, 130.2, 129.6, 129.2, 129.0, 128.9, 42.6, 22.1, 21.4 and 18.1.

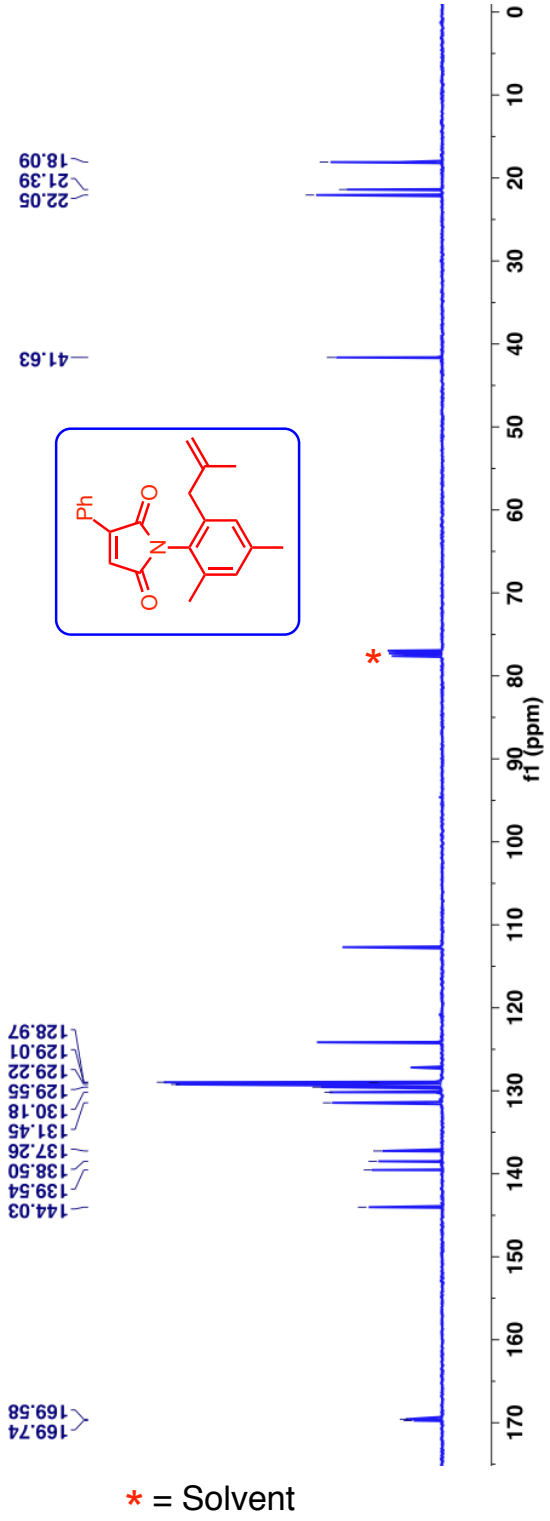

Figure 3.117: ^{13}C-NMR (100 MHz, $CDCl_3$, δ ppm) spectrum of allyl maleimide **205e**.

HPLC analysis conditions:

For analytical conditions,

I). Column : CHIRALPAK-IC

Abs. detector wavelength : 254 nm and 270 nm

Mobile phase : Hexanes:2-propanol = 90:10

Flow rate : 1.0 mL/min

Retention times (min) : ~ 6.12 [(+)-**205e**] and ~ 6.64 [(-)-**205e**]

For preparative conditions,

I). Column : CHIRALPAK-IC

Abs. detector wavelength : 254 nm and 270 nm

Mobile phase : Hexanes:2-propanol = 99:1

Flow rate : 3.0 mL/min

Retention times (min) : ~ 19.53 [(+)-**205e** and ~ 22.10 [(-)-**205e**]

Optical rotation $[\alpha]_D^{22}$:

HPLC retention time (CHIRALPAK-IC) at ~ 6.12 min, (*c* ≈ 1.364 %, $CHCl_3$) = +7.88 deg

HPLC retention time (CHIRALPAK-IC) at ~ 6.64 min, (*c* ≈ 1.364 %, $CHCl_3$) = -7.74 deg.

^{1}H-NMR (400 MHz, $CDCl_3$, δ ppm): 7.27-7.23 (m, 1H), 7.15-7.11 (m, 2H), 5.83-5.72 (m, 1H), 5.54 (s, 1H), 4.99-4.95 (m, 2H), 3.96 (s, 3H), 3.20 (d, J = 6.8, 2H) and 2.10 (s, 3H).

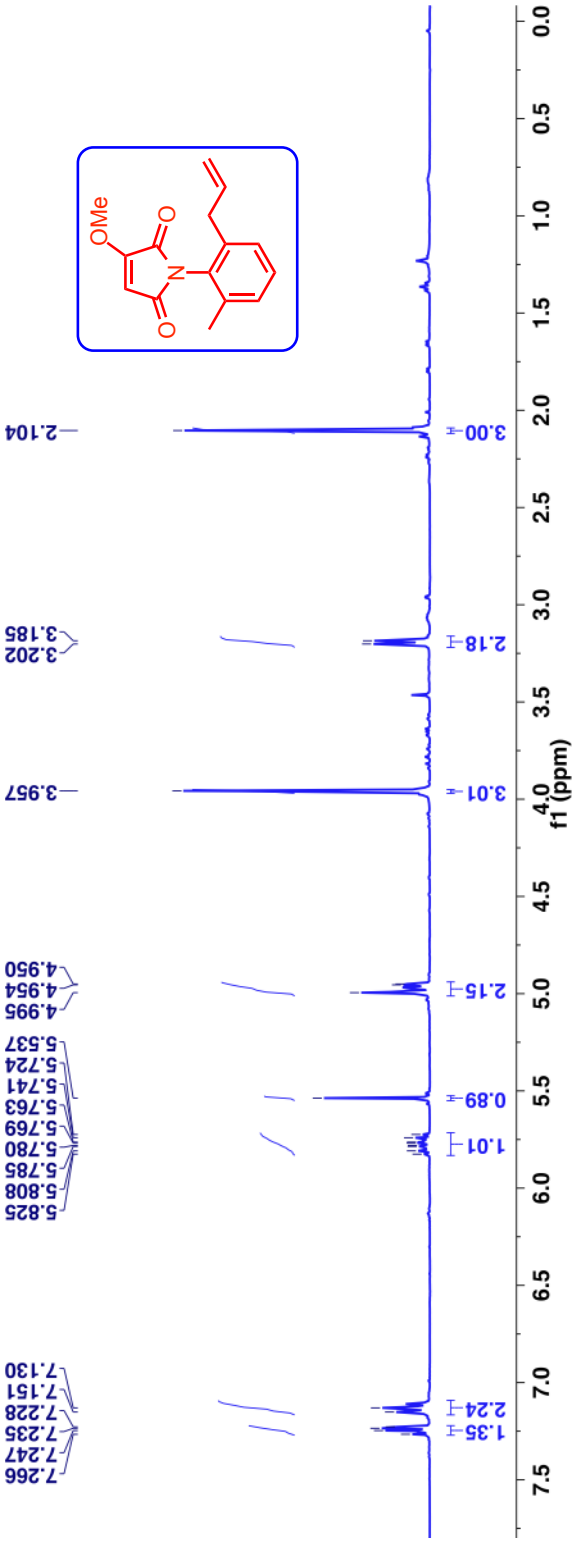

Figure 3.118: ^{1}H-NMR (400 MHz, $CDCl_3$, δ ppm) spectrum of allyl maleimide **205f**.

^{13}C-NMR (100 MHz, $CDCl_3$, δ ppm): 169.3, 164.7, 161.0, 139.4, 137.7, 137.1, 129.8, 129.3, 129.0, 128.2, 116.5, 96.7, 59.2, 36.9 and 18.2.

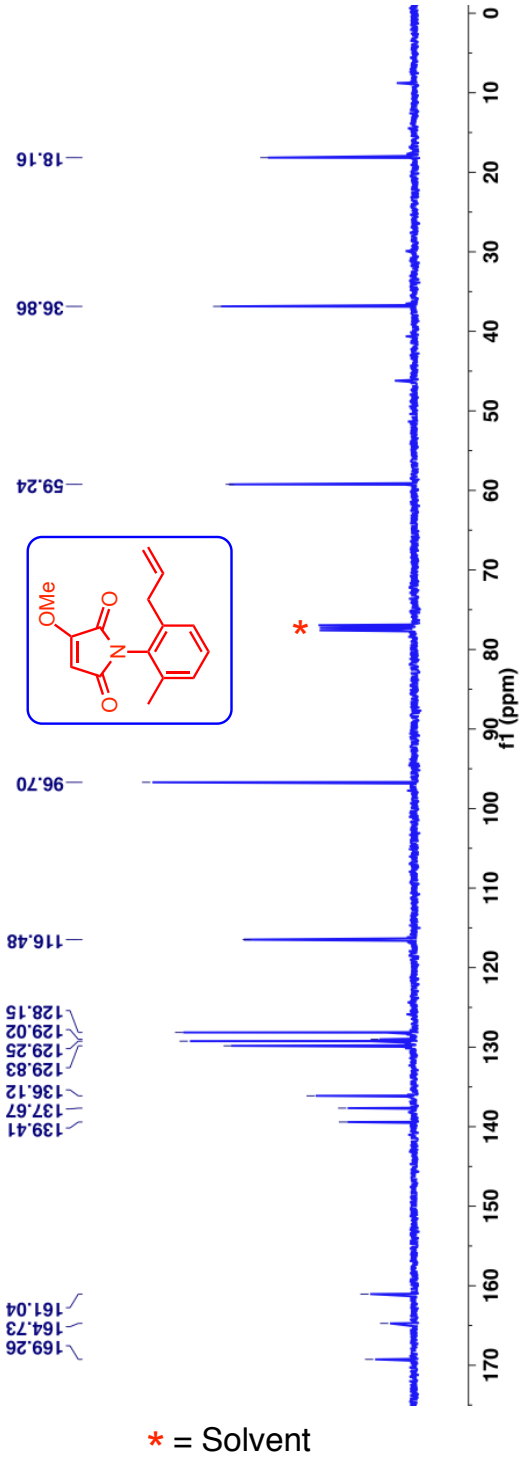

Figure 3.119: ^{13}C-NMR (100 MHz, $CDCl_3$, δ ppm) spectrum of allyl maleimide **205f**.

HPLC analysis conditions:

For analytical conditions,

I). Column : CHIRALPAK-IC

Abs. detector wavelength : 254 nm and 270 nm

Mobile phase : Hexanes:2-propanol = 95:5

Flow rate : 1.0 mL/min

Retention times (min) : ~ 13.59 [(-)-**205f**] and ~ 15.34 [(+)-**205f**]

For preparative conditions,

I). Column : CHIRALPAK-IC

Abs. detector wavelength : 254 nm and 270 nm

Mobile phase : Hexanes:2-propanol = 99:1

Flow rate : 3.0 mL/min

Retention times (min) : ~ 5.64 [(-)**205f** and ~ 18.89 (+)**205f**]

Optical rotation $[\alpha]_D^{24}$:

HPLC retention time (CHIRALPAK-IC) at ~ 13.59 min, (*c* ≈ 0.408 %, $CHCl_3$) = - 3.69 deg

HPLC retention time (CHIRALPAK-IC) at ~ 15.35 min, (*c* ≈ 0.408 %, $CHCl_3$) = +1.89 deg.

^{1}H-NMR (400 MHz, $CDCl_3$, δ ppm): 7.32-7.28 (m, 1H), 7.21-7.15 (m, 2H), 7.09-7.08 (q, J = 5.2Hz, 1H), 5.79-5.69 (m, 1H), 4.99-4.92 (m, 2H), 3.22-3.20 (d, J = 6.8 Hz, 2H) and 2.10 (s, 3H).

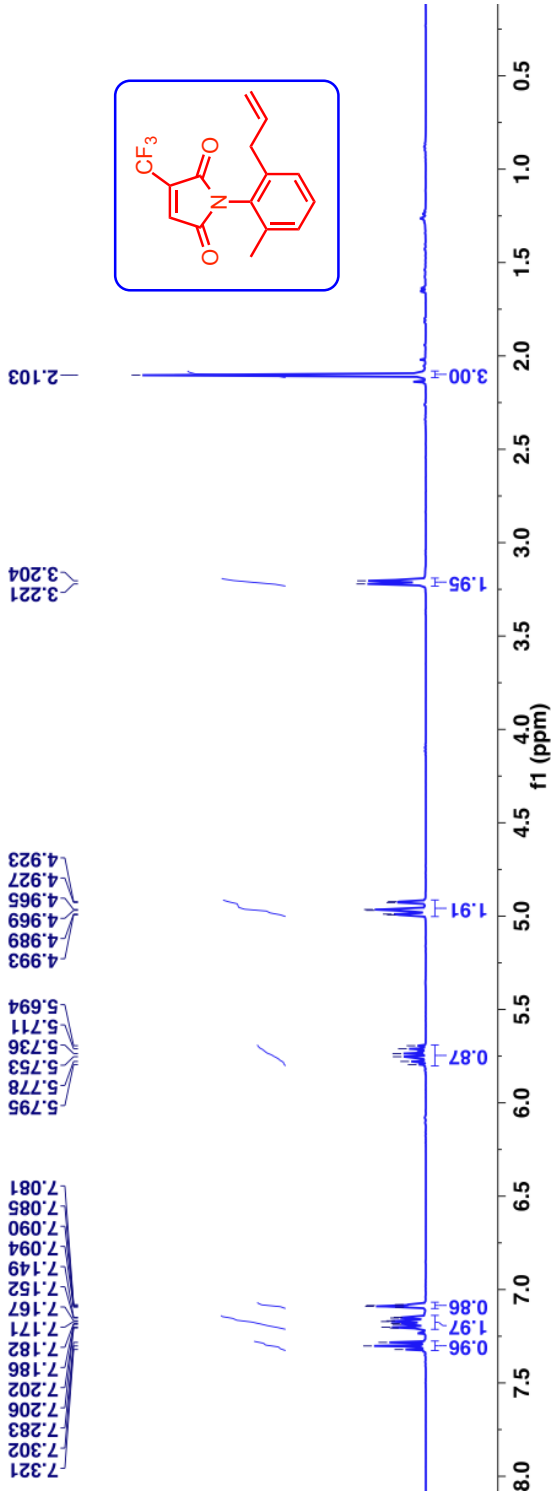

Figure 3.120: ^{1}H-NMR (400 MHz, $CDCl_3$, δ ppm) spectrum of allyl maleimide **205g**.

^{13}C-NMR (100 MHz, $CDCl_3$, δ ppm): 166.2, 163.9, 139.0, 137.5, 136.0, 133.7, 130.3, 129.6, 128.7, 128.5, 120.8, 118.1, 116.5, 37.3 and 17.9.

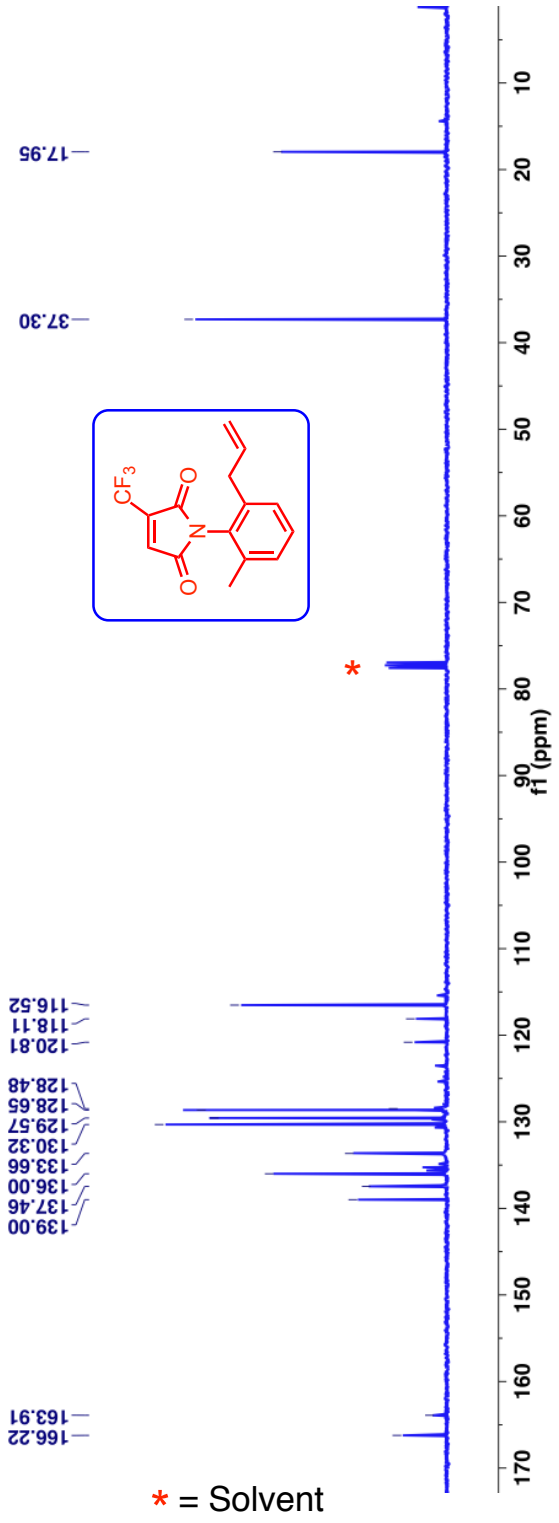

Figure 3.121: ^{13}C-NMR (100 MHz, $CDCl_3$, δ ppm) spectrum of allyl maleimide **205g**.

HPLC analysis conditions:

For analytical conditions,

I). Column : CHIRALPAK-ADH

Abs. detector wavelength : 254 nm and 270 nm

Mobile phase : Hexanes:2-propanol = 95:5

Flow rate : 1.0 mL/min

Retention times (min) : ~ 4.30 [(A)-**205g**] and ~ 5.30 [(B)-**205g**]

For preparative conditions,

I). Column : CHIRALPAK-ADH

Abs. detector wavelength : 254 nm and 270 nm

Mobile phase : Hexanes:2-propanol = 99:1

Flow rate : 3.0 mL/min

Retention times (min) : ~ 10.42 [(A)-**205g**] and ~ 12.42 [(B)-**205g**]

Optical rotation $[\alpha]_D^{24}$:

HPLC retention time (CHIRALPAK-ADH) at ~ 10.42 min, (*c* ≈ 0.283 %, $CHCl_3$) = +7.47 deg

HPLC retention time (CHIRALPAK-ADH) at ~ 12.42 min, (*c* ≈ 0.283 %, $CHCl_3$) = -7.21 deg.

^{1}H-NMR (400 MHz, $CDCl_3$, δ ppm): 7.29-7.25 (m, 1H), 7.18-7.15 (m, 2H), 5.81-5.71 (m, 1H), 4.99-4.93 (m, 2H), 3.20-3.18 (d, J = 6.8 Hz, 2H), 2.11 (s, 3H) and 2.09 (s, 3H).

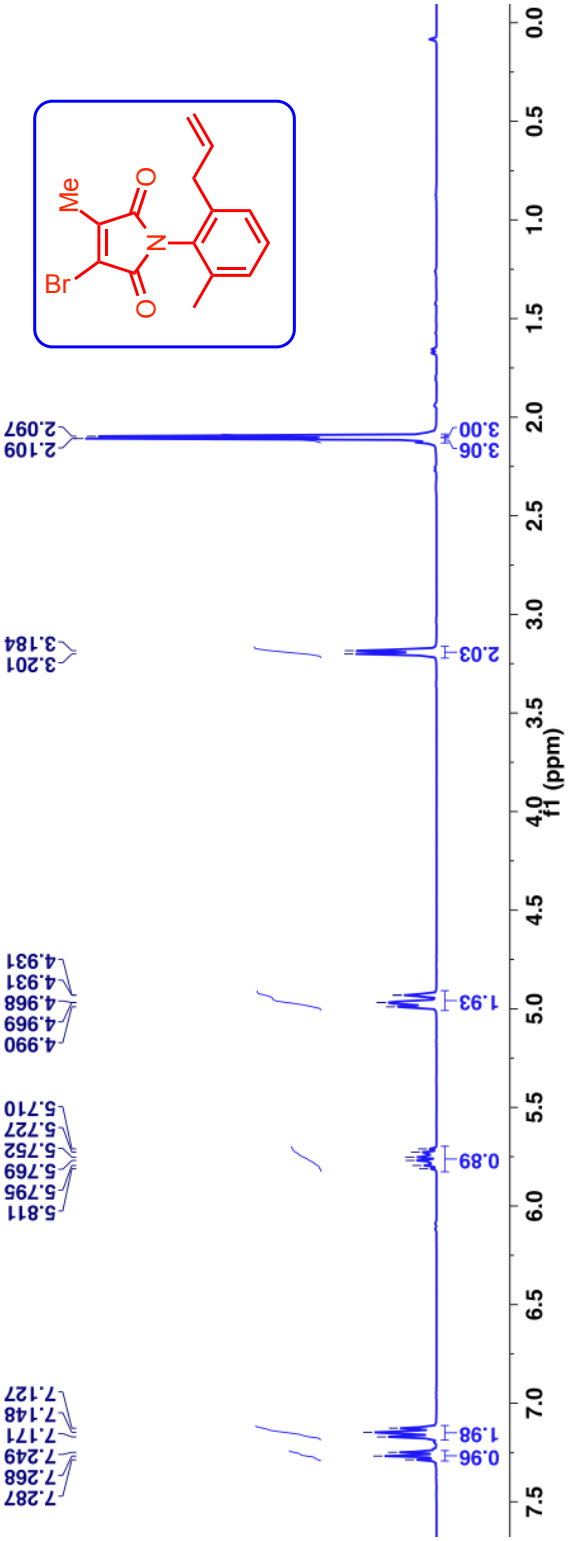

Figure 3.122: ^{1}H-NMR (400 MHz, $CDCl_3$, δ ppm) spectrum of allyl maleimide **205h**.

^{13}C-NMR (100 MHz, $CDCl_3$, δ ppm): 168.5, 164.5, 142.8, 139.2, 137.6, 136.1, 129.9, 129.4, 128.3, 125.5, 116.5, 37.0, 18.2 and 11.2.

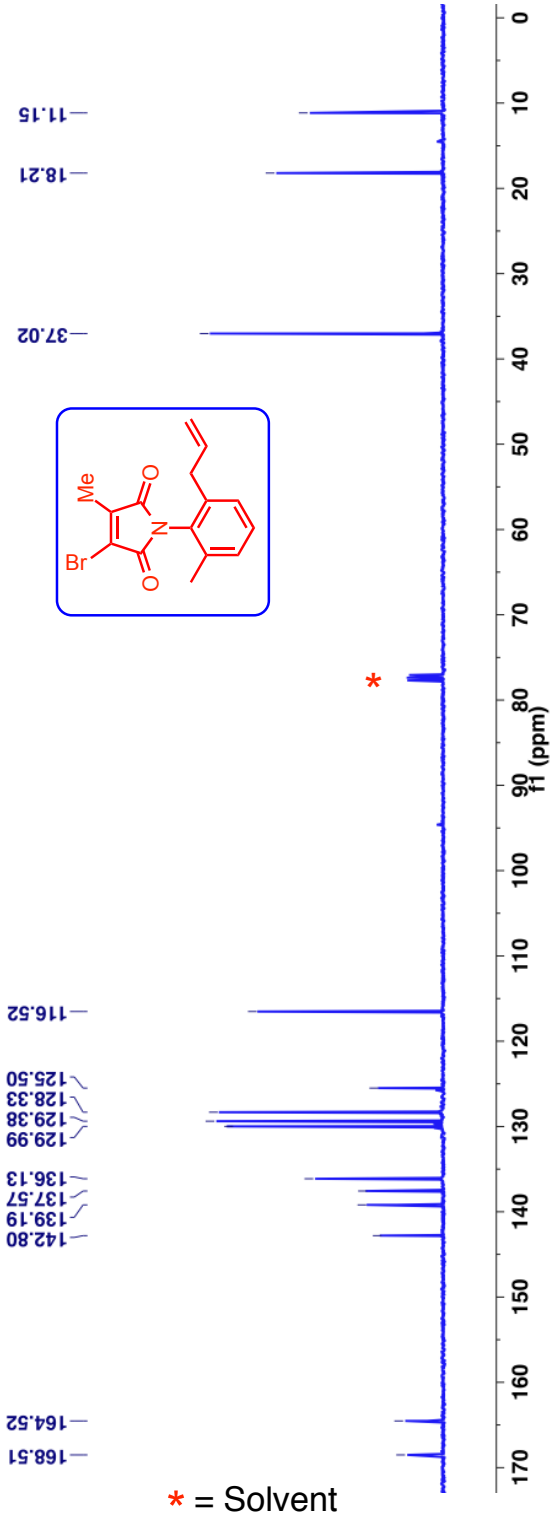

Figure 3.123: ^{13}C-NMR (100 MHz, $CDCl_3$, δ ppm) spectrum of allyl maleimide **205h**.

3.33. UV-Vis Spectrum of atropisomeric maleimides and its photoproducts

The UV-Vis spectra of atropisomeric maleimides and its photoproducts were measured in acetonitrile.

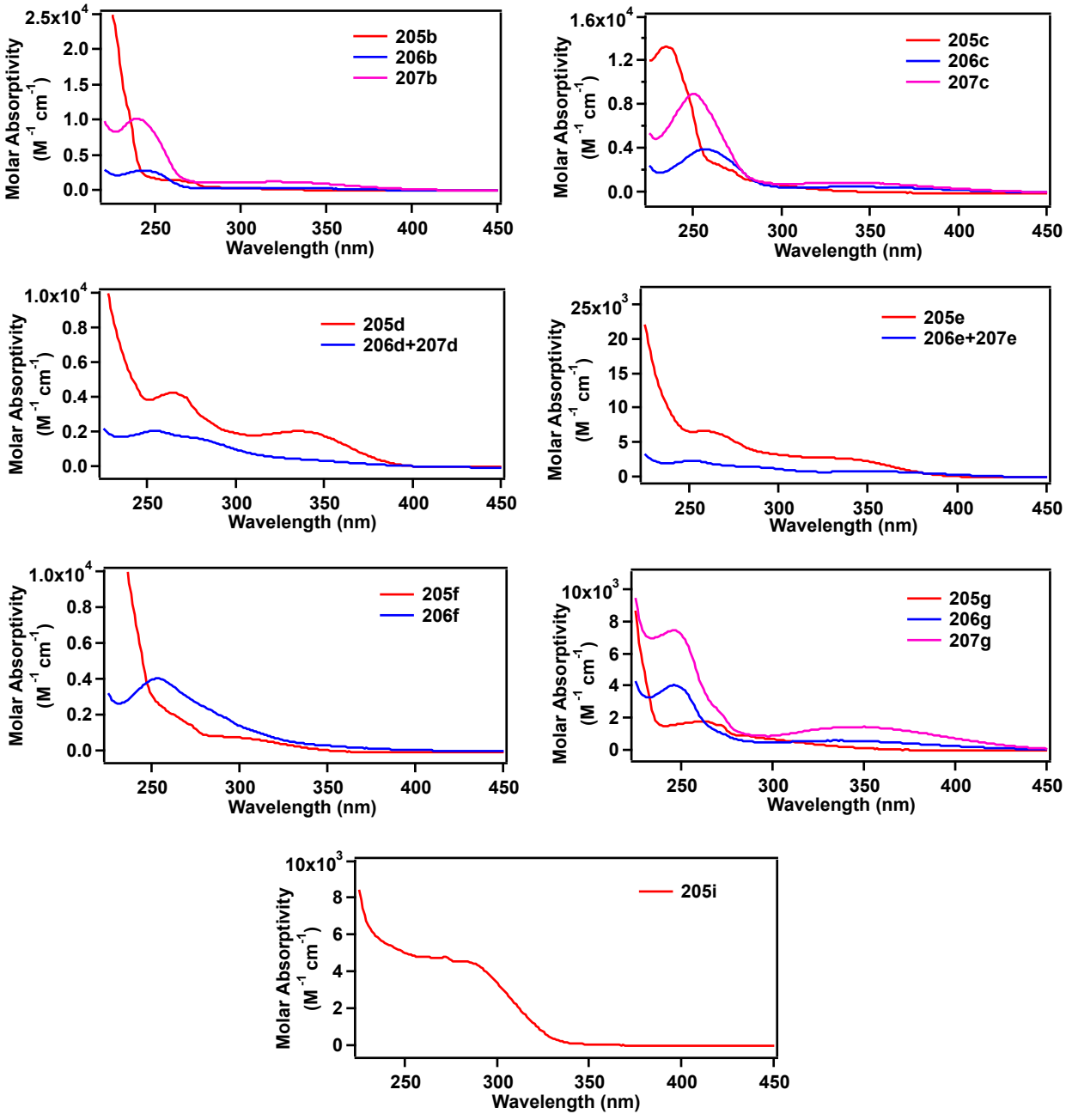

Figure 3.124: UV-Vis spectrum of allyl maleimide **205** and its photoproducts **206** and **207**.

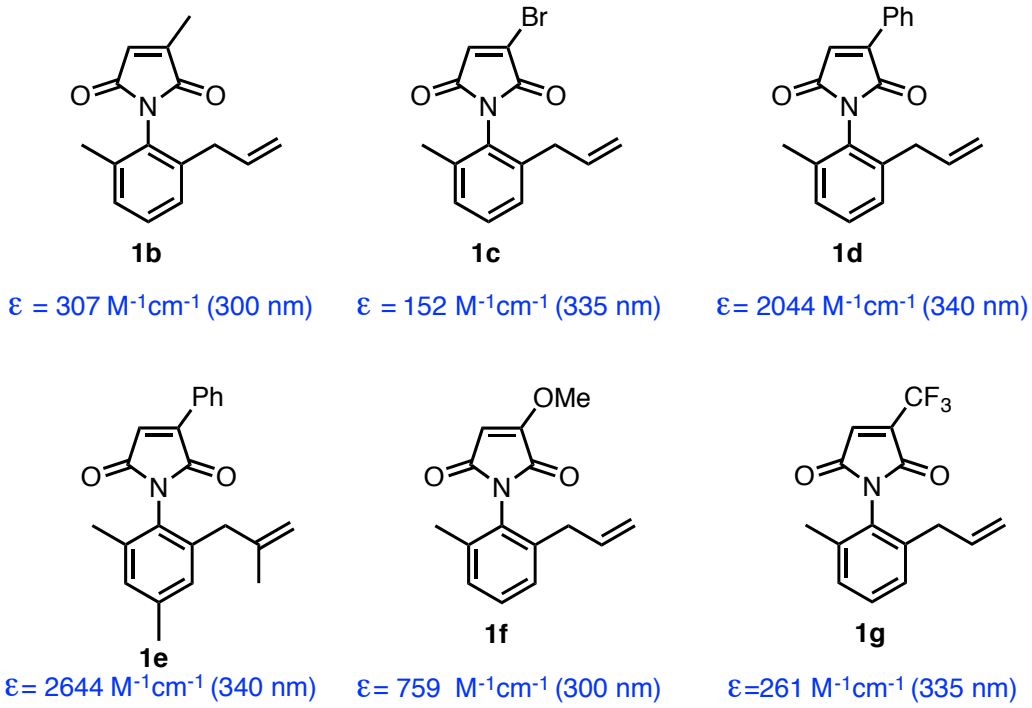

Figure 3.125: Molar absorptivity of **205** at longest absorption wavelength.

Solvatochromic effect: The UV-Vis spectra of atropisomeric maleimide **205d** in various solvent viz. Methyl cyclohexane (MCH), acetonitrile (MeCN) and methanol (MeOH).

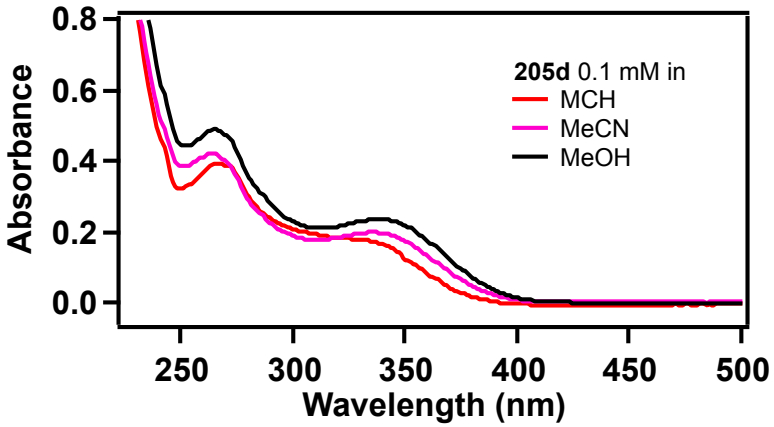

Figure 3.126: Solvatochromic effect of allyl maleimide **205d**.

3.34. General irradiation procedures and characterization of photoproducts

3.34.1. Process for photoreaction of atropisomeric maleimides 205a-l

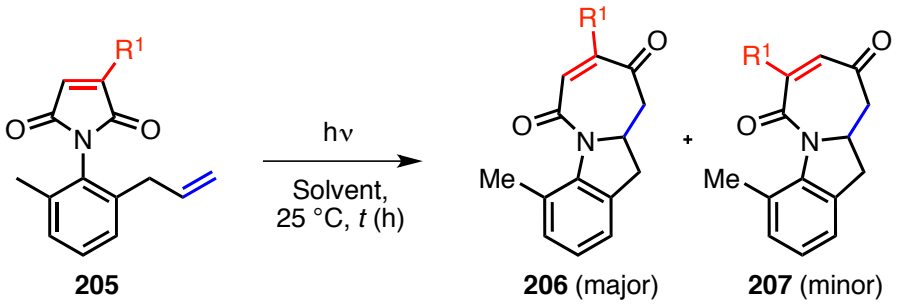

205 **206** (major) **207** (minor)

Scheme 3.56: General irradiation procedure for maleimide derivatives **205a-i**.

Enantiospecific reactions: A solution of optically pure atropisomeric maleimides obtained from HPLC preparative separation on a chiral stationary phase (2.5-4.0 mM or 1 mg/1 mL) in appropriate solvent was irradiated in either one of the following procedures. Irradiated in a Rayonet reactor fitted with bulb of desired wavelength. After the irradiation, the solvent was evaporated under reduced pressure and the photoproducts were isolated by preparative thin layer chromatography and characterized by NMR spectroscopy, mass spectrometry, single crystal XRD, $[\alpha]_D$ and by HPLC. HPLC analysis of the photolysate on a chiral stationary phase gave the optical purity of the photoproducts.

Large-scale reactions: Large-scale reactions were carried out on racemic maleimides as batches (4 × 20 mL test tubes per batch). After the irradiation the solutions were combined and the solvent was evaporated under reduced pressure. The residue was purified by combiflash using a hexanes:ethyl acetate mixture as mobile phase. Conversion and mass balance were obtained from NMR integration of the crude photosylate against triphenylmethane as an internal standard using the equation 2.1 (Chapter 2)

The *dr* of the photoproducts **206** and **207** were calculated from the crude reaction mixture after the photoreaction.

TLC condition - R*f* = 0.30 (80% hexanes:20% ethyl acetate) for **206a**

TLC condition - R*f* = 0.15, 0.2 (80% hexanes:20% ethyl acetate) for **206b** and **207b** respectively

TLC condition - R*f* = 0.30, 0.2 (80% hexanes:20% ethyl acetate) for **206c** and **207c** respectively

TLC condition - R*f* = 0.40 (80% hexanes:20% ethyl acetate) for **206d** and **207d** (single spot)

TLC condition - R*f* = 0.20 (80% hexanes:20% ethyl acetate) for **206g** and **207g** (single spot)

TLC condition - R*f* = 0.10 (50% hexanes:50% ethyl acetate) for **206f**

TLC condition - R*f* = 0.20, 0.10 (80% hexanes:20% ethyl acetate) for **206g** and **207g** respectively

TLC condition - R*f* = 0.40, 0.2 (80% hexanes:20% ethyl acetate) for **206h** and **207h** respectively

^{1}H-NMR (400 MHz, $CDCl_3$, δ ppm): 7.05-7.01 (m, 3H), 6.58-6.6.55 (m, 1H), 6.39-6.36 (m, 1H), 5.08-5.02 (m, 1H), 3.66-3.59 (m, 1H), 3.08-2.99 (m, 1H), 2.78-2.72 (m, 2H) and 2.23 (s, 3H).

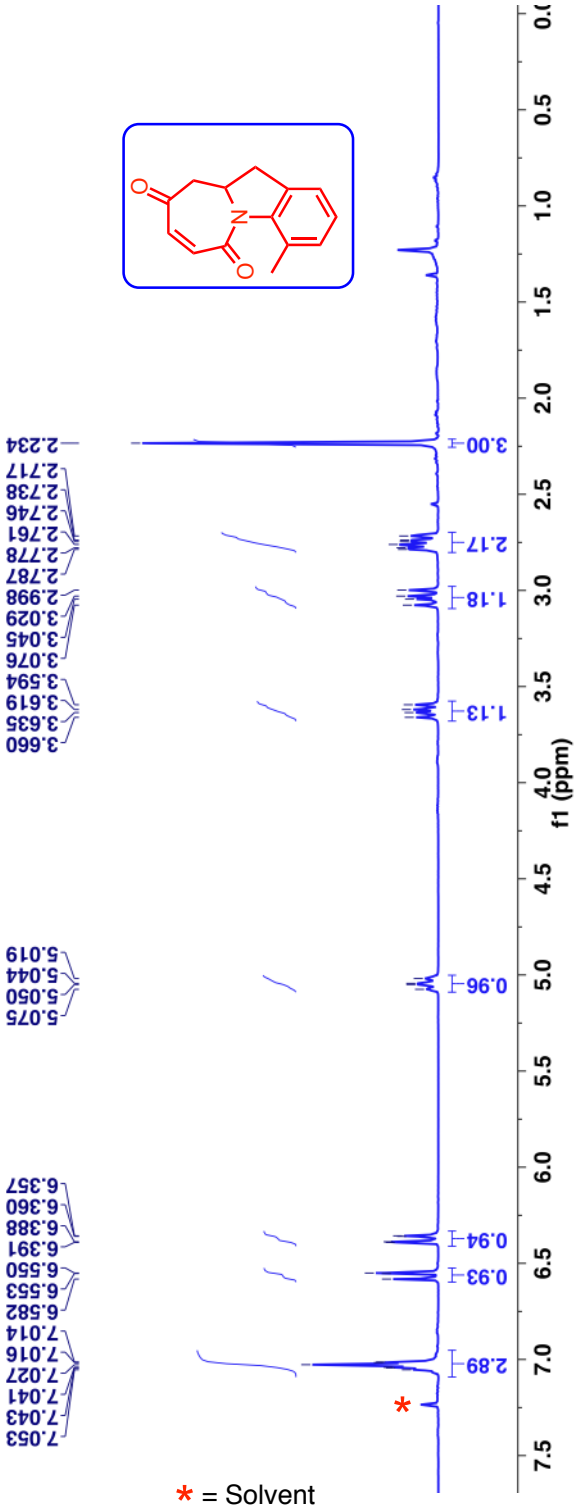

Figure 3.127: ^{1}H-NMR (400 MHz, $CDCl_3$, δ ppm) spectrum of allyl maleimide photoproduct **206a**.

^{13}C-NMR (100 MHz, $CDCl_3$, δ ppm): 209.9, 172.5, 148.9, 146.3, 145.7, 141.5, 141.3, 138.2, 135.7, 132.4, 67.0, 60.9, 44.5 and 31.9.

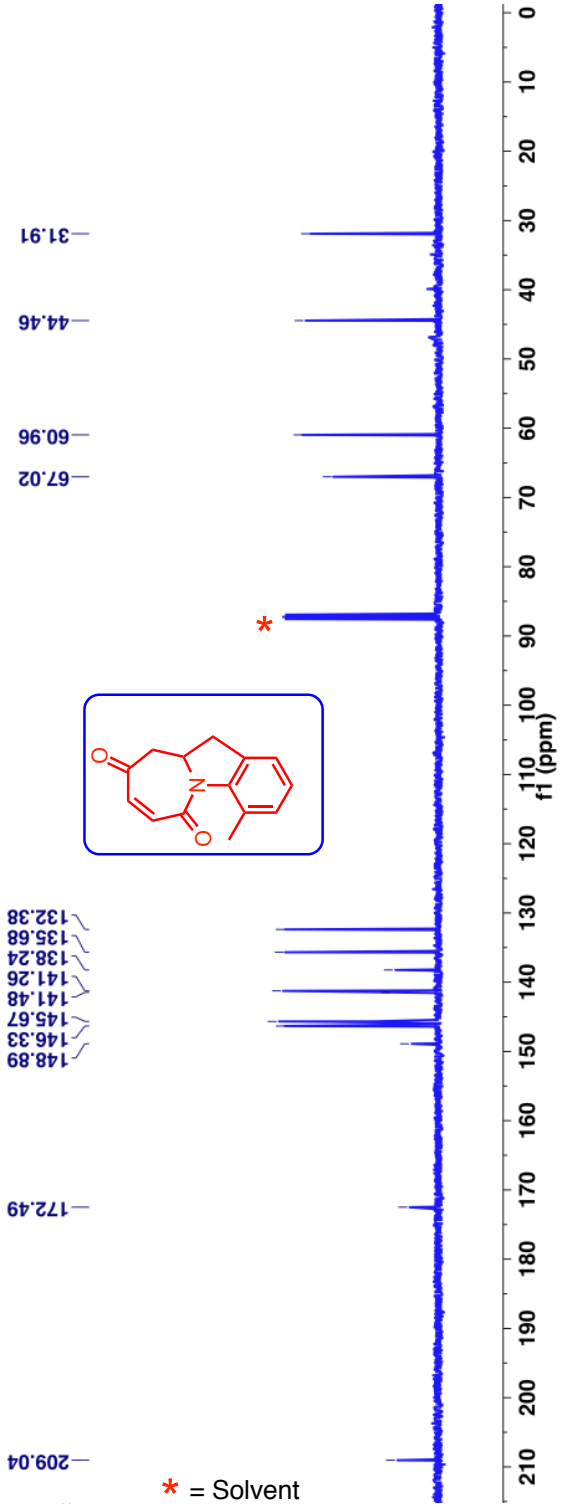

Figure 3.128: ^{13}C-NMR (100 MHz, $CDCl_3$, δ ppm) spectrum of allyl maleimide **206a**.

^{1}H-NMR (400 MHz, $CDCl_3$, δ ppm): 7.03-6.99(m, 3H), 6.46-6.45 (m, 1H), 5.01-4.96 (m, 1H), 3.61-3.54 (m, 1H), 3.07-3.00 (m, 1H), 2.80-2.73 (m, 2H), 2.22 (s, 3H) and 2.05-2.04 (d, J = 4 Hz 3H).

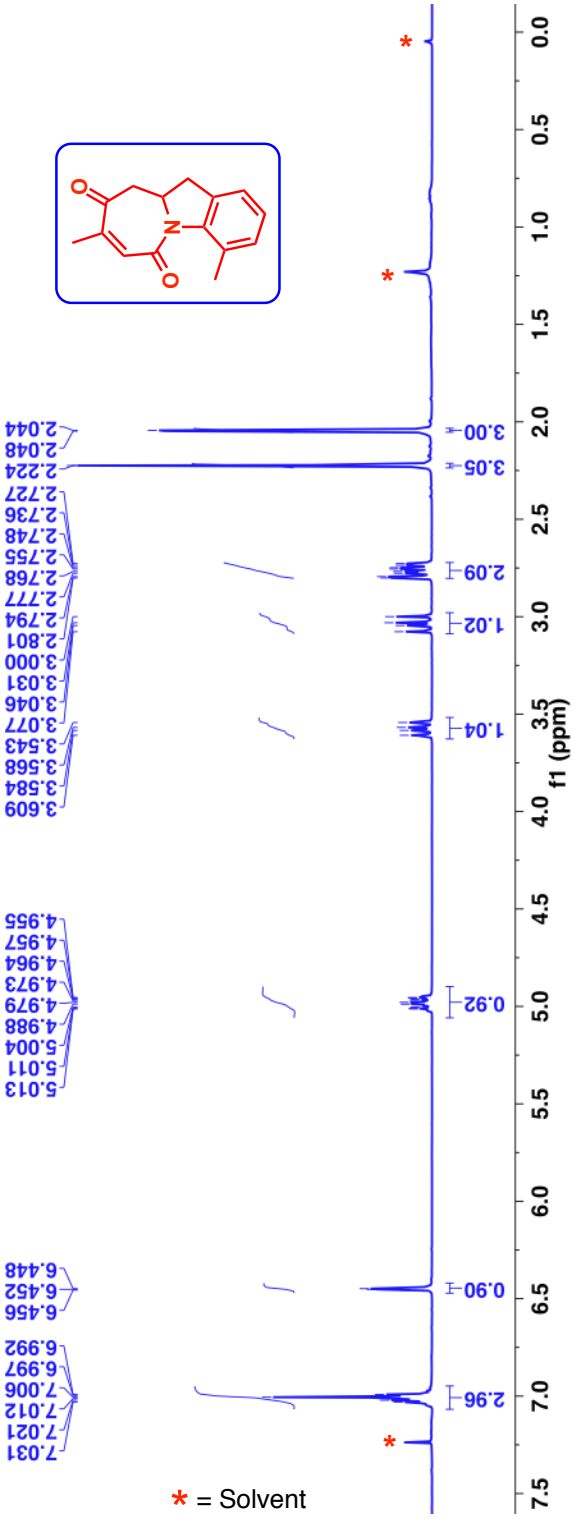

Figure 3.129: ^{1}H-NMR (400 MHz, $CDCl_3$, δ ppm) spectrum of allyl maleimide photoproduct **206b**.

^{13}C-NMR (100 MHz, $CDCl_3$, δ ppm): 200.9, 162.9, 145.3, 139.1, 132.3, 131.4, 131.2, 127.9, 125.4, 122.3, 56.6, 51.3, 34.3, 21.9 and 20.6.

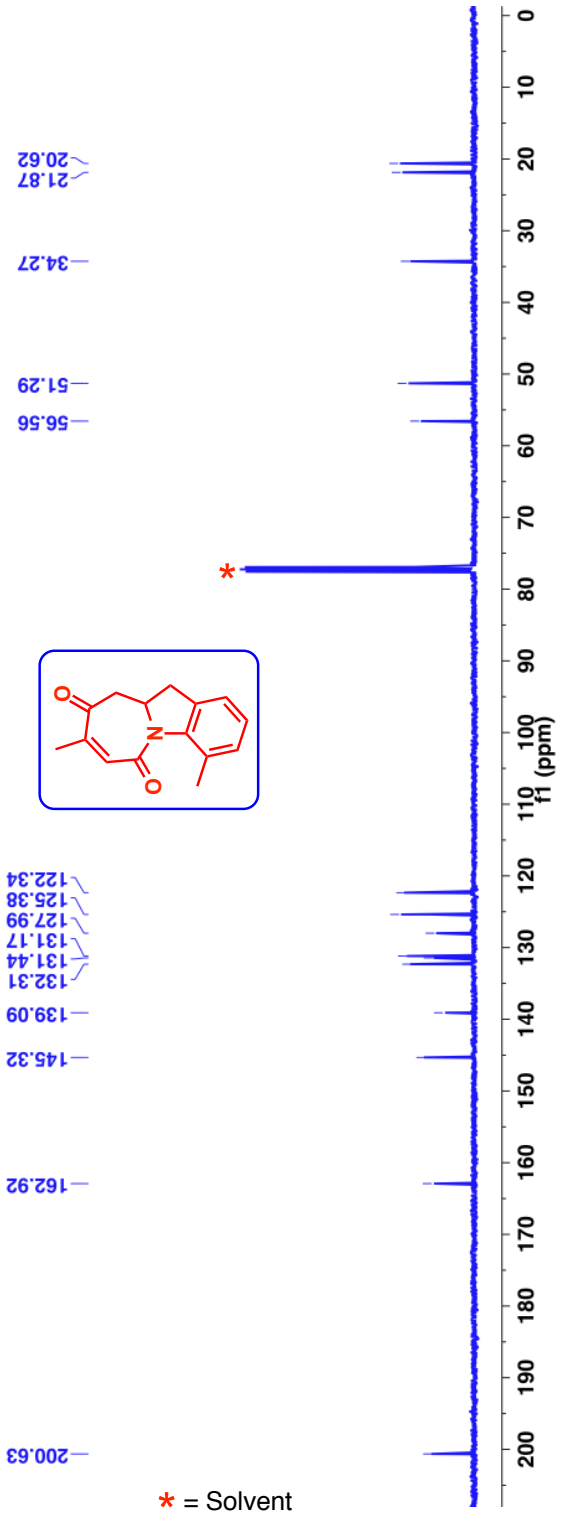

Figure 3.130: ^{13}C-NMR (100 MHz, $CDCl_3$, δ ppm) spectrum of allyl maleimide **206b**.

^{1}H-NMR (400 MHz, $CDCl_3$, δ ppm): 7.07-7.02(m, 3H), 6.37 (s, 1H), 5.05-4.98 (m, 1H), 3.64-3.57 (m, 1H), 2.98-2.90 (m, 1H), 2.78-2.65 (m, 2H), 2.22 (s, 3H) and 2.18 (s, 3H).

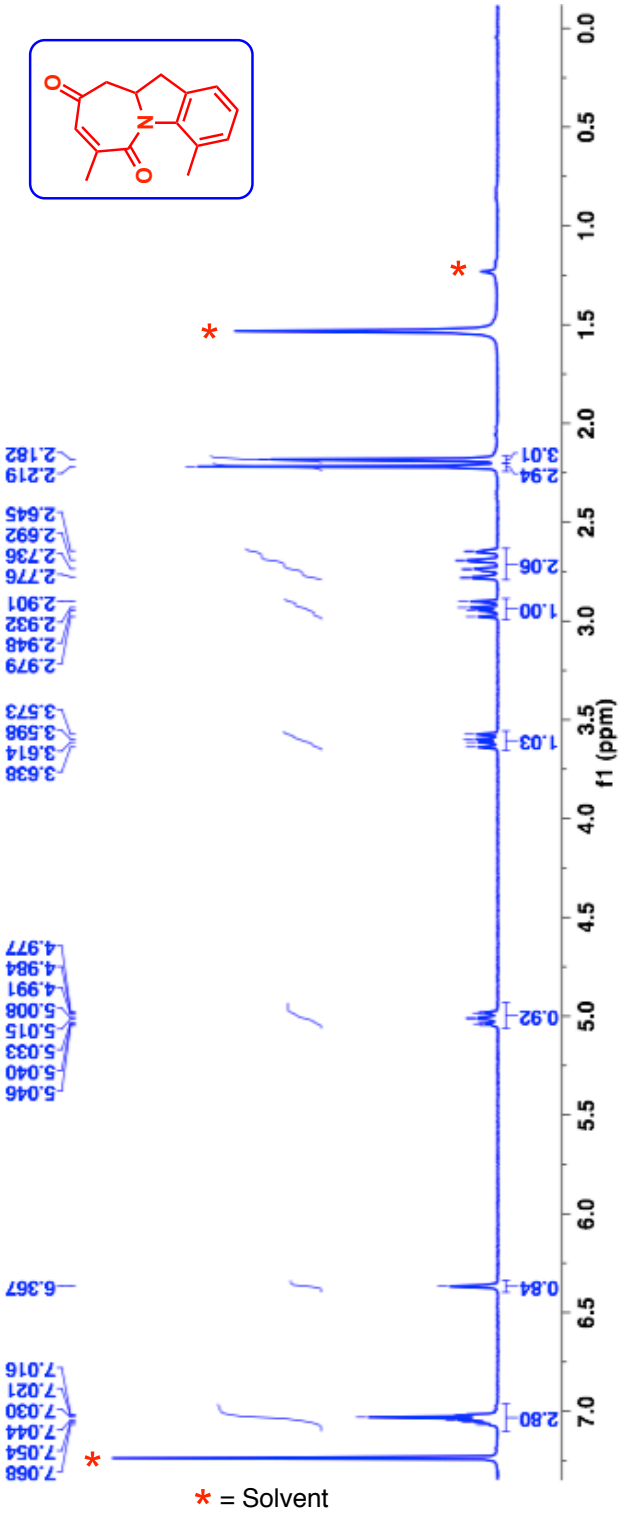

Figure 3.131: ^{1}H-NMR (400 MHz, $CDCl_3$, δ ppm) spectrum of allyl maleimide photoproduct **207b**.

^{13}C-NMR (100 MHz, $CDCl_3$, δ ppm): 199.7, 163.7, 145.1, 138.9, 133.1, 131.6, 131.2, 128.3, 125.5, 122.4, 56.9, 50.6, 34.1, 21.9 and 21.3.

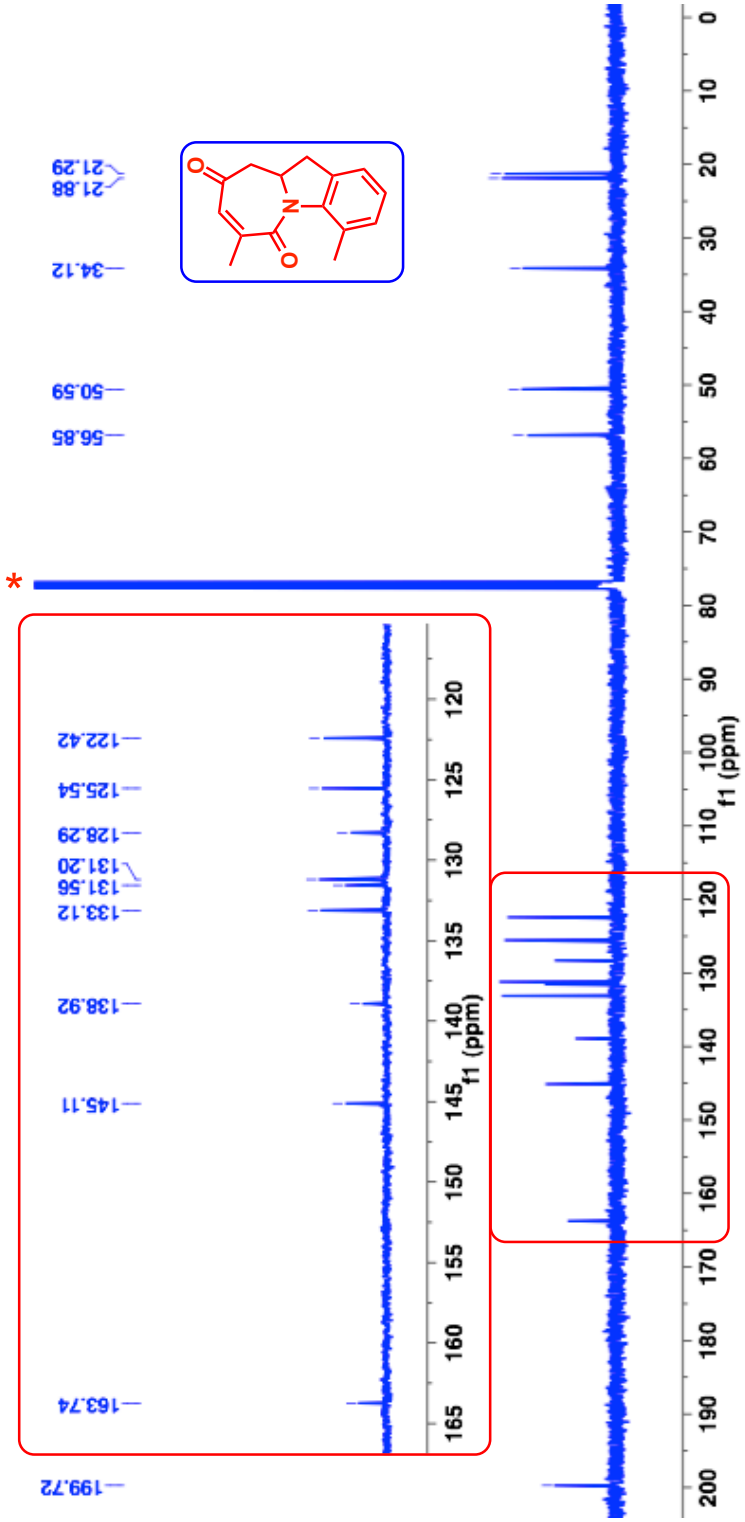

Figure 3.132: ^{13}C-NMR (100 MHz, $CDCl_3$, δ ppm) spectrum of allyl maleimide **207b**.

^{1}H-NMR (400 MHz, $CDCl_3$, δ ppm): 7.19 (s, 1H), 7.05-7.02 (m, 3H), 5.07-4.99 (m, 1H), 3.65-3.58 (m, 1H), 3.19-3.11 (m, 1H), 2.92-2.75 (m, 2H) and 2.22 (s, 3H).

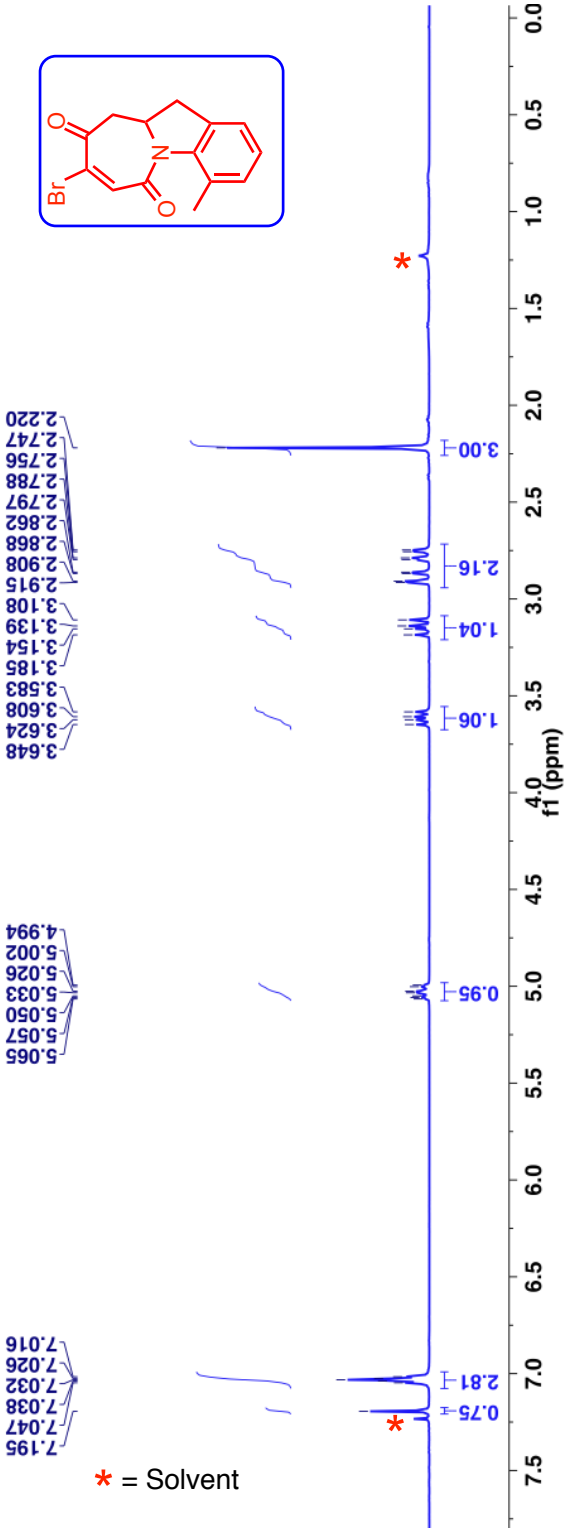

Figure 3.133: ^{1}H-NMR (400 MHz, $CDCl_3$, δ ppm) spectrum of allyl maleimide photoproduct **206c**.

^{13}C-NMR (100 MHz, $CDCl_3$, δ ppm): 192.7, 160.3, 138.5, 137.5, 132.9, 131.4, 131.3, 128.2, 125.9, 122.5, 56.5, 50.3, 34.2 and 21.9.

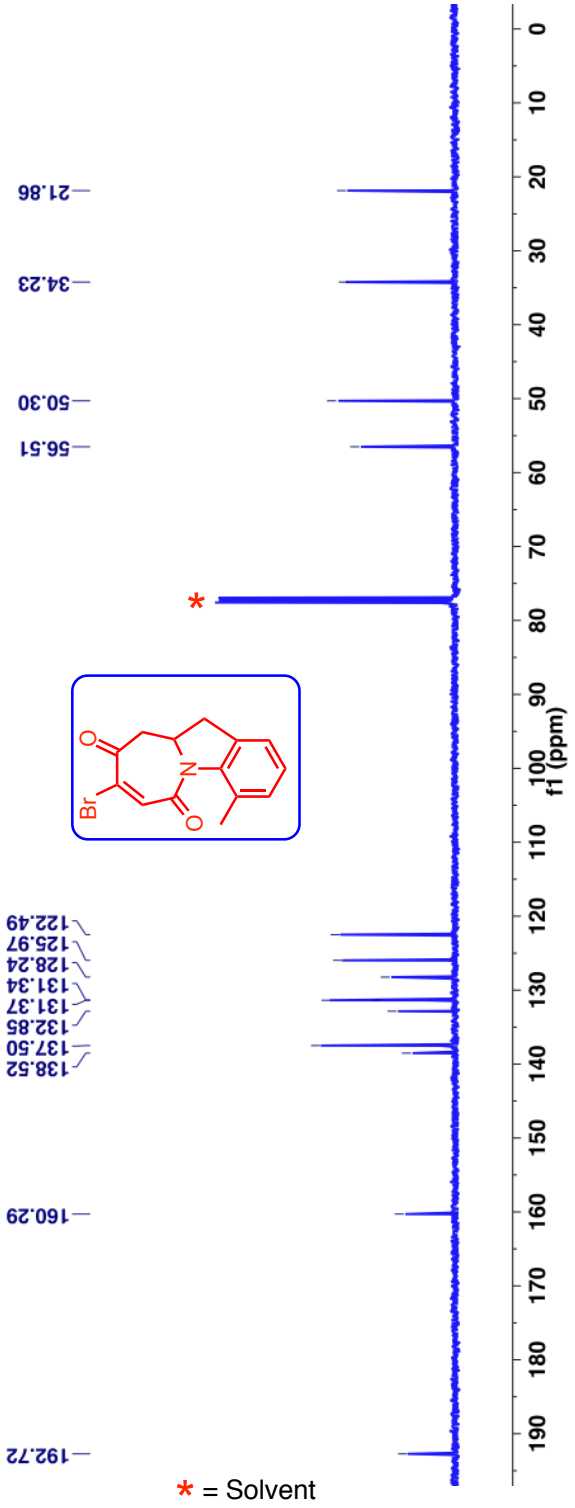

Figure 3.134: ^{13}C-NMR (100 MHz, $CDCl_3$, δ ppm) spectrum of allyl maleimide **206c**.

^{1}H-NMR (400 MHz, $CDCl_3$, δ ppm): 7.08 (s, 1H), 7.07-7.04 (m, 3H), 5.13-5.06 (m, 1H), 3.68-3.61 (m, 1H), 2.99-2.91 (m, 1H), 2.79-2.70 (m, 2H) and 2.23 (s, 3H).

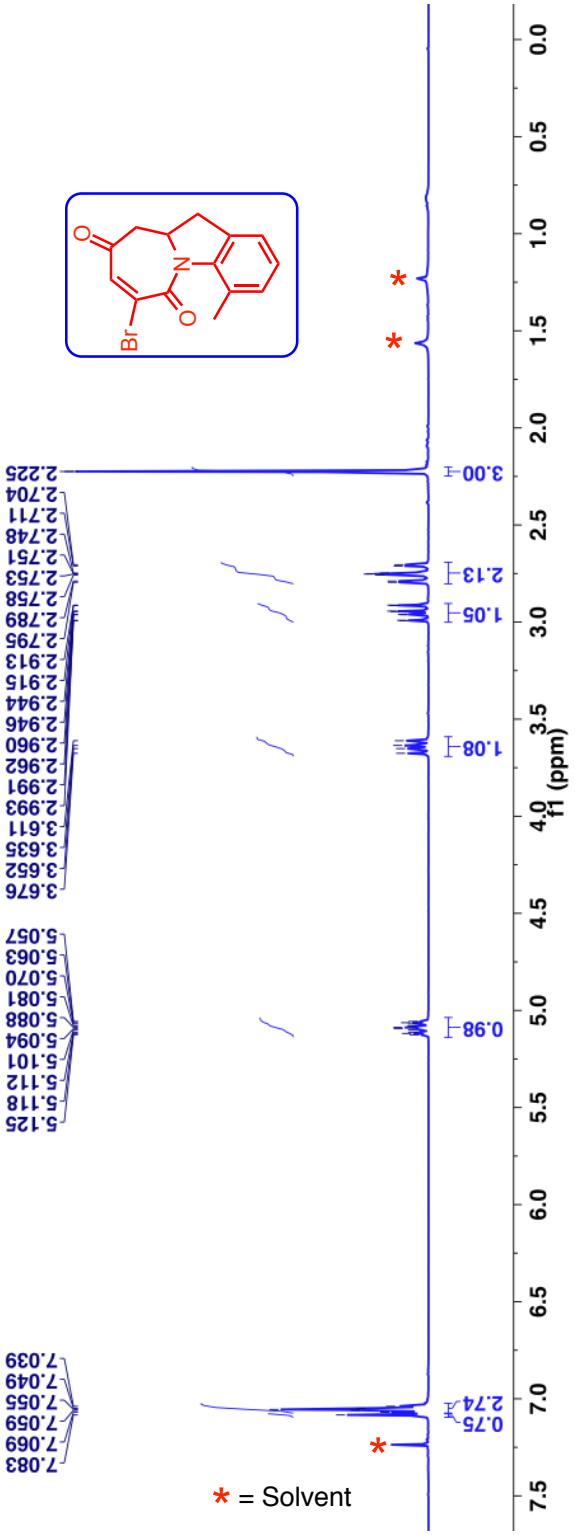

Figure 3.135: ^{1}H-NMR (400 MHz, $CDCl_3$, δ ppm) spectrum of allyl maleimide photoproduct **207c**.

^{13}C-NMR (100 MHz, $CDCl_3$, δ ppm): 196.5, 158.1, 138.3, 137.7, 135.6, 131.4, 128.7, 126.2, 122.6, 57.2, 50.0, 34.1and 21.8.

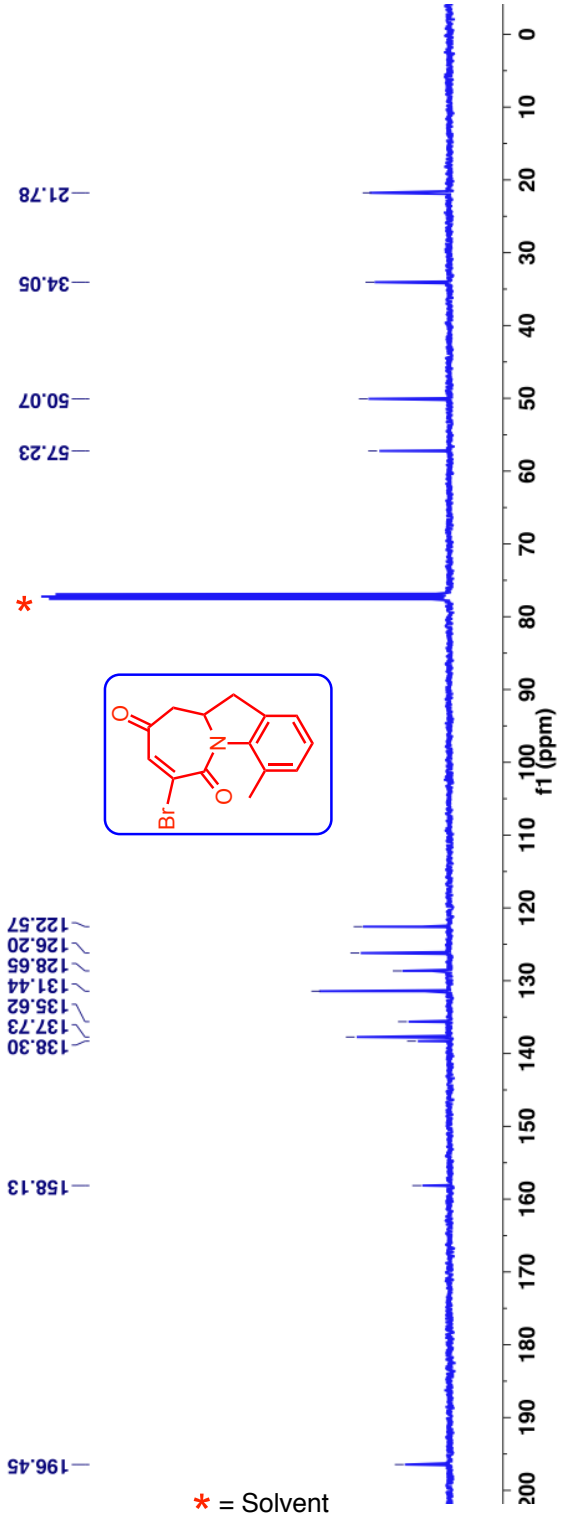

Figure 3.136: ^{13}C-NMR (100 MHz, $CDCl_3$, δ ppm) spectrum of allyl maleimide **207c**.

^{1}H-NMR (400 MHz, $CDCl_3$, δ ppm), (Major **206d** + minor **207d**, 70:30): 7.50-7.27 (m, 16H), 7.06-7.04 (m, 9H), 6.67 (s, 2H), 6.62 (s, 1H), 5.23-5.13 (m, 3H), 3.64-3.58 (m, 3H), 3.18-3.11 (m, 2H), 3.01-2.95(m, 3H), 2.82-2.71 (m, 4H), 2.26 (s,6H) and 2.25 (s, 3H).

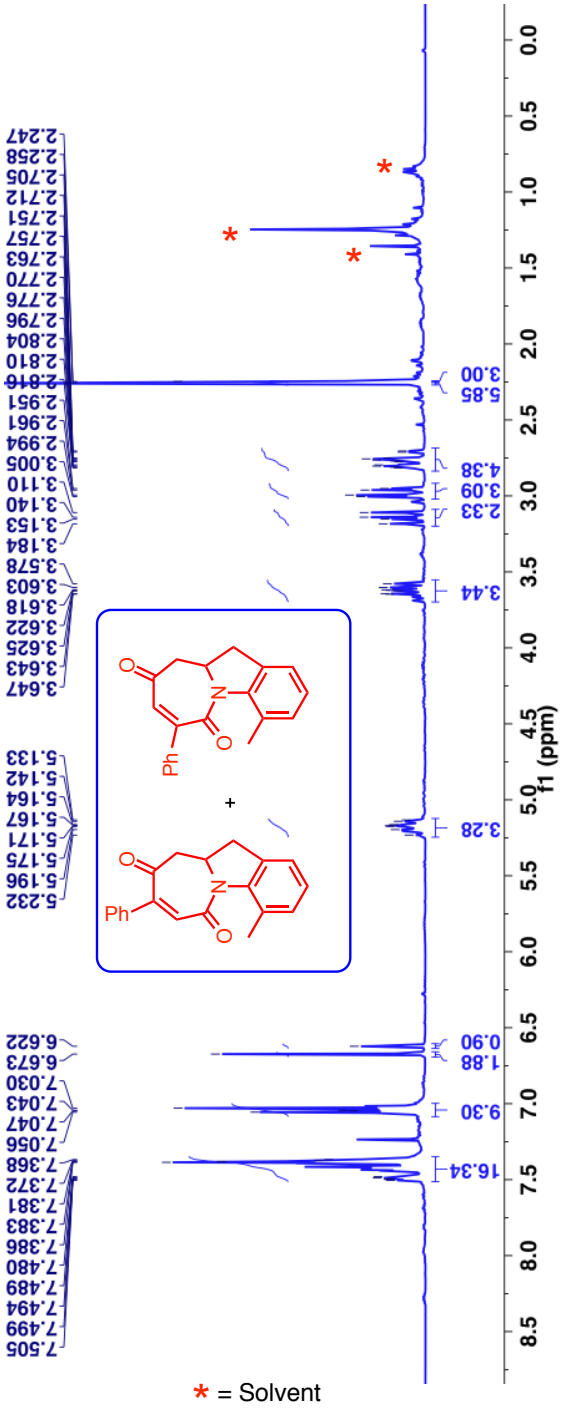

Figure 3.137: ^{1}H-NMR (400 MHz, $CDCl_3$, δ ppm) spectrum of allyl maleimide photoproduct **206d** and **207d**.

^{13}C-NMR (100 MHz, $CDCl_3$, δ ppm), (Major **206d** + minor **207d**, 70:30): 201.9, 200.7, 163.7,162.9, 148.6, 146.6, 138.9, 138.7, 136.8, 135.5, 132.3, 131.8, 131.4, 131.2, 130.1, 129.8, 129.1, 128.8, 128.7, 128.5, 128.1, 128.0, 125.8, 125.5, 122.6, 122.54, 57.1, 57.0, 53.5, 50.8, 36.9, 33.9, 33.7, 29.9, 22.2 and 21.8

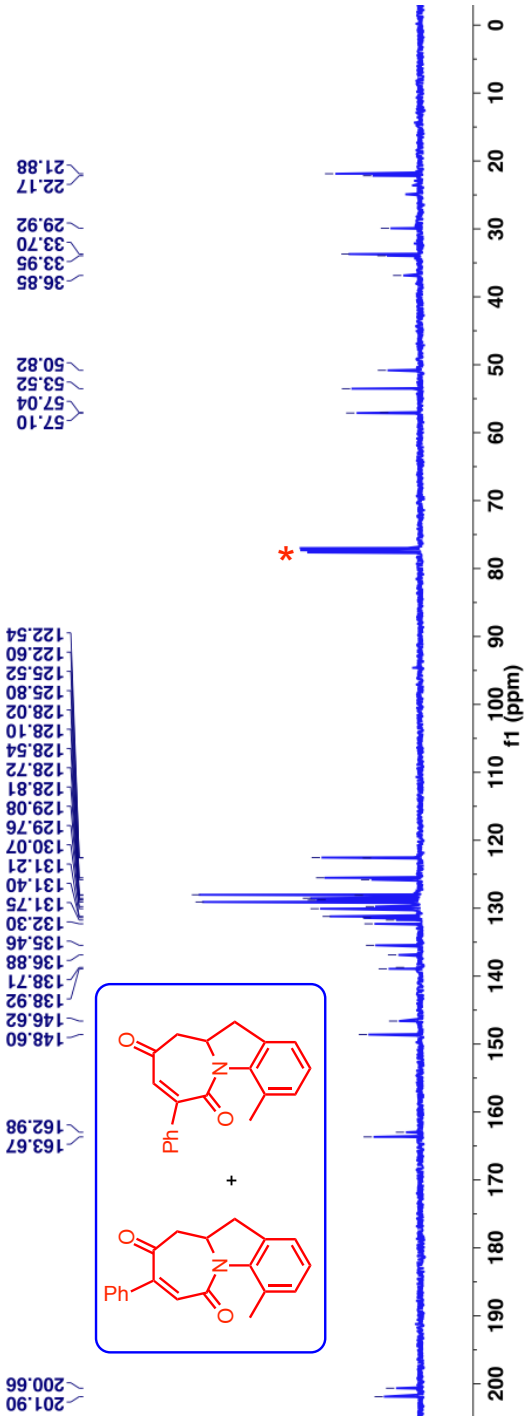

= Solvent

Figure 3.138: ^{13}C-NMR (400 MHz, $CDCl_3$, δ ppm) spectrum of allyl maleimide photoproduct **206d** and **207d**.

^{1}H-NMR (400 MHz, $CDCl_3$, δ ppm), (Major **206e** + minor **207e**, 74:26): 7.57-7.54 (m, 2H), 7.41-7.38 (m, 10H), 7.06 (s, 1H), 6.89-6.87 (m, 5H), 6.48-6.47 (d, J = 2 Hz, 1H), 3.62-3.59 (d, J = 14 Hz, 2H), 3.48-3.45 (d, J = 15 Hz, 3H), 3.38-3.30 (m, 3H), 3.11-3.07 (d, J = 14 Hz, 2H), 2.99-2.92 (m, 2H), 2.86-2.82 (d, J = 15.2 Hz, 2H), 2.29-2.28 (m, 8H), 2.14 (s, 4H), 2.09 (s, 3H), 1.43 (s, 3H) and 1.33 (s, 4H).

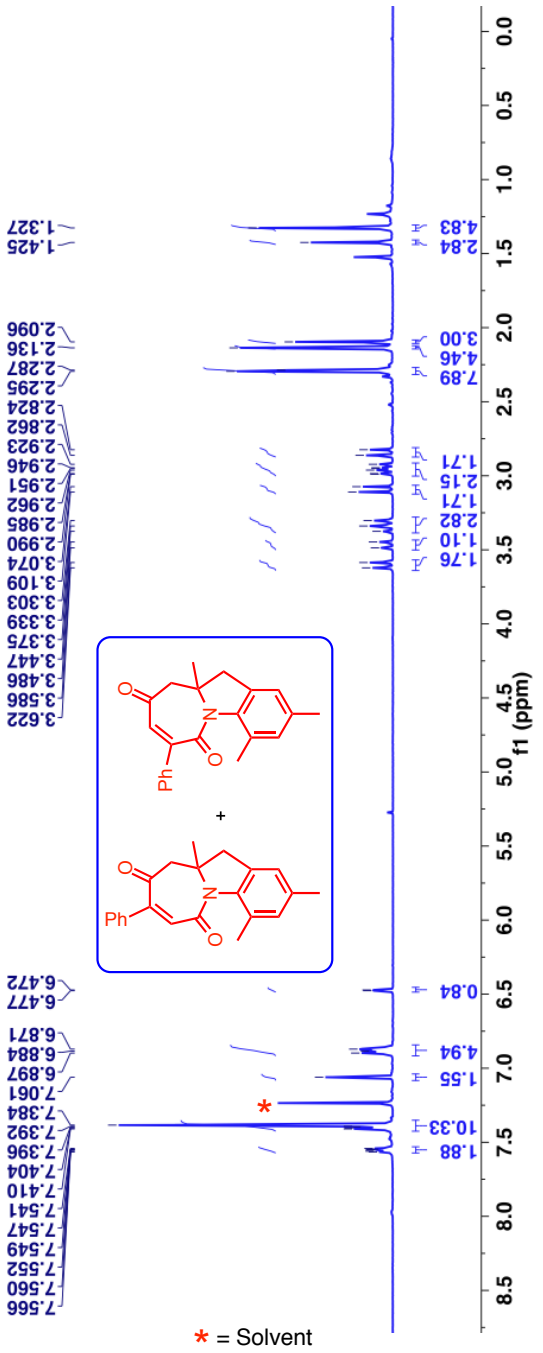

Figure 3.139: ^{1}H-NMR (400 MHz, $CDCl_3$, δ ppm) spectrum of allyl maleimide photoproduct **206e** and **207e**.

^{13}C-NMR (100 MHz, $CDCl_3$, δ ppm), (Major **206e** + minor **207e**, 74:26): 196.5, 195.4, 163.9, 161.7, 152.1, 142.5, 139.4, 138.6, 138.2, 137.8, 135.8, 135.8, 135.4, 132.6, 131.6, 131.4, 131.2, 129.8, 129.2, 129.1, 128.9, 128.96, 128.7, 128.5, 128.48, 128.3, 122.96, 122.90, 64.84, 64.80, 54.2, 53.9, 47.6, 46.9, 23.2, 22.7, 21.8, 21.2, 21.1, 21.0

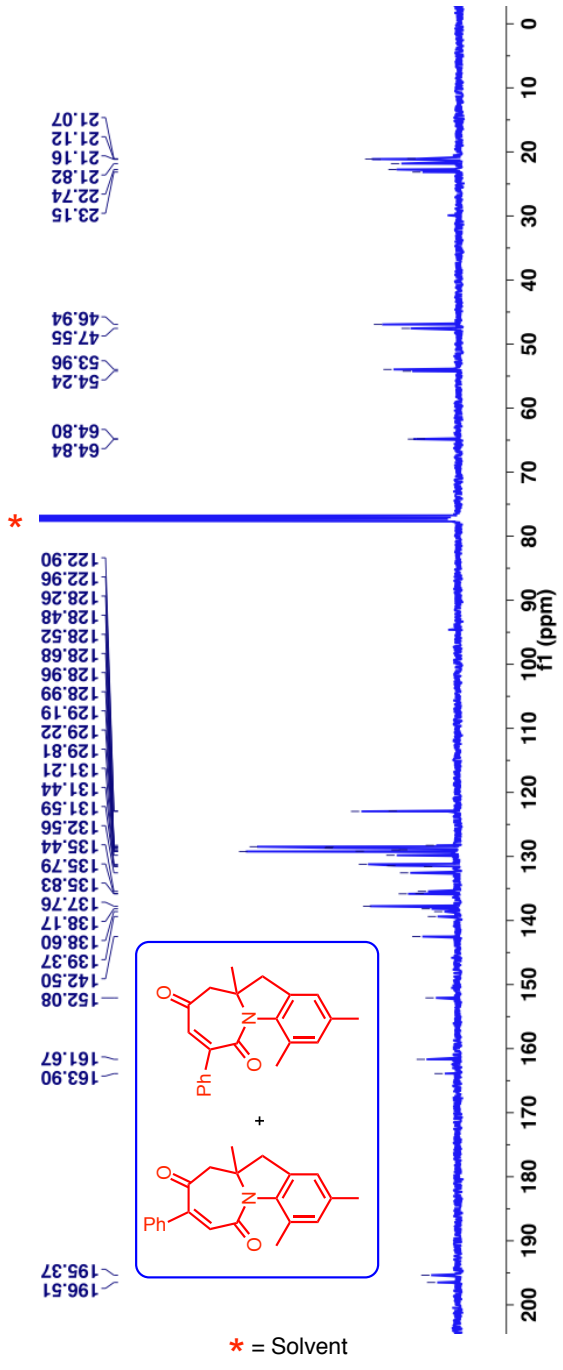

Figure 3.140: ^{13}C-NMR (400 MHz, $CDCl_3$, δ ppm) spectrum of allyl maleimide photoproduct **206e** and **207e**.

^{1}H-NMR (400 MHz, $CDCl_3$, δ ppm): 7.03-6.99 (m, 3H), 5.74 (s, 1H), 5.07-5.02 (m, 1H), 3.76 (s, 3H), 3.65-3.58 (m, 1H), 3.09-3.02 (m, 1H), 2.86-2.70 (m, 2H), and 2.22 (s, 3H).

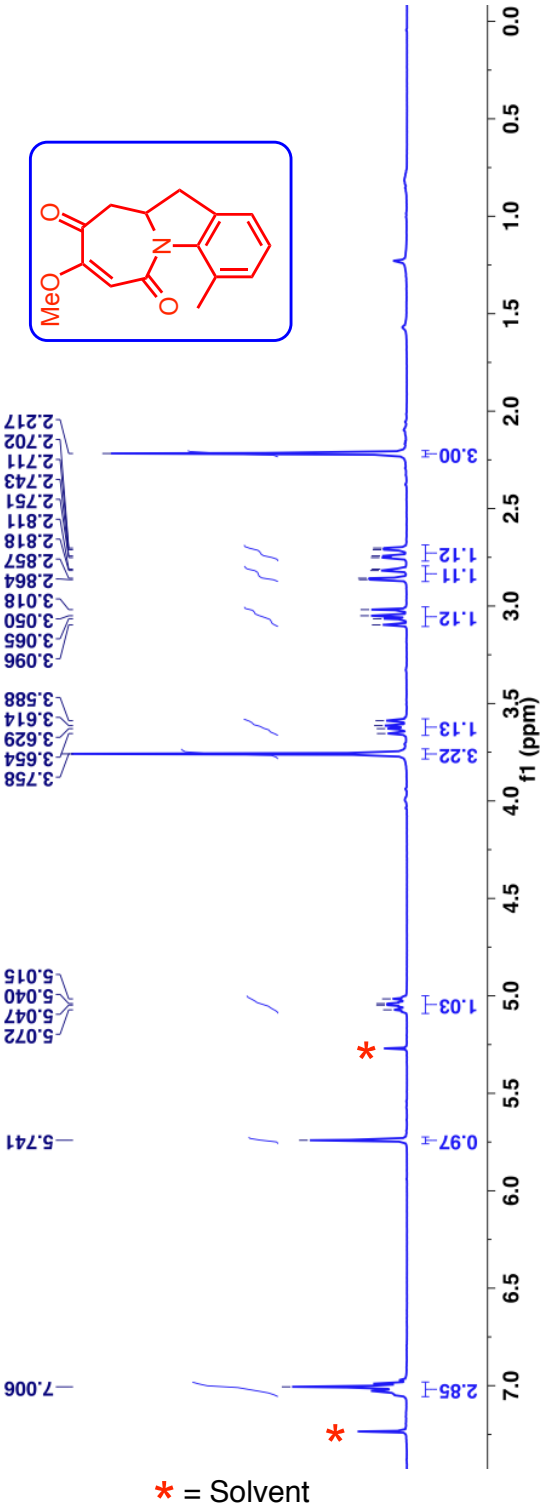

Figure 3.141: ^{1}H-NMR (400 MHz, $CDCl_3$, δ ppm) spectrum of allyl maleimide photoproduct **206f**.

^{13}C-NMR (100 MHz, $CDCl_3$, δ ppm): 194.8, 163.1, 158.9, 139.2, 131.2, 130.9, 131.3, 127.9, 125.2, 122.4, 106.3, 56.4, 56.38, 34.1 and 21.8.

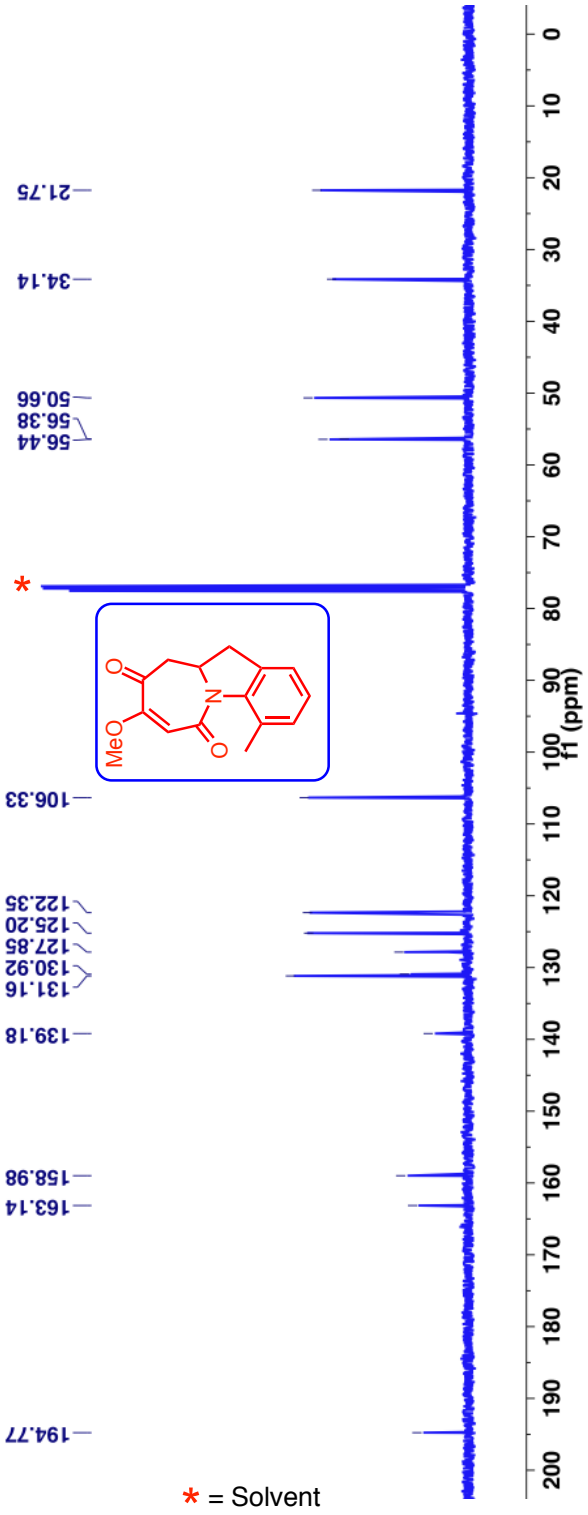

Figure 3.142: ^{13}C-NMR (400 MHz, $CDCl_3$, δ ppm) spectrum of allyl maleimide photoproduct **206f.**

^{1}H-NMR (400 MHz, $CDCl_3$, δ ppm): 7.13-7.09(m, 3H), 6.95 (s, 1H), 5.16-5.09 (m, 1H), 3.76-3.69 (m, 1H), 3.14-3.06 (m, 1H), 2.89-2.82 (m, 2H)) and 2.29 (s, 3H).

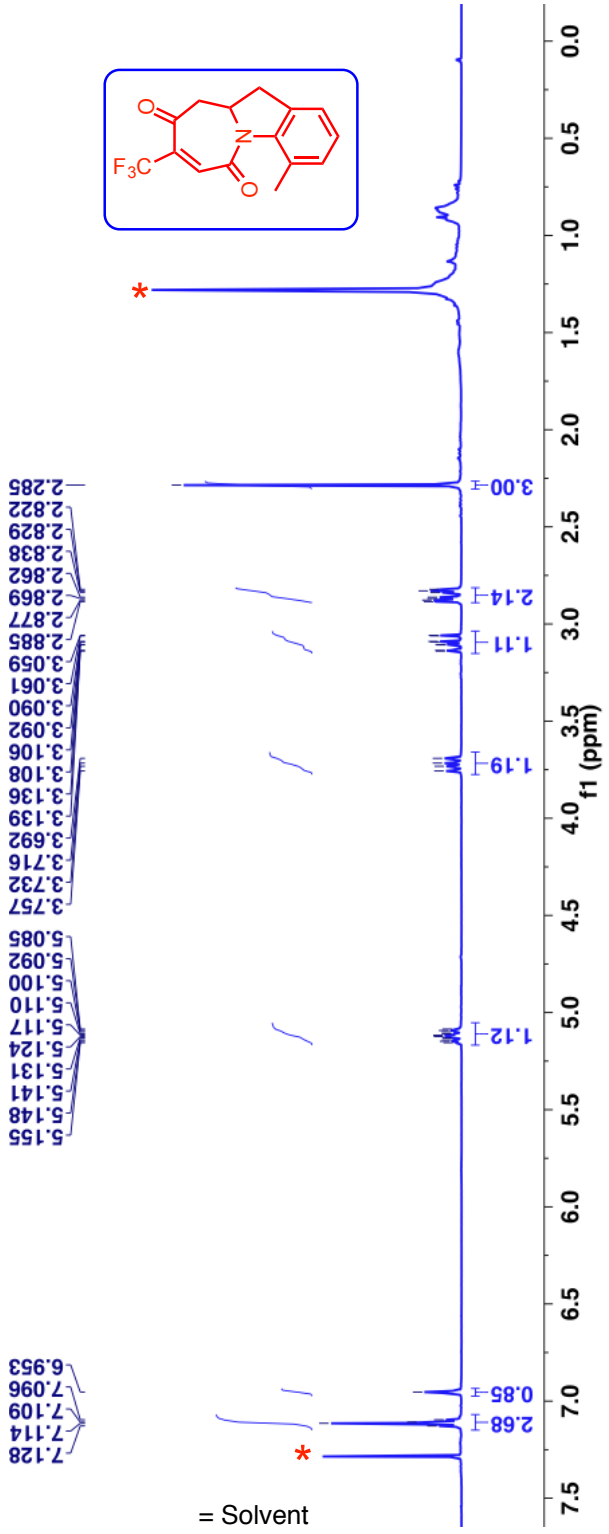

Figure 3.143: ^{1}H-NMR (400 MHz, $CDCl_3$, δ ppm) spectrum of allyl maleimide photoproduct **206g**.

^{13}C-NMR (100 MHz, $CDCl_3$, δ ppm): 197.7, 157.7, 137.9, 135.7, 135.6, 131.3, 131.1, 128.5, 126.1, 122.4, 56.9, 50.6, 33.6, 29.7 and 21.7.

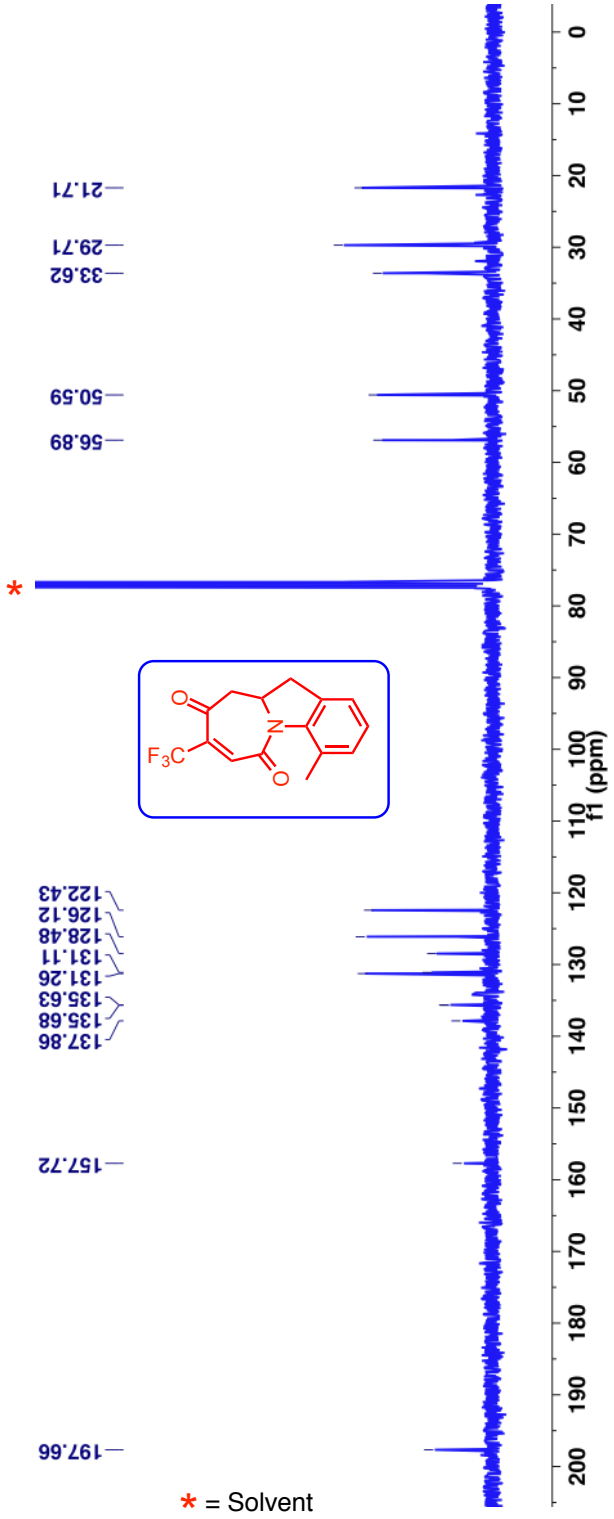

Figure 3.144: ^{13}C-NMR (400 MHz, $CDCl_3$, δ ppm) spectrum of allyl maleimide photoproduct **206g.**

^{1}H-NMR (400 MHz, $CDCl_3$, δ ppm): 7.12-7.09(m, 4H), 5.11-5.04 (m, 1H), 3.72-3.66 (m, 1H),3.22-3.15 (m, 1H), 2.99-2.85 (m, 2H) and 2.29 (s, 3H).

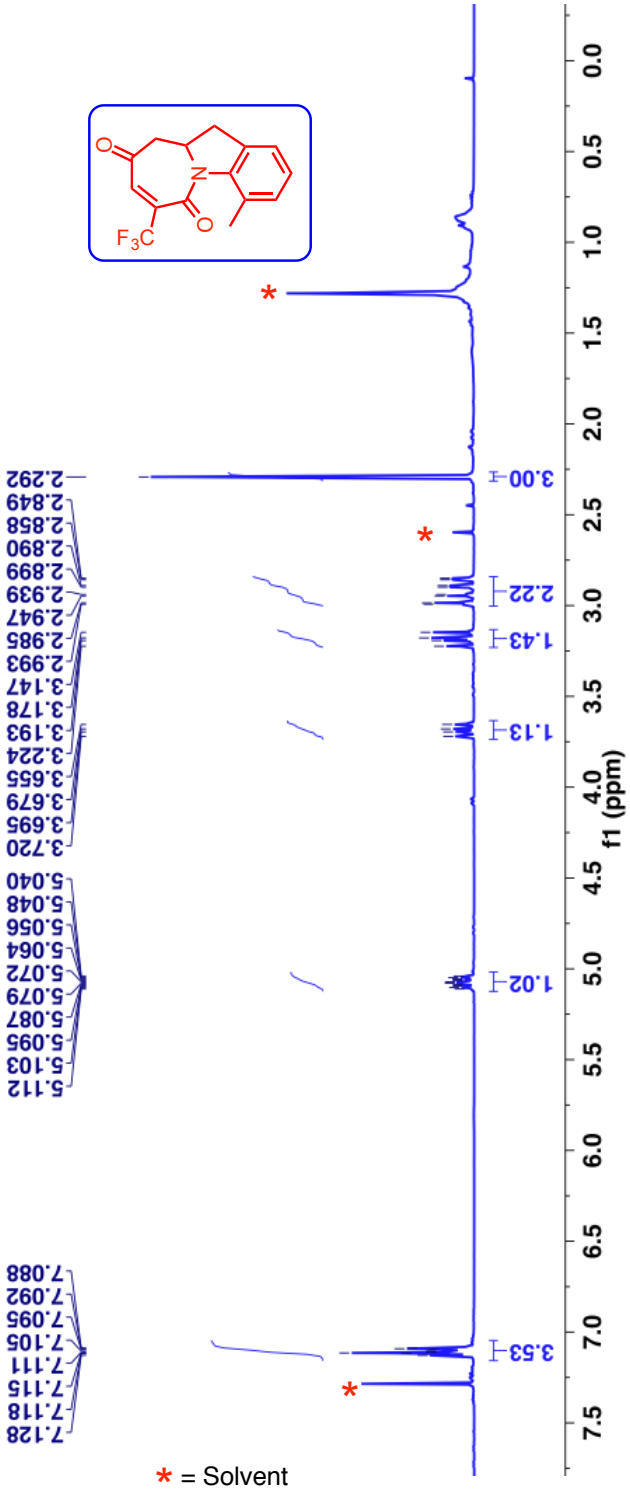

Figure 3.145: ^{1}H-NMR (400 MHz, $CDCl_3$, δ ppm) spectrum of allyl maleimide photoproduct **207g**.

^{13}C-NMR (100 MHz, $CDCl_3$, δ ppm): 193.7, 159.9, 138.1, 135.9, 131.3, 131.2, 128.3, 126.2, 122.4, 119.8, 56.5, 51.6, 33.9, 29.7 and 21.7.

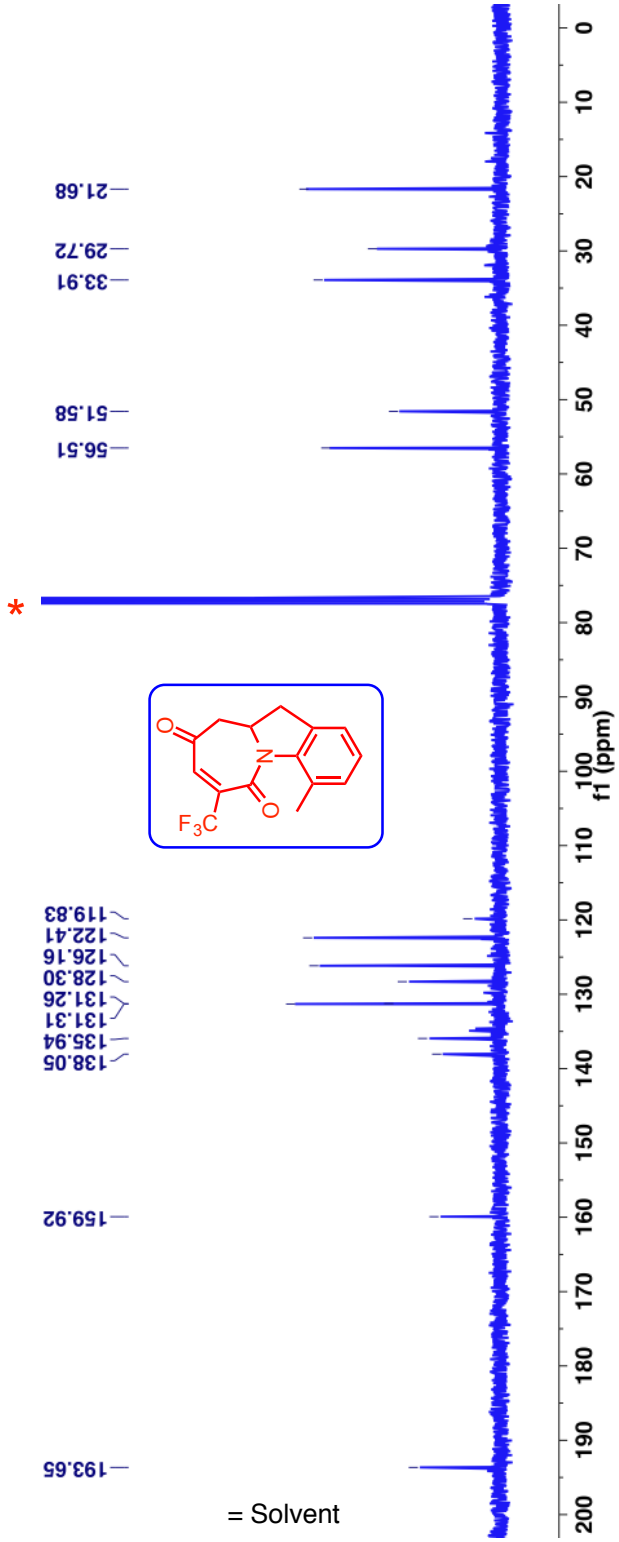

Figure 3.146: ^{13}C-NMR (400 MHz, $CDCl_3$, δ ppm) spectrum of allyl maleimide photoproduct **207g.**

^{1}H-NMR (400 MHz, $CDCl_3$, δ ppm): 7.05-7.02(m, 3H), 5.09-5.02 (m, 1H), 3.63-3.37 (m, 1H), 2.99-2.92 (m, 1H), 2.84-2.73 (m, 2H), 2.24 (s, 3H) and 2.21 (s, 3H).

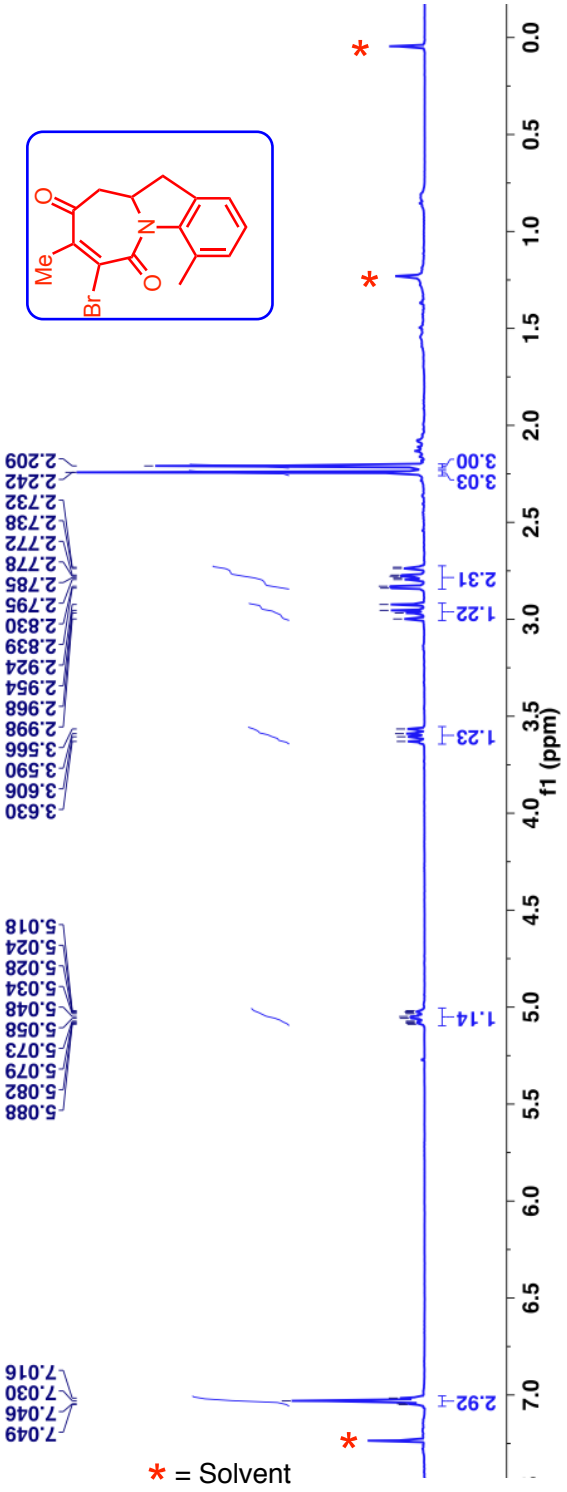

Figure 3.147: ^{1}H-NMR (400 MHz, $CDCl_3$, δ ppm) spectrum of allyl maleimide photoproduct **206h**.

^{13}C-NMR (100 MHz, $CDCl_3$, δ ppm): 199.7, 159.4, 145.9, 138.4, 131.4, 129.3, 128.4, 125.9, 122.6, 56.6, 50.9, 33.5, 22.9 and 21.8.

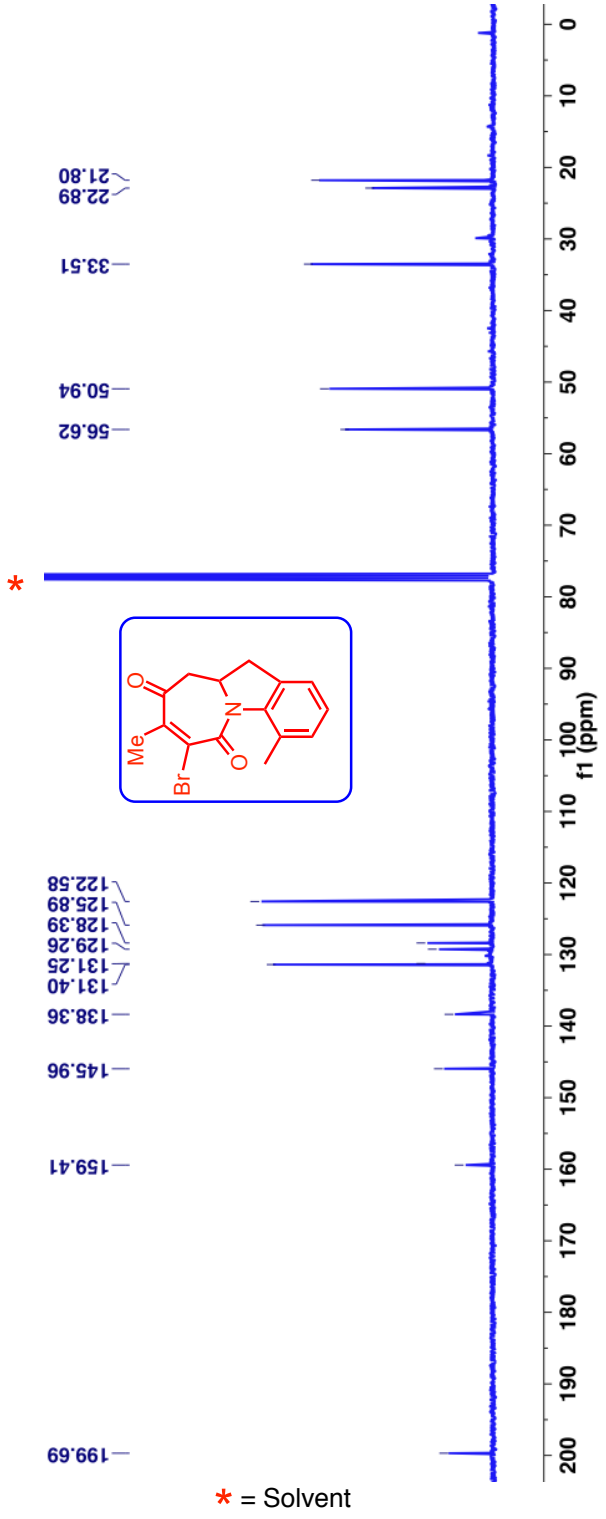

Figure 3.148: ^{13}C-NMR (400 MHz, $CDCl_3$, δ ppm) spectrum of allyl maleimide photoproduct **206h.**

^{1}H-NMR (400 MHz, $CDCl_3$, δ ppm): 7.05-7.02 (m, 3H), 5.04-4.97 (m, 1H), 3.62-3.56 (m, 1H), 3.07-2.99 (m, 1H), 2.89-2.84 (m,1H), 2.79-2.74 (m, 1H), 2.31 (s, 3H) and 2.19 (s, 3H).

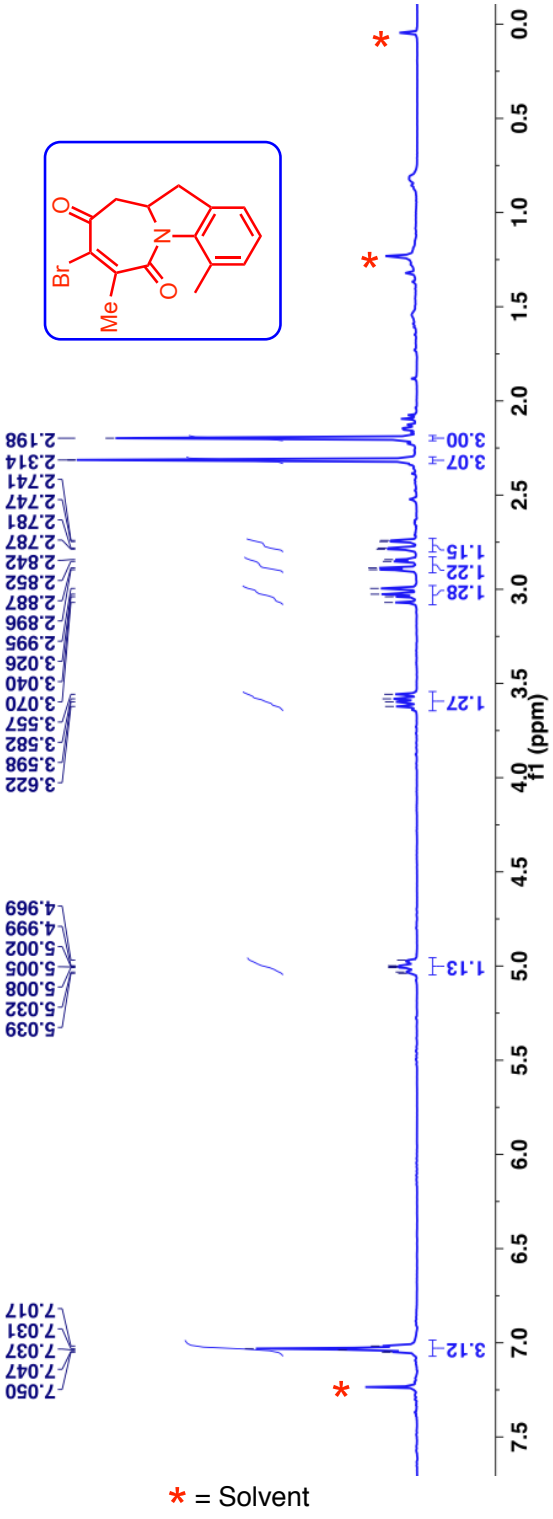

* = Solvent

Figure 3.149: ^{1}H-NMR (400 MHz, $CDCl_3$, δ ppm) spectrum of allyl maleimide photoproduct **207h**.

^{13}C-NMR (100 MHz, $CDCl_3$, δ ppm): 195.2, 161.9, 142.2, 138.3, 131.3, 131.32, 129.4, 128.3, 125.9, 122.6, 56.4, 50.5, 33.5, 21.8 and 21.5.

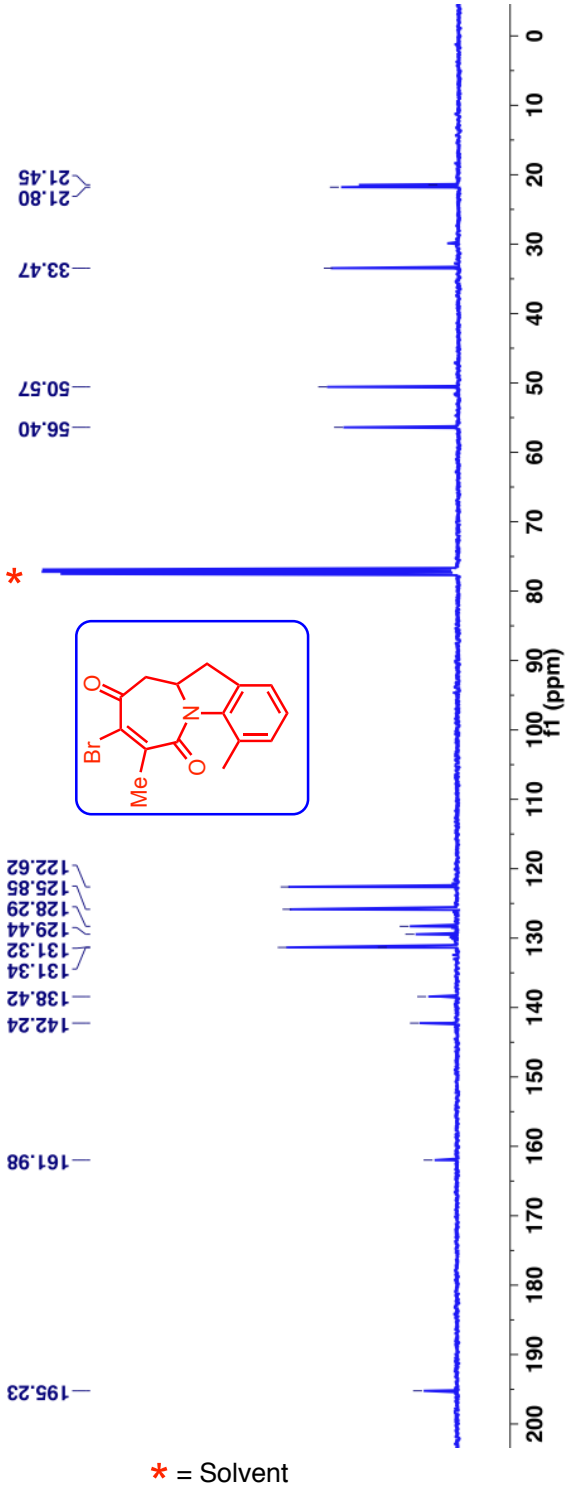

Figure 3.150: ^{13}C-NMR (400 MHz, $CDCl_3$, δ ppm) spectrum of allyl maleimide photoproduct **207h.**

3.34.2. Synthesis of minor methoxy maleimides photoproduct 207f

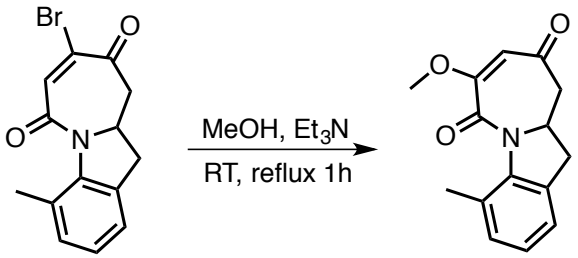

206c **207f**

Scheme 3.57: Synthesis of minor methoxy maleimides photoproduct **207f**.

To a solution of bromo maleimide derivative **206c** (10 mg, 1.0 *equiv.*) in MeOH (5 mL) triethylamine in MeOH (1.1 *equiv.*) was added and the resulting mixture refluxed for 1 h. After the reaction, the solvent was concentrated and the reaction mixture was quenched with DI water. The aqueous layer is extracted with DCM (20 mL). The combined organic layer was dried over *anhyd.* Na_2SO_4, filtered and concentrated under reduced pressure to yield crude product. The crude product was purified by combiflash using a hexanes:ethyl acetate mixture. Since the yield was very low (>0.5 mg was isolated) the product was characterized by mass spectrometry and HPLC.

TLC condition - R*f* = 0.20 (50% hexanes:50% ethyl acetate) for **207f**

HRMS-ESI (m/z) ([M + Na]$^+$): Calculated: 280.0950; Observed: 280.0913; |Δm|: 11 ppm.

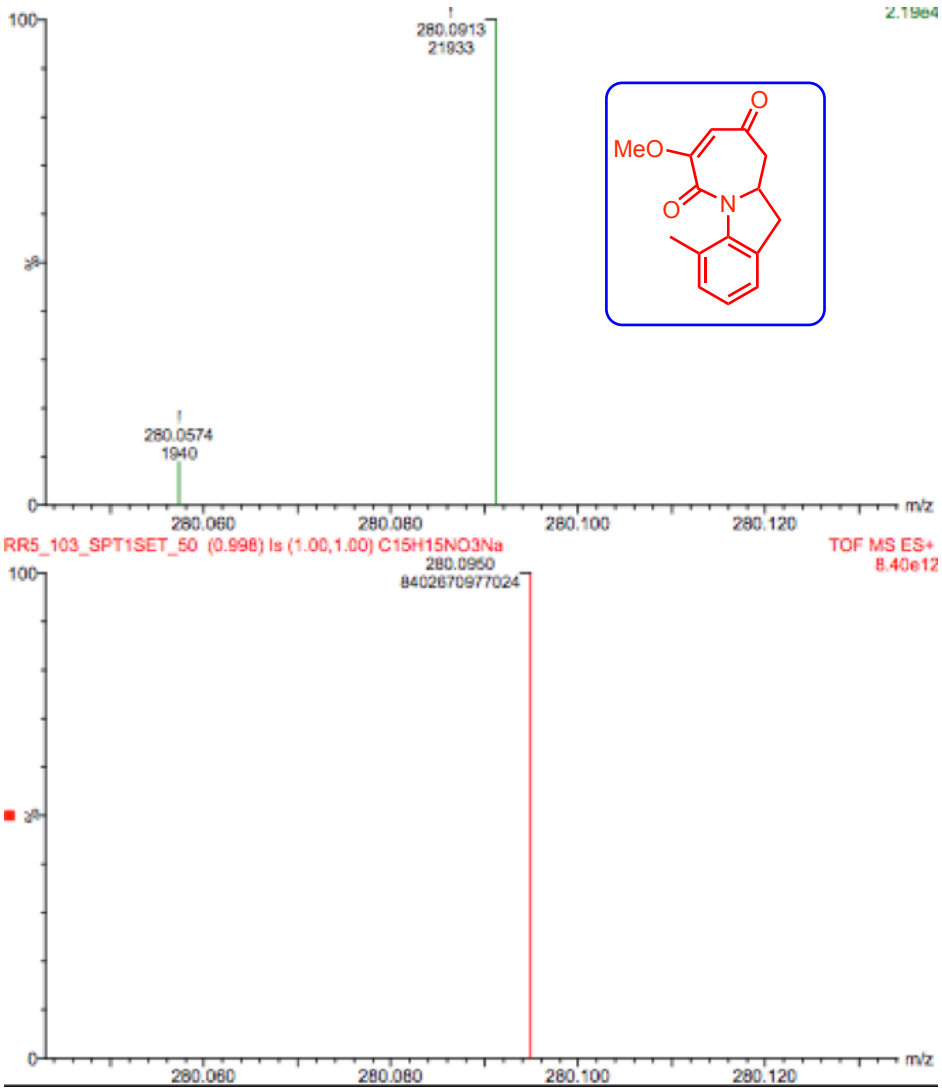

Figure 3.151: HRMS of minor methoxy photoproduct **207f**.

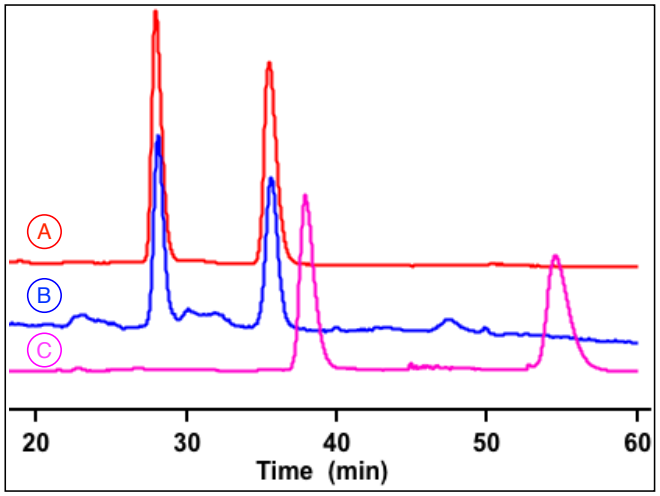

Figure 3.152: HPLC trace of A. Pure major methoxy maleimide photoproduct **206c**, B. Crude photoreaction of **205c** and C. HPLC trace of thermally synthesized **207f**.

3.35. References

(1) Penkett, C. S.; Woolford, J. A.; Day, I. J.; Coles, M. P. The Double [3 + 2] Photocycloaddition Reaction. *J. Am. Chem. Soc.* **2009**, *132*, 4-5.

(2) Cornelisse, J. The Meta Photocycloaddition of Arenes to Alkenes. *Chem. Rev.* **1993**, *93*, 615-669.

(3) Bach, T.; Hehn, J. P. Photochemical Reactions as Key Steps in Natural Product Synthesis. *Angew. Chem. Int. Ed.* **2011**, *50*, 1000-1045.

(4) V, R.: *Photochemistry in Organized and Constrained Media*; Wiley-VCH, New York, , 1991. pp. 429-403.

(5) Mori, R., Weiss. R. G., Inoue. Y. Mediation of Conformationally Controlled Photodecarboxylations of Chiral and Cyclic Aryl Esters by Substrate Structure, Temperature, Pressure, and Medium Constraints. *J. Am. Chem. Soc.* **2004**, *126*, 8961-8975.

(6) Gamlin, J. N.; Jones, R.; Leibovitch, M.; Patrick, B.; Scheffer, J. R.; Trotter, J. The Ionic Auxiliary Concept in Solid State Organic Photochemistry. *Acc. Chem. Res.* **1996**, *29*, 203-209.

(7) Sivaguru, J.; Natarajan, A.; Kaanumalle, L. S.; Shailaja, J.; Uppili, S.; Joy, A.; Ramamurthy, V. Asymmetric Photoreactions within Zeolites:□Role of Confinement and Alkali Metal Ions. *Acc. Chem. Res.* **2003**, *36*, 509-521.

(8) Yang, C., Mori. T., Origane. Y., Ko. Y. H., Selvapalam. N., Kim. K., Inoue. Y. Highly Stereoselective Photocyclodimerization of α-Cyclodextrin-Appended Anthracene Mediated by γ-Cyclodextrin and Cucurbit[8]uril: A Dramatic Steric Effect Operating Outside the Binding Site. *J. Am. Chem. Soc.* **2008**, *130*, 8574-8575.

(9) Ayitou, A. J.-L.; Sivaguru, J. Light-Induced Transfer of Molecular Chirality in Solution: Enantiospecific Photocyclization of Molecularly Chiral Acrylanilides. *J. Am. Chem. Soc.* **2009**, *131*, 5036-5037.

(10) Ayitou, A. J.-L.; Clay, A.; Kumarasamy, E.; Jockusch, S.; Sivaguru, J. Enantiospecific Photochemical 6π-Ring Closure of α-Substituted Atropisomeric Acrylanilides - Role of Alkali Metal Ions. *Photochem. Photobiol. Sci.* **2014**, *13*, 141-144.

(11) Ayitou, A. J.-L.; Sivaguru, J. Reactive Spin State Dependent Enantiospecific Photocyclization of Axially Chiral α-Substituted Acrylanilides. *Chem. Commun.* **2011**, *47*, 2568-2570.

(12) Kumarasamy, E.; Jesuraj, J. L.; Omlid, J. N.; Ugrinov, A.; Sivaguru, J. Light-Induced Enantiospecific 4π Ring Closure of Axially Chiral 2-Pyridones: Enthalpic and Entropic Effects Promoted by H-Bonding. *J. Am. Chem. Soc.* **2011**, *133*, 17106-17109.

(13) Ayitou, A. J. L.; Fukuhara, G.; Kumarasamy, E.; Inoue, Y.; Sivaguru, J. Enantiospecific Photochemical Transformations under Elevated Pressure. *Chem. Eur. J.* **2013**, *19*, 4327-4334.

(14) Kumarasamy, E.; Sivaguru, J. Light-induced stereospecific intramolecular [2+2]-cycloaddition of atropisomeric 3,4-dihydro-2-pyridones. *Chem. Commun.* **2013**, *49*, 4346-4348.

(15) Ayitou, A. J.-L.; Jesuraj, J. L.; Barooah, N.; Ugrinov, A.; Sivaguru, J. Enantiospecific Photochemical Norrish/Yang Type II Reaction of Nonbiaryl Atropchiral α-Oxoamides in Solution: Axial to Point Chirality Transfer. *J. Am. Chem. Soc.* **2009**, *131*, 11314-11315.

(16) Jesuraj, J. L.; Sivaguru, J. Photochemical Type II Reaction of Atropchiral Benzoylformamides to Point Chiral Oxazolidin-4-ones. Axial Chiral Memory Leading to Enantiomeric Resolution of Photoproducts. *Chem. Commun.* **2010**, *46*, 4791-4793.

(17) Burkhard, J. A.; Wuitschik, G.; Rogers-Evans, M.; Müller, K.; Carreira, E. M. Oxetanes as Versatile Elements in Drug Discovery and Synthesis. *Angew. Chem. Int. Ed.* **2010**, *49*, 9052-9067.

(18) Paternò, E. C., G. *Gazz. Chim. Ital.* **1909**, *39*.

(19) Büchi, G.; Inman, C. G.; Lipinsky, E. S. Light-catalyzed Organic Reactions. I. The Reaction of Carbonyl Compounds with 2-Methyl-2-butene in the Presence of Ultraviolet Light. *J. Am. Chem. Soc.* **1954**, *76*, 4327-4331.

(20) Bach, T. Stereoselective Intermolecular [2 + 2]-Photocycloaddition Reactions and Their Application in Synthesis. *Synthesis* **1998**, *5*, 683-703.

(21) Abe, M. Recent Progress Regarding Regio-, Site-, and Stereoselective Formation of Oxetanes in Paternò-Büchi Reactions. *J. Chin. Chem. Soc.* **2008**, *55*, 479-486.

(22) Caldwell, R. A.; Sovocool, G. W.; Gajewski, R. P. Primary Interaction Between Diaryl Ketone Triplets and Simple Alkenes. Isotope Effects. *J. Am. Chem. Soc.* **1973**, *95*, 2549-2557.

(23) Arnold, D. R.; Hinman, R. L.; Glick, A. H. Chemical Properties of the Carbonyl n,π State. The Photochemical Preparation of Oxetanes. *Tetrahedron Lett.* **1964**, *5*, 1425-1430.

(24) Schroeter, S. H.; Orlando, C. M. Photocycloaddition of Various Ketones and Aldehydes to Vinyl Ethers and Ketene Diethyl Acetal. *J. Org. Chem.* **1969**, *34*, 1181-1187.

(25) Griesbeck, A. G.; Stadtmueller, S. Photocycloaddition of Benzaldehyde to Cyclic Olefins: Electronic Control of Endo Stereoselectivity. *J. Am. Chem. Soc.* **1990**, *112*, 1281-1283.

(26) Griesbeck, A. G.; Mauder, H.; Stadtmueller, S. Intersystem Crossing in Triplet 1,4-Biradicals: Conformational Memory Effects on the Stereoselectivity of Photocycloaddition Reactions. *Acc. Chem. Res.* **1994**, *27*, 70-75.

(27) Bach, T.; Schröder, J. Photocycloaddition of N-Acyl Enamines to Aldehydes and Its Application to the Synthesis of Diastereomerically Pure 1,2-Amino Alcohols. *J. Org. Chem.* **1999**, *64*, 1265-1273.

(28) Bach, T. N-Acyl Enamines in the Paternò–Büchi Reaction: Stereoselective Preparation of 1,2-Amino Alcohols by C-C Bond Formation. *Angew. Chem. Int. Ed.* **1996**, *35*, 884-886.

(29) Gotthardt, H.; Lenz, W. Unusally High Asymmetric Induction in the Photochemical Formation of Oxetanes. *Angew. Chem. Int. Ed.* **1979**, *18*, 868-868.

(30) Nehrings, A.; Scharf, H.-D.; Runsink, J. Photochemical Synthesis of an L-Erythrose Building Block and Its use in the Preparation of Methyl 2,3,O-Isopropylidene-β-L-apio-L-furanoside. *Angew. Chem. Int. Ed.* **1985**, *24*, 877-878.

(31) Buschmann, H.; Scharf, H.-D.; Hoffmann, N.; Esser, P. The Isoinversion Principle—a General Model of Chemical Selectivity. *Angew. Chem. Int. Ed.* **1991**, *30*, 477-515.

(32) Bach, T.; Jödicke, K.; Wibbeling, B. Reversal of the Facial Diastereoselectivity in the Paternò-Büchi Reaction of Silyl Enol Ethers Carrying a Chiral Substituent in α-Position. *Tetrahedron* **1996**, *52*, 10861-10878.

(33) Bach, T.; Jödicke, K.; Kather, K.; Fröhlich, R. 1,3-Allylic Strain as a Control Element in the Paternò−Büchi Reaction of Chiral Silyl Enol Ethers:Synthesis of Diastereomerically Pure Oxetanes Containing Four Contiguous Stereogenic Centers. *J. Am. Chem. Soc.* **1997**, *119*, 2437-2445.

(34) Bach, T.; Jödicke, K.; Kather, K.; Hecht, J. Facial Diastereoselectivity in the Paternò–Büchi Reaction of Chiral Silyl Enol Ethers. *Angew. Chem. Int. Ed.* **1995**, *34*, 2271-2273.

(35) Hoffmann, R. W. Allylic 1,3-Strain as a Controlling Factor in Stereoselective Transformations. *Chem. Rev.* **1989**, *89*, 1841-1860.

(36) Sakamoto, M.; Takahashi, M.; Fujita, T.; Watanabe, S.; Nishio, T.; Iida, I.; Aoyama, H. Solid State Photochemical Reaction of N-(α,β-Unsaturated carbonyl)benzoylformamides. *J. Org. Chem.* **1997**, *62*, 6298-6308.

(37) Sakamoto, M.; Aoyama, H.; Omote, Y. Photochemical Reactions of N-Benzoylformyl α,β-Unsaturated Amides. *J. Chem. Soc., Perkin Trans. 1* **1986**, *0*, 1759-1762.

(38) Christian, W. *Dynamic Stereochemistry of Chiral Compounds. Principles and Applications*, *RSC publishing: Cambridge, UK., 2008*.

(39) Tedaldi, L. M.; Aliev, A. E.; Baker, J. R. [2 + 2] Photocycloadditions of Thiomaleimides. *Chem. Commun.* **2012**, *48*, 4725-4727.

(40) Obata, T.; Shimo, T.; Suishu, T.; Somekawa, K. Stereoselective Photo[4+2]-cycloadditions of 2-Pyrone-5-carboxylates with Maleimides in the Solid State and in Solution. *J. Heterocycl. Chem.* **1998**, *35*, 1361-1364.

(41) Cubbage, K. L.; Orr-Ewing, A. J.; Booker-Milburn, K. I. First Higher-Order Photocycloaddition to a C-N Bond: 1,3-Diazepines from Maleimides. *Angew. Chem. Int. Ed.* **2009**, *48*, 2514-2517.

(42) Booker-Milburn, K. I.; Anson, C. E.; Clissold, C.; Costin, N. J.; Dainty, R. F.; Murray, M.; Patel, D.; Sharpe, A. Intramolecular Photocycloaddition of N-Alkenyl Substituted Maleimides: A Potential Tool for the Rapid Construction of Perhydroazaazulene Alkaloids. *Eur. J. Org. Chem.* **2001**, 1473-1482.

(43) Gülten, Ş.; Sharpe, A.; Baker, J. R.; Booker-Milburn, K. I. Use of Temporary Tethers in the Intramolecular [2+2] Photocycloaddition Reactions of Tetrahydrophthalimide Derivatives: A New Approach to Complex Tricyclic Lactones. *Tetrahedron* **2007**, *63*, 3659-3671.

(44) Miller, C. W.; Jönsson, E. S.; Hoyle, C. E.; Viswanathan, K.; Valente, E. J. Evaluation of N-Aromatic Maleimides as Free Radical Photoinitiators:A Photophysical and Photopolymerization Characterization. *J. Phys. Chem. B* **2001**, *105*, 2707-2717.

(45) Roscini, C.; Cubbage, K. L.; Berry, M.; Orr-Ewing, A. J.; Booker-Milburn, K. I. Reaction Control in Synthetic Organic Photochemistry: Switching between [5+2] and [2+2] Modes of Cycloaddition. *Angew. Chem. Int. Ed.* **2009**, *48*, 8716-8720.

(46) Kumarasamy, E. Stereospecific Phototransformations of Atropisomeric Chromophores. North Dakota State University, ND, October 2014.

(47) Kumarasamy, E.; Raghunathan, R.; Jockusch, S.; Ugrinov, A.; Sivaguru, J. Tailoring Atropisomeric Maleimides for Stereospecific [2 + 2] Photocycloaddition—Photochemical and Photophysical Investigations Leading to Visible-Light Photocatalysis. *J. Am. Chem. Soc.* **2014**, *136*, 8729-8737.

(48) Mazzocchi, P. H.; Bowen, M. J.; Narain, N. K. Photochemical Addition of Dienes to N-Alkylphthalimides. *J. Am. Chem. Soc.* **1977**, *99*, 7063-7064.

(49) Mazzocchi, P. H.; Wilson, P.; Khachik, F.; Klingler, L.; Minamikawa, S. Photochemical Additions of Alkenes to Phthalimides. Mechanistic Investigations on the Stereochemistry of Alkene Additions and the Effect of Aryl Substituents on the Regiochemistry of Alkene Additions. *J. Org. Chem.* **1983**, *48*, 2981-2989.

(50) Mazzocchi, P. H.; Minamikawa, S.; Wilson, P.; Bowen, M.; Narian, N. Photochemical Additions of Alkenes to Phthalimides to form Benzazepinediones. Additions of Dienes, Alkenes, Vinyl Ethers, Vinyl Esters, and an Allene. *J. Org. Chem.* **1981**, *46*, 4846-4851.

(51) Mazzocchi, P. H.; Minamikawa, S.; Wilson, P. Photochemical Addition of Alkenes to N-Methylphthalimide. Stereochemistry of the Addition. *J. Org. Chem.* **1979**, *44*, 1186-1188.

(52) Booker-Milburn, K. I.; Costin, N. J.; Dainty, R. F.; Patel, D.; Sharpe, A. Photocycloaddition of N-4-Alkenyl Substituted Unsaturated Imides. *Tetrahedron Lett.* **1998**, *39*, 7423-7426.

(53) Davies, D. M. E.; Murray, C.; Berry, M.; Orr-Ewing, A. J.; Booker-Milburn, K. I. Reaction Optimization and Mechanism in Maleimide [5 + 2] Photocycloaddition:□A Dual Approach Using Tunable UV Lasers and Time-Dependent DFT. *J. Org. Chem.* **2007**, *72*, 1449-1457.

(54) Booker-Milburn, K. I.; Dudin, L. F.; Anson, C. E.; Guile, S. D. Formal Intramolecular [5 + 2] Photocycloaddition Reactions of Maleimides:□A Novel Approach to the CDE Ring Skeleton of (−)-Cephalotaxine. *Org. Lett.* **2001**, *3*, 3005-3008.

(55) T.Matsuo. *Bull. Chem. Soc. Jpn.* **1965**, *38*, 557-562.

(56) Kuang, Y.-Y.; Chen, F.-E. A Convenient and Efficient Asymmetric Synthesis of (s)-α-Arylthiomethyl-α-Hydroxybutyric Acid Esters. *Org. Prep. Proced. Int.* **2005**, *37*, 184-188.

(57) Siqueira, F. A.; Taylor, J. G.; Correia, C. R. D. The FIrst Intramolecular Heck–Matsuda Reaction and its Application in the Syntheses of Benzofurans and Indoles. *Tetrahedron Lett.* **2010**, *51*, 2102-2105.

(58) Görl, C.; Alt, H. G. Iron Complexes with ω-Alkenyl Substituted Bis(arylimino)pyridine Ligands as Catalyst Precursors for the Oligomerization and Polymerization of Ethylene. *J. Mol. Catal. A: Chem.* **2007**, *273*, 118-132.

(59) Choi, D.-S.; Huang, S.; Huang, M.; Barnard, T. S.; Adams, R. D.; Seminario, J. M.; Tour, J. M. Revised Structures of N-Substituted Dibrominated Pyrrole Derivatives and Their Polymeric Products. Termaleimide Models with Low Optical Band Gaps. *J. Org. Chem.* **1998**, *63*, 2646-2655.

(60) Kajigaeshi, S.; Kakinami, T.; Yamasaki, H.; Fujisaki, S.; Okamoto, T. Halogenation Using Quarternary Ammonium Polyhalides. *Bull. Chem. Soc. Jpn.* **1988**, *61*, 600.

(61) Tidwell, J. H.; Buchwald, S. L. Synthesis of Polysubstituted Indoles and Indolines by Means of Zirconocene-Stabilized Benzyne Complexes. *J. Am. Chem. Soc.* **1994**, *116*, 11797-11810.

(62) Yip, K.-T.; Yang, M.; Law, K.-L.; Zhu, N.-Y.; Yang, D. Pd(II)-Catalyzed Enantioselective Oxidative Tandem Cyclization Reactions. Synthesis of Indolines through C−N and C−C Bond Formation. *J. Am. Chem. Soc.* **2006**, *128*, 3130-3131.

CHAPTER 4. PHOTODEGRADATION OF POLYMERIC/OLIGOMERIC MATERIALS DERIVED FROM BIORENEWABLE RESOURCES*

4.1. Introduction

Macromolecular materials derived from renewable resources played a critical role in human civilization before 19th century. We relied on natural polymeric materials such as wood, plant fibers, cotton, silk etc., for utensils, weapons, shelter and clothes for various day-to day activities. However the importance of renewable resource based macromolecules suffered a major setback after the development of non-renewable, coal-based industry and with petrochemical revolution in the 20th century. Within few decades the materials synthesized from non-renewable fossil fuels swamped the world. The decline in the use of renewable resource based products is not only attributed to the development of coal and petroleum based industries, but also to the numerous varieties of synthetic polymeric material synthesized from petroleum based feedstock. For example, last century saw a steep rise in the production of plastics, elastomers, paints, adhesives, resin fibers etc., with superior properties and structures at a low cost compared to the materials derived from renewable resources. This exponential growth on polymers/materials derived from fossil completely filed our daily life such that we are totally dependent on non-renewable polymers.[1,2]

4.2. Decline in fossil fuels and rise of renewable resources

Since the turn of the millennium, the scenario on the dependency of the fossil slowly started to take a turn. Many research efforts were made for developing materials derived from renewable resources. The advance in research not only focused on synthesizing polymers with different properties but also focused on competitive price to polymers derived from renewable resources.

---

*The material in this chapter was co-authored by Saravanakumar Rajendran (SR) Ramya Raghunathan (RR), Ivan Hevus (IH), Retheesh Krishnan (RK), Dr. Angel Ugrinov (AU), Dr. Mukund. P. Sibi (MPS), Dr. Dean C. Webster (DCW) and Dr. J. Sivaguru (JS). SR, RR, RK in consultation with MPS, DCW and JS synthesized all the compounds and carried out all the experiments. AU recorded PXRD data reported in this chapter. IH performed polymer characterization reported in this chapter.

These strenuous efforts rekindled the hope for replacement of fossil fuel by renewable resources. This paradigm shift towards the use of renewable resources is due to the increased awareness on the impact of non-renewable based polymers on the environment. For e.g. between 2010-2015, the worldwide production of plastics will exceed 300 million tons and at least 40% of it are made for short-term usage that will be quickly disposed to environment as landfills.[3] These landfills not only take thousands of years to degrade, but also greatly harm the animal life on land and marine life at sea as they tend to consume the residue of the plastics and perish. Another driving force for the research in renewable polymers is the steep rise in the price of oil and dwindling fossil reserves. About 86 % of the energy and 96% of the organic chemicals are obtained from fossil fuels. With world population increasing from 7.3 billion to about 11.2 billion at the end of the century, and with improved standard of living, the consumption of the fossil fuels will be only be accelerated leading to rapid depletion of fossil fuels that might last only for about 2 more decades.[4-6] Another perilous effects associated with the use of fossil fuel is the emission of CO_2 and other green house gases. With the consumption of more fuels, consumers and the government are alarmed at the rising level of CO_2 emission leading to undesirable global warming and its irreversible destruction to the earth. With these concerns in mind, it becomes imperative to develop polymeric materials from biomass-based resources. Biomass can be defined as materials derived from plants or plants based resources, more specifically defined as lignocellulosic biomass. The major components of lignocellulosic biomass in a plant are polysaccharides, e.g. cellulose, starch, chitin, chitosan, hemicellulose and lignin. Other renewable resources from which monomer for the biobased polymeric materials can be obtained are vegetable oils, terpenoids, polycarboxylic acid, alcohols/polyols, sugars (mono- and disaccharides commonly called as carbohydrates).[2,7,8]

Cellulose:[2,7] Cellulose is undoubtedly the most abundant biopolymer on earth. It is a linear homo polysaccharide comprising of β-D-glucopyranose units linked by glycosidic β (1-4) bonds in a $^4C_1$ conformation **233** (Figure 4.1). The properties of cellulose including its hydrophilic nature, biodegradability are attributed to its unique structure such as the presence of OH group. They display regular intra-inter molecular –O–H•••H–O– hydrogen bonds. Cellulose naturally has fibers like shape, which provides mechanical strength to wood and plants. The pulp industries mainly focus on the chemical extraction of

cellulose fibers and use them in various applications including the production of rayon fibers and films (cellophane) industry.

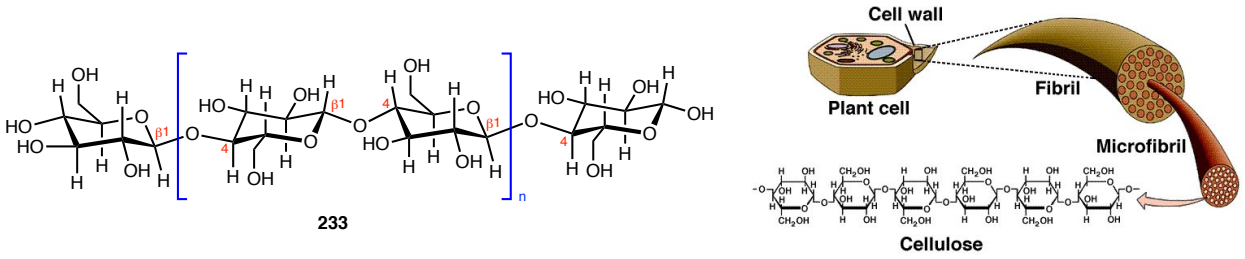

Figure 4.1: Structure of cellulose **233** and the morphology of plant cellulose fibers (right).[9]

Starch:[7,10] It is a polysaccharide similar to cellulose except that it is more granular in nature and plays a role of energy reservoir. Starch is composed of two macromolecules – poly(α-1,4-D-glucopyranose) **234** which is an amylose and α-1,6-branched amylopectin **235** at different proportions depending on the species (Figure 4.2). The structural properties make it easily biodegradable and digestible by humans. Starch based materials plays vital role in thermoplastic starch (TPS) and composites. TPS are generally prepared by subjecting starch granules to a process called gelatinization. The TPS can be molded and used in various applications especially in packaging industries. Many chemical modifications of starch granules are gaining more attention with the aim to develop material composites other than TPS. Most notable research efforts include the synthesis of green adhesives for aluminum by starch-controlled thermolysis.

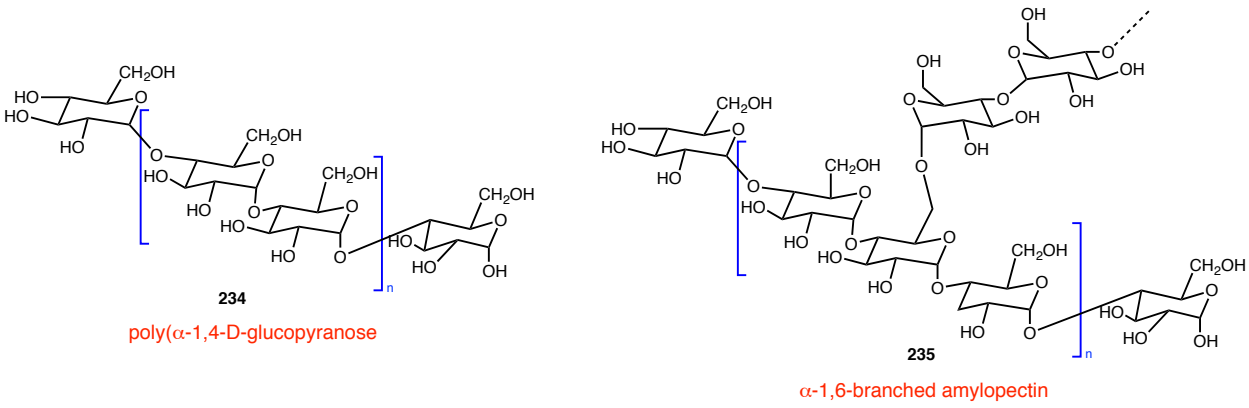

Figure 4.2 : Structure of poly(α-1,4-D-glucopyranose) **234** and α-1,6-branched amylopectin **235**.

Chitin and chitosan:[7,11] These are high molecular weight linear polymers. Chitin is composed of N-acetyl-2-amido-deoxy-D-glucose units **236**, where as chitosan is 2-amido-2-deoxy-D-glucose **237**

obtained from partial deacetylation of chitin (Figure 4.3). Chitosan is widely used in materials due to its ease of processability and chemical modification by simple procedures, which find wide application in the field of biotechnology, pharmaceutics, wastewater treatment, cosmetics and food science.[12] The interest in the chitosan research is gaining momentum after a recent demonstration of water-soluble chitosan derivative used as a coating for paper that improved the quality of the print.[13,14]

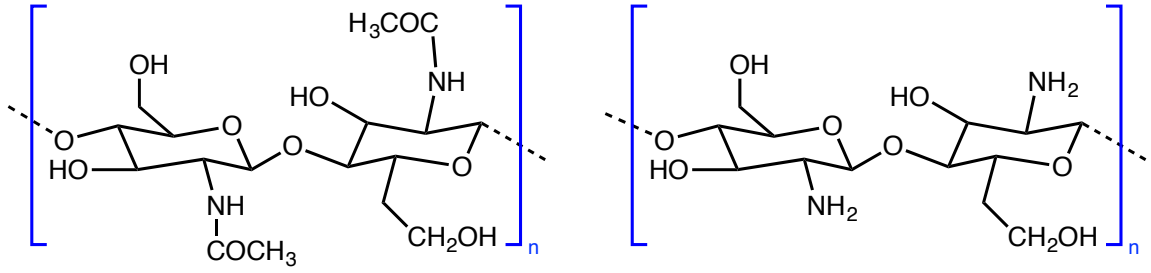

236 Chitin **237** Chitosan

Figure 4.3 : Structure of Chitin **236** and Chitosan **237**.

Hemicellulose:[15] They are polysaccharides with different anhydroglucose unit (AGU) as shown in the Figure 4.4. Due to this structural attribute, hemicelluloses are amorphous in nature and give a gel like texture around cellulose fiber in plants. The primary applications of hemicellulose include, food additives, emulsifications, films and hydrogels. Hemicelluloses are used to prepare films and coatings, which are quite useful in food packaging applications.

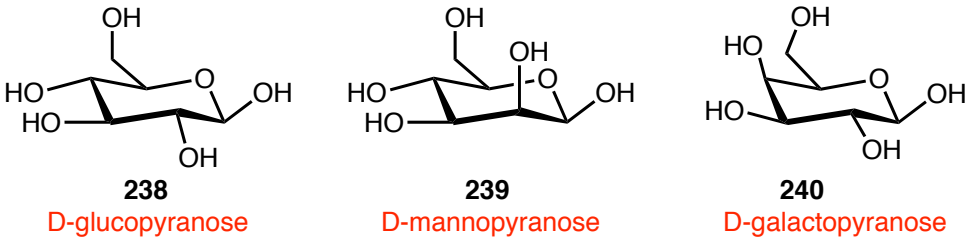

Figure 4.4: Important constituents of hemicelluloses.

Lignin:[7,16] These belong to a family of vegetable biopolymer that has complex macromolecular structures constituting both aromatic and aliphatic moieties (Figure 4.5). In other words, they are complex cross-linked phenolic polymers. These lignins are important for the formation of cell walls most importantly in wood and bark as they provide rigidity to the system. The three basic constituent of lignin are coumaryl alcohol, coniferyl alcohol and sinapyl alcohol (Figure 4.5).

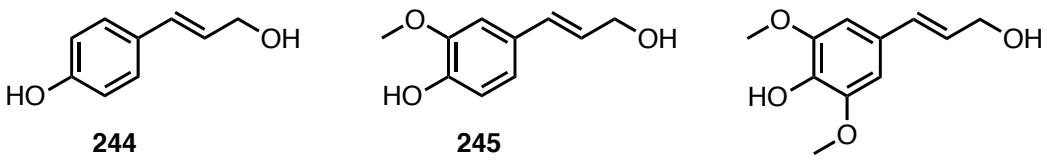

244
Coumaryl alcohol

245
Coumaryl alcohol

246
Sinapyl alcohol

Figure 4.5: The basic constituent of lignins.

These three units are present in various proportions in a plant cell wall. Even though the proportions of lignins are different, polymer chemist showed great interest in exploring these polymers and utilized them for the synthesis of polyester, polyurethanes, polyethers etc., by taking advantage of the functional handle such as phenolic hydroxyl and aliphatic moieties present in them. Several research initiatives on the extraction of fundamental units and their application in the macromolecular materials have been explored. One such interesting study is the conversion of Kraft lignin to vanillin **247**, which is a useful biomass based monomer. It has been used as a precursor in the synthesis of novel aromatic polymers mimicking polyethylene terephthalate (PET) via acetyldihydroferulic acid **250** (Scheme 4.1).[17]

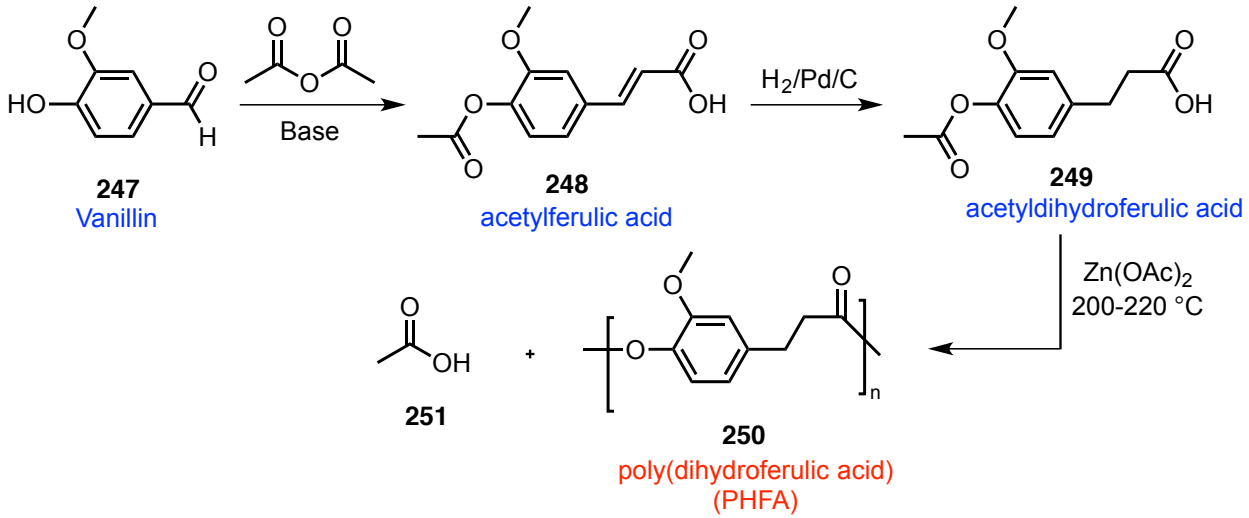

247
Vanillin

248
acetylferulic acid

249
acetyldihydroferulic acid

251

250
poly(dihydroferulic acid)
(PHFA)

Scheme 4.1: Synthesis of poly (dihydroferulic acid) (PHFA) **250** from vanillin **247**.

Other promising monomers derived from renewable resources like vegetable oils (fatty acids derived from vegetable oil like myristic acid, steric acid, oleic acid, etc.,), terpenoids (pinene, limonene, etc.,), polycarboxylic acid (tartaric acid, succinic acid, etc.,), alcohols/polyols (glycerols), sugars (D-glucoisosorbide) are widely used in the synthesis of polyesters, polyurethanes etc., as food additives, lubricants and in the field of cosmetics. Furan-2-carboxaldehyde (furfural) and 5-hydroxymethylfurfural (HMF) are chemically modified product of monosaccharaides (5- and 6-carbon sugars i.e. pentoses and hexoses respectively) and the most important biomass based compounds in the furan family.[1] Among these two, HMF is well explored and attractive to many chemists due to the presence of functional handle on either side of the ring. Dull and Kiermayer reported the first synthesis of HMF independently in the year 1895 and termed the compound as "oxymethylfurfurol".[18,19] Despite its presence from 19th century, its potential as a renewable resource was only identified recently. Since then, there has been a continuous interest and growth in the field of HMF which is evident from the number publications and patens appeared in the literature as shown in Figure 4.6.[20]

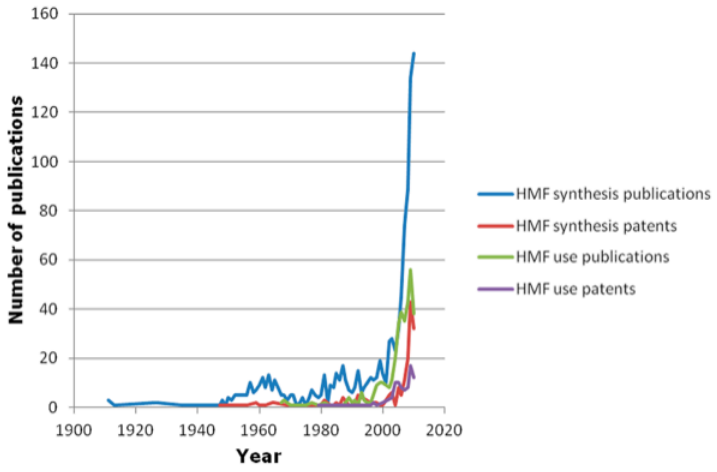

Figure 4.6: Growth of HMF per year as registered by web of science. (Reproduced from reference 20 with permission from American Chemical Society, 2013).

HMF **260** can be synthesized by several methods such as dehydration of fructose in the presence of acid catalyst, high temperature (without catalyst), in the presence of ionic liquids etc.[21] These methods allow us to obtain HMF without losing any carbon from hexoses unlike other platform chemicals such as levulinic acid or bioethanol. It is a key intermediate for many furan/non furanic derivatives, which has widespread application in fuels, and polymers as listed in the Figure 4.7. Due to its versatile applications,

furan derivatives – HMF **260**, furfural, and 2,5-furan dicarboxylic acid **253** are listed in top 14 bio-based chemicals by department of energy (DOE).[20] Though furan is an important intermediate, polymers starting from furan are rare. But HMF is converted into a variety of monomers (Figure 4.8) that are employed in polymer synthesis.

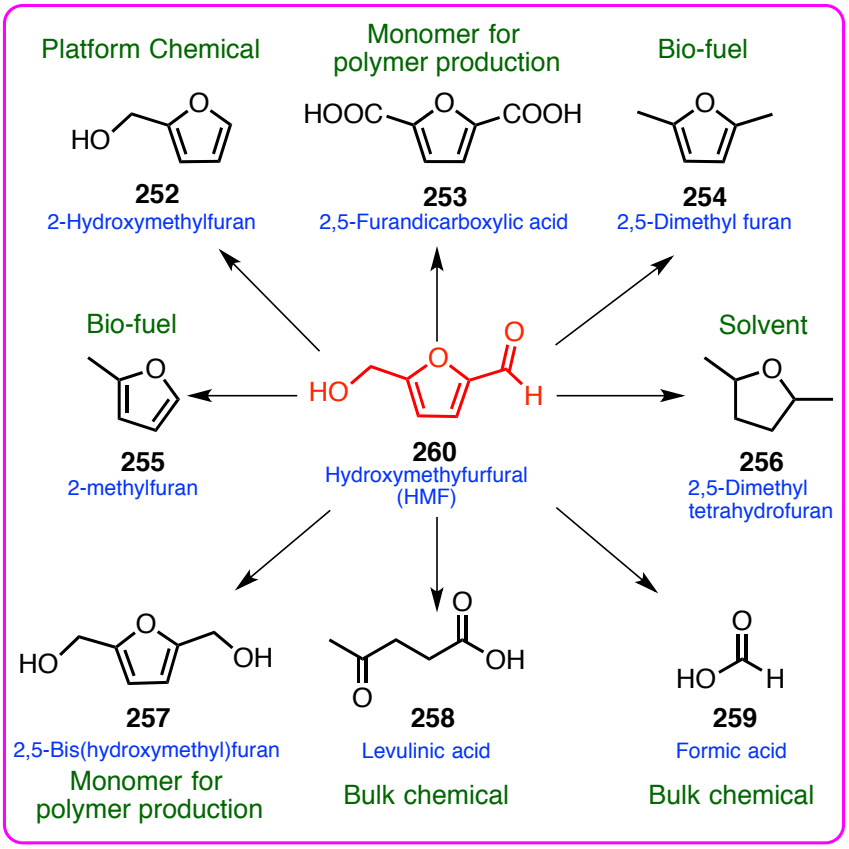

Figure 4.7: HMF as a platform chemical.[20]

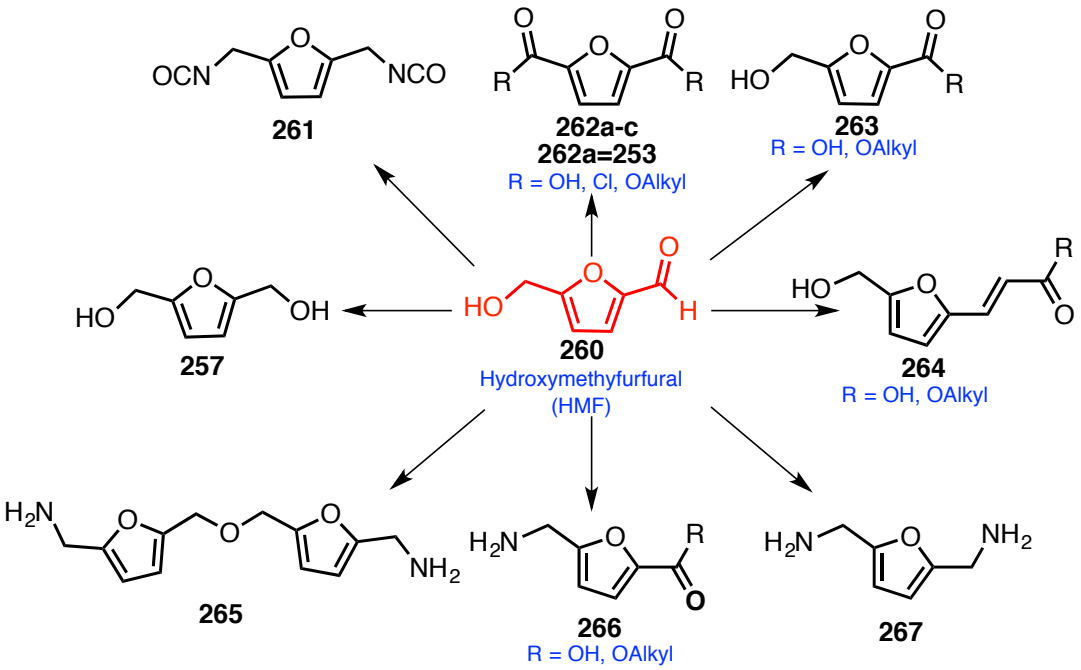

Figure 4.8: Monomers derived from HMF.[22]

The following section discusses few polymers derived from HMF and its derivatives. Detailed discussion on the synthesis of polymers derived from HMF based compounds are reported in various reviews.[20,22-24]

4.3. Polymers from 5-hydroxymethylfurfural derivatives

Gandini and coworkers employed symmetrical aldehyde 2,5-bis(formyl)-furan **268** obtained from the oxidation of HMF as a monomer along with variety of diamine monomers to prepare Schiff base copolymers **270** (Scheme 4.2).[25] The polymers **270** resulting from 2,5-bis(formyl)-furan had a molecular weight M_n of 1500-2500 and are readily soluble in common organic solvents. These categories of polymers resulting from diamines showed good thermal stability and semiconductor properties (10^{-5} to 10^{-4} S cm $^{-1}$).

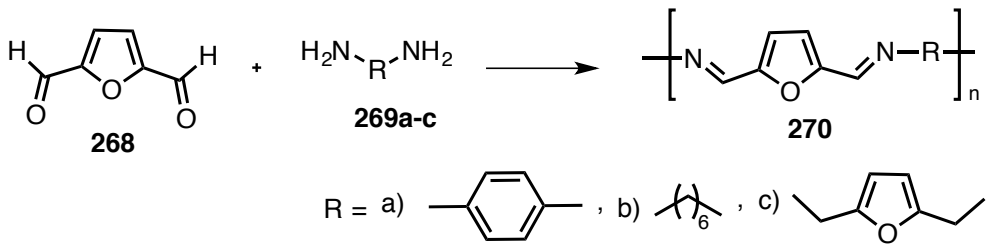

Scheme 4.2: Synthesis of furanic poly Schiff base **270** from 2,5-bis(formyl)furan **268**.

In continuing their efforts towards obtaining polymer with desired structure and good conductivity, the same group worked on condensation of dimerized product of HMF i.e 5, 5'(oxy-bis(methylene))bis-2-furfural (OBMF) **271** with *p*-phenylenediamine **269a** to result in new Schiff polymer **272** (Scheme 4.3).[25] The polymer was stable till 270 °C and showed a semiconductivity of 10^{-6} S cm^{-1} at room temperature.

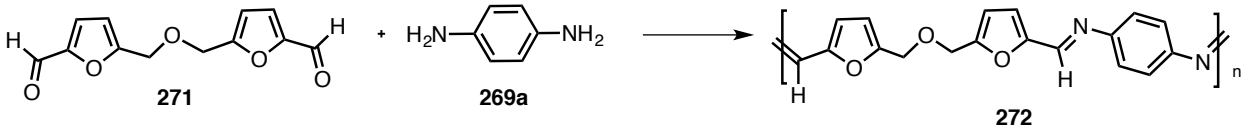

Scheme 4.3: Synthesis of furanic poly Schiff base **272** from 5, 5'(oxy-bis(methylene))bis-2-furfural (OBMF) **271**.

Furan based polyurethanes were prepared by condensation of 2,5-(bishydroxymethyl)furan **257** with various diisocyanates.[25-29] These reactions were performed at 70 °C for 24 h. Initially, a simple hexamethylene diisocyanate **273** was used instead of 2,5-furyl diisocyanate **261** due to its sensitivity to resinification and low stability of urethane. To circumvent the resinification problem, a homologue of 2,5-furyl diisocyanate, furyl methylenediisocyanate was used in the condensation procedure that resulted in stable urethane polymer **275** (Scheme 4.4).

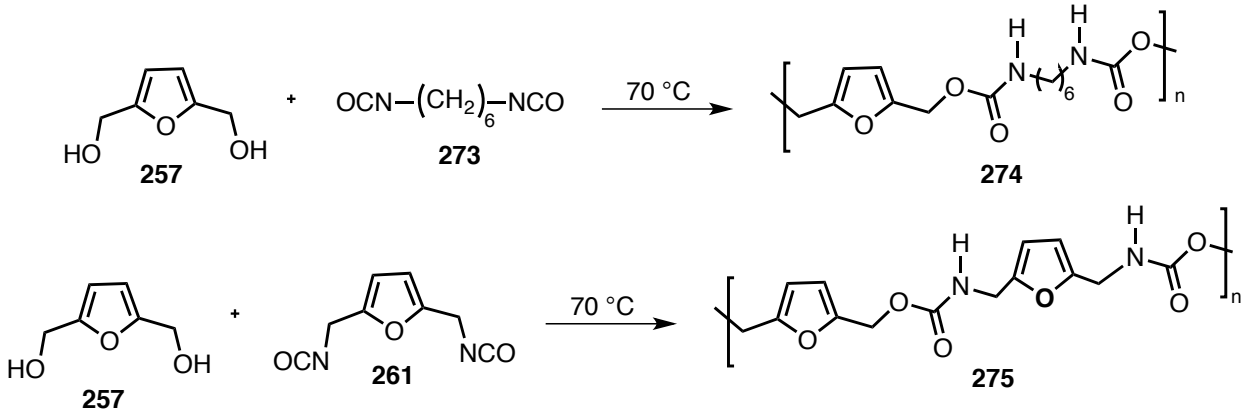

Scheme 4.4: Synthesis of furanic poly urethane from 2,5-bis(formyl)furan **257**.

Lincoln and co-workers reported the preparation of FDCA based polyester in 1951.[30] They demonstrated that that FDCA based polyester can be obtained by heating FDCA and ethylene glycol at 180 °C for 3 h then increasing the temperature to 210 °C and maintaining for 4 h. The melting point of the resulting polyester was found to be 205-210 °C. Later in the year 1978, Moore and Kelly reported a detailed study on the preparation of polyester **277** with FDCA derivative **262a** (Scheme 4.5).[31] They performed trans esterification of FDCA with corresponding diol **276** in the presence of calcium acetate and antimony to obtain polymer of M_n of 7.4 k, M_w = 18 k with PDI of 2.54.

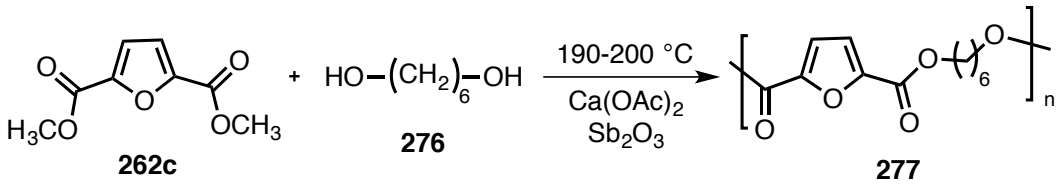

262c **276** **277**

Scheme 4.5: Synthesis of furanic polyester **277** by trans esterification.

Later in 2009, Fehrenbacher and coworkers studied the effect of chain length of diols on the molecular weights and thermal properties of the polyester. They systematically varied the chain length on the diol such as 1,3-propane diol, 1,6-hexane diol, 1,12-dodecane diol, and 1,18-octadocane diol. The analysis showed that that this method produced polyester with low to moderate molecular weight and meting point (Table 4.1)[32]

Table 4.1: Molecular weight and thermal properties of polyester with different diol co-monomer.

Diol co-monomer	M_n (kg/mol)	M_w (kg/mol)	T_m (°C) from DSC
1,3-propane diol	13.9	30.6	176.5
1,6-hexane diol	13.4	22.3	142.7
1,12-dodecane diol	25.3	51.6	109.2
1,18-octadocane diol	22.1	46.8	98.1

In 2009, Gandini and coworkers reported comprehensive comparative studies by analyzing the thermal, spectroscopic characteristics of polyester derived from FDCA **278** and polyethylene terephthalate (PET) **279** (Scheme 4.6).[33] They used diester diol of FDCA **278** subjected to trans esterification in presence of Sb_2O_3 with progressive raise in temperature form 70 to 200 °C. The products were obtained as white powder soluble in trifluoroacetic acid (TFA) and hot tetrachloroethane (TCE). TGA analysis of the polyester PEF showed that it is thermally stable till ~300 °C which is similar to PET and the

DSC analysis showed high degree of crystallinity with melting temperature of 210-215 °C which is ~45 °C lower than PET.

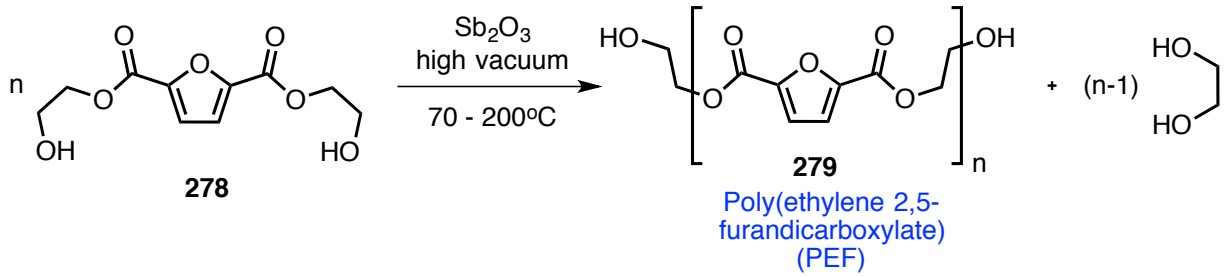

Scheme 4.6: Synthesis of polyethylene(2,5furandicarboxylate)(PEF) **279**.

Based on the extensive research on utilizing renewable resources for the application of materials, it is evident that we have an alternate for the fossil resources. However, once the materials derived from renewable resources gets commercialized, the demand for the renewable sources will increase, their prices will hike, and most importantly, the materials after usage will go back to the environment as landfills. So it is important to find ways to safely decompose them or more desirably recycle them. There are few reports on the degradation of plastics obtained from fossil fuels as well as renewable resources. These methods involve the use of microorganisms, enzymes or catalyst which are expensive, takes longer times and more adversely unsustainable.[34-36] In order to address these deficiencies, we have worked on developing polymeric building blocks that are derived from sustainable materials with built in photocleavable unit that can be excited to initiate the degradation of polymers using a benign reagent "light". In order to validate this proof of concept we have employed FDCA based polymer (section 4.4) incorporated with nitrobenzyl phototrigger (detailed discussion of phototrigger are included in chapter 1) as a chromophore. This light-absorbing unit upon shining light triggers the degradation of polymer releasing the monomer.

Employing nitrophototrigger for the degradation of polymers are reported in the literature. For example Turro and coworkers demonstrated the degradation of star polymer to a linear polymer by incorporating nitrobenzyl phototrigger. Upon UV irradiation of **280** resulted in cleavage giving rise to linear polymer **281** (Scheme 4.7)[37] which has potential application in photolithographic technique, biomaterials etc.,

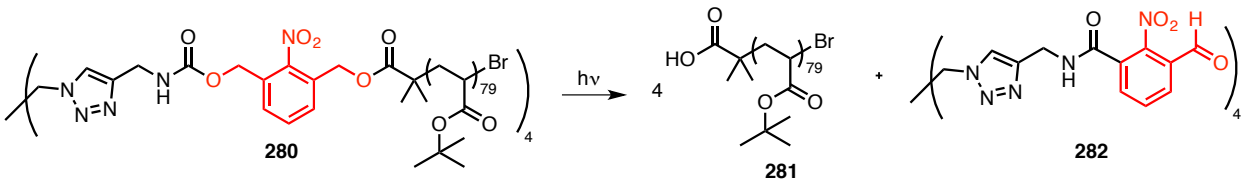

Scheme 4.7: Photoreaction of degradable polymer **280**.

Similarly, nitrobenzyl phototrigger are employed in synthesis of light triggered dissociable block copolymer. These block copolymer are investigated as a nano carrier for the controlled release of drugs. For example, Zhao and coworkers demonstrated release of Nile red dye using two different block co polymer **283** and **286** (Scheme 4.8).[38,39] The release of the Nile red which was efficient in both the polymer.

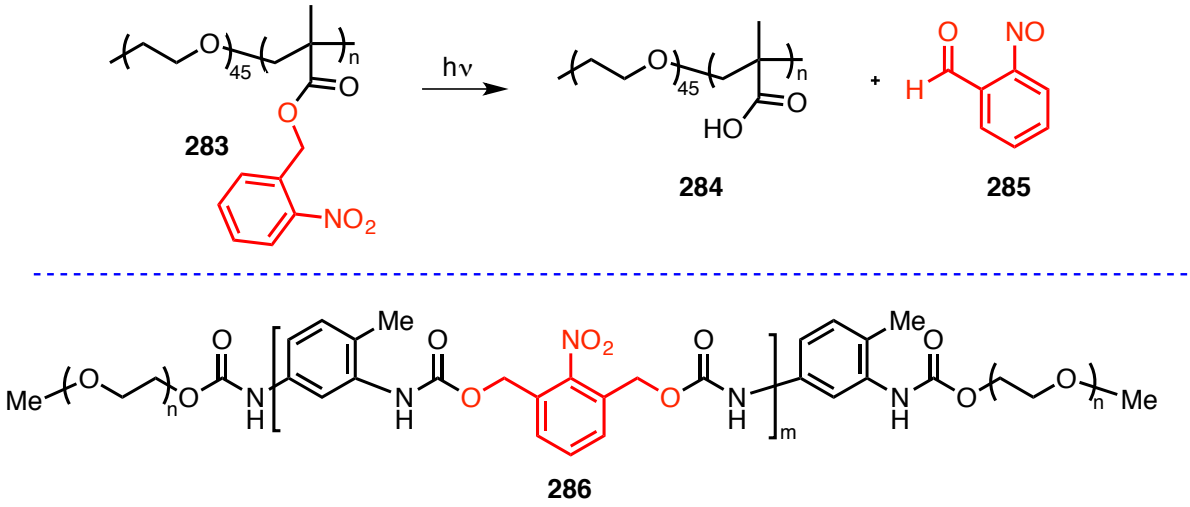

Scheme 4.8: Photoreaction of block copolymer **283** (top). Photodegradable ABA tri block copolymer **286**.

In most of the literature discusses about the cleavage of polymer and also though the nitrobenzyl phototrigger is substituted on both ortho position, the cleavage took place on a mono substituted phototrigger.[40,41] On the contrary, our strategy not only allowed the degradation of the biomass based polymer but also demonstrated the recovery and reuse of monomer when the cleavage of the *ortho*-nitrobenzyl phototrigger occurred at both the position leading to recovery of monomer. This approach alleviates the environmental impact by reducing the amount of landfill. The model compound, polymers and their intermediates used in this study are listed in the Chart 4.1 and were synthesized according to the procedures reported in literature.

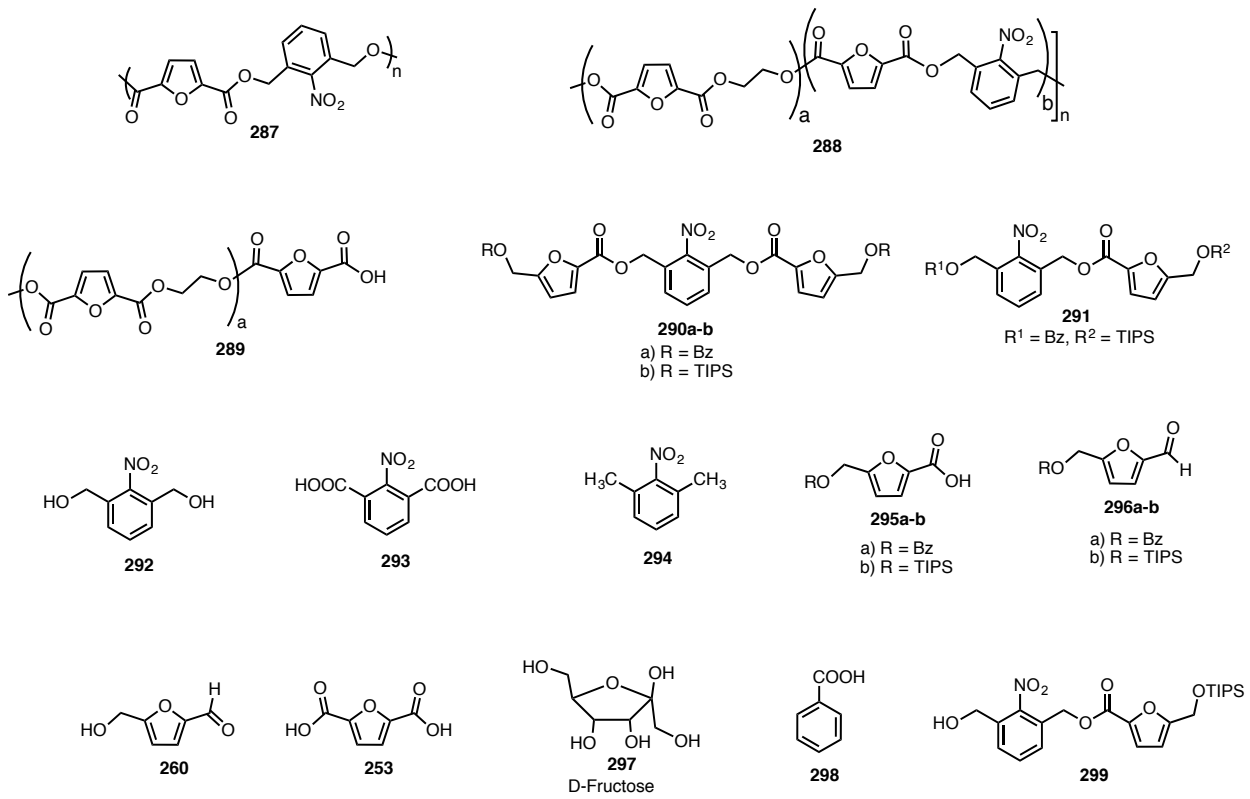

Chart 4.1: Structures of model compounds, polymer, copolymer and the compounds used for their synthesis.

4.4. Synthesis and photodegradation of model compounds

To demonstrate the proof of principle, we began our investigation to optimize the reactions conditions by model compounds employing HMF **260** that is a dehydrated product of fructose **297** (Scheme 4.9). These monomer were functionalized with 2-nitro1,3-benzenedimethanol **292**, which is a phototrigger. We chose to use nitrobenzyl chromophore as a phototrigger as it is one of the well-studied systems and its mechanism of action has been extensively investigated and proved by various research groups. Symmetrical **290** and unsymmetrical model compounds **291** were synthesized to evaluate photodegradation of bio-based polymers. The synthesized polymers were characterized by NMR spectroscopy, and their properties were studied using gel permeation chromatography (GPC), differential scanning calorimetry (DSC), thermogravimetric analysis (TGA), Fourier transform Infrared spectroscopy FTIR and powder X-ray diffraction (XRD).

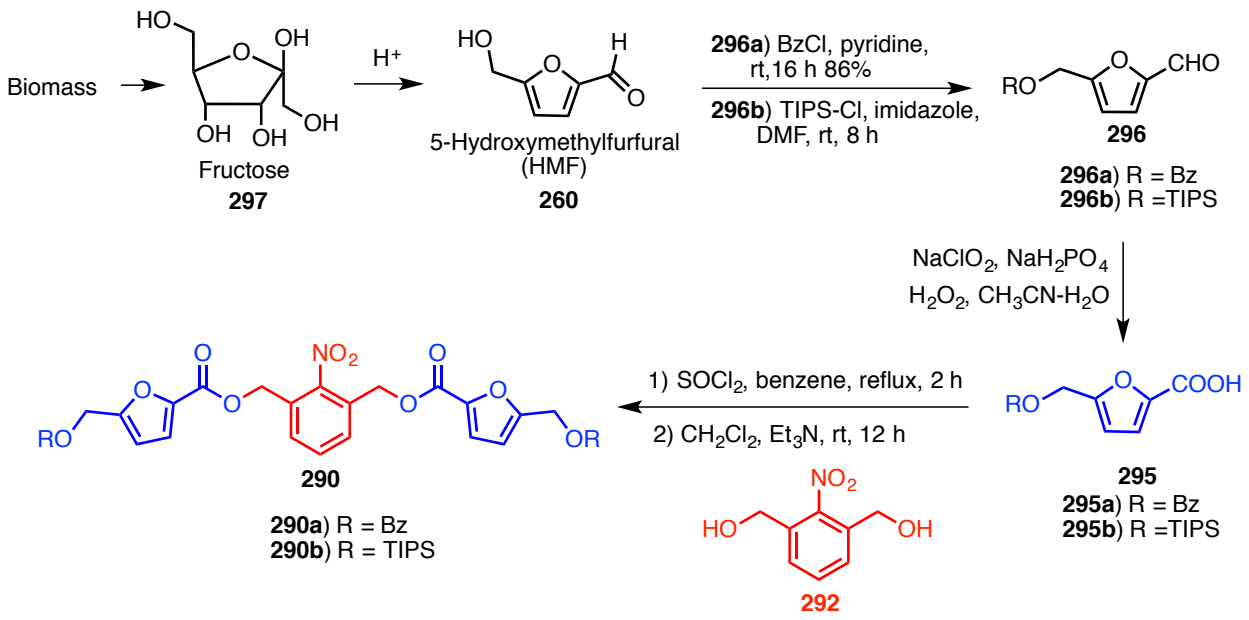

Scheme 4.9: Synthesis of symmetrical model compounds from HMF and 2-nitro1,3-benzenedimethanol.

HMF was obtained from fructose in the presence of acid followed by the protection of alcohol functionality to yield **296**. Upon oxidation of aldehyde **296** followed by reacting with 2-nitro 1,3-benzenediemthanol **292** results in the two model compounds (Scheme 4.9) (detailed synthetic procedure are given in the experimental section). Irradiation of these symmetrical esters **290a-b** was carried out in Rayonet reactor equipped with 350 nm (16 lamps X 14 watts each). Progress of the reaction was monitored by UV-Vis and NMR spectroscopy after an interval of 30 min. The *o*-nitrobenzyl proton at 5.45 ppm was used as a NMR handle to monitor the progress of the reaction. Analysis of the ^{1}H-NMR spectra reveals that the photocleavage was very efficient with mass balance of 89% and 80% respectively (Figure 4.42 and Figure 4.44). As reported in the mechanism of nitrobenzyl phototrigger, the photocleavage of the model ester compounds proceeded via intermediate nitroso aldehyde **300** as the aldehydic resonance at 9.17 ppm was observed during the progress of the reaction, which later decompose to furan carboxylic acid as monitored by the rise of methylene peak at 5 ppm (Scheme 4.10).

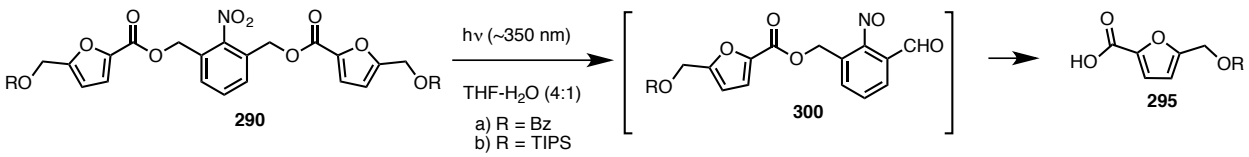

Scheme 4.10: Photoreaction of symmetrical esters model compound **290**.

In order to substantiate the effectiveness of the photocleavage, unsymmetrical model ester compound **291** was also synthesized and subjected to irradiation. Upon irradiation of unsymmetrical ester **291**, photocleavage occurred in a facile manner to give corresponding acid **295b** (Scheme 4.11).

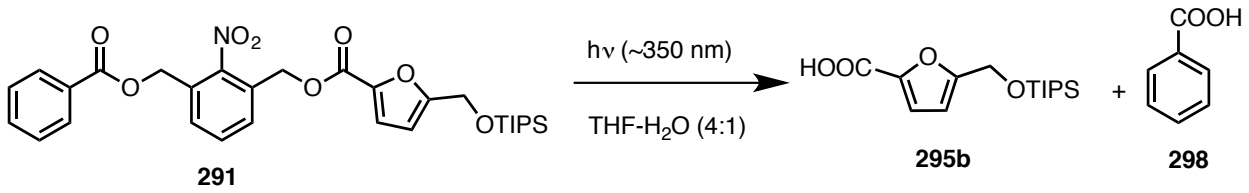

291 **295b** **298**

Scheme 4.11: Photoreaction of unsymmetrical esters model compound **291**.

The study with the model compounds **290** and **291** showed that use of nitrobenzyl as phototrigger can be successfully employed not only for the degradation of polymer but also for recovering the monomer. With the knowledge gained from the prototypical studies we went forward to incorporate this strategy for the degradation of polymer/oligomer derived from FDCA monomer.

4.5. Synthesis and characterization of polymer/oligomer from FDCA monomer

The polymer/oligomers containing the nitrobenzyl phototrigger unit in its backbone were synthesized from FDCA monomer that is an oxidized product of HMF. The polymer was obtained in a one-pot reaction, where the FDCA is converted to its corresponding acid chloride by treating with thionyl chloride, which then reacts with nitrobenzyl phototrigger to yield the desired polymer as a pale brown solid (Scheme 4.12). The insoluble polymer **287** was washed with methanol to remove any unreacted monomer. The resulting polymer further washed with acetone and dichloromethane to remove low molecular weight oligomers. The purified polymer was insoluble and was characterized by NMR spectroscopy, FTIR spectroscopy, GPC, Powder XRD, TGA, DSC analysis.

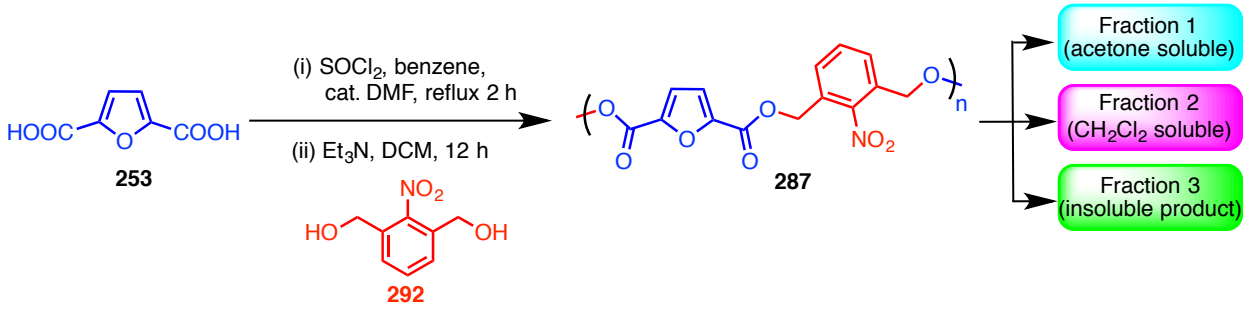

Scheme 4.12: Synthesis of polymer/oligomer **287** derived from FDCA.

Gel permeation chromatographic (GPC) analysis revealed that the product formed was a mixture of polymer with M_w=81000, M_n=54000, PDI=1.5 and oligomer whose M_w= 450, M_n= 340 and PDI=1.3. IR studies clearly revealed the presence of ester functionality as a strong vibration was observed at 1739 cm^{-1} and also the presence of nitro group by indicating the symmetric and asymmetric stretching at 1367 cm^{-1} and 1529 cm^{-1} respectively. As the material is insoluble in most of the common organic solvents (chloroform, ethyl acetate, methanol) it was made soluble by heating the mixture in deuterated DMSO at 80 °C for the ^{1}H-NMR characterization. NMR spectroscopy indicated the presence of furan and phenyl functionalities. Apart from these signature peaks, two distinct singlet resonances were observed at 5.48 ppm and 5.29 ppm, which was assigned to the benzylic functionalities of oligomer and polymer which was in the ratio 11:1. These results substantiated the presence of mixture of oligomer and polymer in the system. TGA analysis of the polymer/oligomer mixture showed that they are thermally stable up to 234 °C without any loss. When the temperature was increased to 302 °C a 50 % loss was observed due to decomposition and decomposition was complete when the temperature was further increased to 648 °C. The first cycle of DSC analysis showed a glass transition temperature (T_g) at 159 °C followed by melting at 184 °C denoting that the polymer /oligomer mixture was a mixture of amorphous and crystalline states. Recrystallization did not show sharp peak due to the absence of crystallinity and the second cycle showed T_g at 113 °C signifying that it is a mostly amorphous oligomer. To corroborate these observations, PXRD was recorded. Inspection of PXRD indicated sharp peaks (2θ values) and the percentage of crystallinity was around 23.34 % using cristobalite (SiO_2) as reference standard. Complete loss of crystallinity was observed upon heating the polymer/oligomer to 200 °C and cooling which was in line with the results observed from DSC analysis (Figure 4.9).

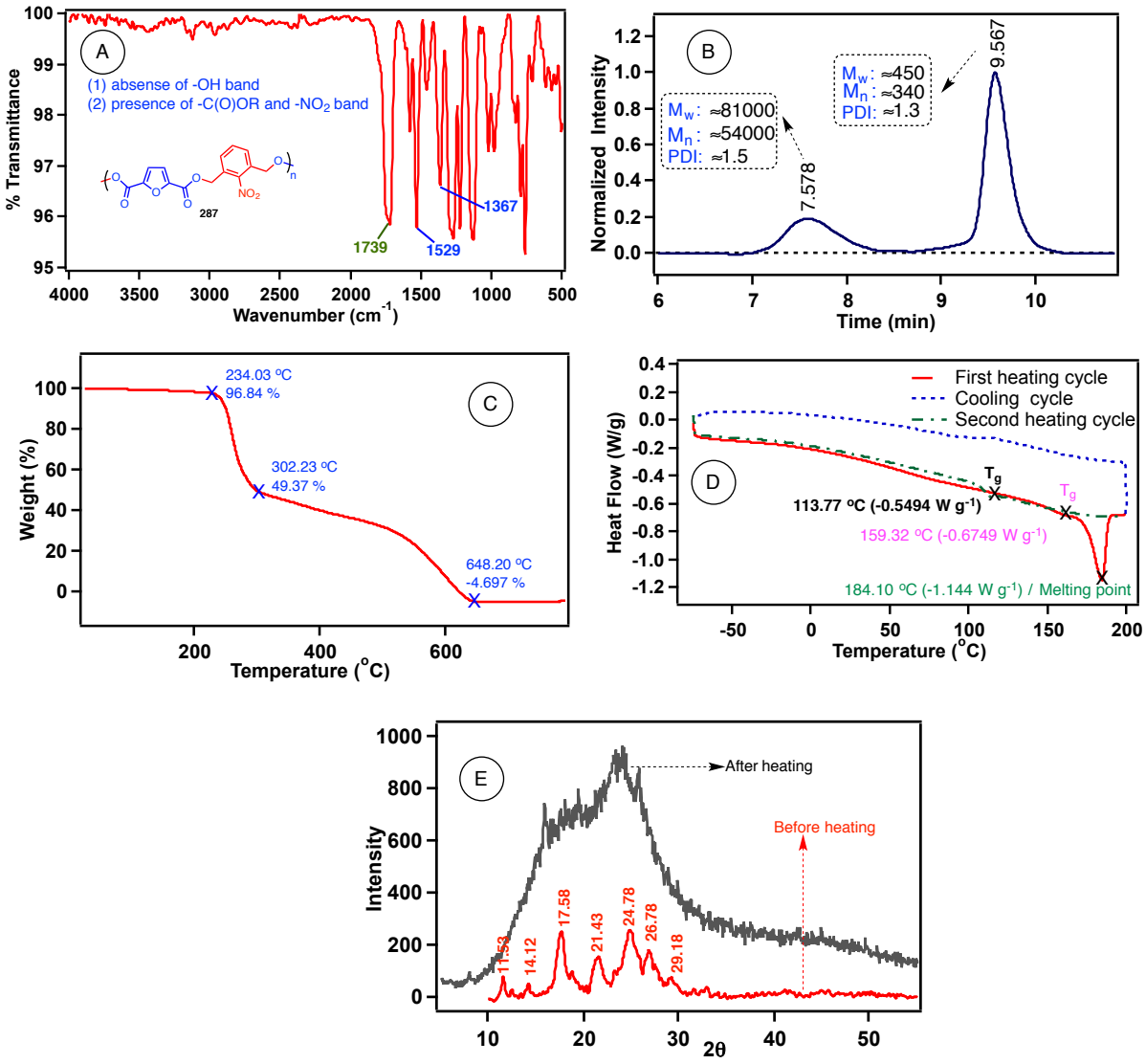

Figure 4.9: Characterization of polymer/oligomer **287**. A) FTIR spectroscopy B) GPC C) TGA D) DSC E) Powder-XRD.

4.6. Photodegradation of polymer/oligomer in solution and solid state

Detailed characterization of the synthesized polymer/oligomer gave insights on the properties of the mixture. Most importantly the crystallinity, which made the polymer/oligomer insoluble in most of the common organic solvents. Therefore to evaluate the photodegradation, polymer/oligomer **287**, it was suspended in THF-H_2O (4:1) mixture and irradiated in Rayonet reactor equipped with ~350 nm bulb (16 bulbs x 14 watt) (Scheme 4.13). The solution was heterogeneous before irradiation, it turned to a turbid

solution after 1 h and become transparent over 3 h of irradiation during which the color of the solution changed from white suspension to yellow solution (Figure 4.10).

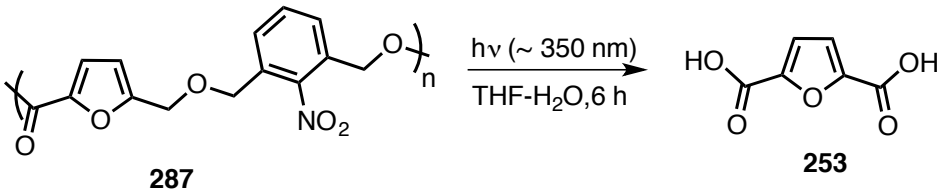

287 **253**

Scheme 4.13: Photodegradation of polymer/oligomer **287** derived from FDCA in solution phase.

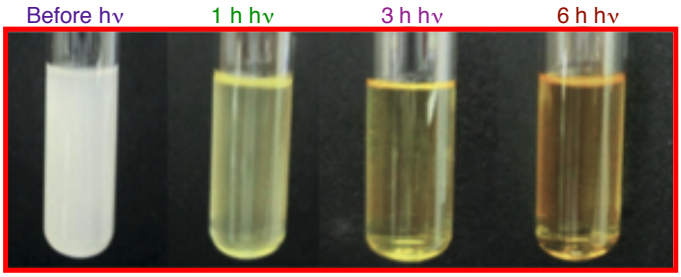

Figure 4.10: Polymer/oligomer **287** a) before irradiation b) irradiated for 1 h c) irradiated for 3 h d) irradiated for 6 h.

The reaction was further continued for 6 h to ensure complete decomposition of the polymeric materials. After 6 h of irradiation, the sample was concentrated and the residue was analyzed by ^{1}H NMR spectroscopy using an internal standard. Analysis of ^{1}H-NMR confirmed (Figure 4.49) complete degradation of the polymer to give FDCA monomer (complete agreement with the NMR spectra of authentic FDCA) with 40±5% recovery.

Since these types of polymers can be potentially made into plastics it becomes important to evaluate the degradation in solid state. Therefore photodegradation was performed in solid state, in both 350 nm lamp as well in ambient conditions (Scheme 4.14)

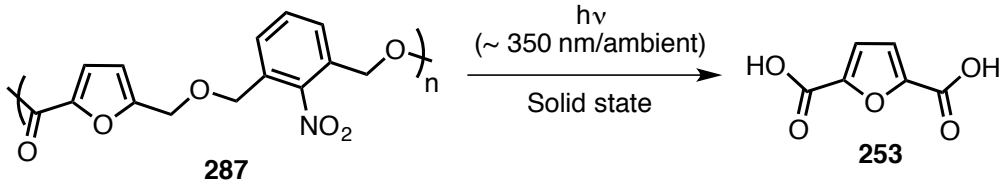

287 **253**

Scheme 4.14: Photodegradation of polymer/oligomer **287** in solid state.

Polymer/oligomer **11** was packed as a thin layer between two 1 mm micro slides made of Swiss glass (purchased from VWR® international). The packed samples were irradiated in Rayonet reactor equipped with ~350 nm bulb (16 bulbs x 14 watt). The reaction was monitored every 6 hour. After 6 h the

sample was analyzed by ^{1}H-NMR spectroscopy as internal standard. The solid sample changed color from pale yellow to dark brown over the period of irradiation (Figure 4.11 left). After 12 h, the recovery of FDCA was found to be 16%. The solid state degradation was slow and resulted in low yield compared to the solution state due to competitive absorption of light by the photoproducts as well as due to light scattering. The above reaction was also performed in ambient conditions (40 W incandescent bulb). No degradation was observed even after 12 h of irradiation (Figure 4.11 Right).

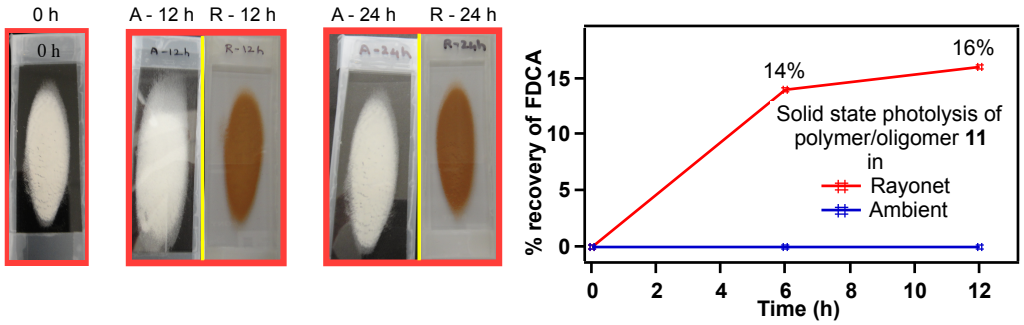

Figure 4.11: Left: Solid-state irradiation of Polymer/oligomer **287** in Rayonet (R) and Ambient (A) Right: % recovery of FDCA determined using ^{1}H NMR spectroscopy in Rayonet reactor and ambient conditions.

4.7. Strategy for recycling the recovered monomer

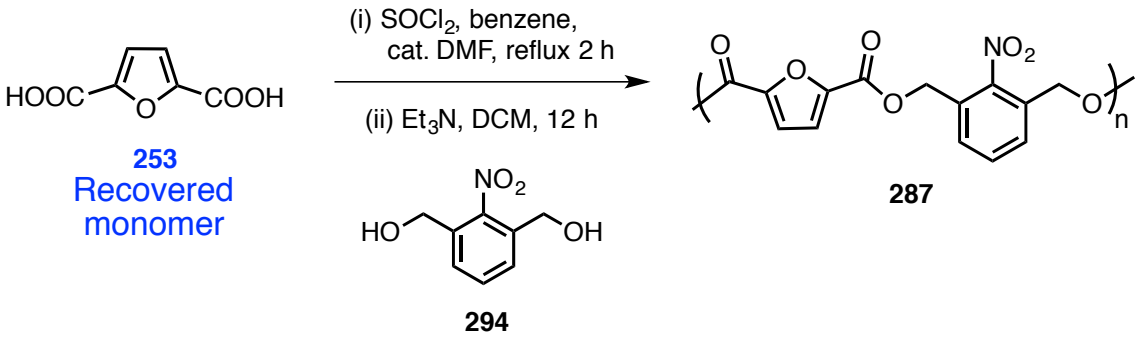

Scheme 4.15: Synthesis of polymer/oligomer **287** in from recovered monomer.

After successfully showcasing the degradation of polymer/oligomer and recovering the monomer (FDCA) it becomes imperative to prove that the recovered monomer can be recycled (Scheme 4.15) to display the viability of the strategy. Hence, large-scale photoreaction (6 batches of 10 mL each) was performed in Rayonet reactor equipped with ~350 nm bulbs (16 bulbs x 14 watt). After the reaction, the resultant mixture was washed with dichloromethane to remove the by-products (FDCA is insoluble in

dichloromethane). The removal of the by-products was monitored by UV-Vis spectrophotometer. The isolated yield was found to be 38 %. The recovered monomer was subjected to polymerization with the procedure reported in Scheme 2.10. The product obtained was analyzed by GPC and compared with the GPC trace of the polymer before photoreaction (Figure 4.12).

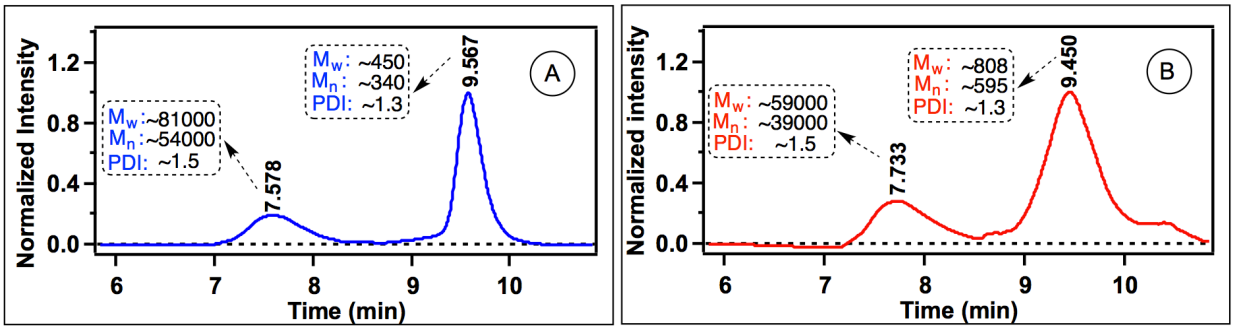

Figure 4.12: GPC trace of polymer/oligomer **287** A) First time synthesized (blue) B) synthesized using the recovered FDCA (red).

4.8. Synthesis, characterization and photodegradation of copolymer

After successfully demonstrating the photodegradation of polymer/oligomer in solution and in solid state followed by its recyclability, we assessed the photodegradation of copolymers including a glycol unit, other than the phototrigger. Copolymer **288** was synthesized in a single pot reaction by converting the FDCA **253** to its corresponding acid chloride and reacting it with glycol and 2-nitro 1,3 benzenedimethanol. After the reaction, methanol was added to the mixture to result the copolymer **288**.

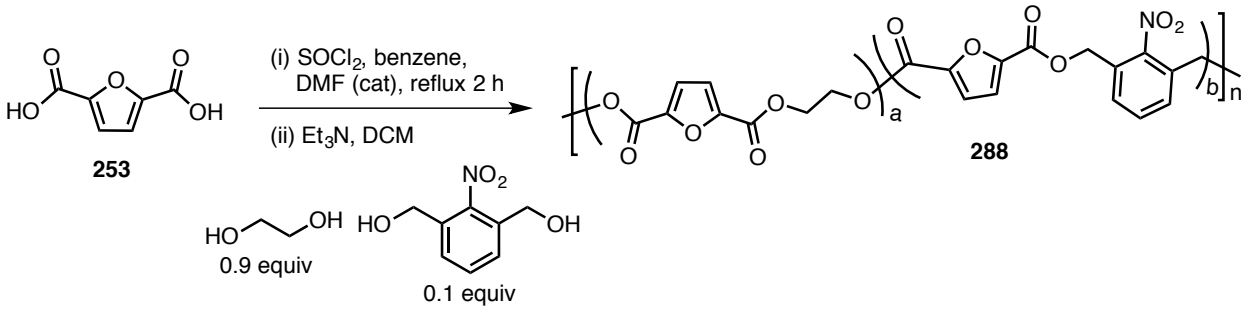

Scheme 4.16: Synthesis of copolymer **288**.

The synthesized copolymer **288** was characterized by NMR spectroscopy, FTIR, GPC, TGA and DSC (Figure 4.13). The copolymer **288** showed better solubility compared to the polymer/oligomer **287** in common organic solvents due to the presence of ethylene units. The polymer was completely soluble in

deuterated DMSO at 75 °C. ^{1}H-NMR analysis showed furan proton resonance at 7.39 ppm and the resonance peaks for nitrophenyl group at 7.76 ppm and 5.45 ppm. Ethylene glycol unit protons appeared at around 4.91, 4.59, 4.28 and 3.56 ppm respectively. FTIR spectra revealed the presence of ester carbonyl at around 1739 cm^{-1} and the symmetric and asymmetric stretching of nitro functionality at 1308 cm^{-1} and 1581 cm^{-1} respectively.

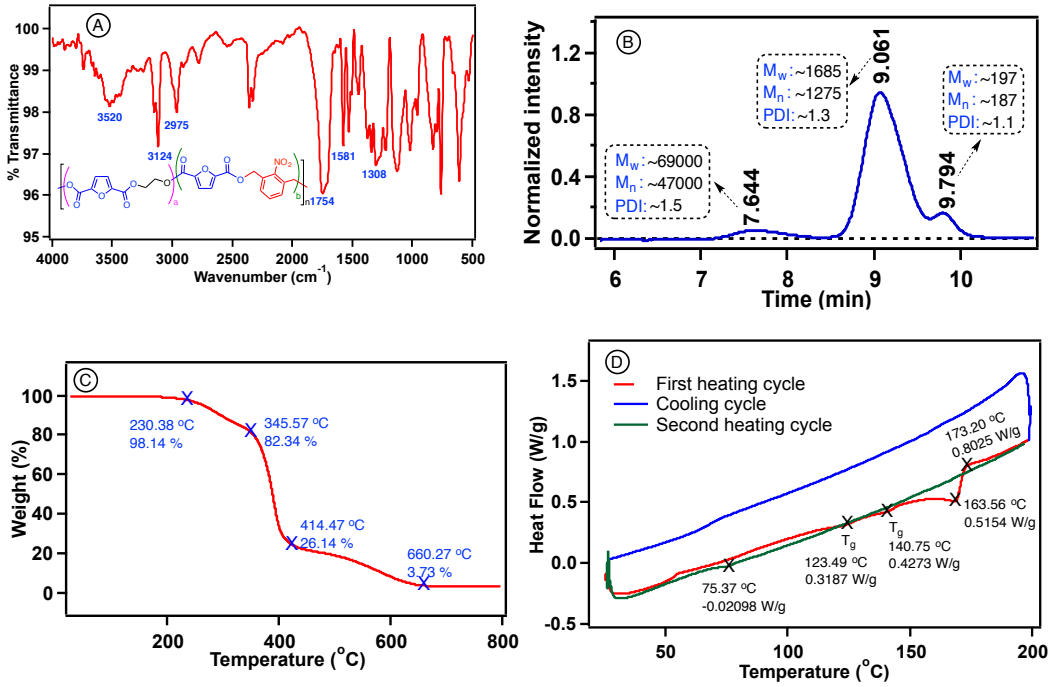

Figure 4.13: Characterization of copolymer **288.** A) FTIR spectroscopy B) GPC C) TGA D) DSC.

Copolymer **288** was sonicated and filtered to record GPC. GPC analysis showed mixture of polymer with M_w=69000, M_n=57000, PDI=1.5 and oligomer whose M_w= 1685, M_n= 1275 and PDI=1.3 along with unreacted 2-nitro-1,3-benzenedimethanol (9.789 min). TGA analysis showed that the synthesized polymer is thermally stable till 230 °C. Up on increasing the temperature to 230-345 °C 13 % loss was observed and further increase to 345-414 °C showed 56 % loss. The copolymer/oligomer was completely decomposed at 660 °C. First cycle of DSC analysis showed two glass transition temperature (T_g) at 123 °C and 140 °C due to the mixture of copolymers (FDCA-glycol-nitrobenzyl and FDCA-glycol). Though there was a endotherm at 168 °C it did not correspond to the melting point as no visible recrystallization was observed. During the second cycle, there was shift in the T_g (75 °C) indicating an amorphous material.

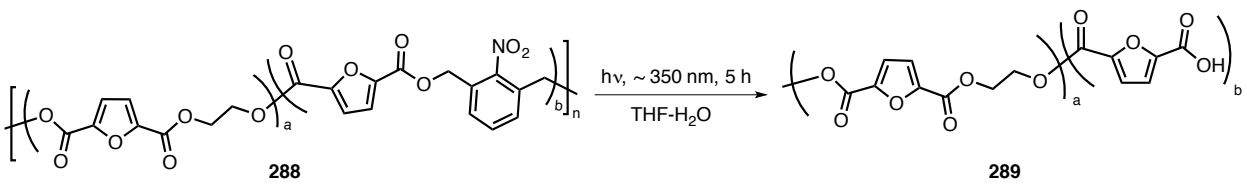

Scheme 4.17: Photodegradation of copolymer **288**.

After characterization, the copolymer was subjected to degradation as a suspension in THF/water (4:1 mixture) with 350 nm light source. Similar to the degradation of polymer/oligomer **287**, The new copolymer **288** also turned from initial turbid to transparent solution after the degradation was complete. After the completion of reaction, the sample was concentrated and the residue was analyzed by ^{1}H-NMR. Analysis of ^{1}H NMR showed that the photodegradation of the copolymer was efficient. Thus proving that the strategy of employing nitrobenzyl unit as a phototrigger to degrade polymer and copolymer was very efficient and also provided avenues to recover and recycle.

4.9. Conclusions

Our strategy of incorporating phototrigger unit in the polymer structure that was derived form biomass to degrade the polymer was substantiated from our studies. We showed that this strategy could be applied for solid-state reaction and also extended to copolymer degradation as well. In addition to the degradation, we have also demonstrated the successful recovery and reuse of the monomer to build the polymer/oligomer. This study opens up avenues to build novel materials from bio renewable resources that can be degraded after use thereby reducing the landfills that affects the environment.

4.10. Experimental section

4.10.1. General methods

All commercially obtained reagents/solvents were used as received; chemicals were purchased from Alfa Aesar®, Sigma-Aldrich®, Acros organics®, TCI America®, Mallinckrodt®, and Oakwood® Products, and were used as received without further purification. Unless stated otherwise, reactions were conducted in oven-dried glassware under nitrogen atmosphere. ^{1}H-NMR and ^{13}C-NMR spectra were recorded on Varian 500 MHz (125 MHz for ^{13}C) or Bruker 400 MHz (100 MHz for ^{13}C) spectrometers.

Data from the ^{1}H-NMR spectroscopy are reported as chemical shift (δ ppm) with the corresponding integration values. Coupling constants (*J*) are reported in hertz (Hz). Standard abbreviations indicating multiplicity were used as follows: s (singlet), b (broad), d (doublet), t (triplet), q (quartet), m (multiplet) and virt (virtual). Data for ^{13}C NMR spectra are reported in terms of chemical shift (δ ppm). High-resolution mass spectrum data in Electrospray Ionization mode were recorded on a Bruker – Daltronics® BioTof mass spectrometer in positive (ESI+) ion mode. IR spectra were recorded in Thermo Scientific Nicolet Nexus 470 FT-IR spectrometer and band positions are reported in reciprocal centimeters. Samples were made as pellet with KBR and IR spectrum was recorded. Absorbance measurements were performed using a Shimadzu® UV-2501PC UV-Vis spectrophotometer and Agilent® Cary 300 UV-Vis spectrophotometer. Tetrahydrofuran (THF) dried over sodium and HPLC graded H_2O (Alfa Aesar®) were used for UV-Vis measurements. Powder X-Ray Diffraction (PXRD) measurements were made in Phillips X'Pert MPD powder X-ray diffractometer (λ = 1.54060) with step size of 0.0500 (2θ) and continuous scan type. 2θ range from 5 to 80°. Thermo Gravimetric Analysis (TGA) were performed in TA instruments Q500 Hi-RES Thermogravimetric analyzer under nitrogen atmosphere with temperature increment of 10 °C/min. Differential Scanning Calorimeter measurements were performed in TA instruments' Q1000 Modulated Differential Scanning Calorimeter. Gel permeation chromatography analysis were performed in Symyx Rapid GPC equipped with ELS detector (PL-ELS1000), two varian PL gel Mixed–β 10 μm 300 x 7.5 mm columns and HP 100 series pump.

4.11. General procedure for the recyclable polymers

4.11.1. Synthesis of 5-hydroxymethylfurfural 260

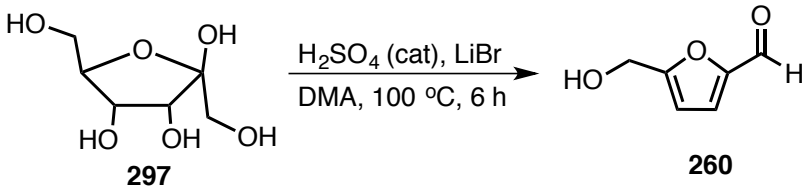

Scheme 4.18: Synthesis of 5-hydroxymethylfurfural **260.**

5-Hydroxymethylfurfural **260** was synthesized according to a procedure reported in the literature.[42] To a solution of D-fructose **297** (10 g, 55.5 mmol, 1 *equiv*.) in *N,N*-dimethylacetamide (DMA, 100 mL) under N_2 atmosphere, LiBr (10 g, 10% wt) was added, followed by catalytic amount of H_2SO_4 (0.326 g, 3.33 mmol, 0.06 *equiv*. 0.17 mL) and stirred at 100 °C for 6 h. After the reaction, the mixture was cooled to room temperature and filtered through celite bed to remove any insoluble residue. Celite bed was washed with ethyl acetate (EtOAc) (3 x 25 mL). Ethyl acetate in the filtrate was removed under reduced pressure, followed by removal of DMA by vacuum distillation. The residue after vacuum distillation was diluted with EtOAc, washed with brine solution, extracted with EtOAc. The organic layer was dried over *anhyd*.Na_2SO_4, and the solvent was removed under reduced pressure. The crude product was purified by column chromatography using hexane-ethyl acetate mixture. 5-hydroxymethylfurfural (HMF, **260**) was obtained as brown viscous oil (which solidifies upon cooling).

TLC condition - R_f = 0.30 (40% hexanes: 60% ethyl acetate) for **260** (Yield = 45 %)

^{1}H-NMR (400 MHz, $CDCl_3$, δ ppm): 3.27 (bs, 1H), 4.68 (s, 2H), 6.49 (d, 1H, *J* = 3.5 Hz), 7.19 (d, 1H, *J* = 3.5 Hz) and 9.53 (s, 1H).

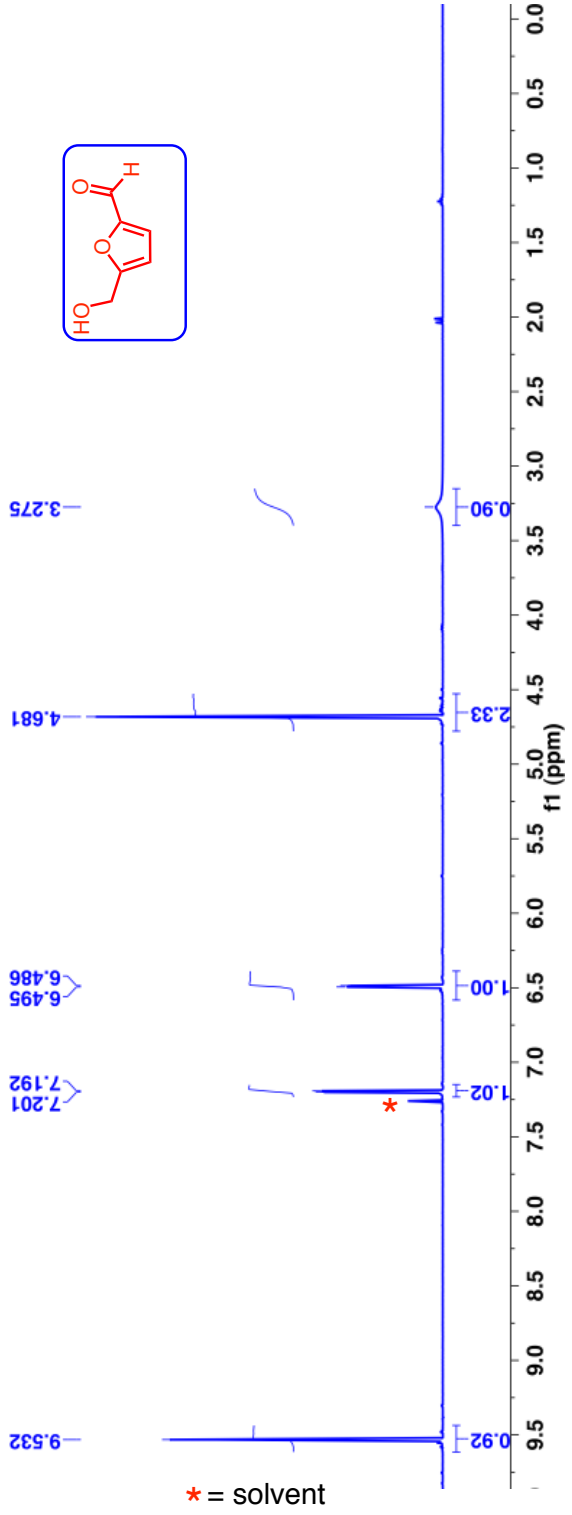

Figure 4.14: ^{1}H-NMR (400 MHz, $CDCl_3$, δ ppm) spectra of HMF **260**.

^{13}C-NMR (100 MHz, $CDCl_3$, δ ppm): 57.6, 110.0, 123.3, 152.3, 161.0 and 177.9.

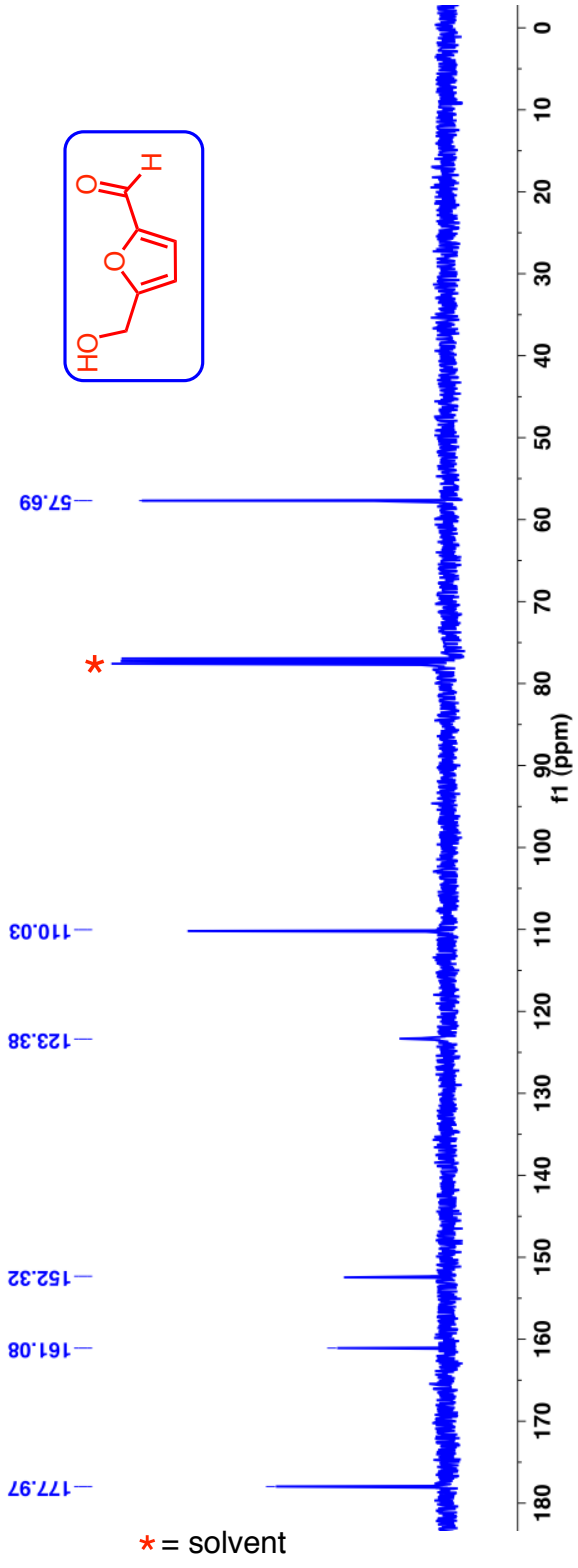

Figure 4.15: ^{13}C-NMR (100 MHz, $CDCl_3$, δ ppm) spectra of HMF **260**.

4.11.2. Synthesis of 2,5-furandicarboxylic acid (FDCA) 253

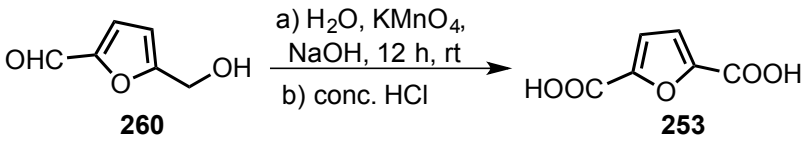

260 **253**

Scheme 4.19: Synthesis of furan dicarboxylic acid **253**.

2,5-Furan dicarboxylic acid (FDCA) was synthesized according to a procedure reported in the literature.[43] To a solution of HMF (**260**) (6.99 g, 0.055 mmol, 1 *equiv*.) in H_2O (370 mL), *aq.* NaOH (51 g, 1.27 mol, 23 equiv. in 93 mL of water) was added followed by the addition of $KMnO_4$ (20.17 g, 0.127 mol, 2.3 equiv. in 92 mL of water) and the reaction mixture was stirred at room temperature for 12 h. After completion the reaction mixture was filtered to remove the insoluble residue. The filtrate was cooled to 0-5 °C and pH of the solution was adjusted to ~1 with *concd.* HCl. The product precipitates as pale yellow solid that was filtered, washed with excess of water and dried in high vacuum at 60 °C to give pure product **253**.

Yield = 64%

HRMS [ESI-MS] *m/z* ([M-OH]): Calculated : 139.0026; Observed : 139.0018; |Δm| : 5.7 ppm

IR (KBr) cm^{-1}: 3026 (ν_{OH}), 1688 ($\nu_{C=O}$), 1221 (ν_{C-O}).

^{1}H-NMR (500 MHz, DMSO-d_6, δ ppm):7.28 (s, 2H).

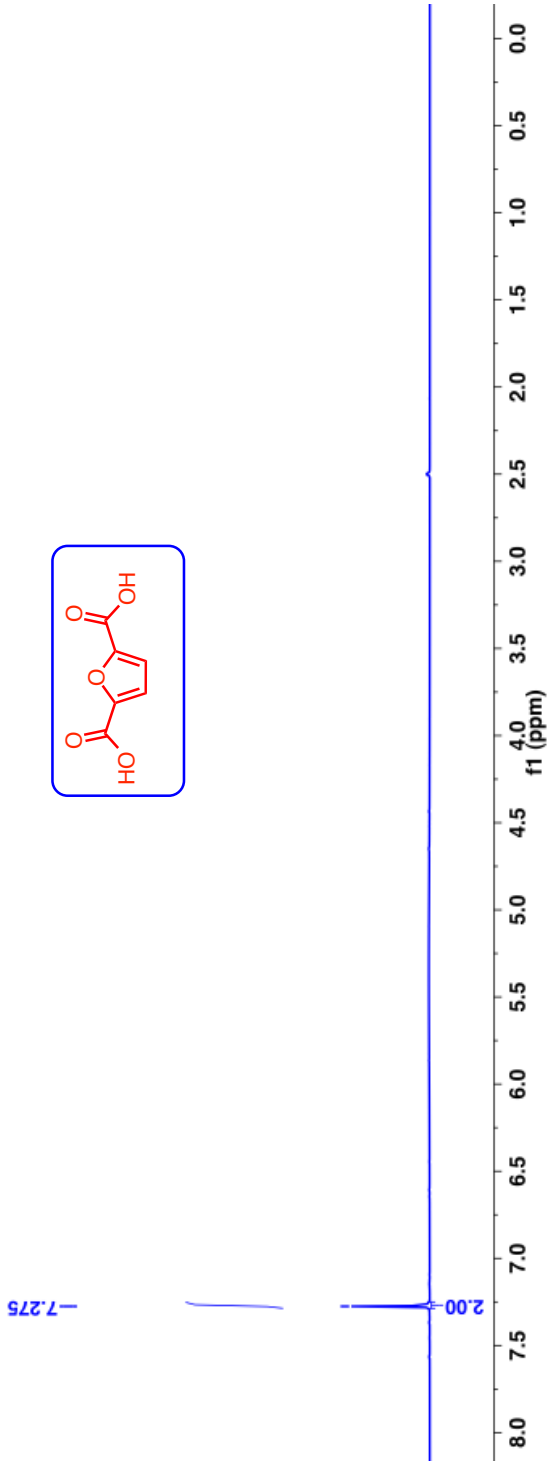

Figure 4.16: ^{1}H-NMR (500 MHz, DMSO-d_6, δ ppm) spectra of FDCA **253**.

^{13}C-NMR (125 MHz, DMSO-d_6, δ ppm): 119.0, 147.6 and 159.6.

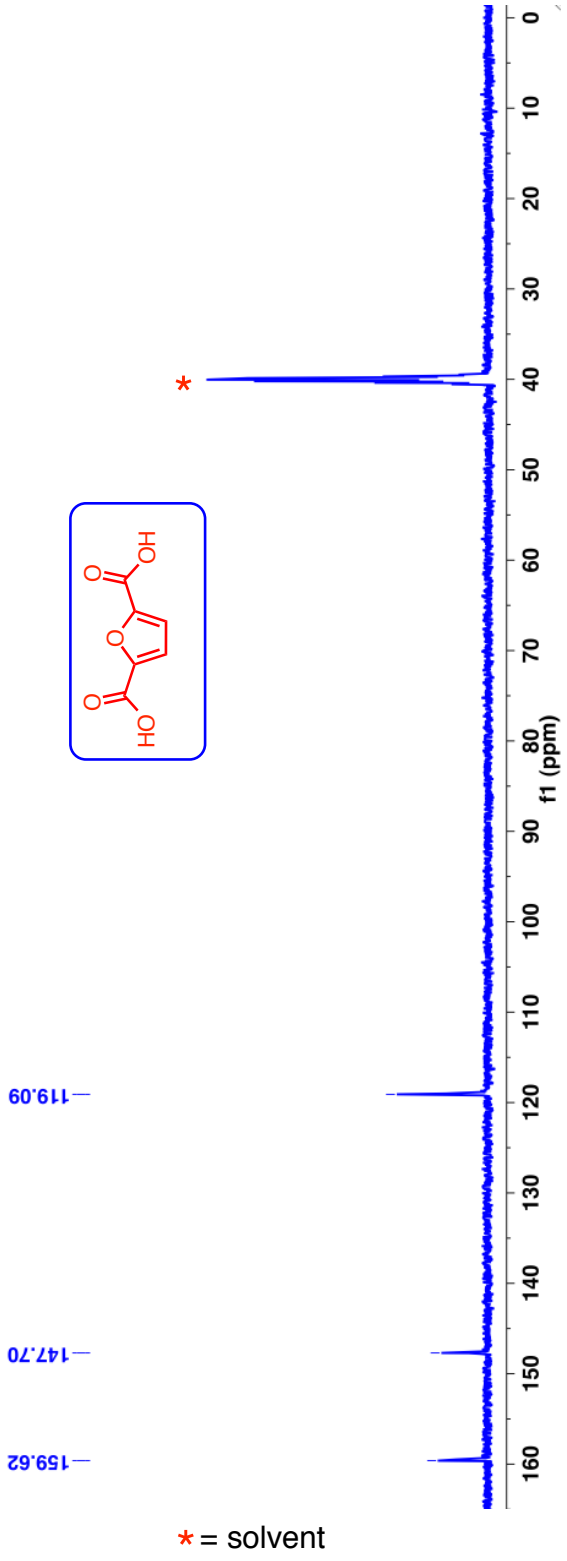

Figure 4.17: ^{13}C-NMR (125 MHz, DMSO-d_6, δ ppm) spectra of FDCA **253**.

4.11.3. Synthesis of benzoyl protected 5-hydroxymethylfurfural 296a

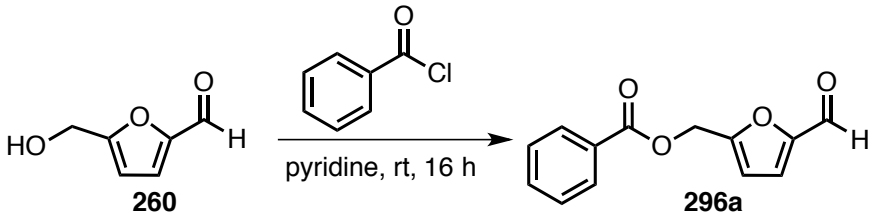

260 **296a**

Scheme 4.20: Synthesis of benzoyl protected 5-hydroxymethylfurfural **296a**.

Compound **296a** was synthesized according to a procedure reported in the literature.[44] To a stirred solution of 5-hydroxymethylfurfural (**260**) (1.5 g, 11.9 mmol, 1 *equiv.)* in pyridine (6 mL), benzoyl chloride (3.35 g, 23.8 mmol, 2 *equiv.,* 2.8 mL) was added drop wise at 0 °C. The resulting mixture was allowed to warm to room temperature over 16 h. After the reaction, the mixture was quenched with cold *dil.* H_2SO_4 (5%) and extracted with CH_2Cl_2 (3 x 25 mL). The combined organic layer was washed with *satd.* $NaHCO_3$ (~30 mL) solution, dried over *anhyd.* Na_2SO_4, and the solvent was removed under reduced pressure. The crude product was purified by column chromatography using hexane-ethyl acetate. Benzoyl protected HMF (**196a**) was obtained as white solid.

TLC condition - R_f = 0.50 (60% hexanes: 40% ethyl acetate) for **296a** (Yield = 86%)

HRMS [ESI-MS] *m/z*([M+Na]): Calculated : 253.0471; Observed : 253.0486; |Δm| : 5.9 ppm

^{1}H-NMR (400 MHz, $CDCl_3$, δ ppm): 5.36 (s, 2H), 6.65 (d, 1H, *J* = 4 Hz), 7.21 (d, 1H, *J* = 4 Hz), 7.40-7.44 (m, 2H), 7.53-7.57 (m, 1H), 8.02-8.05 (m, 2H) and 9.63 (s, 1H).

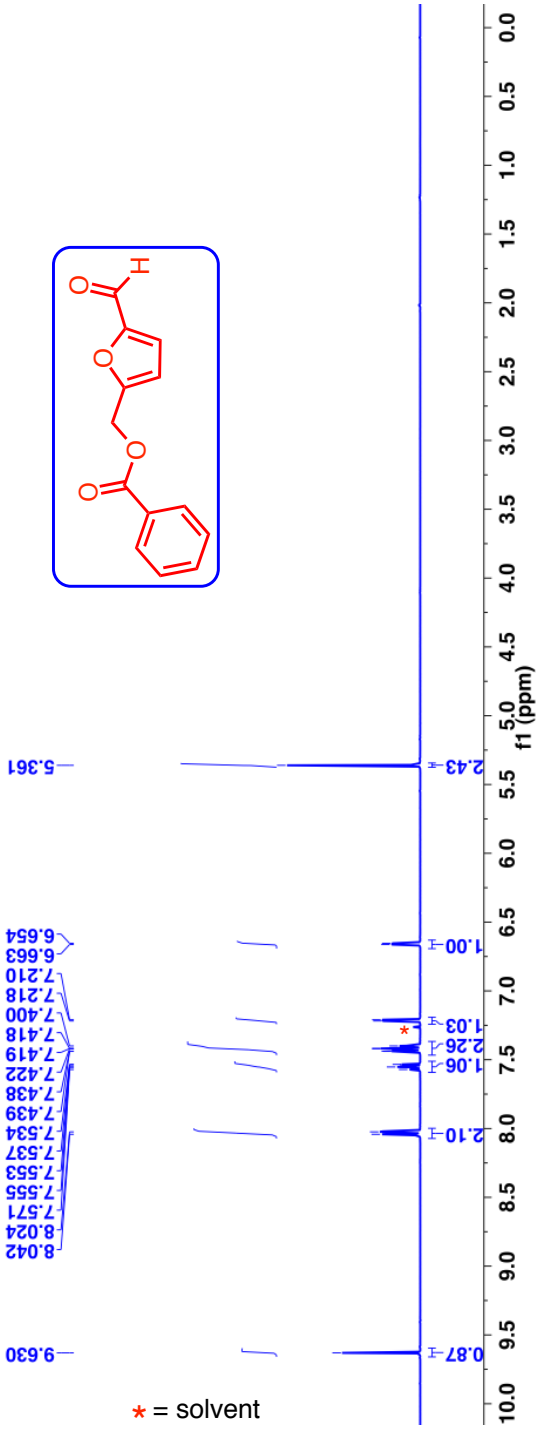

Figure 4.18: ^{1}H-NMR (400 MHz, $CDCl_3$, δ ppm) spectra of benzoyl protected HMF **296a**.

^{13}C-NMR (100 MHz, $CDCl_3$, δ ppm): 58.4, 112.9, 121.9, 128.6, 129.4, 130.0, 133.6, 153.0, 155.7, 166.0 and 178.0.

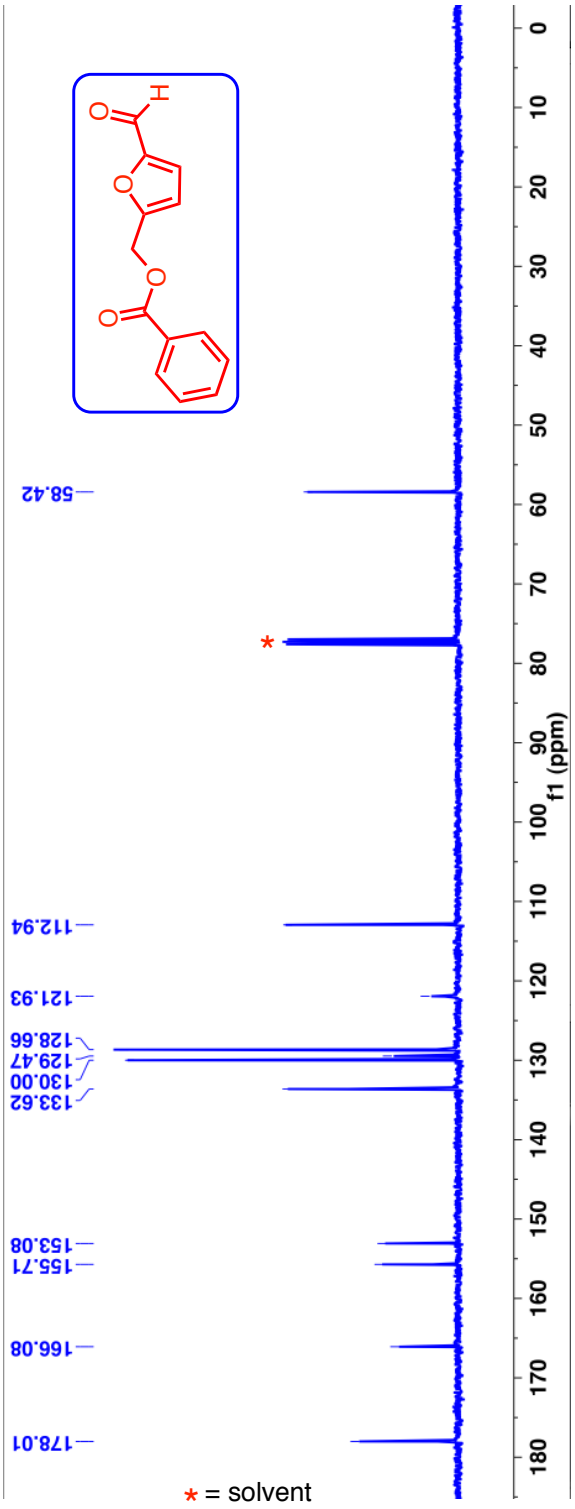

Figure 4.19: ^{13}C-NMR (100 MHz, $CDCl_3$, δ ppm) spectra of benzoyl protected HMF **296a**.

4.11.4. Synthesis of TIPS protected 5-hydroxymethylfurfural 296b

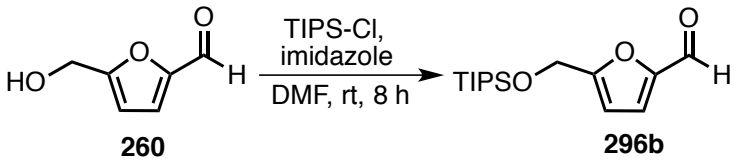

260 **296b**

Scheme 4.21: Synthesis of TIPS protected 5-hydroxymethylfurfural **296b**.

Literature reported procedure was followed for the synthesis of **296b**.[45] To a solution of triisopropylsilyl chloride (1.16 g, 6 mmol, 1.2 *equiv.*,1.28 mL) in DMF (5 mL), imidazole (0.687 g, 10 mmol, 2 *equiv.*), and **260** (0.63 g, 5 mmol, 1 *equiv.*) were added and stirred at room temperature for 8 h. After the reaction, the mixture was diluted with water and extracted with hexane. The organic layer was dried over *anhyd.* Na_2SO_4 and the solvent was removed under reduced pressure. The crude product was purified by column chromatography using hexane-ethyl acetate mixture. Pure compound (**296b**) was obtained as pale yellow viscous liquid.

TLC condition - R_f = 0.80 (85% hexanes: 15% ethyl acetate) for **296b** (Yield = 90%)

HRMS [ESI-MS] *m/z*([M+Na]): Calculated : 305.1543; Observed : 305.1553; |Δm| : 3.3 ppm

^{1}H-NMR (500 MHz, $CDCl_3$, δ ppm): 1.03 (d, 18H, *J* = 7.15 Hz), 1.09-1.16 (m, 3H), 4.80 (s, 2H), 6.47 (d, 1H, *J* = 3.6Hz), 7.18 (d, 1H, *J* = 3.6 Hz) and 9.54 (s, 1H).

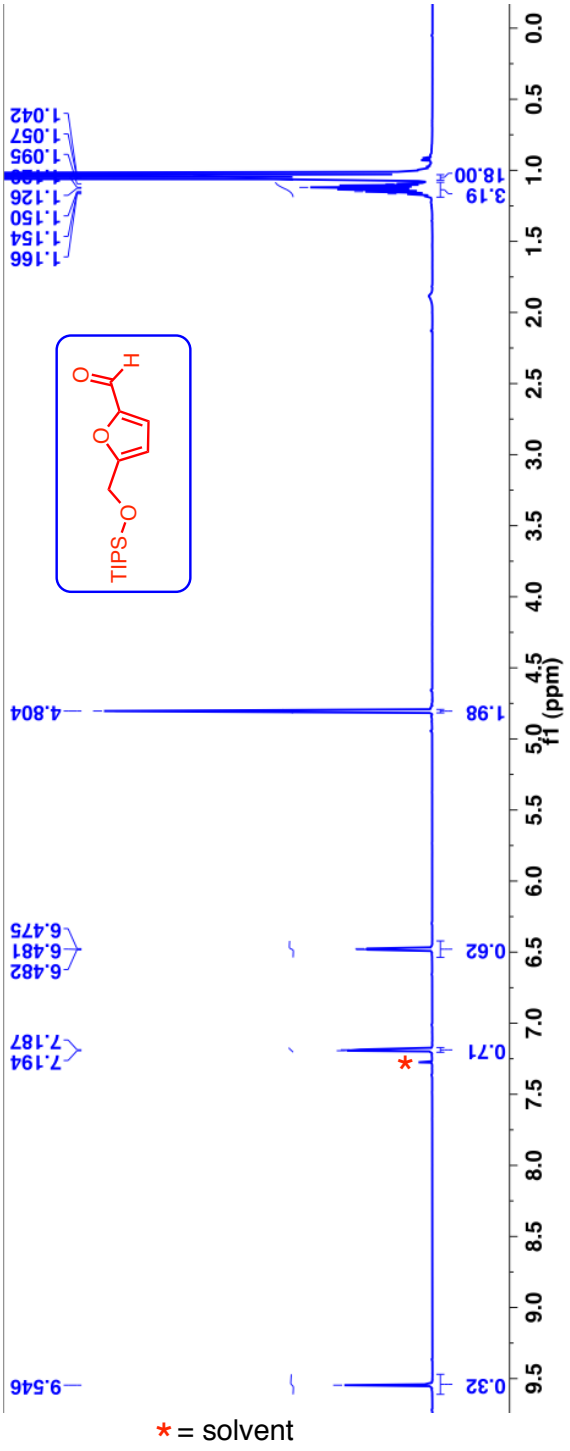

Figure 4.20: ^{1}H-NMR (500 MHz, $CDCl_3$, δ ppm) spectra of TIPS protected HMF **296a**.

^{13}C-NMR (125 MHz, $CDCl_3$, δ ppm): 12.1, 18.0, 59.3, 109.2, 122.7, 152.2, 161.9 and 177.6.

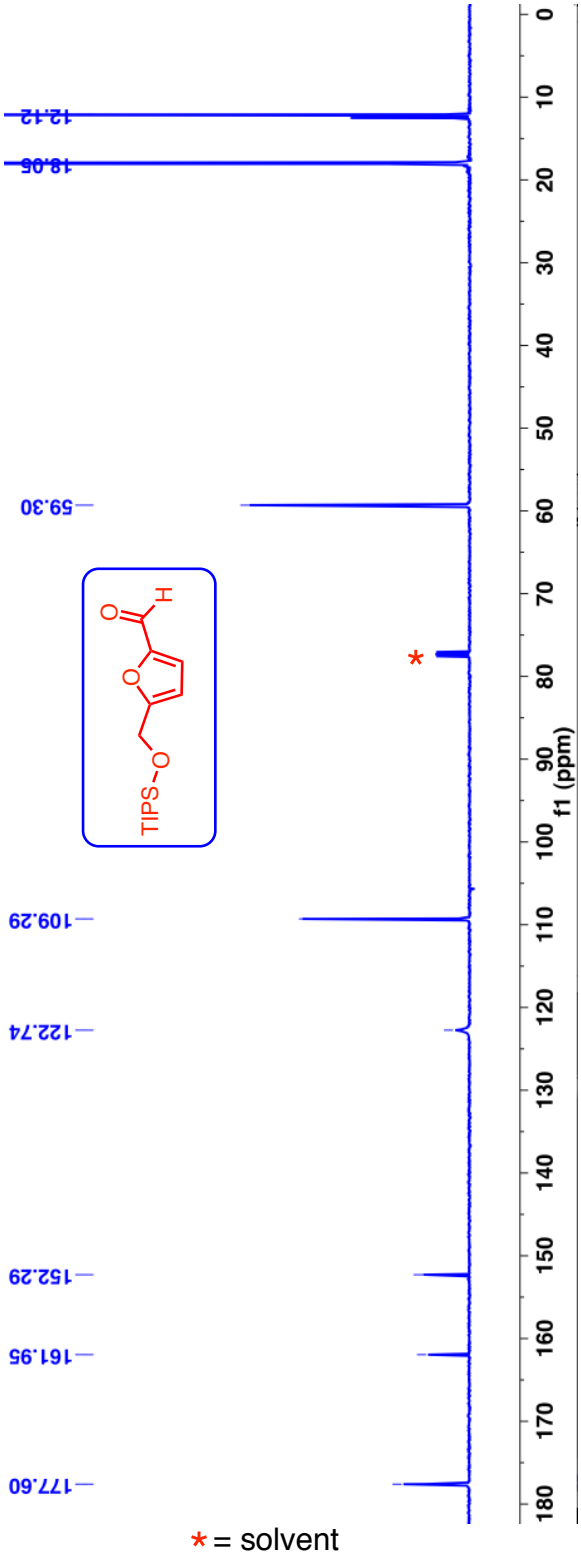

Figure 4.21: ^{13}C-NMR (125 MHz, $CDCl_3$, δ ppm) spectra of TIPS protected HMF **296b**.

4.11.5. Synthesis of 5-((benzoyloxy)methyl)furan-2-carboxylic acid 295a

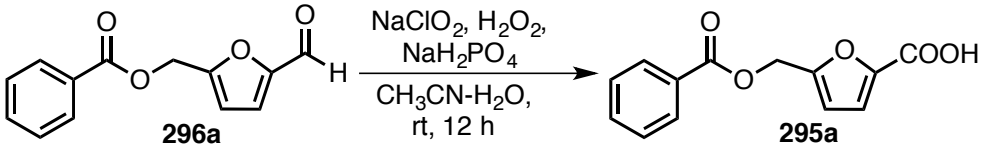

Scheme 4.22: Synthesis of 5-((benzoyloxy)methyl)furan-2-carboxylic acid **295a**.

Literature reported procedure was followed for the synthesis of compound **295a**.[46] To a solution of **296a** (0.23 g, 1 mmol, 1 *equiv.)* in acetonitrile (2 mL) at 0 °C., aq NaH_2PO_4 (50 mg in 0.5 mL of water) was added. To this mixture, 30% aq. H_2O_2 (5 mmol, 5 *equiv.*, 0.6 mL) was added dropwise followed by the addition of aq. $NaClO_2$ (0.135 g, 1.5 mmol, 1.5 *equiv.,2* mL water) over 15 min. The resulting mixture was allowed to warm to room temperature over 12 h. The product precipitated as white solid, which was filtered, washed with excess of water, acetone and dried in high vacuum to give pure product. Compound **295a** was obtained as white solid.

TLC condition - R_f = 0.60 (60% hexanes: 40% ethyl acetate) for **295a** (Yield = 89%)

HRMS [ESI-MS] *m/z*([M+Na]): Calculated : 269.0420; Observed : 269.0430; |Δm| : 3.7 ppm

^{1}H-NMR (500 MHz, DMSO-d_6, δ ppm): 5.33 (s, 2H), 6.64 (d, 1H, *J* = 5 Hz), 6.91 (d, 1H, *J* = 5 Hz), 7.52 (t, 2H, *J* = 10 Hz), 7.66 (t, 1H, *J* = 10 Hz) and 7.96 (d, 2H, *J* = 10 Hz).

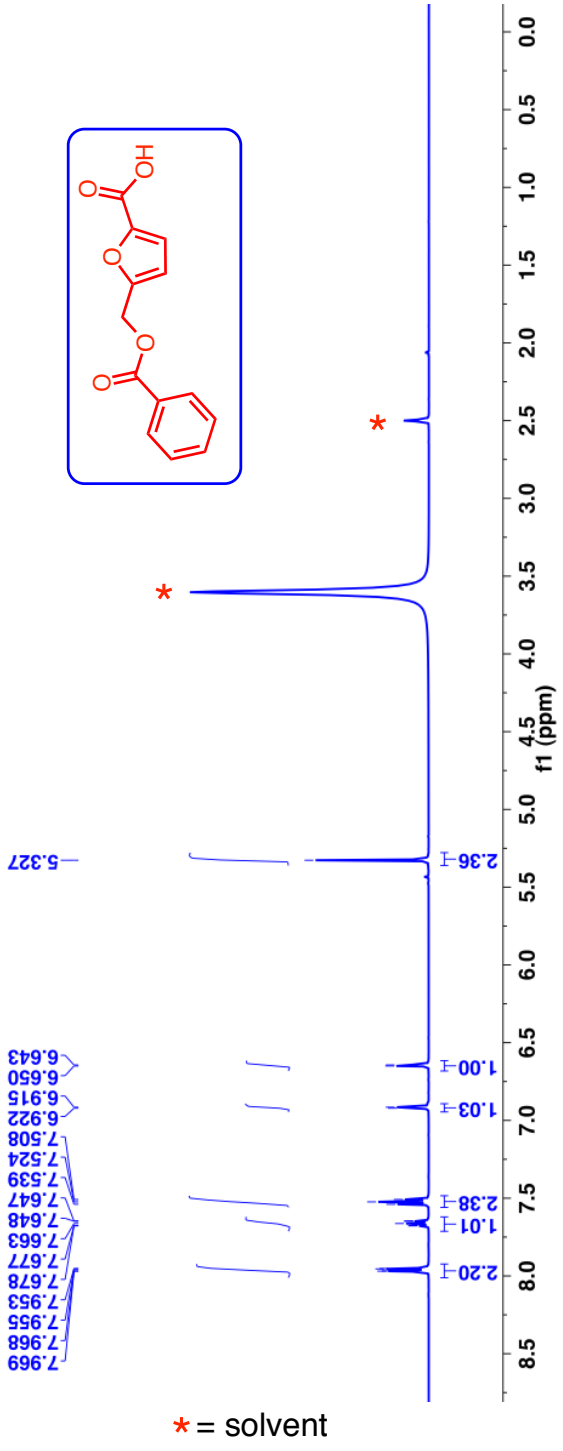

Figure 4.22: ^{1}H-NMR (500 MHz, DMSO-d_6, δ ppm) spectra of acid derivative **295a**.

^{13}C-NMR (125 MHz, DMSO-d_6, δ ppm): 59.1, 113.0, 115.7, 129.6, 129.8, 129.9, 134.2, 150.5, 151.3, 161.2 and 166.0.

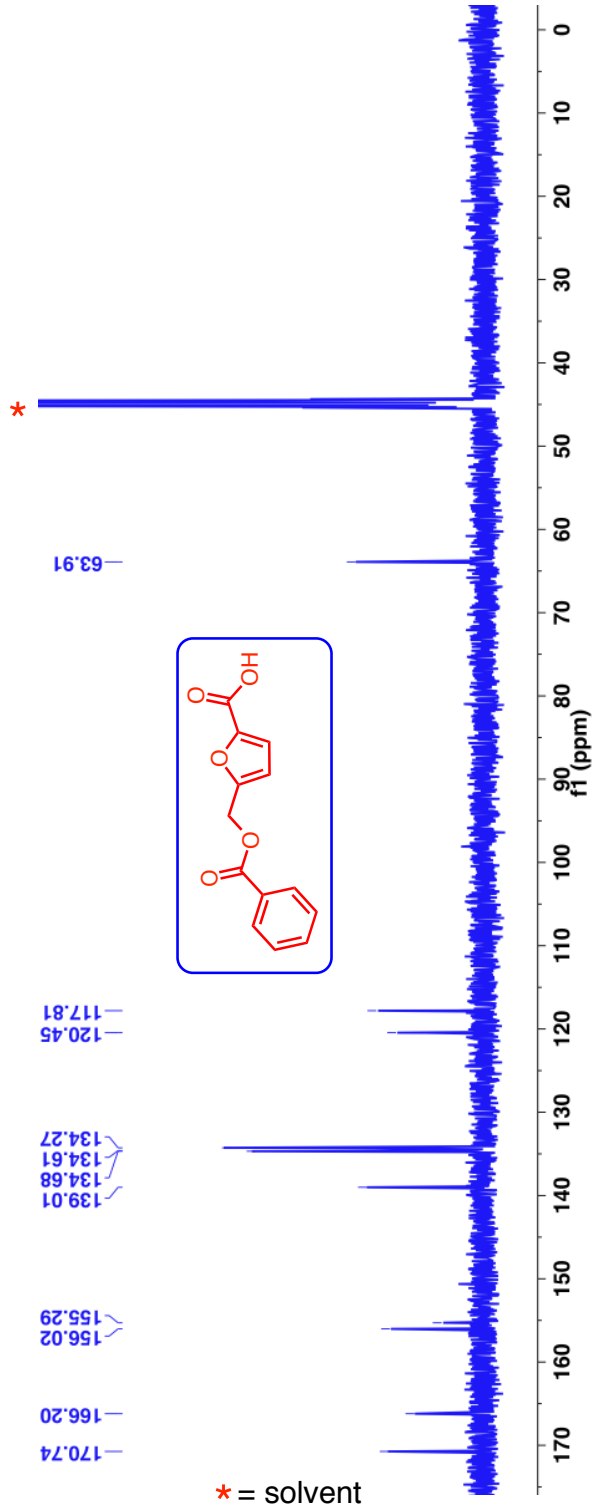

Figure 4.23: ^{13}C-NMR (125 MHz, DMSO-d_6, δ ppm) spectra of acid derivative **295a**.

4.11.6. Synthesis of 5-(((triisopropylsilyl)oxy)methyl)furan-2-carboxylic acid 295b

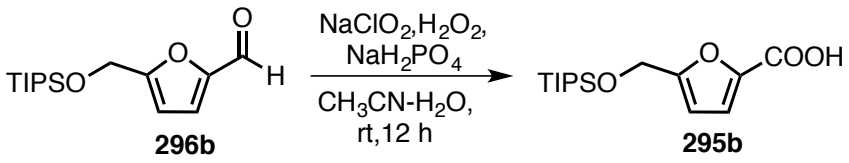

Scheme 4.23: Synthesis of 5-((triisopropylsilyl)methyl)furan-2-carboxylic acid **295b**.

Literature reported procedure was followed for the synthesis of **295b**.[46] To a solution of **296b** (23 g, 0.081 mol, 1 *equiv.*) in acetonitrile (120 mL) at 0 °C, aq. NaH_2PO_4 (7 g in 30 mL of water) was added. To this mixture, 30% aq. H_2O_2 (0.407 mol, 5 *equiv.*, ~50 mL) was added drop wise followed by the drop wise addition of aq. $NaClO_2$ (11.04 g, 0.122 mol, 1.5 *equiv.,*120 mL of water) over 1 h. The resulting mixture was allowed to warm to room temperature over 12 h. After reaction, the mixture was quenched with water and extracted with EtOAc. The organic layer was dried over *anhyd.* Na_2SO_4 and the solvent was removed under reduced pressure to give pure compound **295b** as white semi-solid.

TLC condition - R_f = 0.50 (85% hexanes: 15% ethyl acetate) for **295b** (Yield = 90%)

HRMS [ESI-MS] *m/z*([M+Na]): Calculated : 321.1493; Observed : 321.1491; |Δm| : 0.6 ppm

^{1}H-NMR (500 MHz, $CDCl_3$, δ ppm): 1.09 (d, 18H, *J* = 5 Hz), 1.14-1.21 (m, 3H), 4.85 (s, 2H), 6.47 (d, 1H, *J* = 5 Hz) and 7.30 (d, 1H, *J* = 5Hz).

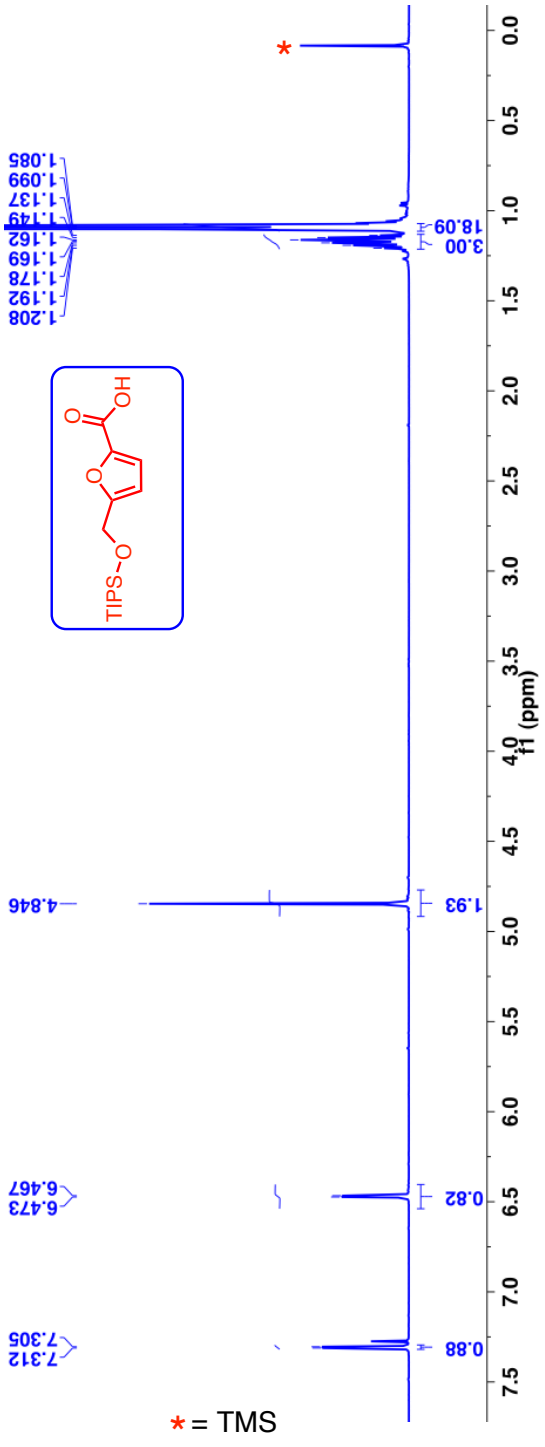

Figure 4.24: ^{1}H-NMR (500 MHz, $CDCl_3$, δ ppm) spectra of TIPS protected acid derivative **295b**.

^{13}C-NMR (100 MHz, $CDCl_3$, δ ppm): 12.1, 18.0, 59.3, 108.9, 121.4, 142.7, 161.0 and 163.8.

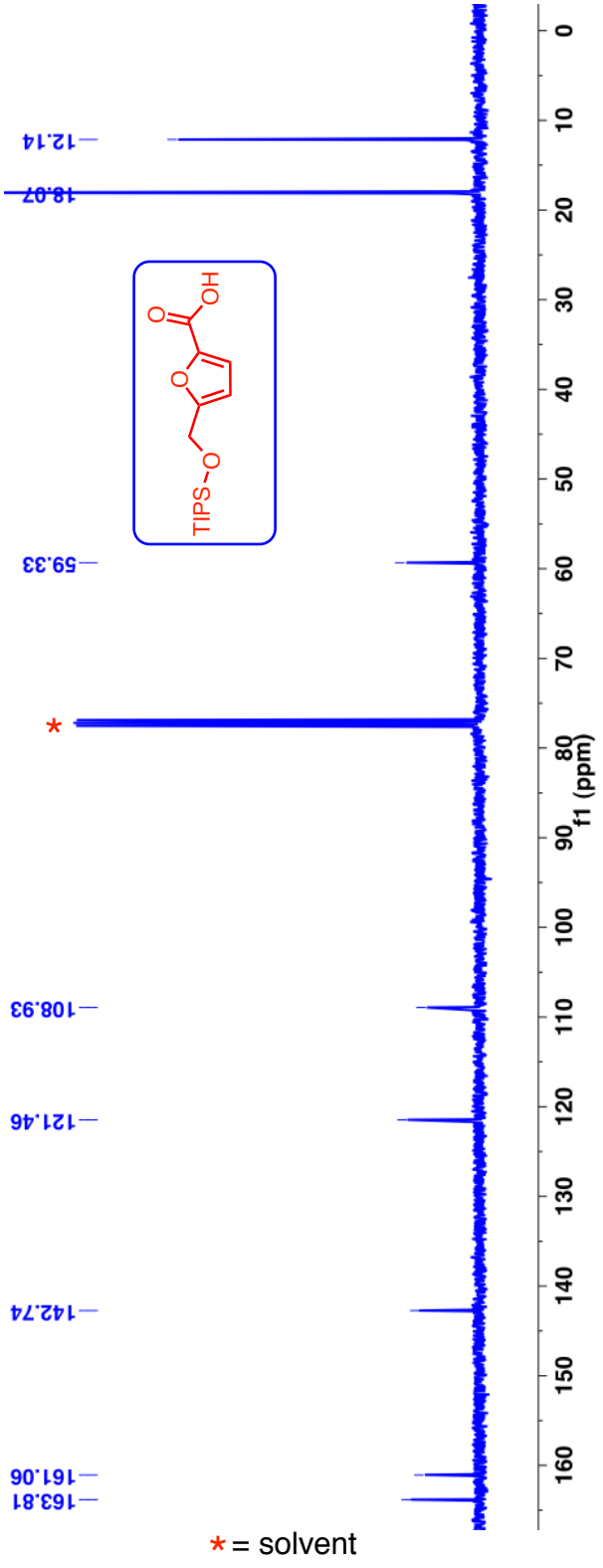

Figure 4.25: ^{13}C-NMR (100 MHz, $CDCl_3$, δ ppm) spectra of TIPS protected HMF **295b**.

4.11.7. Synthesis of 2-nitro-1,3-benzenedicarboxylic acid 293

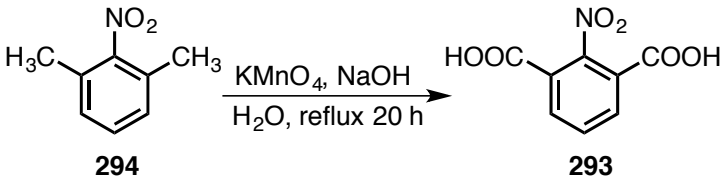

294 **293**

Scheme 4.24: Synthesis of 2-Nitro-1,3-benzenedicarboxylic acid **293**.

Literature reported procedure was followed for the synthesis of **293**.[38] To a stirred solution of 1,3-dimethyl-2-nitrobenzene **294** (15.1 g, 0.1 mol, 1 *equiv.*) in water (750 mL), NaOH (6 g, 0.15 mol, 1.5 *equiv.*) was added and refluxed. To this $KMnO_4$ (60 g, 0.38 mol, 3.8 *equiv.*) was added slowly over a period of 3 h. The resulting mixture was refluxed for 20 h. After the reaction, the mixture was cooled to room temperature and filtered. The filtrate was acidified with *concd.* HCl. The title compound, **293** precipitated out as white solid. The precipitate was filtered, washed with excess water and dried under vacuum.

TLC condition - R_f = 0.60 (90% hexanes: 10% ethyl acetate) for **293** (Yield = 72%)

^{1}H-NMR (500 MHz, DMSO-d_6, δ ppm): 4.91 (s (broad, H_2O + COO*H*), 7.80 (t, 1H, *J* = 10 Hz) and 8.18 (d, 2H, *J* = 10 Hz).

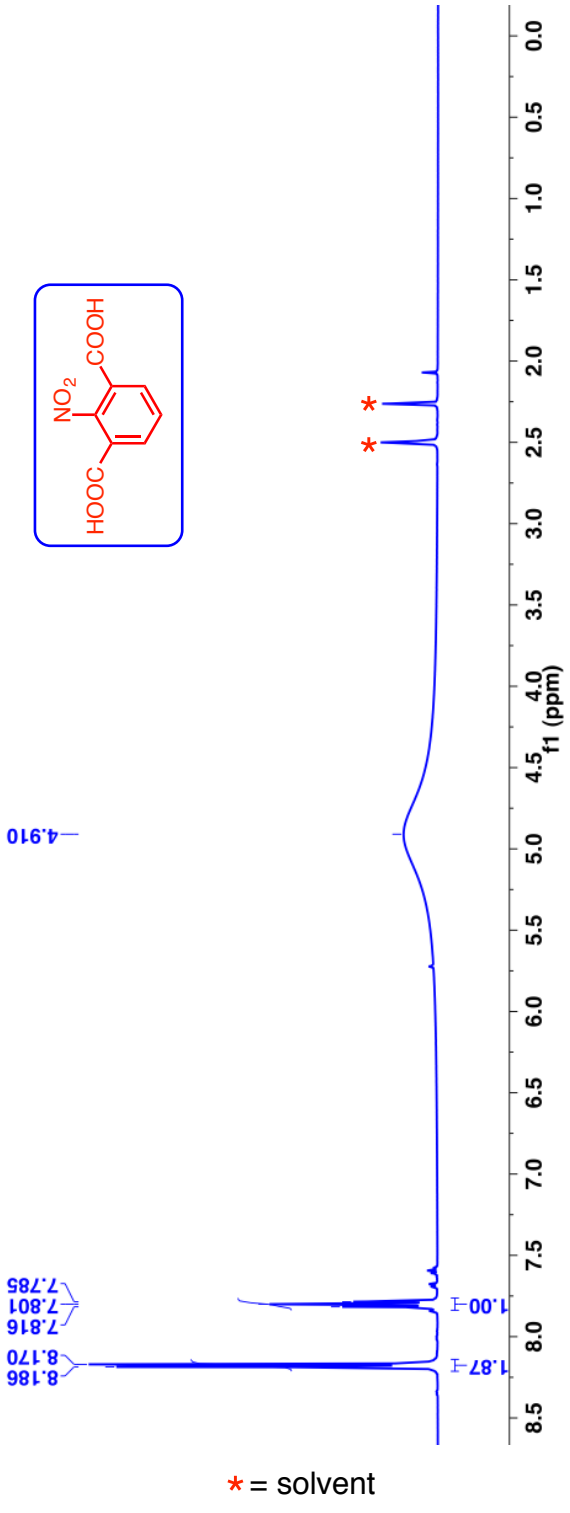

Figure 4.26: ^{1}H-NMR (500 MHz, DMSO-d_6, δ ppm) spectra of nitro acid derivative **293**.

^{13}C-NMR (125 MHz, DMSO-d_6, δ ppm): 125.4, 131.8, 135.2, 149.4 and 164.8.

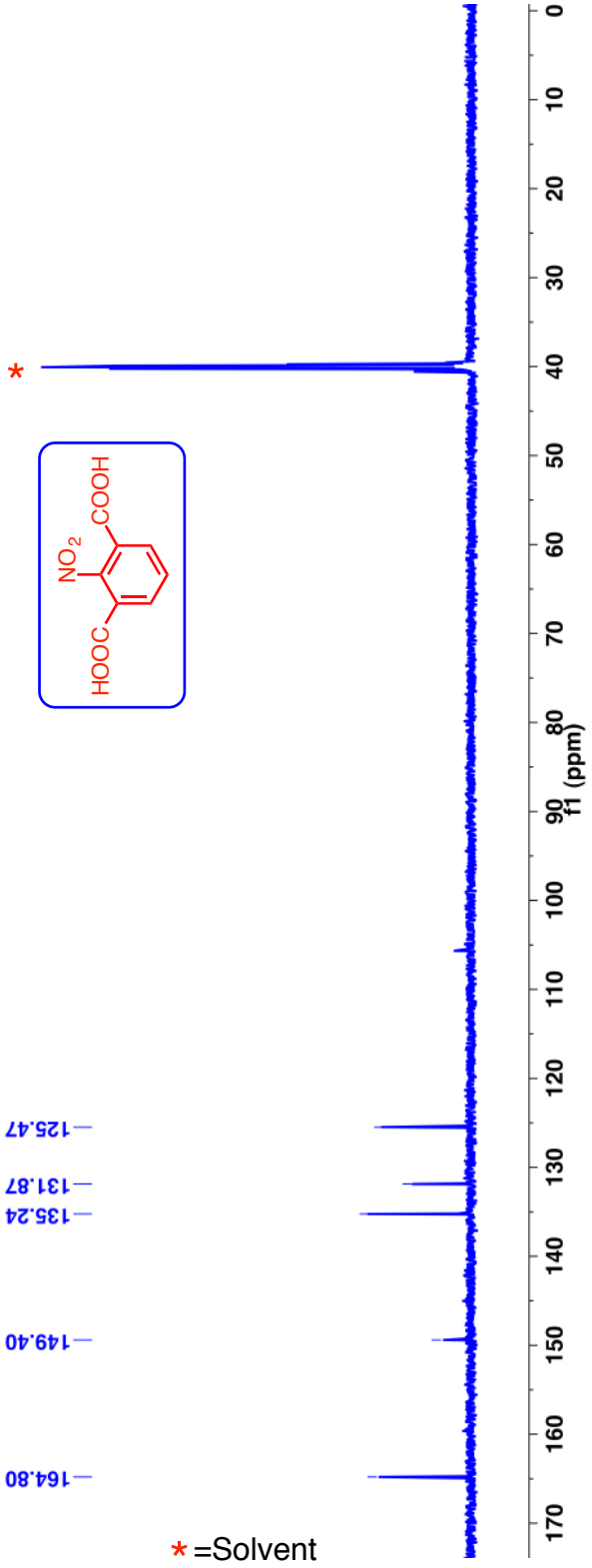

Figure 4.27: ^{13}C-NMR (125 MHz, DMSO-d_6, δ ppm) spectra of nitro acid derivative **293**.

4.11.8. Synthesis of 2-nitro-1,3-benzenedimethanol 292

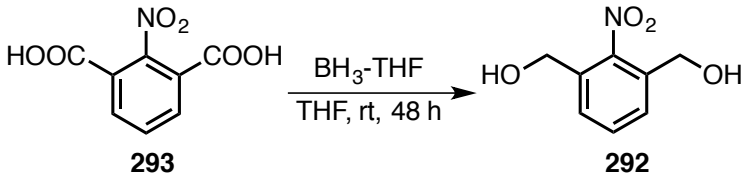

293 **292**

Scheme 4.25: Synthesis of 2-Nitro-1,3-benzenedimethanol **292**.

2-Nitro-1,3-benzenedimethanol **292** was synthesized according to a procedure reported in the literature.[38] To a solution of 2-nitro-1,3-benzenedicarboxylic acid (**293**) (1.25 g, 5.9 mmol, 1 *equiv.*) in THF, BH_3-THF complex (1.0 M in THF. 2.53 g, 29.5 mmol, 5 *equiv*., 29.5 mL) was added at 0 °C over 1 h. The resulting mixture was allowed to warm to room temperature over 48 h. After reaction, THF was removed under vacuum; the reaction mixture was quenched with water, and extracted with EtOAc. The combined organic layer was dried over *anhyd.* Na_2SO_4 and solvent were removed under reduced pressure to give crude product. Crude product was purified by column chromatography (hexane-EtOAc). 2-Nitro-1,3-benzenedimethanol **292** was obtained as a white solid.

TLC condition - R_f = 0.8 (95% DCM: 05% Methanol) for **292** (Yield = 81%)

^{1}H-NMR (500 MHz, DMSO-d_6, δ ppm): 4.53 (d, 4H, *J* = 5 Hz), 5.50 (t, 2H, *J* = 5 Hz) and 7.52-7.57 (m, 3H).

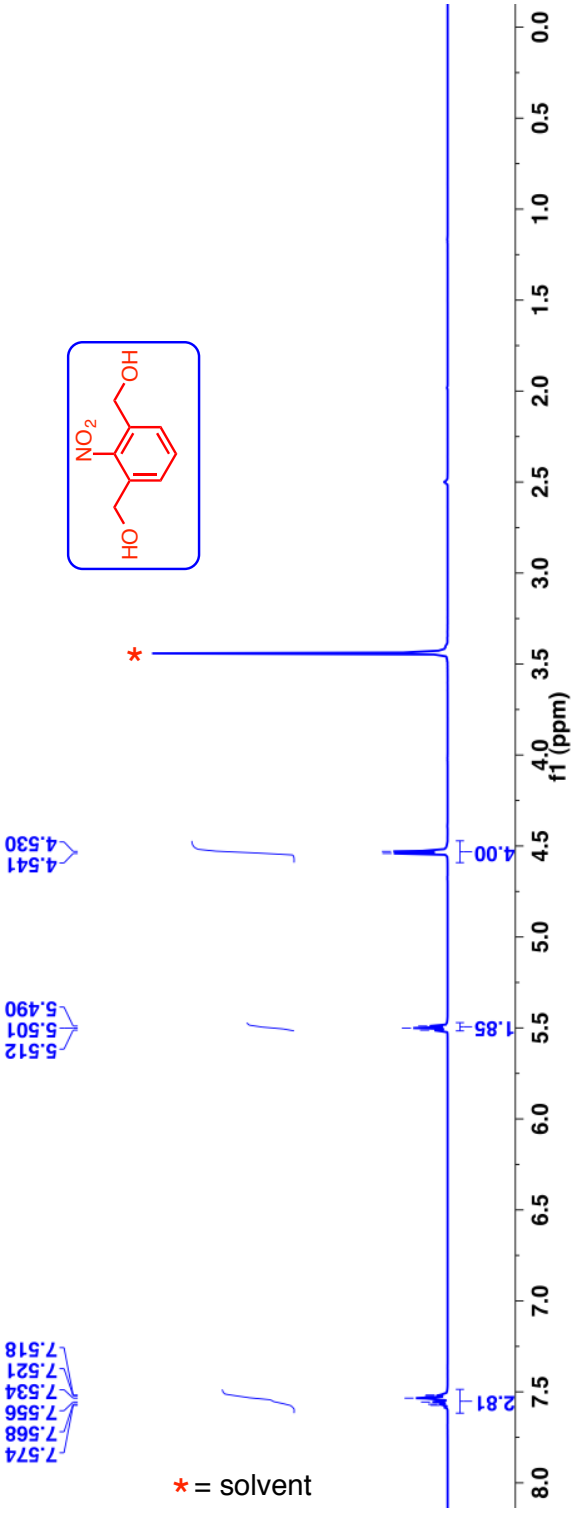

Figure 4.28: ^{1}H-NMR (500 MHz, DMSO-d_6, δ ppm) spectra of alcohol derivative **292**.

^{13}C-NMR (125 MHz, DMSO-d_6, δ ppm): 64.6, 132.9, 136.2, 139.7 and 152.8.

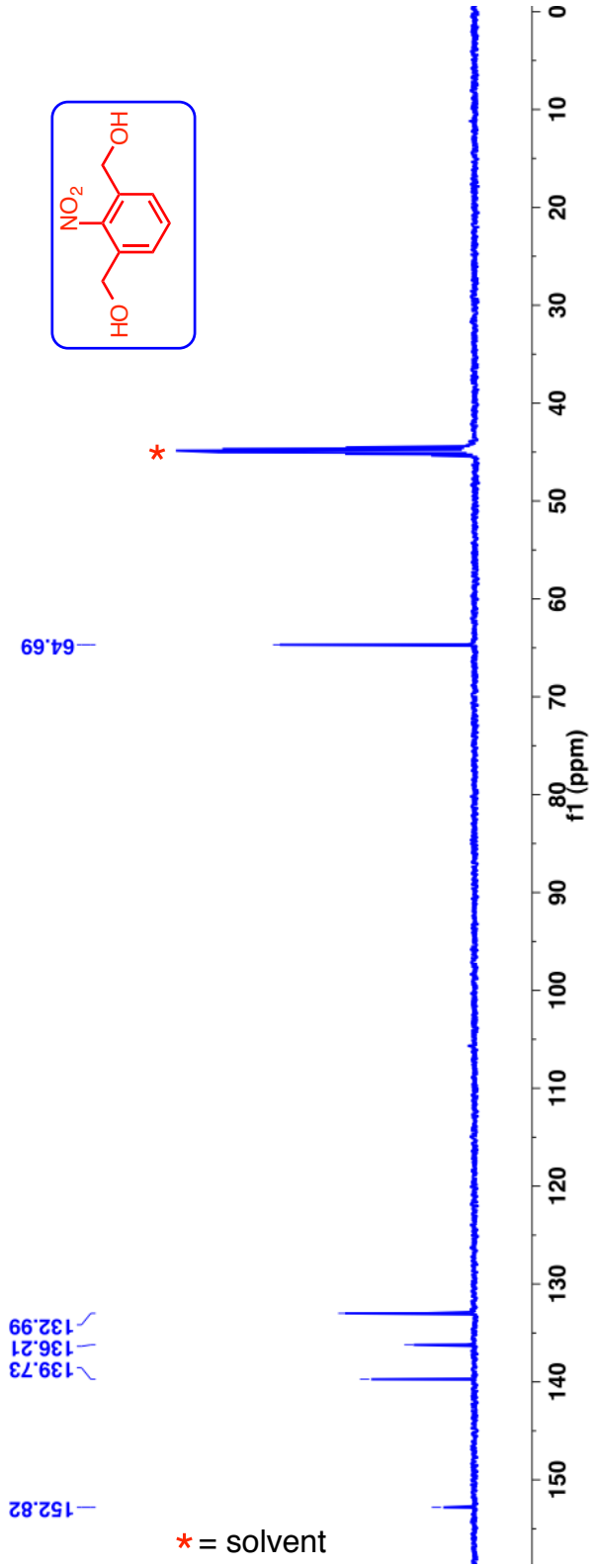

Figure 4.29: ^{13}C-NMR (125 MHz, DMSO-d_6, δ ppm) spectra of alcohol derivative **292**.

4.11.9. Synthesis of ester derivative 290a

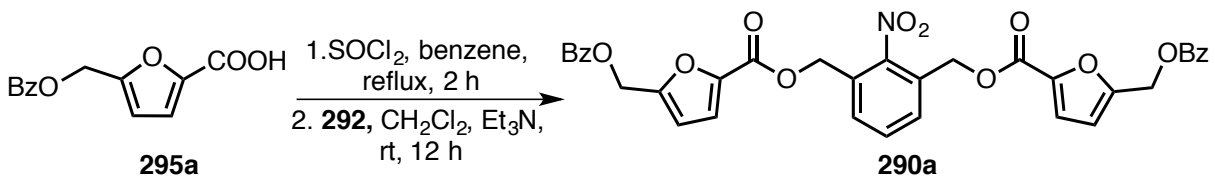

Scheme 4.26: Synthesis of ester derivative **290a**.

To a solution of acid **295a** (2.46 g, 10 mmol, 1 *equiv*.) in benzene (15 mL), $SOCl_2$ (1.784 g, 15 mmol, 1.5 *equiv.* 1.1 mL) was added and refluxed for 2 h. Benzene and excess $SOCl_2$ was removed by distillation and dried under vacuum. The residue was dissolved in CH_2Cl_2 (15 mL) and added drop wise to a solution of 2-nitro-1,3-benzenedimethanol **292** (0.91 g, 5 mmol, 0.5 *equiv.*) and Et_3N (2.53 g, 25 mmol, 2.5 *equiv.*, 3.5 mL) in CH_2Cl_2 (15 mL) and stirred at room temperature for 12 h. After the reaction, the mixture was quenched with water, extracted with CH_2Cl_2. The organic layer was dried over *anhyd.* Na_2SO_4 and the solvent was removed under reduced pressure. The crude product was purified by column chromatography hexanes-EtOAc mixture. The ester **290a** was obtained as white solid.

TLC condition - R_f = 0.30 (60% hexanes: 40% ethyl acetate) for **290a** (Yield = 69%)

HRMS [ESI-MS] *m/z*([M+Na]): Calculated : 662.1269; Observed : 662.1279; |Δm| : 1.5 ppm

FT-IR (KBr) cm^{-1}: 1745 (ν_{CO}, 1532 ($_{asym}\nu_{NO2}$), 1364 ($_{sym}\nu_{NO2}$)

^{1}H-NMR (400 MHz, $CDCl_3$, δ ppm): 5.36 (s, 2H), 5.47 (s, 2H), 6.61 (d, 1H, *J* = 3.45 Hz), 7.19 (d, 1H, *J* = 5 Hz), 7.45 (t, 2H, J = 5 Hz), 7.54-7.61 (m, 3H) and 8.06 (d, 2H, *J* = 5 Hz).

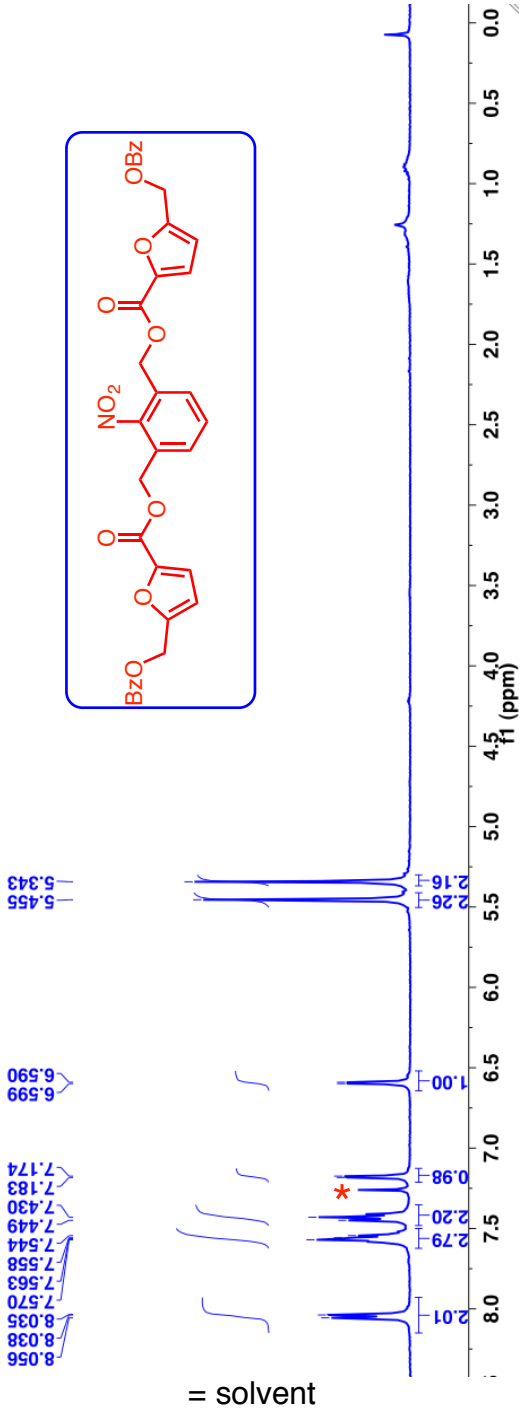

Figure 4.30: ^{1}H-NMR (400 MHz, $CDCl_3$, δ ppm) spectra of ester derivative **290a**.

^{13}C-NMR (100 MHz, $CDCl_3$, δ ppm): 58.4, 62.6, 94.6, 112.6, 119.9, 128.6, 129.5, 129.6, 130.0, 130.3, 131.5, 133.5, 144.0, 154.5, 157.8 and 166.1.

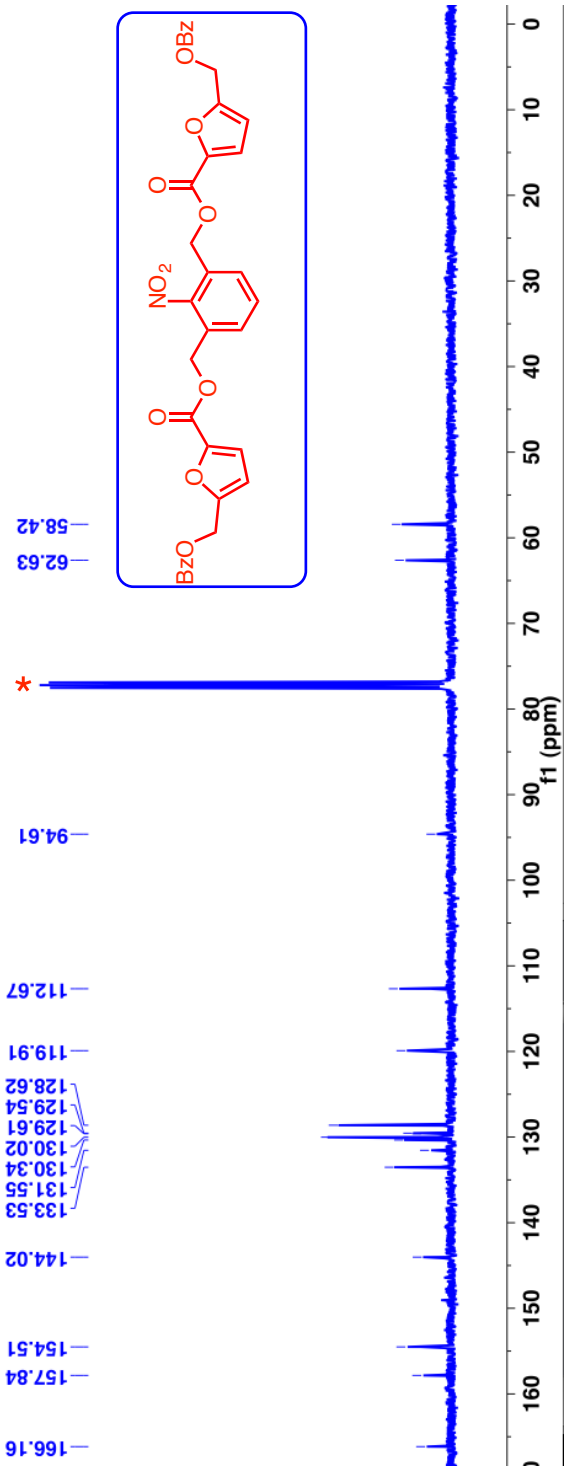

= solvent

Figure 4.31: ^{13}C-NMR (100 MHz, $CDCl_3$, δ ppm) spectra of ester derivative **290a**.

4.11.10. Synthesis of ester derivative 290b

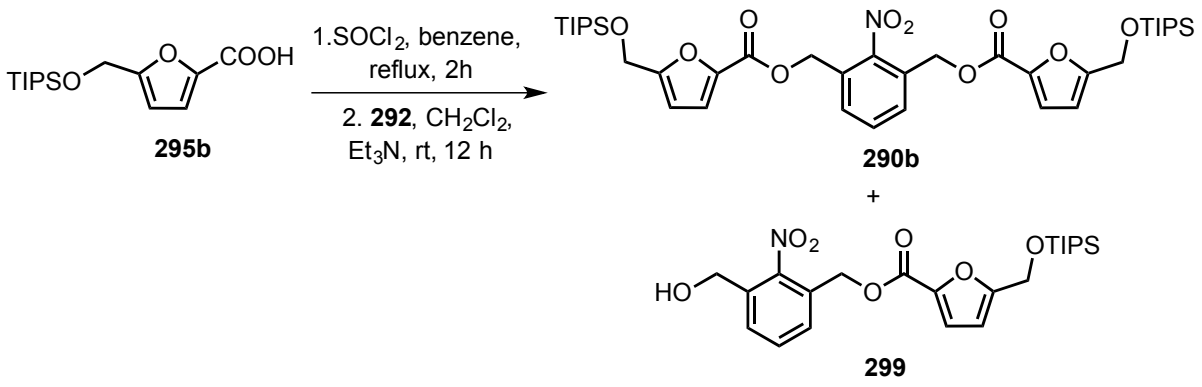

Scheme 4.27: Synthesis of ester derivative **290b**.

To a solution of **295b** (0.149 g, 0.5 mmol, 1 *equiv.*) in benzene (5 mL), $SOCl_2$ (0.089 g, 0.75 mmol, 1.5 *equiv.* 54 µL) was added and refluxed for 2 h. Benzene and excess $SOCl_2$ was distilled and the residue was dried under vacuum. The residue was dissolved in CH_2Cl_2 (5 mL) and added drop wise to a solution of 2-nitro-1,3-benzenedimethanol **292** (0.046 g, 0.25 mmol, 0.5 equiv.) and Et_3N (0.126 g, 1.25 mmol, 2.5 equiv., 0.174 mL) in CH_2Cl_2 (5 mL) and stirred for 12 h at room temperature. After the reaction, the mixture was quenched with water, extracted with CH_2Cl_2. The organic layer was dried over *anhyd.* Na_2SO_4 and concentrated under reduced pressure. Crude product was purified by column chromatography using hexanes-EtOAc mixture. The ester **290b** was obtained as colorless viscous oil and monoester **299** was obtained as minor product.

Compound **290b:**

TLC condition - R_f = 0.60 (60% hexanes: 40% ethyl acetate) for **290b** (Yield = 59%)

HRMS [ESI-MS] *m/z*([M+Na]): Calculated : 766.3413; Observed : 766.3434; |Δm| : 2.7 ppm

^{1}H-NMR (500 MHz, $CDCl_3$, δ ppm): 1.08 (d, 36H, *J* = 10 Hz), 1.12-1.18 (m, 6H), 4.81 (s, 4H), 5.45 (s, 4H), 6.41 (d, 2H, *J* = 5 Hz), 7.17 (d, 2H, *J* = 5 Hz) and 7.53-7.58 (m, 3H).

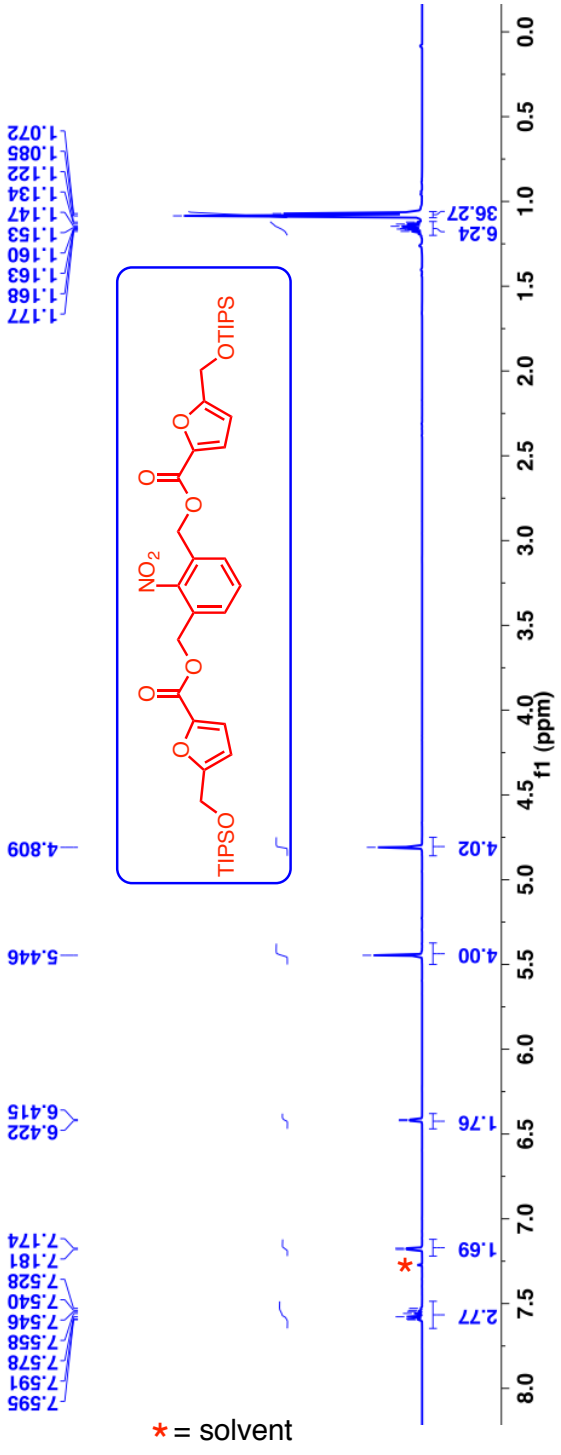

Figure 4.32: ^{1}H-NMR (500 MHz, $CDCl_3$, δ ppm) spectra of ester derivative **290b**.

^{13}C-NMR (125 MHz, $CDCl_3$, δ ppm): 12.1, 18.1, 59.2, 62.3, 108.7, 120.2, 129.7, 130.1, 131.5, 142.7, 148.9, 158.1 and 160.4.

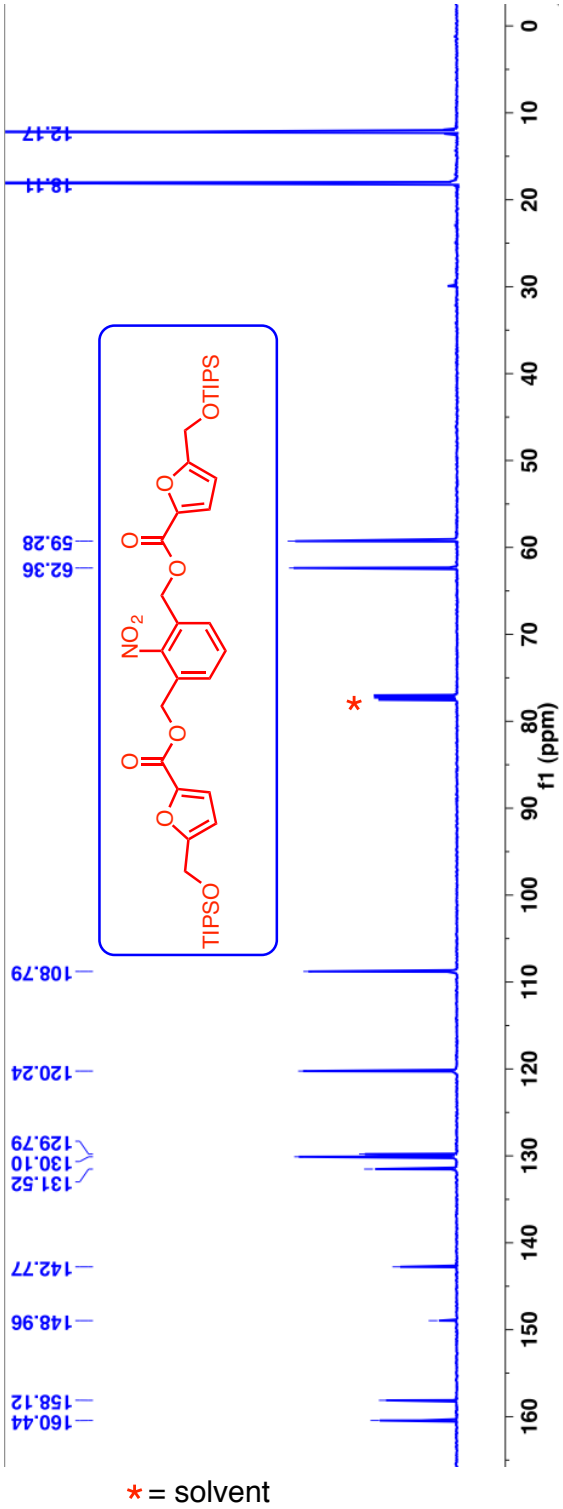

Figure 4.33: ^{13}C-NMR (125 MHz, $CDCl_3$, δ ppm) spectra of ester derivative **290b**.

Compound **299**:

TLC condition - R_f = 0.50 (60% hexanes: 40% ethyl acetate) for **299** (Yield = 10%)

HRMS [ESI-MS] *m/z*([M+Na]): Calculated : 486.1919; Observed : 486.1913; |Δm| : 1.2 ppm

^{1}H-NMR (400 MHz, $CDCl_3$, δ ppm): 1.09 (d, 18H, *J* = 4 Hz), 1.13-1.20 (m, 3H), 2.25, (s (broad), 1H), 4.77 (s, 2H), 4.83 (s, 2H), 5.46 (s, 2H), 6.43 (d, 1H, *J* = 4 Hz), 7.18 (d, 1H, *J* = 4 Hz), 7.56-7.60 (m, 2H) and 7.63-7.65 (m, 1H).

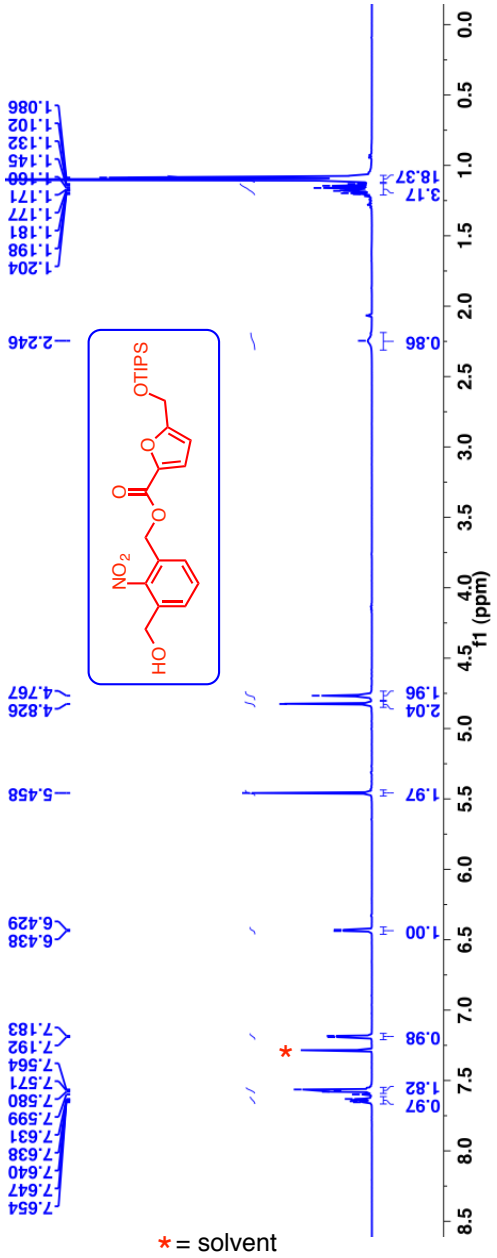

Figure 4.34: ^{1}H-NMR (400 MHz, $CDCl_3$, δ ppm) spectra of alcohol derivative **299**.

^{13}C-NMR (100 MHz, $CDCl_3$, δ ppm): 11.9, 17.8, 59.0, 61.5, 62.2, 108.5, 119.9, 129.3, 129.4, 129.8, 131.6, 134.2, 142.5, 148.5, 157.9 and 160.2.

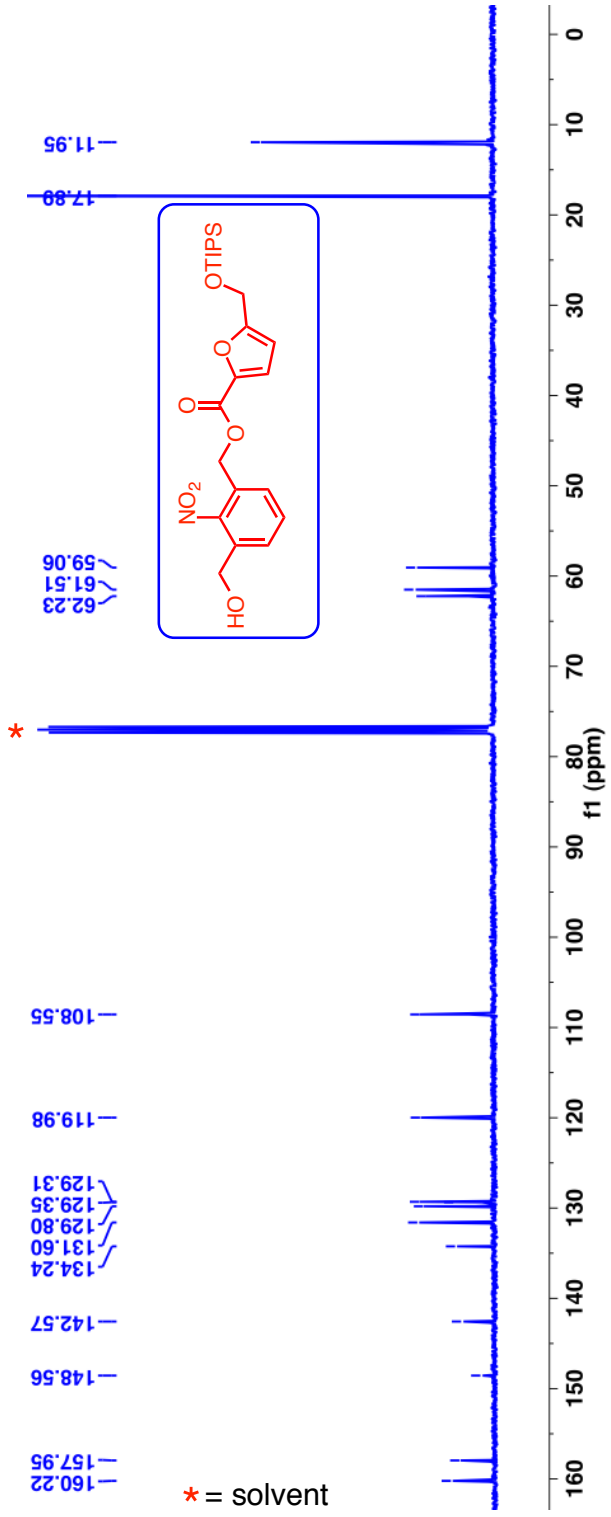

Figure 4.35: ^{13}C-NMR (100 MHz, $CDCl_3$, δ ppm) spectra of alcohol derivative **299**.

4.11.11. Synthesis of ester derivative 291

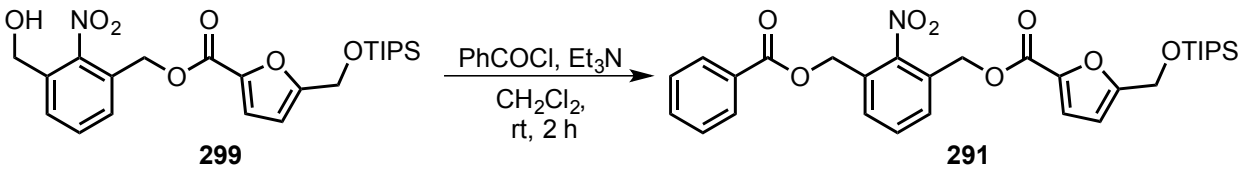

299 **291**

Scheme 4.28: Synthesis of ester derivative **291**.

To a solution of **299** (0.463 g, 1 mmol, 1 *equiv.*) in CH_2Cl_2 (25 mL), Et_3N (0.151 g, 1.5 mmol, 1.5 *equiv.*, 0.21 mL) was added followed by drop wise addition of benzoyl chloride (0.168 g, 1.2 mmol, 1.2 equiv., 0.14 mL). The reaction mixture was stirred for 2 h at room temperature. After the reaction, the mixture was quenched with *satd.* $NaHCO_3$ solution, extracted with CH_2Cl_2. The combined organic layer was dried over *anhyd.* Na_2SO_4 and concentrated under reduced pressure. The crude product was purified by column chromatography using hexanes:EtOAc mixture. The pure compound **291** was obtained as colorless viscous oil (which solidifies upon cooling).

TLC condition - R_f = 0.60 (70% hexanes: 30% ethyl acetate) for **291** (Yield = 93%)

HRMS [ESI-MS] *m/z*([M+Na]): Calculated : 590.2181; Observed : 590.2184; |Δm| : 0.5 ppm

^{1}H-NMR (400 MHz, $CDCl_3$, δ ppm): 1.09 (d, 18H, *J* = 4 Hz), 1.20-1.13 (m, 3H), 4.83 (s, 2H), 5.47 (s, 2H), 5.51 (s, 2H), 6.43 (d, 1H, *J* = 4 Hz), 7.19 (d, 1H, *J* = 4 Hz), 7.45-7.49 (m, 2H), 7.55-7.63 (m, 4H) and 8.04-8.06 (m, 2H).

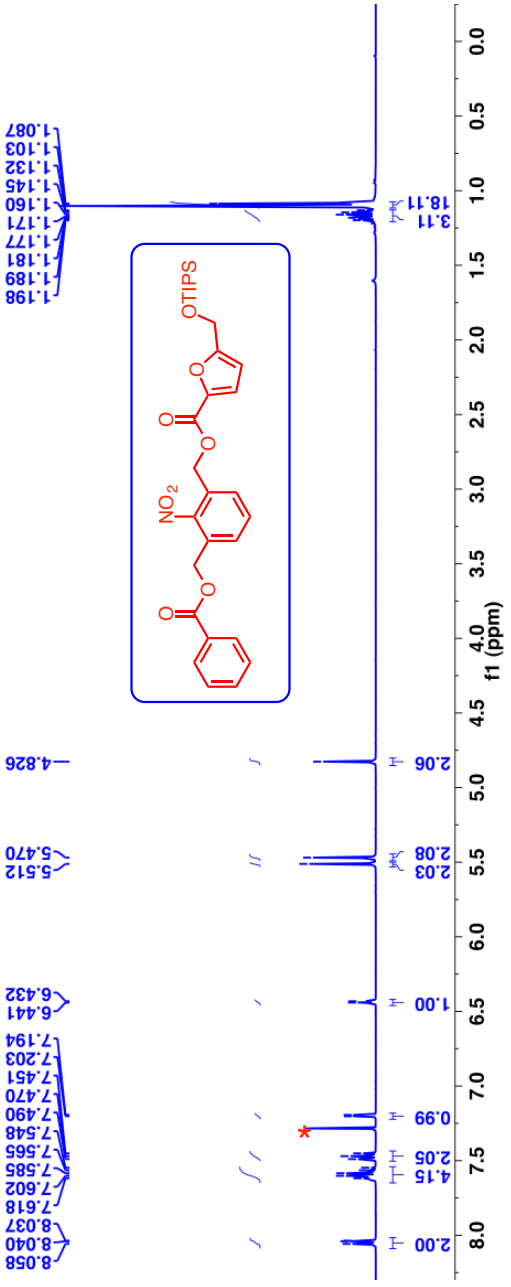

Figure 4.36: ^{1}H-NMR (400 MHz, $CDCl_3$, δ ppm) spectra of ester derivative **291**.

^{13}C-NMR (100 MHz, $CDCl_3$, δ ppm): 11.9, 17.9, 59.0, 62.1, 62.6, 108.5, 120.0, 128.5, 129.3, 129.5, 129.7, 129.8, 129.9, 130.0, 131.2, 133.4, 142.5, 148.9, 157.9, 160.2 and 165.8.

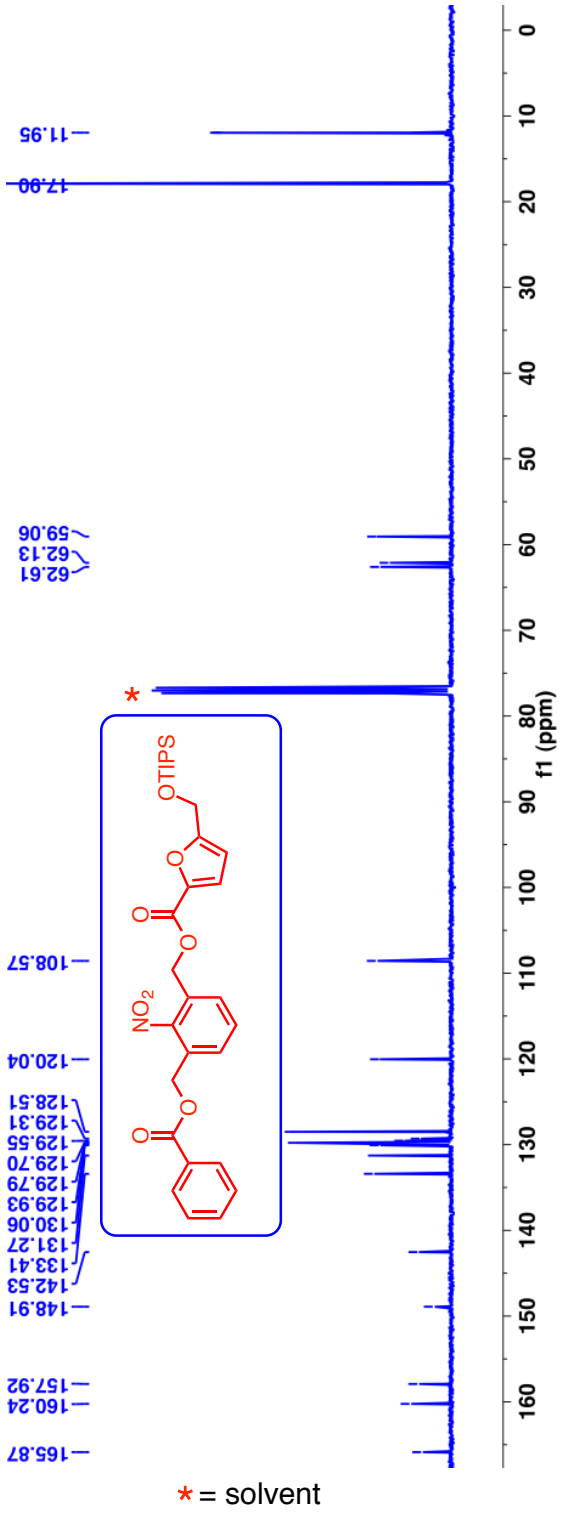

Figure 4.37: ^{13}C-NMR (100 MHz, $CDCl_3$, δ ppm) spectra of ester derivative **291**.

4.11.12. Synthesis of polymer/oligomer 287

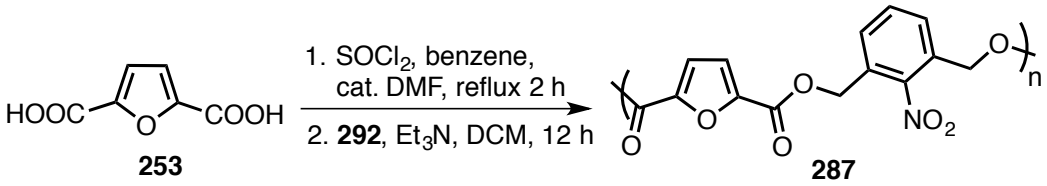

253 287

Scheme 4.29: Synthesis of polymer/oligomer **287**.

To a solution of **253** (0.312 g, 2 mmol, 1 *equiv.*) in dry benzene (15 mL), $SOCl_2$ (0.713 g, 6 mmol, 3 *equiv.* 0.5 mL) and DMF (0.2 mL) were added and were refluxed for 2 h. After 2 h, benzene and excess $SOCl_2$ were distilled and dried under vacuum. The residue was dissolved in CH_2Cl_2 (10 mL) and added drop wise to a solution of 2-nitro-1,3-benzenedimethanol **292** (0.183 g, 1 mmol, 0.5 *equiv.*) and Et_3N (0.606 g, 6 mmol, 3 *equiv.*, 0.8 mL) in CH_2Cl_2 (10 mL) and continued stirring for 12 h at room temperature. After the reaction, pale brown solid was precipitated. It was filtered and washed with methanol (3 x ~25 mL) to remove any unreacted monomer. Followed by washing with DCM (2 x 20 mL) and acetone (2 x 20 mL) to remove low molecular weight oligomer. The insoluble material obtained was pale yellow solid (**287**) in 0.175 g. It was insoluble in common organic solvents such as DMSO, DMF, CH_2Cl_2, EtOAc, MeOH, THF and $CHCl_3$. It was characterized by ^1H, ^{13}C NMR in DMSO-d_6 (the suspension was heated at 60-80 ^oC to make it completely soluble), IR spectroscopy, GPC, TGA, DSC and PXRD. For GPC analysis, the compound was suspended in THF and sonicated for 5 h at room temperature. The residue was filtered and the supernatant was injected in the GPC.

Yield: 0.175 g (insoluble portion)

^{1}H-NMR (400 MHz, DMSO-d_6, δ ppm): 5.29, (s, 0.47 H), 5.48 (s, 4H), 7.41 (s, 2H), 7.54 (s, 0.23 H), 7.64 (d, 0.39 H, J = 8 Hz) and 7.73-7.77 (m, 3H).

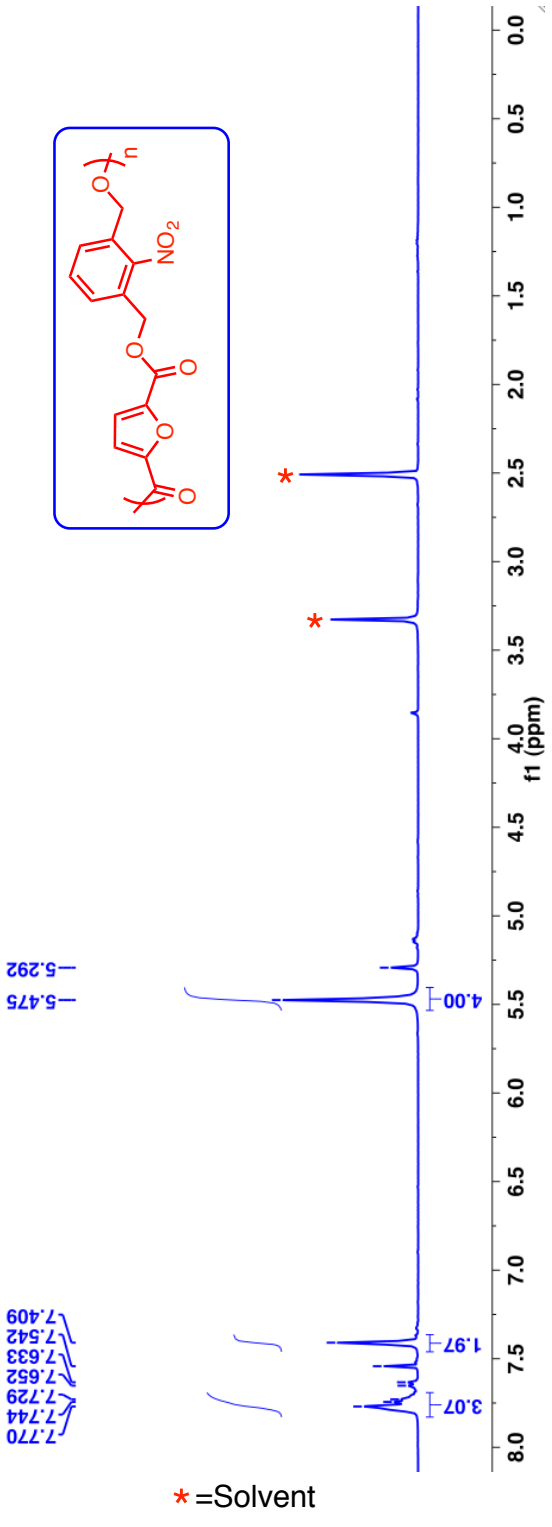

Figure 4.38: ^{1}H-NMR (400 MHz, DMSO-d_6, δ ppm) spectra of polymer/oligomer **287**.

^{13}C-NMR (100 MHz, DMSO-d_6, δ ppm): 63.2, 120.1, 129.1, 131.2, 132.5, 146.1, 148.4 and 157.0.

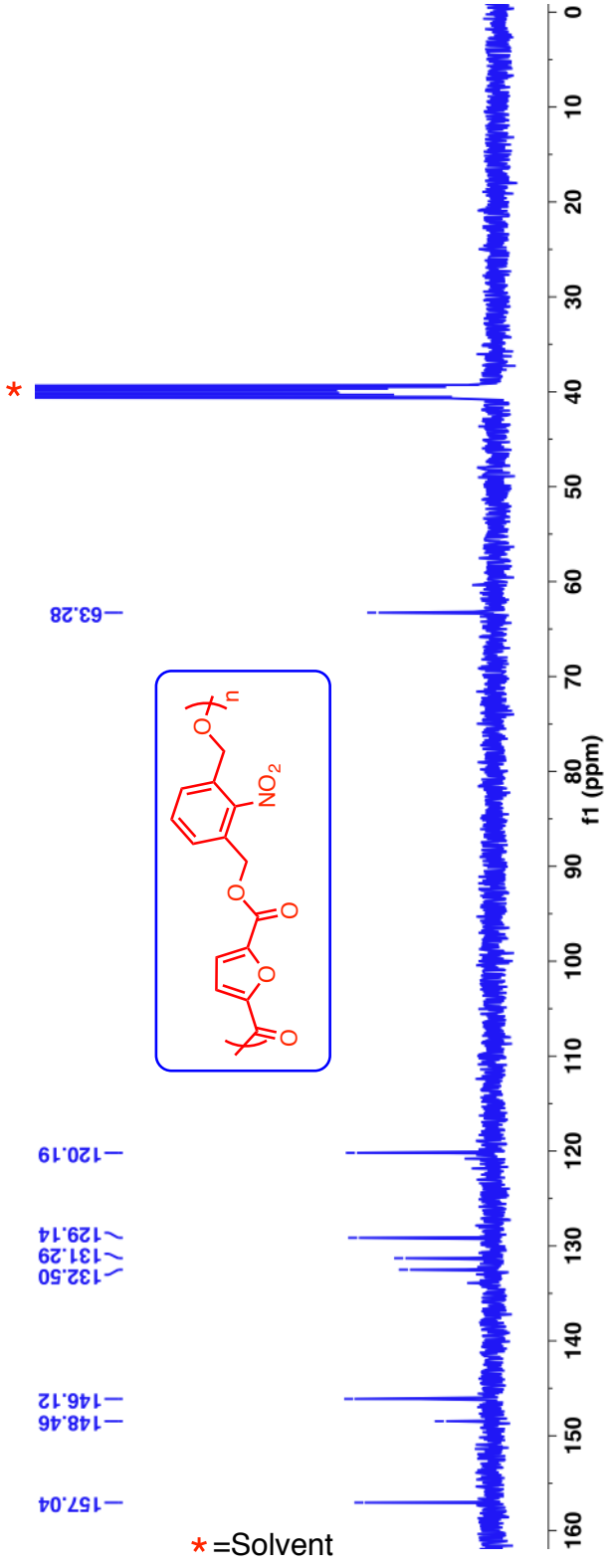

Figure 4.39: ^{13}C-NMR (100 MHz, DMSO-d_6, δ ppm) spectra of polymer /oligomer **287**.

IR (KBr) cm^{-1}: 1739 ($v_{C=O}$), 1529(asym. v_{NO2}), 1367 (sym. $_{NO2}$), 1129 (v_{C-O}).

%Crystallinity of compound **287** was determined by PXRD data It is calculated to be 20.26% with respect to Cristobalite (98% crystallinity) as standard.

The above experiment was repeated at least three times to check the reproducibility of the crystallinity of the product formed. PXRD patterns are almost identical

%Crystallinity of compound **287** synthesized for second and third time are found to be 19.93% and 21.47% respectively.

4.11.13. Synthesis of co-polymer/oligomer 288

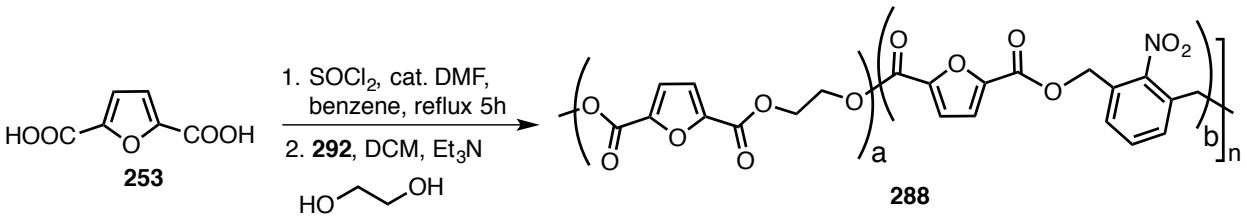

Scheme 4.30: Synthesis of co-polymer/oligomer **288**.

To a solution of 2,5-furan dicarboxylic acid (FDCA) **253** (0.468 g, 3 mmol, 1 *equiv.*) in dry benzene (15 mL), $SOCl_2$ (2.14 g, 18 mmol, 6 *equiv.* 1.3 mL) and catalytic amount of DMF (0.2 mL) were added and refluxed for 3 h. After the reaction, benzene and excess $SOCl_2$ were distilled and dried under reduced pressure. The residue obtained was dissolved in CH_2Cl_2 (10 mL) and added drop wise to a solution of 2-nitro-1,3-benzenedimethanol **292** (0.055 g, 0.3 mmol, 0.1 *equiv.*), ethylene glycol (0.167 g, 2.7 mmol, 0.9 *equiv.*, 0.15 mL) and Et_3N (0.91 g, 9 mmol, 3 *equiv.*, 1.25 mL) in CH_2Cl_2 (10 mL) and continued stirring for 36 h at room temperature. After the reaction, the mixture was concentrated under reduced pressure to obtain crude product as pale brown solid. It was then washed with excess of water (2 x ~200 mL) and methanol (2 x ~50 mL) and dried under vacuum to get off-white solid in 260 mg. The obtained solid was characterized by ^{1}H, ^{13}C NMR, IR spectroscopy, GPC, TGA, DSC and PXRD.

For GPC analysis, the compound was suspended in THF for 5 h at room temperature. The residue was filtered and the supernatant was injected in the GPC.

^{1}H-NMR (500 MHz, DMSO-d_6, δ ppm): 3.66 (s (broad), 4H), 4.27 (s (broad), 4H), 4.59 (s (broad), 28H), 4.91 (s (broad), 2H), 5.45 (s (broad), 4H), 7.40 (s (broad), 15H) and 7.75 (s (broad), 3H).

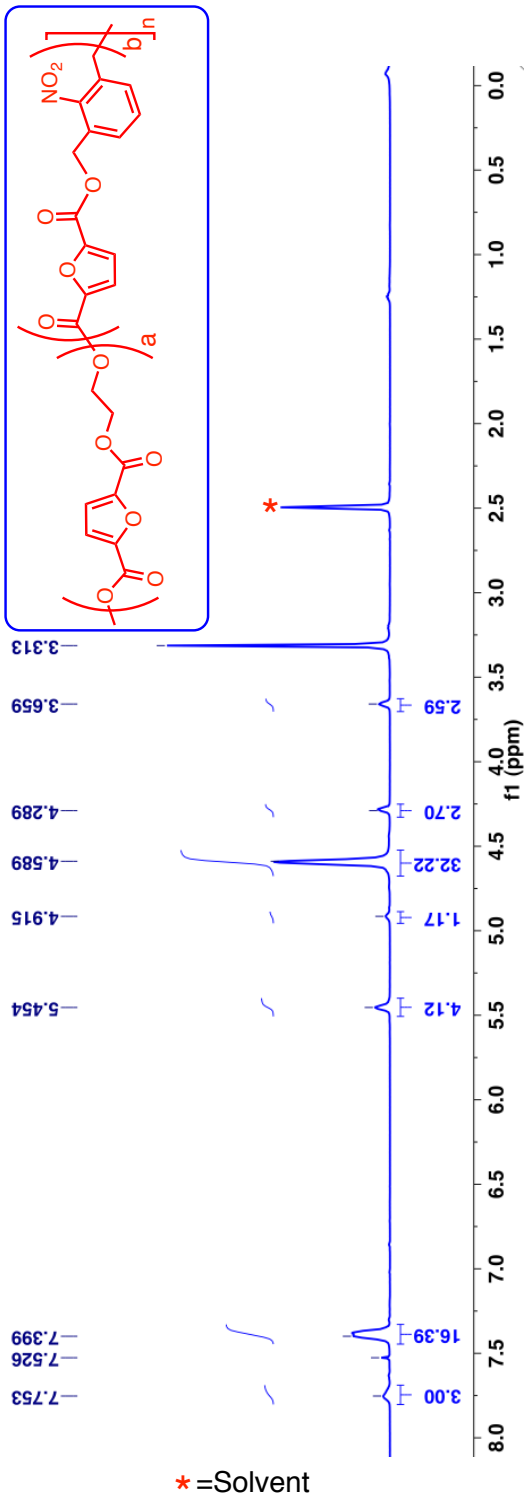

Figure 4.40: ^{1}H-NMR (500 MHz, DMSO-d_6, δ ppm) spectra of copolymer **288**.

^{13}C-NMR (125 MHz, DMSO-d_6, δ ppm): 64.2, 68.5, 72.4, 124.9, 134.1, 151.3 and 162.5. Apart from the above major peaks there are several peaks, which are little above base line: 68.1,124.5, 125.1, 136.2, 137.4, 150.8, 151.1, 151.6, 151.8, 162.0, 162.5, 162.6 and 162.8.

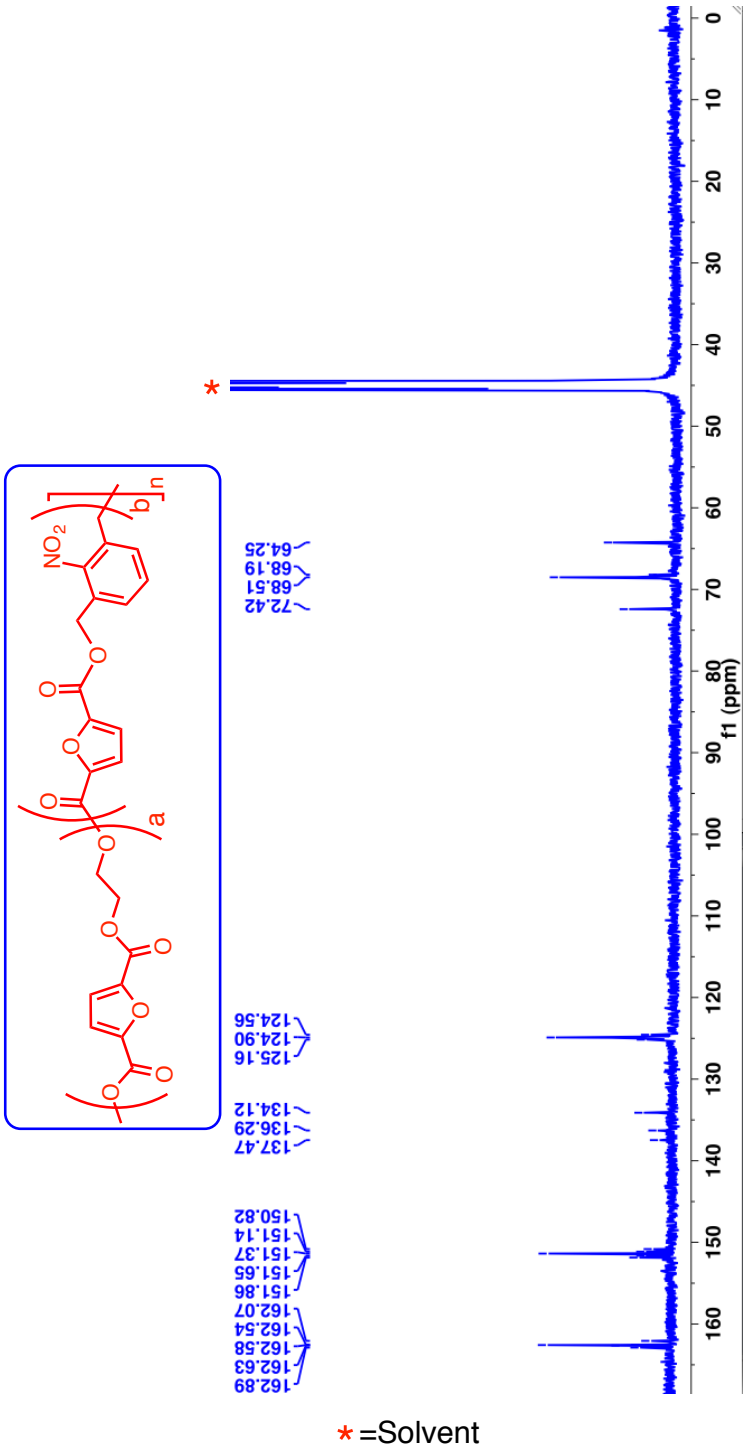

Figure 4.41: ^{13}C-NMR (125 MHz, DMSO-d_6, δ ppm) spectra of copolymer **288**.

ESI-MS sample preparation: Sample was dispersed in THF and sonicated for 5 min and allow to settle down for 2 h. The supernatant solution was analyzed by ESI-MS. A series of peaks appeared in the range of *m/z* 531-839 as binomial series with difference of 44 between every peak which is typical for ethylene glycol unit.

[ESI-MS] *m/z*: 531.4567, 575. 4870, 619.5200, 663. 5516, 707.5837, 751.6145, 795.6462, 839. 6800.

IR (KBr) cm^{-1}: 3520 (b, v_{O-H}), 1754 ($v_{C=O}$), 1581 (asym. v_{NO2}), 1308 (sym. $_{NO2}$), 1124 (v_{C-O}).

% Crystallinity of above copolymer/oligomer was determined by PXRD. It is calculated to be 21.05% with respect to Cristobalite (98% crystallinity) standard

4.12. General procedure and characterization of photocleaved products

Nitrobenzyl phototrigger based model compound **290a-b**, 2**91** and polymeric/oligomeric compounds **287**,co-polymer/oligomeric compound **288** in respective solvent were irradiated for a given time interval in pyrex tube in Rayonet reactor RPR-200 at 350 nm (16 bulbs X 14 Watts). The photocleaved mixture was analyzed by NMR spectroscopy.

Conversion and mass balance after photoreaction: Mass balance and conversion of photocleaved compounds were obtained using triphenylmethane as an internal standard (IS). 1 mL of 10^{-2} M (122 mg in 50 mL of $CHCl_3$) solution of triphenylmethane was added to the crude product and evaporated. To the mixture of Internal standard and the photosylate about ~0.6 mL of deuterated solvent is added and ^{1}H and ^{13}C NMR was recorded. From the integral value of respective peaks, the % conversion and mass balance was calculated using the equation 2.1 (Chapter 2)

Calculation for the recovery of FDCA: Literature reported method was followed for the calculation of FDCA recovery.[47] The recovery of FDCA from the irradiated polymer/oligomer sample was determined with NMR spectroscopy using an internal standard (IS). The mass of the FDCA was calculated from the integrated peak areas using the formula

$$m_{FDCA} = \frac{MW_{FDCA}}{MW_{IS}} \times \frac{N_{FDCA}}{N_{IS}} \times \frac{m_{IS} \times A_{FDCA}}{A_{IS}} \qquad \textbf{(Equation 4.1)}$$

Where m_{FDCA}, m_{IS} are the mass; N_{FDCA}, N_{IS} are the number of nuclei giving rise to the signals; A_{FDCA}, A_{IS} are the areas of the peak and MW_{FDCA}, MW_{IS} are the molecular weights of FDCA and IS respectively.

4.12.1. Photoreaction, mass balance and conversion studies of ester derivative 290a

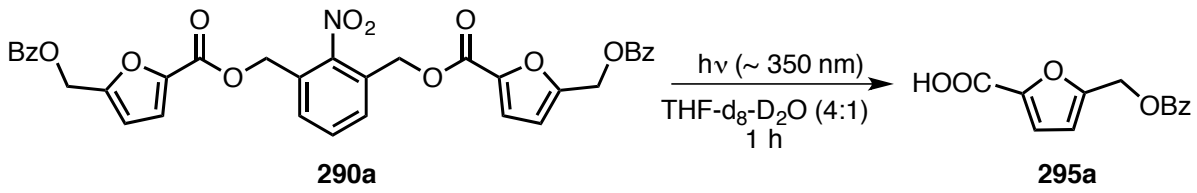

290a **295a**

Scheme 4.31: Photoreaction of ester derivative **290a**.

1 mM solution of **290a** in THF-d_8-D_2O was employed for the mass balance and conversion studies. Schematic representation of procedure was given below

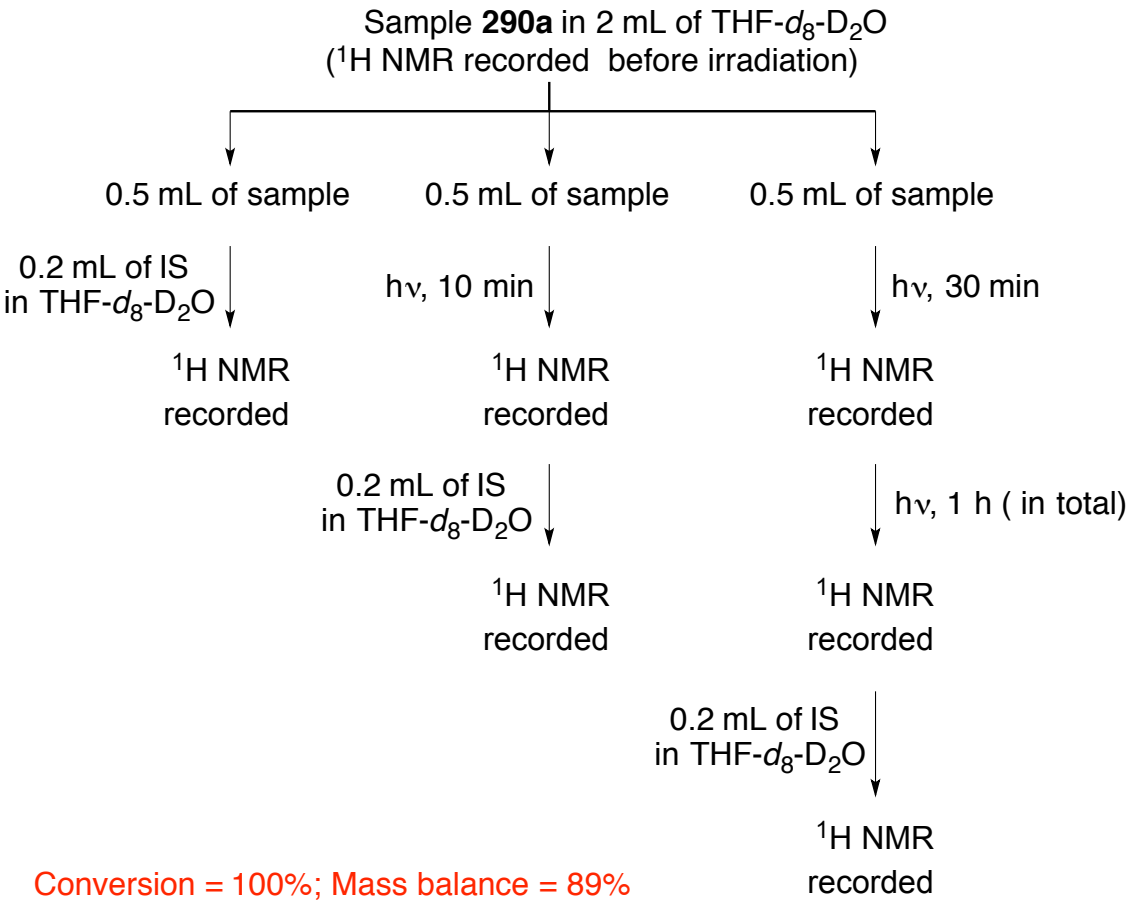

Scheme 4.32: Schematic depiction of photoreaction of ester derivative **290a**.

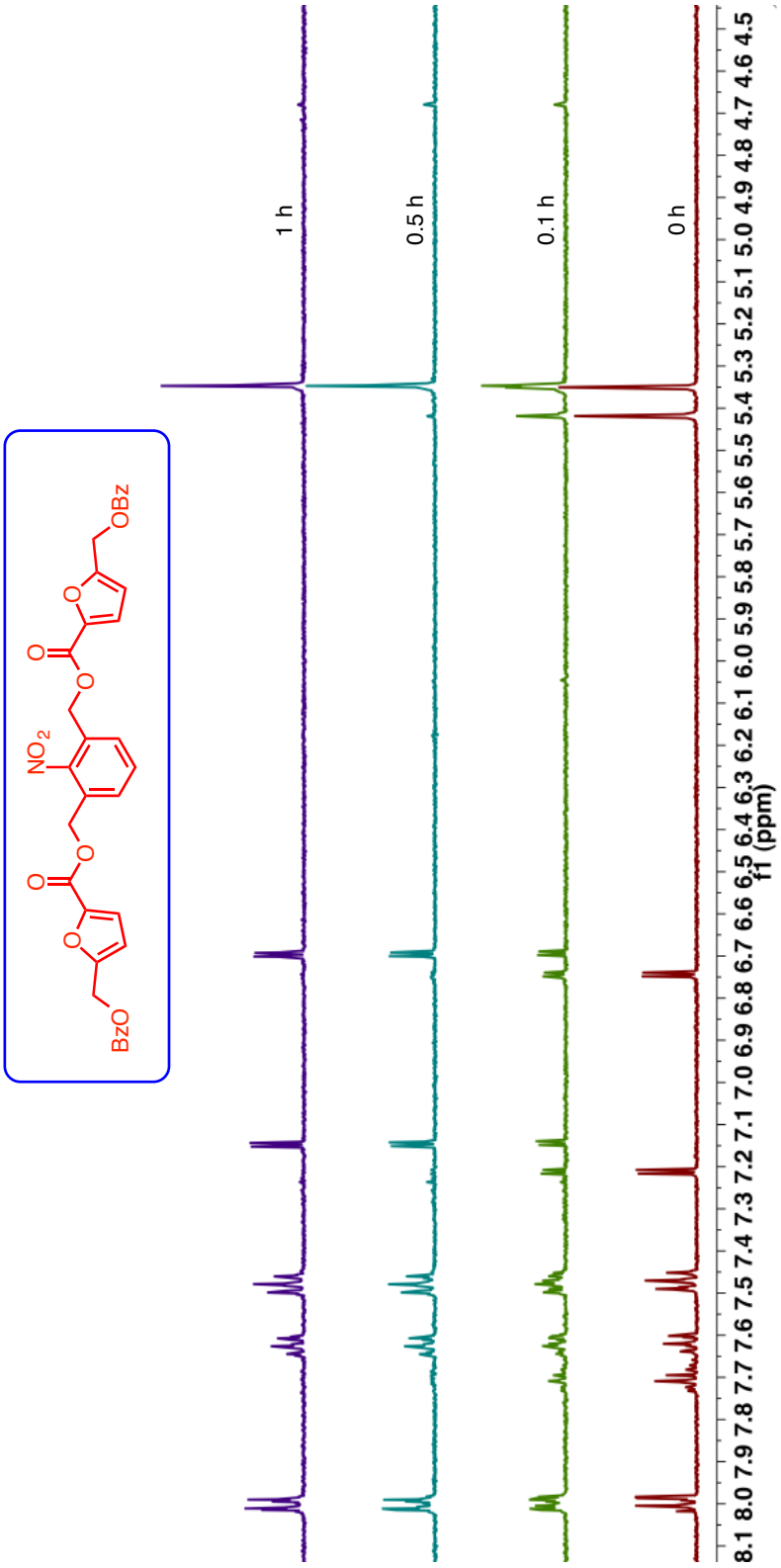

Only part (4.5-8.1 ppm) of ^{1}H NMR spectrum is shown for clarity.

Figure 4.42: ^{1}H-NMR (500 MHz, THF-D_2O, δ ppm) spectra of **290a** inTHF-D_2O (4:1) irradiated at different time interval.

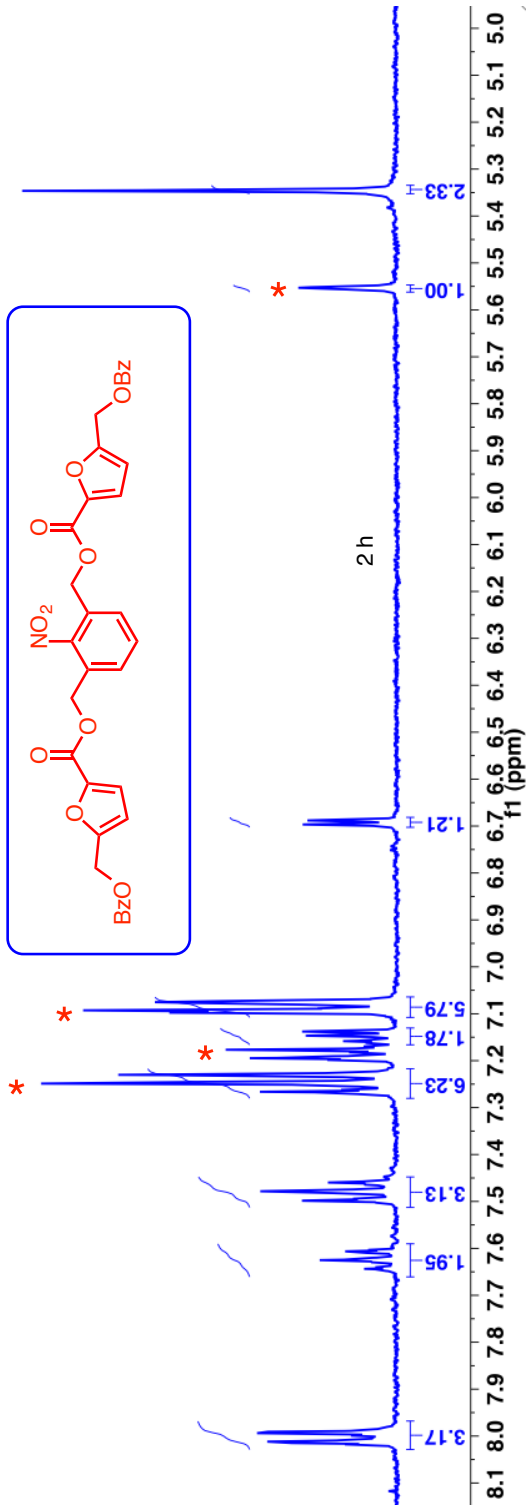

* = Internal standard-triphenyl methane

Only part (5.0-8.1 ppm) of ^{1}H NMR spectrum is shown for clarity.

Figure 4.43: ^{1}H-NMR (400 MHz, THF-D_2O, δ ppm) spectra of **290a** in THF-D_2O (4:1) irradiated at different time interval.

4.12.2. Photoreaction, mass balance and conversion studies of ester derivative 290b

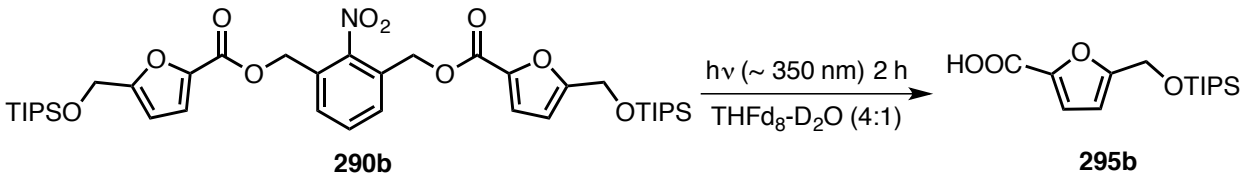

290b **295b**

Scheme 4.33: Photoreaction of ester derivative **290b**.

1 mM solution of **290b** in THF-d_8-D_2O was employed for the mass balance and conversion studies. Schematic representation of procedure was given below

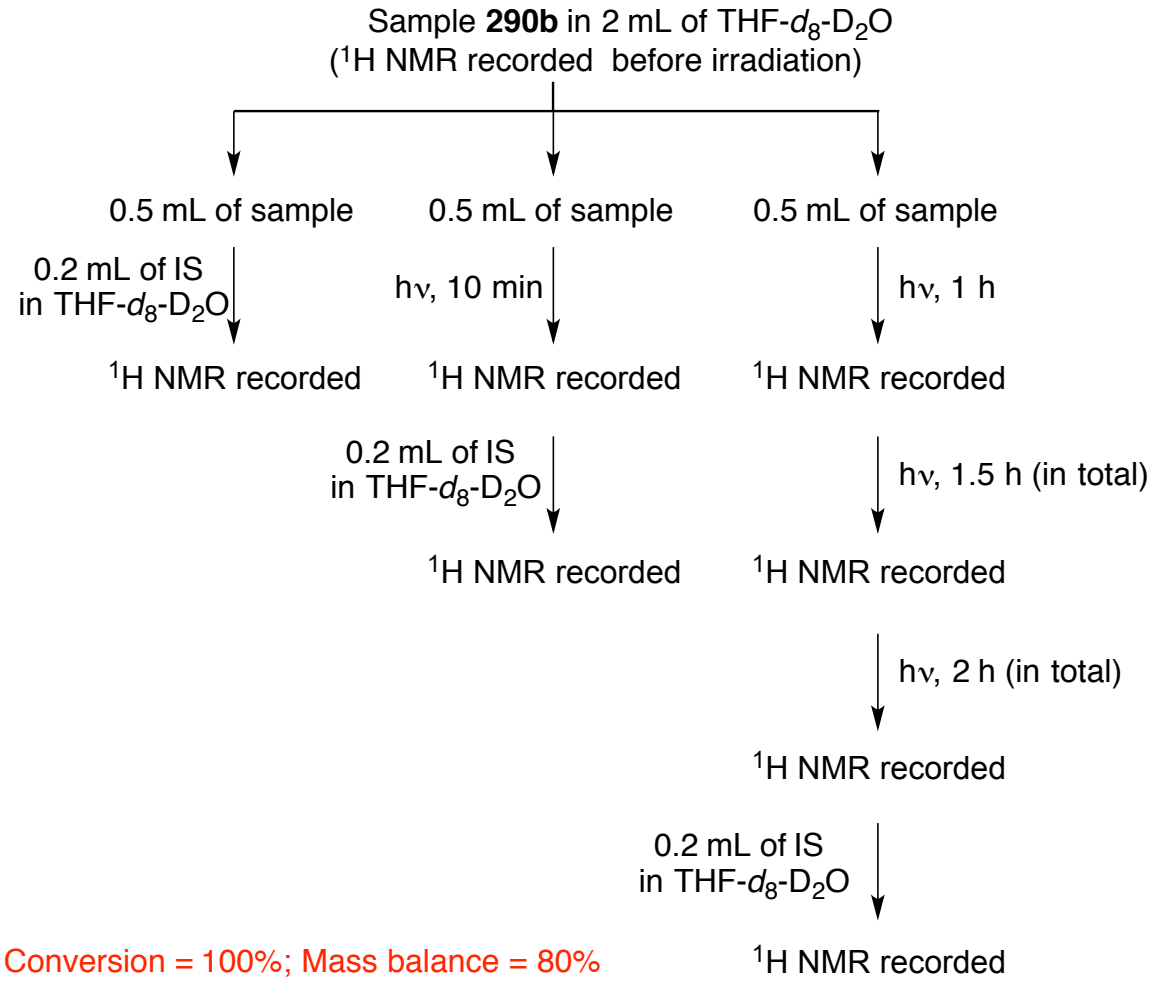

Scheme 4.34: Schematic depiction of photoreaction of ester derivative **290b**.

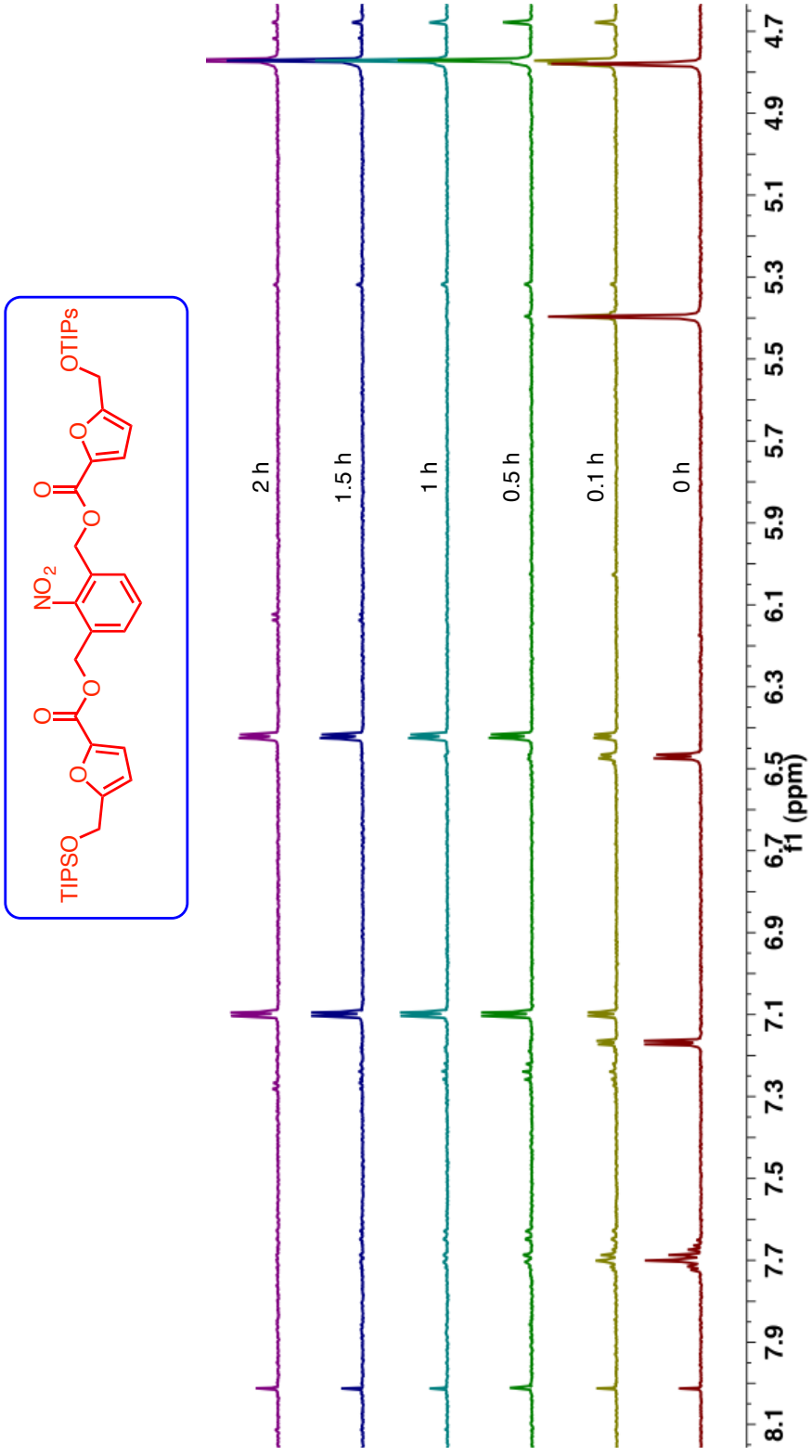

Only part (4.7-8.1 ppm) of ^{1}H NMR spectrum is shown for clarity.

Figure 4.44: ^{1}H-NMR (400 MHz, THF-D_2O, δ ppm) spectra of **290b** in THF-D_2O (4:1) irradiated at different time interval.

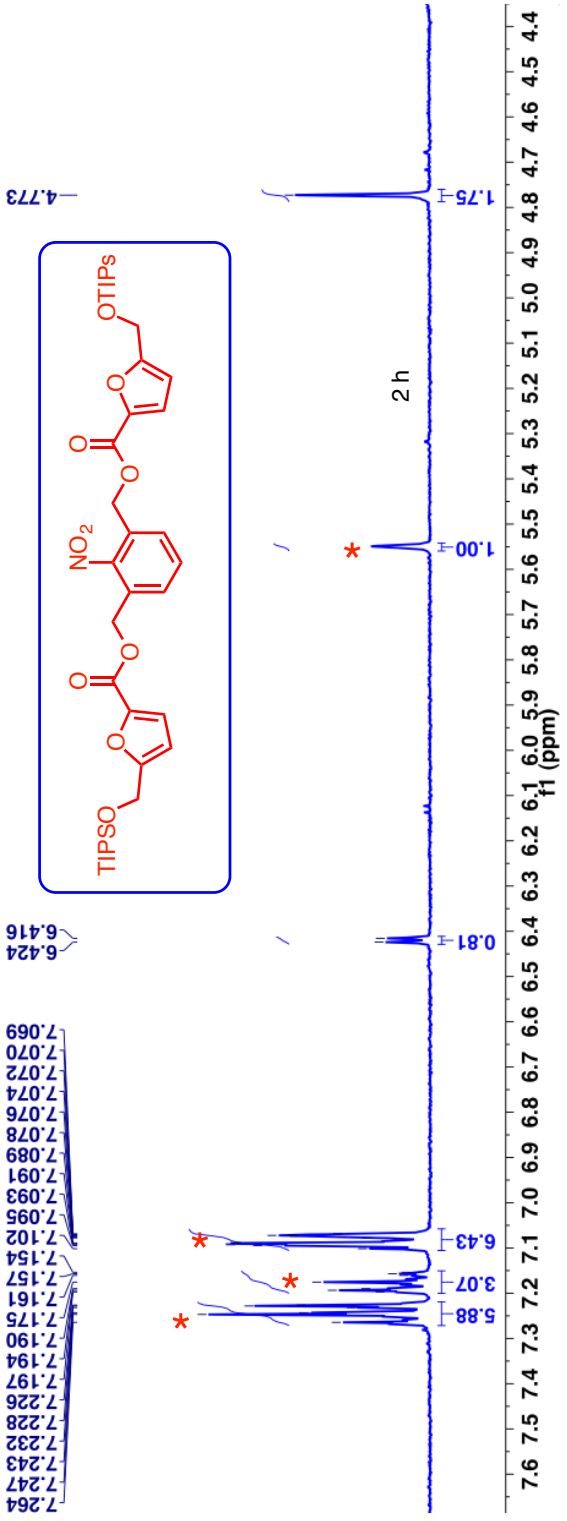

* = Internal standard-triphenyl methane

Only part (4.5-7.4 ppm) of ^{1}H NMR spectrum is shown for clarity.

Figure 4.45: ^{1}H-NMR (400 MHz, THF-D_2O, δ ppm) spectra of **290b** in THF-D_2O (4:1) irradiated at different time interval.

4.12.3. Photoreaction, mass balance and conversion studies of ester derivative 291

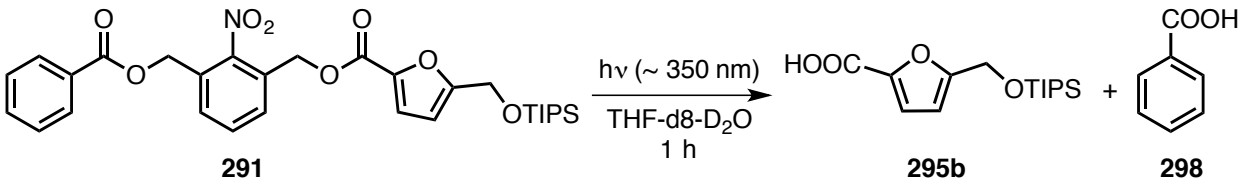

291 **295b** **298**

Scheme 4.35: Photoreaction of ester derivative **291**.

A 5 mM solution of ester **291** in THF-d_8-D_2O (NMR tube) was irradiated for 1 h. For every 0.5 h photocleavage was followed up ^{1}H NMR spectrum. Schematic representation of procedure was given below

Sample **291** in 0.5 mL of THF-d_8-D_2O
(^{1}H NMR recorded before irradiation)

↓ hν, 10 min

^{1}H NMR recorded

↓ hν, 40 min (in total)

^{1}H NMR recorded

↓ hν, 60 min (in total)

^{1}H NMR recorded

↓ 0.2 mL of IS in THF-d_8-D_2O

^{1}H NMR recorded

Conversion = 100%;
Mass balance = 60% (for furan acid, **5b**) and 74% (for benzoic acid, **10**)

Scheme 4.36: Schematic depiction of photoreaction of ester derivative **291**.

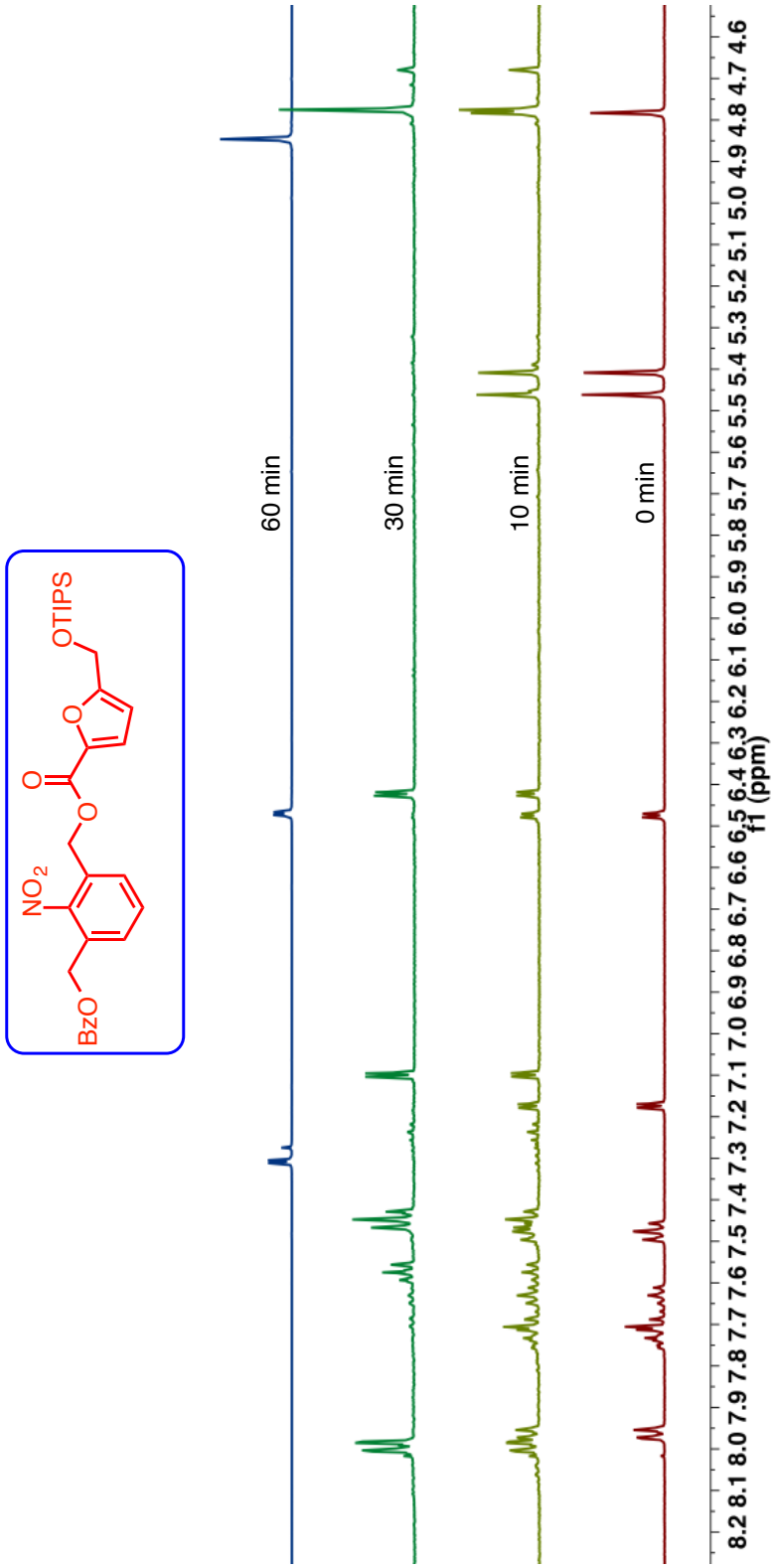

Only part (4.6-8.2 ppm) of ^{1}H NMR spectrum is shown for clarity.

Figure 4.46: ^{1}H-NMR (400 MHz, THF-D_2O, δ ppm) spectra of **291** in THF-D_2O (4:1) irradiated at different time interval.

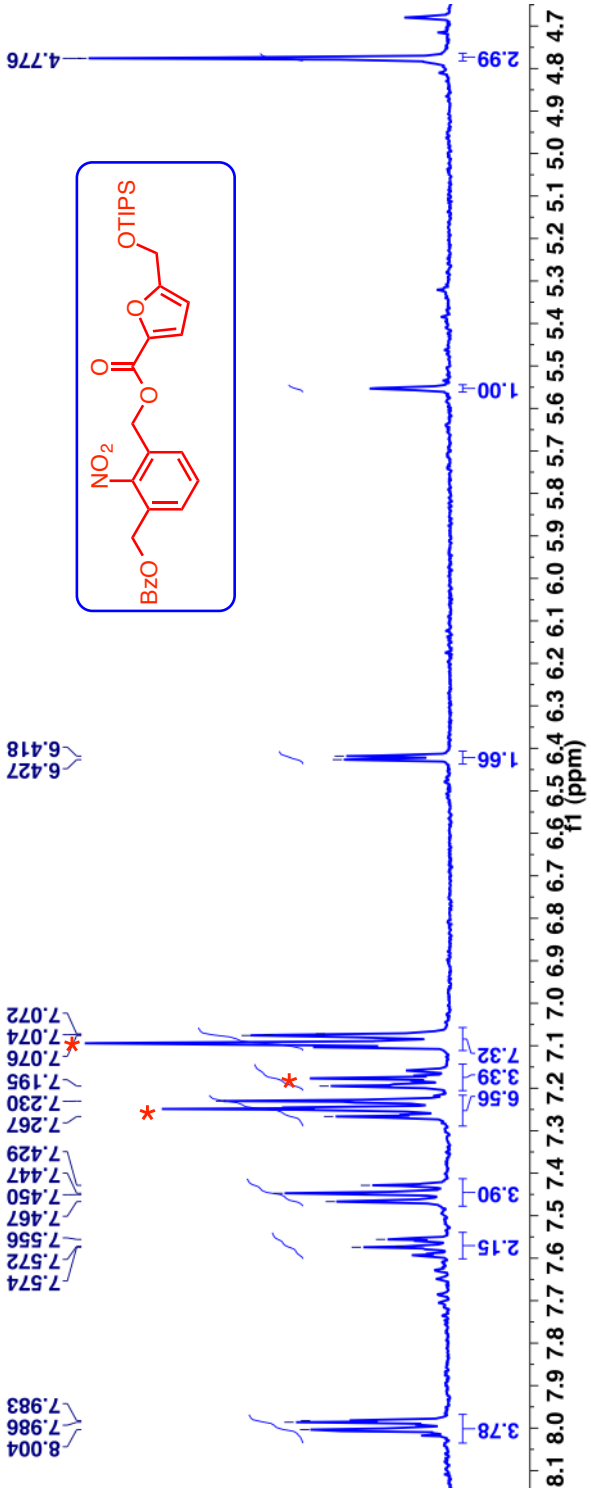

* = Internal standard-triphenylmethane

Only part (4.7-8.1 ppm) of ^{1}H NMR spectrum is shown for clarity.

Figure 4.47: ^{1}H-NMR (400 MHz, THF-D_2O, δ ppm) spectra of **291** in THF-D_2O (4:1) irradiated at different time interval.

4.12.4. Photoreaction and conversion studies of polymer/oligomer 287 in solution

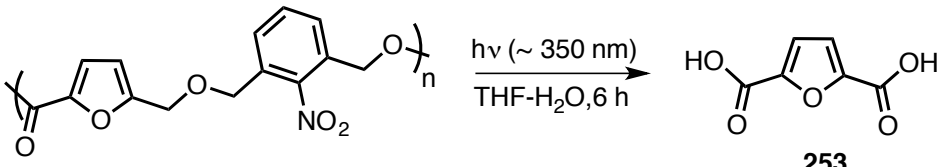

287 **253**

Scheme 4.37: Photoreaction of polymer/oligomer **287** in solution.

30 mg of polymer/oligomer **287** in 60 mL of THF-H_2O (4:1) mixture was divided into 6 x 10 mL and irradiated in Rayonet reactor equipped with ~350 nm bulb (16 bulbs x 14 watt). For every one hour one sample was removed, concentrated and the residue was analyzed by ^{1}H-NMR spectroscopy (such that the last sample was irradiated for 6 h). The solution was heterogeneous before irradiation and become clear over 3 h of irradiation during which the color of the solution changed from white suspension to yellow solution (Figure 4.48). The reaction was further continued for 3 h to ensure complete decomposition of the polymeric materials.

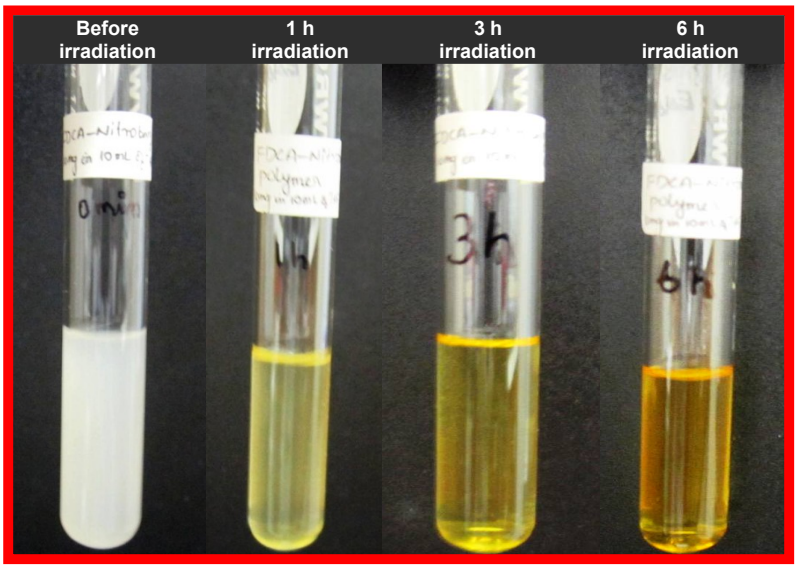

Figure 4.48: Polymer/oligomer **287** a) before irradiation b) irradiated for 1 h c) irradiated for 3 h d) irradiated for 6 h

After 6 h of irradiation the sample was concentrated and the residue was analyzed by ^{1}H NMR spectroscopy using triphenylmethane (10^{-2} M in $CHCl_3$, 1 mL) as an internal standard. Analyzing the ^{1}H and ^{13}C-NMR spectrum of 6 h irradiated sample showed the presence of FDCA (by comparing the

spectra of authentic FDCA sample) and the recovery of FDCA was found to be 40 ±5%. The experiments were performed with two different internal standards (triphenylmethane and maleic acid) and the results are an average of three runs.

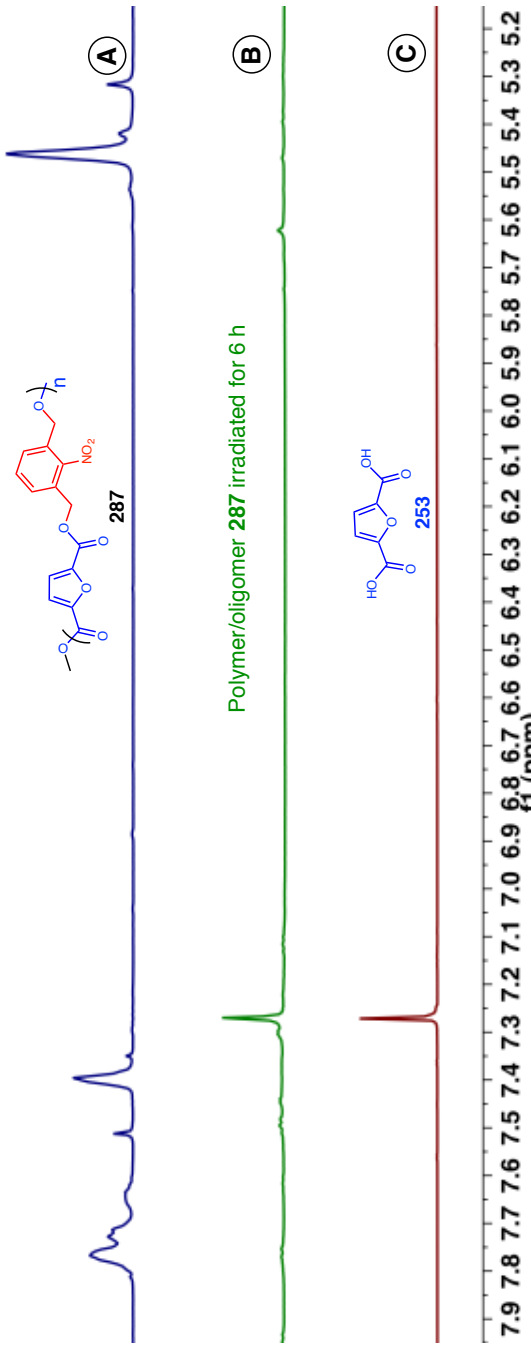

(A) before irradiation and (B) after irradiation.
(C) The authentic FDCA **253** is provided for comparison.

Figure 4.49: ^{1}H-NMR (400 MHz, DMSO-d_6, δ ppm) spectra of polymer/oligomer **287**.

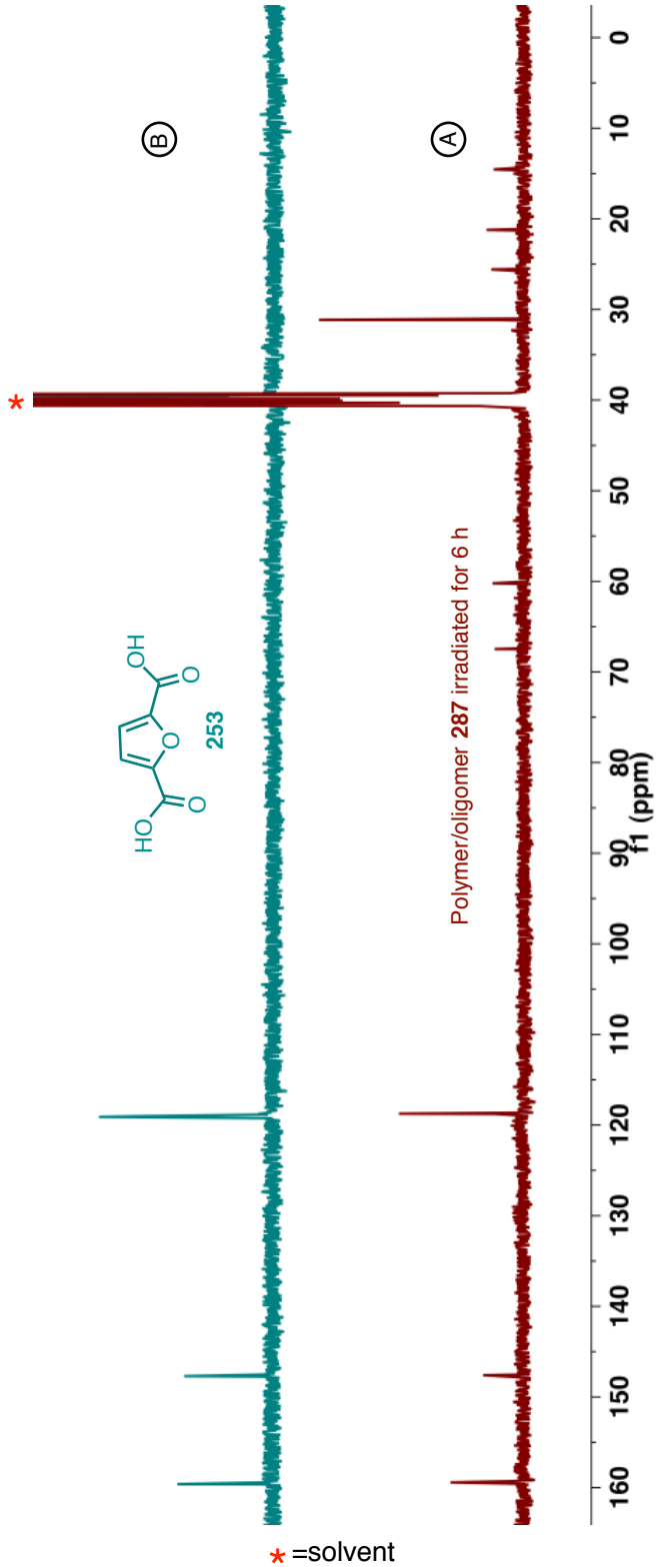

(A) after irradiation for 6 h and (B) The authentic FDCA **253**.

Figure 4.50: ^{13}C-NMR (125 MHz, DMSO-d_6, δ ppm) spectra of polymer/oligomer **287**.

4.12.5. Photoreaction of polymer/oligomer 287 in solid state

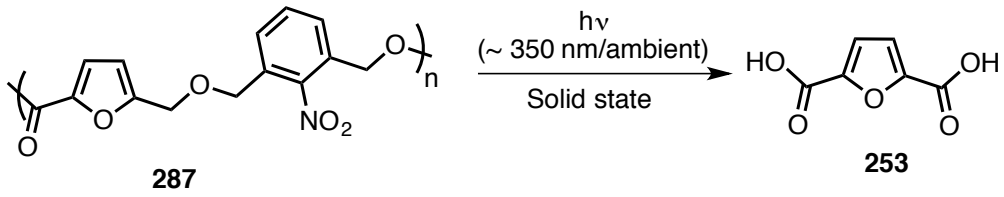

287 **253**

Scheme 4.38: Photoreaction of polymer/oligomer **287** in solid state.

5 mg of polymer/oligomer **287** was packed as a thin layer between two 1 mm micro slides made of Swiss glass (purchased from VWR® international). 3 sets of samples were prepared and were irradiated in Rayonet reactor equipped with ~350 nm bulb (16 bulbs x 14 watt). One sample was kept in dark (0 h sample). For every 6 hour one sample was removed and was analyzed by ^{1}H-NMR spectroscopy with maleic acid as internal standard (such that the last sample was irradiated for 12 h). The solid sample changed color from pale yellow to dark brown over the period of irradiation (Figure 4.51-Left). After 12 h, the recovery of FDCA was found to be 16%. The low yield is due to competitive absorption of light by the photoproducts. The above reaction was also performed in ambient conditions (40 W incandescent bulb). No degradation was observed even after 12 h of irradiation (Figure 4.51-Right)

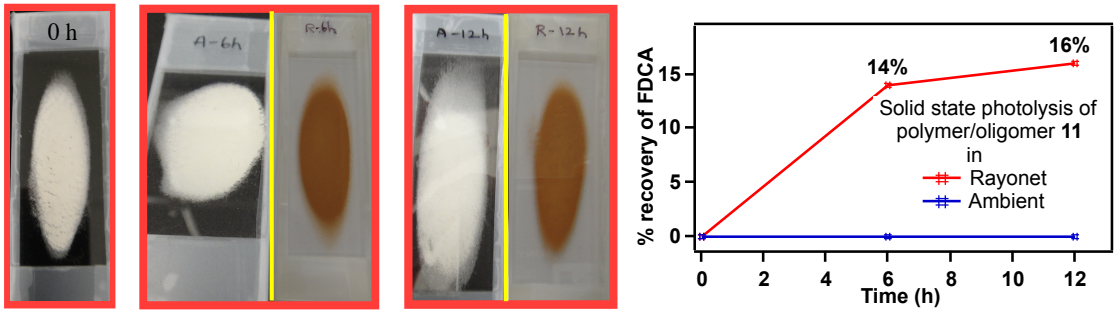

Figure 4.51: Left: Solid-state irradiation of Polymer/oligomer **287** in Rayonet (R) and Ambient (A) Right: % recovery of FDCA determined using ^{1}H NMR spectroscopy in Rayonet reactor and ambient conditions.

4.12.6. Photoreaction of co-polymer/oligomer 288

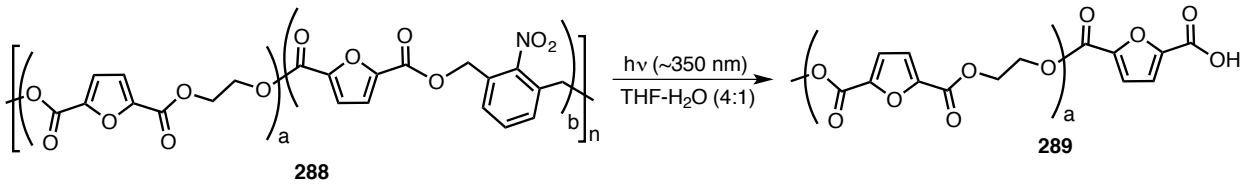

288 **289**

Scheme 4.39: Photoreaction of co-polymer/oligomer **288**.

5 mg of copolymer/oligomer **288** in 10 mL of THF-H_2O (4:1) and irradiated in Rayonet reactor equipped with 350 nm bulb (16 bulbs x 14 watt) for 5 h. After the reaction (appearance of clear solution), the solvent in the mixture was removed under reduced pressure to get crude product as pale yellow solid in 3 mg. It was then analyzed by ^{1}H NMR spectroscopy.

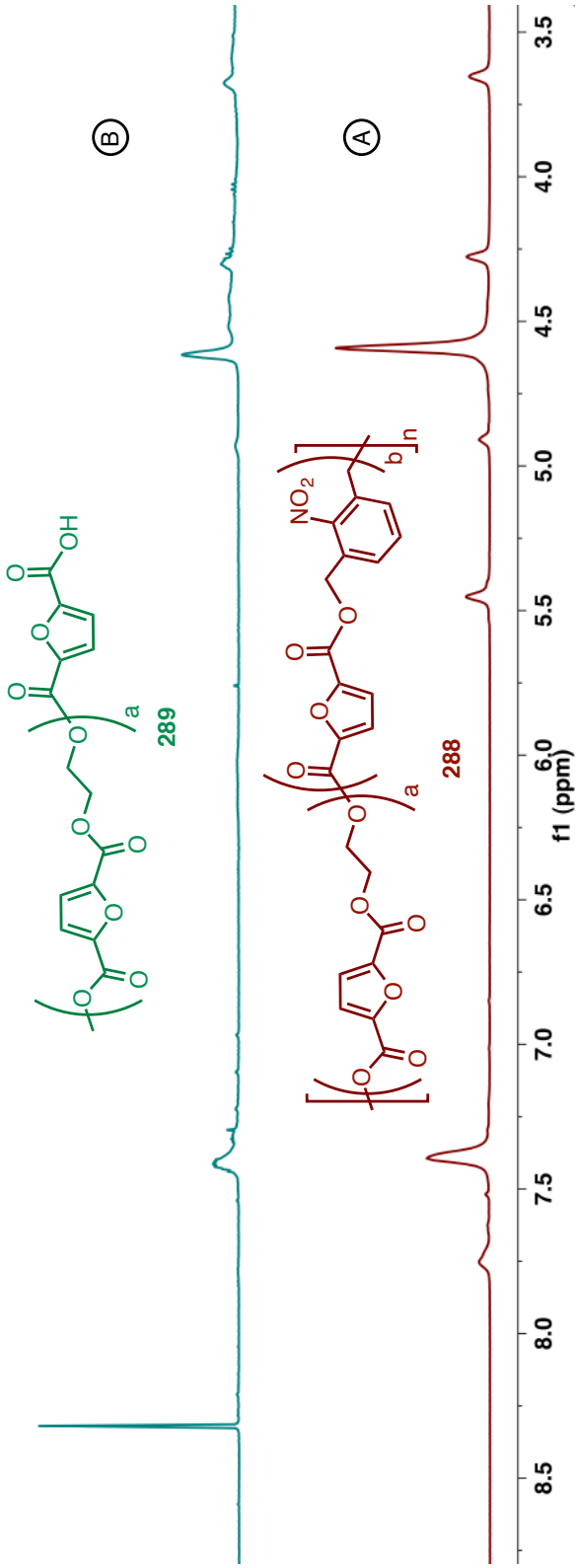

(A) co-polymer/oligomer **288** (B) after irradiation for 5 h **289**.

Figure 4.52: ^{1}H-NMR (500 MHz, DMSO-d_6, δ ppm) spectra of copolymer **288**.

4.13. UV-Vis absorption spectra

4.13.1. UV-Vis spectra of ester 290a-b in THF-H_2O irradiated at different time intervals

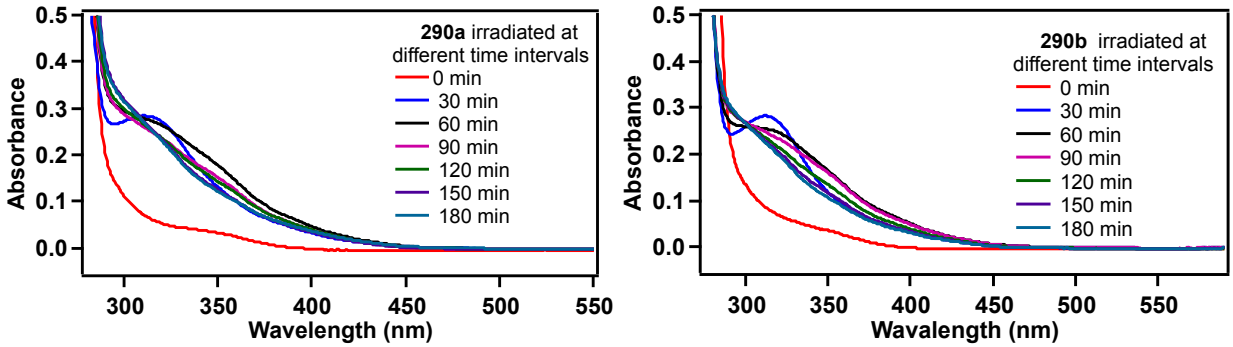

Figure 4.53: UV-Vis spectra of 10^{-4} M solution of ester **290a** (left) and **290b** (right) in THF-H_2O (4:1) at 0 min, 30 min, 60 min, 90 min, 120 min, 150 min and 180 min of irradiation.

4.13.2. UV-Vis spectra of ester 291 in THF-H_2O irradiated at different time intervals

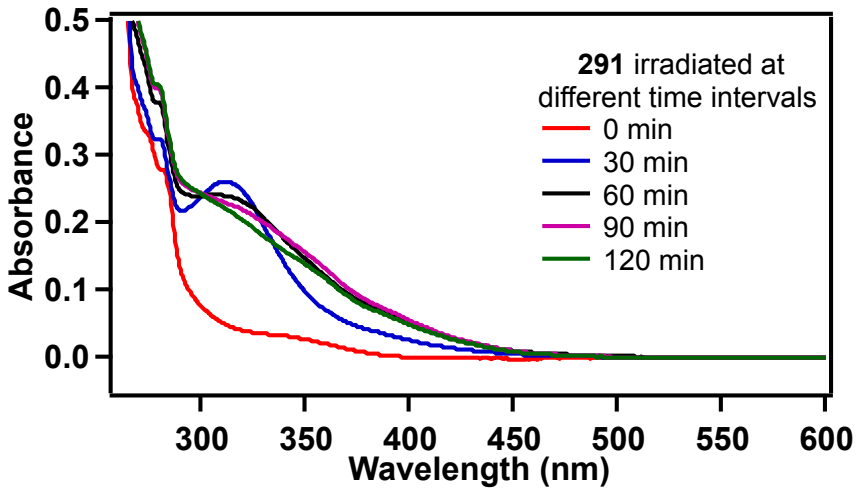

Figure 4.54: UV-Vis spectra of 10^{-4} M solution of ester **291** in THF-H_2O (4:1) at 0 min, 30 min, 60 min, 90 min, 120 min, 150 min and 180 min irradiation.

4.14. Powder X-ray diffraction (PXRD) of 287 and 288

4.14.1. PXRD of polymer/oligomer 287

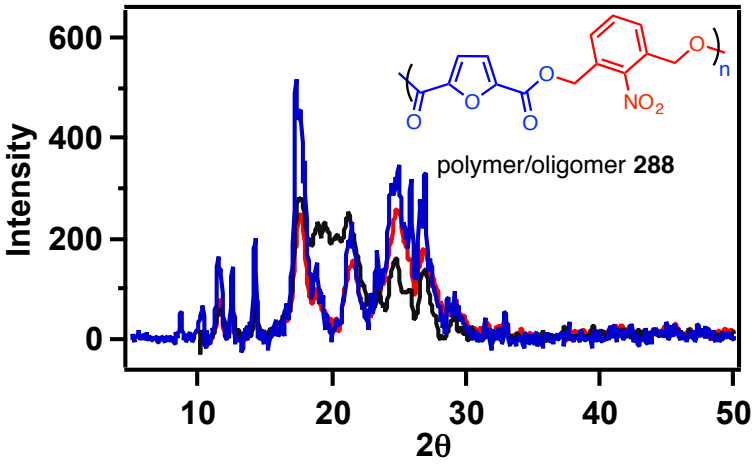

Figure 4.55: Stacked PXRD pattern of polymer/oligomer **287** synthesized first time (Red) second time (black) and third time (blue).

4.14.2. PXRD of co-polymer/oligomer 289

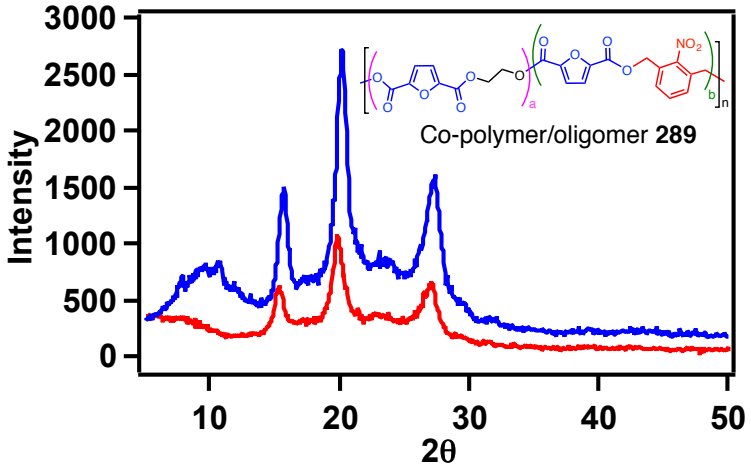

Figure 4.56: Stacked PXRD pattern of co-polymer/oligomer **289** synthesized first time (Red) second time (black) and third time (blue).

4.15. References

(1) Mittal, V.: *Renewable Polymers: Synthesis, Processiong and Technology*; Wiley, New Jersey, 2012.

(2) Gandini, A. Polymers from Renewable Resources: A Challenge for the Future of Macromolecular Materials. *Macromolecules* **2008**, *41*, 9491-9504.

(3) North, E. J. H., R. U. Plastics and Environmental Health: The Road Ahead. *Rev. Environ, Health* **2013**, *28*, 1-8.

(4) Kamm, B. G., P. R.; Kamm, M.: *Biorefineries Industrial Processes and Products*; Wiley-VCH: Weinheim, Germany, 2006.

(5) Facing the Hard Truths about Energy. *U.S. National Petroleum Council: Washington* **2007**.

(6) Henrich, E. D., N.; Dinjus, E.; Sauer, J. The Role of Biomass in a Future World Without Fossil Fuels. *Chem. Ing. Tech.* **2015**, *87*, 1667-1685.

(7) Gandini, A. The Irruption of Polymers from Renewable Resources on the Scene of Macromolecular Science and Technology. *Green Chem.* **2011**, *13*, 1061-1083.

(8) Corma, A.; Iborra, S.; Velty, A. Chemical Routes for the Transformation of Biomass into Chemicals. *Chem. Rev.* **2007**, *107*, 2411-2502.

(9) The Molecules that make Plants Cells.... Different. http://www.bio.miami.edu/dana/226/226F09_2.html. (accessed January 15, 2016).

(10) Carvalho, A. J. F.: Starch: Major Sources, Properties and Applications. In *Monomers, Polymers and Composites from Renewable Resources*; Belgacem, M. N. G., A., Ed.; Elsevier, Amsterdam, 2008; pp 321.

(11) Peniche, C. A.-M., W.; Goycoolea, F. M.: Chitin and Chitosan: Major Sources, Properties and Applications. In *Monomers, Polymers and Composites from Renewable Resources*; Belgacem, M. N. G., A., Ed.; Elsevier, Amsterdam, 2008; pp 517.

(12) Rinaudo, M. Chitin and Chitosan: Properties and Applications. *Prog. Polym. Sci.* **2006**, *31*, 603-632.

(13) Fernandes, S. C. M.; Freire, C. S. R.; Silvestre, A. J. D.; Neto, C. P.; Gandini, A.; Desbriéres, J.; Blanc, S.; Ferreira, R. A. S.; Carlos, L. D. A Study of the Distribution of Chitosan onto and Within a Paper Sheet Using a Fluorescent Chitosan Derivative. *Carbohydr. Polym.* **2009**, *78*, 760-766.

(14) Fernandes, S. C. M.; Freire, C. S. R.; Silvestre, A. J. D.; Desbrières, J.; Gandini, A.; Neto, C. P. Production of Coated Papers with Improved Properties by Using a Water-Soluble Chitosan Derivative. *Ind. Eng. Chem. Res.* **2010**, *49*, 6432-6438.

(15) Spiridon, I. P., V. I.: Major Sources, Properties and Applications,. In *Monomers, Polymers and Composites from Renewable Resources*; Belgacem, M. N. G., A., Ed.; Elsevier, Amsterdam, 2008; pp 289.

(16) Burton, R. A.; Gidley, M. J.; Fincher, G. B. Heterogeneity in the Chemistry, Structure and Function of Plant Cell Walls. *Nat. Chem. Biol.* **2010**, *6*, 724-732.

(17) Mialon, L.; Pemba, A. G.; Miller, S. A. Biorenewable Polyethylene Terephthalate Mimics Derived from Lignin and Acetic Acid. *Green Chem.* **2010**, *12*, 1704-1706.

(18) Dull, G. *Chem. Zeitg.* **1895**, *19*, 216.

(19) Kiermayer. *Chem. Zeitg.* **1895**, *19*, 1003.

(20) van Putten, R.-J.; van der Waal, J. C.; de Jong, E.; Rasrendra, C. B.; Heeres, H. J.; de Vries, J. G. Hydroxymethylfurfural, A Versatile Platform Chemical Made from Renewable Resources. *Chem. Rev.* **2013**, *113*, 1499-1597.

(21) Lewkowaki, J. Synthesis, Chemsitry and Applicaitons of 5-Hydroxymethylfurfural and its Derivatives. *Arkivoc* **2001**, *2001*.

(22) Gandini, A.; Belgacem, M. N. Furans in Polymer Chemistry. *Prog. Polym. Sci.* **1997**, *22*, 1203-1379.

(23) Gandini, A.; Lacerda, T. M. From Monomers to Polymers from Renewable Resources: Recent Advances. *Prog. Polym. Sci.* **2015**, *48*, 1-39.

(24) Gandini, A.; Lacerda, T. M.; Carvalho, A. J. F.; Trovatti, E. Progress of Polymers from Renewable Resources: Furans, Vegetable Oils, and Polysaccharides. *Chem. Rev.* **2016**, *116*, 1637-1669.

(25) Hui, Z.; Gandini, A. Polymeric Schiff Bases Bearing Furan Moieties. *Eur. Polym. J.* **1992**, *28*, 1461-1469.

(26) Belgacem, M. N.; Quillerou, J.; Gandini, A. Urethanes and Polyurethanes Bearing Furan Moieties—3. Synthesis, Characterization and Comparative Kinetics of the Formation of Diurethanes. *Eur. Polym. J.* **1993**, *29*, 1217-1224.

(27) Belgacem, M. N.; Quillerou, J.; Gandini, A.; Rivero, J.; Roux, G. Urethanes and Polyurethanes Bearing Furan Moieties—2. Comparative Kinetics and Mechanism of the Formation of Furanic and other Monourethanes. *Eur. Polym. J.* **1989**, *25*, 1125-1130.

(28) Boufi, S.; Gandini, A.; Belgacem, M. N. Urethanes and Polyurethanes Bearing Furan Moieties: 5. Thermoplastic Elastomers based on Sequenced Structures. *Polymer* **1995**, *36*, 1689-1696.

(29) Boufi, S.; Belgacem, M. N.; Quillerou, J.; Gandini, A. Urethanes and polyurethanes bearing furan moieties. 4. Synthesis, kinetics and characterization of linear polymers. *Macromolecules* **1993**, *26*, 6706-6717.

(30) Drewitt, J. G., N.; Lincoln. J. . US 255173119510508. USA Patent.

(31) Moore, J. A.; Kelly, J. E. Polyesters Derived from Furan and Tetrahydrofuran Nuclei. *Macromolecules* **1978**, *11*, 568-573.

(32) Grosshardt, O. F., U.; Kowallik, K.; Tubke, B.; Digneouts, N.; Wilhelm, M. Synthese und Charakterisierung von Polyestern und Polyamiden auf der Basis von Furan-2,5-dicarbonsaure. *Chemie-Ingenierur-Technik* **2009**, *8*, 1829-1835.

(33) Gandini, A.; Silvestre, A. J. D.; Neto, C. P.; Sousa, A. F.; Gomes, M. The Furan Counterpart of Poly(ethylene terephthalate): An Alternative Material based on Renewable Resources. *J. Polym. Sci., Part A: Polym. Chem.* **2009**, *47*, 295-298.

(34) Shah, A. A.; Hasan, F.; Hameed, A.; Ahmed, S. Biological Degradation of Plastics: A Comprehensive Review. *Biotechnol. Adv.* **2008**, *26*, 246-265.

(35) Koyama, N.; Doi, Y. Miscibility, Thermal Properties, and Enzymatic Degradability of Binary Blends of Poly[(R)-3-hydroxybutyric acid] with Poly(ε-caprolactone-co-lactide). *Macromolecules* **1996**, *29*, 5843-5851.

(36) Rutkowska, M.; Krasowska, K.; Heimowska, A.; Kowalczuk, M. Degradation of the Blends of Natural and Synthetic Copolyesters in Different Natural Environments. *Macromol. Symp.* **2003**, *197*, 421-430.

(37) Johnson, J. A.; Finn, M. G.; Koberstein, J. T.; Turro, N. J. Synthesis of Photocleavable Linear Macromonomers by ATRP and Star Macromonomers by a Tandem ATRP−Click Reaction:Precursors to Photodegradable Model Networks. *Macromolecules* **2007**, *40*, 3589-3598.

(38) Han, D.; Tong, X.; Zhao, Y. Fast Photodegradable Block Copolymer Micelles for Burst Release. *Macromolecules* **2011**, *44*, 437-439.

(39) Jiang, J.; Tong, X.; Morris, D.; Zhao, Y. Toward Photocontrolled Release Using Light-Dissociable Block Copolymer Micelles. *Macromolecules* **2006**, *39*, 4633-4640.

(40) Klán, P.; Šolomek, T.; Bochet, C. G.; Blanc, A.; Givens, R.; Rubina, M.; Popik, V.; Kostikov, A.; Wirz, J. Photoremovable Protecting Groups in Chemistry and Biology: Reaction Mechanisms and Efficacy. *Chem. Rev.* **2012**, *113*, 119-191.

(41) Gaplovsky, M.; Il'ichev, Y. V.; Kamdzhilov, Y.; Kombarova, S. V.; Mac, M.; Schworer, M. A.; Wirz, J. Photochemical Reaction Mechanisms of 2-Nitrobenzyl Compounds: 2-Nitrobenzyl Alcohols form 2-Nitroso Hydrates by Dual Proton Transfer. *Photochem. Photobiol. Sci.* **2005**, *4*, 33-42.

(42) Binder, J. B.; Raines, R. T. Simple Chemical Transformation of Lignocellulosic Biomass into Furans for Fuels and Chemicals. *J. Am. Chem. Soc.* **2009**, *131*, 1979-1985.

(43) Yoon, D.-W.; Gross, D. E.; Lynch, V. M.; Sessler, J. L.; Hay, B. P.; Lee, C.-H. Benzene-, Pyrrole-, and Furan-Containing Diametrically Strapped Calix[4]pyrroles—An Experimental and Theoretical Study of Hydrogen-Bonding Effects in Chloride Anion Recognition. *Angew. Chem. Int. Ed.* **2008**, *47*, 5038-5042.

(44) Bognár, R.; Herczegh, P.; Zsély, M.; Batta, G. Synthesis of 3,4-Dideoxy-dl-hex-3-enopyranosides from 5-Hydroxymethyl-2-furaldehyde. *Carbohydr. Res.* **1987**, *164*, 465-469.

(45) McNelis, B. J.; Sternbach, D. D.; MacPhail, A. T. Synthetic and Kinetic Studies of Substituent Effects in the Furan Intramolecular Diels-Alder Reaction. *Tetrahedron* **1994**, *50*, 6767-6782.

(46) Dalcanale, E.; Montanari, F. Selective Oxidation of Aldehydes to Carboxylic Acids with Sodium Chlorite-Hydrogen Peroxide. *J. Org. Chem.* **1986**, *51*, 567-569.

(47) Rundlöf, T.; Mathiasson, M.; Bekiroglu, S.; Hakkarainen, B.; Bowden, T.; Arvidsson, T. Survey and Qualification of Internal Standards for Quantification by 1H NMR Spectroscopy. *J. Pharm. Biomed. Anal.* **2010**, *52*, 645-651.

CHAPTER 5. EVALUATING *p*-HYDROXY PHENACYL DERIVATIVES AS A BIOMASS DERIVED MODEL PHOTOTRIGGER*

5.1. Introduction

In the previous chapter, we demonstrated the use of *o*-nitrobenzyl derivative as a phototrigger to degrade polymer. Although *o*-nitrobenzyl derivative is one of the most commonly used phototriggers and its mechanism of action is well established in the literature, it has a few shortcomings, and they are (i) the release of leaving group are in the microseconds time regime[1] and (ii) the formation of *o*-nitroso derivative byproduct during the releasing process. The byproduct (nitroso derivative) absorbs more strongly than the parent compound at the irradiation wavelength (~350 nm) which interferes with the release of the leaving group due to competitive absorption.[2] This hindrance becomes more challenging especially in the case of the bio-based polymer discussed in the previous chapter. We believed that the formation of the *o*-nitroso by-product interacts/reacts with the released FDCA monomer thereby reducing its recovery. To alleviate this problem, we looked at alternative phototriggers that could be employed for degradation of polymers and obtain better recovery of the released monomer(s). This chapter describes our attempt towards that goal where we designed and evaluated a model system with *p*-hydroxy phenacyl (*p*HP) as phototrigger with the long-term goal of developing biomass derived compounds and incorporating them in the polymer backbone for programmed photodegradation.

5.2. *p*-Hydroxy phenacyl as a phototrigger

In 1962, Anderson and Reese were the first to report on the use of *p*-hydroxy phenacyl as a phototrigger in the substituted phenacyl chlorides **301** as shown in Scheme 5.1.[3] They performed the reaction in 1% ethanolic solution of the phenacyl chloride and observed the formation of two products: (i) ketone-reduction product **302**, that is formed by the loss of chlorine resulting in ketonyl radical followed by H-abstraction from the solvent and (ii) ester-rearranged product **303**, which is formed via spirodienedione intermediate.

*Dr. Saravanakumar Rajendran (SR) Ramya Raghunathan (RR), in consultation with Dr. Mukund. P. Sibi (MPS) and Dr. J. Sivaguru (JS) synthesized all the compounds reported in this chapter and carried out all the experiments.

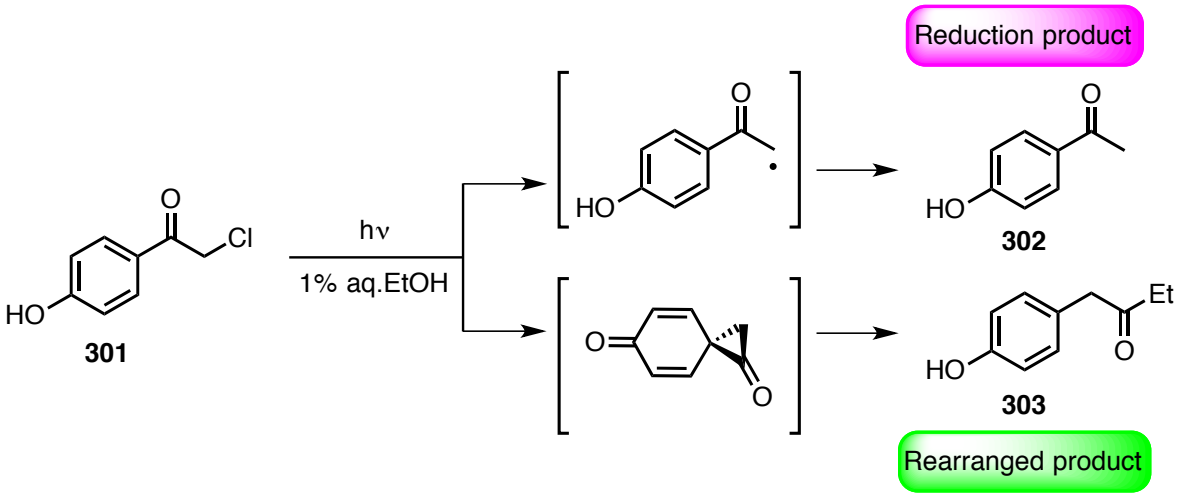

Scheme 5.1: First report on p-hydroxy phenacyl phototrigger **301**.

Later in 1973, Sheehan and Umezwa reported the release of benzoic acid and various amino acid derivatives employing *p*HP derivative as a phototrigger (Scheme 5.2).[4] But unlike the observation made by Anderson and Reese, this group reported that they observed only the reduction product **302**. They demonstrated this observation by irradiating of *p*-methoxy phenacyl derivative **304** in dioxane or in ethanol as solvent. They proposed that the formation of products took place via a homolytic cleavage of carbon-oxygen bond and the solvent served as a hydrogen donor. The reaction proceeded in ethanol more efficiently compared to dioxane as ethanol is a better H-donor solvent then dioxane. For instance, the reaction in ethanol only took 6 h for completion compared to dioxane that took 11-17 h for complete conversion.

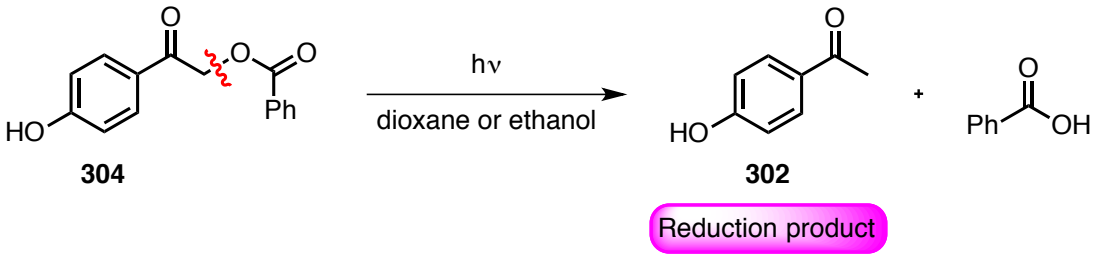

Scheme 5.2: Release of benzoic acid employing phenacyl phototrigger.

Similar observation was noticed by Epstein and Garrossian for the release of ethyl and phenyl phosphate esters from the *p*-methoxy phenacyl phosphates in 1,4-dioxane solvent.[5] This contradiction in the formation of product was attributed to the change in the mechanism involved in the reaction by the employment of non H-donor solvent such as dioxane that did not assist the formation of precursor to form

the rearranged photoproduct (similar to **303**). The influence of the nature of solvent affecting the outcome of the products led to comprehensive study of the phenacyl phototrigger. Along these lines, Givens and coworkers have done extensive studies including the solvent dependent product formation.[6] They examined the release of phosphate esters **305** using *t*-butyl alcohol and methanol as H-donor solvents (Scheme 5.3). The solvents employed for this reaction are more polar in nature compared to dioxane and protic in nature. However, methanol is a much better H-donor solvent compared to *t*-butyl alcohol, which is a poor hydrogen donor. The reaction run in both solvents resulted in rearranged product **306** as the major photoproduct similar to observation made by Anderson and Reese along with the reduction product **302** as a minor. However, the formation of reduction product was 21% in methanol compared to only 14% in *t*-butyl alcohol. So, they further investigated the role of solvent by performing the reaction in deuterated methanol (CD_3OD) and compared with CH_3OH. The formation of reduction product **302** was 5 times lower when the reaction was carried out in CD_3OD compared to CH_3OH. These studies clearly indicated the ability of the solvent to donate hydrogen atom is one of the key factors in determining the formation of reduction product.

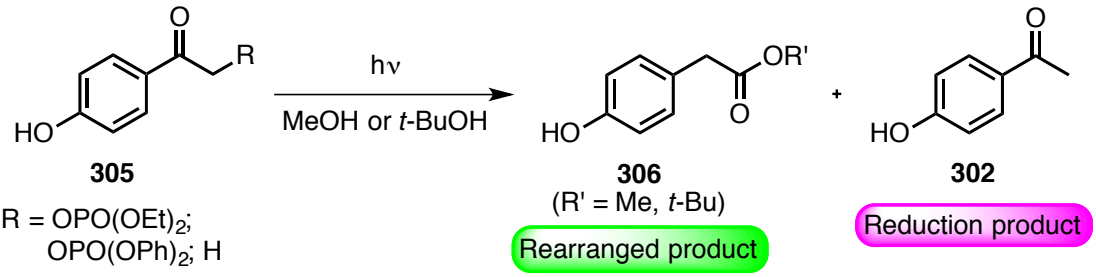

Scheme 5.3: Photo release of phosphates esters **305**.

Based on their extensive work involving solvent, substitution on the phototrigger, Givens and coworkers proposed new mechanistic aspects for the phototrigger, which is depicted in Scheme 5.4.[7] They proposed three plausible mechanistic pathways for the formation of the products. Upon excitation, the compound undergoes a rapid intersystem crossing from singlet to triplet-excited state. In the first pathway, from the triplet-excited state it can either undergo homolytic cleavage to form ketonyl radical, which abstracts a proton from the solvent to form the reduction product. The ketonyl radical can also undergo single electron transfer to form zwitterionic intermediate. The intermediate generates spirodienedione by electrocyclic closure of the intermediate to form rearrangement product. In the second

plausible pathway, a simple heterolytic cleavage resulting in the zwitterionic intermediate followed by spiro derivative to form rearranged product. In the latter case, the release of the leaving group takes place via neighboring group participation leading to the formation of spirodienedione derivative followed by formation of rearranged product. The exact mechanistic pathway of the reaction largely depends on the solvent, substitution on the aryl ring and the leaving group.

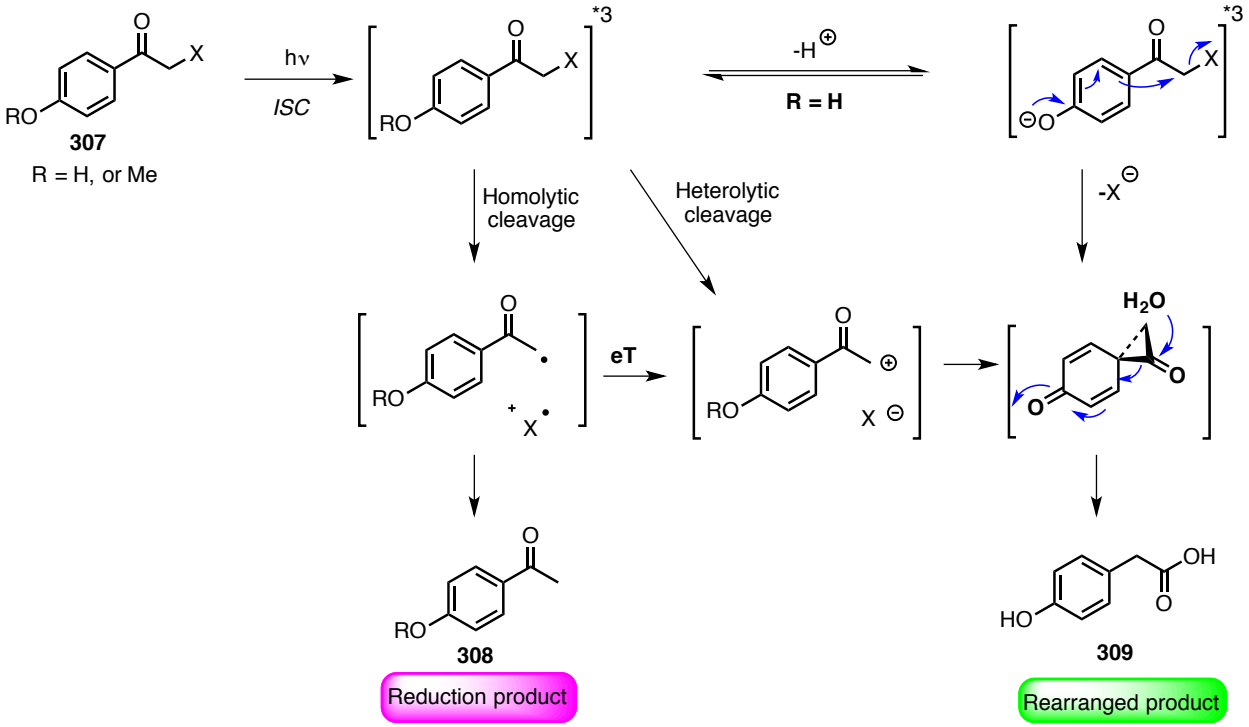

Scheme 5.4: Mechanistic aspect of pHP trigger.

Insights gained from mechanistic analysis on the phototrigger led to widespread use of this approach in the photo protection of thiols, phosphates, acids etc., Apart from its use as photo protecting group, phototriggers were also used in micro pattering of the film by photolithographic technique and biomedical applications like controlled drug delivery. One such application employing the phototrigger was reported by Joy and coworkers (Figure 5.1).[8] They synthesized phenacyl phototrigger based polycarbonates polymer **310**. The polymer film was coated on a silicon surface and irradiated through a 1000 mesh transmission electron microscopy (TEM) grid for 30 min. Upon shining light, the uncovered portion of the polymer film underwent controlled scission leading to TEM grid pattern on the polymer film that was confirmed by AFM and SEM (Figure 5.1 C and D). They had also demonstrated the release of

Nile red nanoparticle loaded in the polymer as a proof of concept for mimicking drug delivery system.[8]

They had performed similar studies by incorporating phototrigger-based polyesters (**311**) as well.[9]

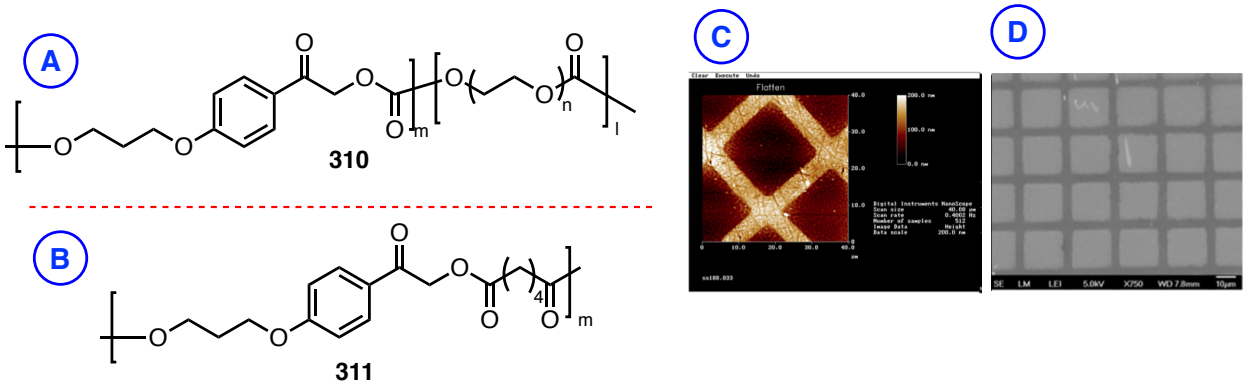

Figure 5.1: A) Phenacyl based polycarbonate polymer. B) Phenacyl based polyesters C) AFM pictures showing the pattern on polycarbonate polymer and D) SEM picture of the pattern. (Reproduced from reference 8 with permission from American Chemical Society, 2012).

While the photodegradable polymers find various applications such as photo patterning, the primary objective in the development of photodegradable polymers was to reduce the wastes caused by the plastics.[10,11] We recently reported one such photodegradable polymers derived form biomass using *o*-nitrobenzyl derivative as a trigger to cleave the polymer. The novelty of our strategy compared to other photodegradable polymers lies in recovering the monomer after the degradation and reusing the monomer to recreate the polymer.[12] Along those lines we have looked at employing *p*HP for the degradation of polymer. In order to evaluate the *p*HP as a phototrigger we initially studied the degradability of the model system. The model system and the precursor listed in Chart 5.1 were synthesized according to procedures reported in the literature.

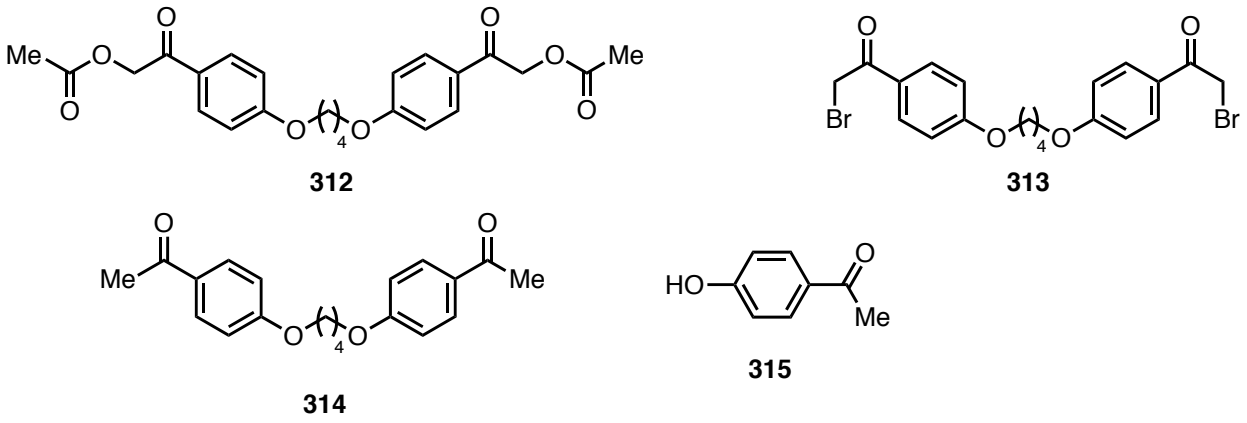

Chart 5.1: Structures of phenacyl trigger based model system and its precursor.

5.3. Synthesis and photodegradation of model compounds

To demonstrate photodegradation of polymer incorporated with *p*HP trigger, we began our investigation by optimizing the reactions conditions employing model compound (**312**). We synthesized the model system starting from hydroxy acetophenone (**315**) as shown in Scheme 5.5.

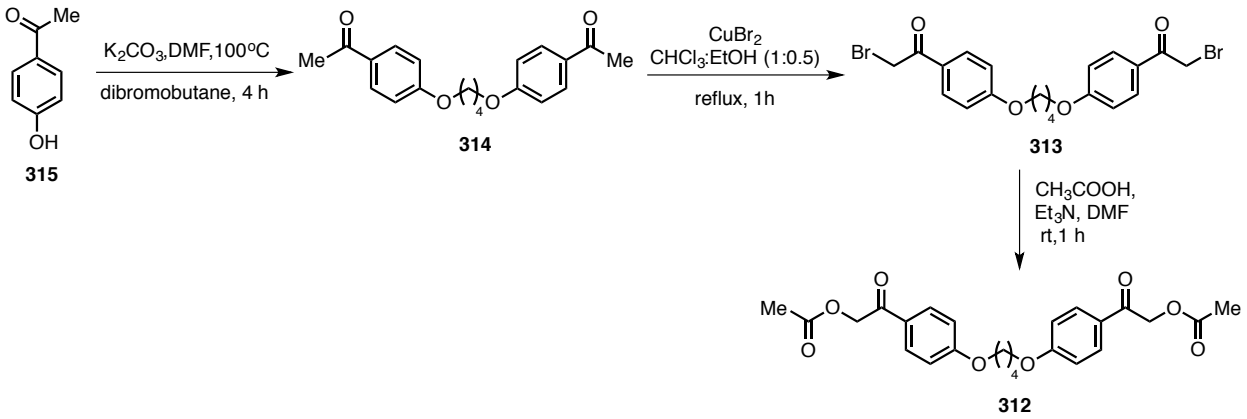

Scheme 5.5: Synthesis of phenacyl based model compound **312**.

Hydroxy acetophenone based model system **312** was obtained by reacting the hydroxy acetophenone **315** in the presence of a base followed by bromination and coupling with the acetic acid (detailed synthetic procedures are given in the experimental section). Irradiation of the ester **312** (Scheme 5.6) was carried out in Rayonet reactor equipped with 300 nm bulbs (16 lamps x 14 watts each). The progress of the reaction was monitored by ^{1}H-NMR spectroscopy after an interval of 15 min. Analysis of the ^{1}H-NMR spectroscopy revealed that the photocleavage was very efficient with complete consumption

of ester (**312**). One of the interesting observations made during the investigation of the model system study is the formation the reduction product (**314**) which was confirmed by comparing the reaction mixture with the authentic sample. The formation of reduction product presents an avenue to recycle the intermediate and use it in the preparation of polymer with the same synthetic procedure shown in Scheme 5.5 as the reduction product (**314**) is one of the intermediate.

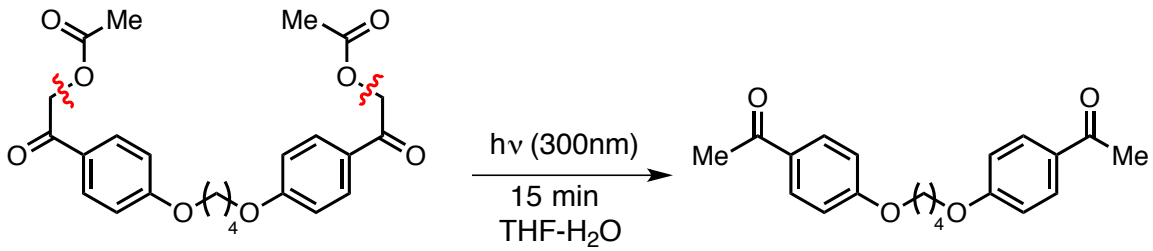

312 **314**

Scheme 5.6: Photoreaction of phenacyl based model system **312**.

The success with the model compounds **312** clearly indicates that the phenacyl as phototrigger could be incorporated in the polymer backbone and can be employed not only for the degradation of polymer but also for recovering and reusing the monomer.

5.4. Conclusions

The use of phenacyl phototrigger was successfully demonstrated in the model system. The photoreaction resulted in the reduction product (**314**), which gives an opportunity recycle and reuse the trigger. In long-term objective, this trigger can be imbibed in the backbone of the polymer to undergo photodegradation, which has the potential to degrade fast and increase the recovery of the trigger derivative.

5.5. Experimental section

5.5.1. General methods

All commercially obtained reagents/solvents were used as received; chemicals were purchased from Alfa Aesar®, Sigma-Aldrich®, Acros organics®, TCI America®, Mallinckrodt®, and Oakwood® Products, and were used as received without further purification. Unless stated otherwise, reactions were

conducted in oven-dried glassware under nitrogen atmosphere. ^{1}H-NMR and ^{13}C-NMR spectra were recorded on Varian 500 MHz (125 MHz for ^{13}C) or Bruker 400 MHz (100 MHz for ^{13}C) spectrometers. Data from the ^{1}H-NMR spectroscopy are reported as chemical shift (δ ppm) with the corresponding integration values. Coupling constants (*J*) are reported in hertz (Hz). Standard abbreviations indicating multiplicity were used as follows: s (singlet), b (broad), d (doublet), t (triplet), q (quartet), m (multiplet) and virt (virtual). Data for ^{13}C NMR spectra are reported in terms of chemical shift (δ ppm). High-resolution mass spectrum data in Electrospray Ionization mode were recorded on a Bruker – Daltronics® BioTof mass spectrometer in positive (ESI+) ion mode.

5.6. General procedure for the model system

5.6.1. Synthesis of hydroxy acetophenone dimer 314

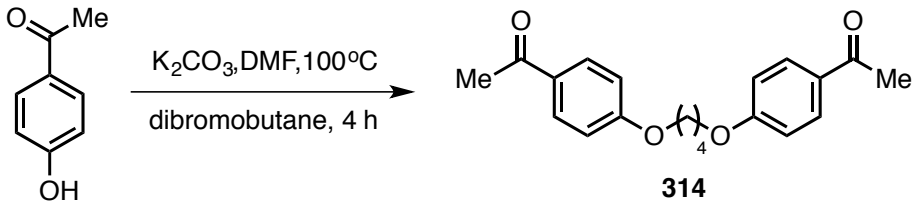

315 **314**

Scheme 5.7: Synthesis of hydroxy acetophenone dimer **314**.

To a solution of *p*-hydroxylphenacyl **315** (6.8 g, 50 mmol, 1 equiv.) in DMF (50 mL), K_2CO_3 (13.6 g, 100 mmol, 2 *equiv*.) and 1,4-dibromobutane (5.4 g, 10 mmol, 0.5 equiv., 2.98 mL) were added and heated at 100 °C for 4 h. Progress of the reaction was monitored by TLC. After completion of the reaction mixture was cooled to room temperature and added to ice cold water upon which white solid precipitated which was filtered, washed with excess of water, methanol (~2 x 25 mL) and dried to get pure product **314** (the obtained compound is pure enough that column chromatography was not necessary) as white solid.

TLC condition - R_f = 0.60 (95% DCM: 5% ethyl acetate) for **314** (Yield = 86 %)

HRMS [ESI-MS] *m/z* ([M+Na]): Calculated: 349.1410; Observed: 349.1409; |Δm|: 0.2 ppm

^{1}H-NMR (500 MHz, $CDCl_3$, δ ppm): 7.95-7.93 (d, 4H, *J* = 10 Hz), 6.94-6.93 (d, 4H, *J* = 5 Hz), 4.13-4.12 (t, 4H, *J* = 5 Hz), 2.57 (s, 6H), 2.04-2.03 (t, 4H, *J* = 5 Hz).

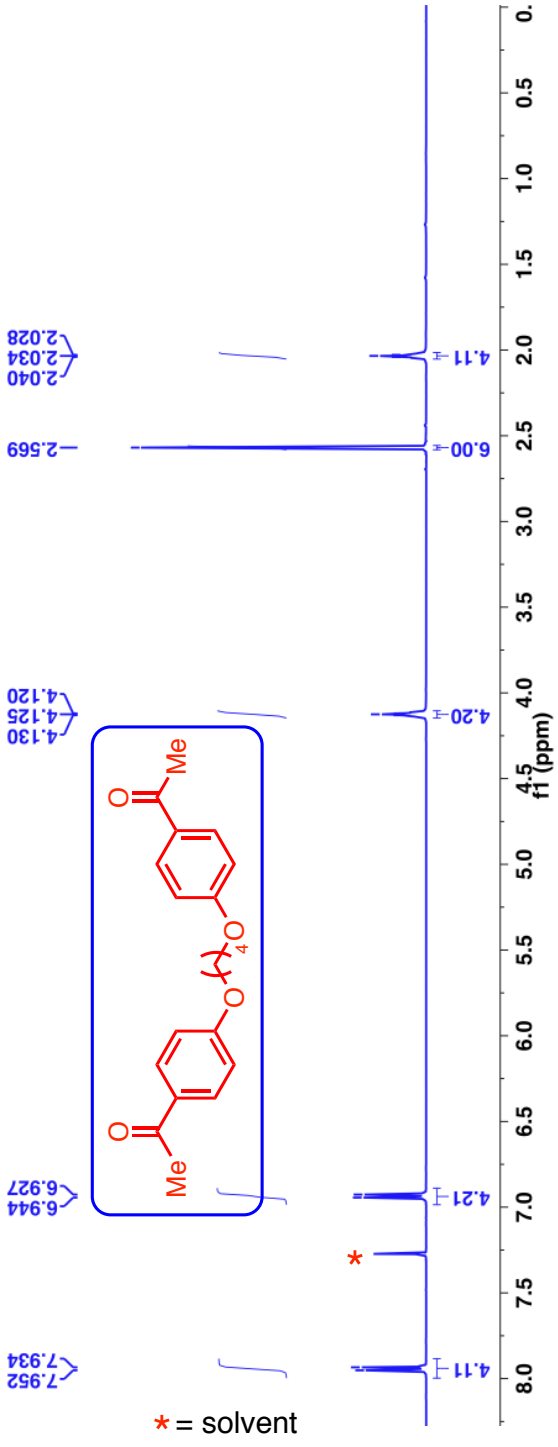

Figure 5.2: ^{1}H-NMR (500 MHz, $CDCl_3$, δ ppm) spectra of hydroxy acetophenone dimer **314**.

^{13}C-NMR (125 MHz, $CDCl_3$, δ ppm): 196.9, 163.0, 130.8, 114.3, 67.8, 26.0.

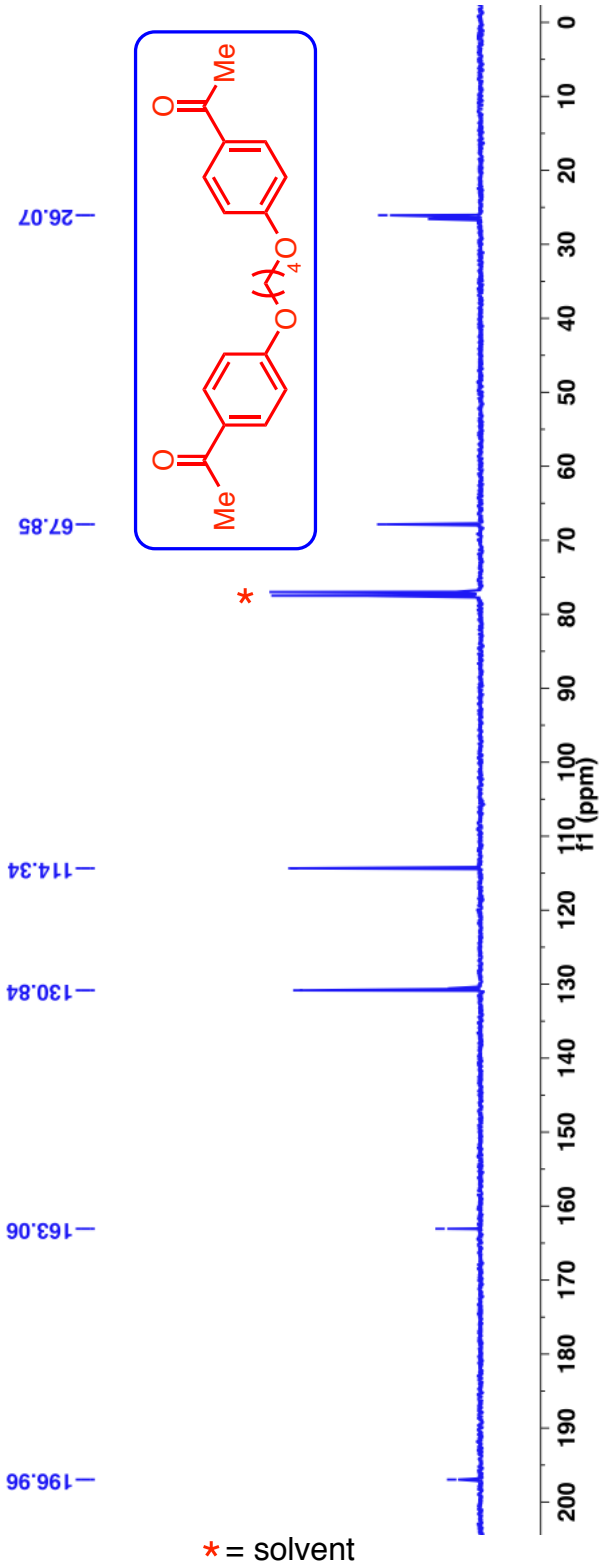

Figure 5.3: ^{13}C-NMR (125 MHz, $CDCl_3$, δ ppm) spectra of hydroxy acetophenone dimer **314**.

5.6.2. Synthesis of bromo derivative 313

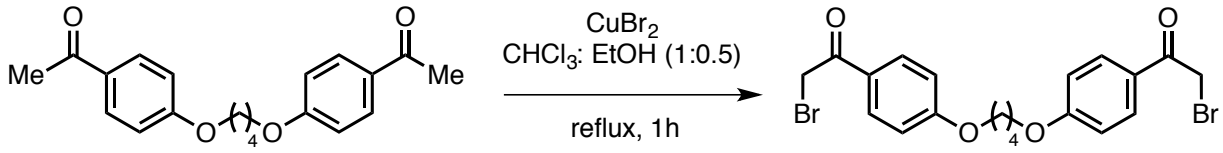

314 **313**

Scheme 5.8: Synthesis of bromo derivative **313**.

Compound **313** was synthesized according to a procedure reported in the literature.[8] $CuBr_2$ (11.16 g, 50 mmol, 5 equiv.) was added to a solution of compound **314** (3.26 g, 10 mmol, 1 equiv.) in $CHCl_3$-EtOH (1:05) (42 mL) and refluxed for 1 h and the progress of the reaction was monitored by TLC. After completion of the reaction mixture was filtered through celite bed and filtrate was concentrated under reduced pressure. The crude product was washed with excess of methanol to get pure product **313** as white solid.

TLC condition - R_f = 0.70 (95% DCM: 5% ethyl acetate) for **313** (Yield = 88%)

HRMS [ESI-MS] *m/z* ([M+Na]): Calculated: 504.9621, 506.9601; Observed: 504.9608, 506.9602; |Δm|: 2.6 ppm and 0.2 ppm

^{1}H-NMR (500 MHz, $CDCl_3$, δ ppm): 7.98-7.97 (d, 4H, *J* = 10 Hz), 6.96-6.95 (d, 4H, *J* = 10 Hz), 4.41 (s, 4H), 4.15-4.14 (t, 4H, *J* = 5 Hz), 2.05-2.04 (t, 4H, *J* = 5 Hz).

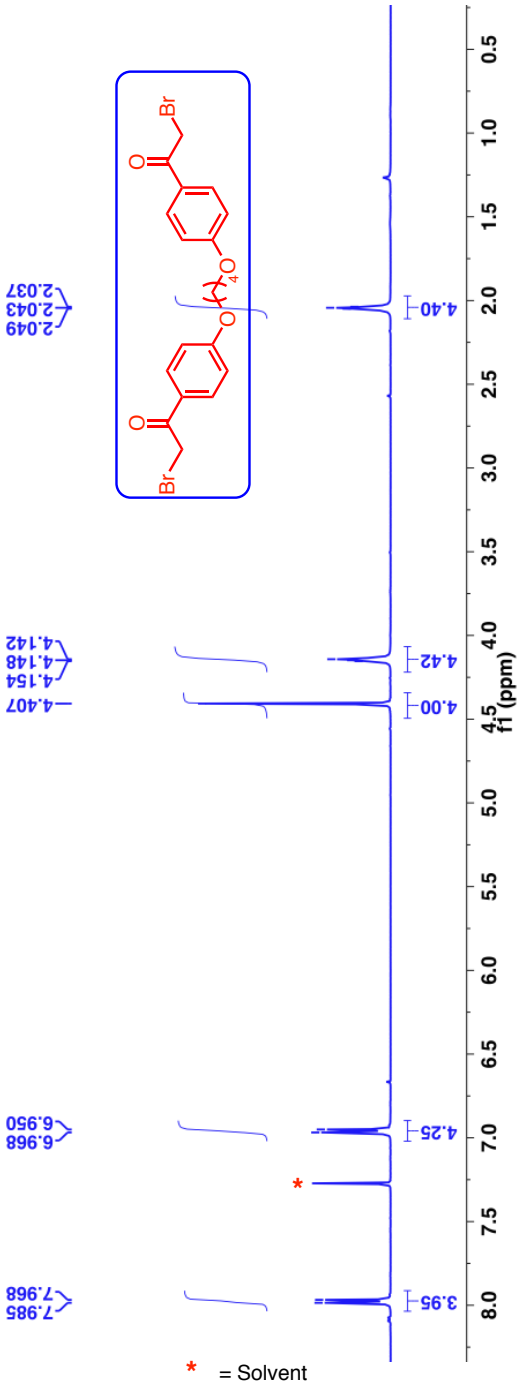

Figure 5.4: ^{1}H NMR (500 MHz, $CDCl_3$, δ ppm) spectra of bromo derivative **313**.

^{13}C-NMR (125 MHz, $CDCl_3$, δ ppm): 190.1, 163.7, 131.6, 127.1, 114.7, 67.9, 30.8, 26.0.

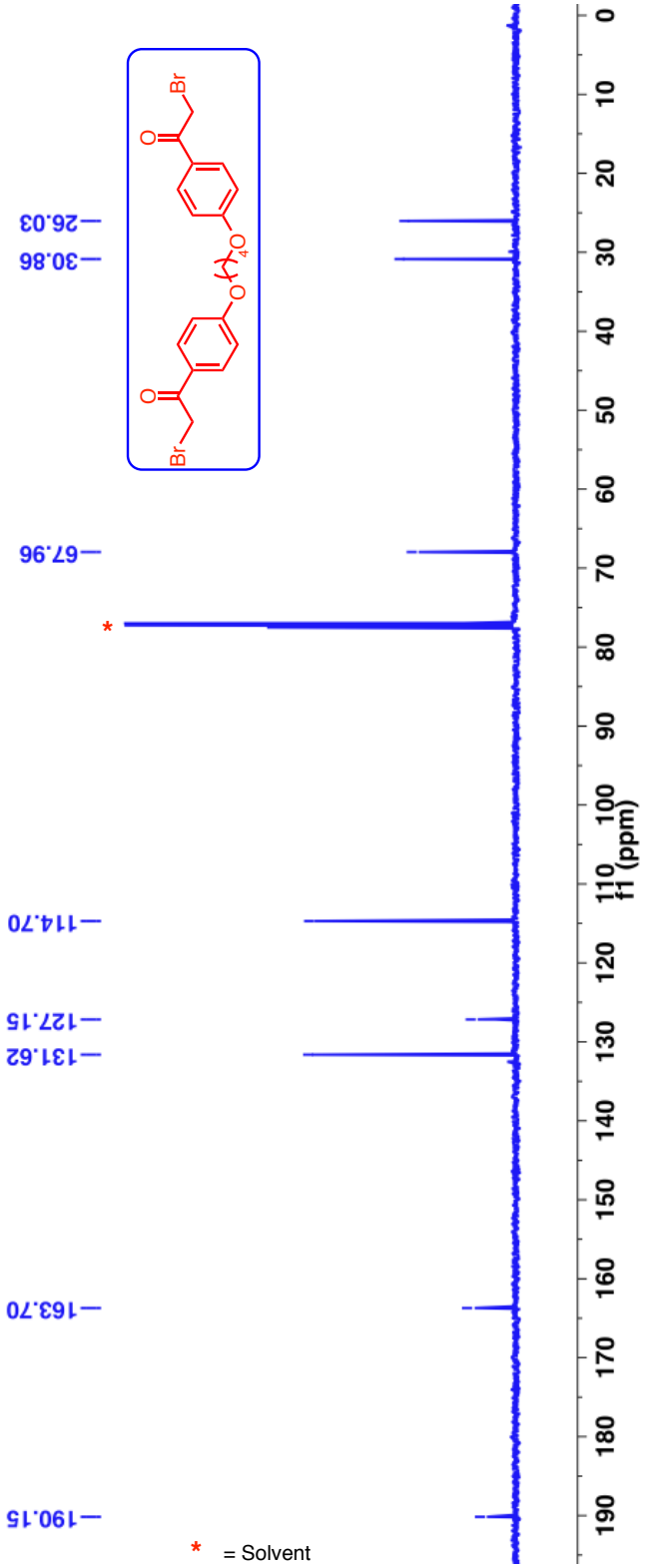

Figure 5.5: ^{13}C-NMR (125 MHz, $CDCl_3$, δ ppm) spectra of bromo derivative **313**.

5.6.3. Synthesis of phenacyl based model system 312

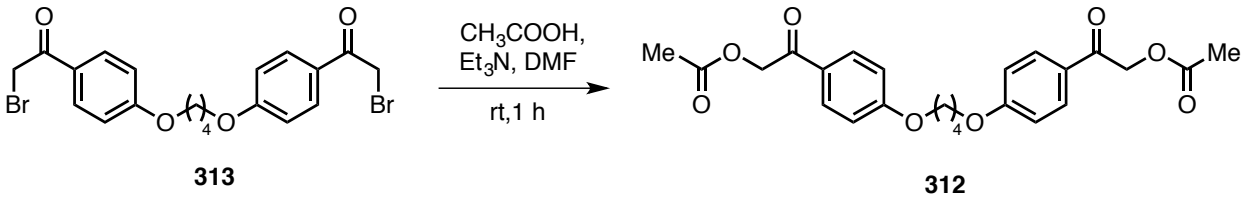

Scheme 5.9: Synthesis of phenacyl based model system **312**.

To a solution of compound **313** (1.21 g, 2.5 mmol, 1 equiv.) in DMF (20 mL), Et_3N (0.758 g, 7.5 mmol, 3 equiv.) followed by acetic acid (0.45 g, 7.5 mmol, 3 equiv., 0.43 mL) were added and stirred at room temperature for 1 h. Progress of the reaction was monitored by TLC. After the reaction, the mixture was quenched with water, extracted with CH_2Cl_2. The organic layer was dried over *anhyd.* Na_2SO_4 and concentrated under reduced pressure. Pure product **312** was obtained after column chromatography using CH_2Cl_2-EtOAc (95:5) as white solid

TLC condition - R_f = 0.30 (95% DCM: 5% ethyl acetate) for **312** (Yield = 27%)

HRMS [ESI-MS] *m/z* ([M+Na]): Calculated: 465.1520; Observed: 465.1520; |Δm|: 0 ppm

^{1}H-NMR (500 MHz, $CDCl_3$, δ ppm): 7.91-7.89 (d, 4H, *J* = 10 Hz), 6.96-6.94 (d, 4H, *J* = 10 Hz), 5.31 (s, 4H), 4.13-4.12 (t, 4H, *J* = 5 Hz), 2.24 (s, 6H), 2.04-2.03 (t, 4H, *J* = 5 Hz).

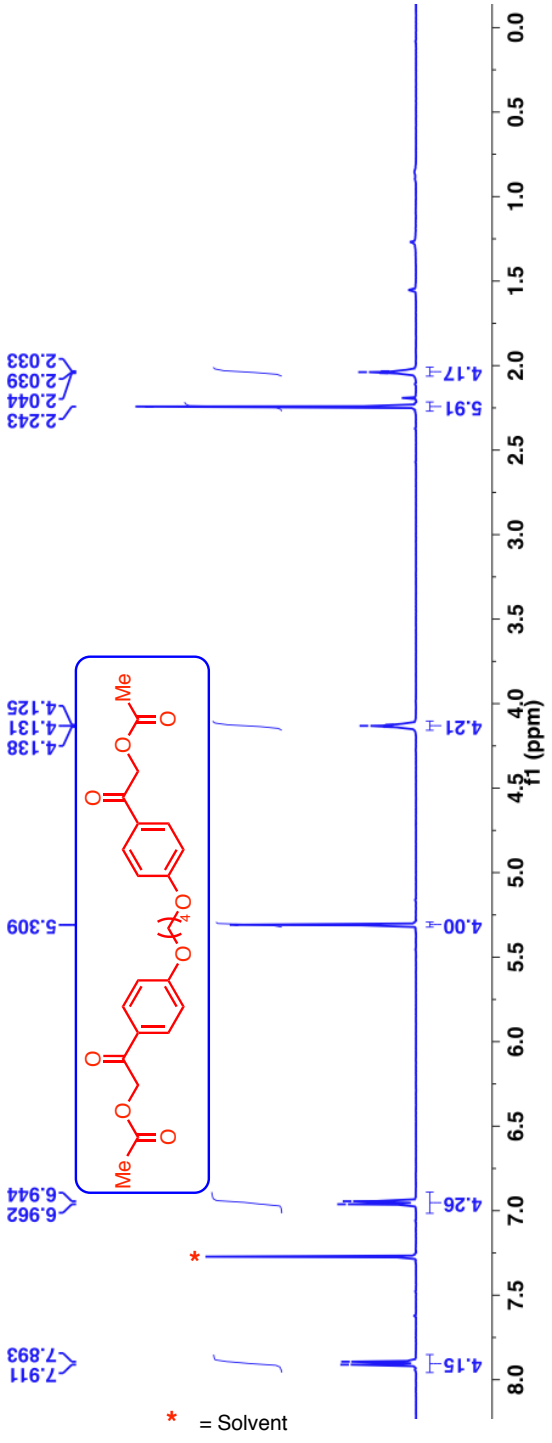

Figure 5.6: ^{1}H-NMR (500 MHz, $CDCl_3$, δ ppm) spectra of ester derivative **312**.

^{13}C-NMR (125 MHz, $CDCl_3$, δ ppm): 190.7, 170.7, 163.6, 130.3, 127.4, 114.7, 67.9, 65.9, 26.0, and 20.9.

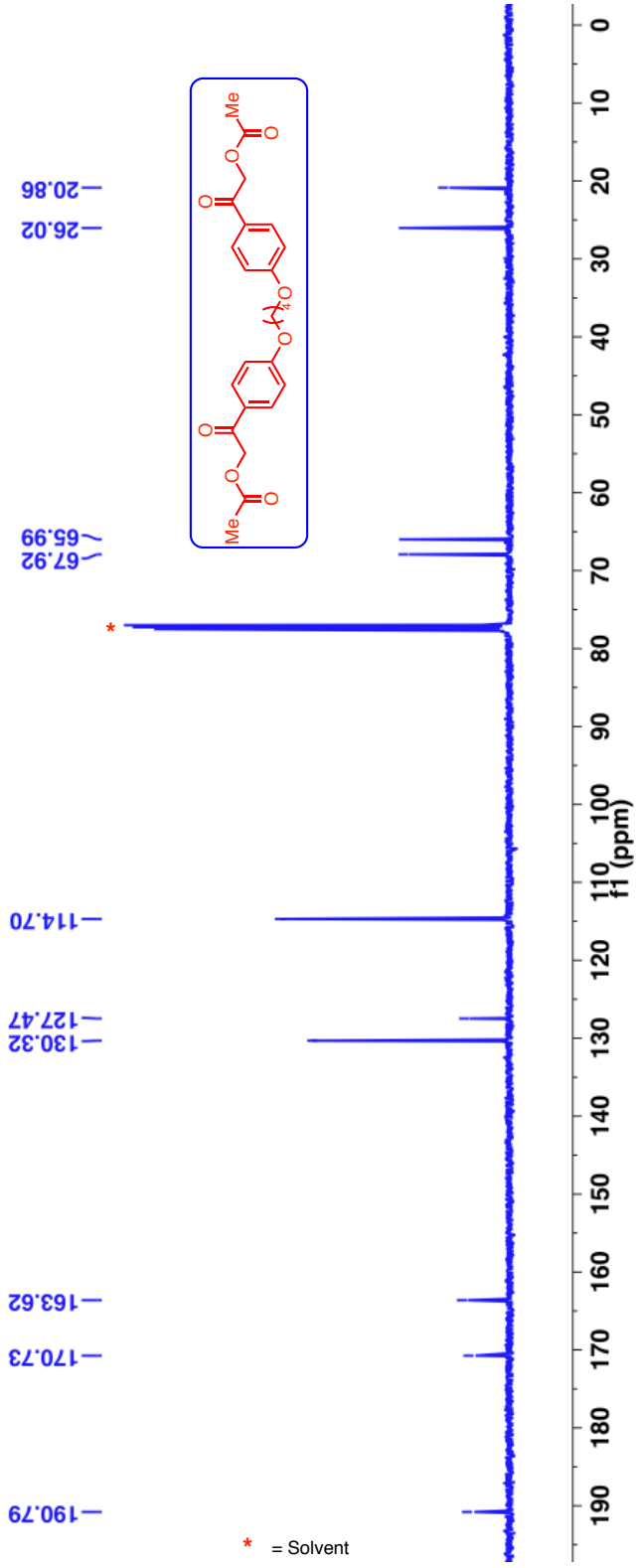

Figure 5.7: ^{13}C-NMR (125 MHz, $CDCl_3$, δ ppm) spectra of ester derivative **312**.

5.7. General procedure and characterization of photocleaved products

Phenacyl phototrigger based model compound **312** in THF-H_2O (4:1) was irradiated for a given time interval in Pyrex tube in Rayonet reactor RPR-200 at 350 nm (16 bulbs x 14 Watts). The photocleaved mixture was analyzed by ^{1}H-NMR spectroscopy.

Conversion and mass balance after photoreaction: Mass balance and conversion of photocleaved compounds were obtained using triphenylmethane as an internal standard (IS). 1 mL of 10^{-2} M (122 mg in 50 mL of $CHCl_3$) solution of triphenylmethane was added to the crude product and evaporated. To the mixture of Internal standard and the photosylate about ~0.6 mL of deuterated solvent is added and ^{1}H-NMR was recorded. From the integral value of respective peaks, the % conversion and mass balance was calculated using the equation 2.1 (Chapter 2)

5.7.1. Photoreaction, mass balance and conversion studies on ester derivative 312

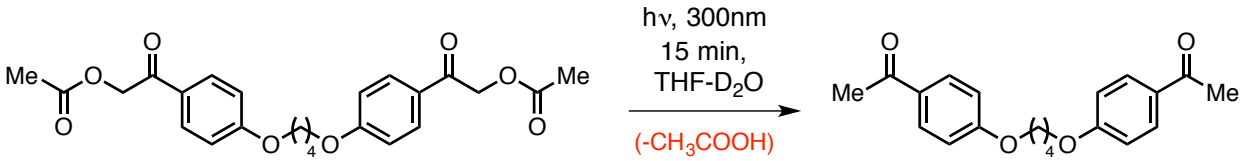

312 **314**

Scheme 5.10: Photoreaction of ester derivative **312**.

A 5 mM (1.0 mg in 0.5 mL of THF-d_8-D_2O (4:1)) solution of ester **312** in THF-d_8-D_2O (4:1) was irradiated at 300 nm and analyzed by ^{1}H-NMR spectroscopy. Photocleavage was completed in 15 min and to the irradiated sample 0.1 mL of 5 mM internal standard (triphenylmethane in THF-d_8-D_2O) was added and ^{1}H-NMR recorded to determine conversion and mass balance.

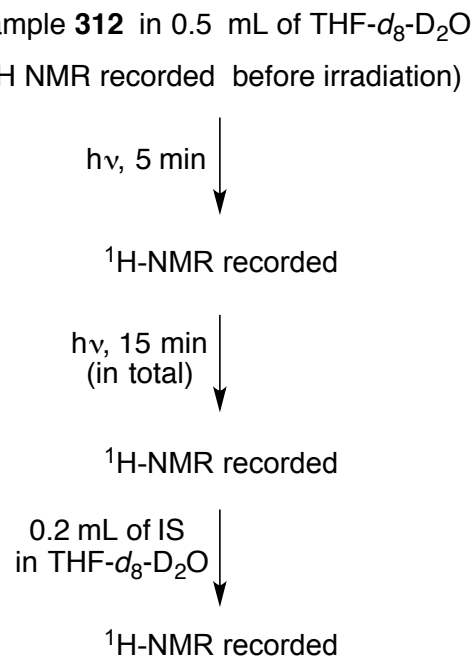

Scheme 5.11: Schematic representation of photoreaction of ester derivative **312**.

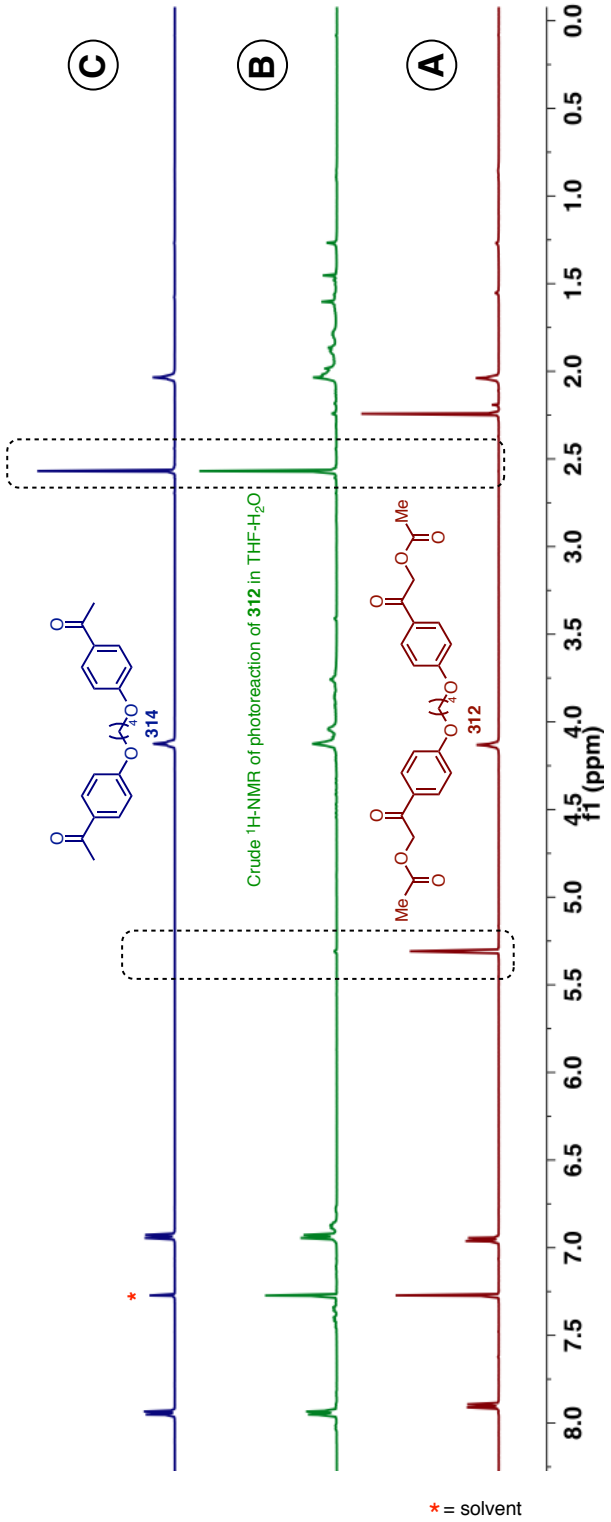

(A) before irradiation and (B) after irradiation.
(C) The authentic **314** is provided for comparison.

Figure 5.8: ^{1}H-NMR (400 MHz, $CDCl_3$, δ ppm) spectra of photoreaction of **312**.

5.8. References

(1) Il'ichev, Y. V.; Schwörer, M. A.; Wirz, J. Photochemical Reaction Mechanisms of 2-Nitrobenzyl Compounds:Methyl Ethers and Caged ATP. *J. Am. Chem. Soc.* **2004**, *126*, 4581-4595.

(2) Givens, R. S.; Rubina, M.; Wirz, J. Applications of *p*-Hydroxyphenacyl (*p*HP) and Coumarin-4-ylmethyl Photoremovable Protecting Groups. *Photochem. Photobiol. Sci.* **2012**, *11*, 472-488.

(3) Anderson, J. C.; Reese, C. B. A Photoinduced Rearrangement Involving Aryl Participation. *Tetrahedron Lett.* **1962**, *3*, 1-4.

(4) Sheehan, J. C.; Umezawa, K. Phenacyl Photosensitive Blocking Groups. *J. Org. Chem.* **1973**, *38*, 3771-3774.

(5) Epstein, W. W.; Garrossian, M. *p*-Methoxyphenacyl Esters as Photodeblockable Protecting Groups for Phosphates. *J. Chem. Soc., Chem. Commun.* **1987**, 532-533.

(6) Givens, R. S.; Athey, P. S.; Matuszewski, B.; Kueper, L. W.; Xue, J.; Fister, T. Photochemistry of Phosphate Esters: α-Keto Phosphates as a Photoprotecting Group for Caged Phosphate. *J. Am. Chem. Soc.* **1993**, *115*, 6001-6012.

(7) Givens, R. S. L., J.-L. The *p*-Hydroxyphenacyl Photoremovable Protecting Group. *J. Photosci.* **2003**, *10*, 37-48.

(8) Sun, S.; Chamsaz, E. A.; Joy, A. Photoinduced Polymer Chain Scission of Alkoxyphenacyl Based Polycarbonates. *ACS Macro Lett.* **2012**, *1*, 1184-1188.

(9) Chamsaz, E. A.; Sun, S.; Maddipatla, M. V. S. N.; Joy, A. Photoresponsive Polyesters by Incorporation of Alkoxyphenacyl or Coumarin Chromophores Along the Backbone. *Photochem. Photobiol. Sci.* **2014**, *13*, 412-421.

(10) Li, S. K. L.; Guillet, J. E. Photochemistry of Ketone Polymers. XIV. Studies of Ethylene Copolymers. *J. Polym. Sci., Polym. Chem.* **1980**, *18*, 2221-2238.

(11) Al-Malaika, S. H., C.; Sheena,; Eds., H. H.: *Photodegradable Polymers*; John Wiley & Sons: New York., 2010.

(12) Rajendran, S.; Raghunathan, R.; Hevus, I.; Krishnan, R.; Ugrinov, A.; Sibi, M. P.; Webster, D. C.; Sivaguru, J. Programmed Photodegradation of Polymeric/Oligomeric Materials Derived from Renewable Bioresources. *Angew. Chem. Int. Ed.* **2015**, *54*, 1159-1163.

CHAPTER 6. FUTURE OUTLOOK

Light plays a vital role in everyday life and has been a great influence in the life sustaining process that takes place around us. We share a close tie with light not only with respect to their influence in biological systems but also with respect to the role they play in the field of medicine, industry, electronics, chemistry etc., This thesis details two such important areas of chemistry i.e. asymmetric transformations of organic molecules and photodegradation of bio-based polymers. Chapter one narrates the role of light in various fields of science; the second and third chapters in this thesis describe strategies to obtain stereoselectivity in photochemical transformations using organophotocatalyst and atropisomeric chromophore respectively. The fourth and fifth chapters details about the use of phototrigger in the degradation of polymer and the reusability of the polymers. With an aim to further explore the above-described aspects in chemistry that utilizes light, this chapter details future goals of the discussed strategies.

Chapter 2 explores the thiourea/urea-based catalyst for enantioselective 6π-photocyclization of acrylanilides. As a continuing effort, evaluation of new catalysts based on non-covalent interactions to enhance the enantioselectivity in the photoproduct(s) is necessary. Also, to broaden the substrate scope, substitution on the β-position of acrylanilides e.g. cyclic enones will give an opportunity to have better hydrogen bonding interaction between the catalyst and the substrate that might influence the %ee in the resulting photoproduct. Varying the substitution on the aryl ring such as electron donating and electron-withdrawing groups, its impact on reactivity and selectivity can be evaluated.

Chapter 3 demonstrates axial-point chiral strategy towards atropselective transformations employing various chromophores such as oxoamides and maleimides. Maleimide chromophore undergoes chain length dependent chemoselective photocycloaddition viz., [2+2] or [5+2] photocycloaddition. Though [2+2] photocycloaddition resulted in high chemical yield, the [5+2]-photocycloaddition resulted in only low yield due to competitive absorption between the reactant and the photoproducts (due to presence of highly conjugated chromophore in the products). In order to address this issue, tandem reactions with conjugated double bond (enones) such as nucleophillic addition, 1,4-conjugate addition using Gilman reagents could be evaluated to increase the yield of the photoproduct

(by removal of the enone chromophore). This in turn also increases the stereocenters in the molecule and also provides a handle to diversify the reactivity.

Chapter 4 and 5 explores the concept of employing phototrigger for programmed degradation of polymers. In chapter 4, nitrophototrigger is employed for photodegradation of polymers. Based on the literature[1-5] reports on nitrophototrigger where the nitrobenzyl derivative features substitution at one of the *ortho* positions, it was established that the presence of nitro group is necessary for the photocleavage resulting in nitroso aldehyde photoproduct. But the studies detailed in chapter 4 were performed with nitrobenzyl compounds that features substitution at both the *ortho* positions of the nitrobenzyl trigger. This makes the break down mechanism more challenging, as the nitroso aldehyde has to initiate the second cleavage for complete decomposition leading to monomer. In order to decipher this, detailed mechanistic investigations needs to be carried out. Preliminary investigation reveals that both oxygen and light are necessary for the second cleavage process. Further studies need to be carried out using laser flash photolysis to identity the reactive intermediate and the excited state(s) involved. Chapter 5 describes the use of phenacyl phototrigger with a model compound to address the shortcomings of the nitrobenzyl phototrigger. Further studies on developing biomass-derived polymers with phenacyl phototrigger needs to carried out to showcase the effectiveness of the strategy.

In summary, light is an environmentally benign reagent that has widespread applications. This dissertation detailed two important areas of chemistry that extensively employs light. Further research along these lines as discussed in this chapter is likely to strengthen the strategies and broaden the scope of the methodologies detailed in this thesis.

6.1. References

(1) Klán, P.; Šolomek, T.; Bochet, C. G.; Blanc, A.; Givens, R.; Rubina, M.; Popik, V.; Kostikov, A.; Wirz, J. Photoremovable Protecting Groups in Chemistry and Biology: Reaction Mechanisms and Efficacy. *Chem. Rev.* **2012**, *113*, 119-191.

(2) Bochet, C. G. Photolabile Protecting Groups and Linkers. *J. Chem. Soc., Perkin Trans. 1* **2002**, 125-142.

(3) Pelliccioli, A. P.; Wirz, J. Photoremovable Protecting Groups: Reaction Mechanisms and Applications. *Photochem. Photobiol. Sci.* **2002**, *1*, 441-458.

(4) Il'ichev, Y. V.; Schwörer, M. A.; Wirz, J. Photochemical Reaction Mechanisms of 2-Nitrobenzyl Compounds:Methyl Ethers and Caged ATP. *J. Am. Chem. Soc.* **2004**, *126*, 4581-4595.

(5) Gaplovsky, M.; Il'ichev, Y. V.; Kamdzhilov, Y.; Kombarova, S. V.; Mac, M.; Schworer, M. A.; Wirz, J. Photochemical Reaction Mechanisms of 2-Nitrobenzyl Compounds: 2-Nitrobenzyl Alcohols form 2-Nitroso Hydrates by Dual Proton Transfer. *Photochem. Photobiol. Sci.* **2005**, *4*, 33-42.